PALACKÝ UNIVERSITY OLOMOUC
Faculty of Science

Structural variability of Photosystem II in land plants

RNDr. Roman Kouřil, Ph.D.

Habilitation thesis

Olomouc 2025

Declaration

I declare that I have prepared this habilitation thesis independently using the literature listed in the reference list at the end of the thesis.

In Olomouc: January 20, 2025   RNDr. Roman Kouřil, Ph.D.

Acknowledgements

Contents

1. Introduction to Photosystem II and its role in photosynthesis

Photosystem II (PSII) is a pivotal component in the photosynthetic process, responsible for the initial step of light-dependent water splitting, which generates oxygen and supplies electrons for the subsequent reactions in the photosynthetic electron transport chain. PSII is embedded in the thylakoid membrane, which forms a flexible, three-dimensional network within chloroplasts. This network is characterized by regular stacks of thylakoids, known as grana, which are interconnected by unstacked stroma thylakoids. The grana and stroma thylakoids create distinct regions within the chloroplast, with the thylakoid lumen enclosed by the membrane and the stroma filling the space outside the thylakoids.

The photosynthetic apparatus within the thylakoid membrane, in addition to PSII, includes several other key membrane protein complexes. Notable among these are Photosystem I (PSI) and the cytochrome (Cyt) b_6/f complex. Together, these components facilitate electron transport, which leads to the reduction of NADP+ to NADPH and to the translocation of protons across the thylakoid membrane. This process generates a transmembrane proton gradient (ΔpH), which ATP synthase then utilizes to produce ATP, an essential energy source for various cellular metabolic processes.

The spatial organization of PSII and PSI within the thylakoid membrane reflects their functional roles. PSII complexes are predominantly found in the grana regions, where they are tightly packed, although a smaller fraction exists as monomers in the stroma thylakoids, participating in the PSII repair cycle. In contrast, PSI complexes are located primarily in the stroma thylakoids and at the grana margins. The spatial segregation of these complexes is influenced by structural factors; for instance, the extrinsic subunits of PSI, which face the stroma, prevent PSI from entering the densely packed grana stacks. ATP synthase is similarly excluded from the grana regions, whereas the Cyt b_6f complex is more uniformly distributed across the thylakoid membrane (Figure 1) (Dekker & Boekema, 2005; **Kouřil et al. 2018**; Nelson & Yocum, 2006)[1].

---

[1]Publications in which I contributed as the main or corresponding author, or as a member of the author team, are highlighted in black bold. Publications included in the Appendix of my habilitation thesis are highlighted in blue bold.
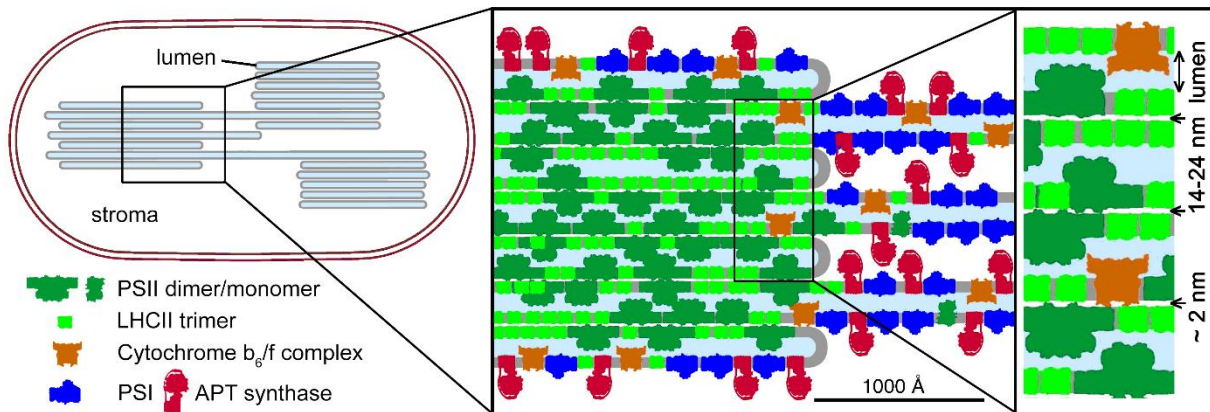
Figure 1. Model of the thylakoid membrane organization within the chloroplast. The model shows a chloroplast with three stacks of grana membranes, connected by stroma membranes. A cross-section of the granum shows a specific distribution of major components of photosynthetic apparatus such as PSII, PSI, cyt *b₆/f* complex, and ATP-synthase (modified from (**Kouřil *et al*. 2018**).

The organization of PSII from green algae and land plants follows a common structural motif, consisting of a core complex and associated peripheral light-harvesting complexes (LHCII). The core complex contains the reaction center and all the cofactors necessary for the primary photochemical reactions, while the peripheral LHCII, composed of Lhcb proteins (Lhcb1-6), optimizes and regulates light harvesting. The core complex of PSII is highly conserved across photosynthetic organisms, but the composition and organization of their LHCII systems exhibit significant variability. The major part of the plant LHCII is represented by LHCII trimers, which consist of three Lhcb proteins (Lhcb1–Lhcb3), and which are associated with the core complex via monomeric antenna proteins Lhcb4 (also called CP29), Lhcb5 (CP26) and Lhcb6 (CP24). Based on the amount of bound LHCII, PSII can assemble into distinct types of supercomplexes. Moreover, PSII can form even larger assemblies, known as megacomplexes formed through the association of multiple PSII-LHCII units. Understanding the structural and functional significance of these supercomplexes is crucial, as they are believed to play important roles in the regulation of photosynthetic efficiency and adaptation to environmental stresses (for reviews see Cao *et al*. 2018; Gao *et al*. 2018; **Kouřil *et al*. 2012**; **Kouřil *et al*. 2018**).

The structural characterization of these large protein assemblies presents significant challenges due to their transient nature and fragility. However, advances in techniques such as clear native polyacrylamide gel electrophoresis (CN-PAGE) and single-particle electron

microscopy (EM) have facilitated the isolation and structural analysis of these complexes, as shown by **Kouřil** *et al.* **(2018)**, who demonstrated the successful combination of CN-PAGE for the separation of pigment-protein complexes with single-particle EM for their structural characterization. This thesis explores the structural variability of PSII in land plants, specifically focusing on *Arabidopsis thaliana* and *Picea abies* as model organisms of angiosperms and gymnosperms, respectively. It focuses on recent experimental approaches and findings that shed light on the organization, function, and physiological significance of these intricate photosynthetic structures.

In this habilitation thesis, I will outline the structural research of photosynthetic complexes, with a primary focus on plant PSII supercomplexes, their assembly into larger megacomplexes, and their organization within the thylakoid membrane. The work begins with a brief overview of key separation techniques commonly employed in EM structural studies, followed by a review of major achievements in the structural analysis of PSII. This habilitation thesis is not intended as an extensive review of the field, but rather as an opportunity to highlight my contributions and scientific papers, obtained in collaboration with my former and current colleagues, and to place these findings within the broader context of PSII structural research.

2. Experimental approaches for the structural analysis of photosynthetic protein complexes

2.1. Isolation and separation of protein complexes for electron microscopy

The preparation of high-quality samples is critical for the success of structural EM studies, as it directly impacts the accuracy and resolution of the final analysis. For cryo-EM in particular, protein complexes must be isolated in a highly pure, concentrated, and structurally intact form. Achieving this level of sample quality typically involves techniques such as sucrose gradient ultracentrifugation, gel filtration chromatography, affinity purification, gel electrophoresis, or their combination. These methods are necessary to ensure that the sample is free of contaminants and possibly breakdown products of particles that might otherwise interfere with structural analysis or introduce artefacts into the reconstruction (Azinas & Carroni, 2023; Stark & Chari, 2016).

In contrast, structural analysis of negatively stained samples imposes less strict requirements on sample purity and concentration. The high contrast provided by negative staining allows different particle types to be easily distinguished and separated during image analysis, even if the sample contains a mixture of proteins (Harris & Horne, 1994; **Kouřil et al. 2005a**). This makes negative staining a useful technique for initial assessments or for studying samples that are difficult to purify to the same degree required for cryo-EM (**Boekema et al. 2009**).

Additionally, EM analysis of photosynthetic protein complexes can be conducted *in situ* on isolated thylakoid membrane fragments. This approach allows researchers to visualize the native distribution and interactions between individual protein complexes, such as PSII, directly within the membrane environment. By examining these complexes in their natural context, valuable insights can be gained into their functional organization and dynamics that might be lost in more isolated preparations (Goral *et al.* 2012; Johnson *et al.* 2011; **Kouřil et al. 2012**; **Kouřil et al. 2011**; **Kouřil et al. 2013**).

In the following section, I briefly review the basic separation techniques commonly used in conjunction with EM structural studies. For more detailed information on these techniques and their applications, readers are encouraged to read the cited publications and review articles.

2.2. Ultracentrifugation on sucrose gradient

Ultracentrifugation on sucrose gradients is a key technique for isolating specific protein complexes, such as PSII or PSI, following the solubilization of thylakoid membranes. After the thylakoid membranes are solubilized with mild detergents like the dodecyl-maltosides (DDM) (the α- and β- anomers) and digitonin, the resulting mixture contains a variety of protein complexes, each with different molecular weights and compositions. To isolate these complexes, the solubilized protein extract is subjected to ultracentrifugation on a sucrose gradient.

The sucrose gradient creates a density gradient within the centrifuge tube, allowing protein complexes to migrate to the region of the gradient where their density matches that of the surrounding sucrose solution. During ultracentrifugation, where samples are typically spun at around 300,000xg, larger and denser complexes, such as PSI and PSII supercomplexes, migrate further through the gradient than smaller or less dense components (e.g., LHCII) due to the greater centrifugal force exerted on complexes with higher molecular mass. This process effectively separates the complexes based on their size and density, enabling the isolation of distinct protein populations in discrete bands within the gradient.

Once the centrifugation is complete, the gradient is carefully fractionated, and the bands corresponding to specific protein complexes are collected for further analysis. Before using a collected fraction for specimen preparation for EM analysis, it is essential to remove excess sucrose to enhance the contrast of the particles in the micrographs. This can be achieved using various techniques, such as dialysis, gel filtration, or buffer exchange. In buffer exchange, short centrifugation is performed using small filters with a molecular weight cut-off of 50–100 kDa, which not only removes sucrose but also concentrates the sample, which is crucial especially for cryo-EM analysis. The success of this approach depends on the careful optimization of the gradient conditions and the solubilization protocol, as these factors directly influence the quality and yield of the isolated protein complexes. This technique is widely used in the study of photosynthetic protein complexes, providing a reliable way to obtain PSII, PSI, and other related complexes in a form that is suitable for detailed structural and functional analysis. This approach was elaborated in detail in our work (**Caffarri *et al*. 2009**), which demonstrated its feasibility for the separation of these complexes and their subsequent functional, biochemical and structural characterization (Figure 2). It has become a reference for further studies (Albanese *et al*. 2016a; Mazor *et al*. 2017; **Opatíková *et al*. 2023**; Sheng *et al*. 2019; Su *et al*. 2017; **van Bezouwen *et al*. 2017**; Wei *et al*. 2016).
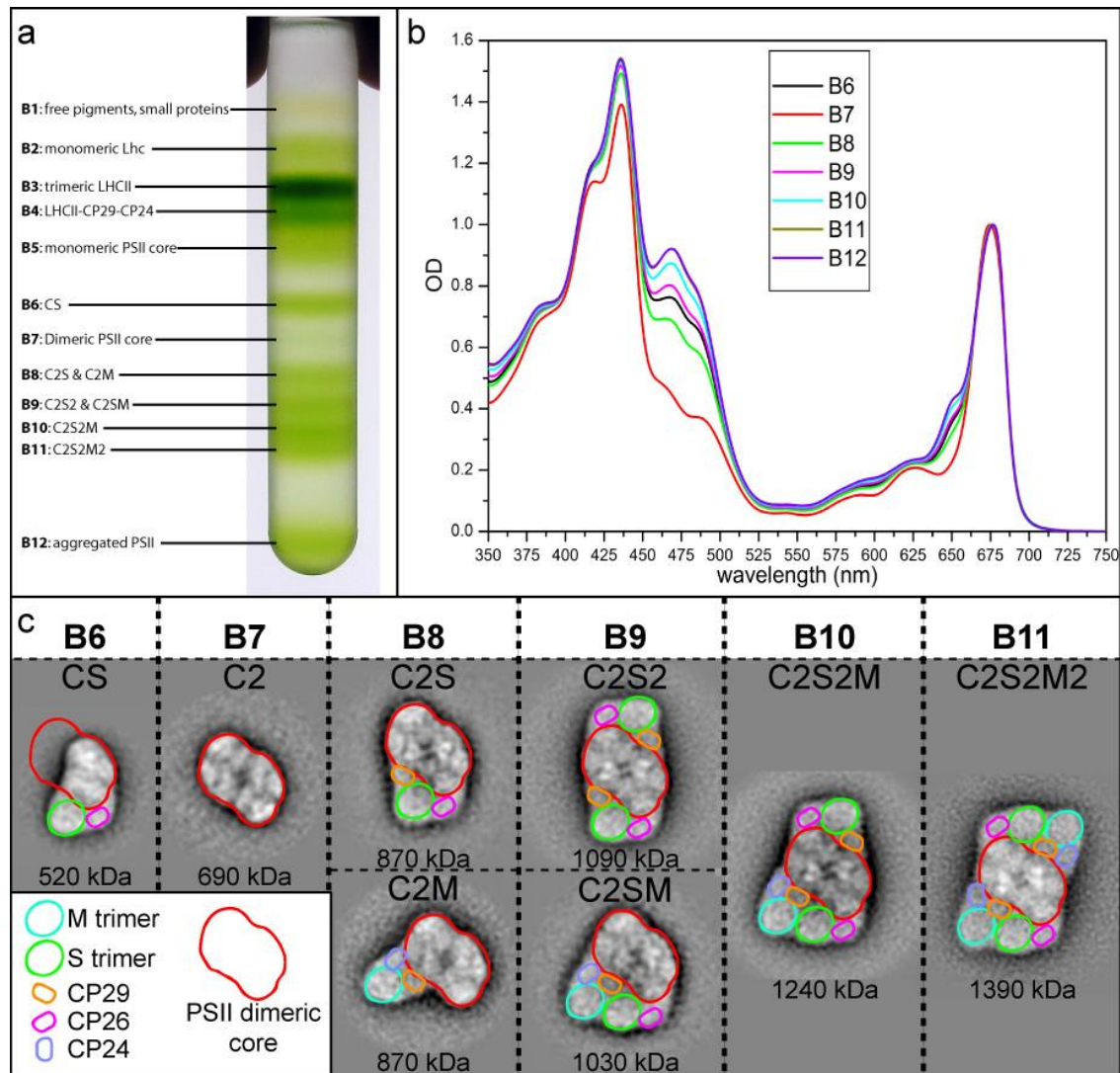
Figure 2. Separation of different forms of PSII supercomplexes by sucrose and their spectral and structural characterization. (a) Sucrose gradient of solubilized PSII membranes, showing specific content of 12 green bands. (b) Absorption spectra of bands 6 to 12. The spectra are normalized to the maximum in the red region. (c) EM analysis of the supercomplexes. The 2D projection maps obtained for bands 6 to 12 are shown. Contours representing the different complexes are superimposed. Legend: C, core; S, LHCII trimer strongly bound; M, LHCII trimer moderately bound. The molecular weight of each particle, calculated on the basis of the protein content as determined by EM and SDS-PAGE, is also reported (modified from **Caffarri et al. 2009**).

2.3. Native gel electrophoresis

Native gel electrophoresis is a widely used method for a separation of membrane protein complexes in their native state. Two common variants are Blue Native PAGE (BN-PAGE) and Clear Native PAGE (CN-PAGE). BN-PAGE uses Coomassie Brilliant Blue (CBB) dye to provide the protein complexes with a uniform negative charge, facilitating their separation based on size and shape (SCHAGGER *et al*. 1994; SCHAGGER & VONJAGOW, 1991). However, this method has certain limitations, especially when applied to fragile protein complexes like photosystem supercomplexes or megacomplexes. One of the main drawbacks of BN-PAGE is that the CBB dye can interfere with protein-protein interactions, potentially destabilizing delicate complexes. Furthermore, based on our experience, spontaneous elution of protein complexes from BN-PAGE gels is often ineffective, making subsequent structural analyses impossible.

In contrast, CN-PAGE offers several advantages for the isolation of photosynthetic protein complexes. Instead of using CBB dye, CN-PAGE employs a mild anionic detergent, such as sodium deoxycholate, to confer a negative charge to the protein complexes (Wittig *et al*. 2007). This approach avoids the potential disruption of weak interactions between protein subunits, making it more suitable for preserving the integrity of large, multi-protein assemblies like PSII and PSI supercomplexes (Wittig & Schägger, 2005).

Moreover, CN-PAGE has proven to be more effective for the spontaneous elution of protein complexes from the gel. This technique allows for the gentle recovery of intact protein complexes, which can then be subjected to further structural analysis, such as single-particle EM or cryo-EM (**Kouřil *et al*. 2014**; Wu *et al*. 2023). The use of deoxycholate in CN-PAGE has been shown to maintain the stability of protein complexes better than CBB, further enhancing its suitability for the separation of photosynthetic supercomplexes (**Kouřil *et al*. 2018**).

Overall, while both BN-PAGE and CN-PAGE are valuable tools for the separation of membrane protein complexes, CN-PAGE offers distinct advantages when working with fragile, multi-protein assemblies. Its ability to preserve the integrity of complexes and facilitate spontaneous elution makes it an excellent choice for preparing samples for structural studies (Figure 3).
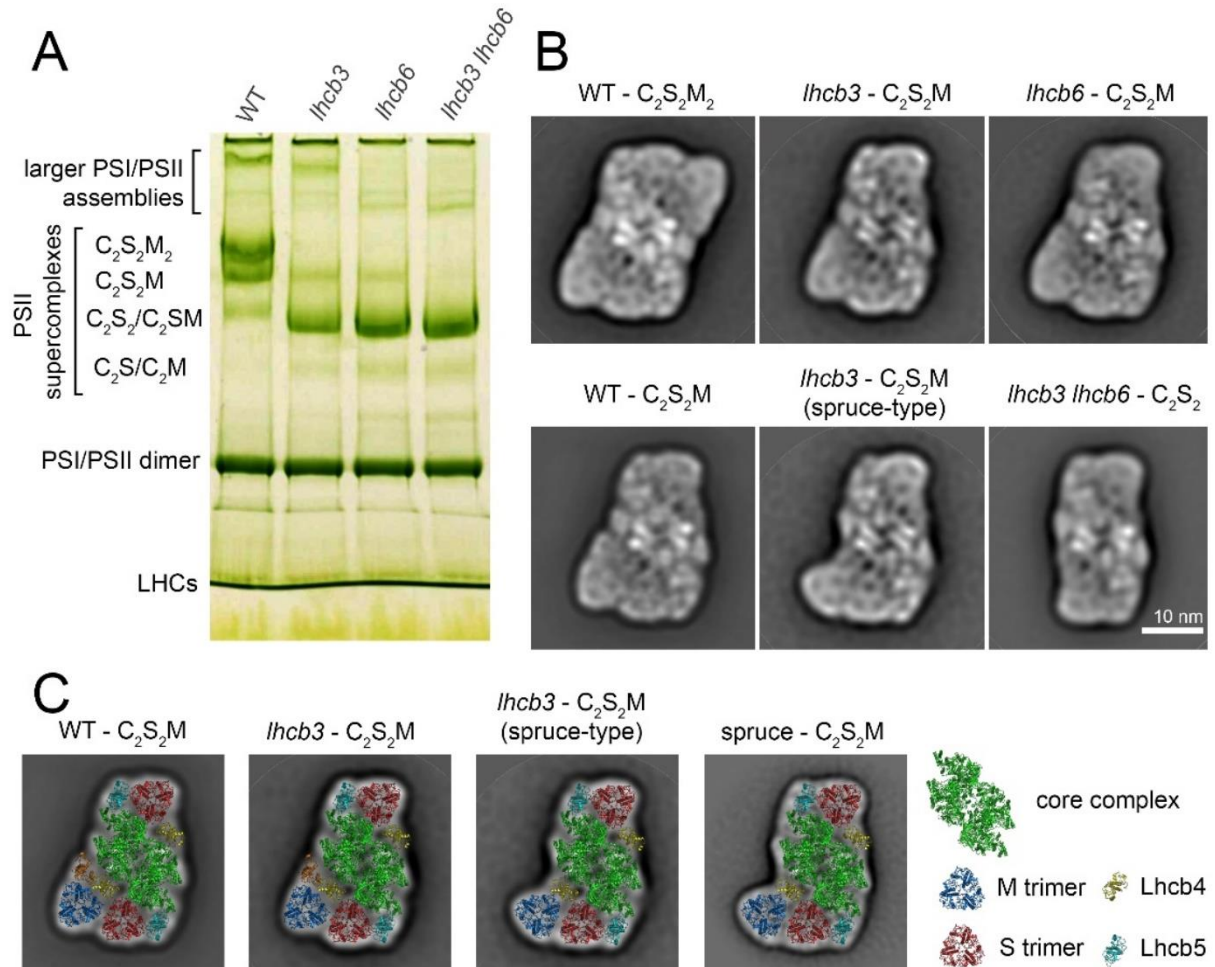
Figure 3. Separation and structural characterization of PSII supercomplexes from WT and mutant plants (lhcb3, lhcb6, lhcb3 lhcb6). (A) CN-PAGE separation of pigment–protein complexes from thylakoid membranes from *A. thaliana* WT, lhcb3, lhcb6, and lhcb3 lhcb6 mutants solubilized by α-DDM. Different forms of separated PSII supercomplexes consist of PSII core dimer (C_2) and one and/or two copies of strongly (S) and moderately (M) bound light-harvesting trimers. (B) Structural characterization of the largest forms of PSII supercomplexes revealed in WT and lhcb3, lhcb6, and lhcb3 lhcb6 mutants. (C) Structural models of C_2S_2M PSII supercomplexes from WT and lhcb3 mutant shown in (B) supplemented with the model of C_2S_2M separated from thylakoid membranes of spruce (**Kouřil *et al*. 2016**). The models were obtained by a fit of the high-resolution structure from **van Bezouwen *et al*. (2017)**. Individual PSII subunits are color-coded (modified from **Ilíková *et al*. 2021**).

2.4. Free-flow electrophoresis

Free-Flow Electrophoresis (FFE) is an advanced technique used for the separation of protein complexes, offering unique advantages in the isolation of large complexes or

supercomplexes that may be challenging to separate using other methods. One of the most significant benefits of FFE is its ability to perform continuous separation under native conditions, which helps preserve the activity and structural integrity of the protein complexes throughout the separation process (Eichacker *et al*. 2015).

What sets FFE apart from other separation techniques is its remarkable speed of separation. This rapid processing is particularly advantageous for isolating transiently formed supercomplexes or those that have a tendency to disintegrate or fall apart over time, such as in the case of the PSI-cytb_6f or PSI-LHCII supercomplexes (**Yadav *et al*. 2017**). In such cases, the quick and gentle nature of FFE ensures that the protein complexes are separated and collected before any significant structural changes can occur. This is crucial for maintaining the functional state of the complexes, allowing for more accurate downstream analyses, such as single-particle EM, where maintaining the native conformation of the protein complexes is essential. Thus, the non-invasive nature of FFE makes it an ideal choice for researchers looking to isolate transiently formed or unstable protein assemblies, ensuring that the complexes remain as close to their native state as possible during the separation process. This technique is particularly useful in the study of photosynthetic protein supercomplexes, where the preservation of intricate protein-protein interactions is critical for understanding their functional mechanisms.

2.5. Size exclusion chromatography

SEC, also known as gel filtration chromatography, is a widely utilized separation technique in the preparation of samples for EM analysis. SEC works on the principle of separation based on the size of the separated molecules as they pass through a column filled with porous beads. Larger molecules elute first because they cannot enter the pores of the beads and thus travel a shorter path, while smaller molecules enter the pores and take longer to pass through the column (Dekker *et al*. 2002; Tokutsu *et al*. 2012; van Roon *et al*. 2000).

This method has been used extensively in the past to prepare samples for EM analysis because it allows efficient purification of protein complexes or membrane fragments by removing aggregates, contaminants and smaller subunits that that could complicate EM analysis. The resulting fractions from SEC are typically of a relatively high purity and homogeneity, which are essential for single-particle EM. Furthermore, SEC is a non-denaturing technique, meaning it preserves the native state of the protein complexes. This characteristic makes SEC an ideal choice for preparing samples for structural analysis by EM, ensuring that

the complexes retain their structural integrity and biological activity during the separation process.

In earlier studies, particularly those involving pilot structural analyses of PSI and PSII complexes (e.g., Boekema *et al*. 1999; **Kouřil *et al*. 2005b**; **Kouřil *et al*. 2005a**; van Roon *et al*. 2000; Yakushevska *et al*. 2001; Yeremenko *et al*. 2004), SEC was commonly used as the primary separation method. These early applications of SEC were essential in achieving the purity needed for the initial EM studies that laid the groundwork for more detailed structural studies.

Today, however, SEC is often used as a secondary or "clean-up" step rather than the main purification method. It is particularly effective for removing contaminants such as residual sucrose or other small molecules that might be present after other purification steps, prior to cryo-EM analysis (Shen *et al*. 2022). This cleaning step is essential to ensure that the sample does not contain any substances that could interfere with the vitrification process or degrade the quality of the cryo-EM images and their subsequent analysis. Thus, although SEC remains an important tool for the separation of protein complexes, its role has evolved over time to support more advanced purification strategies that better meet the requirements of high-resolution structural studies using cryo-EM.

2.6. Affinity chromatography

Affinity purification is a widely used technique for isolating tagged proteins or protein complexes that bind specifically to a ligand immobilized on a column matrix (Block *et al*. 2009; Bumba *et al*. 2005; Büchel *et al*. 2001; Heijbel *et al*. 2004; Spriestersbach *et al*. 2015). This method is highly specific and can provide pure complexes, making it a valuable tool in preparing samples for structural analysis as we have shown for example in the case of PSI analysis (Drop *et al*. 2011; Hansson & Vener, 2003). However, the technique requires that the protein of interest be genetically modified to include a tag, such as a His-tag, FLAG-tag, or Strep-tag, which can then interact with the corresponding ligand on the column (Zhao *et al*. 2013).

Although affinity chromatography is efficient and effective, it is important to note that the addition of a tag can potentially affect the function and structure of the protein. These modifications might influence natural interactions of the proteins, folding, or activity, leading to artifacts that could influence the results of structural studies. For instance, recent studies have highlighted that longer His-tags can induce higher-order oligomerization of proteins through specific tag-mediated interactions (Ayoub *et al*. 2023). This emphasizes the need to carefully

evaluate tag length and its removal to minimize such risks. Therefore, careful experimental design is crucial to minimize these risks. Researchers must ensure that the tag is placed in a region of the protein that is unlikely to disrupt its function or structure. Possible side effects need to be verified. This verification can be achieved by using complementary techniques such as functional assays and comparing their results with measurements on the non-labelled protein to confirm that the labelled protein behaves in the same way as its native counterpart.

2.7. Isolation of grana membranes using a mild solubilization

Mild solubilization of intact thylakoid membranes using digitonin is a widely used method for isolating grana membranes, where PSII complexes are predominantly located. This technique is particularly effective for maintaining PSII *in situ*, which is crucial for detailed structural analyses of PSII localization and interactions using EM, as we have repeatedly demonstrated in several of our studies (**Kouřil *et al*. 2020**; **Nosek *et al*. 2017**), including cryo electron tomography (cryo-ET) (Daum & Kühlbrandt, 2011; Daum *et al*. 2010; **Dlouhý *et al*. 2021**; **Kouřil *et al*. 2011**). The process begins with solubilization of thylakoid membranes using low concentrations of digitonin, which selectively disrupts stromal thylakoids due to the relatively large size of the digitonin molecule. This size allows preferential access to stromal thylakoids and their solubilization, while tightly packed grana stacks remain largely intact and can be easily sedimented by the subsequent centrifugation and further analyzed. Therefore, digitonin allows us to obtain grana membrane fragments with intact PSII supercomplexes, which is particularly useful for studying the structural organization of PSII in its natural membrane environment. Application of a low concentration of alpha-dodecyl maltoside (α-DDM), another mild detergent, prior to specimen preparation for cryo-ET represents another mild solubilization approach. α-DDM gently disrupts intact thylakoid membranes into smaller fragments suitable for tomography, overcoming the size constraints of intact membranes for high-resolution analysis. Cryo-ET analysis of these smaller membrane fragments allows their detailed spatial characterization, including the location of PSII and PSI complexes, and their structural analysis by 3D sub-volume averaging, as demonstrated in our recent cryo-EM study (**Arshad *et al*. 2021**). However, the analysis of intact thylakoid membranes (without detergent application) by cryo-ET is also feasible, but only in areas where the sample thickness is not too large (Daum *et al*. 2010; Grinzato *et al*. 2020) or an advanced technique such as cryo-focused ion beam milling is used to thin the specimen (Bussi *et al*. 2019; Engel *et al*. 2015; Noble & de Marco, 2024) (see also below), so that the sample is permeable to the electron beam. Studying

2. Experimental approaches for the structural analysis of photosynthetic protein complexes

thylakoid membrane samples without detergent represents a situation closer to *in vivo* and possible artifacts due to the presence of detergent can also be avoided.

3. Structural analysis using electron microscopy techniques

Structural analysis by EM technique and especially the method of single-particle EM has revolutionized the structural analysis of protein complexes, providing insights at near-atomic resolution without the need for crystallization. This method is particularly advantageous for studying large macromolecular assemblies, including heterogeneous samples, and dynamic processes in biological systems (Costa *et al.* 2017; Fernández & Vega, 2013; Frank, 2002; Ruprecht & Nield, 2001). The two primary approaches in single-particle EM are negative staining and cryo-EM. Additionally, cryo-ET has emerged as a powerful technique for studying the three-dimensional organization of cellular structures in their native context (Daum & Kühlbrandt, 2011; Hong *et al.* 2023; Koning *et al.* 2018; Staehelin & Paolillo, 2020). The following part explores the principles, methodologies, and applications of these techniques, with a focus on their roles in structural biology.

3.1. Principles of single-particle electron microscopy

Single-particle EM is a powerful technique for determining the 2D and 3D structures of protein complexes. This method involves the collection of thousands of images of individual particles to analyze their structural properties. The image analysis begins with the selection of individual particle projections, which are extracted from micrographs. These projections are then mutually aligned, classified based on their orientations, mass and shape, and averaged into specific 2D classes that represent distinct views of the protein complex under study. For 3D analysis, these 2D class averages are used to reconstruct a 3D density map of the molecule. Unlike traditional crystallography, which depends on the formation of crystalline samples, single-particle EM does not require crystallization. This makes it particularly advantageous for studying large, flexible, or heterogeneous complexes that are often challenging or impossible to crystallize (**Boekema *et al*. 2009**; Ruprecht & Nield, 2001; Serna, 2019; Vinothkumar & Henderson, 2016; Wu & Lander, 2020).

The process of image alignment and classification is facilitated by sophisticated software tools designed for EM image processing. Numerous software packages have been developed to handle the complex tasks of 2D and 3D image analysis, including for instance RELION, EMAN2, SCIPION and CryoSPARC (de la Rosa-Trevín *et al.* 2016; DiIorio & Kulczyk, 2022; Frank, 2002; Sharov *et al.* 2021; Sorzano *et al.* 2018). These tools offer a range of functionalities, from basic 2D alignment and classification of negatively stained specimens to more advanced 3D reconstruction and refinement of cryo-EM datasets. 2D analysis is

particularly useful in the case of negative staining, where the aim is to obtain basic information about the architecture of the protein complex or to assess the quality and homogeneity of the sample before proceeding to more detailed 3D studies (Arthur & Ciferri, 2019; **Boekema *et al.* 2009**; Burgess *et al*. 2004; Harris & Horne, 1994). For cryo-EM, the software must account for the increased complexity of processing images where the particles are preserved in vitreous ice, requiring advanced algorithms to correct for factors such as beam-induced motion and contrast transfer function (CTF) variations (Campbell *et al*. 2012; Li *et al*. 2013; Zhang, 2016; Zheng *et al*. 2017; Zheng *et al*. 2022).

A critical aspect of single-particle EM is the improvement of the signal-to-noise ratio (SNR). In EM, the images are often dominated by noise, making it challenging to discern the structural details of the particles. By averaging a large number of projections of individual particles, random noise is reduced and the true signal - representing the repeated structure of the molecule - is enhanced. This averaging process significantly improves the contrast of the projection maps, allowing for more accurate structure assignment and detailed reconstruction. In cryo-EM, where the particles are embedded in a layer of amorphous ice and preserved in their native state, this improvement in SNR is even more critical, as it allows for the visualization of finer details, ultimately enabling the determination of structures at near-atomic resolution (Lee *et al*. 2014; Sorzano *et al*. 2006).

Overall, single-particle EM, supported by a suite of specialized software and advanced image processing techniques, provides an unparalleled ability to study the structural dynamics of complex biological molecules. Its ability to produce high-resolution 3D reconstructions without the need for crystallization has made it an essential tool in the field of structural biology.

3.2. Negative staining

Negative staining is one of the oldest and most widely used techniques for visualizing macromolecules in EM. Introduced by Brenner and Horne in 1959 (Brenner & Horne, 1959), this method involves embedding the specimen in a heavy metal salt, such as uranyl acetate, which scatters electrons more effectively than the light elements found in organic matter, such as carbon, nitrogen, oxygen, and hydrogen. This scattering provides the necessary contrast for imaging. The stain surrounds the biological molecules, filling the gaps around them and allowing their outlines to be visualized against a dark background.

The process begins with the application of a small drop of the purified protein complex onto a hydrophilic carbon-coated grid. Excess sample is removed by blotting with filter paper, after which the grid is stained with a heavy metal salt solution. Following another blotting step

or air drying, the grid is ready for transfer to the electron microscope for imaging (Figure 4A). Negative staining provides high contrast images, making it ideal for the initial screening of samples to assess their purity, homogeneity, and overall structural integrity. However, the resolution is typically limited to around 10-15 Å due to the grain size of the stain and potential artifacts such as flattening and distortion of the specimen during drying (**Boekema *et al*. 2009**; Harris & Scheffler, 2002; Sawicka *et al*. 2017; Scarff *et al*. 2018).
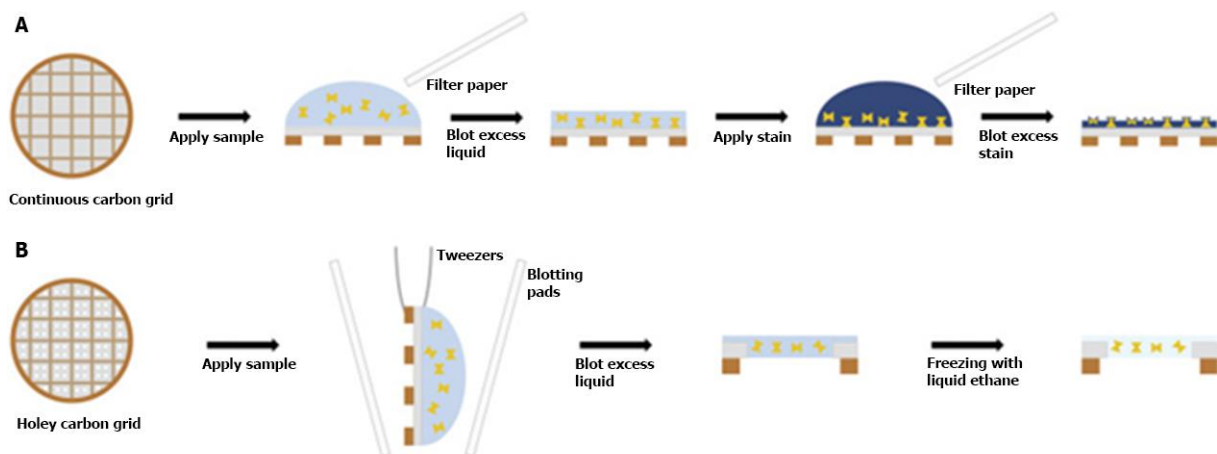
Figure 4. Workflows of specimen preparation for single particle EM. (A) The procedure for preparation of the negatively stained specimen for EM analysis at room temperature using a grid with continuous carbon film. (B) The procedure for preparation of the specimen for cryo-EM analysis using a grid with holey carbon film (modified from Sawicka *et al*. 2017).

3.3. Cryo-electron microscopy

Cryo-EM, pioneered by Jacques Dubochet in the early 1980s, has revolutionized structural biology by enabling the visualization of biological specimens in near-native states. Initially developed to mitigate radiation damage to biological samples, cryo-EM revealed its potential for producing 3D structural maps at near-atomic resolution. This was first demonstrated by Henderson *et al*. in 1990 with their work on bacteriorhodopsin (Henderson *et al*. 1990). The technique involves rapid freezing of samples in vitreous ice, preserving their hydration and structural integrity without requiring staining or dehydration (Dubochet *et al*. 1988; Thompson *et al*. 2016; Xu & Liu, 2020).

Early cryo-EM relied on grids with continuous carbon films, requiring the tilting of grids during imaging to obtain angular views for 3D reconstruction. This method presented challenges, including interference from the film and difficulties in image contrast and

alignment. The development of holey carbon grids revolutionized the field by suspending particles in ice without the interference of a continuous film. These grids enabled the capture of particles in random orientations, simplifying the process of 3D reconstruction (Quispe *et al*. 2007).

The introduction of direct electron detectors (DEDs) was a pivotal advancement, significantly enhancing sensitivity and the signal-to-noise ratio by directly capturing electrons (Mendez *et al*. 2019; Veesler *et al*. 2013). In contrast, conventional CCD detectors relied on an indirect process, converting electrons into photons via a scintillator before detecting them as an electronic signal, and were much slower in data readout (Faruqi & Henderson, 2007). The superior speed of DEDs enabled real-time data acquisition and processing, facilitating advances in motion correction algorithms and dose optimization strategies that further preserved structural details. Together, these innovations led to the 'resolution revolution' of the 2010s, achieving resolutions as fine as 1.5 Å for many macromolecules, with the highest resolution of nearly 1 Å obtained for apoferritin (Yip *et al*. 2020).

The workflow begins with applying a sample onto a holey carbon grid, blotting excess liquid, and rapidly plunging the grid into liquid ethane cooled by liquid nitrogen (Figure 4B). This prevents ice crystal formation and preserves fine structural details. Cryo-EM's advantages over traditional techniques, like X-ray crystallography, include its ability to handle large, flexible, or heterogeneous macromolecular complexes. In recognition of its impact, the Nobel Prize in Chemistry was awarded in 2017 to Jacques Dubochet, Richard Henderson, and Joachim Frank for their pioneering contributions.

3.4. Cryo-electron tomography

Cryo-electron tomography (ET) represents another structural method in the field of EM. Unlike single-particle EM, which involves imaging of isolated particles, cryo-ET is designed to examine the three-dimensional architecture of intact biological samples, such as cellular organelles and their inner compartments, in their native environments (Chakraborty *et al*. 2020; Erdmann *et al*. 2018; Koning *et al*. 2018; Lucic *et al*. 2008; Lucic *et al*. 2013; Turk & Baumeister, 2020; Xu & Liu, 2020).

The process of cryo-ET begins similarly to cryo-EM, with the rapid freezing of the sample in vitreous ice to preserve its native state without introducing artifacts from dehydration or chemical fixation. However, instead of collecting images of multiple identical particles, cryo-ET involves tilting the sample within the electron microscope and collecting a series of 2D projections at different angles. This tilt series is then computationally aligned and reconstructed

into a 3D volume, known as a tomogram, which represents the entire structure of the sample (Figure 5).

Cryo-ET is particularly powerful for studying the structural organization of large macromolecular complexes within the context of their cellular environment. For example, it has been extensively used to visualize the arrangement of photosynthetic complexes within thylakoid membranes (**Arshad *et al*. 2021**; Bussi *et al*. 2019; Daum & Kühlbrandt, 2011; Daum *et al*. 2010; Engel *et al*. 2015; **Kouřil *et al*. 2011**; Nevo *et al*. 2007; Shimoni *et al*. 2005), providing insights into the spatial relationships between different protein complexes that are critical for understanding how photosynthesis is regulated in response to environmental changes.

One of the key advantages of cryo-ET is its ability to capture the native arrangement of macromolecules within a crowded cellular environment, where individual complexes can be observed interacting with one another in real-time. This capability is invaluable for studying dynamic processes such as protein trafficking, organelle biogenesis, and the assembly of large molecular machines. Moreover, cryo-ET can be combined with sub-tomogram averaging to enhance the resolution of specific macromolecular complexes within the tomogram, allowing for detailed structural analysis of complexes that are too heterogeneous or flexible for traditional single-particle EM (Castaño-Díez *et al*. 2012; Castaño-Díez *et al*. 2017; Daum *et al*. 2010; Huang *et al*. 2022; **Kouřil *et al*. 2011**; Ni *et al*. 2022).

Recent advances have further expanded the capabilities of cryo-ET. The integration of cryo-focused ion beam (cryo-FIB) milling has been particularly important. Cryo-FIB milling allows the preparation of electron-transparent lamellae from thick biological samples, such as whole cells or tissues, by precisely thinning regions of interest. This technique minimizes multiple scattering of electrons, which often limits resolution in thicker samples, and enables the detailed imaging of complex cellular structures that were previously inaccessible (Buckley *et al*. 2020; Klumpe *et al*. 2021; Schaffer *et al*. 2019; Tacke *et al*. 2021).

In addition, the development of phase plates has significantly improved image contrast in cryo-ET, especially for low-density or small structures, by reducing phase contrast distortions (Asano *et al*. 2016; Koning *et al*. 2018; Turonová *et al*. 2020). These tools, combined with advanced denoising algorithms, address limitations such as low signal-to-noise ratios and the missing wedge artifact caused by the incomplete angular coverage of tilt series. Machine learning techniques are increasingly employed to enhance tomogram segmentation, automate particle picking, and reconstruct continuous heterogeneity within samples, pushing the boundaries of structural and functional analysis (Furat *et al*. 2019; Zhao *et al*. 2023).

Cryo-ET, like cryo-EM, benefits from the advancements in direct electron detectors and sophisticated image processing software, which have significantly enhanced the quality of tomographic reconstructions. Innovations such as constrained single-particle tomography are bridging the gap between single-particle EM and cryo-ET, providing high-resolution reconstructions of macromolecules within their native environments. These developments are pushing the boundaries of what can be resolved *in situ*, making cryo-ET an important tool for the structural analysis of complex biological systems.

1. Culture cells grown on EM grids

2. Plunge freezing

3. Production of FIB lamella

6. Segmentation

5. Reconstruction

4. Tilt-series collection
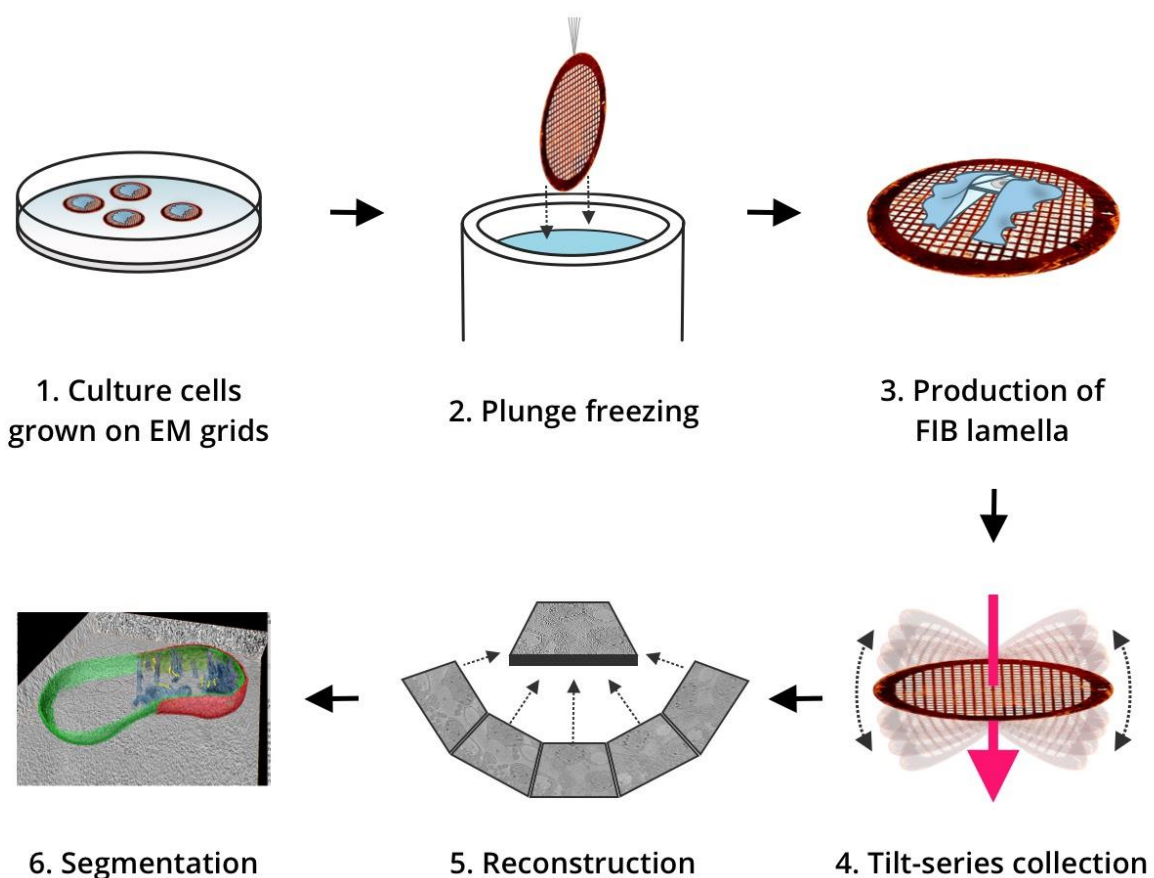
Figure 5: Workflow for cryo-ET of cells. Six steps include growing of the cells on gold grids (1), which are plunge frozen in liquid ethane (2). The thick part of the sample at the region of interest is thinned into a lamella using the cryo-FIB milling (3). This step is not necessary for thin samples such as unstacked or fragmented parts of the thylakoid membrane. The tilt series of images is collected in the cryo-EM (4). The tomogram is reconstructed from the images in the tilt series (5) and segmented to define the structures of interest from the data set (6) (adopted from https://micro.org.au/).

3.5. Challenges and future directions in cryo-electron microscopy

Despite the tremendous success of single-particle EM, several challenges persist that limit its full potential. A primary limitation is the necessity for substantial amounts of purified protein, which can be particularly challenging to obtain for complexes that are unstable or exist in low abundance. The purification process must yield samples that are not only pure but also homogeneous and intact, which makes a bottleneck for structural studies. Additionally, the intrinsic heterogeneity of biological samples presents another challenge. Variations in particle size, conformation, and composition can complicate image processing, potentially reducing the resolution of the final reconstruction. These issues are particularly pronounced in the study of smaller or highly flexible complexes (Drulyte *et al.* 2018; Lyumkis, 2019; Noble & de Marco, 2024). However, recent advancements in image processing software show that flexible complexes and even heterogeneous samples containing different forms of both PSII and PSI, where the protein of interest constitutes approximately 20% of the sample, can yield meaningful results (manuscript in preparation). This clearly highlights the growing potential of single-particle EM to overcome some of its traditional limitations.

Future advancements in single particle cryo-EM and cryo-ET will likely be driven by the integration of artificial intelligence to streamline workflows, enhance image processing, and resolve structural heterogeneity in challenging samples. Hardware innovations, such as improved direct electron detectors, phase plates, and cryo-FIB milling, will continue to push resolution limits and expand the capability to analyze structures within complex native environments. Hybrid approaches that combine single particle EM and cryo-ET are expected to enable comprehensive studies of macromolecular complexes, bridging high-resolution structural insights with *in situ* context. Furthermore, these techniques are poised to impact drug discovery and functional biology by providing detailed visualizations of biomolecular interactions in near-native states, unlocking new possibilities for understanding and leveraging biological complexity (Galaz-Montoya, 2024; Wang *et al.* 2024; Watson & Bartesaghi, 2024).

4. Structural organization of PSII supercomplexes

4.1. Evolution of the structural analysis of PSII using single particle electron microscopy (1995-2000)

Structural analysis of PSII is an important area of research for understanding the molecular basis of photosynthesis. PSII is a multi-subunit protein complex embedded in the thylakoid membranes of chloroplasts and cyanobacteria that plays a key role in the light reactions of photosynthesis by catalyzing water oxidation and plastoquinone reduction. The first studies of the structure of PSII predominantly used EM with negative staining, which laid the foundation for later high-resolution studies using the advanced cryo-EM technique.

In the mid-1990s, structural analysis of PSII was performed primarily using EM negatively stained samples, which provided the first important insights into the structure of PSII and its associated light-harvesting complexes (LHCs). Boekema *et al.* (1995) were among the first to use this technique to investigate the structural organization of PSII supercomplexes in spinach. Their work revealed the dimeric nature of PSII and identified different types of configurations of this supercomplex. This study emphasized the modular nature of PSII and showed that different types of supercomplexes can be formed by changing the number and spatial arrangement of LHCII monomers and trimers around the PSII core. Hankamer *et al.* (1997a) demonstrated that dimeric PSII cores are more stable and exhibit higher oxygen-evolving activity than monomeric cores, supporting the functional advantages of dimerization in PSII. Based on these key findings, Boekema *et al.* (1998) further investigated the structural heterogeneity of PSII in partially solubilized membranes using negative EM staining. This study was important in introducing the concepts of "strongly bound" (S) and "moderately bound" (M) trimers of LHCII, which are now fundamental to our understanding and classification of different types of PSII supercomplexes, such as the $C_2S_2M_2$, C_2S_2M, C_2S_2, C_2SM, C_2S, C_2M, C_2, and CS configurations (Figure 6). By identifying these S and M trimers, Boekema *et al.* established a framework for describing the assembly and variability of PSII supercomplexes and demonstrated that the structural arrangement of these trimers is affected by environmental factors such as light intensity. These findings provided compelling evidence for the structural flexibility of PSII, a property critical for optimizing photosynthetic efficiency under different light conditions.
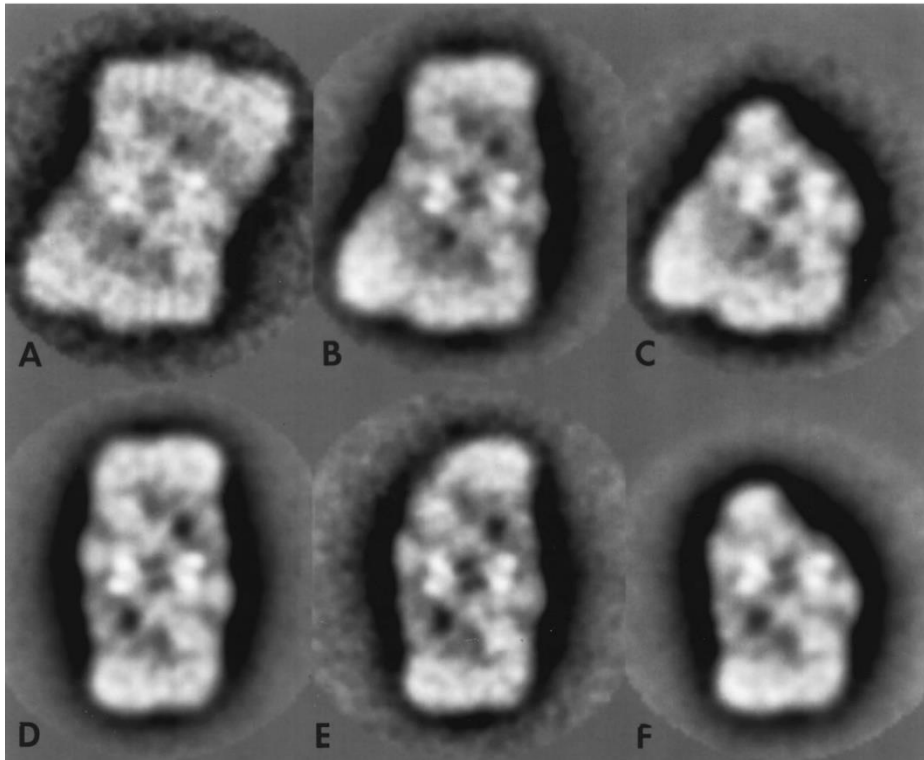
Figure 6: Average projections of the six largest and most abundant types of spinach PSII supercomplexes. The projections represent $C_2S_2M_2$ (A), C_2S_2M (B), C_2SM (C), C_2S_2 (D, E) and C_2S (F) types of supercomplexes. The number of summed images is: 30 (A), 225 (B), 125 (C), 260 (D), 120 (E) and 350 (F) (adopted from Boekema *et al.* 1998). Note that the relatively small number of averaged projections reflects mainly the technical limitations of the time, including the manual recording of micrographs and the hardware limitations of computing clusters, which constrained the analysis to smaller datasets. Despite these limitations, however, it was possible to make a basic description of the structural organization of the PSII supercomplex and its peripheral components.

In a subsequent study, the designation concept of PSII supercomplexes was supplemented with a third type of LHCII binding position, termed "loosely bound" (L) (Figure 7) (Boekema *et al.* 1999). This discovery introduced the "L" designation into the nomenclature of PSII supercomplexes, for example $C_2S_2M_2L_2$, where the L-LHCII trimer represents the next level of adaptation of the PSII supercomplex to external light conditions. The study found that incorporation of this LHCII binding site can create larger and more diverse supercomplexes, such as the C_2S_2ML and C_2S_2L configurations, further illustrating the structural diversity of PSII in response to environmental changes. These findings highlighted the role of PSII structural heterogeneity in regulating energy transfer pathways and adapting to different light

conditions, and pointed to the dynamic assembly process of PSII and its associated LHCII antennae.
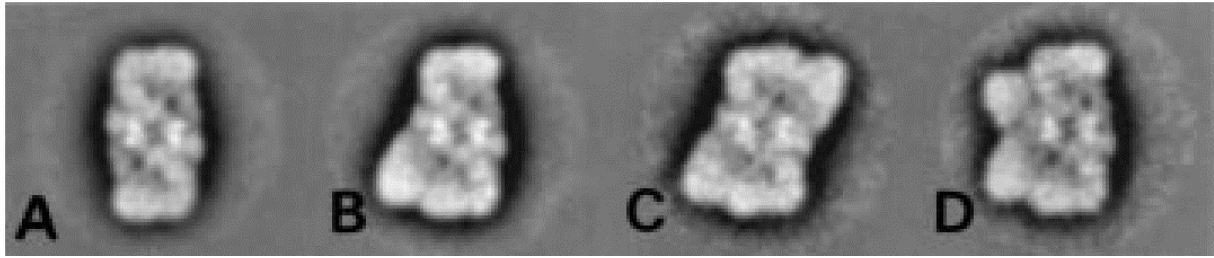
Figure 7: Average projections of spinach PSII supercomplexes showing three different binding positions for LHCII trimers. PSII Average projections of (A) the best 600 C_2S_2, (B) the best 360 C_2S_2M, (C) 91 $C_2S_2M_2$, (D) 86 C_2S_2ML particles (modified from Boekema *et al.* 1999).

4.2. Further progress in understanding the structure of PSII (2000-2009)

The application of cryo-EM to the study of PSII represented a significant advancement in the field, providing a more detailed and native-like view of the PSII supercomplexes. One of the pioneering studies in this area was conducted by Nield *et al.* (2000), which offered the first 3D structure of the PSII supercomplex from higher plants using cryo-EM and single particle analysis. The structure was solved with a resolution of 24 Å, which, although not high resolution by today's standards, was remarkably good for its time and provided, among other things, insights into the spatial arrangement of PSII's core components, including the reaction center proteins D1 and D2, the inner antenna proteins CP43 and CP47, and the positioning of LHCII trimers, and crucial information about the arrangement of the outer oxygen complex (OEC) proteins on the lumenal surface (Nield *et al.* 2000). Importantly, this study highlighted the strong structural similarity between the PSII core complex of higher plants and that of cyanobacteria, underscoring the evolutionary conservation of the PSII architecture. This similarity suggests that the fundamental design of the PSII core has been highly preserved due to its critical role in photosynthetic function. The study also related higher resolution data from electron crystallography (Hankamer *et al.* 1999; Rhee *et al.* 1997) to identify the binding sites of OEC proteins, specifically localizing the 33 kDa OEC protein towards the CP47/D2 side of the reaction center, and the 23/17 kDa proteins near the N-terminus of the D1 protein. These findings marked a significant leap in PSII structural research, laying a robust foundation for understanding how the OEC and its associated components are organized within the supercomplex.

4. Structural organization of PSII supercomplexes

Significant advancements in understanding the structural organization and functional roles of PSII components have been achieved using biochemical and genetic approaches. Negative staining EM analysis of the PSII supercomplexes in Arabidopsis wild-type plants revealed distinctive features such as the strong association of M-type LHCII trimers with the PSII core (Yakushevska *et al*. 2001), which differed from previously studied spinach supercomplexes (Boekema *et al*. 1999; Boekema *et al*. 1998). These findings highlighted the diversity and adaptability of PSII structures across plant species. To further broaden the scope of PSII research, scientists have included species such as the liverwort *Marchantia polymorpha*, one of the oldest lineages of land plants. Harrer *et al*. (2003) used two- and three-dimensional EM to examine the PSII complexes in this early-evolving species, providing valuable insights into its conserved architecture. Their findings demonstrated a conserved PSII architecture across land plants, with tightly associated LHCII trimers and monomeric light-harvesting proteins contributing to structural stability of PSII supercomplexes, underscoring the evolutionary conservation of its characteristic features. Yakushevska *et al*. (2003) advanced the understanding of PSII architecture by localizing the minor antenna proteins CP26 and CP29 using single-particle EM. Their findings showed that these proteins occupy specific positions within the PSII supercomplex, where they play roles in stabilizing its structure and optimizing energy transfer between LHCII and the PSII core. Together, these studies highlight the integral role of minor antenna proteins in the functional flexibility and structural integrity of PSII.

The era of structural research on PSII using negative staining was notionally capped by the study of (**Caffarri *et al*. 2009**), which at the time represented the most detailed characterization of the PSII supercomplex. We used a combination of single-particle EM, biochemical analysis, and mutant studies to resolve the structure of the $C_2S_2M_2$ PSII supercomplex in *Arabidopsis thaliana*, the model organism of land plants, at 12 Å resolution. This study provided a near-complete picture of PSII organization, identifying the precise locations of the S- and M-LHCII trimers as well as the minor antenna proteins CP24, CP26 and CP29 within the supercomplex (Figure 8).
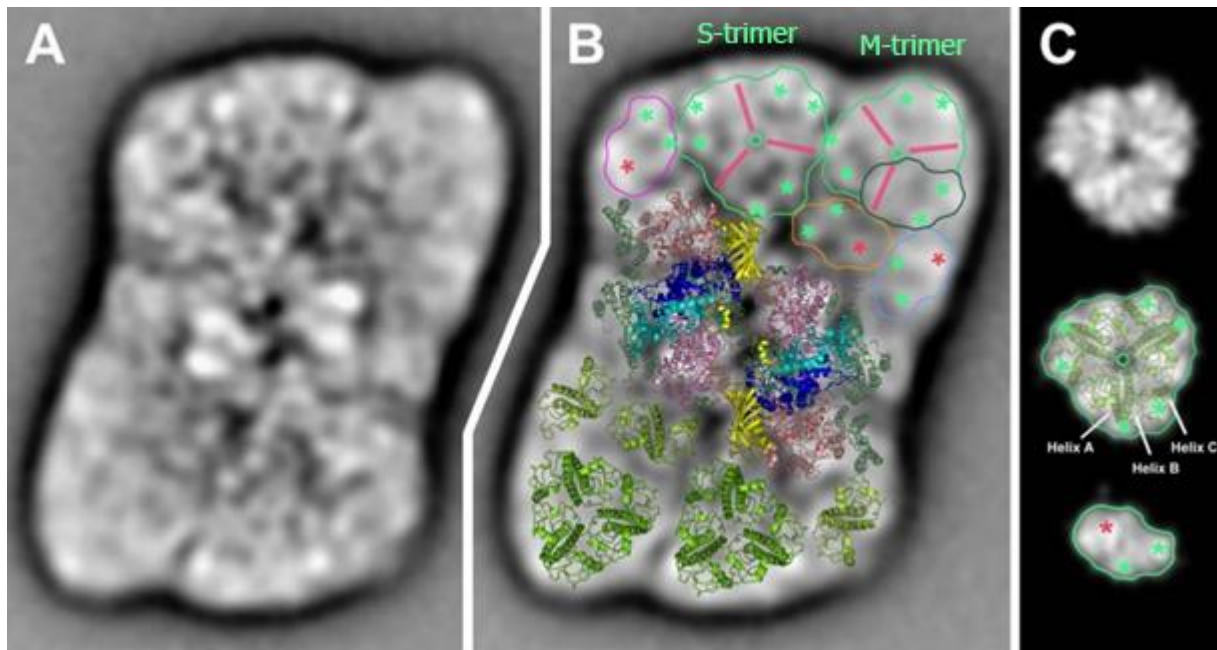
Figure 8: Projection map of the $C_2S_2M_2$ supercomplex. (A) Final projection map of the PSII $C_2S_2M_2$ supercomplex at 12 Å resolution. (B) Assignment of the subunits in the supercomplex by fitting the high-resolution structures of PSII core (Loll *et al*. 2005) (pale-green; subunits D1, D2, CP43, CP47, and extrinsic subunit PsbO are highlighted in blue, cyan, salmon, pink, and yellow, respectively) and Lhcb (Liu *et al*. 2004) (trimeric LHCII and monomeric Lhcb in dark and light-green, respectively). Lhcb3 and the minor antennas, CP24, CP26 and CP29, are schematically depicted in dark green, light blue, magenta, and orange contours, respectively. Green and pink asterisks indicate similar high-densities of trimeric and monomeric LHCII, respectively. Tripod-shaped pink lines indicate a stain-excluded area of LHCII trimer. (C) Generated 2D projection maps of LHCII trimer and monomer from atomic model, truncated at 10 Å resolution. To allow comparison, corresponding densities of LHCII revealed in the EM projection map are indicated in the truncated 2D projection maps (modified from **Caffarri *et al*. 2009**).

Importantly, in **Caffarri *et al*.** we also conducted extensive biochemical experiments to correlate the structural data with functional implications. By using mutants lacking specific Lhcb proteins, we demonstrated the impact of these proteins on the stability and light-harvesting efficiency of the PSII supercomplex under our experimental conditions and revealed the importance of these individual subunits for the supramolecular organization of PSII. At that time, the study by **Caffarri *et al*. (2009)** was particularly notable for its comprehensive approach, combining high quality structural data with functional analyses. Our work established

a detailed framework for understanding how the various components of PSII interact to optimize energy transfer and photoprotection, and to date, this work has been referenced by many researchers in the field of PSII research.

4.3. Organization of PSII supercomplexes in Pinaceae

Further research on the structure of PSII revealed a surprising fact, namely that the structure of PSII is not conserved in all land plants. It was found that the organization of PSII is clearly different in representatives of Pinaceae family belonging to the gymnosperms. Their PSII supercomplexes exhibit a unique organization and composition of light-harvesting complexes compared to angiosperms. We explored the PSII supercomplexes in two species of Pinaceae, Norway spruce and Scots pine, and identified several key differences that underscore the adaptability of PSII across plant lineages (**Kouřil *et al*. 2016**; **Kouřil *et al*. 2020**). Unlike the typical PSII supercomplexes found in angiosperms, which commonly include Lhcb6 and Lhcb3 proteins, the Pinaceae family, and also Gnetales family, lacks these proteins. Instead, they have developed alternative structural configurations that resembles the counterpart in green alga, *Chlamydomonas reinhardtii* (Drop *et al*. 2014), an evolutionarily older organism (Figure 9). Thus, our results broke the generally accepted idea that Lhcb6 and Lhcb3 proteins in the light-harvesting antenna of PSII are an essential characteristic of all land plants (Alboresi *et al*. 2008; Büchel, 2015; de Bianchi *et al*. 2008; Koziol *et al*. 2007). Further research revealed another unexpected specificity of Pinaceae (also representatives Gnetales) that was the presence of only one out of three isoforms of Lhcb4 protein (Lhcb4.1-3), i.e., Lhcb4.3, also known as Lhcb8 (Grebe *et al*. 2019). The presence of the Lhcb8 isoform, which is typically expressed in plants under high light conditions (Albanese *et al*. 2016b; Klimmek *et al*. 2006), supports the interpretation that the photosynthetic apparatus in Pinaceae and Gnetales represents, together with the absence of the Lhcb3 and Lhcb6 proteins, an adaptation to prolonged high light conditions in the past during evolution (**Kouřil *et al*. 2016**; Grebe *et al*. 2019).
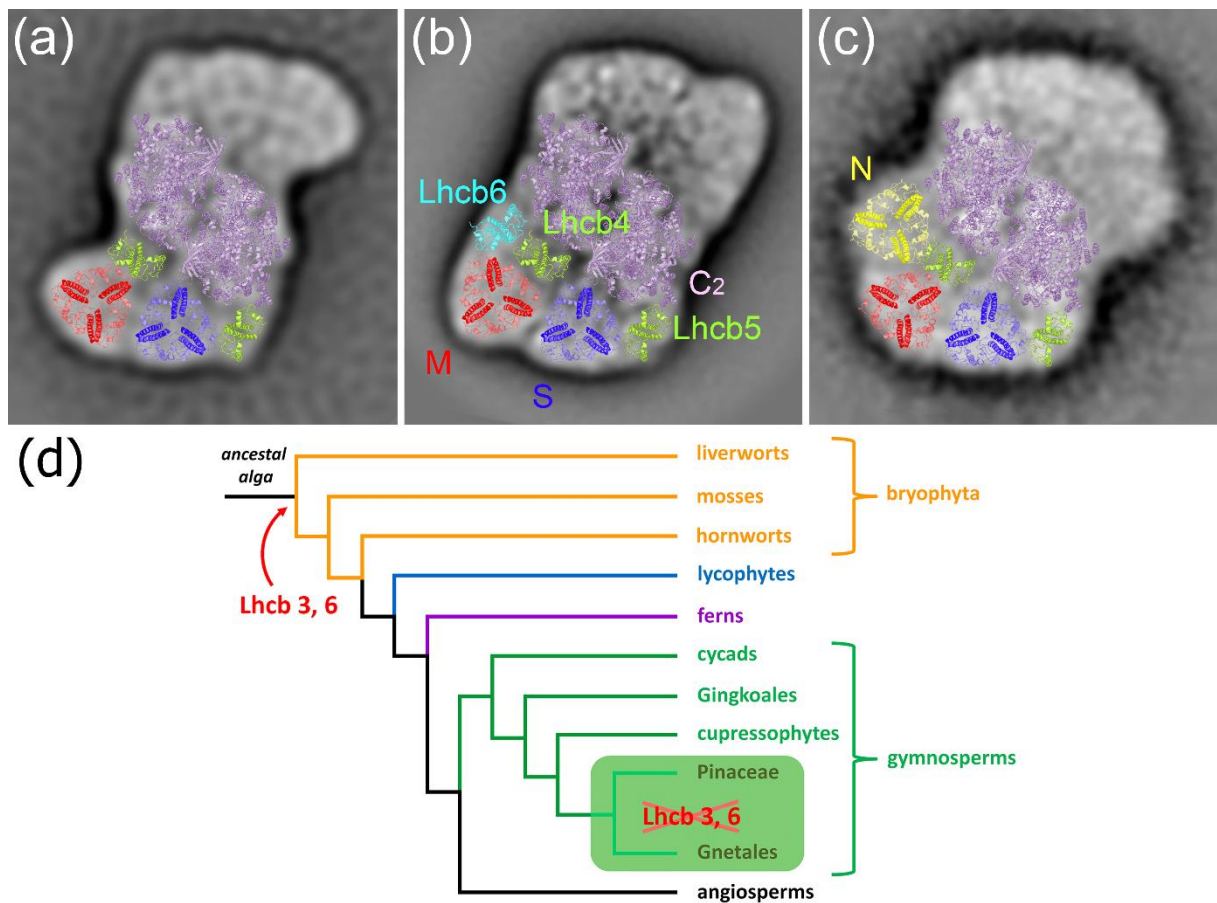
Figure 9: Structural assignment of protein subunits of PSII supercomplexes from different organisms. (a) PSII supercomplexes from Norway spruce (*Picea abies*) and its counterparts from (b) *Arabidopsis thaliana* and (c) *Chlamydomonas reinhardtii*. Averaged projection maps are shown for the $C_2S_2M_2$ supercomplexes from Norway spruce and *A. thaliana*, and $C_2S_2M_2N_2$ from *C. reinhardtii* (adapted from Drop *et al*. 2014). High-resolution structures were fitted to the projection maps; the PSII core complex (C_2, light violet) (Guskov *et al*. 2009), trimeric (the S, M and N trimer in blue, red and yellow, respectively) and monomeric (Lhcb4 and Lhcb5 in green, Lhcb6 in cyan) Lhcb proteins (Liu *et al*. 2004). (d) Phylogenetic tree of land plant groups with indicated appearance and loss of Lhcb3 and Lhcb6 proteins (modified from **Kouřil *et al*. 2016**).

Interestingly, mild solubilization of thylakoid membranes and separation by CN-PAGE revealed apparently another consequence of the absence of Lhcb6 and Lhcb3 in Pinaceae, that is, the possibility of binding multiple LHCII trimers at binding positions not previously observed in other representatives of land plants (Figure 10) (**Kouřil *et al*. 2020**). This increased capacity for LHCII binding was found to allow Pinaceae PSII to form far larger and more

complex supercomplexes, such as the $C_2S_2M_2$ and $C_2S_2M_2L_n$ configurations, compared to e.g., spinach or Arabidopsis. The additional LHCII trimers provide extended light-harvesting antenna and greater flexibility in energy distribution, which can be crucial for adaptation to survive in diverse light environments, such as understory conditions where many Pinaceae species are found. Thus, our study demonstrates how structural adaptations at the supercomplex level enhance the photosynthetic versatility and evolutionary success of Pinaceae.
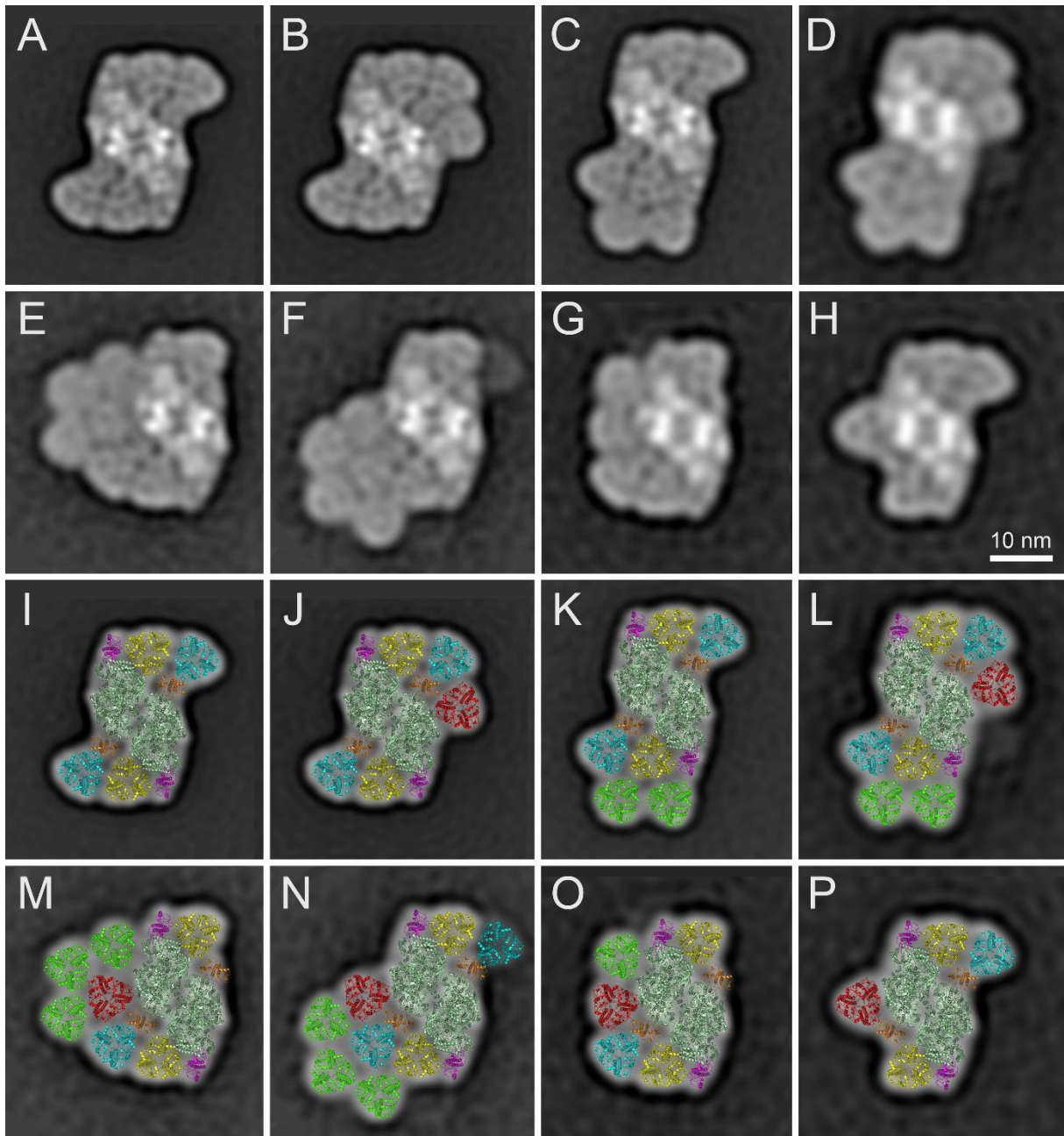
Figure 10: The large PSII supercomplexes from Norway spruce. Projection maps of individual types of the PSII supercomplexes represent the best class averages of: (a) 12015; (b) 9847; (c) 6356; (d) 622; (e) 1298; (f) 1018; (g) 1554; (h) 1219 particles. (i–p) Structural models

of PSII supercomplexes were obtained by a fit of the high-resolution structure (van Bezouwen *et al*. 2017). Individual PSII subunits are color-coded: dark green – core complex; yellow – S trimer; cyan – M trimer; red – N trimer; green – L trimer; magenta – Lhcb5; orange –Lhcb4 (adopted from **Kouřil *et al*. 2020**).

Moreover, these findings have broader evolutionary implications and suggest that the structural diversity observed in Pinaceae PSII is an adaptive response to specific ecological niches. This adaptability illustrates the evolutionary plasticity of PSII, which, while maintaining very conserved PSII core structure across plant lineages, can incorporate variable antenna configurations to optimize light capture and energy transfer efficiency. Our work emphasizes that the structural variations in PSII are not merely biochemical curiosities but represent fundamental strategies that plants use to cope with environmental pressures, reinforcing the view of PSII as a highly dynamic and adaptable photosynthetic complex. This is a challenge for further research into the structural adaptations of PSII, particularly using cryo-EM, which continues to refine our understanding of these sophisticated supercomplexes.

4.4. Advancements in PSII structural analysis using cryo-electron microscopy

The introduction of advanced cryo-EM technique has significantly enhanced our understanding of the structural details of PSII, surpassing the capabilities of earlier method like negative staining EM. Cryo-EM has provided unprecedented resolution, allowing researchers to visualize PSII supercomplexes in near-native states, which has greatly refined our knowledge of their organization and function.

One of the breakthrough studies using cryo-EM was conducted by (Wei *et al*. 2016), who resolved the structure of the PSII C_2S_2 supercomplex from spinach at an impressive resolution of 3.2 Å. This high-resolution structure revealed detailed arrangements of chlorophylls, carotenoids, and most of the PSII protein subunits, including extrinsic subunits PsbO, P, Q, and Tn, which form the oxygen-evolving complex, thus elucidating the energy transfer pathways in the complex. Importantly, this study demonstrated that the structure of the PSII supercomplex is in a good agreement with models proposed in previous lower resolution studies using negative-staining EM. This agreement highlights the reliability and impact of the initial structural insights obtained using negative staining, despite its resolution limitations, while also highlighting the unprecedented level of detail achievable using cryo-EM.

The first high-resolution structural details of the larger $C_2S_2M_2$ supercomplex from the model organism *Arabidopsis thaliana* using cryo-EM with a total resolution of 5.3 Å were

described in our study (**van Bezouwen *et al*. 2017**). In this study, we provided a comprehensive view of this large supercomplex, including the precise binding sites of the S and M-LHCII trimers and their interactions with the PSII core. In particular, the research highlighted the flexibility of the M trimer as well as the smaller antenna proteins Lhcb4 (CP29) and Lhcb6 (CP24). This flexibility highlights the critical role of this antenna domain in optimizing light harvesting and photoprotection, allowing the supercomplex to dynamically adapt to changing light conditions (Betterle *et al*. 2009). In a very short time, Su *et al*. (2017) expanded on these findings by resolving the cryo-EM structure of the PSII $C_2S_2M_2$ supercomplex from *Pisum sativum* at resolution of 2.7 Å. This work further elaborated on the specific interactions between the PSII core and its associated LHCII trimers, as well as minor antenna proteins like CP24 and CP29. They highlighted the importance of these interactions in the dynamic assembly and structural modification of the PSII antenna, emphasizing how such flexibility allows plants to efficiently manage light harvesting and photoprotection under diverse environmental conditions. Subsequently, Graça *et al*. (2021) continued this research and presented an improved cryo-EM model of the PSII $C_2S_2M_2$ supercomplex from Arabidopsis at 2.79 Å resolution. This study not only confirmed the structural configurations observed in earlier cryo-EM studies but also addressed the effect of different extraction methods, such as digitonin (compared to widely used α-DDM), on the stability and protein-protein interactions in the PSII supercomplex (Rantala *et al*. 2017). The findings highlighted several key differences between Arabidopsis and frequently studied species such as pea and spinach. Notably, subunits such as PsbJ, PsbP, and PsbQ were absent in the Arabidopsis PSII structure. This absence was likely due to protocol-specific effects of digitonin or species-specific features, as these subunits were also absent in the earlier Arabidopsis PSII structure reported in our study, where a slightly different isolation procedure was used (**van Bezouwen *et al*. 2017**).

Our next logical contribution in this area of research, given our previous studies on conifers, was a cryo-EM study of the structure of the PSII supercomplex from a gymnosperm, Norway spruce (*Picea abies*) at 2.8 Å resolution (**Opatíková *et al*. 2023**) (Figure 11). This study revealed both similarities and distinct differences between the PSII structures of gymnosperms and angiosperms. While the core dimeric organization is conserved, Norway spruce features unique antenna arrangements, including the replacement of Lhcb4 with Lhcb8 (Grebe *et al*. 2019) and the presence of a homotrimeric LHCII composed solely of Lhcb1, in contrast to the heterotrimeric LHCII found in angiosperms ((Jansson, 1994; Jansson, 1999). These differences reflect gymnosperm-specific adaptations in light-harvesting strategies. A notable discovery was the presence of α-tocopherol (vitamin E) at the interface between LHCII

and the core antenna CP43, a feature not seen in previous PSII structures. This molecule is thought to play a photoprotective role, scavenging reactive oxygen species generated under high light conditions (Krieger-Liszkay & Trebst, 2006; Kruk *et al*. 2000; Kumar *et al*. 2020), indicating a possible adaptation of gymnosperms to mitigate light-induced damage. This structure enhances our understanding of the evolutionary divergence between gymnosperms and angiosperms, revealing how PSII supercomplex organization can vary across plant lineages while maintaining core functional elements. It underscores the flexibility of peripheral antenna configurations in optimizing light harvesting and photoprotection, offering new insights into the structural diversity of PSII across different plant groups.
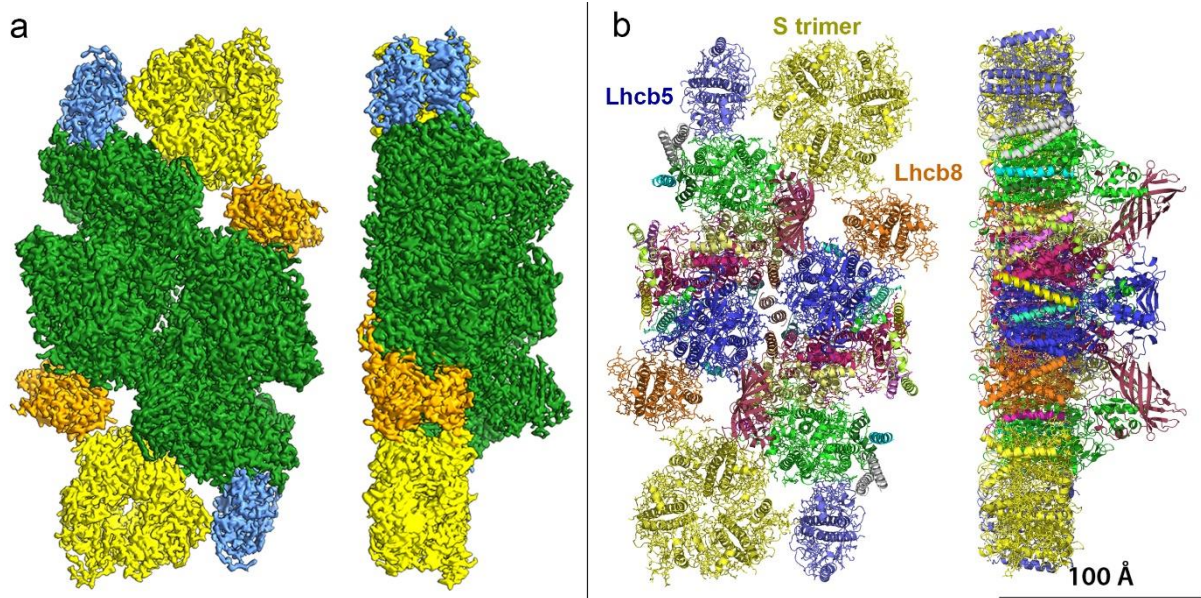
Figure 11: Cryo-EM structure of the spruce PSII supercomplex. (a) 3D cryo-EM density map of the spruce C_2S_2 supercomplex top view from the luminal side (left) and side view along the membrane plane (right). (b) Model of the C_2S_2 supercomplex from the lumenal side with indicated subunits of light-harvesting antenna, Lhcb5, Lhcb8 and the S-LHCII trimer, bound to the dimeric core complex (left) and the side view of the C_2S_2 supercomplex along the membrane plane (right) (modified from **Opatíková *et al*. 2023**).

In summary, cryo-EM will certainly continue to provide more detailed and accurate PSII models, but it is notable that there is strong agreement between cryo-EM and earlier low-resolution data obtained from negative EM. This agreement validates the structural framework established by negative staining EM and demonstrates that the foundational insights regarding the dimeric organization of PSII, core-antenna interactions, and overall supercomplex

organization were accurate. Cryo-EM built on this foundation to resolve finer structural features, such as the precise position of pigments and interactions between subunits, which were beyond the resolving power of negative-staining EM. These advances will enable further detailed functional-structural studies that will lead to a deeper understanding of the principles governing the PSII supercomplex.

4.5. Contribution of molecular dynamics simulations to understanding PSII

Detailed structural models obtained by cryo-EM studies enabled and significantly supported molecular dynamics (MD) simulations, which have contributed significantly to the understanding of the functional dynamics of PSII. Using this approach, for example, the pathways for diffusions of plastoquinone and plastoquinol within the PSII complex were analyzed (Van Eerden *et al*. 2017). These simulations revealed a complex network of entry and exit channels for these electron carriers, illustrating the promiscuous nature of plastoquinone diffusion through PSII. This work demonstrated how PSII structural elements interact dynamically to facilitate efficient electron transport, confirming that the multiple pathways observed in cryo-EM structures are functional under physiological conditions (Van Eerden *et al*. 2017). MD simulations can also provide dynamic insights into protein interactions and the assembly processes of the PSII supercomplex, identifying whether hydrophobic or electrostatic interactions predominantly contribute to LHCII binding to the PSII core or the assembly of the PSII core itself (Mao *et al*. 2023).

Overall, the combination of cryo-EM and MD simulations provides a powerful tool (Bock *et al*. 2024; Nierzwicki & Palermo, 2021) that has the potential to extend our knowledge of PSII beyond static structural descriptions and provides a dynamic view of the photosynthetic function of the PSII supercomplex under near-*in vivo* conditions. These integrated approaches can contribute significantly to elucidating the balance between stability and flexibility required for efficient photosynthesis, reinforcing the value of cryo-EM as a key method for unraveling the complex mechanism of PSII function and regulation in photosynthesis.

4.6. Formation of PSII megacomplexes

Knowledge of PSII supercomplexes forming larger specific assemblies in thylakoid membrane, termed PSII megacomplexes, has advanced significantly over time due to various biochemical and structural studies. They are considered to be important formations in the thylakoid membrane, which play an important role in photosynthesis by optimizing light energy capture and electron transfer. The first evidence of these PSII megacomplexes came from

biochemical techniques such as BN-PAGE, CN-PAGE, and sucrose gradient centrifugation (Albanese *et al*. 2016b; Albanese *et al*. 2016a; Ifuku, 2023; Järvi *et al*. 2011; Kim *et al*. 2020; Kim *et al*. 2023; Suorsa *et al*. 2015), which revealed the presence of high molecular weight bands corresponding to large PSII assemblies, formed by two copies of PSII supercomplexes, or PSII supercomplex associated with PSI complex. However, these methods did not provide detailed structural insight into the nature of these assemblies and thus it was not possible to rule out whether these megacomplexes were the result of random association of solubilized PSII supercomplexes prior to their electrophoretic separation.

EM analysis, particularly in the last decade, has provided a deeper understanding of these specific megacomplex structures and revealed, in general, two distinct types of PSII megacomplexes that differ in their organization and functional roles. The first type of PSII megacomplex involves interactions confined to the plane of a single thylakoid membrane. These megacomplexes are usually formed by association of two PSII supercomplexes, often facilitated by light-harvesting complex (Albanese *et al*. 2016a; Kim *et al*. 2020; Kim *et al*. 2023; **Kouřil *et al*. 2020**; **Nosek *et al*. 2017**). The second type of the PSII megacomplexes originates from interactions between PSII supercomplexes located in adjacent thylakoid membranes. These complexes are organized through the stromal slit, the intermembrane space between stacked grana thylakoids (Albanese *et al*. 2016a; Daum *et al*. 2010; Shan *et al*. 2024). The ability of PSII to form these two types of megacomplexes highlights its remarkable structural flexibility and functional adaptability. Parallel associations within a single membrane optimize photochemical efficiency by enabling energy sharing between neighboring PSII cores. In contrast, the bridging megacomplexes between membranes might play a role in inter-thylakoid communication and stabilization, contributing to the overall resistance and efficiency of the photosynthetic apparatus.

Our major contribution in this area was the structural characterization of specific PSII megacomplexes directly in the thylakoid membrane (Figure 12). Indication of PSII megacomplex formation in the thylakoid membrane has been previously observed through cryo-ET (**Kouřil *et al*. 2011**) and further confirmed by structural analysis of grana membranes using single particle image analysis, which revealed the details of the organization of these PSII megacomplexes (**Kouřil *et al*. 2020**; **Nosek *et al*. 2017**). These studies revealed different configurations of PSII megacomplexes, including parallel and non-parallel associations of PSII supercomplexes, and demonstrated how the S- and M-LHCII trimers and mainly Lhcb5, along with the PSII core subunits contribute to megacomplex formation.
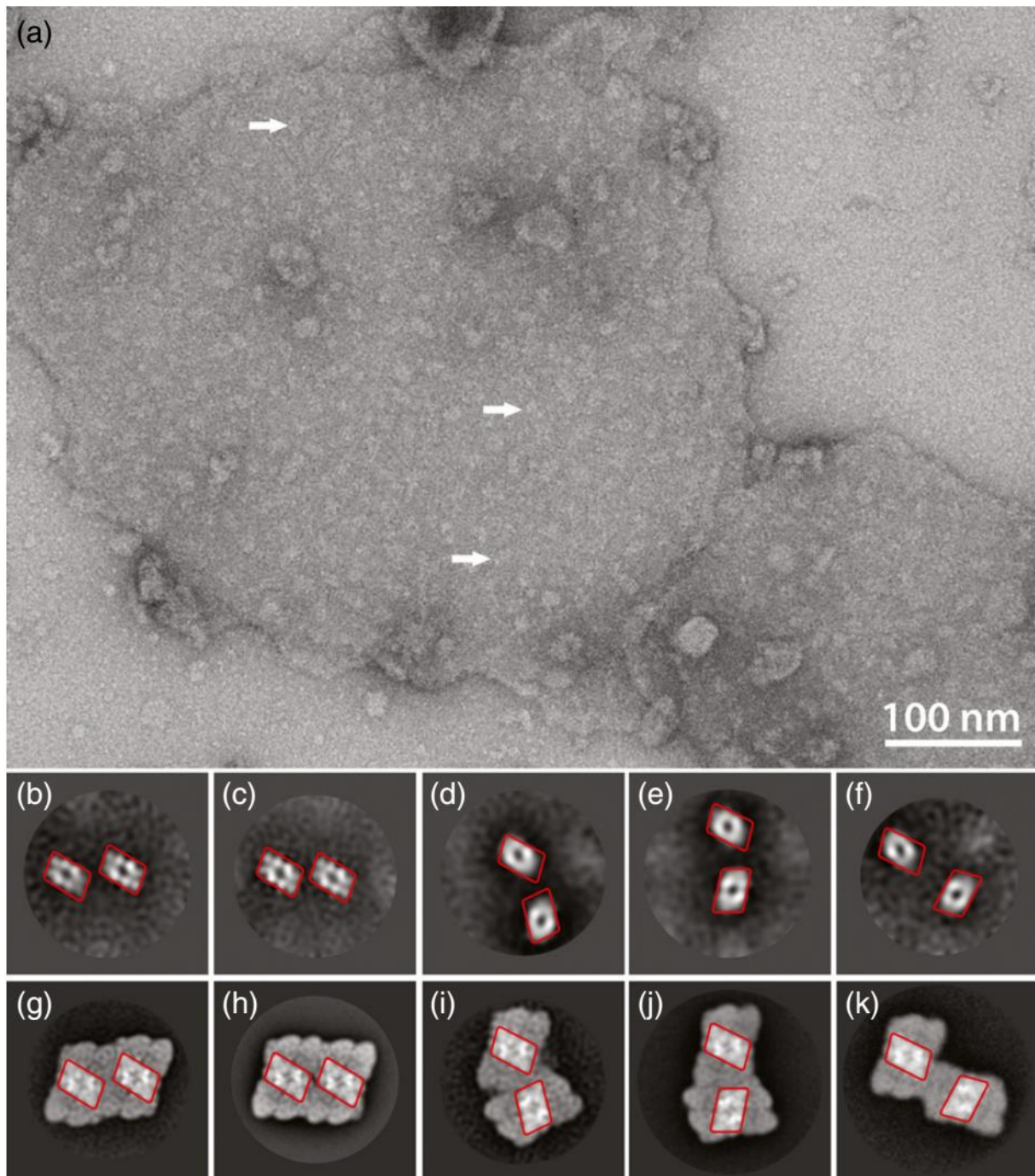
Figure 12. PSII megacomplexes found within an intact thylakoid membrane. (a) An example of an electron micrograph of negatively stained thylakoid membrane isolated from *Arabidopsis thaliana*, with densities corresponding to the PSII core complex indicated by white arrows. (b–f) PSII megacomplexes found within the thylakoid membrane (the number of summed projections was 1838, 2620, 940, 682 and 825, respectively). (g–k) PSII megacomplex analogs found in the sample separated by CN-PAGE. The red frames surround core complexes of individual PSII supercomplexes and highlight that the megacomplexes found in the thylakoid membrane match with those obtained using CN-PAGE (adopted from **Nosek *et al.* 2017**).

In summary, the progression from biochemical identification to detailed structural analysis has significantly deepened our understanding of PSII megacomplexes. These larger assemblies represent a higher level of organization within the photosynthetic membrane, reflecting the complex interplay between structure and function in photosynthesis. PSII megacomplexes, with their dynamic antenna configurations and their ability to facilitate energy spillover, highlight the remarkable adaptability of the photosynthetic machinery to fluctuating environmental conditions.

4.7. Role of individual Lhcb proteins in PSII supercomplex formation

The formation of PSII supercomplexes is a highly regulated process that involves a complex interplay of individual light-harvesting proteins, Lhcb1-6, under specific environmental conditions. Lhcb1-3 proteins are the most abundant and they form several types of trimers. As the ratio between Lhcb1, Lhcb2, and Lhcb3 proteins is about 8:3:1 (Jansson, 1994), this implies that they can form either homotrimers (composed of either Lhcb1 or Lhcb2) or heterotrimers (composed of Lhcb1, Lhcb2 and Lhcb3) (Caffarri *et al.* 2004; Standfuss & Kühlbrandt, 2004). The minor antenna proteins Lhcb4 (CP29), Lhcb5 (CP26), and Lhcb6 (CP24) represent a minor fraction of LHCII and play critical roles in stable binding of LHCII trimers to the PSII core complex and formation of specific types of PSII supercomplexes.

Lhcb1-3 play critical roles in the assembly of LHCII trimers, which are essential for efficient light capture and energy transfer to the reaction center. Lhcb1, the most abundant LHCII protein, is encoded by multiple gene isoforms, including five isoforms (Lhcb1.1–Lhcb1.5) in *Arabidopsis thaliana*, while Lhcb2 is encoded by three isoforms (Lhcb2.1–Lhcb2.3), and Lhcb3 by a single isoform in the same species. Current knowledge indicates that in most land plants, including angiosperms, S-LHCII trimers can consist of either homotrimers or heterotrimers composed of Lhcb1 and Lhcb2. Cryo-EM structures from Arabidopsis, pea, and spinach support this conclusion, as the density maps of S-LHCII indicate the presence of both homo- and heterotrimers. By contrast, in gymnosperms such as Norway spruce, the much better defined cryo-EM map suggests that the S-LHCII trimer is a specific homotrimer consisting solely of Lhcb1, reflecting a distinct adaptation in PSII supercomplex organization (**Opatíková *et al.* 2023**). Knockout studies of Lhcb1 in *Arabidopsis thaliana* revealed significant disruptions in the formation of LHCII trimers, leading to a reduced antenna size of PSII and impaired light-harvesting efficiency (Pietrzykowska *et al.* 2014; Vayghan *et al.* 2022). The M-LHCII trimer, on the other hand, has a specific composition that includes one copy of Lhcb3, along with a combination of Lhcb1 and Lhcb2 (**Caffarri *et al.* 2009**; Su *et al.* 2017;

van Bezouwen *et al*. 2017). Knockout studies in *Arabidopsis thaliana* have shown that the absence of Lhcb3 results in compensatory increases in Lhcb1 and Lhcb2 levels, preserving LHCII trimer formation but altering the orientation of the M-trimer within the PSII supercomplex (Damkjær *et al*. 2009). Interestingly, our recent structural analysis of the Lhcb3 mutant suggests that in the absence of Lhcb3, the M-trimer may bind in a manner similar to that observed in spruce-type PSII supercomplexes (Ilíková *et al*. 2021). The evolutionary conservation of Lhcb3, despite its relatively subtle phenotypic effects, suggests that it plays a role in fine-tuning the photosynthetic apparatus under specific environmental conditions.

Lhcb4 (also called CP29), is one of the most crucial minor antenna proteins for the stability of PSII supercomplexes. In *Arabidopsis thaliana*, Lhcb4 is encoded by three isoforms: Lhcb4.1, Lhcb4.2, and Lhcb4.3 (Jansson, 1999), each specifically contributing to the organization and function of the PSII supercomplex under specific environmental conditions. Under normal light conditions, the PSII supercomplex predominantly incorporates either Lhcb4.1 or Lhcb4.2, ensuring structural stability and binding of the M-LHCII trimer. However, under high-light conditions, Lhcb4.3, a high-light-induced isoform, replaces the other isoforms in the PSII supercomplex (Klimmek *et al*. 2006), leading to a reduction in antenna size due to its inability to support the binding of the M-LHCII trimer (see below). Our study on an Arabidopsis mutant deficient in Lhcb4 revealed that the absence of this protein significantly destabilizes PSII supercomplexes, leading to the formation of only smaller assemblies, such as the C_2S_2 supercomplex, and preventing the assembly of the larger $C_2S_2M_2$ supercomplex (de Bianchi *et al*. 2011). Our preliminary data further confirmed that in the absence of Lhcb4, PSII supercomplexes are highly unstable, with only a low amount of C_2S_2 separable using CN-PAGE under mild conditions. Structural analysis suggests that the core complex in the koLhcb4 mutant can adopt two configurations within the C_2S_2 assembly, though further research is needed to fully understand the structural variations and their implications for PSII function.

The specific role of Lhcb4.3, a high-light-induced isoform, has been increasingly recognized. While Lhcb4.3 shares high homology with Lhcb4.1 and Lhcb4.2, it has a truncated C-terminus and unique structural features (Klimmek *et al*. 2006). In plants exposed to high-light conditions, Lhcb4.3 expression increases significantly, contributing to a shift from larger PSII supercomplexes ($C_2S_2M_2$) to smaller assemblies (C_2S_2), which are better suited for photoprotection (Albanese *et al*. 2016b; Albanese *et al*. 2018; Grinzato *et al*. 2020). Structural studies reveal that Lhcb4.3 affects the interaction of the PSII core with other LHCII subunits, particularly Lhcb6 and M-LHCII trimers. This truncated form reduces the binding affinity for additional M-LHCII trimers, leading to a predominance of the C_2S_2 supercomplex in plants

long-term acclimated to high light (Albanese *et al*. 2016b; Grinzato *et al*. 2020) or allowing the spruce-type binding of the M-trimer as observed in Pinaceae (**Kouřil *et al*. 2016**; **Kouřil *et al*. 2020**; **Opatíková *et al*. 2023**). Together, the three isoforms of Lhcb4, and particularly the high-light-specific Lhcb4.3, play a critical role in stabilizing PSII supercomplexes and enabling plants to adapt dynamically to fluctuating light conditions.

Lhcb5 (CP26) plays a distinct but equally important role in the organization of PSII supercomplexes. While early studies suggested that Lhcb5 might not be essential for PSII supercomplex assembly (Yakushevska *et al*. 2003), subsequent work on Arabidopsis mutants lacking Lhcb5 demonstrated significant difficulties in isolating large PSII $C_2S_2M_2$ supercomplexes (**Caffarri *et al*. 2009**; de Bianchi *et al*. 2008). More recent research (Chen *et al*. 2018) and our preliminary data (**Vanská *et al*.** manuscript in preparation) indicate that PSII supercomplexes can only be isolated from the koLhcb5 mutant under very mild conditions. Furthermore, our preliminary structural EM analysis indicates that the absence of Lhcb5 affects the spatial arrangement of the S- and M-LHCII trimers within the PSII supercomplex. This disruption likely explains the very low stability of the supercomplex and highlights the crucial role of Lhcb5 in ensuring the proper and functional assembly of PSII. Additionally, our previous work suggests that Lhcb5 is crucial for the formation of PSII megacomplexes (**Nosek *et al*. 2017**), underscoring its role in the higher-level organization of PSII within the thylakoid membrane.

Lhcb6 (CP24) is a crucial minor antenna protein that significantly contributes to the structural organization of PSII supercomplexes. Mutants lacking Lhcb6 display a notable reduction in the stability of the M-LHCII trimer, which affects the overall stability of the PSII supercomplex. Studies of the Arabidopsis mutant lacking Lhcb6 have shown that the absence of Lhcb6 predominantly leads to the formation of C_2S_2 supercomplexes (de Bianchi *et al*. 2008; **Ilíková *et al*. 2021**; Kovács *et al*. 2006). As a consequence, the organization of PSII supercomplexes in the thylakoid membrane is heavily affected, leading to the formation of tightly packed PSII arrays that restrict the diffusion of plastoquinone molecules and negatively impact photosynthetic electron transport. Furthermore, under high-light conditions, Lhcb6 is down-regulated, which results in a reduction of PSII antenna size by decreasing the number of bound M-LHCII trimers (**Kouřil *et al*. 2013**). This points to a physiological role of Lhcb6 in dynamically adapting the structure of PSII to environmental light conditions and maintaining optimal photosynthetic efficiency through the proper spatial arrangement of its components in the membrane.

4.8. Organization of PSII in the thylakoid membrane

PSII, a key component of the photosynthetic apparatus, dynamically adjusts its arrangement in the thylakoid membrane in response to changing environmental conditions such as light intensity (Kirchhoff, 2014; Pribil *et al*. 2014; Yamamoto *et al*. 2014; Yoshioka-Nishimura, 2016). This adaptability is crucial for optimizing photosynthetic efficiency and ensuring photoprotection on a larger scale at the thylakoid membrane level. The spatial arrangement of PSII complexes can be divided into two distinct types: random and ordered distributions (Figure 13) (Kirchhoff, 2013; **Kouřil *et al*. 2012**; Miller *et al*. 1976; Staehelin, 2003). Both arrangements are highly dynamic and are influenced not only by environmental factors such as light intensity, but also by the protein composition of PSII, which also reflects environmental conditions.
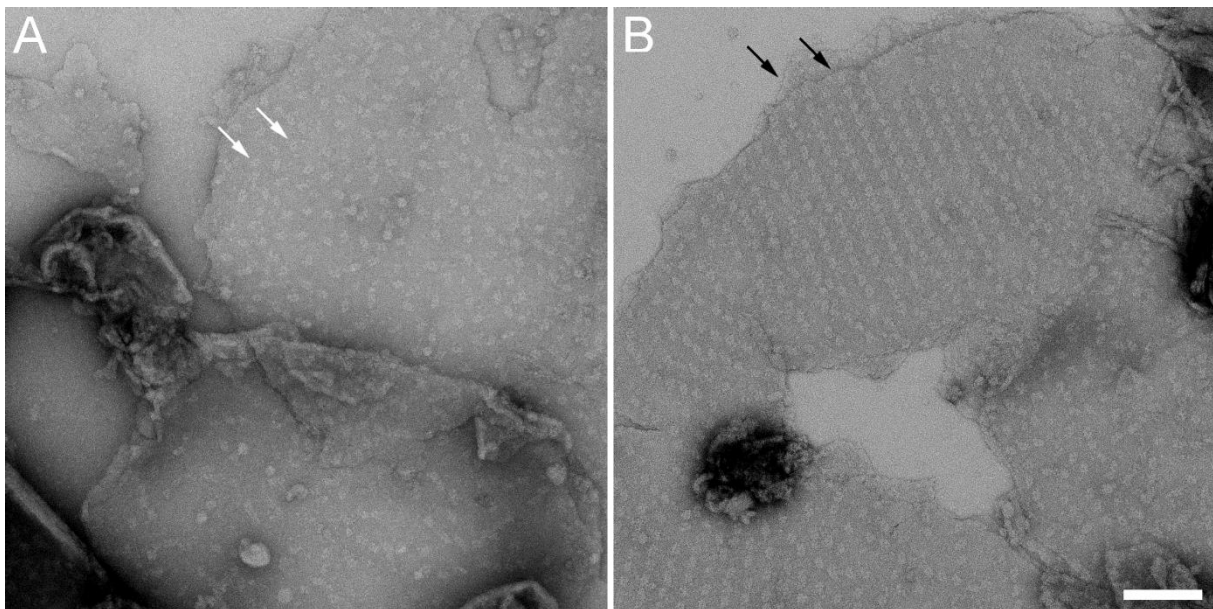
Figure 13. Examples of electron micrographs of negatively stained pairs of grana membranes. Membranes isolated from *Arabidopsis thaliana*. showing either a random (A) or ordered (B) organization of PSII complexes. The white arrows indicate the characteristic densities of PSII core complexes; the black arrows indicate a single piece of a membrane layer. Scale bar is 100 nm (adopted from **Kouřil *et al*. 2013**).

In most cases, PSII complexes are randomly distributed across the grana membranes. This random arrangement allows for (i) efficient capture of light energy and the smooth lateral diffusion of electron carriers, such as plastoquinone (PQ), within the membrane, (ii) flexibility in the lateral mobility of PSII and associated protein complexes, which is essential for processes

such as state transitions (redistribution of LHCII trimers between PSII and PSI), and (iii) the PSII repair cycle, which involves the rapid diffusion of damaged PSII complexes to the stroma lamellae for repair and their subsequent return to the grana. However, this random distribution of PSII may only be apparent. Some fraction of PSII supercomplexes can interact with their neighbors to form specific PSII megacomplexes (see the chapter Formation of PSII megacomplexes). These megacomplexes can be identified at the level of the thylakoid membrane using single particle EM analysis (**Kouřil *et al*. 2020**; **Nosek *et al*. 2017**) or directly visualized using the advanced imaging techniques such as cryo-ET (**Kouřil *et al*. 2011**).

Randomly organized PSII complexes also enable dynamic changes in the composition and size of supercomplexes, including the incorporation or removal of LHCII trimers. This flexibility allows plants to adjust their photosynthetic machinery in response to varying light conditions, increasing the antenna size and absorption cross-section of PSII under low-light conditions while reducing the antenna size and minimizing the risk of photodamage under high-light conditions (Anderson, 1986; Anderson *et al*. 1988; Bailey *et al*. 2001; Ballottari *et al*. 2007; **Kouřil *et al*. 2013**).

Not only the architecture of PSII supercomplexes is modified under different light conditions, but also the density of PSII within the thylakoid membrane. It is well documented using different EM technique that under low-light conditions, PSII density decreases due to the significant enlargement of the pool of LHCII trimers, which helps to increase the cross-section of PSII under this light limiting conditions. In contrast, high-light conditions lead to increased PSII density, particularly in grana membranes, which is enabled by the reversible dissociation of a part of associated antenna, primarily involving the M-LHCII trimer and Lhcb6 and reduction of the entire pool LHCII in the membrane (Bielczynski *et al*. 2016; Kirchhoff *et al*. 2007; **Kouřil *et al*. 2013**). This denser packing promotes both LHCII and PSII clustering, which is associated with induction of photoprotective mechanisms, such as the dissipation of excess light energy via non-photochemical quenching (NPQ) (Goral *et al*. 2010; Goral *et al*. 2012; Johnson *et al*. 2011). However, this clustering has direct impacts on the mobility of proteins in the thylakoid membrane and leads to formation of local diffusion domains where the diffusion is less restricted (Herbstová *et al*. 2012; Johnson *et al*. 2011). On the other hand, there is also light-induced expansion of the thylakoid lumen (Järvi *et al*. 2013; Kirchhoff *et al*. 2011) partially offsets these constraints by providing additional space for the diffusion of luminal proteins like plastocyanin, enhancing electron transport efficiency under high-light conditions.

Thus, at the functional level, the dynamic reorganization of PSII—transitioning between random and clustered states—reflects a finely tuned adaptation to fluctuating light environments. While random distributions support efficient energy capture and mobility under low light, clustering under high light enhances photoprotection, even at the cost of reduced diffusional freedom. This dual strategy ensures that plants can optimize photosynthesis while minimizing photodamage across varying environmental conditions.

In addition to random organization, PSII can adopt an ordered arrangement within the thylakoid membrane, forming two-dimensional (2D) crystalline arrays (Dekker & Boekema, 2005; Garber & Steponkus, 1976; Hankamer *et al*. 1997b; Park & Biggins, 1964; Simpson, 1979; Staehelin, 2003). These arrays are predominantly observed in the grana regions of the thylakoid membrane and are essential for maintaining the structural stability of the photosynthetic machinery under certain conditions (Boekema *et al*. 2000). Although 2D arrays are not the predominant form of PSII arrangement, they can occupy a significant portion of the grana membrane under certain conditions (typically up to 10-20%), with their amount and composition varying depending on light intensity, plant species, and physiological state (typically up to 10-20%) (**Kouřil *et al*. 2012**).

Under low-light conditions, PSII arrays are primarily composed of $C_2S_2M_2$ supercomplexes (Kirchhoff *et al*. 2007; **Kouřil *et al*. 2013**). This configuration enhances the absorption cross-section of PSII, maximizing light-harvesting efficiency under light-limiting conditions. Importantly, arrays of $C_2S_2M_2$ supercomplexes are characterized by the presence of "free highways" that facilitate the diffusion of plastoquinone (PQ) molecules within the thylakoid membrane, enabling efficient electron transport (Kirchhoff *et al*. 2007). In contrast, high-light conditions lead to a transition toward arrays dominated by C_2S_2 supercomplexes, reflecting a reduction in antenna size. However, these tightly packed arrays of C_2S_2 limit PQ diffusion by creating a more restricted environment, which can slow down electron transport rates, activate photosynthetic control and impact photosynthetic efficiency (de Bianchi *et al*. 2008; Morosinotto *et al*. 2006; Tietz *et al*. 2015).

At a functional level, the ordered organization of PSII into 2D arrays represents a finely tuned structural adaptation to optimize photosynthetic performance and photoprotection. These arrays enhance light capture and energy transfer efficiency under low-light conditions, while their reconfiguration under high-light conditions supports photoprotective mechanisms. The balance between structural stability and flexibility ensures that PSII arrays can respond

dynamically to changing environmental conditions, safeguarding photosynthetic efficiency and protecting the plant from light-induced damage.

The formation and stability of 2D arrays of PSII within the thylakoid membrane can be disrupted by several factors, including the expression of PsbS and exposure to high-light conditions (**Kereiche *et al.* 2010**; **Kouřil *et al.* 2013**). PsbS, a critical protein involved in NPQ, plays a significant role in energy dissipation under high-light stress (Li *et al.* 2000). Overexpression of PsbS has been shown to destabilize the semi-crystalline 2D arrays of PSII by promoting the dissociation of LHCII trimers from PSII supercomplexes, leading to a more random distribution of PSII complexes within the membrane (Goral *et al.* 2012; **Kereiche *et al.* 2010**). Similarly, high-light conditions lead to the partial dissociation of antenna proteins resulting in a transition from $C_2S_2M_2$ supercomplexes to C_2S_2 supercomplexes (Grinzato *et al.* 2020; **Kouřil *et al.* 2013**). This modification reduces the ability of PSII to form tight 2D arrays because the uniform structural motif required for these arrays is disrupted (**Kouřil *et al.* 2013**). These disruptions are thought to be adaptive responses, allowing the thylakoid membrane to prioritize photoprotection over structural organization under high-light stress, even though it may lead to reduced photosynthetic efficiency in the short term.

At a functional level, the ordered organization of PSII into 2D arrays represents a finely tuned structural adaptation to optimize photosynthetic performance and photoprotection. These arrays enhance light capture and energy transfer efficiency under low-light conditions, while their reconfiguration under high-light conditions supports photoprotective mechanisms. The balance between structural stability and flexibility ensures that PSII arrays can respond dynamically to changing environmental conditions, safeguarding photosynthetic efficiency and protecting the plant from light-induced damage.

5. Conclusions and future perspectives

Cryo-EM has become an indispensable tool for the structural analysis of photosynthetic supercomplexes, offering unique insights into their organization, dynamics, and functional adaptations. Recent advancements in cryo-EM technology, coupled with significant progress in data processing and analysis software, have made this technique more accessible and user-friendly than ever. Modern cryo-EM approaches, including single particle analysis and cryo-ET, now allow researchers to routinely visualize protein complexes in their near-native state with near-atomic resolution - something that was previously very challenging.

The increased accessibility of cryo-EM has significantly expanded its applications, enabling its integration into larger-scale structure-function studies. These include exploring the effects of different growth conditions, such as stress-induced modifications or genetic mutations, on the photosynthetic apparatus. For example, studying mutants lacking specific subunits can reveal the structural consequences of these absences at high resolution, shedding light on the roles of individual components in maintaining the integrity and functionality of the supercomplex. In addition, cryo-EM has opened new opportunities for investigating or even screening photosynthetic complexes in stress-resistant species. Organisms adapted to extreme conditions, such as drought or high light, may have unique structural characteristics that confer resilience. Understanding these adaptations could serve as a basis for strategies to design stress-tolerant crops, contributing to the sustainability of agriculture in the much-debated era of climate change. In addition, research on previously unexplored photosynthetic organisms also offers potential in uncovering new structural aspects of the photosynthetic apparatus, thereby improving our understanding of the structural and functional diversity of photosynthetic supercomplexes.

Technological advances and applications of cryo-EM demonstrate its fundamental impact on the field of structural biology and its potential to bridge the gap between structural biology and applied science. For this reason, I firmly believe that cryo-EM will undoubtedly remain at the forefront of structural methods, a position it has achieved thanks to its remarkable development over the past decade.

6. References

Albanese, P., Manfredi, M., Meneghesso, A., Marengo, E., Saracco, G., Barber, J.,…Pagliano, C. (2016b). Dynamic reorganization of photosystem II supercomplexes in response to variations in light intensities. *Biochimica et Biophysica Acta-Bioenergetics*, *1857*(10), 1651-1660. https://doi.org/10.1016/j.bbabio.2016.06.011

Albanese, P., Manfredi, M., Re, A., Marengo, E., Saracco, G., & Pagliano, C. (2018). Thylakoid proteome modulation in pea plants grown at different irradiances: quantitative proteomic profiling in a non-model organism aided by transcriptomic data integration. *Plant Journal*, *96*(4), 786-800. https://doi.org/10.1111/tpj.14068

Albanese, P., Nield, J., Tabares, J., Chiodoni, A., Manfredi, M., Gosetti, F.,…Pagliano, C. (2016a). Isolation of novel PSII-LHCII megacomplexes from pea plants characterized by a combination of proteomics and electron microscopy. *Photosynthesis Research*, *130*(1-3), 19-31. https://doi.org/10.1007/s11120-016-0216-3

Alboresi, A., Caffarri, S., Nogue, F., Bassi, R., & Morosinotto, T. (2008). In Silico and Biochemical Analysis of Physcomitrella patens Photosynthetic Antenna: Identification of Subunits which Evolved upon Land Adaptation. *PLOS ONE*, *3*(4), Article e2033. https://doi.org/10.1371/journal.pone.0002033

Anderson, J. (1986). Photoregulation of the composition, function, and structure of thylakoid membranes. *Annual Review of Plant Physiology and Plant Molecular Biology*, *37*, 93-136.

Anderson, J., Chow, W., & Goodchild, D. (1988). Thylakoid membrane organization in sun shade acclimation. *Australian Journal of Plant Physiology*, *15*(1-2), 11-26.

Arshad, R., Calvaruso, C., Boekema, E., Büchel, C., & Kouřil, R. (2021). Revealing the architecture of the photosynthetic apparatus in the diatom *Thalassiosira pseudonana*. *Plant Physiology*, *186*(4), 2124-2136. https://doi.org/10.1093/plphys/kiab208

Arthur, C., & Ciferri, C. (2019). High-Throughput Protein Analysis Using Negative Stain Electron Microscopy and 2D Classification. In *High-throughput protein production and purification* (vol. 2025, pp. 477-485).

Asano, S., Engel, B., & Baumeister, W. (2016). In Situ Cryo-Electron Tomography: A Post-Reductionist Approach to Structural Biology. *Journal of Molecular Biology*, *428*(2), 332-343. https://doi.org/10.1016/j.jmb.2015.09.030

Ayoub, N., Roth, P., Ucurum, Z., Fotiadis, D., & Hirschi, S. (2023). Structural and biochemical insights into His-tag-induced higher-order oligomerization of membrane proteins by cryo-EM and size exclusion chromatography. *Journal of Structural Biology*, *215*(1), Article 107924. https://doi.org/10.1016/j.jsb.2022.107924

Azinas, S., & Carroni, M. (2023). Cryo-EM uniqueness in structure determination of macromolecular complexes: A selected structural anthology. *Current Opinion in Structural Biology*, *81*, Article 102621. https://doi.org/10.1016/j.sbi.2023.102621

Bailey, S., Walters, R., Jansson, S., & Horton, P. (2001). Acclimation of Arabidopsis thaliana to the light environment:: the existence of separate low light and high light responses. *Planta*, *213*(5), 794-801.

Ballottari, M., Dall'Osto, L., Morosinotto, T., & Bassi, R. (2007). Contrasting behavior of higher plant photosystem I and II antenna systems during acclimation. *Journal of Biological Chemistry*, *282*(12), 8947-8958. https://doi.org/10.1074/jbc.M606417200

Betterle, N., Ballottari, M., Zorzan, S., de Bianchi, S., Cazzaniga, S., Dall'Osto, L.,…Bassi, R. (2009). Light-induced Dissociation of an Antenna Hetero-oligomer Is Needed for Non-photochemical Quenching Induction. *Journal of Biological Chemistry*, *284*(22), 15255-15266. https://doi.org/10.1074/jbc.M808625200

Bielczynski, L., Schansker, G., & Croce, R. (2016). Effect of Light Acclimation on the Organization of Photosystem II Super- and Sub-Complexes in Arabidopsis thaliana. *Frontiers in Plant Science*, *7*, Article 105. https://doi.org/10.3389/fpls.2016.00105

Block, H., Maertens, B., Spriestersbach, A., Brinker, N., Kubicek, J., Fabis, R.,…Schäfer, F. (2009). Immobilized-metal affinity chromatography (imac): a review. In *Guide to Protein purification, Second Edition* (Vol. 463, pp. 439-473).

Bock, L., Igaev, M., & Grubmüller, H. (2024). Single-particle Cryo-EM and molecular dynamics simulations: A perfect match. *Current Opinion in Structural Biology*, *86*, Article 102825. https://doi.org/10.1016/j.sbi.2024.102825

Boekema, E., Hankamer, B., Bald, D., Kruip, J., Nield, J., Boonstra, A.,…Rogner, M. (1995). Supramolecular structure of the photosystem-ii complex from green plants and cyanobacteria. *Proceedings of the National Academy of Sciences of the United States of America*, *92*(1), 175-179.

Boekema, E., van Breemen, J., van Roon, H., & Dekker, J. (2000). Arrangement of photosystem II supercomplexes in crystalline macrodomains within the thylakoid membrane of green plant chloroplasts. *Journal of Molecular Biology*, *301*(5), 1123-1133. https://doi.org/10.1006/jmbi.2000.4037

Boekema, E., van Roon, H., Calkoen, F., Bassi, R., & Dekker, J. (1999). Multiple types of association of photosystem II and its light-harvesting antenna in partially solubilized photosystem II membranes. *Biochemistry*, *38*(8), 2233-2239.

Boekema, E., van Roon, H., & Dekker, J. (1998). Specific association of photosystem II and light-harvesting complex II in partially solubilized photosystem II membranes. *FEBS Letters*, *424*(1-2), 95-99.

Boekema, E. J., Folea, M., & Kouřil, R. (2009). Single particle electron microscopy. *Photosynthesis Research*, *102*(2-3), 189-196. https://doi.org/10.1007/s11120-009-9443-1

Brenner, S., & Horne, R. (1959). A negative staining method for high resolution electron microscopy of viruses. *Biochimica et Biophysica Acta*, *34*(1), 103-110.

Buckley, G., Gervinskas, G., Taveneau, C., Venugopal, H., Whisstock, J., & de Marco, A. (2020). Automated cryo-lamella preparation for high-throughput in-situ structural biology. *Journal of Structural Biology*, *210*(2), Article 107488. https://doi.org/10.1016/j.jsb.2020.107488

Bumba, L., Tichy, M., Dobakova, M., Komenda, J., & Vacha, F. (2005). Localization of the PsbH subunit in photosystem II from the Synechocystis 6803 using the His-tagged Ni-NTA Nanogold labeling. *Journal of Structural Biology*, *152*(1), 28-35. https://doi.org/10.1016/j.jsb.2005.08.001

Burgess, S., Walker, M., Thirumurugan, K., Trinick, J., & Knight, P. (2004). Use of negative stain and single-particle image processing to explore dynamic properties of flexible macromolecules. *Journal of Structural Biology*, *147*(3), 247-258. https://doi.org/10.1016/j.jsb.2004.04.004

Bussi, Y., Shimoni, E., Weiner, A., Kapon, R., Charuvi, D., Nevo, R.,…Reich, Z. (2019). Fundamental helical geometry consolidates the plant photosynthetic membrane. *Proceedings of the National Academy of Sciences of the United States of America*, *116*(44), 22366-22375. https://doi.org/10.1073/pnas.1905994116

Büchel, C. (2015). Evolution and function of light harvesting proteins. *Journal of Plant Physiology*, *172*, 62-75. https://doi.org/10.1016/j.jplph.2014.04.018

Büchel, C., Morris, E., Orlova, E., & Barber, J. (2001). Localisation of the PsbH subunit in photosystem II:: A new approach using labelling of His-tags with a Ni2+-NTA gold cluster and single particle analysis. *Journal of Molecular Biology*, *312*(2), 371-379.

Caffarri, S., Croce, R., Cattivelli, L., & Bassi, R. (2004). A look within LHCII: Differential analysis of the Lhcbl-3 complexes building the major trimeric antenna complex of higher-plant photosynthesis. *BiochemistrY*, *43*(29), 9467-9476. https://doi.org/10.1021/bi036265i

Caffarri, S., Kouřil, R., Kereïche, S., Boekema, E., & Croce, R. (2009). Functional architecture of higher plant photosystem II supercomplexes. *EMBO Journal*, *28*(19), 3052-3063. https://doi.org/10.1038/emboj.2009.232

Campbell, M., Cheng, A., Brilot, A., Moeller, A., Lyumkis, D., Veesler, D.,…Grigorieff, N. (2012). Movies of Ice-Embedded Particles Enhance Resolution in Electron Cryo-Microscopy. *Structure*, *20*(11), 1823-1828. https://doi.org/10.1016/j.str.2012.08.026

Cao, P., Su, X., Pan, X., Liu, Z., Chang, W., & Li, M. (2018). Structure, assembly and energy transfer of plant photosystem II supercomplex. *Biochimica et Biophysica Acta-Bioenergetics*, *1859*(9), 633-644. https://doi.org/10.1016/j.bbabio.2018.03.007

Castaño-Díez, D., Kudryashev, M., Arheit, M., & Stahlberg, H. (2012). Dynamo: A flexible, user-friendly development tool for subtomogram averaging of cryo-EM data in high-performance

computing environments. *Journal of Structural Biology*, *178*(2), 139-151. https://doi.org/10.1016/j.jsb.2011.12.017

Castaño-Díez, D., Kudryashev, M., & Stahlberg, H. (2017). Dynamo Catalogue: Geometrical tools and data management for particle picking in subtomogram averaging of cryo-electron tomograms. *Journal of Structural Biology*, *197*(2), 135-144. https://doi.org/10.1016/j.jsb.2016.06.005

Chakraborty, S., Jasnin, M., & Baumeister, W. (2020). Three-dimensional organization of the cytoskeleton: A cryo-electron tomography perspective. *Protein Science*, *29*(6), 1302-1320. https://doi.org/10.1002/pro.3858

Chen, Y., Ma, J., Wu, N., Su, Y., Zhang, Z., Yuan, M.,…Yuan, S. (2018). The roles of Arabidopsis proteins of Lhcb4, Lhcb5 and Lhcb6 in oxidative stress under natural light conditions. *Plant Physiology and Biochemistry*, *130*, 267-276. https://doi.org/10.1016/j.plaphy.2018.07.014

Costa, T., Ignatiou, A., & Orlova, E. (2017). Structural Analysis of Protein Complexes by Cryo Electron Microscopy. In *Bacterial protein secretion systems* (Vol. 1615, pp. 377-413).

Damkjær, J., Kereïche, S., Johnson, M., Kovacs, L., Kiss, A., Boekema, E.,…Jansson, S. (2009). The Photosystem II Light-Harvesting Protein Lhcb3 Affects the Macrostructure of Photosystem II and the Rate of State Transitions in Arabidopsis. *Plant Cell*, *21*(10), 3245-3256. https://doi.org/10.1105/tpc.108.064006

Daum, B., & Kühlbrandt, W. (2011). Electron tomography of plant thylakoid membranes. *Journal of Experimental Botany*, *62*(7), 2393-2402. https://doi.org/10.1093/jxb/err034

Daum, B., Nicastro, D., Il, J., McIntosh, J., & Kühlbrandt, W. (2010). Arrangement of Photosystem II and ATP Synthase in Chloroplast Membranes of Spinach and Pea. *Plant Cell*, *22*(4), 1299-1312. https://doi.org/10.1105/tpc.109.071431

de Bianchi, S., Betterle, N., Kouřil, R., Cazzaniga, S., Boekema, E., Bassi, R., & Dall'Osto, L. (2011). Arabidopsis Mutants Deleted in the Light-Harvesting Protein Lhcb4 Have a Disrupted Photosystem II Macrostructure and Are Defective in Photoprotection. *Plant Cell*, *23*(7), 2659-2679. https://doi.org/10.1105/tpc.111.087320

de Bianchi, S., Dall'Osto, L., Tognon, G., Morosinotto, T., & Bassi, R. (2008). Minor antenna proteins CP24 and CP26 affect the interactions between photosystem II Subunits and the electron transport rate in grana membranes of Arabidopsis. *Plant Cell*, *20*(4), 1012-1028. https://doi.org/10.1105/tpc.107.055749

de la Rosa-Trevín, J., Quintana, A., del Cano, L., Zaldívar, A., Foche, I., Gutiérrez, J.,…Carazo, J. (2016). Scipion: A software framework toward integration, reproducibility and validation in 3D electron microscopy. *Journal of Structural Biology*, *195*(1), 93-99. https://doi.org/10.1016/j.jsb.2016.04.010

Dekker, J., & Boekema, E. (2005). Supramolecular organization of thylakoid membrane proteins in green plants. *Biochimica et Biophysica Acta-Bioenergetics*, *1706*(1-2), 12-39. https://doi.org/10.1016/j.bbabio.2004.09.009

Dekker, J., Germano, M., van Roon, H., & Boekema, E. (2002). Photosystem II solubilizes as a monomer by mild detergent treatment of unstacked thylakoid membranes. *Photosynthesis Research*, *72*(2), 203-210.

DiIorio, M., & Kulczyk, A. (2022). A Robust Single-Particle Cryo-Electron Microscopy (cryo-EM) Processing Workflow with cryoSPARC, RELION, and Scipion. *JOVE-Journal of Visualized Experiments* (179), Article e63387. https://doi.org/10.3791/63387

Dlouhý, O., Karlický, V., Arshad, R., Zsiros, O., Domonkos, I., Kurasová, I.,…Garab, G. (2021). Lipid Polymorphism of the Subchloroplast-Granum and Stroma Thylakoid Membrane-Particles. II. Structure and Functions. *Cells*, *10*(9), Article 2363. https://doi.org/10.3390/cells10092363

Drop, B., Webber-Birungi, M., Fusetti, F., Kouřil, R., Redding, K. E., Boekema, E. J., & Croce, R. (2011). Photosystem I of Chlamydomonas reinhardtii Contains Nine Light-harvesting Complexes (Lhca) Located on One Side of the Core. *Journal of Biological Chemistry*, *286*(52), 44878-44887. https://doi.org/10.1074/jbc.M111.301101

Drop, B., Webber-Birungi, M., Yadav, S., Filipowicz-Szymanska, A., Fusetti, F., Boekema, E., & Croce, R. (2014). Light-harvesting complex II (LHCII) and its supramolecular organization in Chlamydomonas reinhardtii. *Biochimica et Biophysica Acta-Bioenergetics*, *1837*(1), 63-72. https://doi.org/10.1016/j.bbabio.2013.07.012

Drulyte, I., Johnson, R., Hesketh, E., Hurdiss, D., Scarff, C., Porav, S.,…Thompson, R. (2018). Approaches to altering particle distributions in cryo-electron microscopy sample preparation. *Acta Crystallographica Section D-Structural Biology*, *74*, 560-571. https://doi.org/10.1107/S2059798318006496

Dubochet, J., Adrian, M., Chang, J., Homo, J., Lepault, J., McDowall, A., & Schultz, P. (1988). Cryo-electron microscopy of vitrified specimens. *Quarterly Reviews of Biophysics*, *21*(2), 129-228. https://doi.org/10.1017/S0033583500004297

Eichacker, L., Weber, G., Sukop-Köppel, U., & Wildgruber, R. (2015). Free Flow Electrophoresis for Separation of Native Membrane Protein Complexes. In *Proteomic profiling: methods and protocols* (Vol. 1295, pp. 415-425).

Engel, B., Schaffer, M., Cuellar, L., Villa, E., Plitzko, J., & Baumeister, W. (2015). Native architecture of the Chlamydomonas chloroplast revealed by in situ cryo-electron tomography. *Elife*, *4*, Article e04889. https://doi.org/10.7554/eLife.04889

Erdmann, P., Plitzko, J., & Baumeister, W. (2018). Addressing cellular compartmentalization by in situ cryo-electron tomography. *Current Opinion in Colloid & Interface Science*, *34*, 89-99. https://doi.org/10.1016/j.cocis.2018.05.003

Faruqi, A., & Henderson, R. (2007). Electronic detectors for electron microscopy. *Current Opinion in Structural Biology*, *17*(5), 549-555. https://doi.org/10.1016/j.sbi.2007.08.014

Fernández, F., & Vega, M. (2013). Technologies to keep an eye on: alternative hosts for protein production in structural biology. *Current Opinion in Structural Biology*, *23*(3), 365-373. https://doi.org/10.1016/j.sbi.2013.02.002

Frank, J. (2002). Single-particle imaging of macromolecules by cryo-electron microscopy. *Annual Review of Biophysics and Biomolecular Structure*, *31*, 303-319. https://doi.org/10.1146/annurev.biophys.31.082901.134202

Furat, O., Wang, M., Neumann, M., Petrich, L., Weber, M., Krill, C., & Schmidt, V. (2019). Machine Learning Techniques for the Segmentation of Tomographic Image Data of Functional Materials. *Frontiers in Materials*, *6*, Article 145. https://doi.org/10.3389/fmats.2019.00145

Galaz-Montoya, J. (2024). The advent of preventive high-resolution structural histopathology by artificial-intelligence-powered cryogenic electron tomography. *Frontiers in Molecular Biosciences*, *11*, Article 1390858. https://doi.org/10.3389/fmolb.2024.1390858

Gao, J., Wang, H., Yuan, Q., & Feng, Y. (2018). Structure and Function of the Photosystem Supercomplexes. *Frontiers in Plant Science*, *9*, Article 357. https://doi.org/10.3389/fpls.2018.00357

Garber, M., & Steponkus, P. (1976). Alterations in chloroplast thylakoids during cold-acclimation. *Plant Physiology*, *57*(5), 681-686.

Goral, T., Johnson, M., Brain, A., Kirchhoff, H., Ruban, A., & Mullineaux, C. (2010). Visualizing the mobility and distribution of chlorophyll proteins in higher plant thylakoid membranes: effects of photoinhibition and protein phosphorylation. *Plant Journal*, *62*(6), 948-959. https://doi.org/10.1111/j.1365-313X.2010.04207.x

Goral, T., Johnson, M., Duffy, C., Brain, A., Ruban, A., & Mullineaux, C. (2012). Light-harvesting antenna composition controls the macrostructure and dynamics of thylakoid membranes in Arabidopsis. *Plant Journal*, *69*(2), 289-301. https://doi.org/10.1111/j.1365-313X.2011.04790.x

Graça, A., Hall, M., Persson, K., & Schröder, W. (2021). High-resolution model of Arabidopsis Photosystem II reveals the structural consequences of digitonin-extraction. *Scientific Reports*, *11*(1), Article 15534. https://doi.org/10.1038/s41598-021-94914-x

Grebe, S., Trotta, A., Bajwa, A., Suorsa, M., Gollan, P., Jansson, S.,…Aro, E. (2019). The unique photosynthetic apparatus of Pinaceae: analysis of photosynthetic complexes in Picea abies. *Journal of Experimental Botany*, *70*(12), 3211-3225. https://doi.org/10.1093/jxb/erz127

Grinzato, A., Albanese, P., Marotta, R., Swuec, P., Saracco, G., Bolognesi, M.,…Pagliano, C. (2020). High-Light versus Low-Light: Effects on Paired Photosystem II Supercomplex Structural Rearrangement in Pea Plants. *International Journal of Molecular Sciences*, *21*(22), Article 8643. https://doi.org/10.3390/ijms21228643

Guskov, A., Kern, J., Gabdulkhakov, A., Broser, M., Zouni, A., & Saenger, W. (2009). Cyanobacterial photosystem II at 2.9-Å resolution and the role of quinones, lipids, channels and chloride. *Nature Structural & Molecular Biology*, *16*(3), 334-342. https://doi.org/10.1038/nsmb.1559

Hankamer, B., Barber, J., & Boekema, E. (1997b). Structure and membrane organization of photosystem II in green plants. *Annual Review of Plant Physiology and Plant Molecular Biology*, *48*, 641-671.

Hankamer, B., Morris, E., & Barber, J. (1999). Revealing the structure of the oxygen-evolving core dimer of photosystem II by cryoelectron crystallography. *Nature Structural Biology*, *6*(6), 560-564.

Hankamer, B., Nield, J., Zheleva, D., Boekema, E., Jansson, S., & Barber, J. (1997a). Isolation and biochemical characterisation of monomeric and dimeric photosystem II complexes from spinach and their relevance to the organisation of photosystem II in vivo. *European Journal of Biochemistry*, *243*(1-2), 422-429.

Hansson, M., & Vener, A. (2003). Identification of three previously unknown in vivo protein phosphorylation sites in thylakoid membranes of Arabidopsis thaliana. *Molecular & Cellular Proteomics*, *2*(8), 550-559. https://doi.org/10.1074/mcp.M300050-MCP200

Harrer, R. (2003). Associations between light-harvesting complexes and Photosystem II from Marchantia polymorpha L. determined by two- and three-dimensional electron microscopy. *Photosynthesis Research*, *75*(3), 249-258.

Harris, J., & Horne, R. (1994). Negative staining - a brief assessment of current technical benefits, limitations and future possibilities. *Micron*, *25*(1), 5-13.

Harris, J., & Scheffler, D. (2002). Routine preparation of air-dried negatively stained and unstained specimens on holey carbon support films: a review of applications. *Micron*, *33*(5), 461-480, Article PII S0968-4328(01)00039-7.

Heijbel, A., Andersson, L., Bergh, A., Lindgren, H., Lundqvist, J., Torstenson, K., & Oberg, K. (2004). New optimized resin for purification of His-tagged proteins. *FASEB Journal*, *18*(8), C175-C176.

Henderson, R., Baldwin, J., Ceska, T., Zemlin, F., Beckmann, E., & Downing, K. (1990). Model for the structure of bacteriorhodopsin based on high-resolution electron cryomicroscopy. *Journal of Molecular Biology*, *213*(4), 899-929.

Herbstová, M., Tietz, S., Kinzel, C., Turkina, M., & Kirchhoff, H. (2012). Architectural switch in plant photosynthetic membranes induced by light stress. *Proceedings of the National Academy of Sciences of the United States of America*, *109*(49), 20130-20135. https://doi.org/10.1073/pnas.1214265109

Hong, Y., Song, Y., Zhang, Z., & Li, S. (2023). Cryo-Electron Tomography: The Resolution Revolution and a Surge of In Situ Virological Discoveries. *Annual Review of Biophysics*, *52*, 339-360. https://doi.org/10.1146/annurev-biophys-092022-100958

Huang, Q., Zhou, Y., Liu, H., & Bartesaghi, A. (2022, 2022-01-01). Accurate Detection of Proteins in Cryo-Electron Tomograms from Sparse Labels. Computer Vision, ECCV 2022, PT XXI,

Ifuku, K. (2023). Diversity of the PSI-PSII Megacomplexes That Conduct Energy Spillover in Green Plants. *Plant and Cell Physiology*, *64*(8), 844-846. https://doi.org/10.1093/pcp/pcad069

Ilíková, I., Ilík, P., Opatíková, M., Arshad, R., Nosek, L., Karlicky, V.,…Kouřil, R. (2021). Towards spruce-type photosystem II: consequences of the loss of light-harvesting proteins LHCB3 and LHCB6 in Arabidopsis. *Plant Physiology*, *187*(4), 2691-2715. https://doi.org/10.1093/plphys/kiab396

Jansson, S. (1994). The light-harvesting chlorophyll a/b binding-proteins. *Biochimica et Biophysica Acta-Bioenergetics*, *1184*(1), 1-19.

Jansson, S. (1999). A guide to the Lhc genes and their relatives in Arabidopsis. *Trends in Plant Science*, *4*(6), 236-240.

Johnson, M., Goral, T., Duffy, C., Brain, A., Mullineaux, C., & Ruban, A. (2011). Photoprotective Energy Dissipation Involves the Reorganization of Photosystem II Light-Harvesting Complexes in the Grana Membranes of Spinach Chloroplasts. *Plant Cell*, *23*(4), 1468-1479. https://doi.org/10.1105/tpc.110.081646

Järvi, S., Gollan, P., & Aro, E. (2013). Understanding the roles of the thylakoid lumen in photosynthesis regulation. *Frontiers in Plant Science*, *4*, Article 434. https://doi.org/10.3389/fpls.2013.00434

Järvi, S., Suorsa, M., Paakkarinen, V., & Aro, E. (2011). Optimized native gel systems for separation of thylakoid protein complexes: novel super- and mega-complexes. *Biochemical Journal*, *439*, 207-214. https://doi.org/10.1042/BJ20102155

Kereiche, S., Kiss, A., Kouřil, R., Boekema, E., & Horton, P. (2010). The PsbS protein controls the macro-organisation of photosystem II complexes in the grana membranes of higher plant chloroplasts. *FEBS Letters*, *584*(4), 759-764. https://doi.org/10.1016/j.febslet.2009.12.031

Kim, E., Watanabe, A., Duffy, C., Ruban, A., & Minagawa, J. (2020). Multimeric and monomeric photosystem II supercomplexes represent structural adaptations to low- and high-light conditions. *Journal of Biological Chemistry*, *295*(43), 14537-14545. https://doi.org/10.1074/jbc.RA120.014198

Kim, E., Yokono, M., Tsugane, K., Ishii, A., Noda, C., & Minagawa, J. (2023). Formation of a Stable PSI-PSII Megacomplex in Rice That Conducts Energy Spillover. *Plant and Cell Physiology*, *64*(8), 858-865. https://doi.org/10.1093/pcp/pcad037

Kirchhoff, H. (2013). Architectural switches in plant thylakoid membranes. *Photosynthesis Research*, *116*(2-3), 481-487. https://doi.org/10.1007/s11120-013-9843-0

Kirchhoff, H. (2014). Structural changes of the thylakoid membrane network induced by high light stress in plant chloroplasts. *Philosophical Transactions of the Royal Society B-Biological Sciences*, *369*(1640), Article 20130225. https://doi.org/10.1098/rstb.2013.0225

Kirchhoff, H., Haase, W., Wegner, S., Danielsson, R., Ackermann, R., & Albertsson, P. (2007). Low-light-induced formation of semicrystalline photosystem II arrays in higher plant chloroplast. *Biochemistry*, *46*(39), 11169-11176. https://doi.org/10.1021/bi700748y

Kirchhoff, H., Hall, C., Wood, M., Herbstová, M., Tsabari, O., Nevo, R.,…Reich, Z. (2011). Dynamic control of protein diffusion within the granal thylakoid lumen. *Proceedings of the National Academy of Sciences of the United States of America*, *108*(50), 20248-20253. https://doi.org/10.1073/pnas.1104141109

Klimmek, F., Sjödin, A., Noutsos, C., Leister, D., & Jansson, S. (2006). Abundantly and rarely expressed Lhc protein genes exhibit distinct regulation patterns in plants. *Plant Physiology*, *140*(3), 793-804.

Klumpe, S., Fung, H., Goetz, S., Zagoriy, I., Hampoelz, B., Zhang, X.,…Mahamid, J. (2021). A modular platform for automated cryo-FIB workflows. *ELIFE*, *10*, Article e70506. https://doi.org/10.7554/eLife.70506.sa2

Koning, R., Koster, A., & Sharp, T. (2018). Advances in cryo-electron tomography for biology and medicine. *Annals of Anatomy-Anatomischer Anzeiger*, *217*, 82-96. https://doi.org/10.1016/j.aanat.2018.02.004

Kouřil, R., Dekker, J. P., & Boekema, E. J. (2012). Supramolecular organization of photosystem II in green plants. *Biochimica Et Biophysica Acta-Bioenergetics*, *1817*(1), 2-12. https://doi.org/10.1016/j.bbabio.2011.05.024

Kouřil, R., Nosek, L., Bartos, J., Boekema, E. J., & Ilik, P. (2016). Evolutionary loss of light-harvesting proteins Lhcb6 and Lhcb3 in major land plant groups - break-up of current dogma. *New Phytologist*, *210*(3), 808-814. https://doi.org/10.1111/nph.13947

Kouřil, R., Nosek, L., Opatíková, M., Arshad, R., Semchonok, D., Chamrád, I.,…Ilík, P. (2020). Unique organization of photosystem II supercomplexes and megacomplexes in Norway spruce. *Plant Journal 104*(1), 215-225. https://doi.org/10.1111/tpj.14918

Kouřil, R., Nosek, L., Semchonok, D., Boekema, E., & Ilík, P. (2018). Organization of Plant Photosystem II and Photosystem I Supercomplexes. In *Membrane Protein Complexes: Structure and Function* (Vol. 87, pp. 259-286).

Kouřil, R., Oostergetel, G. T., & Boekema, E. J. (2011). Fine structure of granal thylakoid membrane organization using cryo electron tomography. *Biochimica et Biophysica Acta-Bioenergetics*, *1807*(3), 368-374. https://doi.org/10.1016/j.bbabio.2010.11.007

Kouřil, R., Strouhal, O., Nosek, L., Lenobel, R., Chamrád, I., Boekema, E.,…Ilík, P. (2014). Structural characterization of a plant photosystem I and NAD(P)H dehydrogenase supercomplex. *Plant Journal*, *77*(4), 568-576. https://doi.org/10.1111/tpj.12402

Kouřil, R., Wientjes, E., Bultema, J. B., Croce, R., & Boekema, E. J. (2013). High-light vs. low-light: Effect of light acclimation on photosystem II composition and organization in Arabidopsis thaliana. *Biochimica Et Biophysica Acta-Bioenergetics*, *1827*(3), 411-419. https://doi.org/10.1016/j.bbabio.2012.12.003

Kouřil, R., Yeremenko, N., D'Haene, S., Oostergetel, G., Matthijs, H., Dekker, J., & Boekema, E. (2005b). Supercomplexes of IsiA and photosystem I in a mutant lacking subunit PsaL.

Biochimica Et Biophysica Acta-Bioenergetics, *1706*(3), 262-266. https://doi.org/10.1016/j.bbabio.2004.11.008

Kouřil, R., Zygadlo, A., Arteni, A., de Wit, C., Dekker, J., Jensen, P.,…Boekema, E. (2005a). Structural characterization of a complex of photosystem I and light-harvesting complex II of Arabidopsis thaliana. *Biochemistry*, *44*(33), 10935-10940. https://doi.org/10.1021/bi051097a

Kovács, L., Damkjær, J., Kereïche, S., Ilioaia, C., Ruban, A., Boekema, E.,…Horton, P. (2006). Lack of the light-harvesting complex CP24 affects the structure and function of the grana membranes of higher plant chloroplasts. *Plant Cell*, *18*(11), 3106-3120. https://doi.org/10.1105/tpc.106.045641

Koziol, A., Borza, T., Ishida, K., Keeling, P., Lee, R., & Durnford, D. (2007). Tracing the evolution of the light-harvesting antennae in chlorophyll a/b- containing organisms. *Plant Physiology*, *143*(4), 1802-1816. https://doi.org/10.1104/pp.106.092536

Krieger-Liszkay, A., & Trebst, A. (2006). Tocopherol is the scavenger of singlet oxygen produced by the triplet states of chlorophyll in the PSII reaction centre. *Journal of Experimental Botany*, *57*(8), 1677-1684. https://doi.org/10.1093/jxb/erl002

Kruk, J., Schmid, G., & Strzalka, K. (2000). Interaction of α-tocopherol quinone, α-tocopherol and other prenyllipids with photosystem II. *Plant Physiology and Biochemistry*, *38*(4), 271-277.

Kumar, A., Prasad, A., & Pospísil, P. (2020). Formation of α-tocopherol hydroperoxide and α-tocopheroxyl radical: relevance for photooxidative stress in Arabidopsis. *Scientific Reports*, *10*(1), Article 19646. https://doi.org/10.1038/s41598-020-75634-0

Lee, Z., Rose, H., Lehtinen, O., Biskupek, J., & Kaiser, U. (2014). Electron dose dependence of signal-to-noise ratio, atom contrast and resolution in transmission electron microscope images. *Ultramicroscopy*, *145*, 3-12. https://doi.org/10.1016/j.ultramic.2014.01.010

Li, X., Bjorkman, O., Shih, C., Grossman, A., Rosenquist, M., Jansson, S., & Niyogi, K. (2000). A pigment-binding protein essential for regulation of photosynthetic light harvesting. *Nature*, *403*(6768), 391-395.

Li, X., Mooney, P., Zheng, S., Booth, C., Braunfeld, M., Gubbens, S.,…Cheng, Y. (2013). Electron counting and beam-induced motion correction enable near-atomic-resolution single-particle cryo-EM. *Nature Methods*, *10*(6), 584-+. https://doi.org/10.1038/nmeth.2472

Liu, Z., Yan, H., Wang, K., Kuang, T., Zhang, J., Gui, L.,…Chang, W. (2004). Crystal structure of spinach major light-harvesting complex at 2.72 Å resolution. *Nature*, *428*(6980), 287-292. https://doi.org/10.1038/nature02373

Lucic, V., Leis, A., & Baumeister, W. (2008). Cryo-electron tomography of cells: connecting structure and function. *Histochemistry and Cell Biology*, *130*(2), 185-196. https://doi.org/10.1007/s00418-008-0459-y

Lucic, V., Rigort, A., & Baumeister, W. (2013). Cryo-electron tomography: The challenge of doing structural biology in situ. *Journal of Cell Biology*, *202*(3), 407-419. https://doi.org/10.1083/jcb.201304193

Lyumkis, D. (2019). Challenges and opportunities in cryo-EM single-particle analysis. *Journal of Biological Chemistry*, *294*(13), 5181-5197. https://doi.org/10.1074/jbc.REV118.005602

Mao, R., Zhang, H., Bie, L., Liu, L., & Gao, J. (2023). Million-atom molecular dynamics simulations reveal the interfacial interactions and assembly of plant PSII-LHCII supercomplex. *RSC Advances*, *13*(10), 6699-6712. https://doi.org/10.1039/d2ra08240c

Mazor, Y., Borovikova, A., Caspy, I., & Nelson, N. (2017). Structure of the plant photosystem I supercomplex at 2.6 Å resolution. *Nature Plants*, *3*(3). https://doi.org/10.1038/nplants.2017.14

Mendez, J., Mehrani, A., Randolph, P., & Stagg, S. (2019). Throughput and resolution with a next-generation direct electron detector. *IUCRJ*, *6*, 1007-1013. https://doi.org/10.1107/S2052252519012661

Miller, K., Miller, G., & Mcintyre, K. (1976). Light-harvesting chlorophyll-protein complex of photosystem .2. its location in photosynthetic membrane. *Journal of Cell Biology*, *71*(2), 624-638.

Morosinotto, T., Bassi, R., Frigerio, S., Finazzi, G., Morris, E., & Barber, J. (2006). Biochemical and structural analyses of a higher plant photosystem II supercomplex of a photosystem I-less mutant of barley - Consequences of a chronic over-reduction of the plastoquinone pool. *FEBS Journal*, *273*(20), 4616-4630. https://doi.org/10.1111/j.1742-4658.2006.05465.x

Nelson, N., & Yocum, C. (2006). Structure and function of photosystems I and II. *Annual Review of Plant Biology*, *57*, 521-565. https://doi.org/10.1146/annurev.arplant.57.032905.105350

Nevo, R., Charuvi, D., Shimoni, E., Schwarz, R., Kaplan, A., Ohad, I., & Reich, Z. (2007). Thylakoid membrane perforations and connectivity enable intracellular traffic in cyanobacteria. *EMBO Journal*, *26*(5), 1467-1473. https://doi.org/10.1038/sj.emboj.7601594

Ni, T., Frosio, T., Mendonça, L., Sheng, Y., Clare, D., Himes, B., & Zhang, P. (2022). High-resolution in situ structure determination by cryo-electron tomography and subtomogram averaging using emClarity. *Nature Protocols*, *17*(2), 421-+. https://doi.org/10.1038/s41596-021-00648-5

Nield, J., Orlova, E., Morris, E., Gowen, B., van Heel, M., & Barber, J. (2000). 3D map of the plant photosystem II supercomplex obtained by cryoelectron microscopy and single particle analysis. *Nature Structural Biology*, *7*(1), 44-47.

Nierzwicki, L., & Palermo, G. (2021). Molecular Dynamics to Predict Cryo-EM: Capturing Transitions and Short-Lived Conformational States of Biomolecules. *Frontiers in Molecular Biosciences*, *8*, Article 641208. https://doi.org/10.3389/fmolb.2021.641208

Noble, A., & de Marco, A. (2024). Cryo-focused ion beam for in situ structural biology: State of the art, challenges, and perspectives. *Current Opinion in Structural Biology*, *87*, Article 102864. https://doi.org/10.1016/j.sbi.2024.102864

Nosek, L., Semchonok, D., Boekema, E. J., Ilik, P., & Kouřil, R. (2017). Structural variability of plant photosystem II megacomplexes in thylakoid membranes. *Plant Journal*, *89*(1), 104-111. https://doi.org/10.1111/tpj.13325

Opatíková, M., Semchonok, D., Kopecny, D., Ilík, P., Pospísil, P., Ilíková, I.,…Kouřil, R. (2023). Cryo-EM structure of a plant photosystem II supercomplex with light-harvesting protein Lhcb8 and α-tocopherol. *Nature Plants*, *9*(8), 1359-+. https://doi.org/10.1038/s41477-023-01483-0

Park, R., & Biggins, J. (1964). Quantasome - size + composition. *Science*, *144*(362), 1009-+.

Pietrzykowska, M., Suorsa, M., Semchonok, D., Tikkanen, M., Boekema, E., Aro, E., & Jansson, S. (2014). The Light-Harvesting Chlorophyll a/b Binding Proteins Lhcb1 and Lhcb2 Play Complementary Roles during State Transitions in Arabidopsis. *Plant Cell*, *26*(9), 3646-3660. https://doi.org/10.1105/tpc.114.127373

Pribil, M., Labs, M., & Leister, D. (2014). Structure and dynamics of thylakoids in land plants. *Journal of Experimental Botany*, *65*(8), 1955-1972. https://doi.org/10.1093/jxb/eru090

Quispe, J., Damiano, J., Mick, S., Nackashi, D., Fellmann, D., Ajero, T.,…Potter, C. (2007). An improved holey carbon film for cryo-electron microscopy. *Microscopy and Microanalysis*, *13*(5), 365-371. https://doi.org/10.1017/S1431927607070791

Rantala, M., Tikkanen, M., & Aro, E. (2017). Proteomic characterization of hierarchical megacomplex formation in Arabidopsis thylakoid membrane. *Plant Journal*, *92*(5), 951-962. https://doi.org/10.1111/tpj.13732

Rhee, K., Morris, E., Zheleva, D., Hankamer, B., Kuhlbrandt, W., & Barber, J. (1997). Two-dimensional structure of plant photosystem II at 8-angstrom resolution. *Nature*, *389*(6650), 522-526.

Ruprecht, J., & Nield, J. (2001). Determining the structure of biological macromolecules by transmission electron microscopy, single particle analysis and 3D reconstruction. *Progress in Biophysics & Molecular Biology*, *75*(3), 121-164.

Sawicka, M., Aramayo, R., Ayala, R., Glyde, R., & Zhang, X. (2017). Single-Particle Electron Microscopy Analysis of DNA Repair Complexes. In *DNA repair enzymes: structure, biophysics, and mechanism* (Vol. 592, pp. 159-186).

Scarff, C., Fuller, M., Thompson, R., & Iadaza, M. (2018). Variations on Negative Stain Electron Microscopy Methods: Tools for Tackling Challenging Systems. *JOVE-Journal of Visualized Experiments* (132), Article e57199. https://doi.org/10.3791/57199

Schaffer, M., Pfeffer, S., Mahamid, J., Kleindiek, S., Laugks, T., Albert, S.,…Plitzko, J. (2019). A cryo-FIB lift-out technique enables molecular-resolution cryo-ET within native Caenorhabditis elegans tissue. *Nature Methods*, *16*(8), 757-+. https://doi.org/10.1038/s41592-019-0497-5

Schagger, H., Cramer, W., & Vonjagow, G. (1994). Analysis of molecular masses and oligomeric states of protein complexes by blue native electrophoresis and isolation of membrane-protein complexes by 2-dimensional native electrophoresis. *Analytical Biochemistry*, *217*(2), 220-230.

Schagger, H., & Vonjagow, G. (1991). Blue native electrophoresis for isolation of membrane-protein complexes in enzymatically active form. *Analytical Biochemistry*, *199*(2), 223-231.

Serna, M. (2019). Hands on Methods for High Resolution Cryo-Electron Microscopy Structures of Heterogeneous Macromolecular Complexes. *Frontiers in Molecular Biosciences*, *6*, Article 33. https://doi.org/10.3389/fmolb.2019.00033

Shan, J., Niedzwiedzki, D., Tomar, R., Liu, Z., & Liu, H. (2024). Architecture and functional regulation of a plant PSII-LHCII megacomplex. *Science Advances*, *10*(50), Article eadq9967. https://doi.org/10.1126/sciadv.adq9967

Sharov, G., Morado, D., Carroni, M., & de la Rosa-Trevin, J. (2021). Using RELION software within the Scipion framework. *Acta Crystallographica Section D-Structural Biology*, *77*, 403-410. https://doi.org/10.1107/S2059798321001856

Shen, L., Tang, K., Wang, W., Wang, C., Wu, H., Mao, Z.,…Zhang, X. (2022). Architecture of the chloroplast PSI-NDH supercomplex in Hordeum vulgare. *Nature*, *601*(7894), 649-+. https://doi.org/10.1038/s41586-021-04277-6

Sheng, X., Watanabe, A., Li, A., Kim, E., Song, C., Murata, K.,…Liu, Z. (2019). Structural insight into light harvesting for photosystem II in green algae. *Nature Plants*, *5*(12), 1320-+. https://doi.org/10.1038/s41477-019-0543-4

Shimoni, E., Rav-Hon, O., Ohad, I., Brumfeld, V., & Reich, Z. (2005). Three-dimensional organization of higher-plant chloroplast thylakoid membranes revealed by electron tomography. *Plant Cell*, *17*(9), 2580-2586. https://doi.org/10.1105/tpc.105.035030

Simpson, D. (1979). Freeze-fracture studies on barley plastid membranes .3. location of the light-harvesting chlorophyll-protein. *Carlsberg Research Communications*, *44*(5), 305-336.

Sorzano, C., Marabini, R., Pascual-Montano, A., Scheres, S., & Carazo, J. (2006). Optimization problems in electron microscopy of single particles. *Annals of Operations Research*, *148*(1), 133-165. https://doi.org/10.1007/s10479-006-0078-8

Sorzano, C., Vargas, J., de la Rosa-Trevín, J., Jiménez, A., Maluenda, D., Melero, R.,…Carazo, J. (2018). A new algorithm for high-resolution reconstruction of single particles by electron microscopy. *Journal of Structural Biology*, *204*(2), 329-337. https://doi.org/10.1016/j.jsb.2018.08.002

Spriestersbach, A., Kubicek, J., Schäfer, F., Block, H., & Maertens, B. (2015). Purification of His-Tagged Proteins. In *Laboratory methods in enzymology: protein, PT D* (Vol. 559, pp. 1-15).

Staehelin, L. (2003). Chloroplast structure: from chlorophyll granules to supra-molecular architecture of thylakoid membranes. *Photosynthesis Research*, *76*(1-3), 185-196.

Staehelin, L., & Paolillo, D. (2020). A brief history of how microscopic studies led to the elucidation of the 3D architecture and macromolecular organization of higher plant thylakoids. *Photosynthesis Research*, *145*(3), 237-258. https://doi.org/10.1007/s11120-020-00782-3

Standfuss, J., & Kühlbrandt, W. (2004). The three isoforms of the light-harvesting complex II -: Spectroscopic features, trimer formation, and functional roles. *Journal of Biological Chemistry*, *279*(35), 36884-36891. https://doi.org/10.1074/jbc.M402348200

Stark, H., & Chari, A. (2016). Sample preparation of biological macromolecular assemblies for the determination of high-resolution structures by cryo-electron microscopy. *MICROSCOPY*, *65*(1), 23-34. https://doi.org/10.1093/jmicro/dfv367

Su, X., Ma, J., Wei, X., Cao, P., Zhu, D., Chang, W.,…Li, M. (2017). Structure and assembly mechanism of plant C2S2M2-type PSII-LHCII supercomplex. *Science*, *357*(6353), 816-+. https://doi.org/10.1126/science.aan0327

Suorsa, M., Rantala, M., Mamedov, F., Lespinasse, M., Trotta, A., Grieco, M.,…Aro, E. (2015). Light acclimation involves dynamic re-organization of the pigment-protein megacomplexes in non-appressed thylakoid domains. *Plant Journal*, *84*(2), 360-373. https://doi.org/10.1111/tpj.13004

Tacke, S., Erdmann, P., Wang, Z., Klumpe, S., Grange, M., Plitzko, J., & Raunser, S. (2021). A streamlined workflow for automated cryo focused ion beam milling. *Journal of Structural Biology*, *213*(3), Article 107743. https://doi.org/10.1016/j.jsb.2021.107743

Thompson, R., Walker, M., Siebert, C., Muench, S., & Ranson, N. (2016). An introduction to sample preparation and imaging by cryo-electron microscopy for structural biology. *METHODS*, *100*, 3-15. https://doi.org/10.1016/j.ymeth.2016.02.017

Tietz, S., Puthiyaveetil, S., Enlow, H., Yarbrough, R., Wood, M., Semchonok, D.,…Kirchhoff, H. (2015). Functional Implications of Photosystem II Crystal Formation in Photosynthetic

Membranes. *Journal of Biological Chemistry*, *290*(22), 14091-14106. https://doi.org/10.1074/jbc.M114.619841

Tokutsu, R., Kato, N., Bui, K., Ishikawa, T., & Minagawa, J. (2012). Revisiting the Supramolecular Organization of Photosystem II in Chlamydomonas reinhardtii. *Journal of Biological Chemistry*, *287*(37), 31574-31581. https://doi.org/10.1074/jbc.M111.331991

Turk, M., & Baumeister, W. (2020). The promise and the challenges of cryo-electron tomography. *FEBS LETTERS*, *594*(20), 3243-3261. https://doi.org/10.1002/1873-3468.13948

Turonová, B., Hagen, W., Obr, M., Mosalaganti, S., Beugelink, J., Zimmerli, C.,…Beck, M. (2020). Benchmarking tomographic acquisition schemes for high-resolution structural biology. *Nature Communications*, *11*(1), Article 876. https://doi.org/10.1038/s41467-020-14535-2

van Bezouwen, L. S., Caffarri, S., Kale, R. S., Kouřil, R., Thunnissen, A.-M. W. H., Oostergetel, G. T., & Boekema, E. J. (2017). Subunit and chlorophyll organization of the plant photosystem II supercomplex. *Nature Plants*, *3*(7). https://doi.org/10.1038/nplants.2017.80

Van Eerden, F., Melo, M., Frederix, P., Periole, X., & Marrink, S. (2017). Exchange pathways of plastoquinone and plastoquinol in the photosystem II complex. *Nature Communications*, *8*, Article 15214. https://doi.org/10.1038/ncomms15214

van Roon, H., van Breemen, J., de Weerd, F., Dekker, J., & Boekema, E. (2000). Solubilization of green plant thylakoid membranes with n-dodecyl-α,D-maltoside.: Implications for the structural organization of the Photosystem II, Photosystem I, ATP synthase and cytochrome b6f complexes. *Photosynthesis Research*, *64*(2-3), 155-166.

Vayghan, H., Nawrocki, W., Schiphorst, C., Tolleter, D., Hu, C., Douet, V.,…Longoni, F. (2022). Photosynthetic Light Harvesting and Thylakoid Organization in a CRISPR/Cas9 Arabidopsis Thaliana LHCB1 Knockout Mutant. *Frontiers in Plant Science*, *13*, Article 833032. https://doi.org/10.3389/fpls.2022.833032

Veesler, D., Campbell, M., Cheng, A., Fu, C., Murez, Z., Johnson, J.,…Carragher, B. (2013). Maximizing the potential of electron cryomicroscopy data collected using direct detectors. *Journal of Structural Biology*, *184*(2), 193-202. https://doi.org/10.1016/j.jsb.2013.09.003

Vinothkumar, K., & Henderson, R. (2016). Single particle electron cryomicroscopy: trends, issues and future perspective. *Quarterly Reviews of Biophysics*, *49*, 1-25, Article e13. https://doi.org/10.1017/S0033583516000068

Wang, J., Watson, J., & Lisanza, S. (2024). Protein Design Using Structure-Prediction Networks: AlphaFold and RoseTTAFold as Protein Structure Foundation Models. *Cold spring harbor perspectives in biology*, *16*(7), Article a041472. https://doi.org/10.1101/cshperspect.a041472

Watson, A., & Bartesaghi, A. (2024). Advances in cryo-ET data processing: meeting the demands of visual proteomics. *Current Opinion in Structural Biology*, *87*, Article 102861. https://doi.org/10.1016/j.sbi.2024.102861

Wei, X., Su, X., Cao, P., Liu, X., Chang, W., Li, M.,…Liu, Z. (2016). Structure of spinach photosystem II-LHCII supercomplex at 3.2 Å resolution. *Nature*, *534*(7605), 69-+. https://doi.org/10.1038/nature18020

Wittig, I., Karas, M., & Schägger, H. (2007). High resolution clear native electrophoresis for In-gel functional assays and fluorescence studies of membrane protein complexes. *Molecular & Cellular Proteomics*, *6*(7), 1215-1225. https://doi.org/10.1074/mcp.M700076-MCP200

Wittig, I., & Schägger, H. (2005). Advantages and limitations of clear-native PAGE. *Proteomics*, *5*(17), 4338-4346. https://doi.org/10.1002/pmic.200500081

Wu, J., Chen, S., Wang, C., Lin, W., Huang, C., Fan, C.,…Zhang, L. (2023). Regulatory dynamics of the higher-plant PSI-LHCI supercomplex during state transitions. *Molecular Plant*, *16*(12), 1937-1950. https://doi.org/10.1016/j.molp.2023.11.002

Wu, M., & Lander, G. (2020). Present and Emerging Methodologies in Cryo-EM Single-Particle Analysis. *Biophysical Journal*, *119*(7), 1281-1289. https://doi.org/10.1016/j.bpj.2020.08.027

Xu, B., & Liu, L. (2020). Developments, applications, and prospects of cryo-electron microscopy. *Protein Science*, *29*(4), 872-882. https://doi.org/10.1002/pro.3805

Yadav, K. N. S., Semchonok, D. A., Nosek, L., Kouřil, R., Fucile, G., Boekema, E. J., & Eichacker, L. A. (2017). Supercomplexes of plant photosystem I with cytochrome b6f, light-harvesting complex II and NDH. *Biochimica et Biophysica Acta-Bioenergetics*, *1858*(1), 12-20. https://doi.org/10.1016/j.bbabio.2016.10.006

Yakushevska, A., Jensen, P., Keegstra, W., van Roon, H., Scheller, H., Boekema, E., & Dekker, J. (2001). Supermolecular organization of photosystem II and its associated light-harvesting antenna in Arabidopsis thaliana. *European Journal of Biochemistry*, *268*(23), 6020-6028.

Yakushevska, A., Keegstra, W., Boekema, E., Dekker, J., Andersson, J., Jansson, S.,…Horton, P. (2003). The structure of photosystem II in Arabidopsis:: Localization of the CP26 and CP29 antenna complexes. *Biochemistry*, *42*(3), 608-613. https://doi.org/10.1021/bi027109z

Yamamoto, Y., Kai, S., Ohnishi, A., Tsumura, N., Ishikawa, T., Hori, H.,…Ishikawa, Y. (2014). Quality Control of PSII: Behavior of PSII in the Highly Crowded Grana Thylakoids Under Excessive Light. *Plant and Cell Physiology*, *55*(7), 1206-1215. https://doi.org/10.1093/pcp/pcu043

Yeremenko, N., Kouřil, R., Ihalainen, J., D'Haene, S., van Oosterwijk, N., Andrizhiyevskaya, E.,…Dekker, J. (2004). Supramolecular organization and dual function of the IsiA chlorophyll-binding protein in cyanobacteria. *Biochemistry*, *43*(32), 10308-10313. https://doi.org/10.1021/bi048772l

Yip, K., Fischer, N., Paknia, E., Chari, A., & Stark, H. (2020). Atomic-resolution protein structure determination by cryo-EM. *Nature*, *587*(7832), 157-+. https://doi.org/10.1038/s41586-020-2833-4

Yoshioka-Nishimura, M. (2016). Close Relationships Between the PSII Repair Cycle and Thylakoid Membrane Dynamics. *Plant and Cell Physiology*, *57*(6), 1115-1122. https://doi.org/10.1093/pcp/pcw050

Zhang, K. (2016). Gctf: Real-time CTF determination and correction. *Journal of Structural Biology*, *193*(1), 1-12. https://doi.org/10.1016/j.jsb.2015.11.003

Zhao, C., Lu, D., Zhao, Q., Ren, C., Zhang, H., Zhai, J.,…Gong, X. (2023). Computational methods for in situ structural studies with cryogenic electron tomography. *Frontiers in Cellular and Infection Microbiology*, *13*, Article 1135013. https://doi.org/10.3389/fcimb.2023.1135013

Zhao, X., Li, G., & Liang, S. (2013). Several Affinity Tags Commonly Used in Chromatographic Purification. *Journal of Analytical Methods in Chemistry*, *2013*, Article 581093. https://doi.org/10.1155/2013/581093

Zheng, S., Palovcak, E., Armache, J., Verba, K., Cheng, Y., & Agard, D. (2017). MotionCor2: anisotropic correction of beam-induced motion for improved cryo-electron microscopy. *Nature Methods*, *14*(4), 331-332. https://doi.org/10.1038/nmeth.4193

Zheng, S., Wolff, G., Greenan, G., Chen, Z., Faas, F., Barcena, M.,…Agard, D. (2022). AreTomo: An integrated software package for automated marker-free, motion-corrected cryo-electron tomographic alignment and reconstruction. *Journal of Structural Biology -X*, *6*, Article 100068. https://doi.org/10.1016/j.yjsbx.2022.100068

7. List of publications constituting the habilitation thesis

1. Caffarri, S., **Kouřil, R.**, Kereiche, S., Boekema, E.J., Croce, R. (2009) Functional architecture of higher plant photosystem II supercomplexes. *EMBO J* 28: 3052-3063.
2. **Kouřil, R.**, Oostergetel, G.T., Boekema, E.J. (2011) Fine structure of granal thylakoid membrane organization using cryo electron tomography. *Biochim Biophys Acta* 1807: 368-374.
3. de Bianchi, S., Betterle, N., **Kouřil, R.**, Cazzaniga, S., Boekema, E.J., Bassi, R., Dall´Osto, L. (2011) Arabidopsis mutants deleted in the light-harvesting protein Lhcb4 have a disrupted photosystem II macrostructure and are defective in photoprotection. *Plant Cell* 23: 2659-2679.
4. **Kouřil, R.**, Dekker, J.P., Boekema, E.J. (2012) Supramolecular organization of photosystem II in green plants. *Biochim Biophys Acta* 1817: 2-12.
5. **Kouřil, R.**, Wientjes, E., Bultema, J.B., Croce, R., Boekema, E.J. (2013) High-light vs. low-light: effect of light acclimation on photosystem II composition and organization in *Arabidopsis thaliana*. *Biochim Biophys Acta* 1827: 411-419.
6. **Kouřil, R.**, Nosek, L., Bartoš, J., Boekema, E.J., Ilík, P. (2016) Evolutionary loss of light-harvesting proteins Lhcb6 and Lhcb3 in major land plant groups – break-up of current dogma. *New Phytol* 210: 808-814.
7. Nosek, L., Semchonok, D., Boekema, E.J., Ilík, P., **Kouřil, R.** (2017) Structural variability of plant photosystem II megacomplexes in thylakoid membranes. *Plant J* 89: 104-111.
8. van Bezouwen, L.S., Caffarri, S., Kale, R.S., **Kouřil, R.**, Thunnissen, A.M.W.H., Oostergetel, G.T., Boekema, E.J. (2017) Subunit and chlorophyll organization of the plant photosystem II supercomplex. *Nature Plants* 3: 17080.
9. **Kouřil, R.**, Nosek, L., Semchonok, D., Boekema, E.J., Ilík, P. (2018) Organization of plant photosystem II and photosystem I supercomplexes. In: Membrane Protein Complexes: Structure and Function, *Subcellular Biochemistry* 87, J. R. Harris, E. J. Boekema (eds.), Springer Nature Singapore Pte Ltd.
10. **Kouřil, R.**, Nosek, L., Opatíková, M., Arshad, R., Semchonok, D.A., Chamrád, I., Lenobel, R., Boekema, E.J., Ilík, P. (2020) Unique organization of photosystem II supercomplexes and megacomplexes in Norway spruce. *Plant J* 104: 215-225.
11. Ilíková, I., Ilík, P., Opatíková, M., Arshad, R., Nosek, L., Karlický, V., Kučerová, Z., Roudnický, P., Pospíšil, P., Lazár, D., Bartoš, J., **Kouřil, R.** (2021) Towards spruce-type photosystem II: consequences of the loss of light-harvesting proteins LHCB3 and LHCB6 in Arabidopsis. *Plant Physiol* 187: 2691-2715.
12. Opatíková, M., Semchonok, D.A., Kopečný, D., Ilík, P., Pospíšil, P., Ilíková, I., Roudnický, P., Zeljkovic, S.C., Tarkowski, P., Kyrilis, F.L., Hamdi, F., Kastritis, P.L., **Kouřil, R.** (2023) Cryo-EM structure of a plant photosystem II supercomplex with light-harvesting protein Lhcb8 and α-tocopherol. *Nature Plants* 9: 1359-1369.

Attachment: Publications constituting the habilitation thesis

Publication 1

THE
EMBO
JOURNAL

Functional architecture of higher plant photosystem II supercomplexes

Stefano Caffarri[1,2,3,]*, **Roman Kouřil**[4],
Sami Kereïche[4], **Egbert J Boekema**[4]
and Roberta Croce[4,]*

[1]Université Aix Marseille, Faculté des Sciences Luminy, Laboratoire de Génétique et Biophysique des Plantes, Marseille, France, [2]CEA, DSV, iBEB, Marseille, France, [3]CNRS, UMR Biologie Végétale et Microbiologie Environnementales, Marseille, France and [4]Department of Biophysical Chemistry, Groningen Biomolecular Sciences and Biotechnology Institute, University of Groningen, Nijenborgh, Groningen, The Netherlands

Photosystem II (PSII) is a large multiprotein complex, which catalyses water splitting and plastoquinone reduction necessary to transform sunlight into chemical energy. Detailed functional and structural studies of the complex from higher plants have been hampered by the impossibility to purify it to homogeneity. In this work, homogeneous preparations ranging from a newly identified particle composed by a monomeric core and antenna proteins to the largest $C_2S_2M_2$ supercomplex were isolated. Characterization by biochemical methods and single particle electron microscopy allowed to relate for the first time the supramolecular organization to the protein content. A projection map of $C_2S_2M_2$ at 12 Å resolution was obtained, which allowed determining the location and the orientation of the antenna proteins. Comparison of the supercomplexes obtained from WT and Lhcb-deficient plants reveals the importance of the individual subunits for the supramolecular organization. The functional implications of these findings are discussed and allow redefining previous suggestions on PSII energy transfer, assembly, photoinhibition, state transition and non-photochemical quenching.

Introduction

Photosystem II (PSII) is a large pigment–protein supramolecular complex embedded in the thylakoid membrane of plants, algae and cyanobacteria, which splits water into oxygen, protons and electrons during the photosynthetic process (Barber, 2003). This complex thus provides the

*Corresponding authors. R Croce or S Caffarri, Department of Biophysical Chemistry, University of Groningen, Nijenborgh 4, Groningen, 9747 AG, The Netherlands. Tel.: + 31 503 634 214; Fax: + 31 503 634 800; E-mail: R.Croce@rug.nl or or Université Aix Marseille II, Faculté des Sciences de Luminy, LGBP, 163 Avenue de Luminy, 13288 Marseille, France. Tel.: + 33 4 91829562; Fax: + 33 4 91829566; E-mail: stefano.caffarri@univmed.fr

energy and the oxygen, which sustain all life on earth. PSII is present mainly in dimeric form, each monomer consisting of at least 27–28 subunits organized in two moieties: the core complex and the antenna system (Dekker and Boekema, 2005). The core is composed of several proteins: (i) D1 and D2 containing the reaction centre P680 and all the cofactors of the electron transport chain; (ii) CP47 and CP43, which coordinate chlorophyll (Chl) a molecules and act as an inner antenna and (iii) several low molecular subunits whose role has not yet been fully understood (Shi and Schroder, 2004). The structure of the PSII core of cyanobacteria shows 35 Chl a molecules, 2 pheophytins and 12 molecules of β-carotene (Loll *et al*, 2005; Guskov *et al*, 2009). In higher plants, on the lumenal side of the membrane, the products of the *psbO*, *psbP* and *psbQ* genes compose the oxygen evolving complex (OEC33, 23 and 17, respectively), which participates to the stabilization of the Mn cluster required for an efficient oxygen evolution. However, the exact role and locations of these subunits has not been fully clarified yet (Roose *et al*, 2007). The peripheral antenna system has a primary role in light harvesting, transfer of excitation energy to the reaction centre and photosynthesis regulation through photoprotective mechanisms, which dissipate the excess of energy absorbed by the system as heat under stress conditions (non-photochemical quenching) (Schmid, 2008). It is composed of six different complexes, belonging to the Lhcb (light-harvesting complex) multigenic family (Jansson, 1999), which coordinate Chl a, Chl b and xanthophylls, in different ratios. The major antenna complex, LHCII, is organized in heterotrimers composed of the products of the *Lhcb1-3* genes (Caffarri *et al*, 2004), while the three other subunits, CP29 (Lhcb4), CP24 (Lhcb6) and CP26 (Lhcb5) are present as monomers (Dainese and Bassi, 1991).

The supramolecular organization of PSII–LHCII has been studied by electron microscopy (EM) and single particle analysis on heterogeneous preparations obtained directly from mildly solubilized membranes or after a fast purification step, which allows enrichment of the high molecular weight complexes (Boekema *et al*, 1999a; Yakushevska *et al*, 2001). The location of the large core subunits was assigned by cross-linking experiments (Harrer *et al*, 1998) and confirmed by EM on solubilized membranes of plants lacking individual antenna complexes (Yakushevska *et al*, 2003). The larger supercomplex observed in *Arabidopsis thaliana* contains a dimeric core (C_2), two LHCII trimers (trimer S) strongly bound to the complex on the side of CP43 and CP26, and two more trimers, moderately bound (trimer M) in contact with CP29 and CP24. This complex is known as the $C_2S_2M_2$ supercomplex (Dekker and Boekema, 2005). A 3D reconstruction of a smaller supercomplex containing only one trimer per reaction centre and lacking CP24 (C_2S_2) was obtained by cryo-EM at 17 Å resolution (Nield *et al*, 2000c; Nield and Barber, 2006). Although the overall organization of the system is known, the low resolution at which this structure is available does not allow to determine the exact position of the individual complexes,

their respective orientations and the way in which they interact, thus hampering the possibility to understand the molecular details of the complex functioning of the system. This lack of information is mainly due to difficulties in obtaining a homogeneous and stable preparation of the supercomplex. This has not only restricted the possibility for detailed structural analysis but has also limited functional and spectroscopic studies to the level of non-homogeneous grana membrane preparations, which are enriched in PSII–LHCII (Broess *et al*, 2006; Veerman *et al*, 2007).

In this work, we present a protocol to obtain homogeneous preparations of the various types of PSII–LHCII supercomplexes. The possibility to relate the supercomplex organization to the protein content allows determining the role of the individual subunits in the overall organization. The functional implications of these findings for energy transfer, photoprotection, state transition and non-photochemical quenching are discussed.

Results

Isolation and characterization of the PSII supercomplexes

To obtain homogeneous preparations of PSII supercomplexes, we optimized the conditions for solubilization and fractionation of grana membranes. To this aim, the membranes were solubilized with a very low concentration of α-DM and the different complexes were separated on a dense sucrose gradient, which also contained a very low concentration of detergent to avoid destabilization of the complexes during ultracentrifugation. The detergent concentration was about 4–8 times less than what is normally used for a sucrose gradient, but still sufficient to maintain the complexes in solution. All the different steps of the procedure were performed in dim light and in the cold. This is a very important point as the temperature has a large effect on the stability of the complexes (Supplementary Figure S1). Using this procedure we were able to separate 12 distinct bands (B1–12) containing different PSII components and supercomplexes (Figure 1A). The upper bands (B1–5) have been well characterized in previous works (Caffarri *et al*, 2001) and correspond respectively to: (1) free pigments; (2) monomeric Lhcb proteins; (3) trimeric LHCII; (4) CP24/CP29/LHCII (M) trimer complex; (5) monomeric PSII core. The lower bands (B6–12), which from the apparent molecular weight should contain supercomplexes of increasing size, were further characterized by absorption spectroscopy, EM and SDS–PAGE. All fractions were stable in ice for at least 2 days as assessed by measuring the fluorescence emission (Supplementary Figure S1).

In Figure 1B, the absorption spectra of fractions 6–12 are shown. It is worth saying that the absorption spectra of the same bands from different preparations were identical, demonstrating the high reproducibility of the procedure. Chls *b*, bound to Lhc antenna proteins, show two main peaks around 470 and 650 nm, whereas Chls *a* are responsible for the absorption around 435 and 675 nm. The relative intensity of the absorption in the Chl *b* region increases from B7 to B12 suggesting that B7, almost lacking a Chl *b* contribution, corresponds to the dimeric PSII core (B5 being the monomeric core), whereas the fractions from B8 to B11 contain supercomplexes with increasing Lhc content (note that the spectrum of B12 is identical to that of B11). Unexpectedly B6,

which migrates between the monomeric and the dimeric PSII core, shows a strong Chl *b* absorption, indicating that it contains a complex enriched in Lhcb proteins.

To determine the structural organization of the supercomplexes, the fractions (B6–B12) were analysed by EM and single particle image analysis (Figure 1C): B6 contains almost exclusively a small supercomplex, never described before, consisting of monomeric PSII core, LHCII-S trimer and CP26; B7 contains the PSII dimeric core (C_2), as deduced from the absorption spectrum; B8, C_2S and very few C_2M supercomplexes (around 5%); B9, C_2S_2 and C_2SM particles; B10, mainly C_2S_2M; B11, the $C_2S_2M_2$ supercomplex, the biggest one described so far for *Arabidopsis*; B12 contains megacomplexes of $C_2S_2M_2$ (Boekema *et al*, 1999b; Yakushevska *et al*, 2001), which explains why this band has higher mobility than B11 in the gradient, but the same absorption spectrum (Figure 1A and B). Interestingly, the organization of the subunits in fraction B6 is identical to that in the dimeric complex (e.g. compare B6 with B8 in Figure 1C), which indicates that the monomerization does not influence the binding of CP26 and trimer S.

The exact protein composition of each band was determined by SDS–PAGE (Figure 2). The results are in line with the EM analysis, showing an increase of the ratio Lhcb/small-PSII-subunits and of CP24 content, which indicates increasing amounts of the M trimer (which requires CP24 for its binding; Kovacs *et al*, 2006), in bands from B8 to B11. In these fractions, the amount of CP29 and CP26 is identical, suggesting that these subunits are always bound in a 1:1 stoichiometry to the PSII core. B6 contains only core subunits, LHCII and CP26, lacking any trace of CP29. The analysis also reveals the distribution of the OEC proteins in the fractions: PsbO is present in all fractions containing PSII core but also in band 1, where it is not associated with the core. PsbP is detected in the fraction of monomeric PSII core (B5), in low amount in B6 and dimeric PSII core (B7) (where it is however not bound to the complexes, see discussion and Supplementary Figure S2) but is completely lacking in all PSII supercomplexes, in agreement with previous results (Hankamer *et al*, 1997). PsbQ is present in B6, absent in monomeric (B5) and dimeric PSII core (B7), but again present in increasing amounts (correlating with the Lhcb content) in supercomplexes from B8 to B11 (Figure 2).

The availability of two fractions containing either trimer M (B4) or trimer S (B6) allows determining the distribution of Lhcb1, Lhcb2 and Lhcb3 in the trimers. SDS–PAGE (Figure 2) and western blotting (Figure 3) show that Lhcb3 is present only in trimer M. Indeed the amount of Lhcb3 in B4 is very high, whereas this subunit is practically absent in B6 and B8 (note that this last band contains only very few C_2M particles). The opposite is true for Lhcb2, which is absent in B4 but present in B6 thus indicating that Lhcb2 is a specific component of trimer S. Lhcb1 is present in both trimers.

PsbS, the protein involved in the fast phase of non-photochemical quenching (Li *et al*, 2000), was present in fractions B5–B12, as confirmed by western blotting (Figure 3B). Considering that PsbS is a very hydrophobic protein (Dominici *et al*, 2002), the possibility of unspecific association or formation of aggregates with different sizes was investigated by loading equal volumes of all fractions including the intermediate fraction between B11 and B12 (B11/B12 band) on a gel. This fraction does not contain supercom-
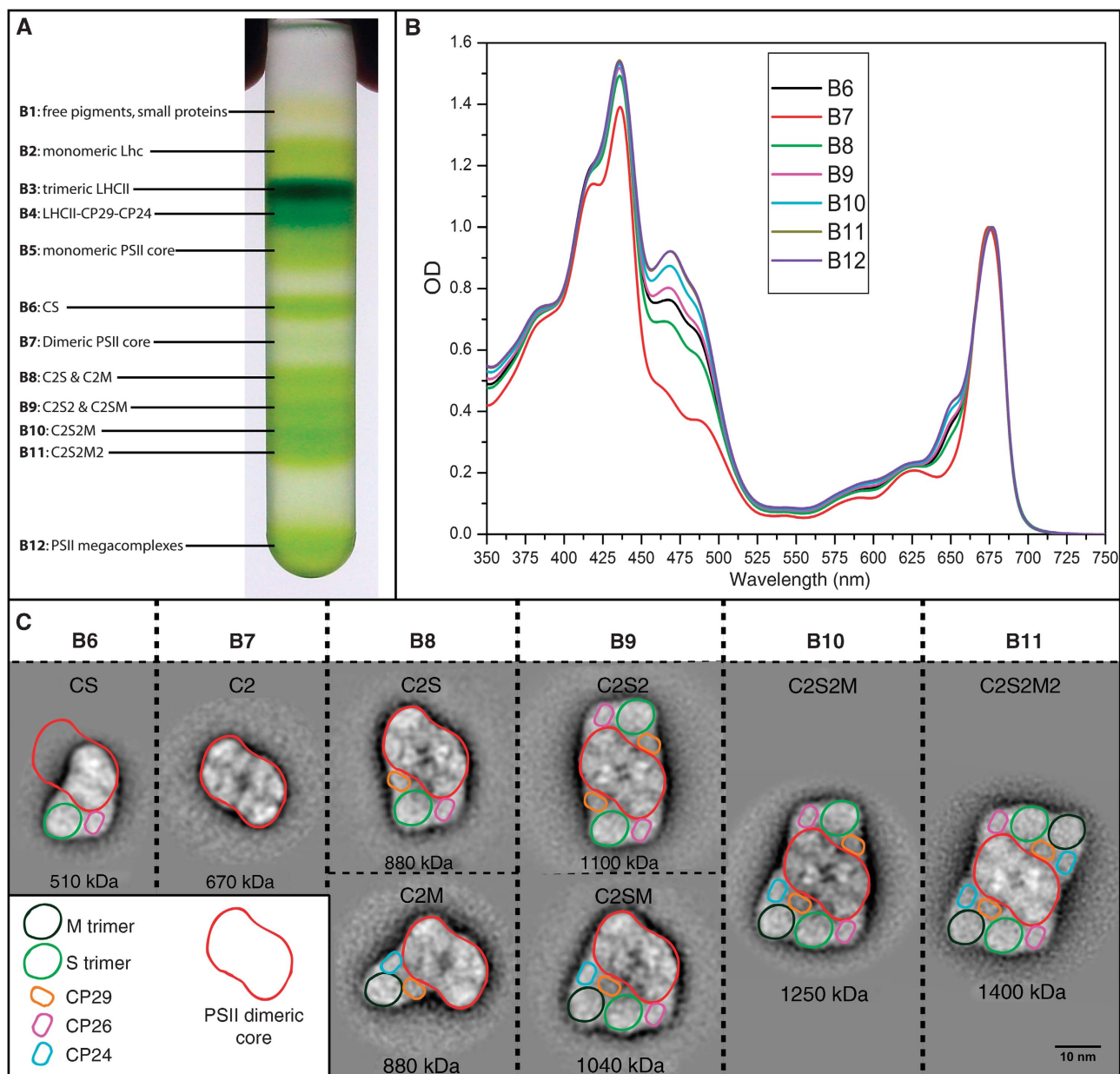
Figure 1 Isolation and characterization of the PSII supercomplexes. (**A**) Sucrose gradient of solubilized membranes, showing 12 green bands. The content of each band is indicated on the basis of earlier work (Caffarri *et al*, 2001) (B1–B5) and this work (B6–B12). (**B**) Absorption spectra of bands 6–12. The spectra are normalized to the maximum in the red region. B11 and B12 are almost superimposed. The Chls b content, which is proportional to the antenna content, is deducible from the intensity of the bands at 470 and 650 nm. (**C**) EM analysis of the supercomplexes. The projections obtained for bands 6–12 are shown. B6 contains a newly identified supercomplex formed by a monomeric core, one LHCII S trimer and the minor antenna CP26. Contours representing the different complexes are superimposed. Also note that the position of the M trimer in the absence of trimer S (C2M in B8) is different. C, core; S, LHCII trimer strongly bound; M, LHCII trimer moderately bound (see text). The molecular weight of each particle, calculated on the basis of the protein content as determined by EM and SDS–PAGE, is also reported.

plexes and therefore should not contain any PsbS if its binding to the supercomplexes is specific. The western blot revealed the presence of similar amounts of PsbS (Figure 3B; Supplementary Figure S2) in all lower fractions, including B11/B12, thus suggesting that this protein is not stably associated with the supercomplexes.

Determination of the supramolecular structure of $C_2S_2M_2$ supercomplex

To determine the supramolecular organization of the $C_2S_2M_2$ supercomplex, fraction B11 was subjected to extensive single

particle EM analysis. In total, a set of 40 000 negatively stained single particle projections was analysed. Repeated alignment steps and classification revealed homogeneous classes of the $C_2S_2M_2$ projections in top-view orientation and few classes with projections in a slightly tilted position. A homogeneous class of about 13 000 top-view projections was summed in the final 2D projection map (Figure 4A; Supplementary Figure S3). The projection map was obtained at 12 Å resolution and it contains ample details to assign the orientation of the individual Lhcb complexes (Figure 4B). The unambiguous assignment of the M and S trimers in the EM
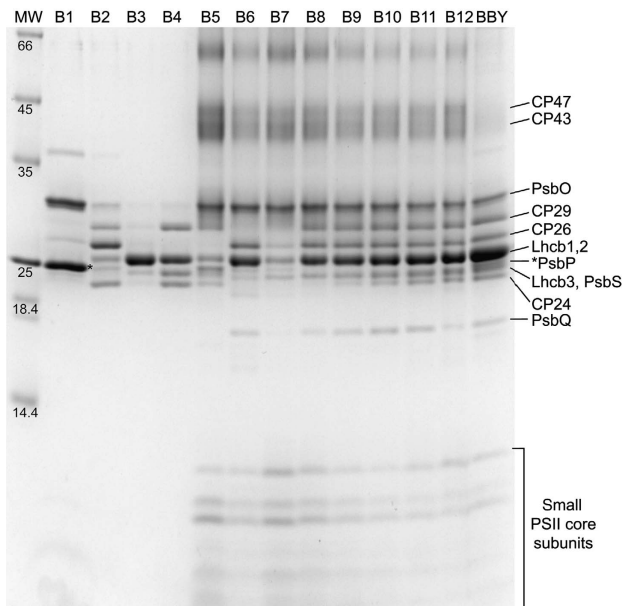
Figure 2 SDS–PAGE analysis of the sucrose gradient fractions. The protein composition of the 12 sucrose gradient fractions was analysed by loading similar amounts of total chlorophylls (3 µg) on the gel (see Materials and methods for details on volumes). The identity of each Coomassie band is indicated. D1 and D2 are not visible in this gel system because they maintain a partial folding during migration, which makes them appearing diffused. Note that PsbP is better visible in lanes B1 and B2 (*). Note the presence of CP26 in B6 together with Lhcb1,2 and the increase of the Lhcb/small-PSII-subunits ratio in the fractions from B8 to B12, according to the increased antenna size of the supercomplexes. PsbQ is absent in the fractions containing PSII core without antennas (B5 and B7).
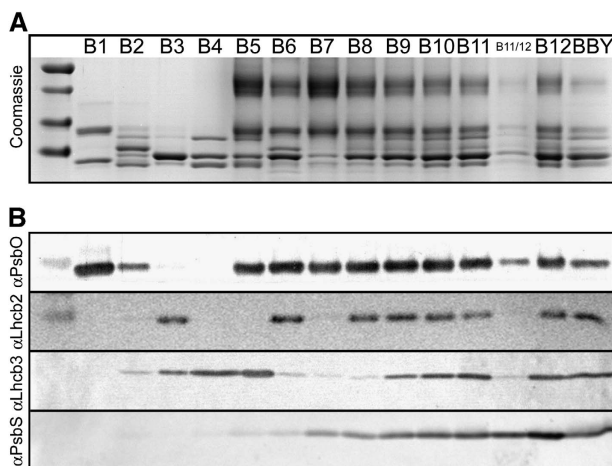
Figure 3 Western blotting analyses of sucrose gradient fractions. Proteins co-migrating in SDS–PAGE were detected by western blotting. (**A**) Coomassie stained gel of sucrose gradient fractions. The B4 used was cleaned of contaminating B3 fraction (LHCII trimers) with a second sucrose gradient. Band B5 was highly contaminated by B4 due to the very low amount of PSII core in our solubilization conditions. Similar amounts of Chls (0.5 µg) were loaded in each line, except for the B11/12 band (the clear gradient fraction between B11 and B12) where a similar volume as adjacent bands was loaded. (**B**) Western blot analyses using antibodies against PsbO, Lhcb2, Lhcb3 and PsbS. The absence of Lhcb2 in trimer M (B4) and of Lhcb3 in trimer S (B6 and B8) is clearly visible. PsbS is present in several fractions, including the fraction between B11 and B12 (B11/12) where a clear decrease in the PSII subunits is evident, but not for PsbS. This indicates that PsbS comigrates with the supercomplexes and it is not specifically bound to them.

projection was facilitated by the localization of corresponding densities in the calculated projection maps of the truncated X-ray high-resolution LHCII structure (Liu *et al*, 2004) (Figure 4C). A tripod-shaped stain-excluded area in the EM projection map of LHCII trimer (Figure 4B, pink lines) can also be recognized in the truncated model (Figure 4C). Further, pairs of high densities revealed in the EM projection map correspond well to the high-density spots of helix A and B, and to the strong density close to helix C (Figure 4B and C, green asterisks). The results indicate that M and S trimer are rotated by 18° with respect to each other.

Assignment of the minor antenna complexes (CP24, CP26 and CP29) was more difficult due to their less pronounced features in the EM projection map. The orientation of these complexes was determined under the assumption that the high densities of monomeric Lhcb in the EM projection map correspond to the pairs of densities observed in LHCII trimers (green asterisks) and a broad density near the end of helix A in the truncated projection of monomeric Lhcb (Figure 4B and C, pink asterisk). A different position of the monomeric Lhcb complexes, in particular a 180° rotation compared with the position in Figure 4, was considered in the modelling. It is noteworthy that neoxanthin protrudes sharply from one side from the monomeric Lhcb complexes (Figure 7, yellow) thus strongly constraining possible subunit orientations. Hence, at present the proposed model is by far the most likely arrangement of the antenna components, because it also brings them in positions close enough to allow fast energy transfer (see discussion). Although no standard criteria are available for fitting X-ray data into 2D EM maps, the resulting pseudo-atomic data can be considered to have a precision extending the resolution of the EM data at 12 Å, in the range of the size of an α helix or a chlorophyll molecule.

Isolation of supercomplexes from Lhcb- and PsbS-deficient mutants

To determine the role of the individual antennas in the architecture and in the stability of the PSII supercomplexes, we have used the solubilization procedure described before on grana membranes prepared from three knock-out (KO) lines lacking Lhcb3, CP24 or CP26. Comparison of the band patterns in the gradients of Lhc-deficient mutants and WT shows significant differences in the supercomplex compositions (Figure 5A). KoLhcb3 and koCP24 lines completely lack the largest supercomplexes (C_2S_2M and $C_2S_2M_2$, B10 and B11 in the WT) and the small complex LHCII(M)/CP24/CP29 (B4). Also, in the case of koCP26 no bands containing high molecular weight supercomplexes are visible and the amount of the fractions containing the smaller supercomplexes (B8 and B9) is extremely reduced. Furthermore, the amount of the PSII dimeric core band (B7) increases as well as that of the band containing LHCII trimers, indicating that supercomplexes lacking CP26 are more sensitive to detergent treatment than those of the WT. Interestingly, all mutants also lack band B6, the monomeric core/LHCII(S)/CP26 complex.

To determine the protein composition in both grana membranes and individual supercomplexes of the antenna-deficient lines, 1D and 2D SDS–PAGE analysis were performed (Figure 6). Unexpectedly, PsbQ was absent in the membranes of all three KO lines and Lhcb3 and CP24 mutants were additionally lacking PsbP (see Figure 6C). The absence of these subunits was also confirmed on stacked thylakoid
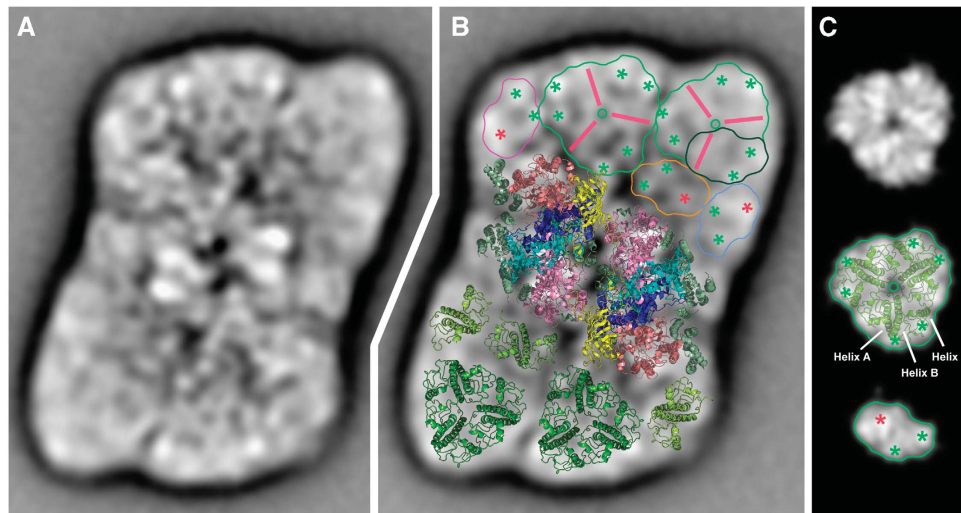
Figure 4 Projection map of the $C_2S_2M_2$ supercomplex. (**A**) Final projection map of the PSII $C_2S_2M_2$ supercomplex at 12 Å resolution. (**B**) Assignment of the subunits in the supercomplex by fitting the high-resolution structures of PSII core (Guskov *et al*, 2009) (subunits D1, D2, CP43, CP47 and extrinsic subunit PsbO are highlighted in blue, cyan, salmon, pink and yellow, respectively) and Lhcb (Liu *et al*, 2004) (trimeric LHCII and monomeric Lhcb in dark and light-green, respectively). Lhcb3 and the minor antennas, CP24, CP26 and CP29, are schematically depicted in dark green, light blue, magenta and orange contours, respectively. Green and pink asterisks indicate similar high densities of trimeric and monomeric LHCII, respectively. Tripod-shaped pink lines indicate a stain-excluded area of LHCII trimer. (**C**) Generated 2D projection maps of LHCII trimer and monomer from atomic model, truncated at 10 Å resolution. To allow comparison, corresponding densities of LHCII revealed in the EM projection map are indicated in the truncated 2D projection maps. Note that the fitting of the CP24 region with the LHCII monomeric structure leaves empty a large density next to helix C towards the outer part of the supercomplex. However, CP24 presents an extremely long helix C–helix A loop (28 amino acids more than LHCII) that would fit perfectly this region.
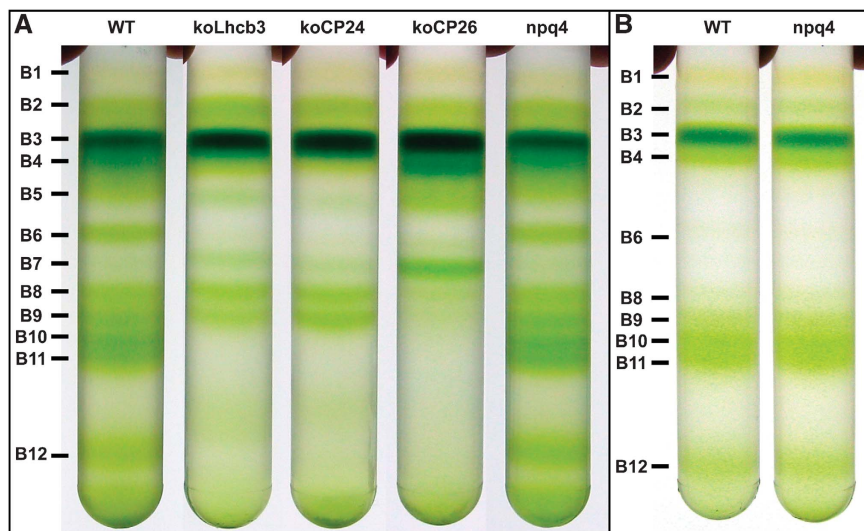
Figure 5 Sucrose gradient fractionation of solubilized grana membranes of WT, Lhcb-depleted lines and *npq4* mutant. (**A**) Supercomplexes were prepared from *Arabidopsis* lines lacking Lhcb3 (koLhcb3), CP24 (koCP24), CP26 (koCP26) and PsbS (*npq4*). Lhcb3 and CP24 mutants lack the small complex containing LHCII-CP24-CP29 (B4) and the high molecular weight supercomplexes corresponding to C_2S_2M (B10) and $C_2S_2M_2$ (B11). koCP26 is lacking almost completely the supercomplexes and shows an intense PSII dimeric core band (B7). All mutants also lack band 6 containing PSII monomeric core/LHCII S-trimer/CP26. The *npq4* mutant lacking the PsbS protein does not show any difference with respect to the WT. (**B**) Sucrose gradient of WT and *npq4* membranes solubilized at pH 5.5. Protonation of PsbS *in vitro* has no effect on the antenna binding to PSII core. Note also that the most abundant bands of supercomplexes correspond to C_2S_2M and $C_2S_2M_2$ complexes (B10 and B11), suggesting that most of the PSII *in vivo* in our grana preparation binds both trimer S and trimer M.

membranes indicating that this was not caused by the harsh grana preparation protocol (Supplementary Figure S4). However, western blotting analysis of the total protein content of the leaf shows the presence of these proteins, suggesting that they have been lost during the preparation of the thylakoid membrane (Supplementary Figure S4). PsbP was absent in the supercomplexes of koCP26 (B8 and B9)

(Figure 6B and D), indicating that this subunit is easily lost on purification as was observed for the WT. The content of CP24 in koLhcb3 was reduced, as was that of Lhcb3 in koCP24 suggesting that fractions B8 and B9 contain C_2S and C_2S_2 particles, respectively (in the WT, C_2M (B8) and C_2SM (B9) complexes were also found). In koCP26, the significant increase of CP24 and Lhcb3 in the faint B8 and
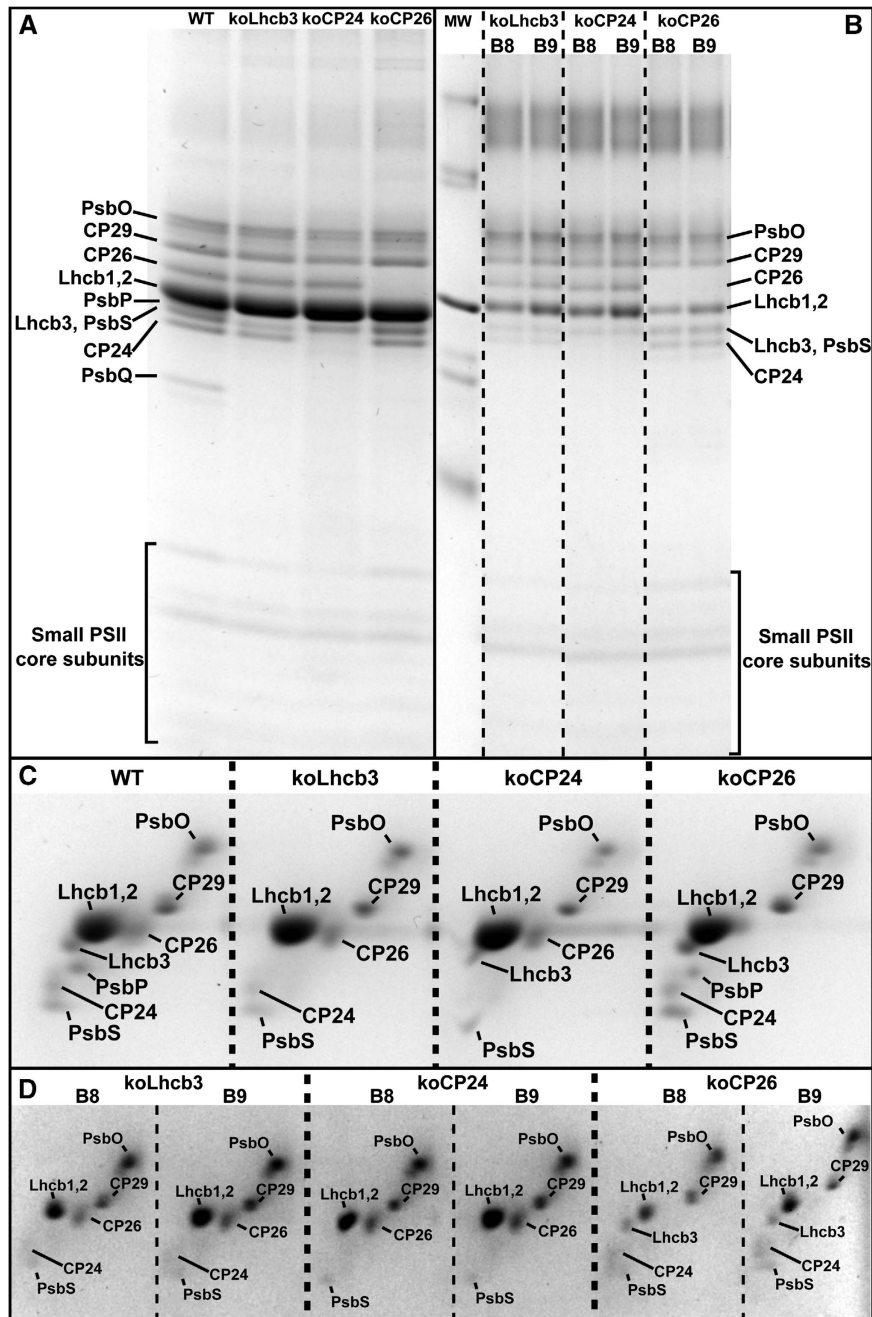
Figure 6 1D and 2D SDS–PAGE of grana membranes and supercomplexes of Lhcb-depleted lines. (**A**) Grana membranes of WT, koLhcb3, koCP24 and koCP26 mutants. Note that PsbQ is absent in the three mutants. (**B**) Supercomplexes (B8 and 9 of Figure 5) of the antenna mutants. (**C**) 2D SDS–PAGE separation of the PsbO-CP24 region of panel A, which allows a better investigation of the protein composition in the membrane of the mutants. Note the lack of PsbP in koLhcb3 and koCP24. (**D**) 2D SDS–PAGE separation of the PsbO-CP24 region of panel B allows highlighting the strong reduction of CP24 in the koLhcb3 supercomplexes, the lack of Lhcb3 in the koCP24 supercomplexes and the significant presence of Lhcb3 and CP24 proteins in the supercomplexes from koCP26.

B9 fractions, as compared with the same bands in the WT, indicates an enrichment of complexes containing LHCII M-trimer (i.e. C_2M) and a strong reduction of C_2S and C_2S_2 complexes.

To investigate the role of PsbS in the supercomplex organization, the *npq4* mutant lacking PsbS was analysed. We found that the absence of PsbS does not influence the supercomplex formation and stability, the gradient bands being identical to those of the WT (Figure 5). In addition, a high-resolution projection map of the $C_2S_2M_2$ supercomplex was obtained by single particle EM of the B11 fraction from

the *npq4* mutant. This projection is identical to that of the WT, thus excluding the possibility that PsbS is part of the supercomplex or strongly associated to it. This is in agreement with the SDS–PAGE analysis, which indicates that PsbS is not specifically associated with the purified supercomplexes in the WT (Figure 2), but it co-migrates with them (Figure 3).

Oxygen evolution

To test the photosynthetic activity of our preparations, oxygen evolution of the grana membranes and PSII supercom-
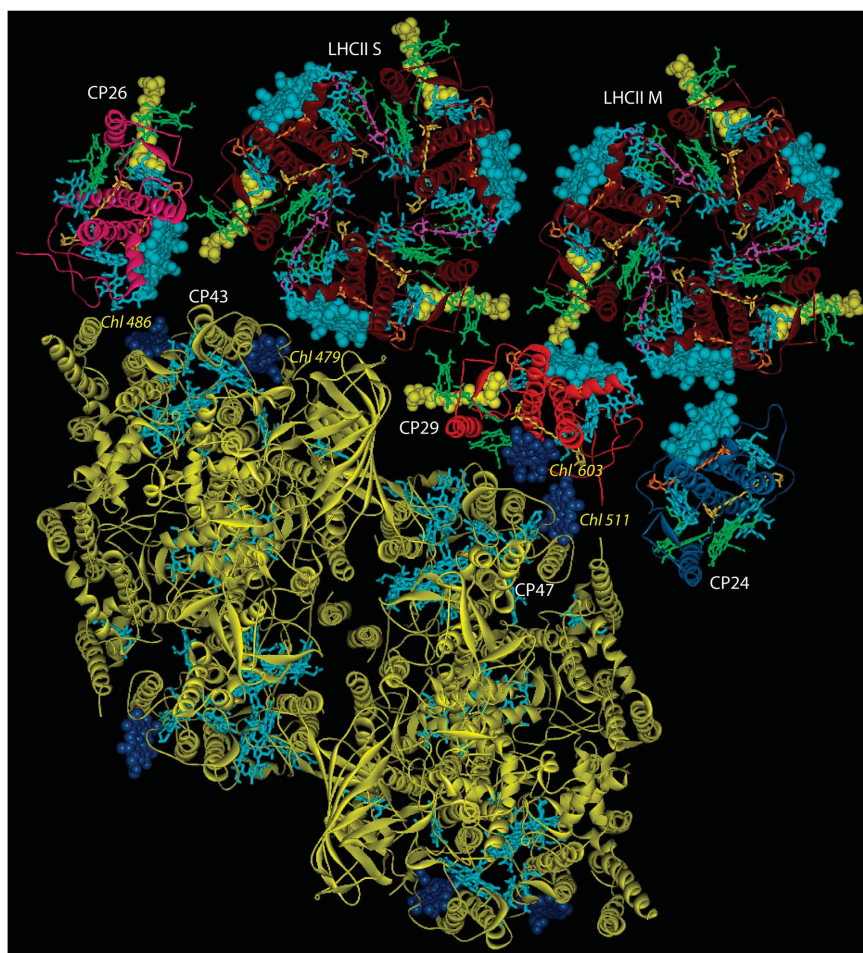
Figure 7 Model of the structure of photosystem II supercomplex $C_2S_2M_2$. The model has been assembled based on the projection map in Figure 4 using the crystal structures of the cyanobacterial PSII core (Guskov *et al*, 2009) (3BZ1 and 3BZ2) and LHCII trimer (Liu *et al*, 2004) (1RWT). For the monomeric antennas, the structure of a monomeric LHCII has been used. Proteins of the core, gold; LHCII, brown; CP24, blue; CP29, red; CP26, magenta; Chls *a*, cyan; Chls *b*, green; Neoxanthin, yellow (spheres); Lutein L1, orange; Lutein L2, dark-yellow. Chls 611 and 612 of all subunits are represented as cyan spheres. Chls 511 (in CP47), 479 and 486 (in CP43) of the core, which are the nearest-neighbour to the outer antenna are represented as blue spheres. Chls 603 of CP29 is also represented as blue spheres. For clarity the phytol chains of the Chls are omitted.

plexes of WT and Lhcb-deficient lines was measured (see Table I). Reduction in oxygen evolution was observed in the membranes of all three KO mutants, with values of 72% for koCP26, 50% for koLhcb3 and 36% for koCP24 as compared with the WT. The data also show that all supercomplexes, including the B6 fraction, evolve oxygen, which clearly indicates that all the preparations are active and can efficiently drive photosynthesis.

Discussion

During the past few years, a tremendous improvement in the knowledge of the organization of photosynthetic components was achieved, because the structures of most of the complexes of the thylakoid membrane could be obtained at atomic or near atomic level (Jordan *et al*, 2001; Stroebel *et al*, 2003; Liu *et al*, 2004; Loll *et al*, 2005; Yamashita *et al*, 2007; Guskov *et al*, 2009). At present, only the structural details of the PSII–LHCII supercomplexes remain partially obscure. This lack of information is primarily due to the impossibility of obtaining stable and homogeneous preparations of PSII–LHCII. In contrast to PSI, the interaction between the core and the outer antenna in PSII is extremely

weak and even mild solubilization leads to the disassembly of the supercomplexes (Caffarri *et al*, 2001). Moreover, the impossibility of obtaining stable and homogeneous preparations of PSII–LHCII has also prevented the study of the light harvesting and energy transfer processes in the system.

In this work, we were able to purify for the first time six homogeneous fractions of PSII–LHCII supercomplexes with increasing antenna sizes, ranging from PSII core to the large $C_2S_2M_2$ supercomplex, which are suitable for biochemical, structural and spectroscopic analysis. All fractions were analysed in detail, combining biochemical methods with single particle EM analysis. This allows, to our knowledge for the first time, to directly relate the presence/absence of individual subunits to the supramolecular organization of the complex and thus to get answers about their roles in the assembly and their positions in the supercomplexes.

12 Å resolution structure of PSII supercomplex ($C_2S_2M_2$)—implication for the energy transfer

The structural organization and the orientation of the different light-harvesting proteins in the PSII $C_2S_2M_2$ supercomplex were determined from a 12 Å resolution projection map obtained by single particle EM and image analysis

Table I Oxygen evolution measurements on sucrose gradient fractions and grana membranes of WT and antenna KO mutants

	A μmol O$_2$ mg(Chl)$^{-1}$ hr^{-1}
(a)	
B6	64.9 ± 5.9
B7	61.6 ± 6.3
B8	72.3 ± 1.3
B9	70.5 ± 3.8
B10	72.9 ± 2.9
B11	72.6 ± 3.4
(b)	
WT	53.1 ± 2.0
koLhcb3	27.0 ± 1.3
koCP24	19.1 ± 1.8
koCP26	38.3 ± 1.3

(a) O$_2$ evolution measurements on gradient fractions from B6 to B11 show similar activity, including the monomeric CS complex (B6).
(b) Measurements on grana membranes from WT and antenna KO plants show a clear decrease in O$_2$ evolution activity in the three mutants, especially for koLhcb3 and koCP24 lacking both the PsbP and PsbQ subunits.
Difference between koLhcb3 and koCP24 could be due to the different membrane organization which influences the diffusion of the plastoquinone (de Bianchi *et al*, 2008).

(Figure 4). This allowed the reconstruction of a 3D pseudo-atomic model of the full PSII–LHCII supercomplex using the crystal structures of the LHCII trimer (Liu *et al*, 2004) and the recent refined structure of the cyanobacteria core (Guskov *et al*, 2009), which presents the full assignment of the small PSII subunits and an improved localization of the cofactors (Figure 7). For the minor antenna complexes, the structure of a monomeric unit of LHCII was used after modification according to the available biochemical data (e.g. pigment content) (Sandona *et al*, 1998; Caffarri *et al*, 2007). This allows the visualization of possible energy transfer pathways in the supercomplex. The model shows that trimer S is in direct contact with Chl 479 of the CP43 subunit to which it can transfer energy through Chls 611/612. These Chls represent the low-energy state in all Lhcb antenna complexes (Mozzo *et al*, 2008) and thus are the most populated ones at thermal equilibrium. CP26 can also transfer energy directly to the core, again through Chls 611/612, which are facing CP43 (Chl 486) in the structure. The nearest-neighbour Chls between CP26 and LHCII S are 604 and 605, which are a Chl *a* at high energy and a Chl *b* (Novoderezhkin *et al*, 2005), respectively, suggesting that there is small exchange of energy between the two subunits. The LHCII M trimer is in contact with CP24 and CP29, but not with the core. In the interaction region, all three complexes expose Chls 611/612, thus forming a pool of Chls *a* at low energy. The present model (Figure 7) suggests that CP24 cannot transfer excitation energy directly to the core, because there are no Chls of CP47 located near CP24. This indicates that the transfer from trimer M and CP24 to the core occurs through CP29. This makes CP29 a very suitable site for the regulation of the excitation energy flow and thus for playing a primary role in the non-photochemical-quenching process. In CP29, Chl 603 (a Chl *a* absorbing around 676 nm (Bassi *et al*, 1999), thus only slightly higher in energy than Chls 611/612) faces CP47 (Chl 511) to which it can transfer excitation energy. However, at the moment we cannot exclude that one of the small higher plant-specific subunits (PsbR or PsbW), which are absent in

the cyanobacteria structure, is accommodated near CP24 and binds Chls, thus allowing CP24 to directly transfer excitation energy to the core. Indeed, the EM projection indicates that there is room in this region for a small extra subunit.

The overall architecture of the antenna system indicates that excitation energy is transferred from the peripheral antenna to the core through specific pathways, which involve only Chl *a* molecules and in particular the low-energy forms. This has the effect of speeding up the energy transfer process, strongly decreasing the migration time and explaining the fast transfer observed in integer membranes (Broess *et al*, 2008). Interestingly, CP29, which is the link between the outer antenna and the core, has the lowest Chl *b* content of all Lhcb's (Sandona *et al*, 1998) and these Chls are located in a region rich in Chl *b* and neoxanthin, between trimers S, M and CP29, thus off the main highway from the antenna to the core.

A new complex shows that monomeric core can bind Lhcb antenna—implication for photoinhibition

In addition to the supercomplexes, a novel complex, composed of a monomeric core, one LHCII S-trimer and CP26 (CS/CP26) was isolated (band B6, Figure 1). No traces of CP29 were detected in this band. This finding is surprising, since so far the association of Lhcb antenna to the core was believed to be possible only for the dimeric conformation (Dekker and Boekema, 2005) and in the presence of CP29 as a docking protein (Yakushevska *et al*, 2003). However, our results show that a complex consisting of a monomeric core, CP26 and one LHCII trimer is stable enough to be purified in high yield. It is active in O$_2$ evolution, strongly suggesting that it could also be present in the membranes. One implication of this finding concerns the D1 protein degradation/repair cycle, a process that replaces the D1 subunit, which has a half-life of about 30 min (Godde *et al*, 1991). It is generally believed that the entire antenna system disassembles before monomerization of the PSII core complex (Adir *et al*, 2003). The newly found particle suggests that this is in principle not necessary: trimer S and CP26 can remain associated to the core, with the advantage of limiting the potentially dangerous presence of isolated antenna complexes in the grana membrane during the repairing cycle. Indeed, it is very likely that only one of the two D1 proteins present in the dimeric PSII is damaged, and needs to be replaced, at a time. The possibility to disassemble only the damaged moiety of the photosystem, leaving the 'healthy' core still in contact with its antenna, which has also a photoprotective function, helps to protect it from photodamage.

Assembly of the PSII–LHCII supercomplex: role of the Lhcb proteins

The analysis of Lhcb-depleted lines allows determining the hierarchy of the binding of the individual subunits within the PSII–LHCII supercomplex. The reduction of Lhcb3 in koCP24 and of CP24 in koLhcb3, suggests a mutual stabilization of these complexes. Furthermore, a complete absence in both mutants of complexes and supercomplexes containing trimer M indicates that CP24 and Lhcb3 have an important function in mediating the association of trimer M with the PSII complex. Indeed, the EM analysis of koCP24 membranes has shown that the supercomplexes of this mutant do not contain trimer M (Kovacs *et al*, 2006; de Bianchi *et al*, 2008). C$_2$S$_2$M$_2$ supercomplexes could be observed (Kereiche *et al*,

2007) in koLhcb3 membranes, but it was shown that the general packing of the trimers differed slightly from that of the WT. Our results indicate that the pseudo-M trimer (trimer M without Lhcb3) observed in the membrane of koLhcb3 (Kereiche *et al*, 2007) is only weakly interacting with the supercomplex as it can easily be lost on mild solubilization. It can be concluded that CP24 and Lhcb3 specifically mediate the binding of the M trimer to the supercomplex, suggesting that Lhcb3 is the monomeric unit facing CP24. This is also supported by sequence comparison of Lhcb3 with Lhcb1 and Lhcb2 (Caffarri *et al*, 2004), which reveals major differences at the end of the B helix, with the insertion of a Trp in Lhcb3, and at the beginning of the loop between helixes B and C. This is exactly the domain of the LHCII monomeric unit facing CP24, as can be seen in the model (Figure 4).

CP24 and Lhcb3 are present only in higher plants (Alboresi *et al*, 2008) where they apparently evolved to increase the antenna size of PSII. Indeed in green algae only C_2S_2 complexes have been observed (Nield *et al*, 2000b; Iwai *et al*, 2008). It can also be concluded that trimer M has an influence on the assembly of trimer S that, in the absence of M or in the presence of the pseudo-M, is less strongly associated to the core, as suggested by the absence of the CS/CP26 complex in the gradients of koCP24 and koLhcb3. On the other hand, trimer M in C_2M is displaced compared with its position in the particles containing also trimer S (Figure 1), indicating that trimer S is influencing the location of trimer M.

In general, the data indicate that the stable connection of an antenna to the supercomplex requires interactions with two different partners. According to the model (Figure 4), association of trimer S to the core complex through CP43 is stabilized by interactions with CP26 and CP29. Although it has been shown that the S trimer is still connected to the supercomplex in the absence of CP26 (Yakushevska *et al*, 2003), our results indicate that its binding is far less stable (Figures 5 and 6). Moreover, the possibility to purify CS/CP26 complexes in the WT shows that the effect of CP26 on the stabilization of the S trimer is at least as high as that of CP29. Previous analysis of plants lacking CP29 showed that no PSII–LHCII supercomplexes could be found even on very mild solubilization (Yakushevska *et al*, 2003). Taken together, these data indicate a clear role of CP29 in the stability of the PSII–LHCII dimer. CP29, bound to one monomeric core, binds the S-trimer of the other monomeric core implicating a general stabilization of the supercomplex, while CP29 *per se* is not required for stable binding of trimer S.

Finally, it could be observed that on solubilization at low pH (Figure 5B) large part of PSII is present in the gradient as C_2S_2M or $C_2S_2M_2$ supercomplexes, while the amount of C_2S_2 is very low. As some M trimers clearly detached during the purification (presence of B4), it can be suggested that in the grana membranes of our plants most of the PSII is present as $C_2S_2M_2$ and not as C_2S_2. However, the detection in the gradient of an intense band of trimeric LHCII (B3) indicates the presence of additional LHCII complexes in the membranes. That fact that the crystalline arrays in *Arabidopsis* have a size compatible with $C_2S_2M_2$ complexes (Yakushevska *et al*, 2001) and that we were not able by very mild solubilization to purify complexes larger than those, supports the idea that LHCII-enriched regions exist in the grana membranes, as suggested earlier (Boekema *et al*, 2000).

State transitions: which trimer?

In agreement with earlier data (Dekker and Boekema, 2005), our results indicate that trimer M can easily be dissociated from the supercomplex. This makes it a good candidate for state transitions, during which some LHCII trimers migrate from grana to stroma lamellae where they associate with PSI (Allen, 1992; Kouril *et al*, 2005). However, it has been shown that Lhcb3 is not present in the stroma lamelle (Bassi *et al*, 1988; Jansson *et al*, 1997). Considering that Lhcb3 is a key component of trimer M and that, as shown here, this trimer has a structural role for the assembly of PSII together with CP24, it can be concluded that it is not responsible for state transitions. In agreement with earlier data, our results show that the association of trimer S with the PSII core is very strong and it is quite doubtful that it can easily detach from it. Moreover, biochemical and EM analysis of the membranes revealed the presence of at least one additional LHCII trimer for PSII monomeric core, probably located in regions enriched in LHCII trimers or loosely bound to the PSII (Boekema *et al*, 2000; Dekker and Boekema, 2005). We suggest that these trimers, instead of M or S associated with the supercomplexes, are involved in state transitions.

Non-photochemical quenching: PsbS is not stably associated to the supercomplexes

PsbS is key player in the process of non-photochemical quenching (Li *et al*, 2000), and it has been proposed to act in synergy with other proteins. Its localization would thus be important for understanding the quenching mechanism. Although several studies have addressed this point (Nield *et al*, 2000a; Thidholm *et al*, 2002; Teardo *et al*, 2007; Fey *et al*, 2008), the high propensity of this protein to form aggregates and to precipitate or to stick to other complexes (Dominici *et al*, 2002) has strongly complicated the interpretation of the results. Recently, it has been suggested that PsbS regulates the interactions between LHCII and PSII in the membranes (Kiss *et al*, 2008; Betterle *et al*, 2009). Our results show that the solubilization has an identical effect on WT and *npq4* mutant membranes (Figure 5A), also at low pH (Figure 5B) when PsbS is protonated and should facilitate the detaching of LHCII from the core *in vivo* (Kiss *et al*, 2008; Betterle *et al*, 2009). Our results thus suggest that the protonation of the two lumenal glutamate residues (Li *et al*, 2004) is not sufficient to activate PsbS and regulate the interactions LHCII-core. Other factors such as a particular ion or the presence of a ΔpH (and not just a low pH as in the *in vitro* experiment) might be necessary for the activation of PsbS.

In addition, the results clearly show that PsbS is not located in or stably associated with the supercomplexes, indicating that either it has a transient binding to them or it is located in the LHCII-enriched membrane regions as suggested earlier (Dekker and Boekema, 2005). However, we cannot exclude that PsbS is located in between two adjacent photosystems and that its binding is not strong enough to survive the purification.

Oxygen evolution: the OEC subunits organization depends on the antenna system

PsbO was present in all fractions containing PSII core indicating a strong binding to the monomeric core, as observed earlier (Hankamer *et al*, 1997; Nield *et al*, 2000c). PsbQ was present only in Lhcb-containing supercomplexes, in amounts

that are roughly proportional to the antenna size. In all these fractions, PsbP was absent, which indicates, in contrast to previous data (Berthold *et al*, 1981), that the binding of PsbQ does not require PsbP. Instead, it requires the peripheral antenna system, or at least the domain composed of CP26/ LHCII(S). This is confirmed by the absence of PsbQ in the membranes of all three Lhcb mutants, indicating that it can be stably associated with the supercomplex only when the outer antenna is perfectly assembled. PsbP was found in the membrane of koCP26, while it was absent in koCP24 and koLhcb3, indicating that the domain formed by CP29/CP24/ trimer M is needed for the assembly of this subunit. These results suggest that the localization of the OEC subunits in the 3D reconstruction of PSII–LHCII (Nield and Barber, 2006) needs to be revised. In addition, the oxygen evolution measurements on isolated membranes, where these subunits are not present, show lower values for koLhcb3 and koCP24 and partially also for koCP26 as compared with the WT, thus confirming that PsbP and PsbQ have an important function in the PSII activity.

Conclusions

In this work, homogeneous and stable PSII supercomplexes with different antenna sizes were isolated. A full gallery of complexes, from the core to the largest $C_2S_2M_2$, was characterized by EM and biochemical methods, which allows relating for the first time their protein content to the supramolecular organization. A new complex containing a monomeric core, a trimeric LHCII(S) and CP26 was isolated, showing that the antenna proteins can stably bind to the monomeric core, in contrast to the current opinion. A projection map at 12 Å resolution of the $C_2S_2M_2$ supercomplex reveals the positions and the orientations of the antenna complexes and allows to suggest the main pathways of excitation energy transfer from the antenna to the core. Comparison of the supercomplexes obtained from WT and Lhcb-deficient plants allowed determining the hierarchy of the assembly and the role of the individual subunits in the supramolecolar organization. The binding of the M trimer depends on interactions between CP24 and Lhcb3, which are proposed to face each other in the supercomplex. CP26 has a strong effect on the stable binding of trimer S, whereas CP29 is mainly involved in the stabilization of the PSII dimer. PsbS has not been found associated to the supercomplexes and its presence does not influence the interactions between core and outer antenna leading to the conclusion that it is located either peripherally or in the LHCII-enriched domains. The data also indicate that the stable binding of PsbQ to the supercomplex requires trimer S, but not PsbP, in contrast to the current view.

Moreover, we show that stable supercomplexes can be obtained, which can be further used for structural and functional analysis, opening the way to a full comprehension of the largest photosynthetic complex.

Materials and methods

PSII supercomplexes preparation

PSII-enriched membranes (grana membranes) were prepared from WT Col0 plants and the following mutants (Columbia ecotype): *npq4.1* (Li *et al*, 2000), koLhcb3 (SALK_051600), koCP26 (T-DNA insertion in the Lhcb5 gene, SALK_014869), koCP24 (T-DNA insertion in the Lhcb6 gene SALK_077953). Results on koCP24

were confirmed (not shown) also on an independent mutant in Landsberg erecta ecotype (Arabidopsis Gene Trap line GT6248). Plants were grown under $100 \, \mu mol \, m^{-2} \, s^{-1}$ of light (8 h/day) at 21°C. Membranes were prepared according to Berthold *et al* (1981) with few modifications. In particular, Arabidopsis leaves were shortly grinded in a solution (B1) containing 20 mM Tricine KOH pH 7.8, 0.4 M NaCl, 2 mM $MgCl_2$ and the protease inhibitors 0.2 mM benzamidine, 1 mM €-aminocaproic acid. Solution was centrifuged 10 min at $1400 \, g$ and pellet resuspended in a solution (B2) containing 20 mM Tricine KOH pH 7.8, 0.15 M NaCl, 5 mM $MgCl_2$ and protease inhibitors as before. This solution was centrifuged 10 min at $4000 \, g$, pellet resuspend in 20 mM Hepes 7.5, 15 mM NaCl, 5 mM $MgCl_2$ (solution B3) and centrifuged again 10 min at $6000 \, g$. Pellet was finally resuspend in a small volume of B3. Chlorophyll concentration was adjusted to 2.5 mg/ml and then PSII membranes were prepared by solubilizing stacked thylakoids at 2.1 mg/ml final concentration with 3/16 volumes of 20% Triton X100 (w/v), 15 mM NaCl, 5 mM $MgCl_2$ for 20 min on ice and soft agitation. To remove non-solubilized material, a 5 min-centrifugation at $3500 \, g$ was done. Surnatant was then centrifuged for 30 min at $40\,000 \, g$, pellet washed once with solution B3 to remove excess detergent and then centrifuged as before. Finally, membranes were resuspended in a small volume of 20 mM Hepes 7.5, 0.4 M sorbitol, 15 mM NaCl, 5 mM $MgCl_2$. BBY membranes can be frozen in liquid nitrogen and stored at −80°C. The entire preparation was done in cold condition.

For the PSII supercomplex preparations, 150 μg of membranes (in Chls) were washed once with 5 mM EDTA, 10 mM Hepes pH 7.5, then with 10 mM Hepes pH 7.5 and finally solubilized at 0.5 mg/ml by adding an equal volume of 0.6% α-DM in 10 mM Hepes 7.5 and vortexing for a few seconds. The solubilized samples were centrifuged at $12\,000 \, g$ for 10 min to eliminate unsolubilized material and then fractionated by ultracentrifugation on a sucrose or maltose gradient in a SW41 rotor, for 14–16 h at 4°C at 41 000 rpm. Gradients were formed directly in the tube by freezing at −80°C and thawing at 4°C a 0.65 M sugar solution containing 0.008% α-DM and 10 mM Hepes pH 7.5. For low pH preparations (Figure 5B), 10 mM MES pH 5.5 (instead of Hepes), 100 μg of membranes and a gradient at 0.01% α-DM were used. Maltose was used for EM experiments for better particle resolution in negative staining of EM samples, thus avoiding a dialysis step to remove the excess of sugar. Band separation and absorption spectra were identical using maltose or sucrose. Keeping the samples at 4°C during the entire preparation (i.e. solubilization in cold conditions, gradient loading in the cold room) was essential to improve significantly the yield of high molecular weight supercomplexes (see also Supplementary Figure S1).

SDS–PAGE

1D electrophoresis was performed using the Tris-Tricine system (Schagger, 2006) at 14.5% acrylamide concentration. Second dimension was realized as in Laemmli (1970) using a 14% acrylamide concentration. Different volumes of each band were loaded on the gel in Figure 2. The values normalized to 1 for band B3 (corresponding to 13 μl) are: B1, 31; B2, 5; B3, 1; B4, 2; B5, 23; B6, 11; B7, 16; B8, 11; B9, 13; B10, 19; B11, 31; B12, 31.

Spectroscopy

Absorption spectra were recorded using a Cary4000 (Varian Inc.). When dilution was necessary, the same solution as for the gradients was used.

Electron microscopy

Samples were negatively stained with 2% uranyl acetate on glow discharged carbon-coated copper grids. EM was performed on a Philips CM120 electron microscope equipped with a LaB_6 filament operating at 120 kV. Images were recorded with a Gatan 4000 SP 4 K slow-scan CCD camera at either $80\,000 \times$ (results shown in Figure 1) or $130\,000 \times$ (results shown in Figure 4) magnification at a pixel size (after binning the images) of 3.75 Å and 2.3 Å, respectively, at the specimen level with GRACE software for semi-automated specimen selection and data acquisition (Oostergetel *et al*, 1998). Single particle analysis was performed using GRIP software including multireference and non-reference alignments, multivariate statistical analysis, and classification, as in Boekema *et al* (1999a). Resolution was measured using Fourier-ring correlation and the 3σ criterion (Vanheel, 1987). X-ray structures of the PSII core (Loll *et al*, 2005) and LHCII complex (Liu *et al*, 2004) (the

PDB accession numbers 2AXT and 1RWT, respectively) were displayed using Pymol software *DeLano Scientific*, San Carlos, CA, USA). Truncated version and 2D projection map of LHCII at 10 Å resolution was generated using routines from the EMAN package (Ludtke *et al*, 1999). For CP24 (Figures 4B and 7), the LHCII monomeric structure depleted in the last 20 AA at the C-terminal was used, according to the sequence difference between these two antennas.

Oxygen evolution

O_2 production was measured in a Clark-type oxygen electrode system on BBY membranes concentrated 50 μg/ml (in Chls) in 0.4 M sorbitol, 15 mM NaCl, 5 mM $MgCl_2$, 10 mM Hepes KOH pH 7.5 at room temperature using $180\,\mu mol\,m^{-2}\,s^{-1}$ white light. O_2 production in supercomplexes was measured on the sucrose fractions diluted at 5 μg/ml (in Chls) at 12°C. Ferricyanide 0.5 mM and DCBQ 0.5 mM were added as electron acceptors. Addition of 5 mM $CaCl_2$ did not change the O_2 evolution both in membranes and supercomplexes.

Conflict of interest

The authors declare that they have no conflict of interest.

References

Adir N, Zer H, Shochat S, Ohad I (2003) Photoinhibition—a historical perspective. *Photosynth Res* **76:** 343–370

Alboresi A, Caffarri S, Nogue F, Bassi R, Morosinotto T (2008) In silico and biochemical analysis of Physcomitrella patens photosynthetic antenna: identification of subunits which evolved upon land adaptation. *PLoS ONE* **3:** e2033.

Allen JF (1992) Protein phosphorylation in regulation of photosynthesis. *Biochim Biophys Acta* **1098:** 275–335

Barber J (2003) Photosystem II: the engine of life. *Q Rev Biophys* **36:** 71–89

Bassi R, Croce R, Cugini D, Sandona D (1999) Mutational analysis of a higher plant antenna protein provides identification of chromophores bound into multiple sites. *Proc Natl Acad Sci USA* **96:** 10056–10061

Bassi R, Rigoni F, Barbato R, Giacometti GM (1988) Light-harvesting chlorophyll a/b proteins (LHCII) populations in phosphorylated membranes. *Biochim Biophys Acta* **936:** 29–38

Berthold DA, Babcock GT, Yocum CF (1981) A highly resolved, oxygen-evolving photosystem II preparation from spinach thylakoid membranes. EPR and electron-transport properties. *FEBS Lett* **134:** 231–234

Betterle N, Ballottari M, Zorzan S, de Bianchi S, Cazzaniga S, Dall'osto L, Morosinotto T, Bassi R (2009) Light induced dissociation of an antenna hetero-oligomer is needed for non-photochemical quenching induction. *J Biol Chem* **284:** 15255–15266

Boekema EJ, van Breemen JF, van Roon H, Dekker JP (2000) Arrangement of photosystem II supercomplexes in crystalline macrodomains within the thylakoid membrane of green plant chloroplasts. *J Mol Biol* **301:** 1123–1133

Boekema EJ, van Roon H, Calkoen F, Bassi R, Dekker JP (1999a) Multiple types of association of photosystem II and its light-harvesting antenna in partially solubilized photosystem II membranes. *Biochemistry* **38:** 2233–2239

Boekema EJ, van Roon H, van Breemen JF, Dekker JP (1999b) Supramolecular organization of photosystem II and its light-harvesting antenna in partially solubilized photosystem II membranes. *Eur J Biochem* **266:** 444–452

Broess K, Trinkunas G, van der Weij-de Wit CD, Dekker JP, van Hoek A, van Amerongen H (2006) Excitation energy transfer and charge separation in photosystem II membranes revisited. *Biophys J* **91:** 3776–3786

Broess K, Trinkunas G, van Hoek A, Croce R, van Amerongen H (2008) Determination of the excitation migration time in Photosystem II—consequences for the membrane organization and charge separation parameters. *Biochim Biophys Acta-Bioenerg* **1777:** 404–409

Caffarri S, Croce R, Breton J, Bassi R (2001) The major antenna complex of photosystem II has a xanthophyll binding site not involved in light harvesting. *J Biol Chem* **276:** 35924–35933

Caffarri S, Croce R, Cattivelli L, Bassi R (2004) A look within LHCII: differential analysis of the Lhcb1-3 complexes building the major trimeric antenna complex of higher-plant photosynthesis. *Biochemistry* **43:** 9467–9476

Caffarri S, Passarini F, Bassi R, Croce R (2007) A specific binding site for neoxanthin in the monomeric antenna proteins CP26 and CP29 of Photosystem II. *FEBS Lett* **581:** 4704–4710

Dainese P, Bassi R (1991) Subunit stoichiometry of the chloroplast photosystem-II antenna system and aggregation state of the component chlorophyll-a/b binding proteins. *J Biol Chem* **266:** 8136–8142

de Bianchi S, Dall'Osto L, Tognon G, Morosinotto T, Bassi R (2008) Minor antenna proteins CP24 and CP26 affect the interactions between photosystem II subunits and the electron transport rate in grana membranes of Arabidopsis. *Plant Cell* **20:** 1012–1028

Dekker JP, Boekema EJ (2005) Supramolecular organization of thylakoid membrane proteins in green plants. *Biochim Biophys Acta* **1706:** 12–39

Dominici P, Caffarri S, Armenante F, Ceoldo S, Crimi M, Bassi R (2002) Biochemical properties of the PsbS subunit of photosystem II either purified from chloroplast or recombinant. *J Biol Chem* **277:** 22750–22758

Fey H, Piano D, Horn R, Fischer D, Schmidt M, Ruf S, Schröder WP, Bock R, Büchel C (2008) Isolation of highly active photosystem II core complexes with a His-tagged Cyt b(559) subunit from transplastomic tobacco plants. *Biochim Biophys Acta-Bioenerg* **1777:** 1501–1509

Godde D, Schmitz H, Weidner M (1991) Turnover of the D-1 reaction center polypeptide from Photosystem-Ii in intact spruce needles and spinach leaves. *Z Naturforsch C* **46:** 245–251

Guskov A, Kern J, Gabdulkhakov A, Broser M, Zouni A, Saenger W (2009) Cyanobacterial photosystem II at 2.9-A resolution and the role of quinones, lipids, channels and chloride. *Nat Struct Mol Biol* **16:** 334–342

Hankamer B, Nield J, Zheleva D, Boekema E, Jansson S, Barber J (1997) Isolation and biochemical characterisation of monomeric and dimeric photosystem II complexes from spinach and their relevance to the organisation of photosystem II *in vivo*. *Eur J Biochem* **243:** 422–429

Harrer R, Bassi R, Testi MG, Schafer C (1998) Nearest-neighbor analysis of a photosystem II complex from Marchantia polymorpha L. liverwort), which contains reaction center and antenna proteins. *Eur J Biochem* **255:** 196–205

Iwai M, Takahashi Y, Minagawa J (2008) Molecular remodeling of photosystem II during state transitions in Chlamydomonas reinhardtii. *Plant Cell* **20:** 2177–2189

Jansson S (1999) A guide to the Lhc genes and their relatives in Arabidopsis. *Trends Plant Sci* **4:** 236–240

Jansson S, Stefansson H, Nystrom U, Gustafsson P, Albertsson PA (1997) Antenna protein composition of PS I and PS II in thylakoid sub-domains. *Biochim Biophys Acta* **1320:** 297–309

Jordan P, Fromme P, Witt HT, Klukas O, Saenger W, Krauss N (2001) Three-dimensional structure of cyanobacterial photosystem I at 2.5 A resolution. *Nature* **411:** 909–917

Kereiche S, Dankjaer J, Kovacs L, Jansson S, Horton P, Boekema EJ (2007) Structural characterization of PSII membranes from an Arabidopsis knock-out mutant lacking Lhcb3 antenna. *Photosynth Res* **91:** 171

Kiss AZ, Ruban AV, Horton P (2008) The PsbS protein controls the organization of the photosystem II antenna in higher plant thylakoid membranes. *J Biol Chem* **283:** 3972–3978

Kouril R, Zygadlo A, Arteni AA, de Wit CD, Dekker JP, Jensen PE, Scheller HV, Boekema EJ (2005) Structural characterization of a complex of photosystem I and light-harvesting complex II of Arabidopsis thaliana. *Biochemistry* **44:** 10935–10940

Kovacs L, Damkjaer J, Kereiche S, Ilioaia C, Ruban AV, Boekema EJ, Jansson S, Horton P (2006) Lack of the light-harvesting complex CP24 affects the structure and function of the grana membranes of higher plant chloroplasts. *Plant Cell* **18:** 3106–3120

Laemmli UK (1970) Cleavage of structural proteins during the assembly of the head of bacteriophage T4. *Nature* **227:** 680–685

Li XP, Bjorkman O, Shih C, Grossman AR, Rosenquist M, Jansson S, Niyogi KK (2000) A pigment-binding protein essential for regulation of photosynthetic light harvesting. *Nature* **403:** 391–395

Li XP, Gilmore AM, Caffarri S, Bassi R, Golan T, Kramer D, Niyogi KK (2004) Regulation of photosynthetic light harvesting involves intrathylakoid lumen pH sensing by the PsbS protein. *J Biol Chem* **279:** 22866–22874

Liu Z, Yan H, Wang K, Kuang T, Zhang J, Gui L, An X, Chang W (2004) Crystal structure of spinach major light-harvesting complex at 2.72 A resolution. *Nature* **428:** 287–292

Loll B, Kern J, Saenger W, Zouni A, Biesiadka J (2005) Towards complete cofactor arrangement in the 3.0 angstrom resolution structure of photosystem II. *Nature* **438:** 1040–1044

Ludtke SJ, Baldwin PR, Chiu W (1999) EMAN: semiautomated software for high-resolution single-particle reconstructions. *J Struct Biol* **128:** 82–97

Mozzo M, Passarini F, Bassi R, van Amerongen H, Croce R (2008) Photoprotection in higher plants: the putative quenching site is conserved in all outer light-harvesting complexes of Photosystem II. *Biochim Biophys Acta-Bioenerg* **1777:** 1263–1267

Nield J, Barber J (2006) Refinement of the structural model for the photosystem II supercomplex of higher plants. *Biochim Biophys Acta-Bioenerg* **1757:** 353–361

Nield J, Funk C, Barber J (2000a) Supermolecular structure of photosystem II and location of the PsbS protein. *Philos Trans R Soc Lond B Biol Sci* **355:** 1337–1344

Nield J, Kruse O, Ruprecht J, da Fonseca P, Buchel C, Barber J (2000b) Three-dimensional structure of Chlamydomonas reinhardtii and Synechococcus elongatus photosystem II complexes allows for comparison of their oxygen-evolving complex organization. *J Biol Chem* **275:** 27940–27946

Nield J, Orlova EV, Morris EP, Gowen B, van Heel M, Barber J (2000c) 3D map of the plant photosystem II supercomplex obtained by cryoelectron microscopy and single particle analysis. *Nat Struct Biol* **7:** 44–47

Novoderezhkin VI, Palacios MA, Van Amerongen H, van Grondelle R (2005) Excitation dynamics in the LHCII complex of higher plants: modeling based on the 2.72 angstrom crystal structure. *J Phys Chem B* **109:** 10493–10504

Oostergetel GT, Keegstra W, Brisson A (1998) Automation of specimen selection and data acquisition for protein electron crystallography. *Ultramicroscopy* **74:** 47–59

Roose JL, Wegener KM, Pakrasi HB (2007) The extrinsic proteins of photosystem II. *Photosynth Res* **92:** 369–387

Sandona D, Croce R, Pagano A, Crimi M, Bassi R (1998) Higher plants light harvesting proteins. Structure and function as revealed by mutation analysis of either protein or chromophore moieties. *Biochim Biophys Acta* **1365:** 207–214

Schagger H (2006) Tricine-SDS–PAGE. *Nat Protoc* **1:** 16–22

Schmid VHR (2008) Light-harvesting complexes of vascular plants. *Cell Mol Life Sci* **65:** 3619–3639

Shi LX, Schroder WP (2004) The low molecular mass subunits of the photosynthetic supracomplex, photosystem II. *Biochim Biophys Acta-Bioenerg* **1608:** 75–96

Stroebel D, Choquet Y, Popot JL, Picot D (2003) An atypical haem in the cytochrome b(6)f complex. *Nature* **426:** 413–418

Teardo E, de Laureto PP, Bergantino E, Dalla Vecchia F, Rigoni F, Szabò I, Giacometti GM (2007) Evidences for interaction of PsbS with photosynthetic complexes in maize thylakoids. *Biochim Biophys Acta-Bioenerg* **1767:** 703–711

Thidholm E, Lindstrom V, Tissier C, Robinson C, Schroder WP, Funk C (2002) Novel approach reveals localisation and assembly pathway of the PsbS and PsbW proteins into the photosystem II dimer. *FEBS Lett* **513:** 217–222

Vanheel M (1987) Angular reconstitution—a posteriori assignment of projection directions for 3-D reconstruction. *Ultramicroscopy* **21:** 111–123

Veerman J, McConnell MD, Vasil'ev S, Mamedov F, Styring S, Bruce D (2007) Functional heterogeneity of photosystem II in domain specific regions of the thylakoid membrane of spinach (Spinacia oleracea L.). *Biochemistry* **46:** 3443–3453

Yakushevska AE, Jensen PE, Keegstra W, van Roon H, Scheller HV, Boekema EJ, Dekker JP (2001) Supermolecular organization of photosystem II and its associated light-harvesting antenna in Arabidopsis thaliana. *Eur J Biochem* **268:** 6020–6028

Yakushevska AE, Keegstra W, Boekema EJ, Dekker JP, Andersson J, Jansson S, Ruban AV, Horton P (2003) The structure of photosystem II in Arabidopsis: localization of the CP26 and CP29 antenna complexes. *Biochemistry* **42:** 608–613

Yamashita E, Zhang H, Cramer WA (2007) Structure of the cytochrome b6f complex: quinone analogue inhibitors as ligands of heme cn. *J Mol Biol* **370:** 39–52

Publication 2

Fine structure of granal thylakoid membrane organization using cryo electron tomography

Roman Kouřil *, Gert T. Oostergetel, Egbert J. Boekema *

Electron microscopy group, Groningen Biomolecular Sciences and Biotechnology Institute, University of Groningen, Groningen, The Netherlands

ARTICLE INFO

ABSTRACT

The architecture of grana membranes from spinach chloroplasts was studied by cryo electron tomography. Tomographic reconstructions of ice-embedded isolated grana stacks enabled to resolve features of photosystem II (PSII) in the native membrane and to assign the absolute orientation of individual membranes of granal thylakoid discs. Averaging of 3D sub-volumes containing PSII complexes provided a 3D structure of the PSII complex at 40 Å resolution. Comparison with a recently proposed pseudo-atomic model of the PSII supercomplex revealed the presence of unknown protein densities right on top of 4 light harvesting complex II (LHCII) trimers at the lumenal side of the membrane. The positions of individual dimeric PSII cores within an entire membrane layer indicates that about 23% supercomplexes must be of smaller size than full $C_2S_2M_2$ supercomplexes, to avoid overlap.

© 2010 Elsevier B.V. All rights reserved.

1. Introduction

Chloroplasts play a central role in the plant energy metabolism known as photosynthesis. They enclose the thylakoid membrane, which forms a unique three-dimensional network with regular stacks of thylakoids, called grana, which are interconnected by single membranes, the stroma thylakoids. The distinct parts of the thylakoid membrane specifically accommodate individual components of photosynthetic apparatus. Photosystem II (PSII) and the light-harvesting complex II (LHCII) are confined mainly to grana stacks, whereas most of Photosystem I (PSI), the light-harvesting complex I and ATP synthase are localized in unstacked stromal thylakoids and grana margins. Distribution of cytochrome b_6f complex in the thylakoid membrane seems to be unrestricted [1].

PSII consists of a dimeric core complex and a peripheral antenna system composed of 6 different complexes, belonging to the Lhcb (Light-harvesting complex) multigenic family [2]. The major antenna complex, LHCII, is organized in heterotrimers composed of the products of the *Lhcb1-3* genes. The three other subunits, CP29 (Lhcb4), CP26 (Lhcb5) and CP24 (Lhcb6) are present as monomers. A variable number of the peripheral antenna proteins can associate with dimeric PSII core complexes to form the so-called PSII-LHCII supercomplexes [3]. Many supercomplexes observed in spinach and *Arabidopsis thaliana* contain a dimeric core (C_2), 2 LHCII trimers (trimer S) strongly bound to the complex on the side of CP43 and CP26, and 2 more trimers, moderately

bound (trimer M), which are in contact with CP29 and CP24. This complex is known as the $C_2S_2M_2$ supercomplex [3]. Occasionally, spinach supercomplexes loosely bind a third trimer (trimer L) around CP24 [4]. A 3D reconstruction of a smaller supercomplex containing only one trimer per reaction center and lacking CP24 (C_2S_2) was obtained by cryo-EM at about 17 Å resolution [5,6]. More recently, a 2D map at 12 Å resolution was obtained and used to generate a pseudo-atomic 3D model. This allowed determination of the location and orientation of individual light-harvesting components and the approximate position of pigments [7].

The lateral distribution of protein complexes within grana membranes is an intriguing topic and was a subject of many structural studies using electron microscopy of either freeze-fractured or negatively stained grana membranes (see [3,8] for reviews), atomic force microscopy [9] or, very recently, by cryo electron tomography [10]. Although in most grana membranes PSII supercomplexes are not highly organized, semi-crystalline domains of PSII supercomplexes or core complexes appear in a minority of the membranes (see [8] for a list of native crystalline arrays, [10]). A study of paired inside-out grana membranes indicated that crystalline arrays of adjacent layers can have a specific interaction in which orientations of opposing PSII complexes have preferred angles. This was found for spinach [11] as well as for *Arabidopsis* membranes [12]. A tomographic study on isolated spinach thylakoid membranes revealed the presence of the PSII crystalline arrays exclusively in stacked grana membranes, indicating the importance of a specific interaction between the stroma membrane surfaces of two adjacent membrane layers for the formation of regular PSII arrays [10]. In addition, recent experiments indicate that the PsbS protein controls the frequency of this crystalline macro-organization in the grana membrane [13]. High levels of PsbS disrupt the macro-organization. However, many other aspects of the PSII distribution,

---

such as possible changes upon state transition or photoinhibition are not known in detail. Recently, however, the mobility of grana membrane proteins was studied by fluorescence recovery after photobleaching [14]. In intact, wild-type chloroplasts a mobile population of grana membrane proteins increases significantly after photoinhibition, which is consistent with a role of protein diffusion in the PSII repair cycle. It was shown that protein phosphorylation switches the membrane system to a more fluid state, thus facilitating the PSII repair cycle [14].

There is a generally accepted idea that the entire thylakoid membrane is folded in such a way that it encloses a single aqueous space, the thylakoid lumen. The space between the thylakoid membrane and the chloroplast envelope is called the stroma. The details of the thylakoid membrane folding and the interconnection of grana stacks with stromal thylakoids have not been totally solved. Early electron microscopy studies of serial sections of chemically fixed thylakoid membranes led to the proposition of several 3D models of thylakoid membrane architecture (reviewed in [15]). Afterward, some of these models were questioned by an electron microscopy study of freeze-substituted chloroplast sections [16]. These models include (i) "the folded membrane model", which proposes a way of a dynamic reversible folding of the thylakoid membrane [17] and (ii) "the helical model", in which the stroma membranes are wound around the granal stacks [15]. It was further proposed that a bifurcation of stromal membranes and a subsequent membrane bending and fusion is involved in grana stack formation [16]. These novel viewpoints of the grana architecture initiated a further discussion with a common consensus that current data still require further refinements to clarify discrepancies between individual models [18–20]. Refining of chloroplast membrane topology models will depend very much on improving of electron microscopy hardware to reach better data acquisition and on perfecting tomography reconstruction techniques, necessary to image complete chloroplasts.

Over the last decade the application of cryo electron tomography on intact frozen-hydrated samples has become a popular technique to visualize cell structures because the method is free of fixation artifacts [21]. In combination with sub-volume averaging, it is nowadays a very feasible approach for studying macromolecules and membrane architecture inside cells, cellular organelles and structures of membrane protein complexes in their native membrane environment [10,22–25]. Because electron tomography is most efficient with thin objects and since there is a direct relation between the size of an object and the theoretical resolution [26], it works the best for small objects up to about 0.5–1 μm. Unfortunately, chloroplasts are substantially larger and also densely packed with membranes. Hence, intact chloroplasts are currently just too large to yield a resolution of about 50–60 Å, which is necessary to unambiguously elucidate structural features of the thylakoid membrane, including its precise folding. In this study, we applied cryo electron tomography to isolated grana membrane stacks. Working with smaller tomography volumes, in contrast to e.g. intact chloroplasts, allowed pushing up the resolution to see interpretable densities of PSII complexes in the granal membrane. This enabled averaging sub-volumes containing PSII and seeing characteristic features of PSII core complexes in the natural membrane at 40 resolution. In addition, single particle 3D averaging revealed a novel density associated with the PSII core complex in multiple copies, which has not been observed before in isolated forms of PSII complexes. Comparison of the 3D structure of the PSII core complex with the recently proposed pseudo-atomic model of the complete, $C_2S_2M_2$ PSII supercomplex [7] revealed a striking fit of the extra densities with the position of LHCII trimers. A possible origin of the novel density is discussed.

2. Materials and methods

2.1. Preparation of the granal thylakoid membranes

Thylakoid membranes were isolated from market, dark adapted spinach according to [27]. The isolated membranes were resuspended in 20 mM Bis-Tris (pH 6.5) with 5 mM $MgCl_2$ at a final concentration of 0.5 mg of Chl/mL and partially solubilized with digitonin at a final concentration of 0.5% (w/v) for 20 min at 4 °C with a slow stirring, followed by centrifugation in an Eppendorf table centrifuge for 15–20 min [28]. The pellet, which contained the non-solubilized granal thylakoid membranes, was used for cryo electron tomography.

2.2. Cryo electron tomography

Granal thylakoid membranes were mixed with 10-nm gold particles as fiducial markers and applied to glow discharged 200 mesh Quantifoil specimen support grids (Quantifoil Micro Tools GmbH) coated with a thin carbon film. Vitrification was performed in liquid ethane using a Vitrobot Mk3 (FEI company, Eindhoven) operating under a 100% humidified atmosphere at room temperature. Electron tomography was performed on a 300 kV G2 Polara electron microscope (FEI) equipped with a Gatan post-column energy filter. Images were recorded with a 2 k × 2 k CCD camera (Gatan) at 8 μm underfocus and 51,750x final magnification, resulting in a pixel size of 0.58 nm at the level of the specimen. Single axis tilt series were recorded at 2° increments over a range of ± 68° with a total dose of about 80 e/Å^2.

2.3. 3D reconstruction and image analysis

Tomograms were calculated using IMOD software [29] and further denoised with 20 iterations by non-linear anisotropic diffusion [30]. Averaging of manually selected sub-volumes with a box size of either 232 × 232 Å or 319 × 319 Å was performed using PEET program (a part of IMOD package). Central coordinates of the sub-volumes were selected using 3dmod program. Surface views of averaged sub-volumes were produced using 3dmod program (a part of the IMOD package). The resolution of the final averaged sub-volume was estimated by Fourier Shell Correlation [31] at 0.3 threshold with EMAN software [32].

3. Results

3.1. Cryo electron tomography of granal thylakoid membranes

Suspensions of isolated granal thylakoid membranes (Supplemental Fig. 1) were directly investigated by cryo electron tomography. Fig. 1 shows four slices of a typical electron tomogram of one granal membrane stack, where four membrane layers were clearly resolved (Fig. 1A to D). This and other tomographic reconstructions revealed distinct densities in all membrane layers, which could be unambiguously assigned to the dimeric PSII complex (see e.g. white arrows in Fig. 1A). Tomographic slices of the middle part of the reconstruction indicate that the membranes form two vesicles, as evident from a pair of strong rims resolved at the edge of the granal membrane (Figs. 1B and C). Close investigation of the tomographic data revealed other interesting features that will be discussed below.

Creation of surface views of individual granal stacks gave good insight into the overall 3D organization. Fig. 2 shows different angular surface views of two granal vesicles like in Fig. 1, with marked positions of individual PSII complexes (Figs. 2A to C, and D to F, respectively). Both vesicles have the shape of a sac and each one is formed by a pair of continuous membranes, which does not have any direct contact with the other. The outer membrane, depicted in green, accommodates PSII complexes in both the upper and bottom membrane layers (Fig. 2, green and blue spheres, respectively). The outer membrane is not (anymore) continuous at the vesicle margin, which is mainly obvious from the top-views (Figs. 2A and D). The inner membrane, depicted in brown, encloses the inner space of the vesicle and accommodates PSII complexes in two layers (Fig. 2, cyan and red spheres). At this moment, it is not clear (due to a resolution-limited membrane tracking) if the inner membrane fully encloses the
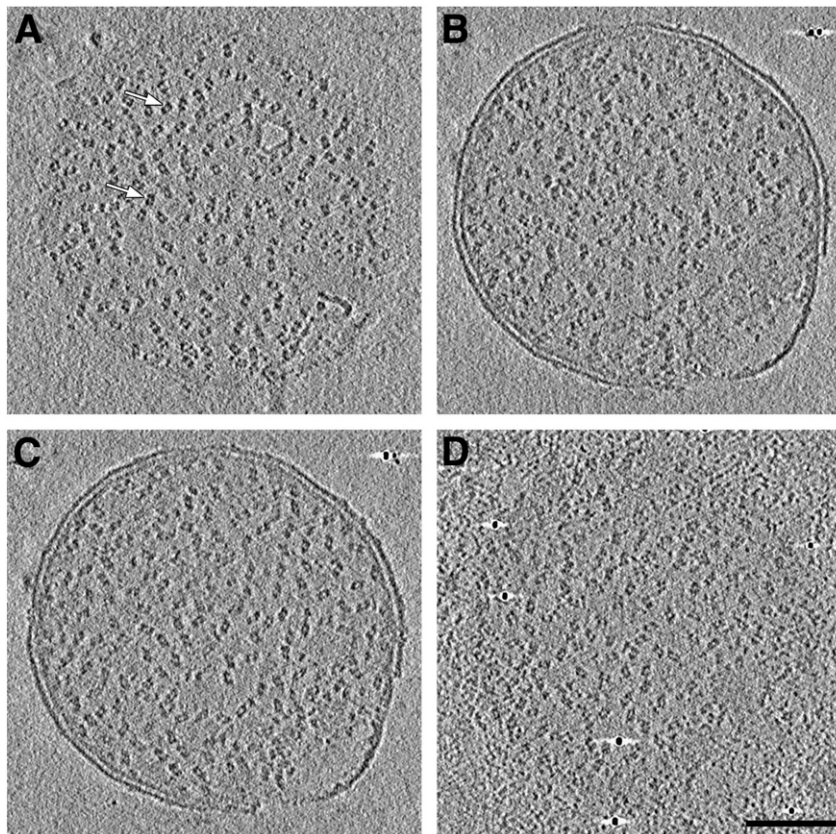
Fig. 1. Tomographic slices of a stack of four granal membranes forming two vesicles. An example of X–Y slices of 2.9 nm thickness along the z-axis projection from tomographic reconstruction of an ice-embedded spinach granal membrane vesicle, which contains four membrane layers: (A) the upper membrane of the granal vesicle. (B–C) adjacent membrane layers in the middle of the granal vesicle. (D) the bottom membrane of the granal vesicle facing a thin carbon support film. PSII complexes were well resolved in all four membrane layers (see e.g. white arrows in A). The bar is 100 nm.

inner space of the vesicle or if there is a narrow gap in the membrane, which would connect the inner space with surroundings. Under the experimental conditions applied, the distance between two outer adjacent PSII layers (one layer formed by the outer and the other formed by the inner membrane) was found in these (Figs. 2A–C and D–F) and similar reconstructions to be rather constant in a range of 14–16 nm. In contrast, the distance between adjacent PSII layers formed only by the inner membrane was highly variable in 8 different reconstructions, of which two extremes are shown (Figs. 2C and F). This is probably because the vesicles of thylakoid membranes can get swollen during isolation procedure (see also [10]). The integrity of grana membrane stacking may also have been altered by the detergent solubilization of the connecting stroma membranes. Nevertheless, some characteristics remain, such as the remarkable flatness of each single membrane leaflet (Fig. 2).

3.2. 3D analysis of PSII complexes

Tomogram sub-volumes of randomly oriented PSII were selected and subjected to 3D analysis and subsequent averaging. Fig. 3 shows the result of the analysis. Averaging of the best 100 sub-volumes revealed the structure of the dimeric PSII core complex (Figs. 3A to C). Views of the PSII complex from the lumenal (Fig. 3A), the stromal side (Fig. 3B) and from a side (Fig. 3C) clearly show the topology of the PSII core part, especially of the extrinsic subunits of the oxygen evolving complex protruding into the lumen. Noteworthy, the 3D analysis revealed a pair of additional spherical densities at the lumenal membrane surface close to the center of the PSII complex (Figs. 3A–C). Comparison of the 3D structure of the PSII complex with the recently proposed pseudo-atomic model of the complete, $C_2S_2M_2$ PSII super-complex [7] indicates an overall structural similarity of the 3D

tomography data with the higher-resolution model of the super-complex (Fig. 3D). Furthermore, the comparison revealed a striking fit of the extra spherical densities with the position of the S-type of LHCII trimers centers. Analysis of the same 100 sub-volumes, but with a larger box size to cover a larger space around the PSII core, revealed another pair of non-membrane embedded densities, which coincided well with the position of the M-type LHCII trimers in the pseudo-atomic model (Fig. 3E). Extension of the box size was, however, at the expense of the resolution, which was computed to be 40 for the core part in case of analysis of smaller sub-volumes. Features of individual LHCII trimers within the membrane could not be revealed, possibly because of low contrast.

4. Discussion

Imaging of organelles in amorphous ice, free of any fixation agent, represents a situation close to the natural state. We have previously shown that it is feasible to average sub-volumes containing large macromolecules from intact organelles, such as dimeric ATP synthase in mitochondria from the alga *Polytomella* [24]. In present study, we investigated a fraction of isolated spinach granal membranes using cryo electron tomography to able to resolve and analyze PSII complexes in their native environment and native form. The reason to work here with fragments was a practical one, because the *Spinacea* chloroplasts turned out to be just too thick to image them as entities. It was already shown that to compensate for this limitation, working with small thylakoid membrane fractions is an appropriate way to yield enough resolution in tomographic reconstruction [10], compared to analysis of thin sections of chemically fixed (reviewed in [15]) or high-pressure frozen, freeze-substituted chloroplast sections [16].
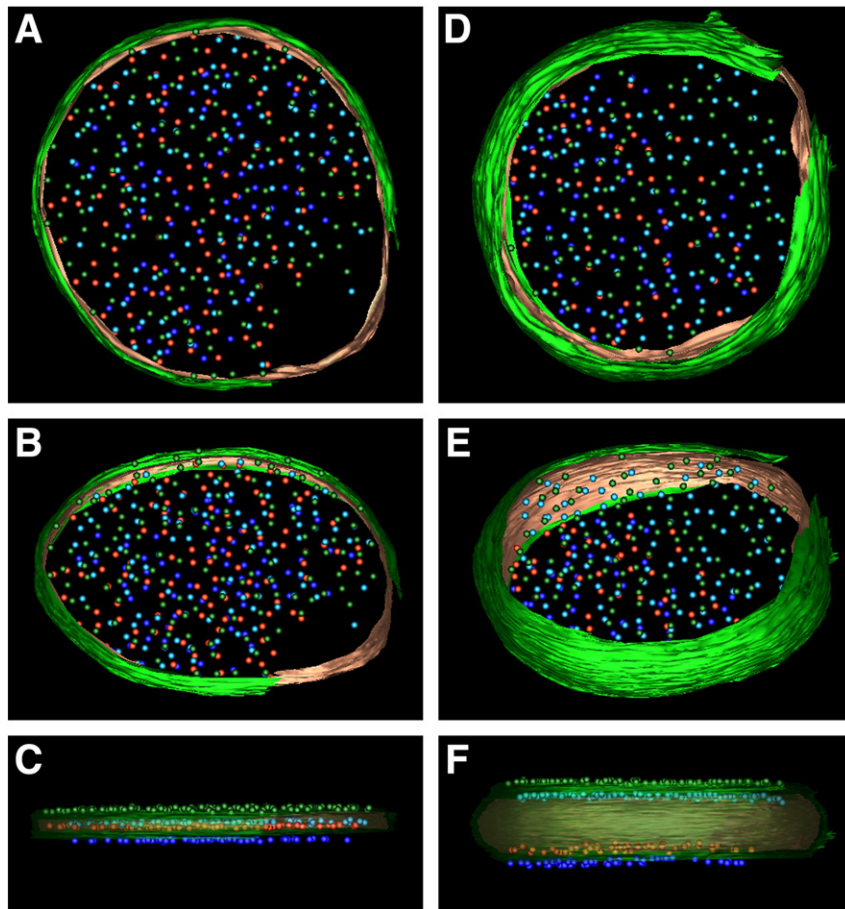
Fig. 2. Surface views of two reconstructed granal stacks (A–C and D–F), composed of two granal membrane vesicles of different thickness. Reconstructions are seen in top view (A, D), tilted view (B, E) and side-view (C, F) orientation, respectively. The outer and inner membranes are depicted in green and brown, respectively. PSII complexes were resolved in four membrane layers and are depicted as green, cyan, red, and blue spheres.
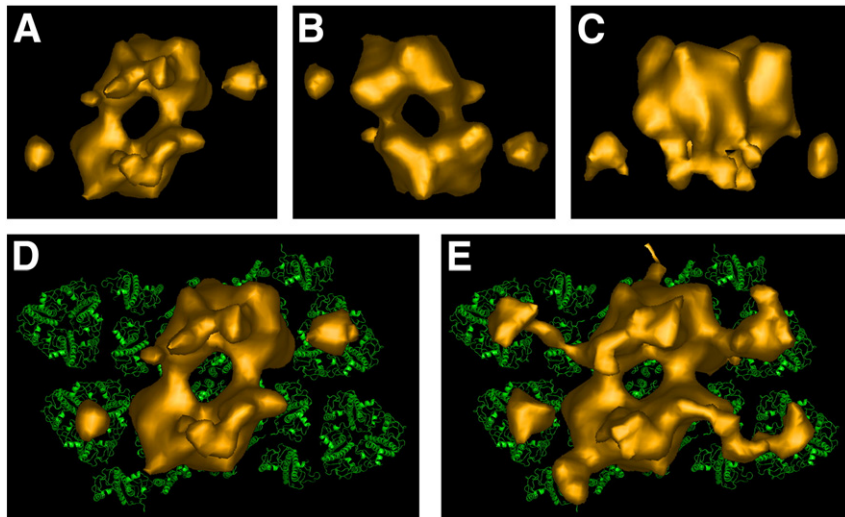
Fig. 3. 3D data of PSII complex and fitting. (A–C) 3D average of the best 100 sub-volumes of PSII complexes selected from tomographic reconstructions viewed from the lumenal and stromal side, and from a side along the membrane plane, respectively. Isosurface model shows the PSII core complex together with extrinsic subunits of oxygen-evolving complex resolved on the lumenal side of the complex. Further, two additional spherical densities were revealed at the lumenal side of the PSII complex. (D) a comparison of the isosurface model of PSII complex with a pseudo-atomic model of the complete PSII supercomplex ($C_2S_2M_2$ supercomplex) [7], viewed from the lumenal side. The fit indicates that the spherical densities coincide with the position of the S-type LHCII trimers. (E) a comparison of the isosurface model of PSII complex obtained from the average of PSII sub-volumes of an increased size (with respect to the model presented in A–D) with the pseudo-atomic model of the complete PSII supercomplex. Analysis of the larger sub-volumes revealed additional, non-membrane embedded spherical densities, which coincide with the position of the M-type LHCII trimers. Analysis of larger sub-volumes was at the expense of the resolution of the PSII core complex and extrinsic subunits of oxygen-evolving complex.

The potency of the cryo electron tomography approach applied on non-chemically fixed chloroplasts is also obvious from the current data. Imaging of single grana discs free of any fixation agent led to a resolution which is far better than previously obtained by thin section studies of chemically fixed chloroplasts. This is evident from the appearance of individual PSII core complexes in the membrane which could not be resolved before. This is mainly due to using smaller volumes [33], but also because of better instrumental performance. Especially, the application of energy filtering to remove inelastically scattered electrons that blur the image is beneficial for a higher resolution in electron tomography [34].

4.1. 3D analysis of PSII complexes revealed novel densities

The high-resolution structure of the PSII core complex of cyanobacteria was recently improved to 2.9 Å resolution [35]. In contrast, the structural analysis of plant PSII supercomplex is impaired mainly by its lability and the complexity of its peripheral antenna system (see Introduction). A novel protocol for obtaining homogeneous fractions of the various types of PSII-LHCII supercomplexes enabled a 2D structural characterization of the largest $C_2S_2M_2$ PSII supercomplex from Arabidopsis at 12 Å resolution [7]. Previously, 3D electron microscopy structural studies yielded a 17 Å resolution 3D map for the smaller C_2S_2 PSII supercomplex [6]. It is known, however, that PSII easily may lose some of its subunits upon purification [36]. Here, we show a 3D analysis of plant PSII complex, which was resolved in the native thylakoid membrane by cryo electron tomography. The averaging of 3D sub-volumes revealed the structure of PSII complex at 40 Å resolution (Fig. 3), which was assigned as the PSII core complex, based on the comparison with the recently proposed pseudo-atomic model of the complete, $C_2S_2M_2$ PSII supercomplex [7]. An overall architecture of lumen-exposed oxygen evolving complex indicates similar features as observed in a 3D map of plant PSII supercomplex [5,6].

The averaging of 3D sub-volumes revealed extra densities on both sides of the dimeric core. These densities must be genuine proteins, because (1) they are at positions related by two-fold rotational symmetry and (2) this symmetry was not imposed during averaging or afterwards. They are too large to be considered as lumen-exposed loops of LHCII. Comparison with the pseudo-atomic structure reveals that these proteins are associated to the PSII supercomplexes, right on top of the S- and M-trimers (Figs. 3D and E). We can be quite confident that most LHCII trimers have the extra lumenal density, because the 3D averaging is performed on all selected sub-volumes, including those who may have LHCII trimers without such densities. If for instance only 25% of the trimers would have a density, then the other 75% would cause that in the final sum this detail would have been more or less lost.

As the extra densities are attached to the lumenal side of the PSII supercomplex (Fig. 3C), they likely represent an enzyme. Although a proteome analysis indicates that the lumen compartment can contain up to 200 different proteins [37] we tentatively propose that the extra densities represent, due to their specific association to LHCII proteins, violaxanthin deepoxidase (VDE). VDE is a soluble lumenal protein, which is involved in the conversion of violaxanthin into zeaxanthin in the xanthophyll cycle and thus in non-photochemical quenching of an excess of excitation energy (see [38] for recent review). It was found that VDE remains attached to the thylakoid membrane at acidic pH, even after several freeze-thaw cycles [39]. Under our experimental conditions, all tomography experiments were performed at pH = 6.5, which was shown to still keep VDE in the bound form [39]. On the other hand, it remains puzzling that each LHCII trimer would have a VDE copy, as enzymes are usually present in much smaller numbers than proteins, such as the LHCII trimers. It will take more effort to assign the nature of the extra densities and the most obvious way to solve the problem is by using Arabidopsis null mutants.

4.2. Nature and distribution of the PSII complexes in the thylakoid membrane

Grana discs were obtained after a short treatment with a mild detergent to get them separated. Tomographic reconstructions revealed that grana discs consist of two concentrically folded membranes, which form a sac with four layers (Figs. 1 and 2). Densities of PSII core complexes were clearly resolved in all four membrane layers. The tomographic data not only revealed the positions of individual PSII complexes within the native membrane, but showed clearly recognizable details of individual molecules. Importantly, the features of dimeric PSII core complexes provide the orientations of the PSII dimers within the membrane plane (Fig. 4). This led us to correlate the map of the large $C_2S_2M_2$ PSII supercomplex with the PSII cores. Hand fitting of this specific supercomplex contour indicates that there would be enough space to accommodate complete PSII supercomplexes on many of the cores (Fig. 4A, green contours). In several cases, however, $C_2S_2M_2$ particles overlap with their neighbors (Fig. 4A, red contours). In most of them, only smaller PSII supercomplexes can be present (e.g. C_2S_2 or C_2S_2M supercomplexes), because of overlapping antennae. The number of smaller
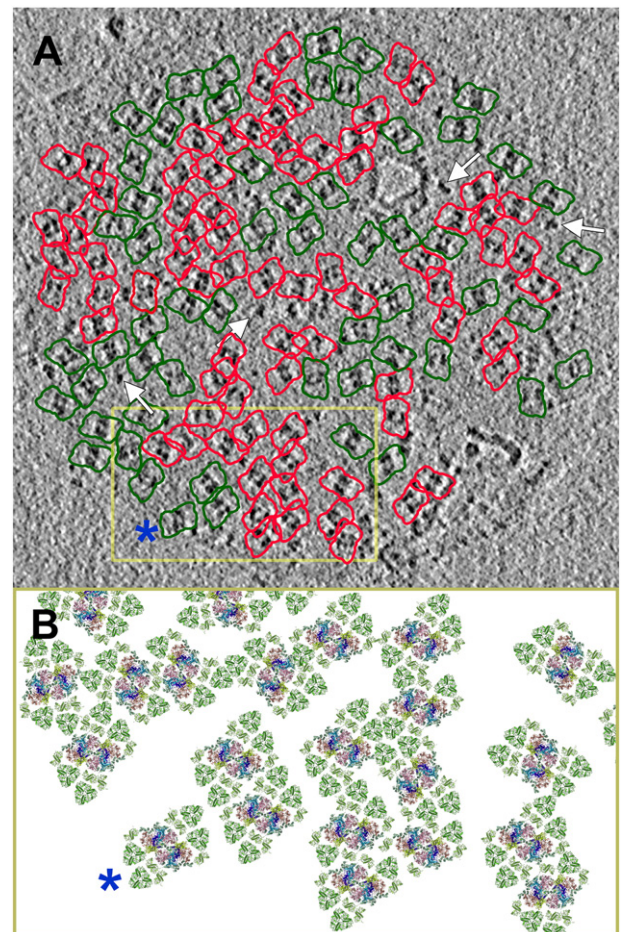
Fig. 4. Distribution of PSII complexes in thylakoid membrane. (A) superimposition of contours of the complete, $C_2S_2M_2$ supercomplex over clearly resolved densities of the PSII core in one membrane layer of the thylakoid stack of Fig. 1. Green and red contours indicate positions of PSII complexes with either no or significant clashes with neighboring PSII complexes, respectively. White arrows indicate smaller, non-assigned densities, which could represent e.g. PSII monomers. (B) example of the higher organization of PSII supercomplexes in the thylakoid membrane based on the experimental data. Blue asterisk indicates the corresponding PSII complex within the selected area of the tomographic data (see yellow box in A).

complexes is estimated to be about half of red marked particles, or 23% of the total. Furthermore, tomographic data revealed also smaller densities, which cannot be assigned to PSII dimers, and likely represent monomeric PSII complexes (Fig. 4A, white arrows). The fact that not all of the PSII core complexes can be surrounded by a complete set of four LHCII trimers is in line with previous work on solubilized spinach chloroplast membranes [40]. However, in that particular study only 1% of the particles was assigned as $C_2S_2M_2$ supercomplexes and the vast majority of PSII particles (70%) was comprised of the smaller C_2S_2 complexes. It is well possible that the absolute amount of supercomplexes became decreased by detergent solubilization; thus our tomographic data provide a closer-to-reality view of the grana membrane (Fig. 4A). However, it should also be realized that light conditions have a strong influence on the amount of free- and bound LHCII [41], which can cause different amounts of individual types of PSII supercomplexes.

It is also evident that regardless of a minor fraction of unassigned densities, PSII supercomplexes do not occupy the whole surface of grana membrane (Fig. 4B). There are several membrane areas, which are very flat and seem to be free of protruding proteins. They can represent membrane lipid areas, which are important for a lateral diffusion of proteins and plastoquinone molecules in the membrane, or they can be partially occupied by free LHCII proteins, as pointed out earlier [3]. Thus, there appears to be ample space for the non-bound fraction of LHCII trimers, as was already suggested two decades ago [42].

Within the reconstructed volumes there were no highly ordered crystalline domains of individual PSII complexes present, except of one tomogram, where some clear rows of PSII molecules were seen (Supplemental Fig. 2). The rows of PSII are similar to those observed before in isolated paired inside-out membranes [11,12]. It is highly unlikely that a mild detergent treatment in the purification procedure has a negative effect on the crystallinity, as the ordered PSII arrays have been observed before in detergent treated samples, including the recent tomography data [10]. However, such crystalline domains usually occupy only a small part of all grana membranes [10,11,13] and their presence is mostly a matter of lateral segregation within the densely packed membranes [3]. Although in these particular membranes the distribution and orientation of PSII complexes is seemingly random, the fitting indicates there is some preference for a parallel alignment (Fig. 4), which is in line with statistical analysis of AFM data [9].

4.3. Architecture of the granal stacks by cryo electron tomography

The total folding of the grana membrane remains certainly an intriguing question to address by any microscopy technique. In our study, we could not address the question of the complete architecture of the granal thylakoids by using cryo electron tomography because the *Spinacea* chloroplasts turned out to be just too thick to image them as

entities. Therefore, we compromised with working on thin grana stacks from disrupted chloroplasts. The use of detergent in our experiments led to removal of stroma thylakoids, which made it impossible to reconstruct how the grana membranes interconnect the unstacked stroma membranes. Disruption probably also lead to an alteration of membrane stacking and thus to variation in the distances between the different membranes (Figs. 2 and 5), as is evident from other studies [43].

Nevertheless, tomographic reconstructions on the thinner moiety of grana stacks revealed that many grana discs consist of two concentrically folded membranes, which form a sac with four layers (Figs. 1, 2 and 5), although some thicker ones were also observed. Densities of PSII core complexes were clearly resolved in all four membrane layers with no obvious sign for a higher ordered organization (Fig. 1 and 4, see below for a discussion). Crucial for a thorough examination of the overall thylakoid structure is the fact that the stroma and lumen sides of the membrane could be established from the PSII orientation, which was derived from 3D analysis of PSII sub-volumes selected from individual membrane layers. 3D analysis clearly indicated that the two folded membranes are facing each other from their lumen sides as illustrated in our schematic models (Fig. 5A,B). The thickness of the lumen space was found rather constant, in a range of 14–16 nm, which is in a range reported for thylakoid membranes isolated from dark adapted plants [3]. In contrast, the dimension of the stroma space was found rather variable (Figs. 2C and F; 5A). Considering the dimensions of the oxygen evolving complex (about 5 nm in a direction perpendicular to the membrane plane), there is no spatial restriction for the distribution of PSII complexes in the adjacent layers. Thus, under applied experimental conditions, a juxtaposition of PSII complexes is also possible. A smaller distance is not expected simply due to the presence of the novel densities on top of the LHCII trimers. Only in the absence of such densities, the PSII supercomplexes would have the possibility to approach closer, as claimed in [10].

Tomographic data further indicate that in the margins of the grana discs the pair of membranes is separated by only 3–4 nm (Figs. 1 and 5) and free of PSII complexes, a firm proof for the hypothesis that the margins are free from the major proteins involved in the light reactions in photosynthesis [3].

The appearance of crystalline arrays, discussed in Section 4.2., is often within two adjacent layers [11,12]. In previous studies, it was found that PSII complexes from two such layers with semi-crystalline arrays also show preferential orientations in their interaction in the stroma [11,12]. This was also confirmed by recent tomography study [10], where it was discussed that electrostatic interactions of LHCII trimers are responsible for this. The 3D data of Fig. 3A allow us to see trends in the lateral distribution of PSII protein complexes of four intact layers. The interaction of PSII complexes of the layers separated by the narrow stromal space (Fig. 2C) could, in principle, also be specific. The current data, however, do not show any obvious relation
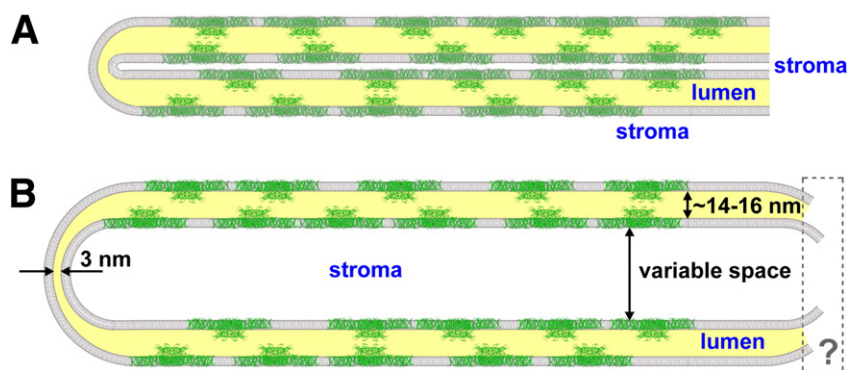
Fig. 5. Scheme of the stacking of membranes in two reconstructed granal stacks of different thickness. The same stacks are presented in Fig. 2. The stroma and lumen sides of the membranes were established from the orientations of the PSII complexes in sub-volumes as indicated in the picture; the $C_2S_2M_2$ supercomplexes are depicted on scale. (A) schematic representation of the granal stack from Fig. 2A. (B) schematic representation of the granal stack from Fig. 2B. The box at the right indicates that the membranes were locally not continuous.

in orientation of PSII complexes from adjacent layers. Apparently, the interaction of single PSII complexes, randomly distributed in grana membranes is different from stacked semi-crystalline arrays.

4.4. Conclusions and outlook

Combination of cryo electron tomography on intact ice embedded samples with 3D analysis of sub-volumes clearly represents a powerful approach for structural studies close to native conditions. It can reveal novel structures of transient and unstable assemblies, which have not been observed before in studies of isolated protein complexes obtained even under optimized conditions. Our tomography data provide the most detailed information on PSII within grana membranes until now. But further investigation of more intact grana stacks is necessary to disclose the nature and formation of their architecture, which will extend our current and simplified views [3,18–20]. In the future, it should be technically feasible to record tomography data on complete chloroplasts at a resolution as provided here, which was performed with current best technology. It should be performed on already existing microscopes equipped with a higher acceleration voltage than the 300 kV applied here to be able to penetrate thicker samples. A more crucial factor necessary to get the good resolution is the use of a direct electron counting camera [44], instead of current CCD camera technology, expected to become available in 2011 and to have a 10x better performance. Thus it may be possible to provide an improved view on grana stacks with interconnected stroma membranes which may lead to refined models of how green plant photosynthesis is carried out at the membrane level.

Supplementary materials related to this article can be found online at doi:10.1016/j.bbabio.2010.11.007.

Acknowledgments

References

[1] P.Å. Albertsson, A quantitative model of the domain structure of the photosynthetic membrane, Trends Plant Sci. 6 (2001) 349–354.
[2] S. Jansson, The light-harvesting chlorophyll a/b binding proteins, Biochim. Biophys. Acta 1184 (1994) 1–19.
[3] J.P. Dekker, E.J. Boekema, Supramolecular organization of the thylakoid membrane proteins in green plants, Biochim. Biophys. Acta 1706 (2005) 12–39.
[4] E.J. Boekema, H. van Roon, F. Calkoen, R. Bassi, J.P. Dekker, Multiple types of association of photosystem II and its Light-Harvesting antenna in partially solubilized Photosystem II membranes, Biochemistry 38 (1999) 2233–2239.
[5] J. Nield, E.V. Orlova, E.P. Morris, B. Gowen, M. van Heel, J. Barber, 3D map of the plant photosystem II supercomplex obtained by cryoelectron microscopy and single particle analysis, Nat. Struct. Biol. 7 (2000) 44–47.
[6] J. Nield, M. Balsera, J. De Las Rivas, J. Barber, Three-dimensional electron cryo-microscopy study of the extrinsic domains of the oxygen-evolving complex of spinach, J. Biol. Chem. 277 (2002) 15006–15012.
[7] S. Caffarri, R. Kouřil, S. Kereïche, E.J. Boekema, R. Croce, Functional architecture of higher plant photosystem II supercomplexes, EMBO J. 28 (2009) 3052–3063.
[8] L. Bumba, F. Vácha, Electron microscopy studies of Photosystem II, Photosynth. Res. 77 (2003) 1–19.
[9] H. Kirchhoff, S. Lenhert, C. Büchel, L. Chi, J. Nield, Probing the organization of photosystem II in photosynthetic membranes by atomic force microscopy, Biochemistry 47 (2008) 431–440.
[10] B. Daum, D. Nicastro, J. Austin, J. McIntosh, W. Kühlbrandt, Arrangement of Photosystem II and ATP Synthase in chloroplast membranes of Spinach and Pea, Plant Cell 22 (2010) 1299–1312.
[11] E.J. Boekema, J.F.L. van Breemen, H. van Roon, J.P. Dekker, Arrangement of PSII supercomplexes in crystalline macrodomains within the thylakoid membrane of green plants, J. Mol. Biol. 301 (2000) 1123–1133.
[12] A.E. Yakushevska, P.E. Jensen, W. Keegstra, H. van Roon, H.V. Scheller, E.J. Boekema, J.P. Dekker, Supermolecular organization of photosystem II and its associated light-harvesting antenna in Arabidopsis thaliana, Eur. J. Biochem. 268 (2001) 6020–6021.
[13] S. Kereïche, A.Z. Kiss, R. Kouřil, E.J. Boekema, P. Horton, The PsbS protein controls the macro-organisation of photosystem II complexes in the grana membranes of higher plant chloroplasts, FEBS Lett. 584 (2010) 759–764.
[14] T.K. Goral, M.P. Johnson, A.P.R. Brain, H. Kirchhoff, A.V. Ruban, C.W. Mullineaux, Visualizing the mobility and distribution of chlorophyll proteins in higher plant thylakoid membranes: effects of photoinhibition and protein phosphorylation, Plant J. 62 (2010) 948–959.
[15] L. Mustardy, G. Garab, Granum revised. A three-dimensional model — where things fall into place, Trends Plant Sci. 8 (2003) 117–122.
[16] E. Shimoni, O. Rav-Hon, I. Ohad, V. Brumfeld, Z. Reich, Three-dimensional organization of higher-plant chloroplast thylakoid membranes revealed by electron tomography, Plant Cell 17 (2005) 2580–2586.
[17] P.O. Arvidsson, C. Sundby, A model for the topology of the chloroplast thylakoid membrane, Aust. J. Plant Physiol. 26 (1999) 687–694.
[18] L. Mustardy, K. Buttle, G. Steinbach, G. Garab, The three-dimensional network of the thylakoid membranes in plants; quasihelical model of the granum-stroma assembly, Plant Cell 20 (2008) 2552–2557.
[19] V. Brumfeld, D. Charuvi, R. Nevo, S. Chuartzman, O. Tsabaki, I. Ohad, E. Shimoni, Z. Reich, A note on three-dimensional models of higher-plant thylakoid networks, Plant Cell 20 (2008) 2546–2549.
[20] G. Garab, C.A. Mannella, Reply: On three-dimensional models of higher-plant thylakoid networks: Elements of consensus, controversies, and future experiments, Plant Cell 20 (2008) 2549–2551.
[21] O. Medalia, I. Weber, A.S. Frangakis, D. Nicastro, G. Gerisch, W. Baumeister, Macromolecular architecture in eukaryotic cells visualized by cryoelectron tomography, Science 298 (2002) 1209–1213.
[22] M. Beck, F. Förster, M. Ecke, J. Plitzko, F. Melchior, G. Gerisch, W. Baumeister, O. Medalia, Nuclear pore complex structure and dynamics revealed by cryoelectron tomography, Science 306 (2004) 1387–1390.
[23] M. Strauss, G. Hofhaus, R.R. Schröder, W. Kühlbrandt, Dimer ribbons of ATP synthase shape the inner mitochondrial membrane, EMBO J. 27 (2009) 1154–1160.
[24] N.V. Dudkina, G.T. Oostergetel, H.P. Braun, E.J. Boekema, Row-like organization of ATP synthase in intact mitochondria determined by cryo-electron tomography, Biochim. Biophys. Acta 1797 (2010) 272–277.
[25] N.V. Dudkina, R. Kouřil, J.B. Bultema, E.J. Boekema, Imaging of organelles by electron microscopy reveals protein–protein interactions in mitochondria and chloroplasts, FEBS Lett. 584 (2010) 2510–2515.
[26] A. Klug, R.A. Crowther, 3-dimensional image reconstruction from viewpoint of information theory, Nature 238 (1972) 435–440.
[27] H. van Roon, J.F.L. van Breemen, F.L. de Weerd, J.P. Dekker, E.J. Boekema, Solubilization of green plant thylakoid membranes with n-dodecyl-D-maltoside. Implications for the structural organization of the Photosystem II, Photosystem I, ATP synthase and cytochrome b6 f complexes, Photosynth. Res. 64 (2000) 155–166.
[28] R. Kouřil, A. Zygadlo, A.A. Arteni, C.D. de Wit, J.P. Dekker, P.E. Jensen, H.V. Scheller, E.J. Boekema, Structural characterization of a complex of photosystem I and light-harvesting complex II of Arabidopsis thaliana, Biochemistry 44 (2005) 10935–10940.
[29] J.R. Kremer, D.N. Mastronarde, J.R. McIntosh, Computer visualization of three-dimensional image data using IMOD, J. Struct. Biol. 116 (1996) 71–76.
[30] A.S. Frangakis, R. Hegerl, Noise reduction in electron tomographic reconstructions using nonlinear anisotropic diffusion, J. Struct. Biol. 135 (2001) 239–250.
[31] M. van Heel, G. Harauz, Resolution criteria for 3-dimensional reconstruction, Optik 73 (1986) 119–122.
[32] S.J. Ludtke, P.R. Baldwin, W. Chiu, EMAN: Semiautomated software for high-resolution single-particle reconstructions, J. Struct. Biol. 128 (1999) 82–97.
[33] A. Leis, B. Rockel, L. Andrees, W. Baumeister, Visualizing cells at the nanoscale, Trends Biochem. Sci. 34 (2009) 60–70.
[34] R. Grimm, D. Typke, W. Baumeister, Improving image quality by zero-loss energy filtering: quantitative assessment by means of image cross-correlation, J. Microsc. 190 (1998) 339–349.
[35] A. Guskov, J. Kern, A. Gabdulkhakov, M. Broser, A. Zouni, A.W. Saenger, Cyanobacterial photosystem II at 2.9-Å resolution and the role of quinones, lipids, channels and chloride, Nat. Struct. Mol. Biol. 16 (2009) 334–342.
[36] E.J. Boekema, J. Nield, B. Hankamer, J. Barber, Localization of the 23 kDa subunit of the oxygen evolving complex of Photosystem II by electron microscopy, Eur. J. Biochem. 252 (1998) 268–276.
[37] J.B. Peltier, O. Emanuelsson, D.E. Kalume, J. Ytterberg, G. Friso, A. Rudella, D.A. Liberles, L. Söderberg, P. Roepstorff, G. von Heijne, K.J. van Wijk, Central functions of the lumenal and peripheral thylakoid proteome of Arabidopsis determined by experimentation and genome-wide prediction, Plant Cell 14 (2002) 211–236.
[38] P. Jahns, D. Latowski, K. Strzalka, Mechanism and regulation of the violaxanthin cycle: The role of antenna proteins and membrane lipids, Biochim. Biophys. Acta 1787 (2009) 3–14.
[39] A. Hager, K. Holocher, Localization of the xanthophyll-cycle enzyme violaxanthin de-epoxidase within the thylakoid lumen and bolition of its mobility by a (light-dependent) pH decrease, Planta 192 (1994) 581–589.
[40] E.J. Boekema, H. van Roon, J.F.L. van Breemen, J.P. Dekker, Supramolecular organization of photosystem II and its light-harvesting antenna in partially solubilized photosystem II membranes, Eur. J. Biochem. 266 (1999) 444–452.
[41] J.M. Anderson, Photoregulation of the composition, function, and structure of thylakoid membranes, Ann. Rev. Plant Physiol. 37 (1986) 93–136.
[42] G.F. Peter, J.P. Thornber, Biochemical evidence that the higher plant photosystem core is organized as a dimer, Plant Cell Physiol. 32 (1991) 1237–1250.
[43] R. Danielsson, P.Å. Albertsson, Fragmentation and separation analysis of the photosynthetic membrane from spinach, Biochim. Biophys. Acta 1787 (2009) 25–36.
[44] A.C. Milazzo, G. Moldovan, J. Lanman, L. Jin, J.C. Bouwer, S. Klienfelder, S.T. Peltier, M.H. Ellisman, A.I. Kirkland, N.-H. Xuong, Characterization of a direct detection device imaging camera for transmission electron microscopy, Ultramicroscopy 110 (2010) 741–744.

Publication 3

Arabidopsis Mutants Deleted in the Light-Harvesting Protein Lhcb4 Have a Disrupted Photosystem II Macrostructure and Are Defective in Photoprotection [C][W]

Silvia de Bianchi,[a,1] Nico Betterle,[a,1] Roman Kouril,[b] Stefano Cazzaniga,[a] Egbert Boekema,[b] Roberto Bassi,[a,c,2] and Luca Dall'Osto[a]

[a] Dipartimento di Biotecnologie, Università di Verona, 37134 Verona, Italy
[b] Department of Biophysical Chemistry, Groningen Biomolecular Sciences and Biotechnology Institute, University of Groningen, 9747 AG Groningen, The Netherlands
[c] Institut für Pflanzenwissenschaften-2, Pflanzenwissenschaften, Forschungszentrum Jülich, D-52425 Juelich, Germany

The role of the light-harvesting complex Lhcb4 (CP29) in photosynthesis was investigated in *Arabidopsis thaliana* by characterizing knockout lines for each of the three Lhcb4 isoforms (Lhcb4.1/4.2/4.3). Plants lacking all isoforms (*koLhcb4*) showed a compensatory increase of Lhcb1 and a slightly reduced photosystem II/I ratio with respect to the wild type. The absence of Lhcb4 did not result in alteration in electron transport rates. However, the kinetic of state transition was faster in the mutant, and nonphotochemical quenching activity was lower in *koLhcb4* plants with respect to either wild type or mutants retaining a single Lhcb4 isoform. *KoLhcb4* plants were more sensitive to photoinhibition, while this effect was not observed in knockout lines for any other photosystem II antenna subunit. Ultrastructural analysis of thylakoid grana membranes showed a lower density of photosystem II complexes in *koLhcb4*. Moreover, analysis of isolated super-complexes showed a different overall shape of the C_2S_2 particles due to a different binding mode of the S-trimer to the core complex. An empty space was observed within the photosystem II supercomplex at the Lhcb4 position, implying that the missing Lhcb4 was not replaced by other Lhc subunits. This suggests that Lhcb4 is unique among photosystem II antenna proteins and determinant for photosystem II macro-organization and photoprotection.

INTRODUCTION

Oxygenic photosynthesis is performed in the chloroplast by a series of reactions that exploits light as an energy source to fuel ATP and NADPH production for CO_2 fixation and synthesis of organic compounds. Light harvesting is the primary process in photosynthesis and consists of absorption of photons by an array of hundreds of chlorophylls (Chls) organized into photosystems. Excitons are transferred among Chls and to the reaction center (RC), where charge separation occurs. In photosystem II (PSII), electrons are transferred to the quinonic acceptor plastoquinone (PQ), leading to charge accumulation in the oxygen evolving complex and water splitting (Nelson and Ben-Shem, 2004). RC of PSII consists of the D1/D2/cytochrome *b*559 complex carrying the cofactors for electron transport, which forms, together with the nearest subunits CP43 and CP47, a core complex (Ferreira et al., 2004). Core complexes form dimers (C_2), which bind an extended system of nuclear-encoded light-harvesting proteins (Lhc), each binding Chl *a*, Chl *b*, and xanthophylls. Lhcb4 (CP29) and Lhcb5 (CP26) are located near the core and mediate the binding of a trimeric LHCII antenna complex called LHCII-S (strongly bound). These components form the basic PSII supercomplex structure, called C_2S_2 (Boekema et al., 1999), which is the major PSII form found in plants grown under high light (HL) (Morosinotto et al., 2006; Frigerio et al., 2007). Under low/moderate light, larger supercomplexes, called $C_2S_2M_2$, are formed: one additional monomeric subunit Lhcb6 (CP24) and two LHCII trimers (LHCII-M and LHCII-L, moderately and loosely bound, respectively) are accumulated to extend the light-harvesting capacity (Melis 1991; Ballottari et al., 2007). In *Arabidopsis thaliana*, single genes encode Lhcb5 (CP26) and Lhcb6 (CP24) subunits, while Lhcb4 (CP29) is encoded by three highly conserved genes. *Lhcb4.1* and *Lhcb4.2* are similarly expressed, while the level of the *Lhcb4.3* messenger is 20 times lower under control conditions (Jansson, 1999). The polypeptide encoded by *Lhcb4.3* is predicted to lack a large part of the C-terminal domain, a peculiar feature of Lhcb4.1 and Lhcb4.2 isoforms, leading to the suggestion of renaming it as Lhcb8 (Klimmek et al., 2006).

A remarkable property of the antenna system is the ability to actively regulate PSII quantum efficiency to avoid the damaging effects of excess light. Indeed, under constant moderate light conditions, the efficiency of energy conversion is high, due to photochemical reactions. On the other hand, fluctuations of light intensity/temperature/water availability may yield into the

excitation of PSII over the capacity for photochemical quenching of Chl singlet excited states (^{1}Chl*). The consequent lifetime increase enhances the probability of Chl triplet (^{3}Chl*) formation by intersystem crossing and yields into single oxygen (^{1}O$_2$) production (Melis, 1999). Since formation of ^{3}Chl* is a constitutive property of Chls (Mozzo et al., 2008), photoprotection mechanisms are activated to prevent damage and improve fitness in the ever-changing environment experienced by plants. Safety systems have evolved to either detoxify the reactive oxygen species (ROS) (Asada, 1999) or to prevent their formation (Niyogi 2000) by (1) downregulating ^{1}Chl* lifetime through the process of nonphotochemical quenching (NPQ) that dissipates excess excited states into heat (Horton 1996); (2) by quenching ^{3}Chl*; and (3) by scavenging ROS. Sustained overexcitation is counteracted by the long-term reduction of PSII antenna size (Anderson, 1986). Additional regulation is activated in limiting light conditions by transferring LHCII complexes between photosystems, which balances excitation delivery to photosystem I (PSI) and PSII (Allen, 1992; Haldrup et al., 2001).

The conservation of the different Lhcb gene products through evolution suggests each has a specific functional role, which, however, is not yet fully clarified. Two major approaches have been used to this aim: namely, the analysis of individual gene products either purified from thylakoids (Bassi et al., 1987; Caffarri et al., 2001) or recombinant (Caffarri et al., 2004; Formaggio et al., 2001) and reverse genetics, by which plants lacking one or more Lhcbs have been produced and characterized (Andersson et al., 2001; Kovács et al., 2006; de Bianchi et al., 2008; Damkjaer et al., 2009). These studies have provided evidence for differential roles of LHCII components (Lhcb1-3) with respect to monomeric subunits (Lhcb4-6). Antisense lines of *Arabidopsis* devoid of Lhcb1+2 (Ruban et al., 2003) showed a reduced fitness for plants grown in the field, while only minor differences were observed for growth rate, PSII quantum yield, photosynthetic rate, and capacity for NPQ in a controlled environment (Andersson et al., 2003). Similar considerations apply to Lhcb3, the major effect of its depletion consisting of a faster kinetic of state I to state II transitions (Damkjaer et al., 2009). More specific effects have been reported for monomeric Lhcb4 and Lhcb5, which have been shown to (1) carry protonatable (DCCD binding) sites (Pesaresi et al., 1997; Walters et al., 1996); and (2) undergo conformation changes upon exchange of violaxanthin (Viola) to zeaxanthin (Zea) in their L2 xanthophyll binding site (Morosinotto et al., 2002), an important feature since Zea is synthesized in excess light conditions and correlates with NPQ (Demmig-Adams et al., 1989). The Zea-dependent allosteric change was shown to affect the properties of these pigment proteins, including a decrease in fluorescence lifetime (Crimi et al., 2001; Moya et al., 2001) and formation of carotenoid radical cations (Ahn et al., 2008; Avenson et al., 2008), suggesting a major role in NPQ. Consistently, *koLhcb6* plants exhibited decreased qE (Kovács et al., 2006; de Bianchi et al., 2008), while *koLhcb5* plants were affected in the slower relaxing component of NPQ called qI. Other properties of Lhcb proteins, which are essential for photoprotection, appear to be redundant. In fact, while the total depletion of Lhcb proteins induces photosensitivity in *ch1* mutants (Kim et al., 2009; Dall'Osto et al., 2010), no individual knockout (KO) lines have shown major impairment in

their capacity to resist HL treatment so far (Ruban et al., 2003; de Bianchi et al., 2008). Lhcb4 antisense lines showed NPQ kinetics and amplitude, photosynthetic electron transport rate, and light sensitivity similar to that of the wild type (Andersson et al., 2001). However, since this work only employed growth in mild conditions, the question is open for the role of Lhcb4 in photoprotection. Indeed, the maintenance of Lhcb4, in HL stress conditions that leads to the reduction of Lhcb6 and LHCII (Ballottari et al., 2007), suggests that Lhcb4 might be a key factor in light harvesting and photoprotection. Lhcb4 phosphorylation in both monocots (Testi et al., 1996) and dicots (Hansson and Vener, 2003; Tikkanen et al., 2006) affects the spectral properties of the protein (Croce et al., 1996) and correlates with higher resistance to HL and cold (Bergantino et al., 1995; Mauro et al., 1997) and water stress (Liu et al., 2009). Although the mechanism of this protective effect is unknown, there is evidence for a link between Lhcb4 and NPQ, since the protein has been identified as an interaction partner of PsbS (Teardo et al., 2007), the pH-dependent trigger of qE (Li et al., 2000), and it is part of a pentameric complex whose dissociation is indispensable for the establishment of NPQ (Betterle et al., 2009). Finally, two Chl ligands in Lhcb4 have been identified as components of the quenching site, which catalyzes the formation of a xanthophyll radical cation (Holt et al., 2005; Avenson et al., 2008).

In this work, we constructed KO mutants for Lhcb4 isoforms in *Arabidopsis* and analyzed their performance in photosynthesis and photoprotection. PSII quantum efficiency and capacity for NPQ were affected by lack of Lhcb4, and, unlike that of any other Lhcb subunit, the capacity of resisting excess light conditions was affected. Although depletion of Lhcb subunits is usually complemented by the overaccumulation of other members of the subfamily (Ruban et al., 2003; de Bianchi et al., 2008), this is not the case for Lhcb4 and PSII supercomplexes isolated from *koLhcb4* that although they retained their C$_2$S$_2$ organization, they lacked Lhcb4. This caused a different mode of binding of LHCII-S trimer within the PSII supercomplex and changed the overall shape of the C$_2$S$_2$ particle. Deletion of either Lhcb4.1 or Lhcb4.2 yielded into a compensatory accumulation of the remaining subunit; instead, the double mutant *koLhcb4.1 4.2* was unable to accumulate Lhcb4.3. We conclude that Lhcb4 is a fundamental component of PSII, which is essential for maintenance of both the function and structural organization of this photosystem.

RESULTS

The construction of a plant without a CP29 complex (hereafter named *koLhcb4*) requires the isolation of KO mutants at three distinct loci, namely, *Lhcb4.1*, *Lhcb4.2*, and *Lhcb4.3* (Jansson, 1999). We identified *koLhcb4.1*, *koLhcb4.2*, and *koLhcb4.3* homozygous plants in T-DNA F5 seed pools, obtained from the European Arabidopsis Stock Centre (NASC), by PCR analysis of genomic DNA using specific primers (Figure 1A). The triple KO mutant *koLhcb4* was obtained by selection of the progeny from crossing single mutants. PCR analysis confirmed that all Lhcb4 coding regions carried a T-DNA insertion in both alleles (Figure 1A), while RT-PCR showed that mRNAs encoding Lhcb4 isoforms were absent in the mutant (Figure 1B).
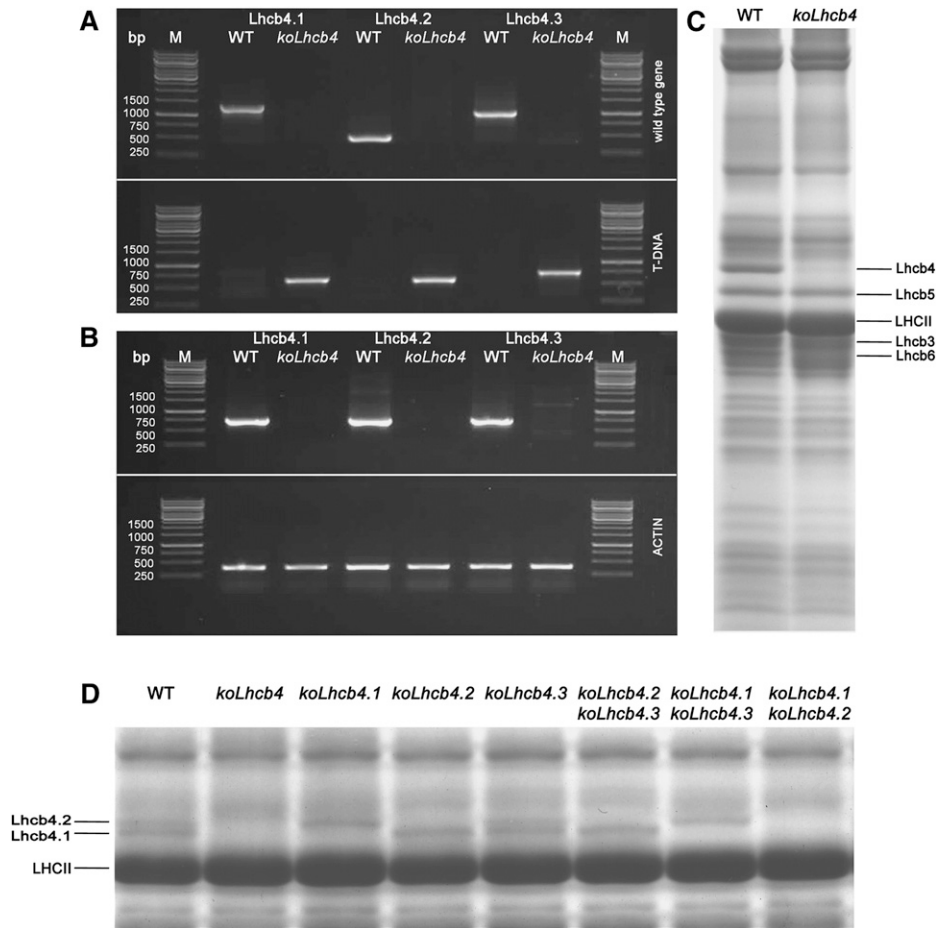
Figure 1. Genetic and Biochemical Characterization of the *koLhcb4* Mutant (Triple Mutant for the Three Isoforms of Lhcb4).

(A) Amplification of *Lhcb4.1*, *Lhcb4.2*, and *Lhcb4.3* loci with allele-specific PCR primers. Top panel: amplification using gene-specific primers. Bands of 1378, 520, and 1046 bp were obtained for the amplification of the *Lhcb4.1*, *Lhcb4.2*, and *Lhcb4.3* loci, respectively. Bottom panel: amplification using T-DNA–specific primers. Bands of 685, 661, and 773 bp were obtained for the amplification of *Lhcb4.1*, *Lhcb4.2*, and *Lhcb4.3* KO loci, respectively. Details of primer sequences are reported in Methods. WT, wild type.

(B) RT-PCR measurement of gene-specific transcripts. Sequences of the oligonucleotides used are reported in Methods. Top panel: for each gene, RNA extracted from the wild type and the corresponding mutant was subjected to reverse transcription, followed by 30 cycles of PCR amplification. Bottom panel: amplification of the housekeeping gene actin2 transcript from the same RNAs used as loading control. M, molecular weight marker. The expected sizes of the PCR products are as follows: Lhcb4.1, 724 bp; Lhcb4.2, 715 bp; Lhcb4.3, 730 bp; and actin, 384 bp. Each RT-PCR measurement was repeated three times.

(C) SDS-PAGE analysis of wild-type and *koLhcb4* mutant thylakoid proteins performed with the Tris-Tricine buffer system (Schägger and von Jagow, 1987). Selected apoprotein bands are marked. Purified thylakoid sample, corresponding to 15 μg of chlorophylls, was loaded in each lane.

(D) SDS-PAGE analysis performed with the Tris-Tricine buffer system with the addition of 7 M urea to the running gel in order to separate Lhcb4 isoforms in the *Lhcb4* KO mutants. Selected apoprotein bands are marked. Fifteen micrograms of chlorophylls were loaded in each lane.

During the course of this work, two additional lines (N124926 and SK32480) with a T-DNA insertion mapped to the *Lhcb4.1* and *Lhcb4.2* genes, respectively, became available. Both lacked the corresponding protein. The lines showed very similar phenotypic characteristics to N376476 (*koLhcb4.1*) and N877954 (*koLhcb4.2*), respectively. Below, we present data from the N376476 and N877954 lines, unless otherwise stated.

By screening the F2 generation, it was possible to isolate double mutants expressing single Lhcb4 isoforms, namely, *koLhcb4.2 4.3* (retaining Lhcb4.1), *koLhcb4.1 4.3* (retaining Lhcb4.2), and *koLhcb4.1 4.2* (retaining Lhcb4.3). All of the isolated genotypes did not show a significant reduction in growth with respect to the wild type under control light conditions (100 μmol photons m^{-2} s^{-1}, 24°C, 8/16 day/night). Electron microscopy analysis of plastids from mesophyll cells of the wild type and mutants was performed to test if the thylakoid structure was changed as an effect of the missing Lhcb (see Supplemental Figure 1 online). All the mutants showed a membrane organization similar to that of wild-type chloroplasts with well-defined grana, containing approximately six discs per granum, as well as

similar amounts of grana, stroma lamellae, and end membranes per plastid (see Supplemental Table 1 online).

Thylakoid membranes isolated from the *koLhcb4* mutant lacked the corresponding gene product (Figure 1C). A better resolution in the 22 to 35 kD molecular mass range was obtained using a gel incorporating 7 M urea, which split Lhcb4 into a doublet in wild-type thylakoids, the upper band corresponding to Lhcb4.2 as shown by comparison with the pattern from double KO genotypes (Figure 1D). The gel without urea (Figure 1C) revealed that an additional band with lower molecular mass was also missing, which corresponded to Lhcb6, as revealed by immunoblotting (Figures 2A and 2B). The pigment content of the *koLhcb4* mutant did not differ from the wild type in either chlorophyll content per leaf area or Chl/Car ratio but showed a significant decrease in the Chl *a*/Chl *b* ratio (Table 1).

To determine whether the capacity of the antenna system and its ability to transfer absorbed energy to RCs was affected by the mutation, the functional antenna size of PSII was measured on thylakoids by estimating the rise time of chlorophyll florescence in the presence of DCMU and nigericin. No significant differences were observed in $t_{2/3}$ F_{max} (see Methods for details) between *koLhcb4* and the wild type (Table 1; see Supplemental Figure 2 online), suggesting that Lhcb4 depletion did not impair the overall light-harvesting capacity. Analysis of the fluorescence induction in dark-adapted leaves (Butler and Strasser, 1978) revealed a higher F_0 value and a significant decrease of maximum quantum efficiency of PSII (F_v/F_m) in *koLhcb4* with respect to the wild type. Thus, a larger fraction of absorbed energy is lost as fluorescence in the mutant, implying that the connection between the major LHCII complex and PSII RC is less efficient in the absence of Lhcb4 (Table 1). Nevertheless, parameter S_m/t_{Fmax}, which is used for quantifying PSII electron transport (ET) activity, was essentially the same in *koLhcb4* and the wild type, suggesting that ET was not limited downstream from Q_A^- in mutant leaves.
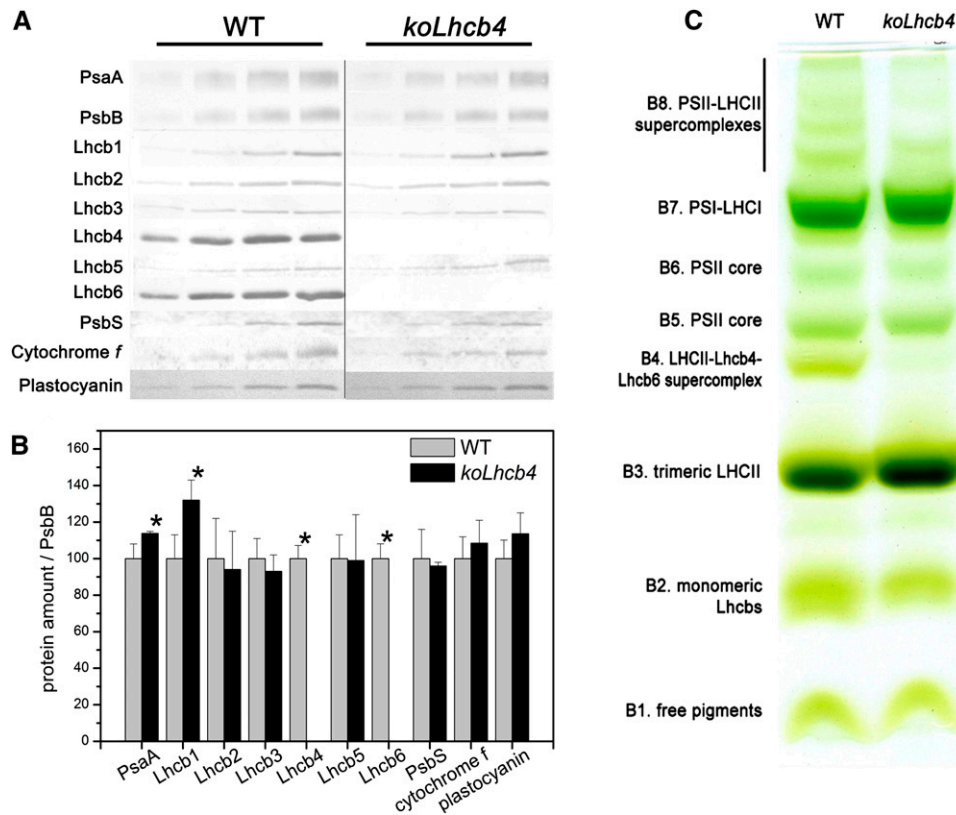
Figure 2. Polypeptide Composition of Thylakoid Membranes from Wild-Type and *koLhcb4* Mutant.

(A) Immunoblotting used for the quantification of photosynthetic subunits in the wild type (WT) and *koLhcb4* thylakoids. Immunoblot analysis was performed with antibodies directed against individual gene products: minor antenna proteins, the LHCII subunit, the PSII core subunit PsbB (CP47), the PSI core subunit (PsaA), cytochrome *f*, and plastocyanin. Thylakoids corresponding to 0.25, 0.5, 0.75, and 1 µg of chlorophyll were loaded for each sample. All samples were loaded on the same SDS-PAGE slab gel.
(B) Results of the immunotitration of thylakoid proteins. Data of PSII antenna subunits were normalized to the core amount, PsbB content (Ballottari et al., 2007), and expressed as a percentage of the corresponding wild-type content. Significantly different values from wild-type membranes are marked with an asterisk.
(C) Thylakoid pigment-protein complexes were separated by nondenaturing Deriphat-PAGE upon solubilization with α-DM. Thylakoids corresponding to 25 µg of chlorophylls were loaded in each lane.
[See online article for color version of this figure.]

Table 1. Chlorophyll Content and Fluorescence Induction Parameters Determined for Leaves of *Arabidopsis* Wild-Type and *koLhcb4* Plants and Mutants Retaining a Single Lhcb4 Isoform

Genotype	Chl a/b	Chl/Car	μg Chl/cm^2	F_o	Fv/Fm	$t_{2/3}$ (ms)	S_m/t_{Fmax} (ms^{-1})
Wild type	3.06 $\pm$ 0.07	3.63 $\pm$ 0.08	20.7 $\pm$ 3.0	0.195 $\pm$ 0.002	0.790 $\pm$ 0.007	182 $\pm$ 6	1.2 $\pm$ 0.1
koLhcb4	2.83 $\pm$ 0.06*	3.58 $\pm$ 0.03	19.0 $\pm$ 1.1	0.253 $\pm$ 0.021*	0.747 $\pm$ 0.021*	176 $\pm$ 8	1.5 $\pm$ 0.3
koLhcb4.2 4.3	2.97 $\pm$ 0.03	3.70 $\pm$ 0.13	22.5 $\pm$ 1.2	0.213 $\pm$ 0.012	0.796 $\pm$ 0.004	182 $\pm$ 5	1.1 $\pm$ 0.4
koLhcb4.1 4.3	2.97 $\pm$ 0.03	3.61 $\pm$ 0.09	22.6 $\pm$ 4.5	0.231 $\pm$ 0.012*	0.777 $\pm$ 0.007*	175 $\pm$ 11	1.6 $\pm$ 0.1
koLhcb4.1 4.2	2.83 $\pm$ 0.09*	3.63 $\pm$ 0.08	22.9 $\pm$ 2.5	0.266 $\pm$ 0.004*	0.745 $\pm$ 0.007*	184 $\pm$ 6	1.4 $\pm$ 0.2

Data are expressed as mean $\pm$ SD ($n > 5$); significantly different values (Student's *t* test, P = 0.05) with respect to the wild type are marked with an asterisk.

Organization and Stoichiometry of Pigment-Protein Complexes

The organization of pigment binding complexes was analyzed by nondenaturing Deriphat-PAGE upon solubilization of wild-type and *koLhcb4* thylakoid membranes with 0.7% dodecyl-α-D-maltoside (α-DM). Seven major green bands were resolved (Figure 2C). In the wild type, the PSI-LHCI complex was found as a major band (B7) in the upper part of the gel, while the components of the PSII-LHCII migrated as multiple green bands with different apparent masses, namely, the PSII core dimer and monomer (B6 and B5, respectively) and the antenna moieties, including the Lhcb4-Lhcb6-LHCII-M supercomplex (B4), LHCII trimer (B3), and monomeric Lhcbs (B2). Four faint green bands with high apparent molecular mass, which contained undissociated PSII supercomplexes of different LHCII composition, were detected in the upper part of the gel (B8). The major differences detected in *koLhcb4* with respect to the wild type were the lack of B4 and a reduced level of PSII supercomplexes. Densitometric analysis of the Deriphat-PAGE showed a higher PSI/PSII ratio in the *koLhcb4* mutant (1.38 $\pm$ 0.11) with respect to the wild type (1.04 $\pm$ 0.03).

To detect possible alterations in the relative amount of protein components of the photosynthetic apparatus, we determined the stoichiometry of several subunits by immunoblotting titration using CP47 (PsbB) as an internal standard (Ballottari et al., 2007). *KoLhcb4* plants lacked both Lhcb4 and Lhcb6 proteins (Figure 2A), while there was a 30% increase in Lhcb1 (Figure 2B) with respect to the wild-type level. The other pigment-protein complexes, as well as cytochrome (cyt) *f* and plastocyanin, were present in wild-type amounts. A slight but significant increase in PsaA content in *koLhcb4* compared with the wild type (Figure 2A) was detected.

We also analyzed the Lhc protein composition in double mutants expressing individual Lhcb4 isoforms (Figure 1D; see Supplemental Table 2 and Supplemental Figure 3 online). The *koLhcb4.2 4.3* mutant retained 87% of wild-type Lhcb4 levels, while *koLhcb4.1 4.3* had a significantly lower amount of Lhcb4 (59%) with respect to the wild type (see Supplemental Table 2 online). The *koLhcb4.1 4.2* mutant did not show any band with mobility similar to Lhcb4.1 and Lhcb4.2 (Figure 1D). Nevertheless, the *Lhcb4.3* gene product is expected to have a molecular mass significantly lower than the 0.1 and 0.2 isoforms. Therefore, we cannot exclude that it migrates together with the bulky LHCII band. Immunoblotting analysis also revealed that the level of

Lhcb6 polypeptide underwent changes in agreement with the amounts of Lhcb4.1 + Lhcb4.2 protein. In the *koLhcb4.1 4.2* mutant, Lhcb6 was not detectable (see Supplemental Table 2 online).

Photosynthesis-Related Functions: ET Rate, State Transition, and P700 Redox State

Since pigment-protein complexes participate in modulating ET between photosystems, PSII and PSI function during photosynthesis was further analyzed by chlorophyll fluorometry. *KoLhcb4* showed no significant differences with respect to wild-type plants either in the linear electron flow (LEF) or in the Q_A redox state (qL), as measured at different light intensities in the presence of saturating CO_2 on leaves (Figures 3A and 3B), thus indicating no limitations in photosynthesis downstream of PSII. This was further confirmed by measuring rates of O_2 evolution in CO_2-saturating conditions: no significant reduction in the quantum yield of photosynthesis was observed in *koLhcb4* versus wild-type plants at any of the light intensities used (Figure 3C).

The capacity for state transitions (Allen, 1992) was measured from the changes in chlorophyll fluorescence on leaves (Jensen et al., 2000). The final amplitude of the state transitions (qT) after a 15-min illumination was the same in both genotypes (0.091 $\pm$ 0.002 and 0.091 $\pm$ 0.006, respectively, in the wild type versus *koLhcb4*) (Figures 3D and 3E). However, the kinetic of the transition from state I to state II upon switching off far-red light was 3 times faster in *koLhcb4* (half-time = 71 $\pm$ 5 s) with respect to the wild type (half-time = 204 $\pm$ 17 s) (Figures 3D and 3E). Furthermore, it was observed that the switching on of far-red light produced a sudden decrease of fluorescence intensity in the wild type but not in *koLhcb4*. In fact, fluorescence level in the latter was already very low, consistent with a faster reoxidation of the PQ pool in *koLhcb4* with respect to the wild type under low-intensity blue light.

Fluorescence induction analysis on intact leaves showed a F_0 value up to 40% higher in *koLhcb4* versus the wild type, implying the absence of Lhcb4 caused a lower efficiency in energy transfer between LHCII and PSII RC (Table 1). Photosynthetic electron flow through PSI during steady state photosynthesis in vivo was measured from the dependence of the P700$^+$/total P700 ratio on intensity of PSI+PSII light (λ = 630 nm; Figure 3F). In the wild type, this value approached saturation level at >1000 μmol photons m^{-2} s^{-1}. In *koLhcb4*, the saturation was observed already at 600 μmol photons m^{-2} s^{-1}, which implies a higher
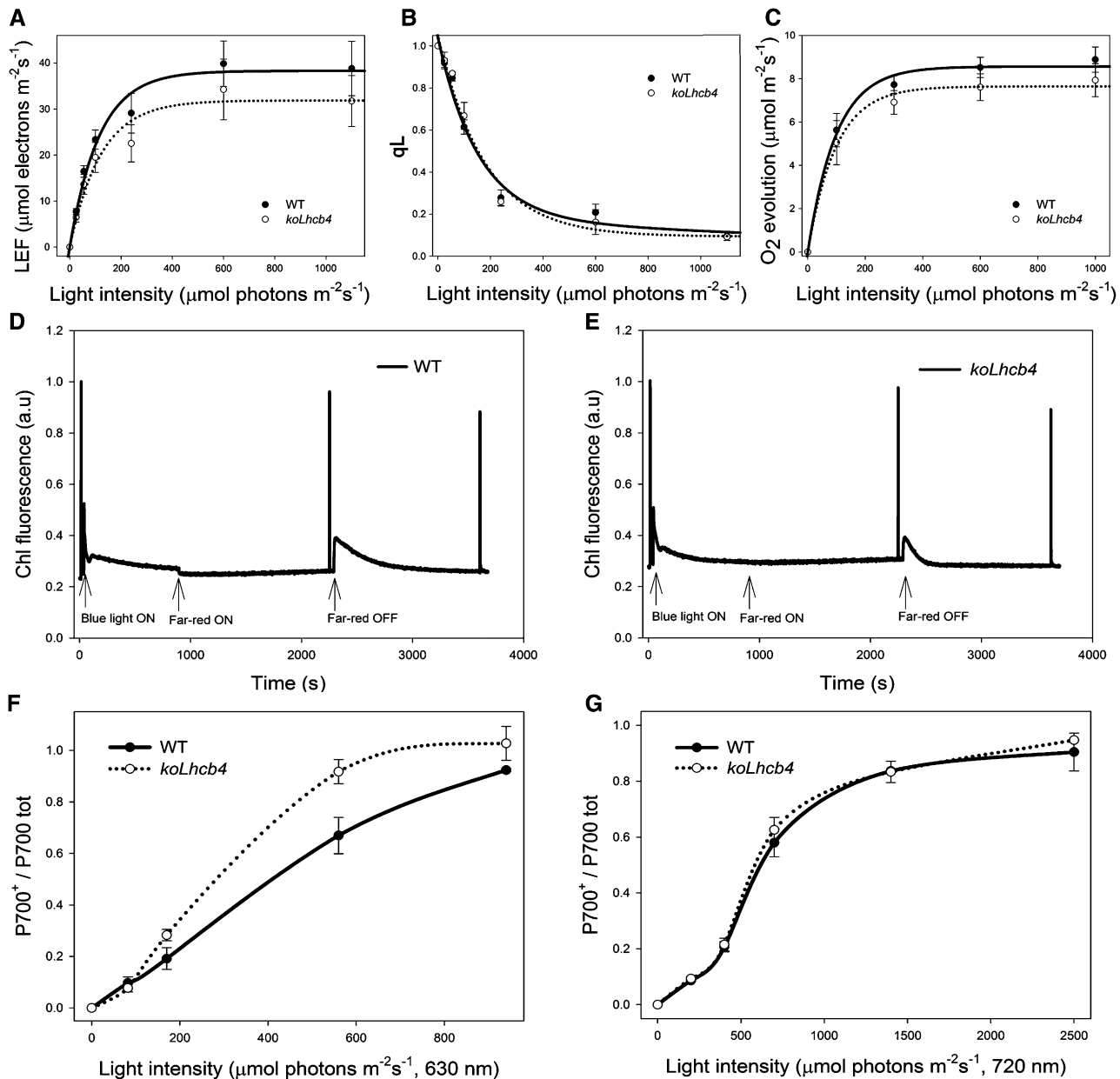
Figure 3. Characterization of Photosynthetic Electron Flow in Wild-Type and *koLhcb4* Plants.

(A) Dependence of the LEF rate on light intensity in wild-type (WT) and *koLhcb4* leaves. LEF rate is calculated as $\phi_{PSII} \cdot PAR \cdot A_{leaf} \cdot fraction_{PSII}$ (see Methods for details).

(B) Photosynthetic oxygen evolution in saturating CO_2. Rate of oxygen evolution was measured on whole leaves during illumination with various levels of actinic red light.

(C) Amplitude of qL measured at different light intensities on wild-type and *koLhcb4* leaves. qL reflects the redox state of the primary electron acceptor Q_A, thus, the fraction of open PSII centers.

(D) and **(E)** Measurement of state I–state II transition in the wild type **(D)** and *koLhcb4* **(E)**. Upon 1-h dark adaptation, plants were illuminated with blue light (40 μmol photons m^{-2} s^{-1}, wavelength <500 nm) for 15 min to reach state II. A far-red light source was then superimposed on the blue light to induce a transition to state I. Values of F_m, F_m', and F_m'' were determined using light saturation pulses (4500 μmol photons m^{-2} s^{-1}, 0.6 s). a.u., arbitrary units.

(F) and **(G)** Dependence of the P700 oxidation ratio ($\Delta A/\Delta A_{max}$) on light intensity. $\Delta A/\Delta A_{max}$ was measured on wild-type and *koLhcb4* leaves at varying actinic intensities, exciting either PSII + PSI ($\lambda = 630$ nm; **[F]**) or PSI only ($\lambda = 730$ nm; **[G]**).

functional antenna size of PSI in mutant leaves. To investigate the origin of this difference, cyclic electron flow (CEF) was determined by following (1) the rereduction of P700$^+$ at 705 nm, upon far-red saturating flashes, on leaves infiltrated with DCMU (see Supplemental Figure 4A online) and (2) the relationship between LEF and the steady state proton flux across the thylakoid membrane (v_{H+}; see Supplemental Figure 4B online). The fast decay component of P700$^+$, which has been attributed to CEF, was the same in both the wild type and *koLhcb4*, as well as the dependence of v_{H+} to LEF. Redox kinetics of cyt b_6 reduction and of cyt f oxidation (see Supplemental Figure 4C online) confirmed that both PQ diffusion and cyt b_6f activities were not significantly affected in *koLhcb4* plants, thus ruling out the possibility that less efficient diffusion of PQ or plastocyanin, or altered activities of the cyt b_6f complex, could account for the faster P700 oxidation. Analysis of the functional antenna size of PSI, measured by the rate coefficient of P700 oxidation in steady far-red light following a saturating flash, did not reveal any difference between the two genotypes (see Supplemental Figure 4D online). To further investigate this point, P700 redox state was measured using PSI light (actinic far red, $\lambda = 720$ nm) rather than PSI+PSII light. The difference in P700 oxidation rate between wild-type and mutant leaves disappeared once measured with far-red light (Figure 3G), implying that PSII components contribute to increase PSI antenna size in *koLhcb4*. To verify this suggestion, we investigated the distribution of Chl b and Chl a absorption forms contributing to PSI and PSII excitation by 77K chlorophyll fluorescence spectroscopy. Wild-type and *koLkcb4* leaves were either dark adapted or illuminated for 5 min (500 μmol photons m^{-2} s^{-1}, room temperature), upon which they where rapidly frozen in liquid nitrogen and grounded in a cooled mortar, diluted to 0.05 absorption units with cold buffer containing 5 mM Mg^{2+}, and finally frozen to 77K. Supplemental Figure 5A online shows the emission spectra from dark-adapted versus light-treated wild-type samples. A small increase in the amplitude of the 685-nm emission peak, from PSII versus the 735-nm peak from PSI was obtained upon illumination, a behavior likely due to a completion of the transition to state I. Illumination of *koLhcb4* leaves, instead, yielded an opposite effect, with a decreased amplitude of the PSII emission peak (see Supplemental Figure 5B online). Consistently, excitation spectra for the PSI emission (735 nm) clearly show that, while the Chl b contribution is essentially the same in dark- versus light-treated wild type, it is increased in the mutant, implying an enhanced LHCII contribution to PSI (see Supplemental Figures 5C and 5D online).

NPQ of Chlorophyll Fluorescence

Thermal energy dissipation is a major photoprotection mechanism in plants. Although a quenching component has been localized in PSII core (Finazzi et al., 2004), most quenching activity was associated to the antenna system (Horton and Ruban, 2005; Havaux et al., 2007). In a previous work (Betterle et al., 2009), we observed that the *koLhcb4* mutant, among other KO mutants for Lhcb genes, cannot assemble the CP29-CP24-LHCII complex (B4C), whose dissociation is essential for triggering of NPQ. Here, we focus on the elucidation of the mechanistic role of Lhcb4 in NPQ and photoprotection. The NPQ activity of *koLhcb4* plants is

shown in Figure 4A. Upon exposure of the wild type to saturating light intensity (1200 μmol photons m^{-2} s^{-1}, 24°C), NPQ showed a rapid rise to 1.4 in the first minute followed by a slower raise, reaching a value of 2.3 after 8 min. Induction of NPQ in *koLhcb4* was slower (0.7 at t = 1 min) and reached a lower amplitude (1.6 at t = 8 min). Recovery in the dark was faster and wider in *koLhcb4* compared with the wild type (Figure 4A), as previously shown (Betterle et al., 2009). NPQ activity of *koLhcb4* reached the wild-type level upon longer light treatment (25 min). When a second illumination period was applied (Figure 4B), the delay in NPQ rise was reduced, while dark recovery was still faster in *koLhcb4*. It should be noted that Zea synthesis had the same kinetic in the wild type and *koLhcb4* (Figure 4C), implying that the delayed NPQ onset was not due to a delayed Zea synthesis.

We also investigated whether the three Lhcb4 isoforms had the same activity in NPQ by analyzing the kinetic of NPQ rise in double mutants retaining one single *Lhcb4* gene. The results reported in Figure 4D show that mutants conserving the *Lhcb4.1* gene had slightly faster onset of NPQ than the wild type, while those retaining *Lhcb4.2* gene were unable to reach the final NPQ level of wild-type plants. Mutant plants retaining only *Lhcb4.3* behaved like *koLhcb4*. The faster fluorescence recovery observed in *koLhcb4* compared with the wild type is present in the mutants retaining only *Lhcb4.2* or *Lhcb4.3* genes, whereas mutant retaining *Lhcb4.1* recovered with the slower wild-type kinetic.

Photosensitivity under Short- and Long-Term Stress Conditions

Treatment of plants with strong light produces photoxidative stress, whose severity is enhanced by low temperature. Under these conditions, enhanced release of $^1O_2$ leads to bleaching of pigments, lipid oxidation, and PSII photoinhibition, which is accompanied by a decrease in F_v/F_m (Zhang and Scheller, 2004). The sensitivity to photoxidative stress of wild-type and Lhcb4-depleted plants was assessed upon transfer from control conditions to HL + low temperature (500 μmol photons m^{-2} s^{-1}, 4°C). The level of F_v/F_m was monitored for 2 d (Figure 5A). In wild-type plants, the F_v/F_m parameter gradually decreased from 0.8 to 0.35 during the treatment, while in *koLhcb4* plants, the decrease was stronger, reaching a value of 0.15 at the end of the treatment. As a reference, we compared the photosensitivity of different antenna mutants, namely, *koLhcb5/Lhcb6*, *koLhcb3*, and LHCII antisense plants (asLHCII). Interestingly, mutants lacking antenna components other than Lhcb4 showed the same level of photoinhibition as wild-type plants, implying that Lhcb4 is the only antenna component indispensable for full level of photoprotection under photoxidative stress (Figure 5A). Measurements of F_v/F_m recovery after photoinhibitory treatment (see Supplemental Figure 6 online) clearly showed that wild-type and *koLhcb4* leaves had the same capacity of PSII quantum efficiency recovery, implying that a higher photosensitivity of mutant plants is due to a less effective photoprotection rather than to impaired PSII repair mechanism (Aro et al., 1994). Loss of Lhcb4 caused a decrease in PSII quantum yield (Figure 5A) that could be caused either by damage of the PSII core complex or by an incomplete excitation transfer to PSII
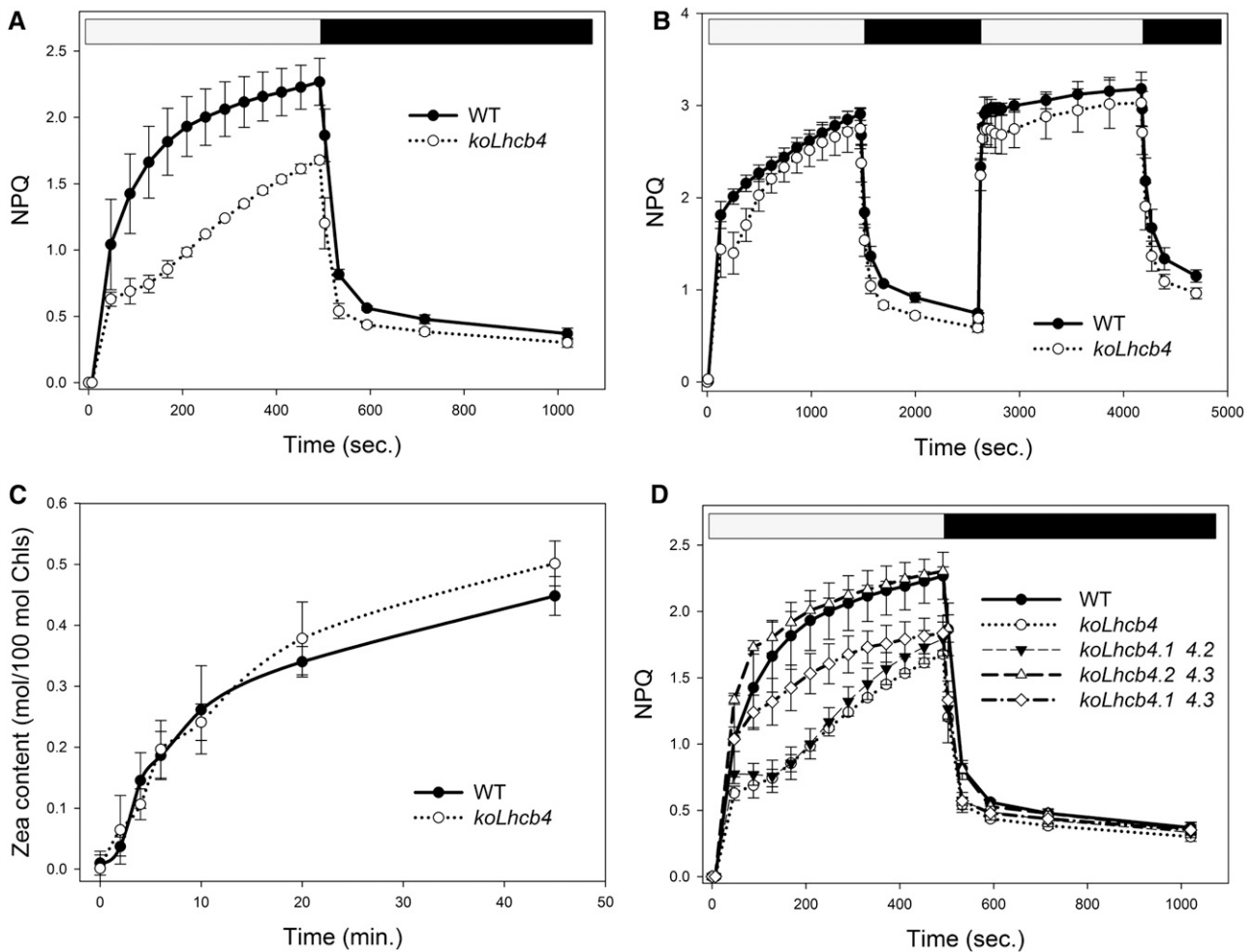
Figure 4. Kinetics of the Formation and Relaxation of Photoprotective Energy Dissipation.

(A) Measurements of NPQ kinetics on wild-type (WT) and *koLhcb4* leaves illuminated with 1200 μmol photons m^{-2} s^{-1}, 24°C.

(B) NPQ kinetics of wild-type and *koLhcb4* plants during two consecutive periods of illumination with white light (1200 μmol photons m^{-2} s^{-1}, 25 min, 24°C) with an 18-min period of darkness in between, as indicated by the white and black bars.

(C) Time course of Viola deepoxidation in wild-type and *koLhcb4* plants. Leaf discs from dark-adapted leaves were illuminated at 1200 μmol photons m^{-2} s^{-1}, 24°C (white actinic light). At different times, discs were frozen in liquid nitrogen and total pigments extracted before HPLC analysis.

(D) NPQ kinetics of the wild type, *koLhcb4*, and mutants retaining single Lhcb4 isoforms. The expression of the isoform Lhcb4.1 (*koLhcb4.2 4.3*) leads to complete compensation of the NPQ phenotype of *koLhcb4*; instead, the expression of the Lhcb4.2 isoform partially recovered the quenching ability in the first minutes of induction; nevertheless the mutant failed to fully match the wild type quenching capacity within 8 min of illumination. The presence of the *Lhcb4.3* gene did not contribute to NPQ activity. Symbols and error bars show means ± SD ($n > 3$).

RC. To provide a more complete characterization of the photodamage, leaf discs from the wild type and *koLhcb4* were submitted to HL + cold stress (1500 μmol photons m^{-2} s^{-1}, 4°C) and the time course of pigment photobleaching and lipid peroxidation was measured (Figures 5B and 5C). Analysis indicates that chlorophyll bleaching was faster and malondialdehyde (MDA) production was higher in *koLhcb4* with respect to wild-type leaves, implying a higher level of lipid peroxidation (Havaux et al., 2005). Photodamage can be caused by the production of ROS, including singlet oxygen ($^1O_2$) (Triantaphylidès et al., 2008). To identify if this species was involved in the

preferential photodamage of *koLhcb4*, we quantified production of $^1O_2$ directly in wild-type and *koLhcb4* leaves using vacuum-infiltrated $^1O_2$-specific probe (see Methods for details). After illumination with strong light at 4°C, *koLhcb4* leaves clearly showed a significantly higher release of singlet oxygen compared with the wild type (Figure 5D).

An interesting question is whether the different Lhcb4 isoforms have a specific importance in photoprotection. We measured the level of PSII photoinhibition on KO mutants retaining individual *Lhcb4* genes. Plants retaining either *Lhcb4.1* or *Lhcb4.2* showed a wild-type level of resistance to HL + cold stress, while those
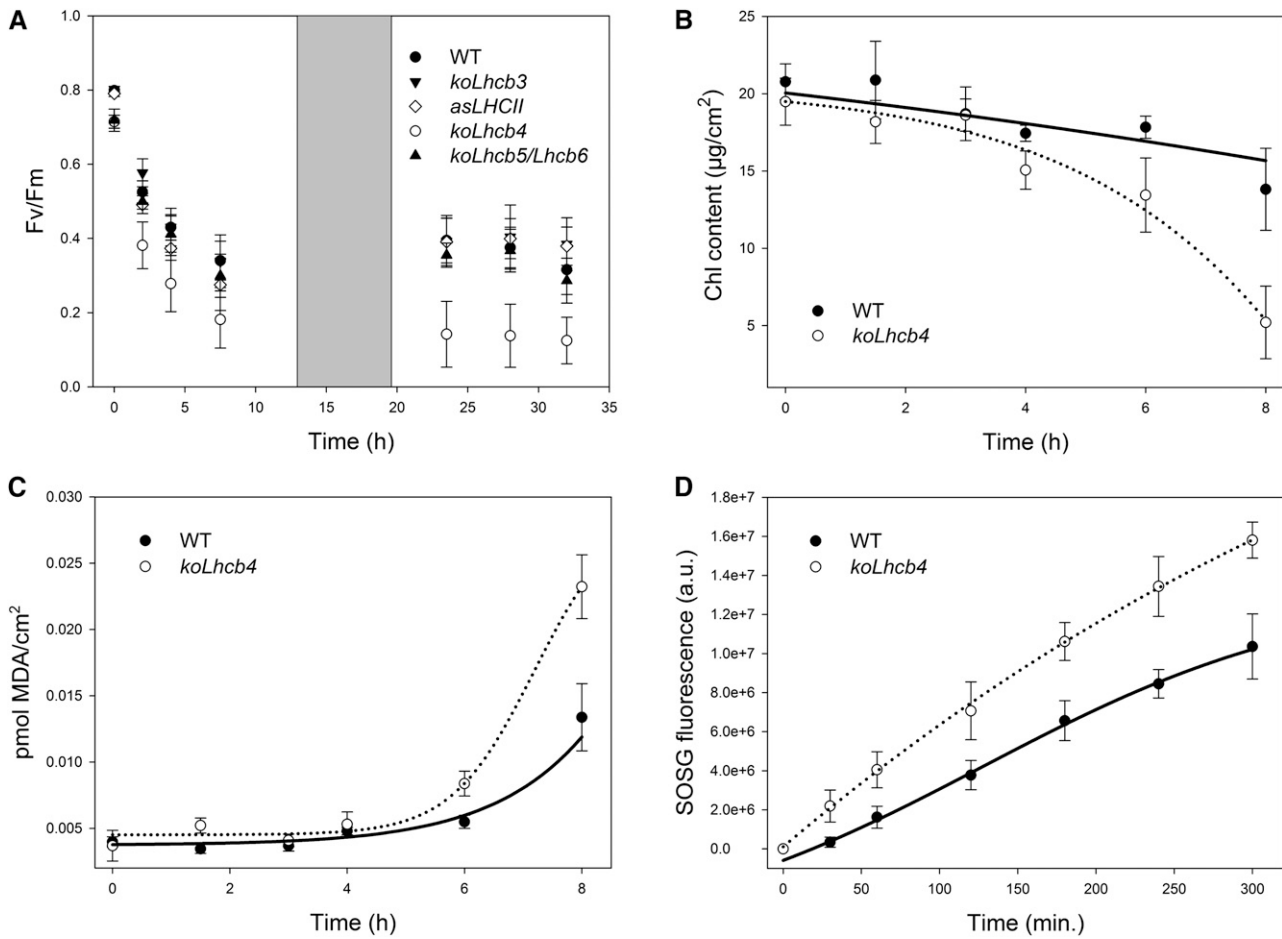
Figure 5. Photooxidation of *Arabidopsis* Wild Type and *koLhcb4* Mutant Exposed to HL and Low Temperature.

(A) PSII photoinhibition (F_v/F_m decay) was followed in the wild type (WT), *koLhcb4*, and antenna-depleted mutant (*koLhcb5 Lhcb6*, *koLhcb3*, and LHCII antisense) plants, treated at 550 μmol photons m^{-2} s^{-1}, 4°C for 30 h with a 6-h period of low light (20 μmol photons m^{-2} s^{-1}) between the 12 h of HL stress; low-light interval permitted the PSII efficiency recovery.

(B) and **(C)** Detached leaves floating on water were treated at 1500 μmol photons m^{-2} s^{-1} at 4°C, and kinetics of chlorophyll bleaching **(B)** and MDA formation **(C)** were recorded.

(D) Wild-type and mutant detached leaves were vacuum infiltrated with 5 μM SOSG, a $^1O_2$-specific fluorogenic probe. SOSG increases its fluorescence emission upon reaction with singlet oxygen. The increase in the probe emission was followed with a fiber optic on the leaf surface during illumination with red actinic light (550 μmol photons m^{-2} s^{-1}) at 4°C. a.u., arbitrary units.

retaining the *Lhcb4.3* gene (*koLhcb4.1 4.2* mutant) were similar to *koLhcb4* (Figure 6). More detailed analysis was performed after 3 and 8 d of treatment by determining the leaf chlorophyll content, a target of photoxidative stress. Mutants *koLhcb4* and *koLhcb4.1 4.2* underwent a significant reduction of leaf chlorophyll content (Table 2), while mutants retaining either Lhcb4.1 or 4.2 did not show this effect. This indicates that a compensatory accumulation of Lhcb4.1 or 4.2 isoforms can restore photoprotection to the wild-type level. Interestingly, the presence of wild-type alleles of Lhcb4.3 as the only Lhcb4 isoform did not restore photoprotection, thus prompting us to get further insight into the Lhcb4.3 expression. We investigated accumulation of the Lhcb4.3 isoform upon several stress conditions, namely, (1) 500 μmol photons m^{-2} s^{-1}, 4°C for 2 d; (2) 900 μmol photons

m^{-2} s^{-1}, 4°C for 10 d; and (3) 1600 μmol photons m^{-2} s^{-1}, 24°C for 10 d. At the end of these treatments, thylakoids were isolated from the wild type, *koLhcb4*, and *koLhcb4.1/4.2* and analyzed by SDS-PAGE/immunoblotting using a polyclonal antibody. Under all experimental conditions, no Lhcb4 immune-reactive bands were detected in the *koLhcb4.1 4.2* sample from all the tested conditions. In order to verify that our antibody was indeed able to detect Lhcb4.3, the three recombinant apoproteins were assayed by the anti-Lhcb4 antibody and were recognized with the same efficiency (see Supplemental Figure 7 online). Based on these experiments, we conclude that plants retaining the *Lhcb4.3* gene only were unable to accumulate the encoded protein to a significant level in the conditions explored in this work.
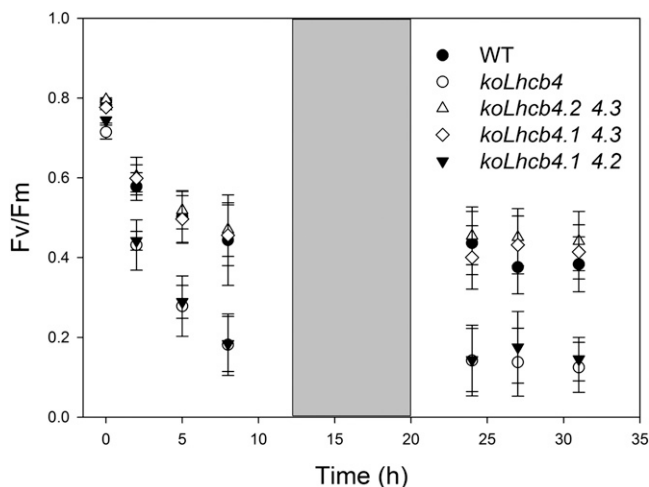
Figure 6. Photoinhibition of the Wild Type and Mutants Retaining a Single Lhcb4 Isoform Exposed to HL and Low Temperature.

Kinetics of F_v/F_m decay were measured on the wild type (WT), *koLhcb4*, *koLhcb4.1 4.2*, *koLhcb4.1 4.3*, and *koLhcb4.2 4.3*. Whole plants were treated as described for Figure 5A.

Role of the Zea–Lhcb4 Interaction in Long-Term Membrane Lipid Photoprotection

Earlier work has shown that Lhcb4 exchanges Viola with Zea both in vitro (Bassi et al., 1997; Morosinotto et al., 2002) and in vivo upon HL treatment (Bassi et al., 1993), which leads to an increased activity of several photoprotection mechanisms, including ROS scavenging, improved Chl triplet quenching (Mozzo et al., 2008), and formation of carotenoid radical cations (Holt et al., 2005; Avenson et al., 2008). In order to investigate the role of Zea on Lhcb4-dependent photoprotection, *koLhcb4* was crossed with *npq1* and selected a genotype lacking both the capacity of producing Zea and Lhcb4. The level of stress caused by HL + cold treatment in the wild type, *npq1*, *koLhcb4*, and *koLhcb4 npq1* was measured from the extent of lipid peroxidation detected by thermoluminescence (TL) (Ducruet and Vavilin, 1999). Figure 7 shows plots of TL amplitudes at different time points during exposure of leaf discs to HL stress (800 μmol photons m^{-2} s^{-1}, 4°C). In *koLhcb4* genotypes, HL treatment produced higher levels of lipid peroxidation with respect to the wild type, while *npq1* behavior was intermediate. Experimental points were fitted using a first-order exponential function (Y = A e^{bx}), and the resulting equations were used to obtain the differential effect of Zea in the presence or absence of Lhcb4 (Figure 7,

inset). Clearly, a much stronger differential effect of the *npq1* mutation was observed in *koLhcb4* versus the wild type background, implying that photoprotection mediated by Lhcb4 is enhanced in the presence of Zea.

Structural Analysis of Isolated Grana Membranes

The above results suggest that the *koLhcb4* mutant was more strongly affected than genotypes lacking other components of the PSII antenna system. Previous work with *koLhcb6* (koCP24) (Kovács et al., 2006; de Bianchi et al., 2008) and *koLhcb3* (Damkjaer et al., 2009) has shown that mutations in members of the Lhcb subfamily can affect the macro-organization of PSII supercomplex and PSII-associated regulatory functions. To verify whether a structural effect was induced by lack of Lhcb4, we analyzed both the organization of PSII supercomplexes in grana membranes and isolated PSII supercomplexes by transmission electron microscopy and single particle analysis. Grana membranes from wild-type and *koLhcb4* plants exhibit randomly distributed tetrameric stain-excluding particles, corresponding to the PSII-OEC complexes exposed on the luminal surface of dimeric PSII core complexes (Figures 8A and 8B) (Boekema et al., 2000; Betterle et al., 2009). In case of the wild type, a density of PSII complexes in the grana membrane was ~1.5 PSII per 1000 nm^2 (Figure 8B). Samples from *koLhcb4* were clearly different (Figure 8A), being characterized by a wider spacing of the tetrameric particles (0.9 PSII particles per 1000 nm^2). To further investigate how the lack of Lhcb4 affects the structure of PSII supercomplex, purified PSII supercomplexes were analyzed by single-particle analysis. To this aim, freshly isolated thylakoids were mildly solubilized with 0.3% α-DM followed by rapid fractionation by gel filtration (Damkjaer et al., 2009). The first eluted fractions, containing membrane fragments and PSII supercomplexes, were analyzed by electron microscopy. Single projections of PSII supercomplexes images, identified on the basis of their shape as determined by earlier work (Caffarri et al., 2009), were collected and subjected to image analysis, including translational and rotational alignments, multivariate statistical analysis, and averaging of homogeneous classes. Figure 8C shows the average projection map from a set of 1024 projections of C_2S_2 supercomplexes from plants lacking Lhcb4. Clearly, the projection map is rather similar to the projection map of the wild-type C_2S_2 supercomplex (Figure 8E). In both genotypes, typical features of the core complex were resolved, together with the S-trimer within the peripheral antenna. However, a detailed comparison between the complexes from *koLhcb4* (Figures 8C and 8D) and from the wild type (Figure 8E) (adopted from Boekema et al., 2000) showed a different mode of binding of

Table 2. Chlorophyll Content of the Wild Type and Lhcb4 Mutants upon 3 and 8 d of Stress (900 μmol Photons m^{-2} s^{-1}, 4°C)

Days of Stress	Wild Type	*koLchb4*	*koLhcb4.2 4.3*	*koLhcb4.1 4.3*	*koLhcb4.1 4.2*
0	21.7 ± 2.86	19.5 ± 0.16	22.5 ± 1.2	21.5 ± 2.1	22.2 ± 2.6
3	19.1 ± 0.7	16.5 ± 1.6*	18.9 ± 2.6*	17.7 ± 0.9*	17.2 ± 1.4*
8	20.3 ± 2.2	13.7 ± 1.7*	19.7 ± 2.0	18.1 ± 2.3	15.8 ± 1.8*

Data are expressed as mean ± SD (n = 5); for each genotype, significantly different values (Student's t test, P = 0.05) with respect to t_0 are marked with an asterisk.
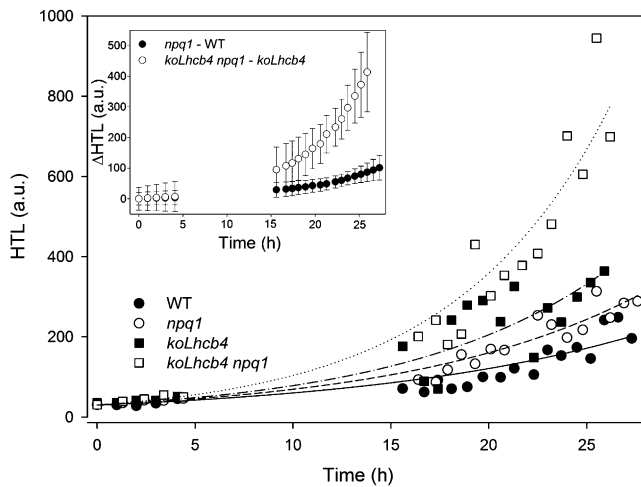
Figure 7. Kinetics of Lipid Peroxidation of *Arabidopsis* Detached Leaves Exposed to HL Stress.

Wild-type, *npq1*, *koLhcb4*, and *koLhcb4 npq1* mutant leaves floating on water were exposed to HL (800 μmol photons m^{-2} s^{-1}, 4°C), and photooxidation was estimated from the extent of lipid peroxidation measured by high-temperature TL. Each experimental point corresponds to a different sample. The kinetic of oxidized lipid accumulation was described by fitting the data set with first-order exponential functions: differential kinetics *npq1*–wild type (WT) and *koLhcb4 npq1*–*koLhcb4* were calculated on the basis of the first-order exponential functions obtained by fitting experimental points (error bars, 95% confidence level). a.u., arbitrary units.

the S-trimer to the core complex and, thus, a different overall shape of the C$_2$S$_2$ particles. In addition, electron density, at the position where Lhcb4 binds in wild-type C$_2$S$_2$ particles, is less evident but still present in *koLhcb4*; however, the space between the core complex and LHCII-S seems to be too small to accommodate an Lhcb subunit, suggesting it could represent a lipid-filled area. The simplest way to interpret this result is that PSII supercomplex associates in the absence of Lhcb4 leading to a reorganization of the overall shape of the particle with partial occlusion of the Lhcb4 area and bending of the LHCII-S mass toward the CP47 complex of the core. To verify this hypothesis, we determined the polypeptide composition and relative amounts in the PSII particles from the wild type versus *koLhcb4*. Grana membranes from wild-type and mutant plants were solubilized with low α-DM concentration (0.3%) and fractionated by nondenaturing Deriphat-PAGE (see Supplemental Figure 8A online), yielding a pattern superimposable to that previously reported (Caffarri et al., 2009). Fractions containing the C$_2$S$_2$M (Band 10) and C$_2$S$_2$M$_2$ (Band 11) supercomplexes were still detectable in *koLhcb4*, albeit their amounts were reduced compared with the wild type (14 and 9% of C$_2$S$_2$M and C$_2$S$_2$M$_2$). We chose to analyze C$_2$S$_2$M supercomplexes (Band 10) since this fraction is homogeneous while fractions with higher mobility contain more comigrating complexes (Caffarri et al., 2009) (see Supplemental Figure 9 online). Band 10, and other bands used as a reference, were eluted from the gel and their protein composition was determined by SDS-PAGE, quantitative protein gel blotting analysis, and densitometry (see Supplemental Figures

8B to 8D online). In the C$_2$S$_2$M supercomplex (Band 10) from the wild type, polypeptides of PSII core were found along with Lhcb4, Lhcb5, and LHCII. In the same fraction from *koLhcb4*, the amounts of Lhcb5 and LHCII with respect to PSII core subunits were the same despite the lack of Lhcb4, implying that this C$_2$S$_2$M supercomplex, although exhibiting a similar overall organization and mobility in green gels, lacked one of its inner subunits. Lhcb4 was not substituted by any other protein component that we could confirm by Coomassie blue staining or immunoblotting (see Supplemental Figure 8 online for details).

DISCUSSION

The Role of Lhcb4/Lhcb6 in the Topology of Grana Membranes and in the Assembly of the PSII-LHCII Supercomplex

Lhcb4 is one of the six homologous Lhc proteins composing the PSII antenna system. These pigment-protein complexes are
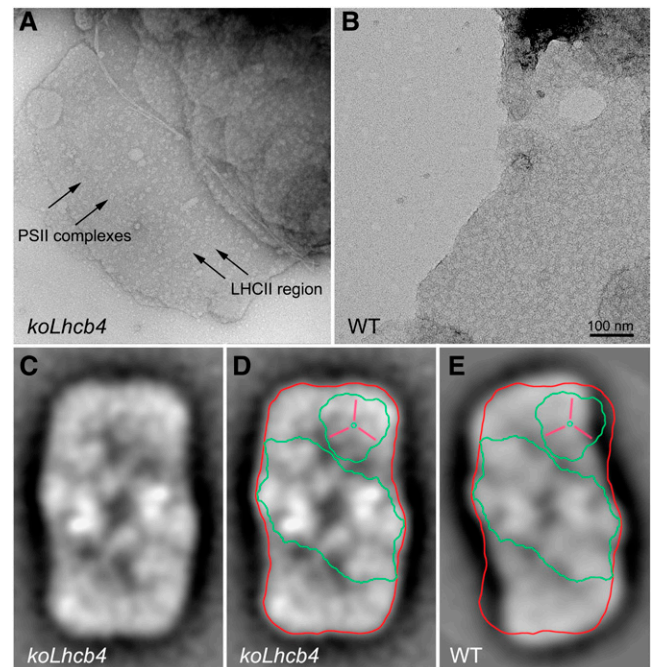
Figure 8. Electron Microscopy of Grana Membranes and PSII Particles.

(A) and **(B)** Electron microscopy of negative staining grana partition membranes were obtained by partial solubilization of thylakoids from *koLhcb4* **(A)** or wild-type (WT) plants **(B)** with α-DM. High-resolution micrographs show the distribution of stain-excluding tetrameric particles (arrows). Grana partitions from *koLhcb4* **(A)** were characterized by the presence of tetrameric particles more widely spaced than wild-type membranes **(B)**. Arrows indicate PSII core complexes (magenta) and LHCII region (violet).

(C) to **(E)** Average projection map of a set of 1024 projections of C$_2$S$_2$ supercomplexes from plants lacking Lhcb4 (**[C]** and **[D]**) and the wild type **(E)**. Contours representing PSII dimeric core (green), Lhcb4 (yellow), and whole wild-type C$_2$S$_2$ supercomplex (red) are superimposed.
[See online article for color version of this figure.]

expected to share a common three-dimensional organization on the basis of the structural data available (Ben Shem et al., 2003; Liu et al., 2004). Previous work with antisense lines has shown a high degree of redundancy among Lhcb subunits; in fact, the PSII supercomplex organization was maintained in the absence of Lhcb1+2 components by overaccumulating Lhcb5 (Ruban et al., 2003). Similarly, plants lacking Lhcb5 and/or Lhcb6 overaccumulated Lhcb1 or Lhcb4 gene products, leading to maintenance of the C_2S_2 central architecture of the PSII supercomplex (de Bianchi et al., 2008). In the case of *koLhcb4*, structural redundancy is broken as shown by the destabilization of all supercomplex bands in green gels (Figure 2C; see Supplemental Figure 3 online) and by the differences in the structure of C_2S_2 particles (Figure 8). These results are consistent with Lhcb4 being the only Lhc subunit that can occupy the position between CP47 and LHCII-M building blocks within the PSII supercomplex (Figures 8C to 8E). This conclusion is supported by the lack of compensation by other gene products in the C_2S_2M of the mutant (see Supplemental Figures 8B to 8D online).

Isolation of the C_2S_2 supercomplex from *koLhcb4* grana membranes shows that antenna proteins can be associated with the core complex in the absence of Lhcb4 as a docking subunit, which is consistent with the recent isolation of a stable monomeric core with CP26 and the LHCII-S trimer complex (Caffarri et al., 2009). Supercomplexes with a similar shape around the Lhcb4 position were previously found after salt treatment (Boekema et al., 2000). We conclude that in the absence of Lhcb4, PSII does assemble in grana membranes. However, because of the missing subunit, the complex is less stable and assumes a different overall structure with a low-density area located in the position where Lhcb4 is present in the wild type, which is likely occupied by lipids. As for the organization of the outer shell of the PSII antenna system, which is formed by LHCII-M, LHCII-L and Lhcb6, it appears to be strongly affected in *koLhcb4*. Titration of the different Lhcb proteins with respect to PSII RC showed that the Lhcb6 complex was completely missing in *koLhcb4* (Figure 2B). Since the *Lhcb6* messenger level was unchanged with respect to the wild type, this implies that removal of Lhcb4 decreases Lhcb6 stability. This is consistent with Lhcb4 being the docking site for Lhcb6 (Andersson et al., 2001; Caffarri et al., 2009), both participating in a pentameric complex called B4C (band 4 complex), which connects inner and outer antenna moieties (Bassi and Dainese, 1992; Betterle et al., 2009). One component of B4C, interacting with Lhcb4 and/or Lhcb6, is Lhcb3 (Betterle et al., 2009), which is still present in *koLhcb4* membranes; this result is consistent with the observation that, besides Lhcb4, Lhcb3 can interact with Lhcb1 and Lhcb2 in complexes containing LHCII-M (see Supplemental Figure 8B online, lanes B9 to B11), while it is absent in complexes containing only LHCII-S, such as CS complexes (lanes B6). Less stable $C_2S_2M_2$ supercomplexes can still form in the *koLhcb4* mutant, which lacks both Lhcb4 and Lhcb6, although their molecular interactions are rather weak and the abundance of this complex is only 5% with respect to the wild type. Previous work with *koLhcb6* has shown that a large part of the outer antenna formed by LHCII-M and LHCII-L is not directly bound to PSII supercomplexes; rather, trimers L and M form LHCII-only domains that segregate from arrays of C_2S_2 particles

(de Bianchi et al., 2008). No such arrays were observed in *koLhcb4* membranes (Figure 8A) nor was PQ diffusion restricted (Figure 3), suggesting that the altered shape of C_2S_2 particles and/or their instability prevents cooperative interactions with arrays. Besides this, the distance between neighbor PSII centers is higher than in the wild type (Figures 8A and 8B), implying a higher number of LHCII trimers is interposed between PSII centers.

Consequences for Photosynthesis: Light Harvesting and ET

The loss of Lhcb4 in *Arabidopsis* did not strongly affect growth rate and pigment compositions under control light conditions (Figure 3, Table 1). Indeed, linear and cyclic ET rates were similar to those in wild-type plants, as well as the functional antenna size. However, alterations in the PSII macrostructure in mutant plants did result in differences in chlorophyll fluorescence parameters (Table 1). Increased F_0 (Table 1) showed that the efficiency of excitation energy transfer from the antenna to the PSII RC is decreased in mutant plants. In grana membranes from the wild type (Figure 8B), the distribution of PSII particles is homogeneous through the whole surface. This is not the case for *koLhcb4*, whose grana membranes contained discrete patches of LHCII trimers interspersed by fewer, randomly distributed PSII cores (Figure 8A); therefore, in some discrete areas of *koLhcb4* grana membranes, the LHCII/PSII core ratio is increased. In these domains, LHCII fluorescence is probably not efficiently photochemically quenched, thus yielding higher F_0 (Table 1). This is consistent with the results obtained in KO mutants for Lhcb5 and Lhcb6 (Kovács et al., 2006; de Bianchi et al., 2008), while no such effect was observed in asLHCII (Andersson et al., 2003). Increased F_0 suggests that vacancy of Lhcb4 forces the excitation energy to follow restricted pathways from the peripheral antenna to the core; indeed, the migration time of excitations from antenna to the PSII RC was significantly reduced in *koLhcb4* with respect to the wild type (van Oort et al., 2010). Thus, despite the fact that fluorescence induction in the presence of DCMU showed no changes in functional antenna size, the number of LHCII per PSII RC in grana membranes was higher (Figures 8A and 8B). We conclude that in the absence of a well-organized PSII-LHCII supercomplex, the efficiency of excitation energy trapping in *koLhcb4* was lower than in the wild type and that the compensatory increase in peripheral LHCII complexes (Figures 2A and 2B) contributed with lower efficiency to light harvesting.

Although functional measurements indicate that there was no major perturbation of PSII and PSI functions, a slight increase in the PSI/PSII ratio was observed in *koLhcb4* (Figure 2). The consequences of a lower PSII level were not strong: the parameter S_m/t_{Fmax}, expressing the average fraction of open RCs during the time needed to complete closure of centers, was similar in *koLhcb4* and wild-type plants, as well as the LEF and Q_A redox state at several light intensities (Figures 3A and 3B), thus making ET restriction unlikely.

The major effect of the mutation on ET activity was a faster saturation of the P700 oxidation ratio in *koLhcb4* with respect to the wild type (Figure 3F). Since both LEF and CEF are not affected in the mutant, we propose that this effect could be related to the higher PSI functional antenna size of the mutant in

HL. Indeed, when measurements were performed by changing the quality of actinic light (PSI rather than PSI+PSII light), differences in P700 oxidation rate between wild-type and mutant leaves disappeared (Figure 3G), implying the increase of PSI functional antenna size in HL is due to PSII components. This is consistent with an increased level of spillover in *koLhcb4* at higher light intensity. This suggestion was verified by 77K fluorescence spectroscopy (see Supplemental Figure 5 online), showing that HL treatment induces an increased contribution of LHCII to PSI excitation in *koLhcb4* but not in the wild type. Since the amplitude of the state I–state II transition is the same in the wild type and in the mutant and, moreover, the stn7 kinase is inhibited in HL (Tikkanen et al., 2006), this spectral change cannot be attributed to state transitions. Instead, we interpret these results as evidence of spillover of excitation from LHCII to PSI. We suggest that this effect ensues from the lower stability of PSII-LHCII supercomplexes in the mutant, with the disappearance of the B4 complex (Figure 2C) and the faster kinetic of state transitions (Figures 3D and 3E). In *koLhcb4*, an overall weakening of interactions between the PSII core and LHCII would make weakly bound LHCII at the grana margins able to contribute to PSI antenna size particularly in HL, when grana membrane reorganization occurs with segregation of LHCII-rich domains (Kirchhoff, 2008; Betterle et al., 2009; Johnson et al., 2011).

Consequences for Regulation of Light Harvesting: State Transitions

State transition is the mechanism by which the complement of LHCII is balanced between PSII and PSI, depending on the reduction state of the intermediate electron carrier PQ, through its reversible phosphorylation, which induces its disconnection from PSII and binding to PSI (Allen and Nilsson, 1997; Jensen et al., 2000). Lhcb4 can be phosphorylated in monocots (Bergantino et al., 1995; Bergantino et al., 1998) and in *Arabidopsis* (Hansson and Vener, 2003). In *Chlamydomonas reinhardtii*, P-Lhcb4 was found to be connected to PSI-LHCI supercomplexes in state II conditions (Takahashi et al., 2006), and Lhcb4-depleted cells showed changes in state transitions (Tokutsu et al., 2009). Thus, changes in state transitions can be expected in Lhcb4-less plants. Results displayed in Figures 3D and 3E show that *koLhcb4* was not affected in its state transition total activity, in agreement with the similar reduction state of the PQ pool at all light intensities (Figure 3B) (Bellafiore et al., 2005). We observed that in *koLhcb4* the fluorescence changes, upon switching off the far-red light, are faster than in the wild type, implying that the transiently reduced state of the free PQ pool is more promptly relaxed by migration of the LHCII to PSI. The same state transition phenotype has been described for *koLhcb6* and *koLhcb5 Lhcb6* plants (de Bianchi et al., 2008), and this is a clear indication that the connection between the PSII core and the bulk trimeric LHCII is weaker in these mutants with respect to the wild type. In the case of the *koLhcb6* plants, the faster state transition was attributed to the displacement of the M-trimer from the PSII macrostructure, thus enhancing its migration to PSI. We suggest that, in the *koLhcb4* mutant, the weaker binding of S trimer (and, possibly, of the M trimer) and the higher amount of weakly connected LHCII trimers available increase

the probability of migrating toward PSI upon phosphorylation. In *C. reinhardtii*, state transitions do not only fulfill the role of balancing light absorption between photosystems, they also increase PSI electron flow at the expense of PSII, acting as a switch between LEF and CEF (Vallon et al., 1991). This was not the case in *Arabidopsis* since, despite an effect on state transitions (Figures 3D and 3E), no changes in linear (Figure 3A) versus CEF rates (see Supplemental Figures 4A and 4B online) were observed.

Nonphotochemical Fluorescence Quenching

Nonphotochemical dissipation of excess energy is affected in *koLhcb4* plants with respect to the wild type: mutant plants showed a delayed rise and a lower NPQ amplitude after 8 min of light (Figure 4A). Upon prolonged illumination and/or upon repeated light treatments (Figure 4B), the amplitude of NPQ was similar to that of the wild type. A similar effect was previously observed in the *koLhcb5 Lhcb6* double mutant (de Bianchi et al., 2008). Since Lhcb6 is destabilized in *koLhcb4* (Figure 2), this mutant phenocopies a double *koLhcb4 Lhcb6* mutant. NPQ kinetic can be modified by changes in the trans-thylakoid ΔpH gradient (de Bianchi et al., 2008), by changes in the level of the pH sensor PsbS (Li et al., 2002, 2004), or by changes in the number/relative abundance of protein subunits hosting quenching sites (Bonente et al., 2008). Changes in luminal pH appear unlikely; in fact, the kinetics of Zea synthesis, catalyzed by the pH-dependent enzyme VDE (Yamamoto and Higashi, 1978), were the same in wild-type and mutant leaves (Figure 4C). Moreover, the level of PsbS was unchanged (Figure 2B), leaving modification in the abundance and identity of quenching sites localized in Lhcb proteins as the most likely cause for the observed phenotype. We interpret our results in the framework of the recently proposed model (Miloslavina et al., 2008; de Bianchi et al., 2010), based on the formation of quenching sites within each of two distinct domains in grana discs: (1) C_2S_2 particles (containing PSII RC, Lhcb4, Lhcb5, and LHCII-S) and (2) the peripheral antenna, including Lhcb6, LHCII-M, and LHCII-L (Miloslavina et al., 2008; Betterle et al., 2009), which segregate because of the action of PsbS. Zea-dependent quenching activity has been detected within monomeric Lhcb4, b5, and b6 in detergent solution (Avenson et al., 2008), while, in LHCII, it was activated by aggregation and was independent from Zea (Ruban et al., 2007). The similar NPQ kinetics of *koLhcb4* and of *koLhcb5 Lhcb6* can thus be explained because they both retain a quenching site within the C_2S_2 domain; the faster quenching kinetic upon repeated illumination is due to the enhancement by Zea of the quenching activity (Niyogi et al., 1998) associated with Lhcb4 (Figure 4) or Lhcb5. This is consistent with the capacity of exchanging Viola with Zea in binding site L2 observed in monomeric Lhcbs (Morosinotto et al., 2002; Wehner et al., 2006) rather than in trimeric LHCII. In *koLhcb5 Lhcb6*, the recovery of NPQ upon the initial delay is faster and more complete than in *koLhcb4*, implying that Lhcb4 is more active as a quencher than Lhcb6 and Lhcb5 (de Bianchi et al., 2008). If there are two distinct quenching domains within PSII antenna (Miloslavina et al., 2008) and monomeric Lhcb4-6 proteins are the only sites of quenching in vivo, the peripheral antenna domain should remain unquenched in both *koLhcb5 Lhcb6* (de Bianchi et al., 2008) and

koLhcb4 because they both lack Lhcb6. Since both genotypes reach NPQ levels similar to the wild type, although with a delayed kinetic, it is likely that some kind of quenching does occur in the peripheral antenna domain disconnected from C_2S_2 particles in these genotypes. Previous work with *koLhcb6* has shown that this component has a quenching effect on the major LHCII antenna (van Oort et al., 2010); here, we observe that, even in the absence of Lhcb6, the overall quenching activity is high, consistent with quenchers being activated in both PSII antenna domains, and conclude that LHCII is likely to contribute to NPQ in vivo, in spite of the fact that it does not exhibit the spectroscopic and structural features of quenching sites (Ahn et al., 2008; Avenson et al., 2008). Thus, it likely activates quenching by a different mechanism (Ruban et al., 2007). Consistent with this view is the finding that a red-shifted fluorescence lifetime component was observed in vivo under NPQ conditions (Müller et al., 2010), which has properties similar to LHCII aggregated in vitro.

While differences in qE were minimized by prolonged/repeated illumination, we observed that the qI component, which is responsible for the slowly relaxing component of quenching, is equally decreased upon short/long or repeated light treatments (Figure 4B). Previous work suggested that qI was specifically due to Zea binding to Lhcb5 (Dall'Osto et al., 2005); instead, removal of Lhcb6 has a negligible effect on qI amplitude, since the double mutant *koLhcb5 Lhcb6* did not further decrease its qI level (de Bianchi et al., 2008). Here, we show that removal of Lhcb4 reduces the extent of qI, implying that qI is modulated by both Lhcb4 and Lhcb5.

Consequences for Photoprotection: Resistance to Photooxidative Stress Is Decreased in koLhcb4 Plants with Respect to the Wild Type

Lhcb4-less plants showed a reduced photoprotection capacity when exposed to high irradiance at low temperature. The highest sensitivity to photooxidative stress of *koLhcb4*, among all other Lhcb KO mutants, is consistent with the higher reduction in fitness of plants lacking Lhcb4 (Andersson et al., 2001; Ganeteg et al., 2004), supporting the importance of this gene product for PSII performance and chloroplast photoprotection. The structural integrity of photosynthetic supramolecular complexes is essential for the resistance to photooxidative stress (Horton and Ruban, 2005), although the reasons are not completely clear. Depletion of light-harvesting antennae has been reported to favor photoinhibition of both PSI (Alboresi et al., 2009) and PSII (Kim et al., 2009; Dall'Osto et al., 2010). *KoLhcb4* mutant plants are more sensitive to photooxidative stress than the wild type (Figure 5), and this effect is associated with increased production of $^1O_2$. This effect cannot be ascribed to a pleiotropic effect on photosynthetic ET efficiency, since lack of Lhcb4 does not significantly affect either the rate or the regulation of photosynthetic ET (Figures 3A to 3C). A putative mechanism for photoinhibition is the reduction of $^1Chl^*$ dissipation (qE and qI) (Johnson et al., 2007); however, in *koLhcb4*, qE activity is affected at the onset of illumination, while it is similar to the wild type on a longer timescale. Since our photoinhibitory light treatment was performed at constant light intensity, we conclude

that photosensitivity of *koLhcb4* plants is not due to differences in qE or qI.

The connection between the PSII core complex and outer LHCII was partially impaired. Indeed, a steady increase in F_0 was measured in *koLhcb4* plants with respect to the wild type (Table 1); a higher $^1Chl^*$ level might lead to $^3Chl^*$ formation through intersystem crossing. Although we cannot exclude that the inefficient connection of LHCII to PSII RC could contribute to the higher photosensitivity of *koLhcb4*, we notice that the *koLhcb5 Lhcb6* double mutant was as resistant as wild-type plants (Figure 5A) despite a F_v/F_m reduction comparable to that of Lhcb4-less plants (de Bianchi et al., 2008). Since photoprotection in *koLhcb5 Lhcb6* plants was similar to that in the wild type (Figure 5A), neither the increase in F_0 per se nor the absence of Lhcb6 can be the cause of higher photosensitivity of *koLhcb4* plants. Instead, this effect appears to be specific for the absence of Lhcb4, implying that this gene product is of particular importance in providing PSII photoprotection (Figure 5A). Indeed, Lhcb4 appears to be the most conserved among Lhc proteins associated with PSII (Koziol et al., 2007), and it maintains its stoichiometry with the RC even under stressful growth conditions that lead to a depletion of Lhcb1, 2, and 6 (Ballottari et al., 2007). The most obvious peculiarity of Lhcb4 is that it cannot be replaced in PSII supramolecular architecture by other Lhcbs and is thus required for allowing structural integrity of PSII (Boekema et al., 1999) (Figures 8C to 8E). Thus, the higher photosensitivity in *koLhcb4* could be the effect of a less stable PSII supercomplex; indeed, the extreme photosensitivity of *Arabidopsis* mutants such as *ch1* (Dall'Osto et al., 2010) can be ascribed to the absence of light-harvesting complexes surrounding the PSII RC, leaving the PSII core complex exposed to the lipid phase, where radical chain reactions of peroxy-lipids occur during photooxidative stress.

Measurement of lipid peroxidative damage by thermoluminescence in intact leaves of wild type versus *koLhcb4* and *koLhcb4 npq1* plants showed that Zea and Lhcb4 are synergistically active in protection from photodamage (Figure 7). Therefore, it appears that a specific effect for Zea in providing efficient photoprotection is preferentially amplified when bound to Lhcb4. This observation is consistent with a previous report of a protective effect of Zea (Dall'Osto et al., 2010) in addition to qE enhancement (Niyogi et al., 1998) and to ROS scavenging in the lipid phase (Havaux and Niyogi, 1999; Baroli et al., 2003, 2004; Havaux et al., 2007). Upon light-induced synthesis, Zea enters the protein-bound xanthophyll pool by binding to the L2 site of minor Lhc (Avenson et al., 2008; Jahns et al., 2009) and to the V1 site of LHCII (Caffarri et al., 2001), in addition to the accumulating in the lipid phase. The molecular mechanism of enhanced resistance to photooxidation by Zea is not yet clear. The hypotheses include (1) draining excitation energy from the PS core by xanthophylls bound at the interface with Lhcbs; (2) quenching of $^3Chl^*$ energy from RC, possibly by the Dexter exchange mechanism (Nayak et al., 2002) by Zea located in site L2 on specific Lhcs; and (3) preferential scavenging of $^1O_2$ by Zea into site V1 of LHCII (Johnson et al., 2007). Although all of these mechanisms are plausible for explaining the higher photosensitivity of *koLhcb4*, their relative contribution needs further investigation.

Effect of the Accumulation of the Individual Isoforms on koLhcb4 Phenotype

The attenuation of the F_0 and NPQ phenotypes produced by the triple koLhcb4 mutations is different in the three double koLhcb4 mutants. Retention of Lhcb4.1 restores F_v/F_m and NPQ to wild-type levels, while Lhcb4.2 is only partially effective in this function, Lhcb4.3 is completely inefficient (Figures 4D and Figure 6, Table 1). Indeed, plants retaining only *Lhcb4.3* show the same reduction in Chl *a/b* ratio (Table 1), increased photosensitivity (Figure 6), and delayed NPQ kinetic as the triple *koLhcb4*. Although we cannot exclude that Lhcb4.1, 4.2, and 4.3 gene products are intrinsically different, the penetration of the phenotype appears to be essentially due to the level of the gene product. Indeed, levels of Lhcb4.1, Lhcb4.2, and Lhcb4.3 in the three double mutant are 1, 0.6, and 0, respectively, per PSII RC (see Supplemental Table 2 online). In fact, although *Lhcb4.3* transcription is lightly increased under stress conditions (Alboresi et al., 2011), we were unable to detect the corresponding protein even by keeping plants under a variety of stress conditions, implying it is either not translated or rapidly turned over.

The *Lhcb4.3* gene appeared recently in plant genome. Its sequence is not present in algal genomes, and no orthologs were found in the moss *Physcomitrella patens*; therefore, it appeared only at later stages in the evolution of the green lineage (Alboresi et al., 2008). It seems unlikely that a new gene conserved in higher plants has no function or is not translated at all. EST data from *Arabidopsis* show that *Lhcb4.3* is expressed at low levels (Jansson, 1999), and its transcription seems to be confined to dicots (Goff et al., 2002; Yu et al., 2002); furthermore, clustering analysis of Lhc superfamily expression data (Klimmek et al., 2006) confirmed that *Lhcb4.3* is regulated in an opposite way with respect to *Lhcb4.1* and *Lhcb4.2*. The putative Lhcb4.3 protein is shorter than other Lhcb4 isoforms, and its sequence is considerably different from both Lhcb4.1 and Lhcb4.2 isoforms, suggesting it might have a different function in the stress conditions in which this gene is actively transcribed. However, we cannot exclude that the Lhcb4.3 isoform might accumulate in special and still uninvestigated environmental/developmental conditions; so far, the role of this isoform remains elusive.

We have shown that Lhcb4 has a specific function in protecting PSII from photoinhibition, which accounts for the increased sensitivity of *koLhcb4* to HL stress. This gene product, different from any other PSII antenna component, cannot be replaced by homologous subunits in the PSII-LHCII supramolecular complex. This leads to the formation of incomplete PSII particles with a gap in the position normally occupied by Lhcb4, a modified shape and a lower stability. This is consistent with evidence that a core group of antenna proteins developed prior to green algal diversification (Koziol et al., 2007) and included Lhcb4 protein associated with PSII RC. The weaker interaction between PSII-LHCII components leads to a faster migration of LHCII complexes to the stroma membrane upon phosphorylation, similar to the case of *koLhcb6* and *koLhcb3*. Although PSII activity is not impaired in moderate light conditions, there is a lower level of PSII RC in grana membranes, probably because the PSII core complex is less strongly retained within grana discs, because one of the two monomeric Lhcbs that bridges it to LHCII is

missing. Under stress conditions, *koLhcb4* is photoinhibited, and this effect is selectively enhanced in the absence of Zea, which is active in preventing the synthesis of ROS species and promoting their scavenging. By binding in between LHCII trimers and the CP47 subunit of PSII, Lhcb4 is crucial for the protection of PSII RC from ROS produced during photosynthesis either by neighbor damaged PSII complexes (Krieger-Liszkay et al., 2008) or by overexcited antennae (Santabarbara et al., 2002; Mozzo et al., 2008). Thus, the absence of a specific antenna subunit, although it does not restrict light harvesting and photosynthetic ET rate, impairs PSII photoprotection capacity through its effect on the assembly of supercomplexes. This is an example of optimization of the building blocks of photosynthetic complexes and the tuning of their interactions with each other toward overcoming the inhibitory effect of increasing oxygen concentration over evolution time. It is worth noting that functional alterations described in *koLhcb4* plants likely result from the reduced ability of PSII macroassemblies to undergo proper organization in low versus high light, thus confirming the crucial role of Lhcb4 in modulating structural and functional flexibility of grana membranes.

METHODS

Plant Material and Growth Conditions

Arabidopsis thaliana T-DNA insertion mutants (Columbia ecotype) GK Line ID282A07 (insertion into the *Lhcb4.1* gene), SAIL_910_D12 (insertion into the *Lhcb4.2* gene), and SALK_032779 (insertion into the *Lhcb4.3* gene) were obtained from NASC collections (Alonso et al., 2003). Homozygous plants (Betterle et al., 2009) were identified by PCR analysis using the following primers: forward 5′-TCACCAGATAACGCAGAGTTTAATAG-3′ and reverse 5′-CACATGATAATGATTTTAAGATGAGGAG-3′ for the *Lhcb4.1* sequence, 5′-CATCATACTCATTGCTGATCCATG-3′ for the insertion; forward 5′-GCGTTTGTGTTTAGCGTTTCGACATCTGTCTG-3′ and reverse 5′-GGTACCCGGGTGGTTTCCGACATTAGC-3′ for the *Lhcb4.2* sequence, 5′-GCCTTTTCAGAAATGGATAAATAGCCTTGCTTCC-3′ for the insertion; forward 5′-GTGAGCTGATCCATGGAAGGTGG-3′ and reverse 5′-GGCCGGTTTTGAACGATTGATGTGAC-3′ for the *Lhcb4.3* sequence, and 5′-GCGTGGACCGCTTGCTGCAACT-3′ for the insertion. Genotypes *koLhcb4*, *koLhcb4.1 4.2*, *koLhcb4.2*, *koLhcb4.3*, and *koLhcb4.1 4.3* were obtained by crossing single mutant plants and selecting progeny by PCR analysis. For RT-PCR, total RNA was isolated from 4-week-old plants with the Trizol protocol. Reverse transcription was performed using M-MLV reverse transcriptase with oligo(dT) primer and 1.5 μg of total RNA. For normalization purposes, actin2 was chosen as an endogenous control. The primers used were as follows: 5′-GTGGCTCCCGGTATCCATCC-3′ and 5′-TTGAACCGCGAATCCCAAGAAGG-3′ for *Lhcb4.1* cDNA; 5′-GGTTTCCGACATTAGCTCCAATTC-3′ and 5′-CTGAACCGCAAAACCCA-AGAATC-3′ for *Lhcb4.2* cDNA; 5′-CCGGTTCGGGGTTCAGTTTCGG-3′ and 5′-GGCAAGGAAGCTGACAGGGC-3′ for *Lhcb4.3* cDNA; and 5′-CCTCATGCCATCCTCCGTCTTG-3′ and 5′-GAGCACAATGTTACCGTA-CAGATCC-3′ for actin2 cDNA.

The *Arabidopsis* T-DNA insertion mutant *koLhcb3* (SALK_020342) from NASC was obtained by selecting progeny by immunoblotting using a specific antibody against the Lhcb3 subunit; asLHCII (Andersson et al., 2003) was obtained from the NASC. The double mutant *koLhcb4 npq1* was obtained by crossing single mutants and selecting progeny by immunoblotting (with the α-Lhcb4 antibody) and HPLC upon HL treatment of leaves. Insertion mutants *koLhcb6* and *koLhcb5 Lhcb6* were isolated as previously described (de Bianchi et al., 2008). Mutants were

grown for 5 weeks at 100 μmol photons m^{-2} s^{-1}, 23°C, 70% humidity, and 8 h of daylight.

Stress Conditions

Short-term HL treatment was performed at 1200 μmol photons m^{-2} s^{-1}, 45 min, and room temperature (24°C), to measure the kinetics of Zea accumulation, on detached leaves floating on water. Samples were rapidly frozen in liquid nitrogen prior to pigment extraction. Longer photooxidative stress was induced by exposing whole plants to either 550 μmol photons m^{-2} s^{-1} at 4°C for 2 d, 900 μmol photons m^{-2} s^{-1} at 4°C for 10 d, or 1600 μmol photons m^{-2} s^{-1} at 24°C for 10 d. Light was provided by halogen lamps (Focus 3; Prisma) and filtered through a 2-cm recirculation water layer to remove infrared radiation.

Pigment Analysis

Pigments were extracted from leaf discs, either dark adapted or HL treated, with 85% acetone buffered with Na_2CO_3, and then separated and quantified by HPLC (Gilmore and Yamamoto, 1991).

Membrane Isolation

Functional thylakoids were isolated from dark-adapted or HL-treated leaves as previously described (Casazza et al., 2001).

Gel Electrophoresis and Immunoblotting

SDS-PAGE analysis was performed with the Tris-Tricine buffer system (Schägger and von Jagow, 1987), with the addition of 7 M urea to the running gel to separate Lhcb4 isoforms. Nondenaturing Deriphat-PAGE was performed following the method developed by Peter et al. (1991) with modification described by Havaux et al. (2004). Thylakoids concentrated at 1 mg/mL chlorophylls were solubilized in a final concentration of 1% α/β-DM, and 25 mg of chlorophyll were loaded in each lane. For immunotitration, thylakoid samples corresponding to 0.25, 0.5, 0.75, and 1 μg of chlorophyll were loaded for each sample and electroblotted on nitrocellulose membranes, and proteins were detected with alkaline phosphatase-conjugated antibody according to Towbin et al. (1979). Signal amplitude was quantified ($n = 4$) using GelPro 3.2 software (Bio-Rad). To avoid any deviation between different immunoblots, samples were compared only when loaded in the same slab gel.

In Vivo Fluorescence and NPQ Measurements

PSII function during photosynthesis was measured through chlorophyll fluorescence on whole leaves at room temperature with a PAM 101 fluorimeter (Heinz-Walz) (Andersson et al., 2001), a saturating light pulse of 4500 μmol photons m^{-2} s^{-1}, 0.6 s, and white actinic light of 100 to 1100 μmol photons m^{-2} s^{-1}, supplied by a KL1500 halogen lamp (Schott). NPQ, ϕ_{PSII}, qP, qL, and LET were calculated according to the following equations (Van Kooten and Snel, 1990; Baker, 2008): NPQ = $(F_m - F_m')/F_m'$, $\phi_{PSII}= (F_m' - F_s)/F_m'$, qP = $(F_m' - F_s)/(F_m' - F_0')$, qL = qP·$F_0'/F_s$, LET = ϕ_{PSII}·PAR·A_{leaf}·fraction$_{PSII}$, where F_0/F_0' is the minimal fluorescence from dark/light-adapted leaf, F_m/F_m' is the maximal fluorescence from dark/light-adapted leaves measured after the application of a saturating flash, F_s the stationary fluorescence during illumination, and PAR the photosynthetic active radiation; A_{leaf} (leaf absorptivity) was 0.67 $\pm$ 0.05 for the wild type, 0.62 $\pm$ 0.04 for *koLhcb4*; fraction$_{PSII}$ was measured by quantitative immunoblot: wild type, 0.50 $\pm$ 0.01; *koLhcb4*, 0.47 $\pm$ 0.06.

State transition experiments were performed using whole plants according to established protocols (Jensen et al., 2000). Preferential PSII excitation was provided by illumination with blue light (40 μmol photons m^{-2} s^{-1}), excitation of PSI was achieved using far-red light from an LED light source (Heinz-Walz; 102-FR) applied for 15 min simultaneously with blue light. F_m level in state I (F_m') and state II (F_m'') was determined at the end of each cycle by the application of a saturating light pulse. The parameter qT (PSII cross-section changes) was calculated as $(F_{m1} - F_{m2})/F_{m1}$ (where $F_{m1/2}$ is the maximal fluorescence yield in state I/II).

Fluorescence induction kinetics was recorded with a home-built apparatus to measure functional antenna size on leaves. S_m/t_{Fmax} was calculated from variable fluorescence curves induced with green light (1100 μmol photons m^{-2} s^{-1}) (Strasser et al., 1995). For measurements of PSII functional antenna size, variable fluorescence was induced with a green light of 15 μmol photons m^{-2} s^{-1}, on thylakoids (10 μg Chls/mL) in a measuring buffer containing 10 mM HEPES, pH 7.8, 5 mM $MgCl_2$, 30 μM DCMU, and 50 μM nigericin. The reciprocal of time corresponding to two-thirds of the fluorescence rise ($T_{2/3}$) was taken as a measure of the PSII functional antenna size (Malkin et al., 1981). For measurements of the PSII repair process, whole plants were illuminated at 900 μmol photons m^{-2} s^{-1}, 4°C for 4 h to induce photoinhibition of PSII, and restoration of the F_v/F_m ratios was subsequently followed at irradiances of 20 μmol photons m^{-2} s^{-1}, 4°C (Aro et al., 1994).

Analysis of P700 Redox State

All in vivo spectroscopic measurements were performed using a LED spectrophotometer (JTS10; Biologic Science Instruments) in which absorption changes are sampled by weak monochromatic flashes (10-nm bandwidth) provided by LEDs. P700$^+$ reduction following a flash was assayed as detailed by Golding et al. (2004). Leaves were infiltrated with 50 μM DCMU in 150 mM sorbitol. A 400-ms saturating flash of red light (λ_{max} = 630 nm; 3000 μmol photons m^{-2} s^{-1}) was delivered to the leaf, and changes in absorbance at 705 nm were used to measure the kinetics of P700$^+$ reduction. Oxidized P700 (ΔA_{max}) was recorded during far-red light illumination (2500 μmol photons m^{-2} s^{-1}, λ_{max} = 720 nm). The level of oxidized P700 in the leaf (ΔA) was determined during illumination with either orange light (630 nm, from 50 to 980 μmol photons m^{-2} s^{-1}, λ_{max} = 720 nm) or far-red light (720 nm, from 200 to 2500 μmol photons m^{-2} s^{-1}) (Zygadlo et al., 2005). Antenna size of PSI was estimated according to Kim et al. (2009).

Analysis of Cytochrome b_6f Redox Kinetics

Absorption transients were measured on thylakoids (30 μg Chls/mL) in a measuring buffer containing 10 mM HEPES, pH 7.8, 5 mM $MgCl_2$, 1 mM sodium ascorbate, 20 μM nigericin, and 50 μM methylviologen (Kirchhoff et al., 2000). Cytochrome redox changes were measured in continuous light (630 nm, 300-ms pulse, 560 μmol photons m^{-2} s^{-1}) at four wavelengths: 548, 554, 563, and 573 nm; redox changes of cytochromes *b* and *f* were calculated according to Joliot and Joliot (1984).

Analysis of Steady State Proton Flux across Thylakoid Membranes

Light-induced pmf was estimated on intact leaves, from DIRK changes in absorbance associated with the ECS at 520 nm, as described previously (Livingston et al., 2010). ECS was induced with orange (630 nm) actinic intensities ranging from 15 to 960 μmol photons m^{-2} s^{-1}. Relative values of steady state proton flux across the thylakoid membrane (v_H^+) was estimated from the initial slope of the ECS decay upon rapid light–dark transitions.

Gas Exchange Measurement

Measurements of O_2 evolution in saturating CO_2 were performed using an S101 O_2 electrode (Qubit System). Light response curves were determined using broadband red light.

Determination of the Sensitivity to Photooxidative Stress

Photooxidative stress was induced in detached leaves by HL treatment at low temperature. Detached leaves floating on water were exposed to 1500 μmol photons m^{-2} s^{-1} for 8 h, in a growth chamber at 4°C, and then immediately frozen in liquid nitrogen. Photooxidative stress was assessed by measuring MDA formation as an indirect quantification of lipid peroxidation (Havaux et al., 2005). Lipid peroxidation was measured on whole plants by TL with a custom-made apparatus (Ducruet, 2003). The amplitude of the TL peak at 135°C was used as an index of lipid peroxidation (Havaux, 2003). Measurements of singlet oxygen production from leaves were performed with SOSG (Molecular Probes), a $^1O_2$-specific fluorogenic probe, as described by Dall'Osto et al. (2010).

Electron Microscopy

Samples were negatively stained with 2% uranyl acetate on glow discharged carbon-coated copper grids. Electron microscopy was performed on a Philips CM120 electron microscope equipped with a LaB6 tip operating at 120 kV. Images were recorded with a Gatan 4000 SP 4 K slow-scan CCD camera at 80,000 magnification at a pixel size (after binning the images) of 0.375 nm at the specimen level with GRACE software for semiautomated specimen selection and data acquisition (Oostergetel et al., 1998). Single-particle analysis of a data set of 1350 PSII particles was performed using Groningen Image Processing software, including multireference and no-reference alignments, multivariate statistical analysis, classification, and averaging of homogeneous classes (van Heel et al., 2000).

Accession Numbers

Sequence data from this article can be found in the Arabidopsis Genome Initiative or GenBank/EMBL databases under accession numbers At5g01530 (Lhcb4.1), At3g08940 (Lhcb4.2), At2g40100 (Lhcb4.3), At5g54270 (Lhcb3), At4g10340 (Lhcb5), At1g15820 (Lhcb6), At1g08550 (npq1), and At3g18780 (actin2). The KO lines mentioned in the article can be obtained from the NASC under the stock numbers N376476 (*koLhcb4.1*), N877954 (*koLhcb4.2*), N532779 (*koLhcb4.3*), N520342 (*koLhcb3*), N514869 (*koLhcb5*), N577953 (*koLhcb6*), and N6363 (asLHCII).

Supplemental Data

The following materials are available in the online version of this article.

Supplemental Figure 1. Transmission Electron Micrographs of Plastid from Mesophyll Cells of the Wild type and Mutants.

Supplemental Figure 2. Induction Curves of Chl Fluorescence Measured on Thylakoids Treated with DCMU.

Supplemental Figure 3. Biochemical Characterization of *koLhcb4* Mutants.

Supplemental Figure 4. P700 Measurements: Cyclic Electron Transport, PSI Functional Antenna Size, and Cytochrome b_6f Redox Kinetics.

Supplemental Figure 5. Low-Temperature Fluorescence Spectra of Chloroplasts.

Supplemental Figure 6. PSII Repair Efficiency under Photoxidative Stress.

Supplemental Figure 7. Insights on the Lhcb4.3 Expression and Function.

Supplemental Figure 8. Insights on the PSII Supercomplex Composition.

Supplemental Figure 9. Schematic Panel of Wild-Type and *koLhcb4* PSII Supercomplex Composition.

Supplemental Table 1. Quantitative Analysis of Thylakoid Morphological Traits.

Supplemental Table 2. Polypeptide Composition of Thylakoid Membranes from Wild-Type and KO Mutant Expressing Single Lhcb4 Isoform.

AUTHOR CONTRIBUTIONS

S.d.B. isolated single KO mutants, carried out the crossings to obtain all the genotypes used, and performed a biochemical and physiological characterization of their photosynthetic apparatus. S.C., N.B., and L.D. were involved in the photoxidative treatments and stress measurements, in the spectroscopy investigation on thylakoids or isolated complexes, and in data analysis. R.K., E.B., and N.B. carried out electron microscopy structural analysis of isolated grana and PSII particles. R.B. and L.D. conceived the study, participated in its design and coordination, and helped to draft the manuscript.

REFERENCES

Ahn, T.K., Avenson, T.J., Ballottari, M., Cheng, Y.C., Niyogi, K.K., Bassi, R., and Fleming, G.R. (2008). Architecture of a charge-transfer state regulating light harvesting in a plant antenna protein. Science **320:** 794–797.

Alboresi, A., Ballottari, M., Hienerwadel, R., Giacometti, G.M., and Morosinotto, T. (2009). Antenna complexes protect Photosystem I from photoinhibition. BMC Plant Biol. **9:** 71.

Alboresi, A., Caffarri, S., Nogue, F., Bassi, R., and Morosinotto, T. (2008). In silico and biochemical analysis of *Physcomitrella patens* photosynthetic antenna: Identification of subunits which evolved upon land adaptation. PLoS ONE **3:** e2033.

Alboresi, A., Dall'osto, L., Aprile, A., Carillo, P., Roncaglia, E., Cattivelli, L., and Bassi, R. (2011). Reactive oxygen species and transcript analysis upon excess light treatment in wild-type *Arabidopsis thaliana* vs a photosensitive mutant lacking zeaxanthin and lutein. BMC Plant Biol. **11:** 62.

Allen, J.F. (1992). Protein phosphorylation in regulation of photosynthesis. Biochim. Biophys. Acta **1098:** 275–335.

Allen, J.F., and Nilsson, A. (1997). Redox signalling and the structural basis of regulation of photosynthesis by protein phosphorylation. Physiol. Plant. **100:** 863–868.

Alonso, J.M., et al. (2003). Genome-wide insertional mutagenesis of *Arabidopsis thaliana*. Science **301:** 653–657.

Anderson, J.M. (1986). Photoregulation of the composition, function and structure of thylakoid membranes. Annu. Rev. Plant Physiol. **37:** 93–136.

Andersson, J., Walters, R.G., Horton, P., and Jansson, S. (2001).

Antisense inhibition of the photosynthetic antenna proteins CP29 and CP26: Implications for the mechanism of protective energy dissipation. Plant Cell **13:** 1193–1204.

Andersson, J., Wentworth, M., Walters, R.G., Howard, C.A., Ruban, A.V., Horton, P., and Jansson, S. (2003). Absence of the Lhcb1 and Lhcb2 proteins of the light-harvesting complex of photosystem II - Effects on photosynthesis, grana stacking and fitness. Plant J. **35:** 350–361.

Aro, E.M., McCaffery, S., and Anderson, J.M. (1994). Recovery from photoinhibition in peas (*Pisum sativum* L.) acclimated to varying growth irradiances (role of D1 protein turnover). Plant Physiol. **104:** 1033–1041.

Asada, K. (1999). The water-water cycle in chloroplasts: Scavenging of active oxygens and dissipation of excess photons. Annu. Rev. Plant Physiol. Plant Mol. Biol. **50:** 601–639.

Avenson, T.J., Ahn, T.K., Zigmantas, D., Niyogi, K.K., Li, Z., Ballottari, M., Bassi, R., and Fleming, G.R. (2008). Zeaxanthin radical cation formation in minor light-harvesting complexes of higher plant antenna. J. Biol. Chem. **283:** 3550–3558.

Baker, N.R. (2008). Chlorophyll fluorescence: A probe of photosynthesis in vivo. Annu. Rev. Plant Biol. **59:** 89–113.

Ballottari, M., Dall'Osto, L., Morosinotto, T., and Bassi, R. (2007). Contrasting behavior of higher plant photosystem I and II antenna systems during acclimation. J. Biol. Chem. **282:** 8947–8958.

Baroli, I., Do, A.D., Yamane, T., and Niyogi, K.K. (2003). Zeaxanthin accumulation in the absence of a functional xanthophyll cycle protects *Chlamydomonas reinhardtii* from photooxidative stress. Plant Cell **15:** 992–1008.

Baroli, I., Gutman, B.L., Ledford, H.K., Shin, J.W., Chin, B.L., Havaux, M., and Niyogi, K.K. (2004). Photo-oxidative stress in a xanthophyll-deficient mutant of Chlamydomonas. J. Biol. Chem. **279:** 6337–6344.

Bassi, R., and Dainese, P. (1992). A supramolecular light-harvesting complex from chloroplast photosystem-II membranes. Eur. J. Biochem. **204:** 317–326.

Bassi, R., Høyer-Hansen, G., Barbato, R., Giacometti, G.M., and Simpson, D.J. (1987). Chlorophyll-proteins of the photosystem II antenna system. J. Biol. Chem. **262:** 13333–13341.

Bassi, R., Pineau, B., Dainese, P., and Marquardt, J. (1993). Carotenoid-binding proteins of photosystem II. Eur. J. Biochem. **212:** 297–303.

Bassi, R., Sandona, D., and Croce, R. (1997). Novel aspects of chlorophyll a/b-binding proteins. Physiol. Plant. **100:** 769–779.

Bellafiore, S., Barneche, F., Peltier, G., and Rochaix, J.D. (2005). State transitions and light adaptation require chloroplast thylakoid protein kinase STN7. Nature **433:** 892–895.

Ben-Shem, A., Nelson, N., and Frolow, F. (2003). Crystallization and initial X-ray diffraction studies of higher plant photosystem I. Acta Crystallogr. D Biol. Crystallogr. **59:** 1824–1827.

Bergantino, E., Dainese, P., Cerovic, Z., Sechi, S., and Bassi, R. (1995). A post-translational modification of the photosystem II subunit CP29 protects maize from cold stress. J. Biol. Chem. **270:** 8474–8481.

Bergantino, E., Sandonà, D., Cugini, D., and Bassi, R. (1998). The photosystem II subunit CP29 can be phosphorylated in both C3 and C4 plants as suggested by sequence analysis. Plant Mol. Biol. **36:** 11–22.

Betterle, N., Ballottari, M., Zorzan, S., de Bianchi, S., Cazzaniga, S., Dall'osto, L., Morosinotto, T., and Bassi, R. (2009). Light-induced dissociation of an antenna hetero-oligomer is needed for non-photochemical quenching induction. J. Biol. Chem. **284:** 15255–15266.

Boekema, E.J., van Breemen, J.F., van Roon, H., and Dekker, J.P. (2000). Conformational changes in photosystem II supercomplexes upon removal of extrinsic subunits. Biochemistry **39:** 12907–12915.

Boekema, E.J., Van Roon, H., Van Breemen, J.F., and Dekker, J.P. (1999). Supramolecular organization of photosystem II and its light-harvesting antenna in partially solubilized photosystem II membranes. Eur. J. Biochem. **266:** 444–452.

Bonente, G., Howes, B.D., Caffarri, S., Smulevich, G., and Bassi, R. (2008). Interactions between the photosystem II subunit PsbS and xanthophylls studied in vivo and in vitro. J. Biol. Chem. **283:** 8434–8445.

Butler, W.L., and Strasser, R.J. (1978). Effect of divalent cations on energy coupling between the light-harvesting chlorophyll a/b complex and photosystem II. In Photosynthesis '77: Proceedings of the Fourth International Congress on Photosynthesis, D.A. Hall, J. Coombs, and T.W. Goodwin, eds (London: The Biochemical Society), pp. 11–20.

Caffarri, S., Croce, R., Breton, J., and Bassi, R. (2001). The major antenna complex of photosystem II has a xanthophyll binding site not involved in light harvesting. J. Biol. Chem. **276:** 35924–35933.

Caffarri, S., Croce, R., Cattivelli, L., and Bassi, R. (2004). A look within LHCII: differential analysis of the Lhcb1-3 complexes building the major trimeric antenna complex of higher-plant photosynthesis. Biochemistry **43:** 9467–9476.

Caffarri, S., Kouril, R., Kereïche, S., Boekema, E.J., and Croce, R. (2009). Functional architecture of higher plant photosystem II supercomplexes. EMBO J. **28:** 3052–3063.

Casazza, A.P., Tarantino, D., and Soave, C. (2001). Preparation and functional characterization of thylakoids from *Arabidopsis thaliana*. Photosynth. Res. **68:** 175–180.

Crimi, M., Dorra, D., Bösinger, C.S., Giuffra, E., Holzwarth, A.R., and Bassi, R. (2001). Time-resolved fluorescence analysis of the recombinant photosystem II antenna complex CP29. Effects of zeaxanthin, pH and phosphorylation. Eur. J. Biochem. **268:** 260–267.

Croce, R., Breton, J., and Bassi, R. (1996). Conformational changes induced by phosphorylation in the CP29 subunit of photosystem II. Biochemistry **35:** 11142–11148.

Dall'Osto, L., Caffarri, S., and Bassi, R. (2005). A mechanism of nonphotochemical energy dissipation, independent from PsbS, revealed by a conformational change in the antenna protein CP26. Plant Cell **17:** 1217–1232.

Dall'Osto, L., Cazzaniga, S., Havaux, M., and Bassi, R. (2010). Enhanced photoprotection by protein-bound vs free xanthophyll pools: A comparative analysis of chlorophyll b and xanthophyll biosynthesis mutants. Mol. Plant **3:** 576–593.

Damkjaer, J.T., Kereïche, S., Johnson, M.P., Kovacs, L., Kiss, A.Z., Boekema, E.J., Ruban, A.V., Horton, P., and Jansson, S. (2009). The photosystem II light-harvesting protein Lhcb3 affects the macrostructure of photosystem II and the rate of state transitions in *Arabidopsis*. Plant Cell **21:** 3245–3256.

de Bianchi, S., Ballottari, M., Dall'osto, L., and Bassi, R. (2010). Regulation of plant light harvesting by thermal dissipation of excess energy. Biochem. Soc. Trans. **38:** 651–660.

de Bianchi, S., Dall'Osto, L., Tognon, G., Morosinotto, T., and Bassi, R. (2008). Minor antenna proteins CP24 and CP26 affect the interactions between photosystem II subunits and the electron transport rate in grana membranes of *Arabidopsis*. Plant Cell **20:** 1012–1028.

Demmig-Adams, B., Winter, K., Kruger, A., and Czygan, F.-C. (1989). Light stress and photoprotection related to the carotenoid zeaxanthin in higher plants. In Photosynthesis. Plant Biology Vol. 8, W.R. Briggs, ed (New York: Alan R. Liss), pp. 375–391.

Ducruet, J.M. (2003). Chlorophyll thermoluminescence of leaf discs: Simple instruments and progress in signal interpretation open the way to new ecophysiological indicators. J. Exp. Bot. **54:** 2419–2430.

Ducruet, J.M., and Vavilin, D. (1999). Chlorophyll high-temperature thermoluminescence emission as an indicator of oxidative stress: Perturbating effects of oxygen and leaf water content. Free Radic. Res. **31** (suppl.): S187–S192.

Ferreira, K.N., Iverson, T.M., Maghlaoui, K., Barber, J., and Iwata, S. (2004). Architecture of the photosynthetic oxygen-evolving center. Science **303:** 1831–1838.

Finazzi, G., Johnson, G.N., Dall'Osto, L., Joliot, P., Wollman, F.A., and Bassi, R. (2004). A zeaxanthin-independent nonphotochemical quenching mechanism localized in the photosystem II core complex. Proc. Natl. Acad. Sci. USA **101:** 12375–12380. Erratum. Proc. Natl. Acad. Sci. USA **101:** 17322.

Formaggio, E., Cinque, G., and Bassi, R. (2001). Functional architecture of the major light-harvesting complex from higher plants. J. Mol. Biol. **314:** 1157–1166.

Frigerio, S., Campoli, C., Zorzan, S., Fantoni, L.I., Crosatti, C., Drepper, F., Haehnel, W., Cattivelli, L., Morosinotto, T., and Bassi, R. (2007). Photosynthetic antenna size in higher plants is controlled by the plastoquinone redox state at the post-transcriptional rather than transcriptional level. J. Biol. Chem. **282:** 29457–29469.

Ganeteg, U., Külheim, C., Andersson, J., and Jansson, S. (2004). Is each light-harvesting complex protein important for plant fitness? Plant Physiol. **134:** 502–509.

Gilmore, A.M., and Yamamoto, H.Y. (1991). Zeaxanthin formation and energy-dependent fluorescence quenching in pea chloroplasts under artificially mediated linear and cyclic electron transport. Plant Physiol. **96:** 635–643.

Goff, S.A., et al. (2002). A draft sequence of the rice genome (*Oryza sativa* L. ssp. *japonica*). Science **296:** 92–100.

Golding, A.J., Finazzi, G., and Johnson, G.N. (2004). Reduction of the thylakoid electron transport chain by stromal reductants—Evidence for activation of cyclic electron transport upon dark adaptation or under drought. Planta **220:** 356–363.

Haldrup, A., Jensen, P.E., Lunde, C., and Scheller, H.V. (2001). Balance of power: A view of the mechanism of photosynthetic state transitions. Trends Plant Sci. **6:** 301–305.

Hansson, M., and Vener, A.V. (2003). Identification of three previously unknown in vivo protein phosphorylation sites in thylakoid membranes of *Arabidopsis thaliana*. Mol. Cell. Proteomics **2:** 550–559.

Havaux, M. (2003). Spontaneous and thermoinduced photon emission: New methods to detect and quantify oxidative stress in plants. Trends Plant Sci. **8:** 409–413.

Havaux, M., Dall'osto, L., and Bassi, R. (2007). Zeaxanthin has enhanced antioxidant capacity with respect to all other xanthophylls in Arabidopsis leaves and functions independent of binding to PSII antennae. Plant Physiol. **145:** 1506–1520.

Havaux, M., Dall'Osto, L., Cuiné, S., Giuliano, G., and Bassi, R. (2004). The effect of zeaxanthin as the only xanthophyll on the structure and function of the photosynthetic apparatus in *Arabidopsis thaliana*. J. Biol. Chem. **279:** 13878–13888.

Havaux, M., Eymery, F., Porfirova, S., Rey, P., and Dörmann, P. (2005). Vitamin E protects against photoinhibition and photooxidative stress in *Arabidopsis thaliana*. Plant Cell **17:** 3451–3469.

Havaux, M., and Niyogi, K.K. (1999). The violaxanthin cycle protects plants from photooxidative damage by more than one mechanism. Proc. Natl. Acad. Sci. USA **96:** 8762–8767.

Holt, N.E., Zigmantas, D., Valkunas, L., Li, X.P., Niyogi, K.K., and Fleming, G.R. (2005). Carotenoid cation formation and the regulation of photosynthetic light harvesting. Science **307:** 433–436.

Horton, P. (1996). Nonphotochemical quenching of chlorophyll fluorescence. In Light as an Energy Source and Information Carrier in Plant Physiology, R.C. Jennings, ed (New York: Plenum Press), pp. 99–111.

Horton, P., and Ruban, A. (2005). Molecular design of the photosystem II light-harvesting antenna: Photosynthesis and photoprotection. J. Exp. Bot. **56:** 365–373.

Jahns, P., Latowski, D., and Strzalka, K. (2009). Mechanism and regulation of the violaxanthin cycle: The role of antenna proteins and membrane lipids. Biochim. Biophys. Acta **1787:** 3–14.

Jansson, S. (1999). A guide to the Lhc genes and their relatives in Arabidopsis. Trends Plant Sci. **4:** 236–240.

Jensen, P.E., Gilpin, M., Knoetzel, J., and Scheller, H.V. (2000). The PSI-K subunit of photosystem I is involved in the interaction between light-harvesting complex I and the photosystem I reaction center core. J. Biol. Chem. **275:** 24701–24708.

Johnson, M.P., Goral, T.K., Duffy, C.D., Brain, A.P., Mullineaux, C.W., and Ruban, A.V. (2011). Photoprotective energy dissipation involves the reorganization of photosystem II light-harvesting complexes in the grana membranes of spinach chloroplasts. Plant Cell **23:** 1468–1479.

Johnson, M.P., Havaux, M., Triantaphylidès, C., Ksas, B., Pascal, A.A., Robert, B., Davison, P.A., Ruban, A.V., and Horton, P. (2007). Elevated zeaxanthin bound to oligomeric LHCII enhances the resistance of Arabidopsis to photooxidative stress by a lipid-protective, antioxidant mechanism. J. Biol. Chem. **282:** 22605–22618.

Joliot, P., and Joliot, A. (1984). Electron transfer between the two photosystem. I. Flash excitation under oxidizing conditions. Biochim. Biophys. Acta **765:** 210–218.

Kim, E.H., Li, X.P., Razeghifard, R., Anderson, J.M., Niyogi, K.K., Pogson, B.J., and Chow, W.S. (2009). The multiple roles of light-harvesting chlorophyll a/b-protein complexes define structure and optimize function of Arabidopsis chloroplasts: A study using two chlorophyll b-less mutants. Biochim. Biophys. Acta **1787:** 973–984.

Kirchhoff, H. (2008). Molecular crowding and order in photosynthetic membranes. Trends Plant Sci. **13:** 201–207.

Kirchhoff, H., Horstmann, S., and Weis, E. (2000). Control of the photosynthetic electron transport by PQ diffusion microdomains in thylakoids of higher plants. Biochim. Biophys. Acta **1459:** 148–168.

Klimmek, F., Sjödin, A., Noutsos, C., Leister, D., and Jansson, S. (2006). Abundantly and rarely expressed Lhc protein genes exhibit distinct regulation patterns in plants. Plant Physiol. **140:** 793–804.

Kovács, L., Damkjaer, J., Kereïche, S., Ilioaia, C., Ruban, A.V., Boekema, E.J., Jansson, S., and Horton, P. (2006). Lack of the light-harvesting complex CP24 affects the structure and function of the grana membranes of higher plant chloroplasts. Plant Cell **18:** 3106–3120.

Koziol, A.G., Borza, T., Ishida, K., Keeling, P., Lee, R.W., and Durnford, D.G. (2007). Tracing the evolution of the light-harvesting antennae in chlorophyll a/b-containing organisms. Plant Physiol. **143:** 1802–1816.

Krieger-Liszkay, A., Fufezan, C., and Trebst, A. (2008). Singlet oxygen production in photosystem II and related protection mechanism. Photosynth. Res. **98:** 551–564.

Li, X.P., Björkman, O., Shih, C., Grossman, A.R., Rosenquist, M., Jansson, S., and Niyogi, K.K. (2000). A pigment-binding protein essential for regulation of photosynthetic light harvesting. Nature **403:** 391–395.

Li, X.P., Gilmore, A.M., Caffarri, S., Bassi, R., Golan, T., Kramer, D., and Niyogi, K.K. (2004). Regulation of photosynthetic light harvesting involves intrathylakoid lumen pH sensing by the PsbS protein. J. Biol. Chem. **279:** 22866–22874.

Li, X.P., Gilmore, A.M., and Niyogi, K.K. (2002). Molecular and global time-resolved analysis of a psbS gene dosage effect on pH- and xanthophyll cycle-dependent nonphotochemical quenching in photosystem II. J. Biol. Chem. **277:** 33590–33597.

Liu, W.J., Chen, Y.E., Tian, W.J., Du, J.B., Zhang, Z.W., Xu, F., Zhang, F., Yuan, S., and Lin, H.H. (2009). Dephosphorylation of photosystem

II proteins and phosphorylation of CP29 in barley photosynthetic membranes as a response to water stress. Biochim. Biophys. Acta **1787:** 1238–1245.

Liu, Z., Yan, H., Wang, K., Kuang, T., Zhang, J., Gui, L., An, X., and Chang, W. (2004). Crystal structure of spinach major light-harvesting complex at 2.72 A resolution. Nature **428:** 287–292.

Livingston, A.K., Cruz, J.A., Kohzuma, K., Dhingra, A., and Kramer, D.M. (2010). An *Arabidopsis* mutant with high cyclic electron flow around photosystem I (hcef) involving the NADPH dehydrogenase complex. Plant Cell **22:** 221–233.

Malkin, S., Armond, P.A., Mooney, H.A., and Fork, D.C. (1981). Photosystem II photosynthetic unit sizes from fluorescence induction in leaves. Correlation to photosynthetic capacity. Plant Physiol. **67:** 570–579.

Mauro, S., Dainese, P., Lannoye, R., and Bassi, R. (1997). Cold-resistant and cold-sensitive maize lines differ in the phosphorylation of the photosystem II subunit, CP29. Plant Physiol. **115:** 171–180.

Melis, A. (1991). Dynamics of photosynthetic membrane composition and function. Biochim. Biophys. Acta **1058:** 87–106.

Melis, A. (1999). Photosystem-II damage and repair cycle in chloroplasts: What modulates the rate of photodamage? Trends Plant Sci. **4:** 130–135.

Miloslavina, Y., Wehner, A., Lambrev, P.H., Wientjes, E., Reus, M., Garab, G., Croce, R., and Holzwarth, A.R. (2008). Far-red fluorescence: A direct spectroscopic marker for LHCII oligomer formation in non-photochemical quenching. FEBS Lett. **582:** 3625–3631.

Morosinotto, T., Baronio, R., and Bassi, R. (2002). Dynamics of chromophore binding to Lhc proteins in vivo and in vitro during operation of the xanthophyll cycle. J. Biol. Chem. **277:** 36913–36920.

Morosinotto, T., Bassi, R., Frigerio, S., Finazzi, G., Morris, E., and Barber, J. (2006). Biochemical and structural analyses of a higher plant photosystem II supercomplex of a photosystem I-less mutant of barley. Consequences of a chronic over-reduction of the plastoquinone pool. FEBS J. **273:** 4616–4630.

Moya, I., Silvestri, M., Vallon, O., Cinque, G., and Bassi, R. (2001). Time-resolved fluorescence analysis of the photosystem II antenna proteins in detergent micelles and liposomes. Biochemistry **40:** 12552–12561.

Mozzo, M., Dall'Osto, L., Hienerwadel, R., Bassi, R., and Croce, R. (2008). Photoprotection in the antenna complexes of photosystem II: Role of individual xanthophylls in chlorophyll triplet quenching. J. Biol. Chem. **283:** 6184–6192.

Müller, M.G., Lambrev, P., Reus, M., Wientjes, E., Croce, R., and Holzwarth, A.R. (2010). Singlet energy dissipation in the photosystem II light-harvesting complex does not involve energy transfer to carotenoids. ChemPhysChem **11:** 1289–1296.

Nayak, L., Raval, M.K., Biswal, B., and Biswal, U.C. (2002). Topology and photoprotective role of carotenoids in photosystem II of chloroplast: A hypothesis. Photochem. Photobiol. Sci. **1:** 629–631.

Nelson, N., and Ben-Shem, A. (2004). The complex architecture of oxygenic photosynthesis. Nat. Rev. Mol. Cell Biol. **5:** 971–982.

Niyogi, K.K. (2000). Safety valves for photosynthesis. Curr. Opin. Plant Biol. **3:** 455–460.

Niyogi, K.K., Grossman, A.R., and Björkman, O. (1998). Arabidopsis mutants define a central role for the xanthophyll cycle in the regulation of photosynthetic energy conversion. Plant Cell **10:** 1121–1134.

Oostergetel, G.T., Keegstra, W., and Brisson, A. (1998). Automation of specimen selection and data acquisition for protein electron crystallography. Ultramicroscopy **74:** 47–59.

Pesaresi, P., Sandonà, D., Giuffra, E., and Bassi, R. (1997). A single point mutation (E166Q) prevents dicyclohexylcarbodiimide binding to the photosystem II subunit CP29. FEBS Lett. **402:** 151–156.

Peter, G.F., Takeuchi, T., and Thornber, J.P. (1991). Solubilization and two-dimensional electrophoretic procedures for studying the organization and composition of photosynthetic membrane polypeptides. Methods **3:** 115–124.

Ruban, A.V., Berera, R., Ilioaia, C., van Stokkum, I.H., Kennis, J.T., Pascal, A.A., van Amerongen, H., Robert, B., Horton, P., and van Grondelle, R. (2007). Identification of a mechanism of photoprotective energy dissipation in higher plants. Nature **450:** 575–578.

Ruban, A.V., Wentworth, M., Yakushevska, A.E., Andersson, J., Lee, P.J., Keegstra, W., Dekker, J.P., Boekema, E.J., Jansson, S., and Horton, P. (2003). Plants lacking the main light-harvesting complex retain photosystem II macro-organization. Nature **421:** 648–652.

Santabarbara, S., Bordignon, E., Jennings, R.C., and Carbonera, D. (2002). Chlorophyll triplet states associated with photosystem II of thylakoids. Biochemistry **41:** 8184–8194.

Schägger, H., and von Jagow, G. (1987). Tricine-sodium dodecyl sulfate-polyacrylamide gel electrophoresis for the separation of proteins in the range from 1 to 100 kDa. Anal. Biochem. **166:** 368–379.

Strasser, R.J., Srivastava, A., and Govindjee. (1995). Polyphasic chlorophyll a fluorescence transient in plants and cyanobacteria. Photochem. Photobiol. **61:** 32–42.

Takahashi, H., Iwai, M., Takahashi, Y., and Minagawa, J. (2006). Identification of the mobile light-harvesting complex II polypeptides for state transitions in *Chlamydomonas reinhardtii*. Proc. Natl. Acad. Sci. USA **103:** 477–482.

Teardo, E., de Laureto, P.P., Bergantino, E., Dalla Vecchia, F., Rigoni, F., Szabò, I., and Giacometti, G.M. (2007). Evidences for interaction of PsbS with photosynthetic complexes in maize thylakoids. Biochim. Biophys. Acta **1767:** 703–711.

Testi, M.G., Croce, R., Polverino-De Laureto, P., and Bassi, R. (1996). A CK2 site is reversibly phosphorylated in the photosystem II subunit CP29. FEBS Lett. **399:** 245–250.

Tikkanen, M., Piippo, M., Suorsa, M., Sirpiö, S., Mulo, P., Vainonen, J., Vener, A.V., Allahverdiyeva, Y., and Aro, E.M. (2006). State transitions revisited-a buffering system for dynamic low light acclimation of Arabidopsis. Plant Mol. Biol. **62:** 779–793. Erratum. Plant Mol. Biol. **62:** 795.

Tokutsu, R., Iwai, M., and Minagawa, J. (2009). CP29, a monomeric light-harvesting complex II protein, is essential for state transitions in *Chlamydomonas reinhardtii*. J. Biol. Chem. **284:** 7777–7782.

Towbin, H., Staehelin, T., and Gordon, J. (1979). Electrophoretic transfer of proteins from polyacrylamide gels to nitrocellulose sheets: Procedure and some applications. Proc. Natl. Acad. Sci. USA **76:** 4350–4354.

Triantaphylidès, C., Krischke, M., Hoeberichts, F.A., Ksas, B., Gresser, G., Havaux, M., Van Breusegem, F., and Mueller, M.J. (2008). Singlet oxygen is the major reactive oxygen species involved in photooxidative damage to plants. Plant Physiol. **148:** 960–968.

Vallon, O., Bulte, L., Dainese, P., Olive, J., Bassi, R., and Wollman, F.A. (1991). Lateral redistribution of cytochrome b6/f complexes along thylakoid membranes upon state transitions. Proc. Natl. Acad. Sci. USA **88:** 8262–8266.

van Heel, M., Gowen, B., Matadeen, R., Orlova, E.V., Finn, R., Pape, T., Cohen, D., Stark, H., Schmidt, R., Schatz, M., and Patwardhan, A. (2000). Single-particle electron cryo-microscopy: Towards atomic resolution. Q. Rev. Biophys. **33:** 307–369.

Van Kooten, O., and Snel, J.F.H. (1990). The use of chlorophyll fluorescence nomenclature in plant stress physiology. Photosynth. Res. **25:** 147–150.

van Oort, B., Alberts, M., de Bianchi, S., Dall'Osto, L., Bassi, R., Trinkunas, G., Croce, R., and van Amerongen, H. (2010). Effect of antenna-depletion in Photosystem II on excitation energy transfer in *Arabidopsis thaliana*. Biophys. J. **98:** 922–931.

Walters, R.G., Ruban, A.V., and Horton, P. (1996). Identification of proton-active residues in a higher plant light-harvesting complex. Proc. Natl. Acad. Sci. USA **93:** 14204–14209.

Wehner, A., Grasses, T., and Jahns, P. (2006). De-epoxidation of violaxanthin in the minor antenna proteins of photosystem II, LHCB4, LHCB5, and LHCB6. J. Biol. Chem. **281:** 21924–21933.

Yamamoto, H.Y., and Higashi, R.M. (1978). Violaxanthin de-epoxidase. Lipid composition and substrate specificity. Arch. Biochem. Biophys. **190:** 514–522.

Yu, J., et al. (2002). A draft sequence of the rice genome (*Oryza sativa* L. ssp. *indica*). Science **296:** 79–92.

Zhang, S., and Scheller, H.V. (2004). Photoinhibition of photosystem I at chilling temperature and subsequent recovery in *Arabidopsis thaliana*. Plant Cell Physiol. **45:** 1595–1602.

Zygadlo, A., Jensen, P.E., Leister, D., and Scheller, H.V. (2005). Photosystem I lacking the PSI-G subunit has a higher affinity for plastocyanin and is sensitive to photodamage. Biochim. Biophys. Acta **1708:** 154–163.

Publication 4

Review

Supramolecular organization of photosystem II in green plants ☆

Roman Kouřil [a], Jan P. Dekker [b],*, Egbert J. Boekema [a]

[a] *Electron microscopy group, Groningen Biomolecular Sciences and Biotechnology Institute, University of Groningen, Nijenborgh 7, 9747 AG Groningen, The Netherlands*
[b] *Faculty of Sciences, Division of Physics and Astronomy, VU University Amsterdam, De Boelelaan 1081, 1081 HV Amsterdam, The Netherlands*

ARTICLE INFO

ABSTRACT

Green plant photosystem II (PSII) is involved in the light reactions of photosynthesis, which take place in the thylakoid membrane of the chloroplast. PSII is organized into large supercomplexes with variable amounts of membrane-bound peripheral antenna complexes. These supercomplexes are dimeric and contain usually 2–4 copies of trimeric LHCII complexes and have a further tendency to associate into megacomplexes or into crystalline domains, of which several types have been characterized. This review focuses on the overall composition and structure of the PSII supercomplex of green plants and its organization and interactions within the photosynthetic membrane. Further, we present the current knowledge how the thylakoid membrane is three-dimensionally organized within the chloroplast. We also discuss how the supramolecular organization in the thylakoid membrane and the PSII flexibility may play roles in various short-term regulatory mechanisms of green plant photosynthesis. This article is part of a Special Issue entitled: Photosystem II.

© 2011 Elsevier B.V. All rights reserved.

1. Introduction

Photosystem II (PSII) is one of the key proteins of the light reactions of photosynthesis. It is universally distributed throughout prokaryotes and eukaryotes capable of oxygenic photosynthesis, including higher plants, macroalgae, diatoms, dinoflagelates, and the oxyphotobacteria (cyanobacteria and prochlorophytes), but not in archea [1]. In this review we will focus on the green plant system. The function of PSII and its role in the light reactions of photosynthesis cannot be understood without a detailed knowledge of its structure, including its peripheral antenna. Over the last two decades a substantial effort has been put on solving medium (4–10 Å) to high-resolution (<3 Å) structures of intact PSII complexes [2–7], single subunits [8–12] and light-harvesting complex II (LHCII) [13,14], which forms part of the peripheral antenna. Most of the high resolution information, however, has been obtained with cyanobacterial PSII complexes, which are generally more stable than the complexes from plants. There is also an increasing emphasis on the interaction of these complexes into higher order associates, like supercomplexes. This is not unique for the chloroplast, since also in the (plant) mitochondrion the existence of several supercomplexes has been described, such as a dimeric form of the ATP synthase [15] and a supercomplex consisting of monomeric complex I and dimeric complex III [16].

A good understanding of the reactions performed by PSII does, however, not only require a deep knowledge of its structure including the peripheral light-harvesting complexes, it requires also knowledge

of how PSII works together with the other main protein complexes such as photosystem I (PSI) and the cytochrome b_6f complex in the photosynthetic membrane to perform the primary light reactions. This is particularly relevant for the light-harvesting function and its regulation. During evolution green plants have adapted different strategies to develop and survive in very diverse environmental conditions characterized by high light or low light, strongly fluctuating light conditions, conditions in which the incoming light is spectrally altered due to shading by water or other photosynthetic organisms or certain types of stress conditions.

To understand how PSII works in the photosynthetic or thylakoid membrane we have to study this membrane in detail within the intact chloroplast. The thylakoid membrane forms a physically continuous three-dimensional network that encloses a single aqueous space, the thylakoid lumen. A characteristic feature of this membrane is its extensive folding. As a consequence, the thylakoid membranes of vascular plants and some green algae are structurally inhomogeneous. They consist of two main domains: the grana, which are stacks of thylakoids, and the stroma lamellae, which are unstacked thylakoids and connect the grana stacks. Three-dimensional models of the spatial relationship between grana and stroma thylakoids show that PSII and LHCII reside mainly in the grana membranes, while PSI and ATPase reside predominantly in the stroma and the cytochrome b_6/f complex is distributed about evenly between the two types of membranes. It is important to realize that protein–protein interactions determine for a major part the shape and folding pattern of the thylakoid membrane [17]. In other words, we need to know the precise interactions of PSII with its neighbors within the intact chloroplast to fully comprehend how the light reactions of photosynthesis occur under changing light and environmental conditions.

This review focuses on the overall composition and structure of the PSII supercomplex of green plants and its organization and interactions within the photosynthetic membrane. Further, we present the current knowledge how the thylakoid membrane is three-dimensionally organized within the chloroplast and finally how this organization can play roles in the various photosynthetic regulation mechanisms.

2. Molecular organization of photosystem II

2.1. Peripheral antenna

In higher plants, the peripheral antenna consists of a number of pigment–protein complexes belonging to the Lhc super-gene family [18]. Two types of peripheral antenna proteins associated to PSII can be distinguished. The most abundant complex is the so-called "major" LHCII antenna complex. This complex occurs in a trimeric oligomerization state and consists of various combinations of three very similar proteins, encoded by the Lhcb1, Lhcb2 and Lhcb3 genes, which usually occur in a ratio of about 8:3:1 [19]. In addition, there are three "minor" antenna complexes, which are called Lhcb4 (CP29), Lhcb5 (CP26) and Lhcb6 (CP24) and usually occur in monomeric states. All these complexes bind various pigment molecules and the high-resolution structures of the major trimeric LHCII complex and CP29 have been solved [12–14]. It is likely that the minor complexes CP26 and CP24 adopt rather similar overall three-dimensional organizations.

2.2. PSII–LHCII supercomplexes

A variable number of peripheral antenna proteins can associate with dimeric PSII core complexes to form PSII–LHCII supercomplexes [17]. These supercomplexes have been denoted according to their composition. A dimeric core, C_2, can associate with up to four copies of peripheral LHCII trimers. Connection of the first two LHCII S-trimers extends a C_2 complex to a C_2S_2 supercomplex, and two further M-trimers are bound in a $C_2S_2M_2$ supercomplex [20]. Spinach supercomplexes may bind a third type of L-trimer, but the resulting $C_2S_2M_2L_{1-2}$ supercomplexes are rare. The C_2S_2 supercomplex contains almost all PSII core proteins [21], but from the peripheral antenna the Lhcb3 and CP24 proteins appear to be absent [22]. A three-dimensional structure of this supercomplex from spinach was constructed using a low-resolution 3D electron density map obtained by single particle cryo electron microscopy [23]. A recent analysis concerns the larger, $C_2S_2M_2$ supercomplex of *Arabidopsis thaliana* and shows details at 12 Å resolution [24], permitting a more accurate fitting of the peripheral antenna proteins, based on the known LHCII structure. The combination of high-resolution structures of components with the low-resolution provided by electron microscopy is useful because the precision of fitting an X-ray structure into an EM density map is much better than the resolution of the EM data [25]. The model is presented in Fig. 1 and shows how within the PSII–LHCII supercomplex the innermost LHCII S-trimer is attached to a dimeric PSII via CP29, binding to one PSII core monomer and CP26 to the other. Indeed, monomeric cores with a full set of peripheral antenna particles have never been observed in disrupted grana, although recently a particle consisting of a monomeric core plus CP26 and one LHCII trimer was found in *Arabidopsis* [24]. The need for dimeric core configuration also explains why the peripheral antenna proteins easily detach from PSII during the transition from dimer to monomer. No intact supercomplexes could be isolated from *Arabidopsis* plants expressing antisense constructs to CP29 [26], although recently small numbers of PSII–LHCII supercomplexes with empty Lhcb4 binding sites could be found [S. de Bianchi, N. Betterle, R. Kouřil, S. Cazzaniga, E. J. Boekema, R. Bassi and L. Dall'Osto, Plant Cell, in press]. This suggests that CP29 occupies a unique position in the PSII macrostructure and that in contrast to CP26 its presence is essential for the formation of PSII–LHCII supercomplexes. Both the CP29 and CP26 antisense mutants showed a rather normal photosynthetic performance, although the mutants showed slightly different fluorescence characteristics and an increased number of PSII centers [27]. This suggests that the organization of PSII and LHCII into supercomplexes is not absolutely required for photosynthetic performance, at least under normal physiological conditions and light levels.

A more peripheral LHCII trimer (M-trimer) is attached via CP24 and CP29. CP24 is necessary for binding the M-trimer because *Arabidopsis* plants depleted of CP24 do not form $C_2S_2M_2$ supercomplexes [28]. In the green alga *Chlamydomonas reinhardtii*, which lacks CP24, only C_2S_2 supercomplexes could be detected [17]. Some small core subunits, such as PsbW, are also necessary for intact supercomplexes [29], but their localization is not yet clear.

Analysis of supercomplexes isolated from *Arabidopsis* plants expressing an antisense construct to Lhcb2 revealed that the LHCII binding sites are not unique for the various types of trimers [30]. In these plants, not only was the synthesis of Lhcb2 almost completely
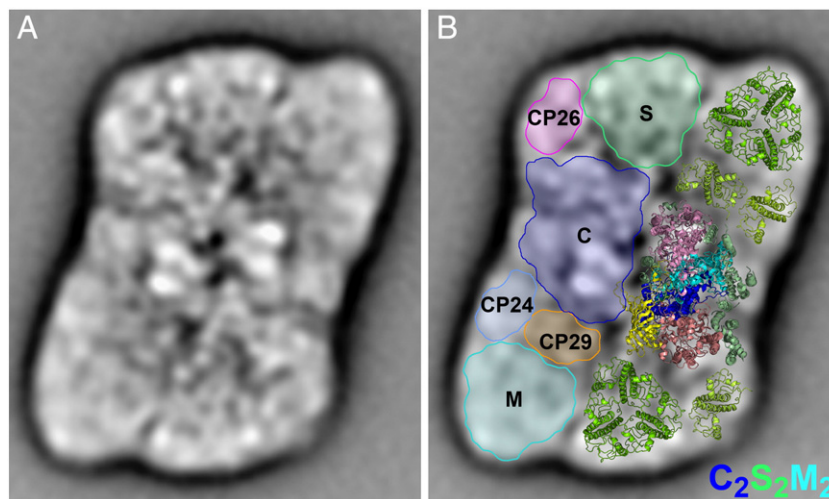
Fig. 1. Projection map and a structural model of the PSII $C_2S_2M_2$ supercomplex. (A) Top view projection map of the $C_2S_2M_2$ supercomplex from *Arabidopsis thaliana* obtained from single particle electron microscopy. (B) Assignment of the subunits of the supercomplex by fitting the high-resolution structures of PSII core [7] (subunits D1, D2, CP43, CP47 and extrinsic subunit PsbO are highlighted in blue, cyan, salmon, pink and yellow, respectively) and Lhcb [13] (trimeric LHCII and monomeric Lhcb in dark and light green, respectively). PSII core monomer, "C"-, "S"- and "M"-type of LHCII trimers and the minor antennas, CP24, CP26 and CP29, are schematically depicted in blue, light green, cyan, light blue, magenta and orange contours, respectively. Adapted from Ref. [24].

abolished, but also that of the strongly related Lhcb1 protein [31]. It appeared that in these plants, the expression of the antisense Lhcb2 construct resulted in strongly increased levels of CP26 and (to a minor extent) Lhcb3, and that supercomplexes were formed with trimers consisting of Lhcb5 and Lhcb3 at the S- and M-binding positions [30]. This replacement is unique, because expression of antisense constructs to the minor peripheral antenna proteins and to the peripheral antenna proteins of PSI did not lead to increased synthesis of other proteins, and stresses the importance of the particular organization of PSII and LHCII in supercomplexes.

2.3. Energy transfer

The recent structures of PSII–LHCII supercomplexes allow a more detailed description of the energy transfer routes from the peripheral antenna to the core antenna and the reaction center. Fig. 2 shows the chlorophylls and carotenoids of one half of the $C_2S_2M_2$ supercomplex, based on data reported in Ref. [24], with chlorophylls a in green and chlorophylls b in blue to point out the major routes of energy transfer between the pigment–protein complexes, based on a relatively close proximity of chlorophylls a in adjacent complexes (arrows Fig. 2). Chlorophylls b are probably only to minor extents involved in energy transfer between complexes, because their energies are at least 2 k_BT higher than those of chlorophylls a. The figure shows that within each PSII core monomer, there are two major routes of energy transfer, i.e., from CP47 to the RC and from CP43 to the RC (yellow arrows), and that within the supercomplex there are also two major routes of energy transfer to the PSII core (blue arrows). The first route goes from S-LHCII and/or CP26 to CP43 and the PSII core monomer on the left in Fig. 2, the other route goes from M-LHCII and CP24 via CP29 to CP47 and the other PSII core monomer on the right in Fig. 2. Along the sides of the PSII core, there is a rim of pigment-free low-molecular mass proteins (indicated by grey bars in Fig. 2), which prevents a close
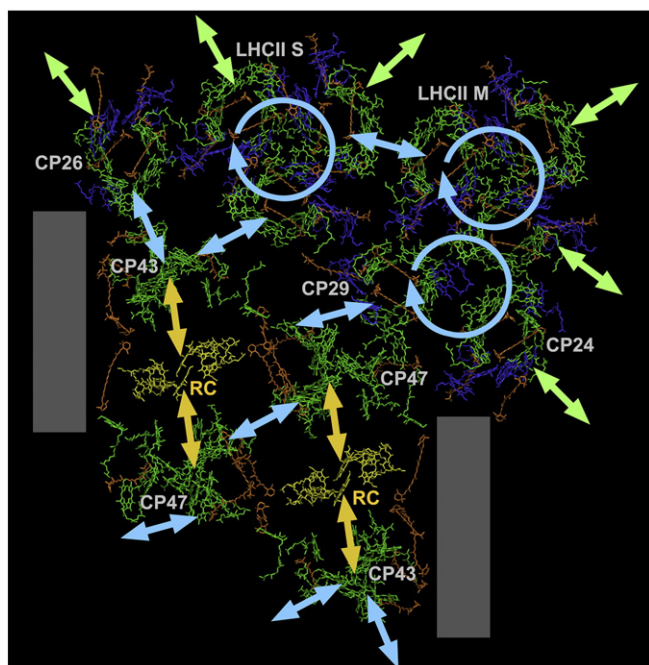
Fig. 2. Energy transfer routes within the PSII $C_2S_2M_2$ supercomplex. The chlorophylls and carotenoids of one half of the $C_2S_2M_2$ supercomplex are depicted, with chlorophylls a in green, chlorophylls b in blue and carotenoids in orange. The six central chlorophylls and pheophytins of the PSII RC are depicted in yellow. The arrows indicate major routes of energy transfer between (i) the RC and the core antenna proteins CP43 and CP47, (yellow arrows), (ii) within the supercomplex (blue arrows), and (iii) to or from possible neighboring (super)complexes within the membrane (green arrows). Grey bars indicate a rim of pigment-free low-molecular mass protein subunits. The model is based on data reported in Ref. [24].

proximity of chlorophylls between neighboring complexes and therefore makes energy transfer through this part of the structure less likely. This means that energy transfer to the supercomplexes within the membrane will predominantly flow through the peripheral antenna (green arrows) and not among dimeric PSII core complexes. This structural arrangement could be advantageous for the effectiveness of regulatory processes of light harvesting (such as high-energy quenching, see below).

3. Organization of supercomplexes in stacked grana membranes

There is quite some variation in the numbers and distribution of the PSII supercomplexes over the grana membranes. Most grana membranes show a rather random organization (Fig. 3A), but in some conditions, which are still not exactly understood, large parts of the membranes occur in semi-crystalline domains and row-like associations (Fig. 3B, C). The formation of semi-crystalline domains in the membrane requires a physical separation of PSII supercomplexes from the other membrane proteins, e.g. free LHCII proteins or PsbS (see also the Section 5.2), which can hamper a specific ordering of PSII supercomplexes into 2D arrays. However, the forces which lead to the protein separation, remain to be elucidated. It is likely that the ordered configuration is energetically favorable and that the random configuration is entropically favorable, and so it is possible that the network of forces at work in the membranes is balanced in such a way that relatively large structural changes (from disorder to order and vice versa) become possible with minimal energetic changes, thus allowing functional modifications.

Crystalline 2D arrays of dimeric PSII have been observed decades ago after freeze-etching and freeze-breaking of green plant photosynthetic membranes (see Refs. [17,22,32] for recent reviews). There is quite some variation in these crystalline arrays, which depends on factors like temperature and biochemical composition of the grana membranes. At least three types of supercomplexes can form the crystals (C_2S_2, C_2S_2M and $C_2S_2M_2$), see Ref. [17] and moreover, these different types of particles can arrange in several different types of packing, which means that the interaction with neighbors is different. A recent novel type of packing of $C_2S_2M_2$ found in *Arabidopsis* is presented in Fig. 3D. The relevance of such crystals was not clear until recently when Kirchhoff et al. could relate the crystals to light conditions [33]. They found a remodeling of the photosynthetic machinery induced by growing spinach plants under low light intensities. This caused an up-regulation of light-harvesting complexes and down-regulation of PSII and cytochrome b_6f complexes in intact thylakoids and isolated grana membranes [33]. The antenna size of PSII increased by 40–60% as estimated by fluorescence induction and LHCII/PSII stoichiometry. These low light-induced changes in the protein composition were accompanied by the formation of ordered PSII complexes in grana thylakoids as detected by electron microscopy. They suggested that the supramolecular reorganization in ordered arrays in low light grana thylakoids is a strategy to overcome potential diffusion problems in this crowded membrane [33].

A further variation in the organization of supercomplexes is caused by the occurrence of pairs of supercomplexes. Image analysis of these pairs has indicated that the supercomplexes can laterally associate to each other in rather specific ways to form megacomplexes. In spinach three types of megacomplexes (dimers of supercomplexes) have been observed thus far, while in *Arabidopsis* a fourth type was found [17]. Some of these megacomplexes appear to be similar to two building blocks within the crystalline arrays [17].

Finally, the higher association of supercomplexes is not restricted to one grana membrane. It appeared that ordered PSII arrays are formed in two adjacent membranes, which are in a specific contact through their stromal sides. There are preferential angles between rows in opposing membranes, both in spinach and in *Arabidopsis*
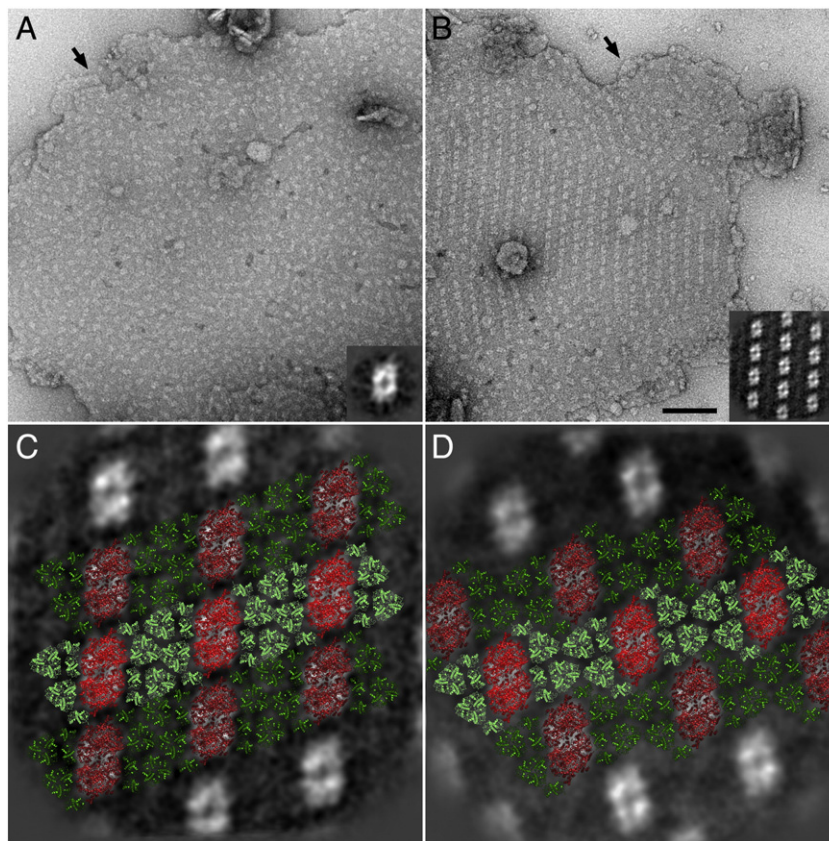
Fig. 3. The higher organization of PSII complexes in the thylakoid membrane. Examples of electron micrographs of negatively stained pairs of thylakoid membranes isolated from *Arabidopsis thaliana* with either a random (A) or ordered (B) organization of PSII complexes. Detergent treatment removed the margins; the black arrows point at remaining single membranes at the periphery. The inset in (A) shows the result of single particle analysis of 224 PSII particles selected from the electron micrograph. The projection map shows a typical density of the PSII core complex. The inset in (B) shows the result of single particle analysis of 96 sub-areas of ordered arrays of PSII complexes selected from the electron micrograph. (C) Assignment of the 2D array of PSII from (B) by the fitting of the structural model of the PSII $C_2S_2M_2$ supercomplex according to Ref. [24]. (D) A novel type of packing of the PSII $C_2S_2M_2$ supercomplexes. Scale bar for the electron micrographs in (A, B) is 100 nm.

[17,34]. At these angles the overlap of LHCII trimers is optimized, at least for the central part of the domains. For spinach the preferential angles were about 3° and 46° [35] or about 90° [34], and for *Arabidopsis* they were about 32° and 58° [36]. The fact that optimal angles are different for these two plant species is related to different basic units (C_2S_2M and $C_2S_2M_2$, respectively). These crystals indicate that the organization of the complexes in one membrane affects the organization of complexes in the opposing membrane and in particular, the preferential angles induce a strong overlap of LHCII trimers of adjacent layers (Fig. 4).

Much of the earlier work on the organization of PSII–LHCII supercomplexes in grana membranes was performed on detergent-derived membrane fragments, the so-called BBY preparations [37]. It was recently shown that the protein packing ratio in these membranes is about 80%, which is slightly higher than the ratio of 70% found in intact grana thylakoids [38], and that dilution of BBY membranes with lipids down to the ratio of 70% resulted in an increased antenna size and enhanced connectivity between reaction centers. Further dilution resulted in a functional disconnection between PSII and LHCII, suggesting that a packing ratio of about 70% brings about optimal photosynthetic performance, by keeping on one hand the distance between the various antenna and PSII core complexes as short as possible to allow fast excitation energy transfer kinetics, and on the other to allow sufficient structural flexibility to allow long-range transport of plastoquinone and to respond optimally to short-term physiological adaptations (e.g., high-energy quenching, state transitions, D1 repair).

In line of this, it was recently shown that excitation energy transfer in PSII is somewhat slower in intact thylakoids than in isolated PSII

membranes [39], suggesting on average a larger distance between PSII and a part of the peripheral antenna in physiological conditions. It was furthermore shown that PSII fluorescence lifetimes were similar in wild-type thylakoids and in thylakoids obtained from a mutant lacking CP26, whereas longer PSII fluorescence lifetimes were observed in mutants lacking CP29 or CP24 [39]. It was discussed above that mutants lacking CP26 retain the supramolecular organization of PSII and LHCII, whereas in mutants lacking CP29 the supercomplexes are much less stable [26], so this result suggests that an organization of PSII and LHCII in supercomplexes facilitates the transfer of excitation energy to the PSII core complexes. The absence of CP24 prevents the formation of $C_2S_2M_2$ supercomplexes but retains the possibility to form C_2S_2 supercomplexes [28], suggesting that in particular the additional M-LHCII–CP24–CP29 energy transfer route (Fig. 2) is important for allowing fast energy transfer between peripheral and core antenna.

4. Overall chloroplast membrane topology

The thylakoid membrane of higher plants forms a very characteristic network consisting of grana stacks interconnected by stroma thylakoids. The 3D architecture of the granum–stroma assembly and the entire thylakoid membrane network is intriguing, especially because of the ability of the membranes to undergo reversible changes in folding and organization under varying environmental conditions [40,41]. In the next sections we will focus on the most recent efforts to determine the overall 3D organization of the thylakoid membranes, of which the capacity to form grana stacks is a well-known aspect. In a previous review we discussed several aspects of the stacking, such as the factors
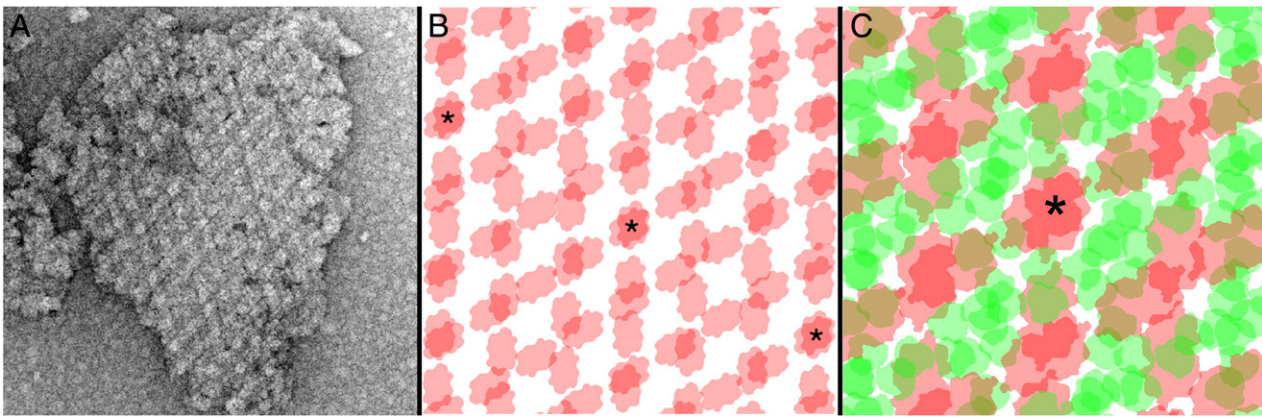
Fig. 4. Example of preferential stacking in paired inside-out grana membranes from *Arabidopsis thaliana*. (A) Electron micrograph of a negatively stained grana fragment of a 58°-type in which the layers make an angle of about 58°. (B) Simulation of the overlap pattern in the 58°-type crystal, based on 150 averaged crystals [36]. Asterisks indicate positions where PSII core complexes (in red) of adjacent layers match optimally. (C) The specific positions of the core complexes of two layers cause a strong local overlap of part of the LHCII trimers (light green).

that sustain the grana and stroma division the protein distribution within the stacks and the location of the cytochrome b_6/f complex [17]. Some are worth to repeat briefly, to better appreciate novel findings about changes in response to stress and other factors.

One of the main consequences of stacking is the physical separation of PSI and PSII. The stacking not only prevents spill-over of excitation energy, but it also provides the chloroplast the means to fine-regulate the light requirements for photosynthesis and provides PSII a very large functional antenna, in which excitation energy can flow within a thylakoid membrane and between two stacked membranes until an 'open' PSII reaction center is found. In addition, it provides an easy means to adapt to low light conditions, in which both the amount of LHCII and the extent of stacking have been shown to increase [17]. It is also possible that a physical separation of PSII and PSI is required to fine-tune the balance between linear and cyclic electron transport, as discussed before in more detail [17].

4.1. Architecture of chloroplast thylakoid membrane

Despite considerable efforts to get a detailed view of the 3D organization of the thylakoid membranes using different experimental approaches (employing conventional electron microscopy, state-of-the-art cryo electron tomography or atomic force microscopy), there is not yet a consistent view of the overall membrane architecture. Discrepancies in the interpretation of structural data can be caused by technical limitations of different experimental approaches and thus in the resolution of 3D reconstructions, or by the flexibility of the plant material. A major obstacle is the size of the entire thylakoid membrane system within an intact chloroplast. This size is just exceeding the limits of the penetration power of a medium-voltage transmission electron microscope and thus makes their direct visualization in an intact form unachievable. Analysis of either thin sections or partially solubilized thylakoid membranes can be applied to overcome the sample thickness limitation [42], however, at the cost of loss of intactness of the 3D membrane architecture.

In the last 40 years, several models of the thylakoid membrane organization have been proposed (see Ref. [43]). Two of them, the helical model and the fork or folded membrane model (Fig. 5), can be discussed as appropriate models of the thylakoid membrane architecture.

4.1.1. Helical model

In the helical model, which was derived from EM studies of thin sections and serial sections of chemically fixed thylakoid membranes [44], the tilted stroma thylakoids are wound around the granal stacks in the form of multiple right-handed helices, where each granum

thylakoid is connected to an average of seven stroma thylakoids (Fig. 5A). The helical arrangement of the stroma thylakoids around grana was further supported by other electron microscopy techniques including scanning electron microscopy [45] and freeze-fracture EM [46]. More recently further evidence came from a number of electron tomography studies: (i) on serial sections of chemically fixed membranes [47], (ii) on high pressure frozen and freeze-substituted sections of chloroplasts [48], and (iii) on high pressure frozen vitreous sections of isolated chloroplasts and thylakoid membranes [34]. In addition, these new tomography data revealed new and unexpected features. For instance, the periodicity of the connections between the stroma and grana thylakoids appeared to be more variable than previously proposed. Furthermore, there are fewer connections between one particular granum thylakoid and its surrounding stroma thylakoids [48]. Also the number of connected grana thylakoids in a stack by one spiral stromal thylakoid seems to be lower than previously thought [34,48]. Finally, dimensions of the connections between the stroma and grana thylakoids were found wider and also more variable in size [34,48]. Thus, their possible role in a regulation of the flow of ions, membrane molecules and proteins between stroma and grana thylakoids was suggested [48]. On the other hand, the observed variable dimensions of membrane connections can be accidental and thus these variations do not necessarily point to a regulatory role.

4.1.2. Fork model

In the fork or folded membrane model, which was originally proposed to illustrate the lateral heterogeneity in the distribution of PSII and PSI in the thylakoid membrane [49], the stroma membranes bifurcate and make a fork, which connects two adjacent grana thylakoids within a stack (Fig. 5B). The model became popular in the field especially due to its ability to illustrate in a simple and understandable way a principle of a dynamic reversible folding/unfolding of the thylakoid membrane [50]. Although the proposition of the fork model was not based on direct structural data, the fork motif was observed in many micrographs, including those of thin serial sections, which were, however, interpreted in favor of the helical model, due to a low depth resolution of serial sectioning [47]. Strong evidences for the existence of the fork at the granum–stroma assembly were provided by cryo tomography on cryo immobilized and freeze-substituted sections of intact leaves [42] and high pressure frozen vitreous sections [34]. The former work further indicates that the adjacent grana membranes fuse both at the margin of and within grana stacks, which is important for granum formation [42]. However, the formation of such membrane bridges would put significant constraints on the reversible membrane folding/unfolding. Structural
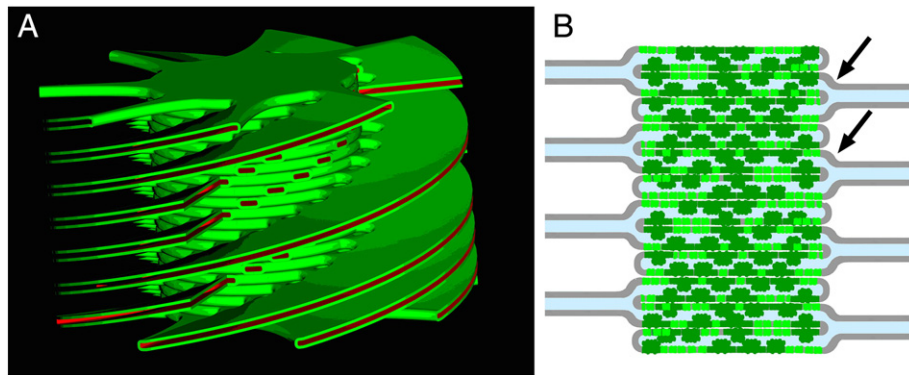
Fig. 5. Two current models for the 3D organization of thylakoid membranes in plant chloroplasts. (A) The helical model (from Ref. [43]). (B) The fork model (based on earlier drawings first presented in Ref. [49]) with a schematic presentation of PSII and LHCII trimers in dark and light green, respectively. The black arrows indicate a fork formation.

studies of thylakoid membrane rearrangements during state transitions indicate that a significant alteration of the membrane organization is accompanied by a reversible membrane fission and fusion [51]. Interestingly, recent tomography data suggest the existence of tubular interconnections between adjacent parallel stroma thylakoids [48].

4.1.3. Conclusions of overall 3D structure

In the light of these novel findings, it is evident that our current structural models are still rather limited and there is a clear need for further improvements of our structural knowledge of the thylakoid membrane architecture to better understand dynamic changes in the membrane folding. Earlier models of the thylakoid membrane organization, which have been obtained using conventional microscopy techniques, are now challenged by new tomography data [47,52,53]. Undoubtedly, a study of intact frozen-hydrated samples (free of fixation artifacts) using cryo electron tomography on a high-voltage electron microscope is an approach that could shed light on the grana structure, the granum–stroma assembly and the grana dynamics, because it visualizes the protein complexes within the membranes and therefore can provide insight in the molecular interactions that underlie the membrane architecture. However, any further refinement of current models will depend very much on the performance of electron microscopy hardware to reach better data acquisition and on perfecting tomography reconstruction techniques, necessary to image complete chloroplasts.

4.2. Dynamic rearrangements within the grana stacks

Besides the enigmatic 3D organization of the entire thylakoid membrane, the individual grana stacks possess other intriguing features. Firstly, although the diameter of single grana discs usually varies within a rather narrow range between 300 and 600 nm [43,54], the extent of grana membrane stacking is highly alterable under different and often varying environmental conditions [55]. Shade-type plants are characteristic for much broader grana with more stacked thylakoids per granum compared to sun-type plants [56]. Even a short exposure of plants to a lower light intensity results in a loss of small grana and formation of larger ones. The opposite is observed under a higher light intensity, although the total changes of the grana membrane stacking (a grana disc area) did not exceed 20% [57]. Surprisingly, a high light treatment induced a similar effect on grana membrane stacking, which was observed under a low light intensity. The observed effect of light quantity on the grana membrane stacking was attributed to a structural alteration that occurs in the thylakoid membrane during state transitions, as they were found to be controlled by the light intensity, not exclusively by a spectral light quality [58]. However, further studies showed that state transitions induced by light of a specific spectral composition can

bring about a structural rearrangement of the thylakoid membrane even at a larger scale [51]. It is also intriguing that the extent of *in vitro* thylakoid membrane unstacking can be further enhanced by e.g. low salt conditions or elevated temperature, when a complete reversible unstacking of the thylakoid membrane can be observed [50,54,59,60]. It clearly indicates that the thylakoid membrane represents a dynamic system, which can undergo under different conditions of highly variable structural rearrangements. It remains to be answered whether only one or more factors are involved in a regulation of the induced membrane rearrangements.

Secondly, the vertical distances between the stacked grana membranes are highly variable [41]. On the stromal side, the grana membranes are very flat, as their protein constituents (PSII, LHCII, cyt b_6/f complex) do not possess any protruding stromal domains. These structural features allow a very close stromal contact between two adjacent layers, which facilitates the stacking of these membranes (reviewed in Ref. [17]). The width of the stromal gap, estimated from thin sections of plastic-embedded chloroplasts, was found to vary between 2 nm and 4 nm. A value of 2.6 nm was determined from an atomic force microscopy study [61], which seems to represent a situation of displaced organization of PSII complexes in two adjacent membranes. Analysis of cryo tomography data indicates an average width of the stromal gap 3.2 nm [34], which most likely represents a spatial limit for a juxtaposition of PSII complexes. Calculation of electrostatic surfaces from the X-ray structure of LHCII [14] and their fitting into the tomography data proved that the stromal gap of 3.2 nm is sufficient to accommodate N terminal peptides of two adjacent LHCII trimers upon their interdigitation [34]. In contrast, at the lumenal side, the distance between the membranes is (i) much larger due to the presence of large membrane-protruding subunits of the PSII core and cytochrome b_6/f complex and (ii) much more variable. The lumen width derived from plastic-embedded thin-sectioned chloroplasts varies roughly from 6 to 16 nm (reviewed in Ref. [17]). Recently, cryo tomography data reported a lumen width within the above range [42,62], although a tighter contact of about 5 nm was also reported in cryo tomography [34] and an atomic force microscopy study [61]. The observed variation is related to the light-induced acidification of the lumen, which was accompanied by a shrinking of the lumen volume [34,41,63,64]. However, the observed effect of light on the lumen width seems to represent a more complex response, as the opposite light effect was observed during state transitions. Under state 2 light conditions, a swelling of the lumen volume up to about 24 nm was observed [51], which strikingly differs from e.g. ~5 nm lumen width observed in plants adapted to growing light conditions [34]. It was hypothesized that the observed variation of the lumen volume is mediated by the light-induced structural rearrangement of the oxygen-evolving-complex (OEC) of PSII [65], which represents the largest membrane-protruding domain at the lumenal side and thus the main spatial barrier determining the lumen

space. Under optimal light conditions, when PSII is photochemically active, a fully assembled OEC complex can closely interact in the lumen with the OEC of the opposite PSII complex. Under unfavourable light conditions, which lead to an inhibition of the photochemical activity of PSII complex, the OEC complex and its interaction with the opposite OEC are destabilized, which results in an expansion of the lumen. Namely PsbQ, an extrinsic subunit of OEC of PSII, was proposed to be a key subunit involved in the above-mentioned interactions as well as in the structure and dynamics of grana membrane stacking [65]. However, considering the height of OEC complex (about 4.5 nm), the hypothesis can only explain a shrinkage of the lumen up to 9 nm for a juxtaposition of PSII complexes. Reported values of the lumen width under 9 nm have to indicate a displacement of OECs of opposing PSII complexes. Although a mechanism and reason of the lumenal volume variation is not fully understood yet, shrinkage of the lumen space could severely hinder the mobility of the complexes in both membranes [61] and also limit the available volume for lumenal proteins. On the contrary, a lumen swelling under e.g. state 2 conditions [51] could facilitate a lateral diffusion of phosphorylated LHCII in the grana membrane. The finding of novel densities attached to the lumenal side of LHCII trimers in supercomplexes (see below in Section 4.3.2 and Fig. 6) further constrains possible large-scale shrinkage of lumen widths.

4.3. Higher organization of PSII in situ

4.3.1. Possibilities and limitations of freeze-fracture EM and AFM

The possibility of studying the 3D organization of photosynthetic proteins in situ, within the thylakoid membrane has been a long standing dream, because it would give an opportunity to obtain information about their distribution and their higher organization. As will be explained in the next section, this possibility was only realized recently. For many years, freeze-fracture EM was the only way to obtain basic information about a lateral distribution of photosynthetic proteins within different compartments of thylakoid membrane from a metal replica of split lipid bilayer (see Ref. [32] for a review). Although the resolution of the technique is rather limited, it allows monitoring the protein density and distances of neighboring complexes in the membrane. Using this approach, an interesting observation was recently made by a study of PSII rearrangements under either low light or high light intensities, which were found to induce a decrease in the density of PSII in the grana thylakoid membrane [66,67]. Moreover, the former study revealed the formation of rows of ordered PSII particles in low light grana thylakoids. Freeze-fracture EM was also used to show that the formation of a photoprotective state induced by a short-term exposure of plants to high light is accompanied by rapid and reversible structural rearrangements of photosynthetic proteins in the membrane. These rearrangements involve the dissociation of LHCII from PSII followed by LHCII aggregation and a tighter clustering of PSII particles [68]. Atomic force microscopy is another technique to study proteins in native membranes, by means of their surface properties. Because of a higher lateral resolution, in the range of about 4 nm, it can determine not only the position of individual PSII complexes within unfixed grana membranes, but also their orientation, which was found to be often in a parallel alignment [61, K. Sznee, J.P. Dekker, R.T. Dame, H. van Roon, G.J.L. Wuite and R.N. Frese, manuscript in preparation]. In particular, height differences can be determined quite accurately.

4.3.2. Emerging technique of cryo electron tomography

Although the AFM technique can provide structural data in three dimensions, it is basically limited to register the surface topology of objects with height differences. Hence the amount of structural information about, e.g., a three-dimensional membrane stack is rather limited. In contrast, cryo electron tomography can provide full 3D information and is currently the most promising technique with a great potential to fully extend our structural knowledge of intact biological objects in three dimensions close to in vivo conditions [69]. Cryo electron tomography is most efficient with thin objects because there is a direct relation between the size of an object and the theoretical resolution [70]. Objects up to about 0.5–1 μm can be studied at reasonable resolution, but for larger objects the thickness causes problems, engraved by multiple scattering of electrons. To overcome the specimen thickness limitation, large objects can be cut into a series of thin vitrious sections, which are examined separately. An alternative approach is to slightly disrupt organelles. The loss of in vivo conditions is compensated by a possibility to reach a higher resolution in a tomographic reconstruction. The latter approach was
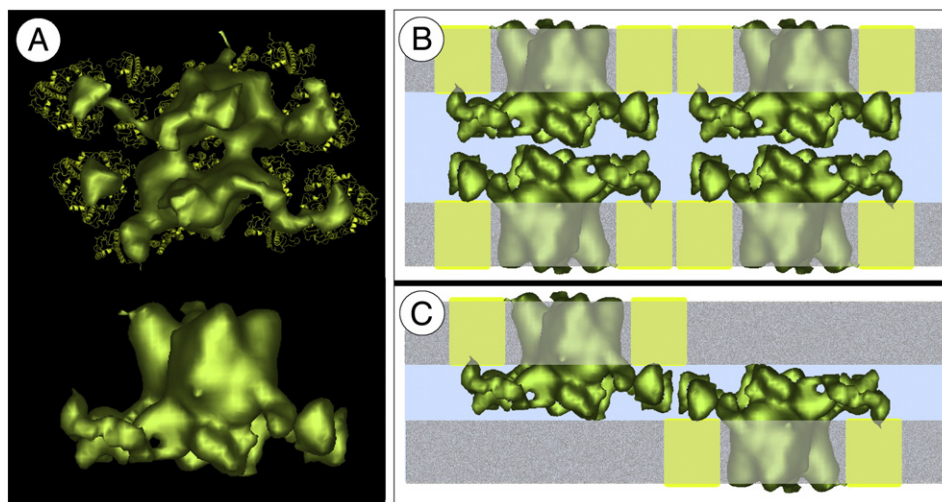
Fig. 6. 3D model of the PSII core complex and its possible organization in a pair of grana membranes. (A) 3D average of subvolumes of PSII complexes selected from tomographic reconstructions, viewed from the lumenal side and from a side along the membrane plane (from the top to bottom, respectively) [62]. Isosurface model shows the PSII core complex together with extrinsic subunits of oxygen-evolving complex resolved on the lumenal side of the complex. Further, four additional spherical densities were revealed at the lumenal side of the PSII complex. A comparison of the isosurface model of PSII complex with a pseudo-atomic model of the complete PSII supercomplex [24] viewed from the lumenal side indicates that the spherical densities coincide with the position of LHCII trimers. (B, C) Possibilities in the variation of the lumenal width at different positions of opposing PSII complexes. (B) A juxtaposition position of PSII complexes of two opposing grana membranes results in a large lumenal space. Extrinsic subunits of oxygen-evolving complex and novel lumenal densities revealed by cryo tomography represent a physical barrier of a closer contact between the opposing grana membranes. (C) Shrinkage of lumenal space is only possible upon a full lateral displacement of opposing PSII complexes.

recently successfully used for the first study of PSII arrangement *in situ*, inside the isolated thylakoid membrane [34,62]. Typical densities of the extrinsic parts of PSII core complexes were clearly distinguished in tomograms of different preparations of stacked thylakoid membranes, including mild digitonin solubilization or osmotic shock. PSII core complexes were found to be either randomly distributed within the thylakoid membrane [34,62] or they were organized in 2D arrays of C_2S_2 supercomplexes. Interestingly, 2D arrays of PSII complexes were merely found in pairs, in two adjacent membrane layers, which were in a contact through their stromal sides [34]. Analysis of PSII interactions in those adjacent layers indicates multiple specific interactions between PSII subunits, including PSII reaction centers, LHCII trimers and minor antennae, which all might contribute to the grana stacking [17,34]. Analysis of positions of randomly distributed PSII cores and their distances from neighboring complexes within an entire membrane layer indicated that about one quarter of supercomplexes in spinach must be of smaller size than full $C_2S_2M_2$ supercomplexes, to avoid overlap [62]. This is consistent with earlier EM studies of grana membranes, where in case of crystalline arrays the C_2S_2M units were found to be predominant [35]. Tomography data further showed that regardless of a minor fraction of unassigned densities, there were several membrane areas, which were very flat and free of PSII supercomplexes or other protruding proteins [62]. Similar areas were found by AFM (Sznee et al., manuscript in preparation). It was suggested that they can be occupied by free LHCII proteins [17]. Calculations by Kirchhoff [71] on the numbers of lipids and proteins exclude the presence of large lipid-only areas. It should be pointed out that light growing conditions have a strong influence on the amount of free and bound LHCII [55], which can modify a relative ratio between different types of PSII supercomplexes (e.g. $C_2S_2M_2$, C_2S_2M, C_2S_2).

The fact that PSII core densities can be traced in tomograms offers the possibility to perform 3D averaging of hundreds of subvolumes containing such large proteins. In this way electron tomography can reveal details of protein structures *in situ* [34,62]. This opportunity will make sure that in the future electron tomography will fill the gap between high-resolution structures on the one side and low-resolution information of cellular structures on the other side. In the study of Kouřil et al., the PSII complex was resolved at 40 Å resolution, which revealed novel protein densities associated with the PSII supercomplexes, which were not observed before in isolated forms of PSII complexes (Fig. 6). Similar densities were also observed in recent AFM data (Sznee et al., manuscript in preparation). The nature of these protein densities, however, has to be established.

5. Structural rearrangements of protein complexes upon short-term adaptation

In most habitats, plants are exposed to a wide variety of irradiance intensities. There are two major short-term acclimations to changing light quantities and quality in which PSII supercomplexes are involved. A redistribution of absorbed light energy between PSI and PSII by means of a reversible redistribution of mobile LHCII trimers is called 'state transitions' (see Refs. [72–76] for reviews). Besides a redistribution, the formation of LHCII aggregates seems also to mediate the energy balance [76]. The other main fast acclimation is non-photochemical quenching (NPQ) when the light intensity exceeds the plant's capacity for photosynthesis [77]. Without proper protection, the accumulation of excited states will result in the accumulation of harmful oxygen species, which can damage the membranes, pigments and proteins of the photosynthetic organism [78,79]. The ability of plants in high light conditions to harmlessly dissipate excess excitation energy into heat is called high-energy quenching (qE) and is one of the main features of NPQ. Recent reports suggest that qE quenching involves dissociation of a complex consisting of CP24, CP29 and M-LHCII [80]. Thus it has been

speculated that the formation of energy-dissipative LHCII aggregates is relevant for both qE and state transitions, at least in the green alga *C. reinhardtii* [76]. If such energy-dissipative aggregation is facilitated by acidification of the lumen and/or reinforced by PsbS, the quenching could be classified as qE; if it is induced by redox-controlled LHCII phosphorylation, the quenching could be classified as a state transition [76,81,82].

5.1. State transitions

State transitions refer to a mechanism by which excitation energy is redistributed among PSI and PSII when they become exposed to light conditions that preferably excite either PSI or PSII. There is general consensus now about the basic features of this process. When PSII is preferentially excited by 'light 2', the plastoquinone pool becomes more reduced, which leads to a conformational change of the cytochrome b_6/f complex, which in turn activates a kinase bound to the b_6/f complex. A number of kinases have been characterized [75] and they all have in common a single transmembrane α-helix and a large extrinsic part at the stromal side of the membrane, suggesting that these kinases cannot occur in the grana stacks because of steric hinderance and thus are located in the stroma membranes. The kinase is then released from b_6/f, after which it can migrate to the margins between stroma and grana membranes, where it meets LHCII and promotes its phosphorylation. Phosphorylated LHCII has a decreased affinity for the grana stacks because of the charges on the phosphate groups and thus a lateral movement of phosphorylated LHCII from grana to stroma occurs where it can meet PSI, to form a PSI–LHCII supercomplex [83]. Such a move can explain the shift from 'state 1' (induced by 'light 1') to 'state 2' (induced by 'light 2') in plants.

There are several aspects of this mechanism that interfere with the supramolecular organization of PSII and PSI supercomplexes in the thylakoid membranes. Recent studies have focussed on the green alga *C. reinhardtii*, rather than on green plants, because the overall state transition effect is much larger in this particular species [84]. Gel filtration and electron microscopy of affinity-purified *C. reinhardtii* particles showed that a PSII–LHCII megacomplex was predominant in state 1, whereas the PSII core complex was predominant in state 2, indicating LHCII trimers dissociate from PSII upon a state 1-to-2 transition. Moreover, in state 2, strongly phosphorylated LHCII was found in the supercomplex, but not in the megacomplex. Phosphorylated minor LHCIIs (CP26 and CP29) were only found in the unbound form. The PSII subunits including the CP43 and D2 proteins were most phosphorylated in the core complex. Based on these observations, a 3-step model was proposed for the PSII remodeling during a state 1-to-2 transition [76]. Initially, unphosphorylated LHCIIs stabilize the megacomplex (State 1), then in step 1: the phosphorylation of LHCII in a LHCII trimer triggers the division of the megacomplex, resulting in individual C_2S_2 supercomplexes; step 2: the phosphorylation of CP26 and CP29, as well as the PSII core subunits D2 and CP43, induce the undocking of all the LHCIIs from PSII; and in step 3: the dissociated LHCIIs reassociate with the PSI–LHCI supercomplex yielding state 2.

Although this is a plausible mechanism for the state transitions in *C. reinhardtii*, we would like to make a few critical notes. First, there is to our knowledge and unlike in plants no solid evidence for the binding of trimeric LHCII to PSI in state 2. After the publication of our electron microscopic analysis of PSI complexes of *C. reinhardtii* [85] it appeared that these complexes were obtained from membranes poised in a mixture of state 1 and state 2 (J.A. Ihalainen, unpublished observations). In this analysis, we found two types of PSI supercomplexes, but the size difference was consistent with a monomeric LHC-type of protein, and certainly not by a trimeric complex. Second, it is clear that the PSII protein CP29 has considerable affinity for the PSI complex of *C. reinhardtii*, which in turn influences the association of the PSII–LHCII supercomplex. All association–dissociation processes are equilibria, and when CP29 (a complex that is crucial for the stability of

the PSII–LHCII supercomplex—see above) is taken away by binding to PSI, it will result in a shift of the equilibrium of PSII–LHCII formation towards the dissociated form. Third, free LHCII complexes don't need to be firmly bound to PSI to induce excitation energy transfer to PSI. In artificially unstacked thylakoid membranes from spinach, a considerable part of the energy transfer from LHCII to PSI was 'slow' (in the order of 150 ps), in contrast to 'fast' energy transfer from LHCII to PSI in a PSI–LHCII complex (in the order of 30 ps) [60], but both contribute to the increased absorption cross-section of PSI and both contribute therefore to the state transition.

Although green plants and *C. reinhardtii* have similar PSII complexes and peripheral antenna components, we speculate that the molecular mechanisms for the state transitions are quite different. In plants most of the LHCII is not accessible for the kinase, probably because a tight stacking of grana membranes restricts the LHCIIs that can be phosphorylated to those near the margins. In addition, the direct binding of an LHCII trimer to PSI induces a relatively large change in antenna cross section of PSI, and so the state transition mechanism is basically meant to provide PSI a larger absorption cross-section in state 2. In *C. reinhardtii*, a much larger part of PSII is accessible for the kinase, perhaps because of a less tight stacking of the thylakoid membrane. In view of the disappearance of the organization in supercomplexes, the main effect of the state transition is to provide PSII a smaller absorption cross-section in state 2, rather than to increase the absorption cross-section of PSI, because the permanent peripheral antenna of *C. reinhardtii* PSI is already much larger than in plant PSI.

Molecular details of the state transition mechanism have to be further studied, for instance, it is not yet clear how a protein like Lhcb3 (part of the M-LHCII trimer) modulates the state transitions [86].

5.2. High-energy quenching

The process of qE is triggered by acidification of the thylakoid lumen, which activates violaxanthin de-epoxidase, the enzyme that converts violaxanthin into zeaxanthin [87]. There is currently no consensus on the precise physical mechanism of quenching, nor on the site or sites in the PSII–LHCII macrostructure where the quenching occurs. Some authors favor a major role of the minor complexes (in particular CP24) [88,89], others prefer also an important role for the major trimeric complex LHCII [90].

How the structural changes underlying the quenching take place is not known in detail. It became clear, however, that the association and dissociation of a five-subunit membrane complex, composed of CP29 and CP24 and the trimeric LHCII-M, named B4C, is an important step [80]. Dissociation of this supercomplex seems essential for the onset of non-photochemical fluorescence quenching in high light, possibly because it makes quenching sites available for the switch to an energy-quenching conformation. These association and dissociation changes are reversible and do not require protein synthesis and degradation, thus allowing for rapid changes in light adaptation.

The process also requires the presence of the PsbS protein [91] as well as its protonation by the acidification of the thylakoid lumen [92]. There is no clear evidence yet for a direct structural role for PsbS in the quenching, also because it is not present in PSII–LHCII supercomplexes and also not in PSII–LHCII supercomplexes organized in 2D arrays [93]. A clear indirect effect of PsbS is in the macro-organization of PSII within the grana membranes. The amount of PsbS determines the proportion of supercomplexes that are organised into semi-crystalline arrays, and in addition determines the precise shape of the psi-type CD signal [94], that thus can be used as a spectroscopic fingerprint of ordered arrays in the thylakoid membranes (see also the discussion in Ref. [95]). In *Arabidopsis* mutants with overexpressed PsbS such arrays are absent [93,94] and the capacity for qE is increased by around two-fold [96], whereas in a mutant lacking PsbS there are significantly more crystals. Thus the vital role of PsbS in qE may be

explained in such a way that the changes in conformation and/or interactions between LHCII subunits that are required for the formation of the quenching state require a loose association of PSII supercomplexes. This may also be considered as the fully functional photosynthetic state that is fully competent in electron transport and able to rapidly and reversibly switch between the light harvesting and photoprotective state (see Fig. 3 from Ref. [93]). When the tendency for strong interaction is present, giving rise to an increased proportion of crystalline arrays, these changes in conformation are inhibited and qE prevented. Specifically, the dissociation of the aggregate of CP29, CP24 and the M-LHCII trimer, mentioned above and considered to be an obligatory event in qE formation [80], would be prevented. Further work is, however, necessary to test the hypothesis that qE involves a PsbS-catalyzed re-organisation of PSII supercomplexes in the grana membrane, mediating the transition between the unquenched and quenched states.

6. Outlook

With recent progress by single particle electron microscopy, atomic force microscopy and tomographic reconstructions of intact and fragmented chloroplasts we have provided insight in the supramolecular organization of PSII and how the thylakoid membranes are organized in the chloroplast. The final question is then what should come next? Tomography of complete chloroplasts is still at the level of membranes. One would like to see in the near future a completely reconstructed chloroplast at the level of individual proteins and protein–protein interactions. This is not impossible, but heavily relying on further improvements in hardware to increase resolution in electron tomography [97].

There is also a strong demand for higher-resolution data of the plant supercomplex, to understand in more detail excitation energy transfer and phenomena like state transitions and NPQ in the peripheral antenna. There are several questions to be solved in the core part of PSII but it should be emphasized that the high-resolution structures of the core complex of cyanobacteria cannot compensate for the lack of a high-resolution model of the plant core complex, because their proteins differ in their primary sequence and they have even a different subunit composition. For instance, the higher plants contain three small proteins (PsbR, PsbTn, and PsbW) that are not present in cyanobacteria [98], and both their localization and functional properties remain unclear. X-ray diffraction is the most obvious way to solve protein structures. However, for large, fragile structures like the PSII supercomplex this may be a very tedious enterprise. Single particle analysis has become an alternative in the case of large, water-soluble protein complexes [99] and large virus structures can be solved at high resolution. The $C_2S_2M_2$ supercomplex was, however, found to be flexible which limited the finally obtained resolution to only 12 Å [24]. Before single particle analysis became the most-popular way of performing EM analysis, electron crystallography was already an established technique and maybe this technique can provide higher resolution in the particular case of PSII. Noteworthy, this technique resulted in an LHCII structure [100], long before the X-ray structures became available.

In conclusion, structure determination has to go on to provide insight to one of the basic aspects of an enzyme, to fully understand and appreciate the light reactions of photosynthesis.

References

[1] A. Williamson, B. Conlan, W. Hillier, T. Wydrzynski, The evolution of photosystem II: insights into the past and future, Photosynth. Res. 107 (2011) 71–86.

[2] A. Zouni, H.T. Witt, J. Kern, P. Fromme, N. Krauss, W. Saenger, P. Orth, Crystal structure of photosystem II from *Synechococcus elongatus* at 3.8 angstrom resolution, Nature 409 (2001) 739–743.

[3] N. Kamiya, J.R. Shen, Crystal structure of oxygen-evolving photosystem II from Thermosynechococcus vulcanus at 3.7-angstrom resolution, Proc. Natl. Acad. Sci. U.S.A. 100 (2003) 98–103.

[4] K.N. Ferreira, T.M. Iverson, K. Maghlaoui, J. Barber, S. Iwata, Architecture of the photosynthetic oxygen-evolving center, Science 303 (2004) 1831–1838.

[5] B. Loll, J. Kern, W. Saenger, A. Zouni, B. Biesiadka, Towards complete cofactor arrangement in the 3.0 angstrom resolution structure of photosystem II, Nature 438 (2005) 1040–1044.

[6] F. Müh, T. Renger, A. Zouni, Crystal structure of cyanobacterial photosystem II at 3.0 Å resolution: a closer look at the antenna system and the small membrane-intrinsic subunits, Plant Physiol. Biochem. 46 (2008) 238–264.

[7] A. Guskov, J. Kern, A. Gabdulkhakov, M. Broser, A. Zouni, A.W. Saenger, Cyanobacterial photosystem II at 2.9-Å resolution and the role of quinones, lipids, channels and chloride, Nat. Struct. Mol. Biol. 16 (2009) 334–342.

[8] K.U. Cormann, J.A. Bangert, M. Ikeuchi, M. Rögner, R. Stoll, M.M. Nowaczyk, Structure of Psb27 in solution: implications for transient binding to photosystem II during biogenesis and repair, Biochemistry 48 (2009) 8768–8770.

[9] P.D. Mabbitt, G.J. Rautureau, C.L. Day, S.M. Wilbanks, J.J. Eaton-Rye, M.G. Hinds, Solution structure of Psb27 from cyanobacterial photosystem II, Biochemistry 48 (2009) 8771–8773.

[10] S.A. Jackson, R.D. Fagerlund, S.M. Wilbanks, J.J. Eaton-Rye, Crystal structure of PsbQ from Synechocystis sp. PCC 6803 at 1.8 Å: implications for binding and function in cyanobacterial photosystem II, Biochemistry 49 (2010) 2765–2767.

[11] Y. Yang, T.A. Ramelot, J.R. Cort, D. Wang, C. Ciccosanti, K. Hamilton, R. Nair, B. Rost, T.B. Acton, R. Xiao, J.K. Everett, G.T. Montelione, M.A. Kennedy, Solution NMR structure of photosystem II reaction center protein Psb28 from Synechocystis sp. strain PCC 6803, Proteins 79 (2011) 340–344.

[12] X. Pan, M. Li, T. Wan, L. Wang, C. Jia, Z. Hou, X. Zhao, J. Zhang, W. Chang, Structural insights into energy regulation of light-harvesting complex CP29 from spinach Nature Struct, Mol. Biol. 18 (2011) 309–315.

[13] Z. Liu, H. Yan, K. Wang, T. Kuang, J. Zhang, L. Gui, X. An, W. Chang, Crystal structure of spinach light-harvesting complex at 2.72 Å resolution, Nature 428 (2004) 287–292.

[14] R. Standfuss, A.C. Terwissscha van Scheltinga, M. Lamborghini, W. Kuhlbrandt, Mechanisms of photoprotection and nonphotochemical quenching in pea light-harvesting complex at 2.5 Å resolution, EMBO J. 24 (2005) 919–928.

[15] H. Schägger, Respiratory chain supercomplexes of mitochondria and bacteria, Biochim. Biophys. Acta 1555 (2002) 154–159.

[16] N.V. Dudkina, H. Eubel, W. Keegstra, E.J. Boekema, H.-P. Braun, Structure of a mitochondrial supercomplex formed by respiratory chain complexes I and III, Proc. Natl. Acad. Sci. U.S.A. 102 (2005) 3225–3229.

[17] J.P. Dekker, E.J. Boekema, Supermolecular organization of the thylakoid membrane proteins in green plants, Biochim. Biophys. Acta 1706 (2005) 12–39.

[18] S. Jansson, A guide to the Lhc genes and their relatives in Arabidopsis, Trends Plant Sci. 4 (1999) 236–240.

[19] S. Jansson, The light-harvesting chlorophyll a/b binding proteins, Biochim. Biophys. Acta 1184 (1994) 1–19.

[20] E.J. Boekema, H. van Roon, F. Calkoen, R. Bassi, J.P. Dekker, Multiple types of association of photosystem II and its light-harvesting antenna in partially solubilized photosystem II membranes, Biochemistry 38 (1999) 2233–2239.

[21] B. Hankamer, E. Morris, J. Nield, A. Carne, J. Barber, Subunit positioning and transmembrane helix organisation in the core dimer of photosystem II, FEBS Lett. 504 (2001) 142–151.

[22] B. Hankamer, J. Barber, E.J. Boekema, Structure and membrane organization of photosystem II in green plants, Annu. Rev. Plant Physiol. Plant Mol. Biol. 48 (1997) 641–671.

[23] J. Nield, J. Barber, Refinement of the structural model for the photosystem II supercomplex of higher plants, Biochim. Biophys. Acta 1757 (2006) 353–361.

[24] S. Caffarri, R. Kouřil, S. Kereïche, E.J. Boekema, R. Croce, Functional architecture of higher plant photosystem II supercomplexes, EMBO J. 28 (2009) 3052–3063.

[25] M.G. Rossmann, Fitting atomic models into electron-microscopy maps, Acta Crystallogr. D56 (2000) 1341–1349.

[26] A.E. Yakushevska, W. Keegstra, E.J. Boekema, J.P. Dekker, J. Andersson, S. Jansson, A.V. Ruban, P. Horton, The structure of photosystem II in Arabidopsis: localization of the CP26 and CP29 antenna complexes, Biochemistry 42 (2003) 806–813.

[27] J. Andersson, R.G. Walters, P. Horton, S. Jansson, Antisense inhibition of the photosynthetic antenna proteins CP29 and CP26: implications for the mechanism of protective energy dissipation, Plant Cell 13 (2001) 1193–1204.

[28] L. Kovacs, J. Damkjær, S. Kereïche, C. Ilioaia, A. Ruban, E.J. Boekema, S. Jansson, P. Horton, Lack of the light-harvesting complex CP24 affects the structure and function of the grana membranes of higher plant chloroplasts, Plant Cell 18 (2006) 3106–3120.

[29] J.G. García-Cerdán, L. Kovács, T. Tóth, S. Kereïche, E. Aseeva, E.J. Boekema, E. Mamedov, C. Funk, W.P. Schröder, The PsbW protein stabilizes the supramolecular organization of photosystem II in higher plants, Plant J. 65 (2011) 368–381.

[30] A.V. Ruban, M. Wentworth, A.E. Yakushevska, J. Andersson, P.J. Lee, W. Keegstra, J.P. Dekker, E.J. Boekema, S. Jansson, P. Horton, Plants lacking the main light-harvesting complex retain photosystem II macro-organization, Nature 421 (2003) 648–652.

[31] J. Andersson, M. Wentworth, R.G. Walters, C.A. Howard, A.V. Ruban, P. Horton, S. Jansson, Absence of the Lhcb1 and Lhcb2 proteins of the light-harvesting complex of photosystem II—effects on photosynthesis, grana stacking and fitness, Plant J. 35 (2003) 350–381.

[32] L.A. Staehelin, Chloroplast structure: from chlorophyll granules to supramolecular architecture of thylakoid membranes, Photosynth. Res. 76 (2003) 185–196.

[33] H. Kirchhoff, W. Haase, S. Wegner, R. Danielsson, R. Ackermann, P.A. Albertsson, Low-light-induced formation of semicrystalline photosystem II arrays in higher plant chloroplasts, Biochemistry 46 (2007) 11169–11176.

[34] B. Daum, D. Nicastro, J. Austin, J. McIntosh, W. Kühlbrandt, Arrangement of photosystem II and ATP synthase in chloroplast membranes of spinach and pea, Plant Cell 22 (2010) 1299–1312.

[35] E.J. Boekema, J.F.L. van Breemen, H. van Roon, J.P. Dekker, Arrangement of photosystem II supercomplexes in crystalline macrodomains within the thylakoid membrane of green plant chloroplasts, J. Mol. Biol. 301 (2000) 1123–1133.

[36] A.E. Yakushevska, P.E. Jensen, W. Keegstra, H. van Roon, H.V. Scheller, E.J. Boekema, J.P. Dekker, Supermolecular organization of photosystem II and its associated light-harvesting antenna in Arabidopsis thaliana, Eur. J. Biochem. 268 (2001) 6020–6021.

[37] D.A. Berthold, G.T. Babcock, C.F. Yocum, A highly resolved, oxygen-evolving photosystem II preparation from spinach thylakoid membranes. EPR and electron transport properties, FEBS Lett. 134 (1981) 231–234.

[38] S. Haferkamp, W. Haase, A.A. Pascal, H. van Amerongen, H. Kirchhoff, Efficient light harvesting by photosystem II requires an optimized protein packing density in grana thylakoids, J. Biol. Chem. 285 (2010) 17020–17028.

[39] B. van Oort, M. Alberts, S. de Bianchi, L. Dall'Osto, R. Bassi, G. Trinkunas, R. Croce, H. van Amerongen, Effect of antenna-depletion in photosystem II on excitation energy transfer in Arabidopsis thaliana, Biophys. J. 98 (2010) 922–931.

[40] C.W. Mullineaux, Function and evolution of grana, Trends Plant Sci. 10 (2005) 521–525.

[41] J.M. Anderson, W.S. Chow, J. de las Rivas, Dynamic flexibility in the structure and function of photosystem II in higher plant thylakoid membranes: the grana enigma, Photosynth. Res. 98 (2008) 575–587.

[42] E. Shimoni, O. Rav-Hon, I. Ohad, V. Brumfeld, Z. Reich, Three-dimensional organization of higher-plant chloroplast thylakoid membranes revealed by electron tomography, Plant Cell 17 (2005) 2580–2586.

[43] L. Mustardy, G. Garab, Granum revisited. A threedimensional model—where things fall into place, Trends Plant Sci. 8 (2003) 117–122.

[44] D.J. Paolillo, 3-Dimensional arrangement of intergranal lamellae in chloroplasts, J. Cell Sci. 6 (1970) 243–255.

[45] L.A. Mustardy, A.G.S. Janossy, Evidence of helical thylakoid arrangement by scanning electron-microscopy, Plant Sci. Lett. 16 (1979) 281–284.

[46] L.A. Staehelin, G.W.M. van der Staay, Structure, composition, functional organisation and dynamic properties of thylakoid membranes, in: D.R. Ort, C.F. Yocum (Eds.), Oxygenic Photosynthesis: The Light Reactions, Kluwer Academic Publishers, Dordrecht, The Netherlands, 1996, pp. 11–30.

[47] L. Mustardy, K. Buttle, G. Steinbach, G. Garab, The three-dimensional network of the thylakoid membranes in plants: quasihelical model of the granum–stroma assembly, Plant Cell 20 (2008) 2552–2557.

[48] J.R. Austin, L.A. Staehelin, Three-dimensional architecture of grana and stroma thylakoids of higher plants as determined by electron tomography, Plant Physiol. 155 (2011) 1601–1611.

[49] B. Andersson, J.M. Anderson, Lateral heterogeneity in the distribution of chlorophyll–protein complexes of the thylakoid membranes of spinach chloroplasts, Biochim. Biophys. Acta 593 (1980) 427–440.

[50] P.O. Arvidsson, C. Sundby, A model for the topology of the chloroplast thylakoid membrane, Aust. J. Plant Physiol. 26 (1999) 678–694.

[51] S.G. Chuartzman, R. Nevo, E. Shimoni, D. Charuvi, V. Kiss, I. Ohad, V. Brumfeld, Z. Reich, Thylakoid membrane remodeling during state transitions in Arabidopsis, Plant Cell 20 (2008) 1029–1039.

[52] V. Brumfeld, D. Charuvi, R. Nevo, S. Chuartzman, O. Tsabaki, I. Ohad, E. Shimoni, Z. Reich, A note on three-dimensional models of higher-plant thylakoid networks, Plant Cell 20 (2008) 2546–2549.

[53] G. Garab, C.A. Mannella, Reply: on three-dimensional models of higher-plant thylakoid networks: elements of consensus, controversies, and future experiments, Plant Cell 20 (2008) 2549–2551.

[54] D. Kaftan, V. Blumfeld, R. Nevo, A. Scherz, Z. Reich, From chloroplasts to photosystems: in situ scanning force microscopy on intact thylakoid membranes, EMBO J. 21 (2002) 6146–6153.

[55] J.M. Anderson, Photoregulation of the composition, function and structure of thylakoid membranes, Annu. Rev. Plant Physiol. Plant Mol. Biol. 37 (1986) 93–136.

[56] H.K. Lichtenthaler, C. Buschmann, M. Döll, H.J. Fietz, T. Bach, U. Kozel, D. Meier, U. Rahmsdorf, Photosynthetic activity, chloroplast ultrastructure, and leaf characteristics of high-light and low-light plants and of sun and shade leaves, Photosynth. Res. 2 (1981) 115–141.

[57] P.R. Rozak, R.M. Seiser, W.F. Wacholtz, R.R. Wise, Rapid, reversible alterations in spinach thylakoid appression upon changes in light intensity, Plant Cell Environ. 25 (2002) 421–429.

[58] E. Rintamaki, P. Martinsuo, S. Pursiheimo, E.M. Aro, Cooperative regulation of light-harvesting complex II phosphorylation via the plastoquinol and ferredoxin–thioredoxin system in chloroplasts, Proc. Natl. Acad. Sci. U.S.A. 97 (2000) 11644–11649.

[59] K. Gounaris, A.P.R. Brain, P.J. Quinn, W.P. Williams, Structural and functional changes associated with heat-induced phase-separations of non-bilayer lipids in chloroplast thylakoid membranes, FEBS Lett. 153 (1983) 47–52.

[60] C.D. van der Weij-de Wit, J.A. Ihalainen, R. van Grondelle, J.P. Dekker, Excitation energy transfer in native and unstacked thylakoid membranes studied by low temperature and ultrafast fluorescence spectroscopy, Photosynth. Res. 93 (2007) 173–182.

[61] H. Kirchhoff, S. Lenhert, C. Büchel, L. Chi, J. Nield, Probing the organization of photosystem II in photosynthetic membranes by atomic force microscopy, Biochemistry 47 (2008) 431–440.

[62] R. Kouřil, G.T. Oostergetel, E.J. Boekema, Fine structure of granal thylakoid membrane organization using cryo electron tomography, Biochim. Biophys. Acta 1807 (2011) 368–374.

[63] S. Murakami, L. Packer, Protonation and chloroplast membrane structure, J. Cell Biol. 47 (1970) 332–351.

[64] P.Å. Albertsson, Interaction between the lumenal sides of the thylakoid membrane, FEBS Lett. 149 (1982) 186–190.

[65] J. De Las Rivas, P. Heredia, A. Roman, Oxygen-evolving extrinsic proteins (PsbO, P, Q, R): bioinformatic and functional analysis, Biochim. Biophys. Acta 1767 (2007) 575–582.

[66] H. Kirchhoff, I. Tremmel, W. Haase, U. Kubitscheck, Supramolecular photosystem II organization in grana thylakoid membranes: evidence for a structured affangement, Biochemistry 43 (2004) 9204–9213.

[67] T.K. Goral, M.P. Johnson, A.P.R. Brain, H. Kirchhoff, A.V. Ruban, C.W. Mullineaux, Visualizing the mobility and distribution of chlorophyll proteins in higher plant thylakoid membranes: effects of photoinhibition and protein phosphorylation, Plant J. 62 (2010) 948–959.

[68] M.P. Johnson, T.K. Goral, C.D.P. Duffy, A.P.R. Brain, C.W. Mullineaux, A.V. Ruban, Photoprotective energy dissipation involves the reorganization of photosystem II light-harvesting complexes in the grana membranes of spinach chloroplasts, Plant Cell 23 (2011) 1468–1479.

[69] O. Medalia, I. Weber, A.S. Frangakis, D. Nicastro, G. Gerisch, W. Baumeister, Macromolecular architecture in eukaryotic cells visualized by cryoelectron tomography, Science 298 (2002) 1209–1213.

[70] A. Klug, R.A. Crowther, Three-dimensional image reconstruction from the viewpoint of information theory, Nature 238 (1972) 435–440.

[71] H. Kirchhoff, U. Mukherjee, H.J. Galla, Molecular architecture of the thylakoid membrane: lipid diffusion space for plastoquinone, Biochemistry 41 (2002) 4872–4882.

[72] F.A. Wollman, State transitions reveal the dynamics and flexibility of the photosynthetic apparatus, EMBO J. 20 (2001) 3623–3630.

[73] A. Haldrup, P.E. Jensen, C. Lunde, H.V. Scheller, Balance of power: a view of the mechanism of photosynthetic state transitions, Trends Plant Sci. 6 (2001) 301–305.

[74] J.F. Allen, State transitions—a question of balance, Science 299 (2003) 1530–1532.

[75] S. Lemeille, J.-D. Rochaix, State transitions at the crossroad of thylakoid signalling pathways, Photosynth. Res. 106 (2010) 33–46.

[76] J. Minagawa, State transitions—the molecular remodeling of photosynthetic supercomplexes that controls energy flow in the chloroplast, Biochim. Biophys. Acta 1807 (2011) 897–905.

[77] I. Szabó, E. Bergantino, G.M. Giacometti, Light and oxygenic photosynthesis: energy dissipation as a protection mechanism against photo-oxidation, EMBO Rep. 7 (2005) 629–634.

[78] J. Barber, B. Andersson, Too much of a good thing: light can be bad for photosynthesis, Trends Biochem. Sci. 17 (1992) 61–66.

[79] P. Horton, A.V. Ruban, R.G. Walters, Regulation of light-harvesting in green plants, Annu. Rev. Plant Physiol. Plant Mol. Biol. 47 (1996) 655–684.

[80] N. Betterle, M. Ballottari, S. Zorzan, S. de Bianchi, S. Cazzaniga, L. Dall'Osto, T. Morosinotto, R. Bassi, Light-induced dissociation of an antenna hetero-oligomer is needed for non-photochemical quenching induction, J. Biol. Chem. 284 (2009) 15255–15266.

[81] M. Iwai, M. Yokono, N. Inada, J. Minagawa, Live-cell imaging of photosystem II antenna dissociation during state transitions, Proc. Natl. Acad. Sci. U.S.A. 107 (2010) 2337–2342.

[82] D.M. Kramer, The photonic "smart grid" of the chloroplast in action, Proc. Natl. Acad. Sci. U.S.A. 107 (2010) 2729–2730.

[83] R. Kouřil, A. Zygadlo, A.A. Arteni, C.D. de Wit, J.P. Dekker, P.E. Jensen, H.V. Scheller, E.J. Boekema, Structural characterization of a complex of photosystem I and light-harvesting complex II of Arabidopsis thaliana, Biochemistry 44 (2005) 10935–10940.

[84] M. Iwai, Y. Takahashi, J. Minagawa, Molecular remodeling of photosystem II during state transitions in Chlamydomonas reinhardtii, Plant Cell 20 (2008) 2177–2189.

[85] M. Germano, A.E. Yakushevska, W. Keegstra, H.J. van Gorkom, J.P. Dekker, E.J. Boekema, Supramolecular organization of photosystem I and light-harvesting complex I in Chlamydomonas reinhardtii, FEBS Lett. 525 (2002) 121–125.

[86] J.T. Damkjær, S. Kereïche, M.P. Johnson, L. Kovacs, A.Z. Kiss, E.J. Boekema, A.V. Ruban, P. Horton, S. Jansson, The photosystem II light harvesting protein Lhcb3 affects the macrostructure of photosystem II and the rate of state transitions in Arabidopsis, Plant Cell 21 (2009) 3245–3256.

[87] B. Demmig-Adams, W.W. Adams III, The role of xanthophyll cycle carotenoids in the protection of photosynthesis, Trends Plant Sci. 1 (1996) 21–26.

[88] S. de Bianchi, L. Dall'Osto, G. Tognon, T. Morosinotto, R. Bassi, Minor antenna proteins CP24 and CP26 affect the interactions between photosystem II subunits and the electron transport rate in grana membranes of Arabidopsis, Plant Cell 20 (2008) 1012–1028.

[89] F. Passarini, E. Wientjes, R. Hienerwadel, R. Croce, Molecular basis of light harvesting and photoprotection in CP24, J. Biol. Chem. 284 (2009) 29536–29546.

[90] A.V. Ruban, R. Berera, C. Ilioaia, I.H.M. van Stokkum, J.T.M. Kennis, A.A. Pascal, H. van Amerongen, B. Robert, P. Horton, R. van Grondelle, Identification of a mechanism of photoprotective energy dissipation in higher plants, Nature 450 (2007) 575–578.

[91] X.P. Li, O. Björkman, C. Shih, A.R. Grossman, M. Rosenquist, S. Jansson, K.K. Niyogi, A pigment-binding protein essential for regulation of photosynthetic light harvesting, Nature 403 (2000) 391–395.

[92] X.P. Li, A.M. Gilmore, S. Caffarri, R. Bassi, T. Golan, D. Kramer, K.K. Niyogi, Regulation of photosynthetic light harvesting involves intrathylakoid lumen pH sensing by the PsbS protein, J. Biol. Chem. 279 (2004) 22866–22874.

[93] S. Kereïche, A.Z. Kiss, R. Kouřil, E.J. Boekema, P. Horton, The PsbS protein controls the macro-organisation of photosystem II complexes in the grana membranes of high plant chloroplasts, FEBS Lett. 584 (2010) 759–764.

[94] A.Z. Kiss, A.V. Ruban, P. Horton, The PsbS protein controls the organisation of the photosystem II antenna in higher plant thylakoid membranes, J. Biol. Chem. 283 (2008) 3972–3988.

[95] G. Garab, H. van Amerongen, Linear and circular dichroism in photosynthesis research, Photosynth. Res. 101 (2009) 135–146.

[96] X.P. Li, P. Muller-Moule, A.M. Gilmore, K.K. Niyogi, PsbS-dependent enhancement of feedback de-excitation protects photosystem II from photoinhibition, Proc. Natl. Acad. Sci. U.S.A. 99 (2002) 15222–15227.

[97] N.V. Dudkina, G.T. Oostergetel, H.P. Braun, E.J. Boekema, Row-like organization of ATP synthase in intact mitochondria determined by cryo-electron tomography, Biochim. Biophys. Acta 1797 (2010) 272–277.

[98] L.X. Shi, W.P. Schröder, The low molecular mass subunits of the photosynthetic supracomplex, photosystem II, Biochim. Biophys. Acta 1608 (2004) 75–96.

[99] E.J. Boekema, M. Folea, R. Kouřil, Single particle electron microscopy, Photosynth. Res. 102 (2009) 189–196.

[100] W. Kühlbrandt, D.N. Wang, Y. Fujiyoshi, Atomic model of plant light-harvesting complex by electron crystallography, Nature 367 (1994) 614–621.

Publication 5

High-light vs. low-light: Effect of light acclimation on photosystem II composition and organization in *Arabidopsis thaliana*

Roman Kouřil [a,b,*], Emilie Wientjes [c], Jelle B. Bultema [a,1], Roberta Croce [c], Egbert J. Boekema [a]

[a] *Department of Biophysical Chemistry, Groningen Biomolecular Sciences and Biotechnology Institute, University of Groningen, Nijenborgh 7, 9747 AG Groningen, The Netherlands*
[b] *Centre of the Region Haná for Biotechnological and Agricultural Research, Department of Biophysics, Faculty of Science, Palacký University, Šlechtitelů 11, 783 71 Olomouc, Czech Republic*
[c] *Department of Physics and Astronomy, Faculty of Sciences, VU University Amsterdam, De Boelelaan 1081, 1081 HV Amsterdam, The Netherlands*

ARTICLE INFO

ABSTRACT

The structural response of photosystem II (PSII) and its light-harvesting proteins (LHCII) in *Arabidopis thaliana* after long-term acclimation to either high or low light intensity was characterized. Biochemical and structural analysis of isolated thylakoid membranes by electron microscopy indicates a distinctly different response at the level of PSII and LHCII upon plant acclimation. In high light acclimated plants, the $C_2S_2M_2$ supercomplex, which is the dominating form of PSII in *Arabidopsis*, is a major target of structural re-arrangement due to the down-regulation of Lhcb3 and Lhcb6 antenna proteins. The PSII ability to form semi-crystalline arrays in the grana membrane is strongly reduced compared to plants grown under optimal light conditions. This is due to the structural heterogeneity of PSII supercomplexes rather than to the action of PsbS protein as its level was unexpectedly reduced in high light acclimated plants. In low light acclimated plants, the architecture of the $C_2S_2M_2$ supercomplex and its ability to form semi-crystalline arrays remained unaffected but the density of PSII in grana membranes is reduced due to the synthesis of additional LHCII proteins. However, the $C_2S_2M_2$ supercomplexes in semi-crystalline arrays are more densely packed, which can be important for efficient energy transfer between PSII under light limiting conditions.

© 2012 Elsevier B.V. All rights reserved.

1. Introduction

Photosynthesis is carried out in the thylakoid membrane, which accommodates the photosynthetic apparatus. Photosystem II (PSII) and its accessory light harvesting complex II (LHCII) reside mainly in the stacks of thylakoids, called grana, which are interconnected by stromal thylakoids, where photosystem I (PSI) and ATP-synthase are mainly confined. They form, together with the cytochrome b_6f complex, the core of the photosynthetic apparatus [1,2].

PSII of higher plants is a multiple protein supercomplex. The core complex consists of D1 and D2 and the inner antenna proteins CP43 and CP47. A dimer of the core complex interacts with a variable number of additional light harvesting complexes (Lhcb1–6). Lhcb1–3 form several types of heterotrimers. They interact specifically with the PSII core via monomeric antenna proteins Lhcb4 (also called CP29), Lhcb5 (CP26) and Lhcb6 (CP24) to form PSII-LHCII supercomplexes (see [3] for a recent review). The largest PSII–LHCII supercomplex in *Arabidopsis*, the so-called $C_2S_2M_2$ supercomplex, consists of the PSII core dimer (C_2), two strongly bound LHCII trimers (S_2) at the side of CP26 and two moderately bound LHCII trimers (M_2), which interact with the core via CP29 and CP24 [4,5]. A 2D projection map of the $C_2S_2M_2$ supercomplex was obtained by single particle electron microscopy (EM) at 12 Å resolution [6], which allowed the reconstruction of a 3D pseudo atomic model of the PSII-LHCII and the visualization of possible energy transfer pathways in the supercomplex [7]. Biochemical evidence suggests that in the thylakoid membrane up to eight LHCII trimers can be present per PSII core dimer [8–10]. This indicates the presence of a pool of "extra" LHCII, which has unknown location with respect to PSII.

It is obvious that more detailed studies of the molecular architecture of the PSII-LHCII supercomplex are important for a deeper understanding of its role in the primary reactions of photosynthesis. There is gathering evidence that the higher organization of PSII and LHCII in the thylakoid membrane is of equal relevance for the regulation and optimization of photosynthetic process. Pioneering freeze-fracture and freeze-etch EM studies revealed first glimpses about a random or well-ordered organization of PSII complexes in the thylakoid membrane [3,11–13]. More recently, both mathematical simulations and data from atomic force microscopy confirm that the PSII distribution in the grana membranes is not completely random [14–16]. Details of the packing and the molecular composition of PSII in these arrays are known from EM analysis of negatively stained grana membranes, which revealed that the arrays consist of C_2S_2, C_2S_2M or $C_2S_2M_2$ supercomplexes [17,18]. Although factors like cold acclimation [16,19], low light acclimation [20], lack of PsbS and

* Corresponding author at: Centre of the Region Haná for Biotechnological and Agricultural Research, Department of Biophysics, Faculty of Science, Palacký University, Šlechtitelů 11, 783 71 Olomouc, Czech Republic. Tel.: +420 58 5634179; fax: +420 58 5225737.
  E-mail address: roman.kouril@upol.cz (R. Kouřil).
[1] Present address: Department of Microbiology, Groningen Biomolecular Sciences and Biotechnology Institute, University of Groningen, Nijenborgh 7, 9747 AG Groningen, The Netherlands.

absence of specific Lhcb antenna proteins [21–23] were found to increase the population of semi-crystalline arrays, their physiological significance is not understood. Recently, cryo electron tomography extended our knowledge about the higher organization of PSII complexes into the third dimension, which provides, among others, unique information about the interaction between PSII complexes in adjacent layers of grana membranes [24,25]. These tomography data indicate that the formation of semi-crystalline arrays *in situ* depends on the interaction of the stroma exposed membrane surface of two adjacent layers, which both contain ordered arrays of PSII complexes [24].

In nature, plants are continuously exposed to varying environmental conditions on a daily or seasonal time scale. Light is for photosynthetic organisms which is one of the most important factors to cope with. As short-term response to varying light intensity and spectral quality, plants had to evolve different mechanisms (i) to protect themselves from photooxidative damage under high light (Non-Photochemical Quenching (NPQ), reviewed by e.g. [26]) and (ii) to optimize photosynthetic function under low light (state transitions, reviewed by e.g. [27]). There are experimental indications that these mechanisms involve structural changes at the level of PSII, LHCII and their higher organization in the thylakoid membrane [28].

Long-term acclimation to different light intensities is accompanied by a regulation of the amount of LHC proteins and PSII/PSI ratio [29]. Under high light, the amount of LHC is reduced, whereas the PSII content increases compared to PSI. The opposite effect is observed under low light, where the lower PSII/PSI ratio reflects a lower amount of PSII complexes, which associate with a larger amount of LHCII proteins [30–32]. Current structural data about the higher organization of PSII in grana membranes are limited to low light conditions, when down-regulation of the PSII content led to a formation of specifically ordered rows of PSII in the grana membrane [20].

The aim of this work is to extend our knowledge about structural aspects of long-term acclimation of plants to either high or low light intensity at the level of PSII supercomplexes and their higher organization in the thylakoid membrane of *Arabidopsis thaliana*. Biochemical analysis of plants acclimated to different light conditions indicates a specific alteration of the composition of PSII supercomplexes and the amount of LHCII proteins. Thorough analysis of electron micrographs revealed a specific response of acclimated plants at the level of both well-ordered and randomly distributed PSII supercomplexes in the thylakoid membrane. We addressed the question whether a long-term acclimation of plants to different light intensities favors the formation of semi-crystalline arrays of PSII supercomplexes in the grana membrane and whether PSII associations in such arrays are characteristic to specific light conditions. Furthermore, analysis of randomly distributed PSII supercomplexes in the grana membrane gave us information about the strategy used by the plant to acclimate to different light intensities.

2. Materials and methods

2.1. Plant material

A. thaliana (Col) plants were grown in a growth chamber (Plant Climatics Percival Growth Chamber, Model AR-36L, Germany) at 100 µE/m^2/s, 70% humidity, 22 °C, and 8 h of daylight and 16 h of dark period. After four weeks, control plants were grown for additional 2.5 weeks at 100 µE/m^2/s (NL) and plants acclimated to low light (LL) and high light (HL) were grown under 20 µE/m^2/s and 800–1100 µE/m^2/s, respectively, for additional four weeks.

2.2. Isolation of thylakoid membranes

A. thaliana leaves were harvested at the end of a dark period. Thylakoid membranes were prepared according to [33], with modifications described in [6]. The membranes were resuspended in 20 mM HEPES,

pH = 7.5, 0.4 M sorbitol, 15 mM NaCl, 5 mM MgCl$_2$, quickly frozen in liquid N$_2$ and stored at 193 K until use.

2.3. Polyacrylamide gel electrophoresis and immunoblot analysis

SDS-PAGE was performed with the Tris–Tricine system [34] at a 14.5% acrylamide concentration. To estimate the level of Lhcb1,2 per CP29 the gels were digitized with a Fujifilm LAS 300 scanner after Coomassie Brilliant Blue staining, and the optical density integrated on the area of the CP29 and Lhcb1,2 band was quantified using the GEL-PRO Analyzer (Media Cybernetics). The number of Lhcb1,2 copies per CP29 was quantified as described by [35], as one CP29 is present per PSII core [18], this gives the Lhcb1,2/PSII core ratio. One Lhcb3 is present per M trimer [6,36,37] and thus per PSII core in NL and LL plants, while based on immunoblot analysis the Lhcb3 level is reduced to 0.5 per PSII in HL plants. These values were used to calculate the amount of LHCII trimers (Lhcb1,2 + Lhcb3)/3 per PSII core. Double amounts are present per PSII core dimer. Immunoblot analysis was performed as in [38] with antibodies from Agrisera (Sweden).

2.4. Electron microscopy of grana membranes

Prior to the solubilization step, thylakoids were thawed on ice and resuspended in an excess of buffer A (20 mM HEPES, pH = 7.5 and 5 mM MgCl$_2$) and spun down using an Eppendorf table centrifuge (5 min, max. speed, 4 °C) to remove the sorbitol. After this washing step, thylakoid membranes were solubilized using digitonin (0.5 mg of chls/ml, 0.5% digitonin in buffer A) for 20 min at 4 °C while slowly stirred, followed by centrifugation in an Eppendorf table centrifuge (5 min, max. speed, 4 °C). The pellet, with the non-solubilized grana thylakoid membranes, was washed once more with buffer A, spun down again for 5 min and then used for EM analysis.

Specimens were prepared by negative staining with 2% uranyl acetate on glow-discharged carbon-coated copper grids. Electron microscopy was performed on a Philips CM120 electron microscope equipped with a LaB$_6$ tip and operated at 120 kV. Images were recorded with a Gatan 4000 SP 4 K slow-scan CCD camera at 80,000 magnification with a pixel size of 0.375 nm at the specimen level after binning the images to 2048 × 2048 pixels. GRACE software was used for semi-automated data acquisition [39]. Electron micrographs were band-pass filtered prior analysis to improve an image contrast. Sub-areas of semi-crystalline arrays of PSII supercomplexes were analyzed using a single particle approach with the Groningen Image Processing (GRIP) software including reference alignments and averaging of aligned projections. Sub-areas (256 × 256 pixels) of PSII arrays were selected from individual electron micrographs and analyzed separately. To determine the minimal distance between PSII complexes and the density of PSII complexes in the membrane area, mid-mass positions of the PSII core complexes were marked manually using GRIP. To determine the minimal distance, coordinates of about 5000 PSII complexes were selected for each examined sample and analyzed with Microsoft Excel.

3. Results

3.1. Long-term acclimation to different light intensities induces changes in the composition of the PSII light harvesting antenna and modifies the level of PsbS

Biochemical analysis of plants acclimated to different light intensities revealed a diverse regulation of both the composition and size of the antenna system of PSII and also the level of the PsbS protein. The modification in the content of CP24, CP29 and Lhcb3 (a component of the M trimer of LHCII) was monitored by immunoblotting and normalized to the amount of Chl content and CP43 (a PSII core protein). Fig. 1 shows that in HL plants the level of CP43/Chl was significantly higher than in both NL and LL plants, due to a reduced level of LHCII proteins
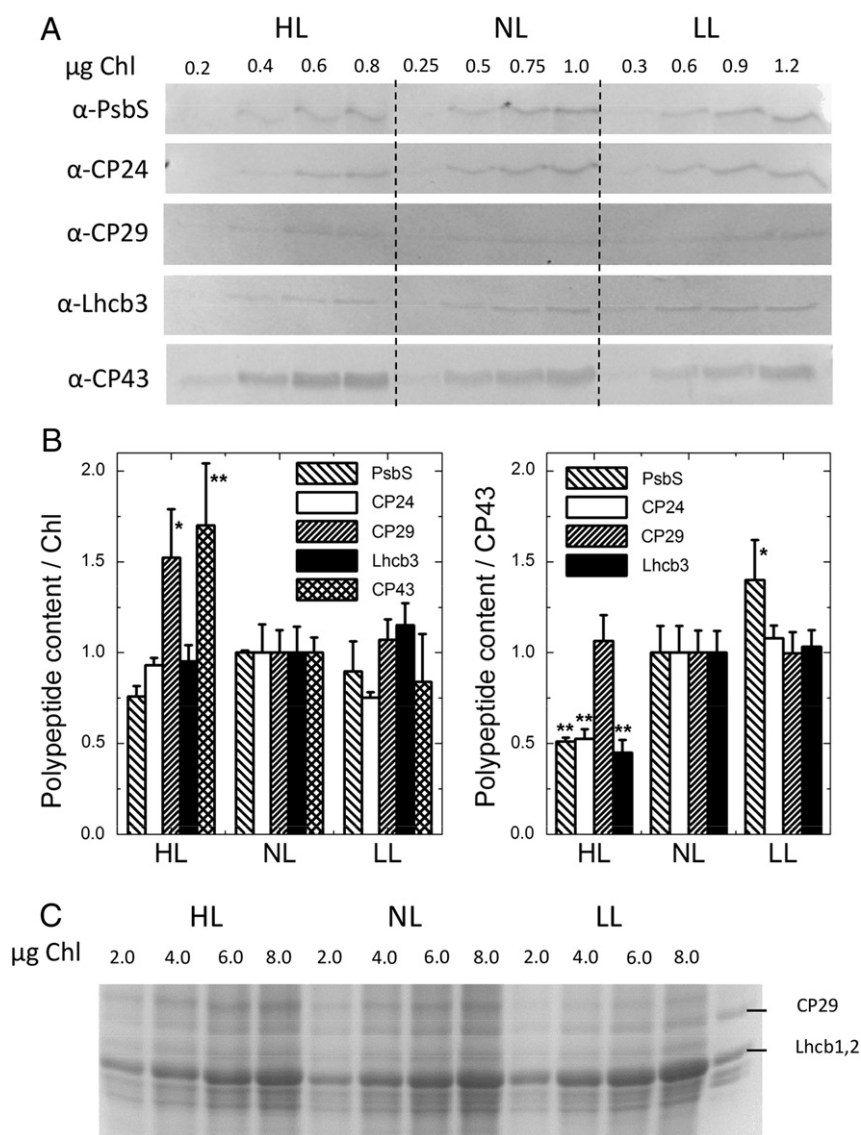
Fig. 1. Quantification of light harvesting proteins of photosystem II and PsbS in plants acclimated to different light conditions. (A) Immunoblotting was performed with antibodies against CP43, CP24, CP29, Lhcb3, and PsbS. The sample was loaded at four different Chls concentrations. Note: it was needed to load different quantities of high light (HL), control (NL) and low light (LL) samples to have similar amounts of CP43 protein. (B) Quantification of immunoblot data. Results are presented relative to the amount of Chl and relative to the PSII core (CP43, quantified by the same method on the same gel; for CP43 per Chl the average from the different gels is shown). Data were normalized to the polypeptide content in the NL sample, the standard deviation is given (n = 3 or 4). Error bars indicate SE (n = 3 or 4); *, ** indicate statistically significant differences at P = 0.05 and P<0.01 levels, respectively, determined using the Student's test. (C) Determination of Lhcb1 and Lhcb2 content per CP29. SDS-PAGE gel after Coomassie staining. The sample was loaded at four different Chls concentrations to ensure a linearity of the signal.

(see below, Table 1) and probably due to a higher PSII/PSI ratio [30–32]. For that reason, analysis of the polypeptide levels per CP43 was also performed. Obtained data for HL plants indicate an about 50% suppression of both CP24/CP43 and Lhcb3/CP43 content compared to the NL sample, while the amount of CP29/CP43 was unaffected. Analysis of LL plants shows the same amounts of those proteins per PSII core as in NL plants.

Lhcb1 and Lhcb2 levels were quantified by SDS-PAGE and used to estimate the total antenna size per PSII core complex (Fig. 1C, Table 1). In NL plants there are on average 4.8 LHCII trimers per PSII core dimer. As expected, acclimation to HL led to a reduction of the antenna size (3.8 LHCII per PSII core dimer), whereas the opposite effect was observed upon acclimation to LL (7.4 LHCII per PSII core dimer) (Table 1). In line with these results, analysis of the Chl a/b ratio also indicates a reduction of the Chl b-rich Lhcb antenna in HL plants (chl a/b = 3.4) compared to NL plants (chl a/b = 3.0), whereas under LL conditions, plants possess a larger PSII antenna (chl a/b = 2.7) (Table 1). Considering that there are 4 LHCII per PSII core dimer in the $C_2S_2M_2$ supercomplex, then in NL and

Table 1
Chlorophyll a/b ratio and amounts of trimeric LHCII complexes in plants acclimated to different light intensities. Chl a/b ratio determined by a fitting of the 80% acetone extract spectra (SD<0.1). Amounts of both bound and "extra" LHCII trimers per PSII core complex were estimated from gels (see Fig. 1 and Section 2.3. for details).

Sample	Chl a/b	Bound LHCII/PSII core	"Extra" LHCII/PSII core	Total LHCII/PSII core
Low light (LL)	2.7	4	3.4	7.4
Normal light (NL)	3.0	4	0.8	4.8
High light (HL)	3.4	3	0.8	3.8

LL plants there are 0.8 (NL) and 3.4 (LL) "extra" LHCII's. In HL plants we observed a 50% reduction of CP24 and Lhcb3 (Fig. 1A, B). As Lhcb3 is predominantly or exclusively present in M trimer and that there is one copy per trimer [6,36,37], it can be assumed that in HL there is a 50% reduction in the number of M trimers. This implies that there are 3 LHCII and 0.8 "extra" LHCII per PSII core dimer in HL plants.

The level of PsbS present in membranes of acclimated plants was analyzed. The result was unexpected, as we found a strong reduction of PsbS per PSII core in HL plants (about 50%), whereas its level increased in LL plants in comparison to NL plants (Fig. 1A, B). When the level of PsbS was normalized to the Chl content, as it is usually done, a reduced level of the PsbS was still observed in HL plants (Fig. 1B).

In summary, biochemical data indicate that plant acclimation to HL conditions leads to a reduction of the antenna size of PSII and of the amount of large $(C_2S_2M_2)$ PSII supercomplexes. The amount of the "extra" LHCII remains at the same level as in NL plants. Acclimation to LL does not affect the ability of PSII to form large supercomplexes and further, it leads to an increase of the "extra" LHCII pool. Finally, acclimation of plants to HL led to the unexpected significant reduction of PsbS per PSII core, whereas acclimation to LL led to a partial increase of the PsbS level. Interestingly, PsbS was reduced to the same level as CP24 and Lhcb3 proteins.

3.2. Electron microscopy revealed both random and well-ordered organization of PSII complexes in grana membranes

We analyzed the organization of PSII complexes and their antenna proteins in the thylakoid membranes in plants acclimated to HL, NL, and LL. Isolation of thylakoid membranes under stacking conditions was performed after mild solubilization using digitonin. In these conditions, non-appressed membranes are well accessible to detergent and are preferentially solubilized, in contrast to appressed (grana) membranes, which remain intact and appear in the pellet after a short centrifugation. EM of the negatively stained pellet fraction revealed pairs of grana membranes, where characteristic densities of PSII core complexes were clearly visible. Inspection of several hundred of electron micrographs of grana membranes, isolated from plants acclimated to different light intensities, revealed that PSII complexes are mostly randomly distributed, but a subset of them is organized into ordered semi-crystalline arrays (Fig. 2).

3.3. The frequency of semi-crystalline arrays of PSII complexes depends on light conditions

As a semi-crystalline array we consider an array of at least three rows of PSII with at least three PSII complexes in each row. The frequency of semi-crystalline arrays was determined from the number of recorded micrographs where semi-crystalline arrays appeared. The analysis revealed a significant difference between the samples. Under NL and LL conditions, semi-crystalline arrays were found in about 7–8% of the recorded micrographs. In the HL sample, the frequency was significantly reduced to less than 3% (Table 2). Image analysis of sub-areas of 2D arrays revealed that in all analyzed samples the semi-crystalline arrays were composed of PSII $C_2S_2M_2$ supercomplex (Fig. 3). Only under HL conditions, a smaller type of PSII supercomplex (the C_2S_2 complex), was also found to be involved in semi-crystalline arrays formation (Table 1, see below for further details).

3.4. Analysis of semi-crystalline arrays of PSII complexes reveals subtle variations in the crystalline lattice under different light conditions

Semi-crystalline arrays of PSII $C_2S_2M_2$ supercomplexes were further analyzed to see whether different light conditions specifically affect their architecture. At first, semi-crystalline arrays were characterized by the lattice parameters, which were determined from raw micrographs. To be accurate, the lattice constants a and b of the unit cell, which contains one $C_2S_2M_2$ supercomplex, were calculated over several rows of PSII complexes from center to center of the mass of the PSII core (see Fig. 3A for a definition of the lattice). We also measured the lattice angle α to calculate the unit cell area (Table 3). The lattice constants a and b fluctuated in a range of 18–22 nm and 24–29 nm, respectively, seemingly without any noticeable dependence on different light conditions. Obtained values are within the range of previously reported data [13].

Secondly, image analysis of small sub-areas of the semi-crystalline arrays was performed to reveal how the PSII supercomplexes interact in these arrays. Fig. 3 shows a gallery of semi-crystalline arrays found under different light conditions. Small insets in the raw electron micrographs represent averaged projection maps of a particular 2D array, which was further assigned by fitting of the pseudo-atomic model of the PSII supercomplex [6]. The assignments indicate overall similar positions and interactions between PSII supercomplexes, independent on light acclimation conditions. A closer look revealed only subtle variations in PSII interactions. For instance, in Fig. 3C and E the cores are lined up in vertical position, whereas in Fig. 3A they slightly incline to the left and in Fig. 3D the inclination is even stronger. This results e.g. in a different interaction between CP24 and CP26 of neighboring PSII supercomplexes (Fig. 3, see white arrowheads).

Another way to compare unit cells is to look at their surface (Table 3). Since the unit cell of the 2D arrays is composed of just one $C_2S_2M_2$ supercomplex, variation in the surface of the unit cell may tell something about the tightness of packing, since the shape of the supercomplex itself is considered to be rigid. There are indeed clear
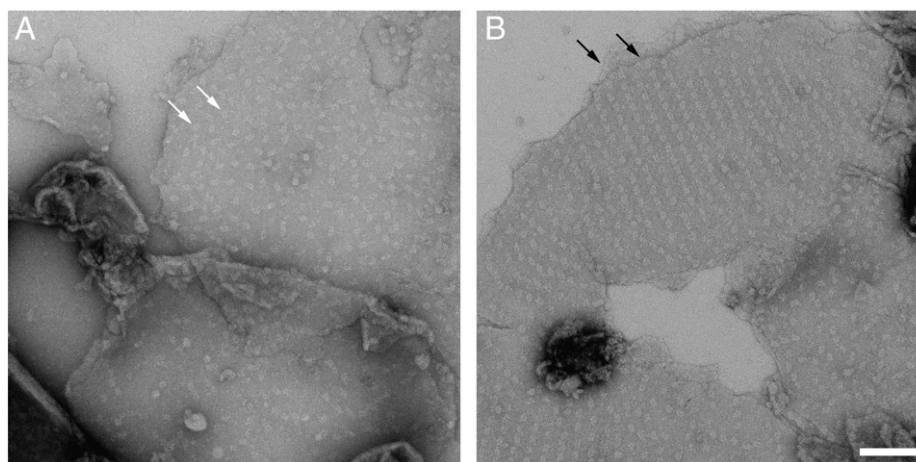
Fig. 2. Examples of electron micrographs of negatively stained pairs of grana membranes isolated from *Arabidopsis thaliana* showing either a random (A) or ordered (B) organization of PSII complexes. The white arrows indicate the characteristic densities of PSII core complexes; the black arrows indicate a single piece of a membrane layer. Scale bar is 100 nm.

Table 2

Frequency and type of semi-crystalline arrays of PSII supercomplexes found in grana membranes of the HL, LL, and NL plants. A total number of recorded micrographs is indicated. Under HL conditions, a majority of semi-crystalline arrays were formed by the C2S2M2 supercomplex (about 90%); only 10% of semi-crystalline arrays were formed by the C2S2 complex.

Sample	HL	LL	NL
Number of recorded micrographs	545	378	555
Micrographs with 2D PSII arrays [%]	2.8	8.5	7.4
Type of PSII supercomplexes involved in a 2D array formation	$C_2S_2M_2$ C_2S_2	$C_2S_2M_2$	$C_2S_2M_2$

differences in the packing surfaces. The strongest, statistically significant difference in the averaged surface is between the LL and NL crystals, with averaged surface of 503 nm^2 and 524 nm^2, respectively (Table 3). The average HL crystal has a surface of 519 nm^2, but only a small number has been determined, due to the low frequency. The smaller surface of the LL crystals indicates a closer packing of the PSII supercomplexes under LL conditions.

3.5. Randomly organized PSII supercomplexes undergo specific rearrangements in the membrane upon acclimation to different light conditions

The major part of the electron micrographs (>90%) shows randomly distributed PSII complexes (see Fig. 2A). To see whether different light conditions have an influence on the random distribution, both the minimal distance between neighboring PSII complexes and their density in the membrane area were determined.

Minimal distances between randomly distributed PSII complexes under HL, LL, and NL conditions were calculated for about 5000 particles which were manually selected from electron micrographs (see Section 2.4. for details). Analysis of HL and NL samples indicates a very similar minimal distance distribution. Most PSII complexes have a minimal distance to the closest neighbor of about 22 nm (Fig. 4). Analysis of LL sample revealed a slightly different distribution with frequency maximums between 19 nm and 21 nm and amplitudes about 20% lower compared to HL and NL samples. Further, LL conditions led to a larger separation of PSII complexes in the membrane, which can be seen from a larger population of PSII complexes with a minimal distance over 26 nm (Fig. 4). Interestingly, LL conditions do not preclude close contact between PSII complexes, as the frequency of PSII complexes with minimal distances below e.g. 18 nm was very similar to the distribution obtained for the HL and NL samples.

Analysis of HL and NL samples shows a rather uniform distribution of PSII complexes in the grana membranes with a density of about 1400 to 1900 PSII complexes per μm^2 (Fig. 5). Analysis of LL plants revealed a considerably lower density, which typically reached a value between 600 and 1300 PSII complexes per μm^2 (Fig. 5). Moreover, electron micrographs of the LL sample revealed a tendency of PSII complexes to specifically associate into rows (Fig. 5C), as observed previously [20].

4. Discussion

4.1. Both bound and "extra" LHCII undergo a specific regulation under plant acclimation to different light intensities

Analysis of plants acclimated to different light intensities indicates a very specific regulation of PSII antenna size at the level of individual proteins. In line with previously published data [31,32], our work confirms a down-regulation of Lhcb1–3 and CP24 proteins in HL plants, while Lhcb1,2 were up-regulated in LL plants.
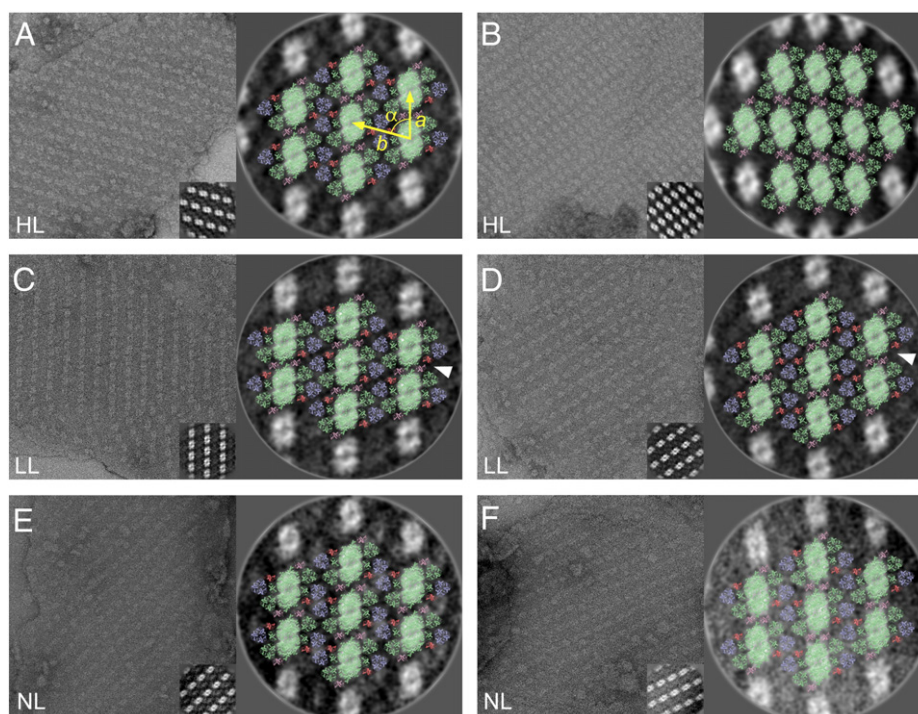
Fig. 3. A gallery of electron micrographs of negatively stained grana membranes with semi-crystalline arrays of PSII supercomplexes from *Arabidopsis thaliana* grown under high light (HL) (A, B), low light (LL) (C, D) and under optimal light intensity (NL) (E, F). The insets show the results of image analysis of sub-areas of ordered arrays of PSII supercomplexes selected from the electron micrographs. Averaged projections were assigned by the fitting of the structural pseudo-atomic model of the PSII $C_2S_2M_2$ supercomplex according to [6] (PSII core complex, the minor antenna CP29 and S-type of light harvesting trimer are depicted in light green, M-type of light harvesting trimer, minor antennae CP24 and CP26 are depicted in light blue, dark salmon and light pink, respectively). Semi-crystalline arrays consist of $C_2S_2M_2$ type of PSII supercomplex. In the high light sample, semi-crystalline array of the C_2S_2 type of PSII supercomplex was also found (B). White arrowheads in (C) and (D) indicate a different interaction between minor antenna proteins CP26 and CP24. The right part of Fig. (A) indicates the definition of lattice parameters, a, b, and the intermediate angle α.

Table 3

Lattice parameters of semi-crystalline arrays. In total, 93 semi-crystalline arrays of the PSII C2S2M2 supercomplexes from HL, LL, and NL plants were characterized. Presented are the unit cell parameters of the lattice and the surface of the unit cell. Lattices are sorted by (1) an ascending angle α between lattice parameters a and b and (2) the ascending length of a (see Fig. 3 for lattice parameters assignment). No. value indicates a number of semi-crystalline arrays with given lattice parameters. Average values of the surface of the lattice cells are 519 nm^2, 503 nm^2 ***, and 524 nm^2 for HL, LL and NL plants, respectively. Asterisks indicate a statistically significant difference between LL and NL plants at P<0.001 determined using the Student's test.

α [°]	HL a [nm]	b [nm]	Surface [nm^2]	No.	LL a [nm]	b [nm]	Surface [nm^2]	No.	NL a [nm]	b [nm]	Surface [nm^2]	No.
65					19	28	490	1				
					20	28	509	1				
66									20	29	528	1
67	21	28	529	1	18	29	490	1	20	28	517	2
					19	28	488	2	21	27	523	1
68	21	28	544	2	19	28	495	5	19	28	513	1
					20	28	502	2	20	28	507	1
69					19	28	499	1	20	29	532	6
					20	28	510	1	21	28	541	2
									22	26	552	1
70					19	28	508	1	19	28	502	1
					20	28	508	4	20	28	517	3
71	20	27	515	2	19	28	503	2	19	28	507	1
	22	26	533	1	21	26	527	1	20	27	517	3
									21	28	551	1
72	20	26	500	1	20	28	518	2	20	26	499	1
	21	27	530	3	21	25	498	3	21	27	533	1
									22	25	530	1
73	21	26	521	1	20	25	490	1	19	28	512	2
					21	26	503	1	20	26	511	1
									21	26	527	3
									22	26	535	1
74	21	25	507	1	20	26	511	3	21	26	524	2
					21	26	525	1				
75	20	25	491	1	20	25	497	1	20	26	514	1
	21	25	498	1	21	25	510	1	21	26	529	2
76									21	26	535	1
77	21	24	489	1	20	25	490	1				
78					18	27	488	1				
81					20	26	520	1				

In HL acclimated plants, immunoblot titration shows about 50% reduction of both Lhcb3 and CP24 proteins (Fig. 1A, B), indicating a 50% reduction of the M trimer. This can fully account for the observed reduction of Lhcb1 and Lhcb2 proteins (which form 2/3 of the M trimer). Down-regulation of the M trimer should lead to the reduction of PSII–LHCII supercomplex (the $C_2S_2M_2$ type) into smaller forms (e.g.C_2S_2M or C_2S_2). Indeed, semi-crystalline arrays of the C_2S_2 type of PSII supercomplex were observed only in HL plants (Fig. 3B). Interestingly,

the "extra" LHCII pool remains at the same level as in NL plants. On the contrary, in LL plants, the stoichiometry between the components of the PSII-LHCII supercomplex remains unaffected (Fig. 1A,B). This implies that the strong up-regulation of Lhcb1 and 2 leads to an enlargement of the "extra" LHCII pool. Indeed, EM analysis of LL acclimated plants shows large areas without PSII complexes (Fig. 5C), which most likely represent LHCII regions. In summary, our data indicate that PSII-associated antenna proteins are the main targets of regulation in HL
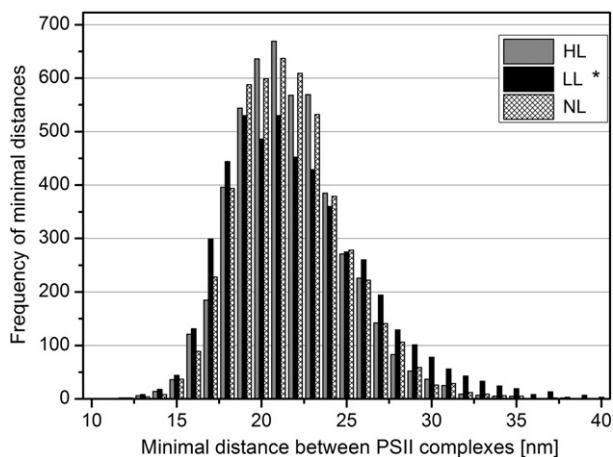
Fig. 4. A frequency of minimal distances between PSII complexes determined from electron micrographs of grana membranes isolated from the high-light (HL), low-light (LL), and control (NL) samples. About 5000 single particles were analyzed for each type of the sample. * indicates statistically significant difference at P = 0.05 determined using the Student's test.
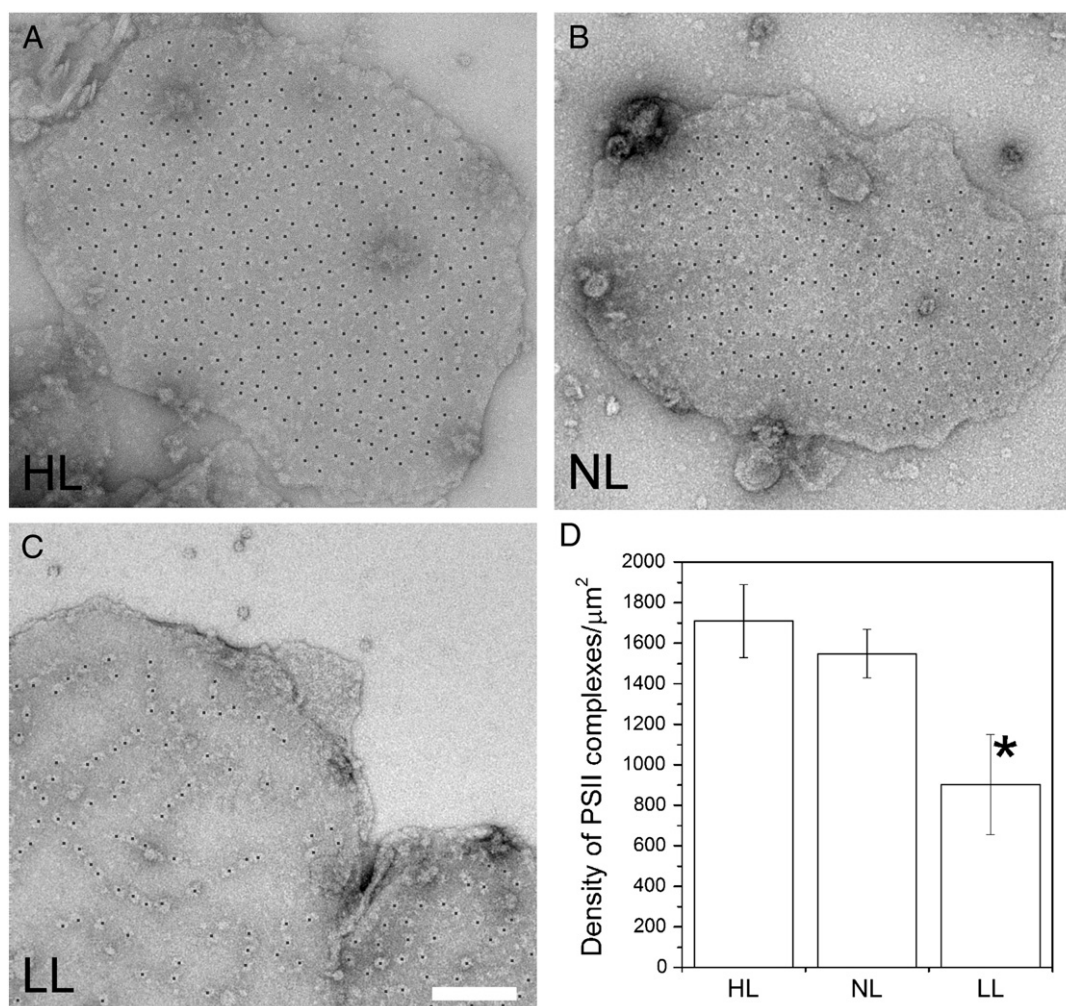
Fig. 5. Density of PSII complexes (grey dots) in the grana membranes of the high-light (HL) (A), low-light (LL) (B), and control (NL) (C) samples. Scale bar is 100 nm. (D) Density of PSII complexes determined for 8 electron micrographs of grana membranes from the HL, LL, and NL samples. A significantly different value from control sample is marked with an asterisk. Error bars indicate SE (n = 8); * indicates statistically significant difference at P = 0.05 determined using the Student's test.

plants. Plant acclimation to LL is accompanied by a regulation of the "extra" LHCII pool, whereas the antenna bound to PSII remains unaffected.

4.2. Frequency of semi-crystalline arrays of PSII is strongly reduced in HL plants

In many structural studies different EM techniques have highlighted the enigmatic organization of PSII complexes into semi-crystalline arrays in the thylakoid membrane. Our data show that the frequency of PSII 2D arrays in the thylakoid membrane depends on growing light intensity. We observed a significant reduction in frequency of PSII 2D arrays in HL plants (about three times) compared to NL (Table 2). Acclimation of plants to LL led to only a minor increase in the frequency of semi-crystalline arrays compared to NL plants. Thus our data did not prove a strong stimulating effect of low light intensity on a formation of ordered arrays of PSII in the membrane as was reported earlier [20]. A possible explanation of this discrepancy is in the way of defining 2D arrays. In contrast to work of Kirchhoff et al. [20], we did not consider single rows of PSII complexes as 2D arrays, although such rows were frequently seen in LL plants (Fig. 5C).

What can be the trigger for a reduced frequency of 2D arrays observed in HL plants? One possibility is the effect of PsbS. It was reported that an elevated level of PsbS in *Arabidopsis* mutant L17 completely suppresses the formation of semi-crystalline arrays, whereas a lack of the PsbS

protein in *Arabidopsis npq4* mutant increases their frequency [22,23]. However, the above observation is seemingly inconsistent with our data, as acclimation of plants to HL led to a decrease in both PsbS level (Fig. 1) and frequency of semi-crystalline arrays (Table 2). Thus, although PsbS has an influence on the 2D array frequency, the array decrease observed here is not due to an increase in the content of PsbS. Before we discuss this topic further on, we like to point out that our finding of a reduced level of PsbS in HL plants is in disagreement with other reports, where either nearly unchanged [40,41] or strongly increased levels of PsbS were reported [32,42]. Although, part of observed discrepancies in the determination of PsbS level in HL plants is due to the normalization method (either to PSII core protein or Chl content), it should be mentioned that in our case the amount of PsbS decreases in HL plants in respect to both the core protein and the total chl content.

In general, one can assume that the formation of 2D arrays in the thylakoid membrane requires a locally homogenous population of PSII supercomplexes. Indeed, in the case of barley PSI-less mutant *viridis zb63*, where PSII complexes are only present in the form of C_2S_2, the grana membranes are organized into large semi-crystalline arrays of up to 0.7 μm in diameter [43,44]. Similarly a very high frequency of semi-crystalline was observed in the CP24KO mutant, where only C_2S_2 complexes were present [45,46]. The presence of a mixture of different types of PSII supercomplexes, like e.g. $C_2S_2M_2$, C_2S_2M, and C_2S_2, can hamper the formation of semi-crystalline arrays. In HL plants, we observed a reduction of CP24 and components of the M trimer, which

implies the presence of smaller PSII supercomplexes than the $C_2S_2M_2$ supercomplex in the thylakoid membrane. Further, analysis of the LL sample indicates that the presence of the "extra" LHCII proteins is not hampering the formation of semi-crystalline arrays. Therefore, we can conclude that the structural heterogeneity of the PSII supercomplexes is the main reason for a lower frequency of PSII semi-crystalline arrays in the thylakoid membrane.

4.3. Unit cell surface of semi-crystalline array of PSII is significantly reduced in LL plants

In all previous EM studies where image processing was performed on 2D arrays, final average 2D maps of semi-crystalline arrays were obtained by taking together the information of many membrane patches. In this study, however, we analyzed for the first time the lattices of *single* crystals.

A thorough analysis of 2D arrays and their assignment by a fitting of the pseudo-atomic model of the PSII supercomplex revealed a significant difference in a tightness of packing of PSII supercomplexes. A smaller unit cell surface indicates a closer contact between PSII supercomplexes in LL plants compared to NL/HL plants (Table 3). Apparently, LL plants prefer (and benefit) keeping PSII complexes tightly clustered either in semi-crystalline arrays or row-like structures. This can be relevant for an optimal performance of the photosynthetic apparatus under light limiting conditions, facilitating energy transfer between supercomplexes. On the contrary, a wider spacing between PSII supercomplexes (a larger unit cell surface) in NL and HL plants can facilitate the diffusion of PQ molecules under light saturating conditions. It remains unclear what helps plants to control the spacing between supercomplexes. Analysis of the lattice parameters revealed their independence on light acclimation conditions (Table 3). Therefore the spacing is not controlled by a specific interaction between PSII supercomplexes. We can speculate that the lipid to protein ration is probably of relevance.

Acknowledgements

References

[1] P.Å. Albertsson, A quantitative model of the domain structure of the photosynthetic membrane, Trends Plant Sci. 6 (2001) 349–354.
[2] N. Nelson, C.F. Yocum, Structure and function of Photosystems I and II, Annu. Rev. Plant Biol. 57 (2006) 521–565.
[3] R. Kouřil, J.P. Dekker, E.J. Boekema, Supramolecular organization of photosystem II in green plants, Biochim. Biophys. Acta 1817 (2012) 2–12.
[4] E.J. Boekema, B. Hankamer, D. Bald, J. Kruip, J. Nield, A.F. Boonstra, J. Barber, M. Rögner, Supramolecular structure of the photosystem II complex from green plants and cyanobacteria, Proc. Natl. Acad. Sci. U. S. A. 92 (1995) 175–179.
[5] E.J. Boekema, H. van Roon, J.P. Dekker, Specific association of photosystem II and light-harvesting complex II in partially solubilized photosystem II membranes, FEBS Lett. 424 (1998) 95–99.
[6] S. Caffarri, R. Kouřil, S. Kereïche, E.J. Boekema, R. Croce, Functional architecture of higher plant photosystem II supercomplexes, EMBO J. 28 (2009) 3052–3063.
[7] R. Croce, H. van Amerongen, Light-harvesting and structural organization of photosystem II: from individual complexes to thylakoid membrane, J. Photochem. Photobiol. B 104 (2011) 142–153.
[8] G.F. Peter, J.P. Thornber, Biochemical composition and organization of higher plant photosystem II light-harvesting pigment-proteins, J. Biol. Chem. 266 (1991) 16745–16754.
[9] K. Broess, G. Trinkunas, A. van Hoek, R. Croce, H. van Amerongen, Determination of the excitation migration time in photosystem II — consequences for the membrane organization and charge separation parameters, Biochim. Biophys. Acta 1777 (2008) 404–409.
[10] B. van Oort, M. Alberts, S. de Bianchi, L. Dall'Osto, R. Bassi, G. Trinkunas, R. Croce, H. van Amerongen, Effect of antenna-depletion in photosystem II on excitation energy transfer in *Arabidopsis thaliana*, Biophys. J. 98 (2010) 922–931.
[11] K.R. Miller, G.J. Miller, K.R. McIntyre, Light-harvesting chlorophyll-protein complex of photosystem 2. Its location in photosynthetic membrane, J. Cell Biol. 71 (1976) 624–638.
[12] L.A. Staehelin, Chloroplast structure: from chlorophyll granules to supra-molecular architecture of thylakoid membranes, Photosynth. Res. 76 (2003) 185–196.
[13] J.P. Dekker, E.J. Boekema, Supramolecular organization of thylakoid membrane proteins in green plants, Biochim. Biophys. Acta 1706 (2005) 12–39.
[14] H. Kirchhoff, I. Tremmel, W. Haase, U. Kubitscheck, Supramolecular photosystem II organization in grana thylakoid membranes: evidence for a structured arrangement, Biochemistry 43 (2004) 9204–9213.
[15] H. Kirchhoff, S. Lenhert, C. Büchel, L. Chi, J. Nield, Probing the organization of photosystem II in photosynthetic membranes by atomic force microscopy, Biochemistry 47 (2008) 431–440.
[16] K. Sznee, J.P. Dekker, R.T. Dame, H. van Roon, G.J. Wuite, R.N. Frese, Jumping mode atomic force microscopy on grana membranes from spinach, J. Biol. Chem. 256 (2011) 39164–39171.
[17] E.J. Boekema, J.F.L. van Breemen, H. van Roon, J.P. Dekker, Arrangement of photosystem II supercomplexes in crystalline macrodomains within the thylakoid membrane of green plant chloroplasts, J. Mol. Biol. 301 (2000) 1123–1133.
[18] A.E. Yakushevska, P.E. Jensen, W. Keegstra, H. van Roon, H.V. Scheller, E.J. Boekema, J.P. Dekker, Supermolecular organization of photosystem II and its associated light-harvesting antenna in *Arabidopsis thaliana*, Eur. J. Biochem. 268 (2001) 6020–6021.
[19] M.P. Garber, P.L. Steponkus, Alterations in chloroplast thylakoids during cold acclimation, Plant Physiol. 57 (1976) 681–686.
[20] H. Kirchhoff, W. Haase, S. Wegner, R. Danielsson, R. Ackermann, P.A. Albertsson, Low-light-induced formation of semicrystalline photosystem II arrays in higher plant chloroplasts, Biochemistry 46 (2007) 11169–11176.
[21] A.V. Ruban, M. Wentworth, A.E. Yakushevska, J. Andersson, P.J. Lee, W. Keegstra, J.P. Dekker, E.J. Boekema, S. Jansson, P. Horton, Plants lacking the main light-harvesting complex retain photosystem II macro-organization, Nature 421 (2003) 648–652.
[22] S. Kereïche, A.Z. Kiss, R. Kouřil, E.J. Boekema, P. Horton, The PsbS protein controls the macro-organisation of photosystem II complexes in the grana membranes of higher plant chloroplasts, FEBS Lett. 584 (2010) 759–764.
[23] T.K. Goral, M.P. Johnson, C.D. Duffy, A.P. Brain, A.V. Ruban, C.W. Mullineaux, Light-harvesting antenna composition controls the macrostructure and dynamics of thylakoid membranes in *Arabidopsis*, Plant J. 69 (2012) 289–301.
[24] B. Daum, D. Nicastro, J. Austin, J.R. McIntosh, W. Kühlbrandt, Arrangement of photosystem II and ATP synthase in chloroplast membranes of spinach and pea, Plant Cell 22 (2010) 1299–1312.
[25] R. Kouřil, G.T. Oostergetel, E.J. Boekema, Fine structure of granal thylakoid membrane organization using cryo electron tomography, Biochim. Biophys. Acta 1807 (2011) 368–374.
[26] A.V. Ruban, M.P. Johnson, C.D. Duffy, The photoprotective molecular switch in the photosystem II antenna, Biochim. Biophys. Acta 1817 (2012) 167–181.
[27] J. Minagawa, State transitions — the molecular remodeling of photosynthetic supercomplexes that controls energy flow in the chloroplast, Biochim. Biophys. Acta 1807 (2011) 897–905.
[28] M.P. Johnson, T.K. Goral, C.D.P. Duffy, A.P.R. Brain, C.W. Mullineaux, A.V. Ruban, Photoprotective energy dissipation involves the reorganization of photosystem II light-harvesting complexes in the grana membranes of spinach chloroplasts, Plant Cell 23 (2011) 1468–1479.
[29] J.M. Anderson, Photoregulation of the composition, function, and structure of thylakoid membranes, Annu. Rev. Plant Physiol. 37 (1986) 93–136.
[30] J.M. Anderson, W.S. Chow, D.J. Goodchild, Thylakoid membrane organization in sun/shade acclimation, Aust. J. Plant Physiol. 15 (1988) 11–26.
[31] S. Bailey, R.G. Walters, S. Jansson, P. Horton, Acclimation of *Arabidopsis thaliana* to the light environment: the existence of separate low light and high light responses, Planta 213 (2001) 794–801.
[32] M. Ballottari, L. Dall'Osto, T. Morosinotto, R. Bassi, Contrasting behavior of higher plant photosystem I and II antenna systems during acclimation, J. Biol. Chem. 282 (2007) 8947–8958.
[33] H.H. Robinson, C.F. Yocum, Cyclic photophosphorylation reactions catalyzed by ferredoxin, methyl viologen and anthraquinone sulfonate — use of photochemical-reactions to optimize redox poising, Biochim. Biophys. Acta 590 (1980) 97–106.
[34] H. Schagger, Tricine-SDS-PAGE, Nat. Protoc. 1 (2006) 16–22.
[35] S.W. Hogewoning, E. Wientjes, P. Douwstra, G. Trouwborst, W. van Ieperen, R. Croce, J. Harbinson, Photosynthetic quantum yield dynamics: from photosystems to leaves, Plant Cell 24 (2012) 1921–1935.
[36] P. Dainese, R. Bassi, Subunit stoichiometry of the chloroplast photosystem II antenna system and aggregation state of the component chlorophyll a/b binding proteins, J. Biol. Chem. 266 (1991) 8136–8142.
[37] B. Hankamer, J. Nield, D. Zheleva, E.J. Boekema, S. Jansson, J. Barber, Isolation and biochemical characterisation of monomeric and dimeric photosystem II complexes from spinach and their relevance to the organisation of photosystem II in vivo, Eur. J. Biochem. 243 (1997) 422–429.
[38] E. Wientjes, G.T. Oostergetel, S. Jansson, E.J. Boekema, R. Croce, The role of Lhca complexes in the supramolecular organization of higher plant photosystem I, J. Biol. Chem. 284 (2009) 7803–7810.
[39] G.T. Oostergetel, W. Keegstra, A. Brisson, Automation of specimen selection and data acquisition for protein electron crystallography, Ultramicroscopy 74 (1998) 47–59.
[40] M. Lindahl, C. Funk, J. Webster, S. Bingsmark, I. Adamska, B. Andersson, Expression of ELIPs and PS II-S protein in spinach during acclimative reduction of the photosystem II antenna in response to increased light intensities, Photosynth. Res. 54 (1997) 227–236.

[41] Y. Mishra, H.J. Jänkänpää, A.Z. Kiss, C. Funk, W.P. Schröder, S. Jansson, Arabidopsis plants grown in the field and climate chambers significantly differ in leaf morphology and photosystem components, BMC Plant Biol. 12 (2012) 6.

[42] M. Tikkanen, M. Piippo, M. Suorsa, S. Sirpiö, P. Mulo, J. Vainonen, A.V. Vener, Y. Allahverdiyeva, E.M. Aro, State transitions revised — a buffering system for dynamic low light acclimation of *Arabidopsis*, Plant Mol. Biol. 62 (2006) 779–793.

[43] D.J. Simpson, Freeze-fracture studies on barley plastid membranes. VI. Location of the P700-chlorophyll a-protein 1, Eur. J. Cell Biol. 31 (1983) 305–314.

[44] T. Morosinotto, R. Bassi, S. Frigerio, G. Finazzi, E. Morris, J. Barber, Biochemical and structural analysis of a higher plant photosystem II supercomplex of a photosystem I-less mutant of barley, FEBS J. 273 (2006) 4616–4630.

[45] L. Kovács, J. Damkjær, S. Kereïche, C. Ilioaia, A.V. Ruban, E.J. Boekema, S. Jansson, P. Horton, Lack of the light-harvesting complex CP24 affects the structure and function of the grana membranes of higher plant chloroplasts, Plant Cell 18 (2006) 3106–3120.

[46] S. de Bianchi, L. Dall'Osto, G. Tognon, T. Morosinotto, R. Bassi, Minor antenna proteins CP24 and CP26 affect the interactions between photosystem II subunits and the electron transport rate in grana membranes of *Arabidopsis*, Plant Cell 20 (2008) 1012–1028.

Publication 6

Rapid report

Evolutionary loss of light-harvesting proteins Lhcb6 and Lhcb3 in major land plant groups – break-up of current dogma

Author for correspondence:
Roman Kouřil
Tel: +420 585634837
Email: roman.kouril@upol.cz

Received: *7 January 2016*
Accepted: *25 February 2016*

Roman Kouřil[1], Lukáš Nosek[1], Jan Bartoš[2], Egbert J. Boekema[3] and Petr Ilík[1]

[1]Department of Biophysics, Centre of the Region Haná for Biotechnological and Agricultural Research, Faculty of Science, Palacký University, Šlechtitelů 27, 783 71 Olomouc, Czech Republic; [2]Centre of the Region Haná for Biotechnological and Agricultural Research, Institute of Experimental Botany, Šlechtitelů 31, 783 71 Olomouc, Czech Republic; [3]Electron Microscopy Group, Groningen Biomolecular Sciences and Biotechnology Institute, University of Groningen, Nijenborgh 7, 9747 AG Groningen, the Netherlands

Summary

- Photosynthesis in plants and algae relies on the coordinated function of photosystems (PS) I and II. Their efficiency is augmented by finely-tuned light-harvesting proteins (Lhcs) connected to them. The most recent Lhcs (in evolutionary terms), Lhcb6 and Lhcb3, evolved during the transition of plants from water to land and have so far been considered to be an essential characteristic of land plants.
- We used single particle electron microscopy and sequence analysis to study architecture and composition of PSII supercomplex from Norway spruce and related species.
- We have found that there are major land plant families that lack functional *lhcb6* and *lhcb3* genes, which notably changes the organization of PSII supercomplexes. The Lhcb6 and Lhcb3 proteins have been lost in the gymnosperm genera *Picea* and *Pinus* (family Pinaceae) and *Gnetum* (Gnetales). We also revealed that the absence of these proteins in Norway spruce modifies the PSII supercomplex in such a way that it resembles its counterpart in the alga *Chlamydomonas reinhardtii*, an evolutionarily older organism.
- Our results break a deep-rooted concept of Lhcb6 and Lhcb3 proteins being the essential characteristic of land plants, and beg the question of what the evolutionary benefit of their loss could be.

Introduction

A key reaction of oxygenic photosynthesis, the photooxidation of water to molecular oxygen, is carried out by photosystem II (PSII), a multi-subunit pigment-protein supercomplex. It consists of a highly conserved core and light harvesting antenna (Kouřil *et al.*, 2012). The latter is much more prone to evolutionary changes (Büchel, 2015). The huge variability of the antenna system was crucial during the evolutionary adaptation of photosynthetic organisms to different conditions (Jansson, 2006). The colonization of land by plants required the presence of an efficient and dynamic mechanism to control safe utilization of absorbed light under variable environmental conditions.

Electron microscopy studies revealed that in land plants, the largest stable PSII supercomplex consists of a PSII core dimer (C_2) bound by four trimeric light-harvesting proteins (LHCIIs), encoded by the *lhcb1–3* genes (*lhcbm* for evolutionarily older species). Two trimers (S_2) are bound strongly to the dimeric PSII core, while the other two are bound only moderately (M_2). The LHCIIs are specifically connected to PSII core via monomeric antenna proteins Lhcb4–6 (Caffarri *et al.*, 2009). This PSII supercomplex, denoted as $C_2S_2M_2$, has been observed in liverworts (Harrer, 2003), the oldest land plants, as well as in angiosperms (Caffarri *et al.*, 2009; Kouřil *et al.*, 2012) (see later Fig. 2b), which belong to the most recent land plants. These findings led to a formulation of the current concept that the $C_2S_2M_2$ PSII supercomplex has been conserved throughout the evolution of land plants. In green algae, their ancestors, the structure of the PSII supercomplex is somewhat different (Tokutsu *et al.*, 2012; Drop *et al.*, 2014) – the M trimers have a different orientation and two additional LHCII trimers (N_2) are attached to form the $C_2S_2M_2N_2$ structure (see later Fig. 2c). Since green algae lack Lhcb6 proteins

that mediate the attachment of the M trimers, the N trimers may substitute their role by stabilizing the $C_2S_2M_2N_2$ supercomplex (Tokutsu *et al.*, 2012; Drop *et al.*, 2014).

The Lhcb6 protein was found to be unique to land plants (Alboresi *et al.*, 2008). Another monomeric antenna protein, Lhcb3, which is a part of the M trimer (Dainese & Bassi, 1991), is also exclusive to land plants. Current knowledge strongly implies that land plants benefit from the presence of both these proteins. The interaction between Lhcb6 and Lhcb3 is important for the stable attachment of M to C_2S_2 (Kovács *et al.*, 2006; Caffarri *et al.*, 2009; Kouřil *et al.*, 2013). The proteins therefore enable a flexible enlargement of the PSII antenna size, leading to an optimal macro-organization of PSII supercomplexes and to more efficient connectivity between PSII cores (Kovács *et al.*, 2006; Caffarri *et al.*, 2009). These factors are important in achieving maximum efficiency of PSII photochemistry as well as for effective photoprotective dissipation of absorbed light energy (so-called nonphotochemical quenching) (Kovács *et al.*, 2006). Thus, the appearance of both Lhcb6 and Lhcb3 is considered as a milestone in the evolution of the PSII supercomplex, allowing the transition of photosynthesizing organisms from the relatively stable water habitat to land (Koziol *et al.*, 2007; Alboresi *et al.*, 2008; de Bianchi *et al.*, 2008; Büchel, 2015). However, here we show that there are representatives of gymnosperms that lack functional *lhcb6* and *lhcb3* genes. Thus, our work breaks the current concept that Lhcb6 and Lhcb3 proteins in the light-harvesting antenna of PSII are an essential characteristic of all land plants.

Materials and Methods

Plant material and sample preparation

Norway spruce (*Picea abies* (L.) Karst.) (Semenoles, Liptovský Hrádok, Slovakia) seedlings were grown in a growth chamber with 16 h : 8 h, light : dark photoperiod at 21°C. Plants were illuminated with white light at 100 μmol photons m^{-2} s^{-1} (400–700 nm). PSII-enriched membranes were isolated from 18-d-old spruce seedlings according to Caffarri *et al.* (2009). Chlorophyll content in the final suspension was determined spectrophotometrically in 80% acetone according to Lichtenthaler & Buschmann (2001). For the electrophoretic separation of PSII supercomplexes, PSII membranes containing 10 μg of chlorophyll were solubilized with *n*-dodecyl-β-D-maltoside (β-DDM) at chlorophyll : β-DDM mass ratio of 12, supplemented with sample buffer (50 mM HEPES (4-(2-hydroxyethyl)-1-piperazineethanesulfonic acid) pH 7.2, 400 mM sucrose, 15 mM sodium chloride (NaCl), 10% glycerol) to a final volume of 30 μl. Nonsolubilized membranes were removed by centrifugation (20 000 *g*, 10 min, 4°C) and samples were directly loaded onto the gel. The clear native polyacrylamide gel electrophoresis (CN-PAGE) separation procedure described by Wittig *et al.* (2007) was used with 4–8% gradient separation gel and 4% stacking gel. The separation started at a constant current of 4 mA for 15 min and continued at a constant current of 7 mA until the front reached the bottom of the gel.

Electron microscopy and image processing

PSII supercomplexes were eluted from excised CN-PAGE gel bands according to Kouřil *et al.* (2014); the solution with eluted supercomplexes was then directly used for electron microscopy specimen preparation by negative staining with 2% uranyl acetate on glow-discharged carbon-coated copper grids. Electron microscopy was performed on a Tecnai G2 20 Twin electron microscope (FEI, Eindhoven, the Netherlands) equipped with a LaB_6 cathode, operated at 200 kV. Images were recorded with an UltraScan 4000 UHS CCD camera (Gatan, Pleasanton, CA, USA) at ×13 000 magnification with a pixel size of 0.224 nm at the specimen level after binning the images to 2048 × 2048 pixels. GRACE software (Oostergetel *et al.*, 1998) was used for semi-automated acquisition of 4200 images, from which *c.* 80 000 particle projections were selected. Single particle analysis was performed using GRIP software (Groningen, the Netherlands) including multireference and nonreference alignments, multivariate statistical analysis and classification.

The projection map with best resolution (14 Å) was obtained for the C_2S_2M supercomplex (Fig. 1d) and therefore this map was used for the construction of a pseudo-atomic model of the PSII
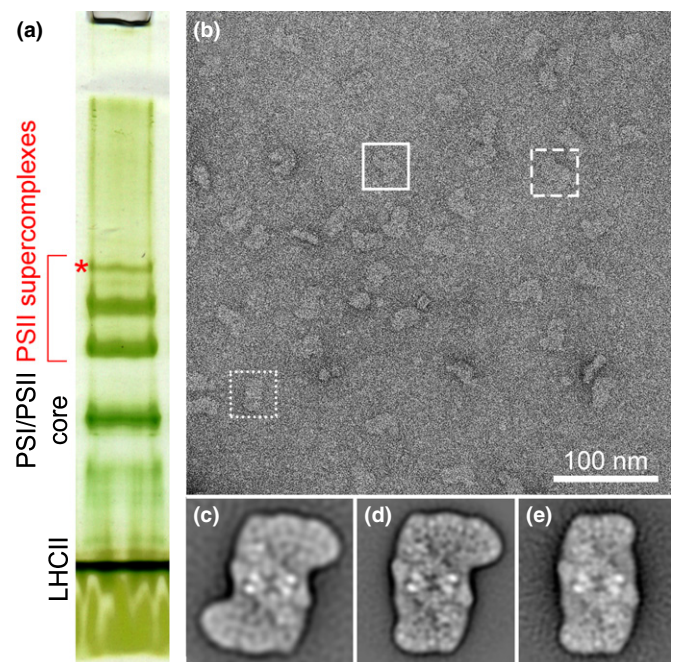
Fig. 1 Separation and structural characterization of photosystem II (PSII) supercomplexes. (a) Separation of PSII supercomplexes from Norway spruce (*Picea abies*) by clear native polyacrylamide electrophoresis. PSII-enriched membranes from spruce seedlings were solubilized in *n*-dodecyl-β-D-maltoside. The red star indicates the band with the largest form of PSII supercomplex, which was analyzed by electron microscopy. (b) Example of raw electron micrograph of a negatively-stained specimen; three different forms of the PSII supercomplexes are indicated: $C_2S_2M_2$ (solid line), C_2S_2M (dashed line) and C_2S_2 (dotted line). (c–e) Averaged projection maps of supercomplexes (c) $C_2S_2M_2$ (sum of 1048 particles), (d) C_2S_2M (sum of 10 000 particles) and (e) C_2S_2 (sum of 4608 particles) revealed by single particle electron microscopy.

supercomplex and for the estimation of the mutual position of the M and S trimers. The constructed model was also used for the fitting of the spruce $C_2S_2M_2$ supercomplex (Fig. 2a). The resolution was measured using Fourier-ring correlation and the 3σ criterion (Vanheel, 1987).

Identification of Lhcb homologs

Amino acid sequences of Lhcb1–6 proteins identified in *Arabidopsis thaliana* (Lhcb1 isoforms: Lhcb1.1, AT1G29920.1; Lhcb1.2, AT1G29910.1; Lhcb1.3, AT1G29930.1; Lhcb1.4, AT2G34430.1; Lhcb1.5, AT2G34420.1; Lhcb2 isoforms: Lhcb2.1, AT2G05100.1; Lhcb2.2, AT2G05070.1; Lhcb2.3, AT3G27690.1; Lhcb3, AT5G54270.1; Lhcb4 isoforms: Lhcb4.1, AT5G01530.1; Lhcb4.2, AT3G08940.2; Lhcb4.3, AT2G40100.1; Lhcb5, AT4G10340.1; Lhcb6, AT1G15820.1) were downloaded from the TAIR.10 database (Lamesch *et al.*, 2012; https://www.arabidopsis.org/) and used for homology search against the *Picea abies* genome and transcriptomes of the species listed later, using the TBLASTN algorithm. The spruce genome (Nystedt *et al.*, 2013) was downloaded from the Congenie database (http://congenie.org/). Transcriptomes of Norway spruce and closely related *Picea* and *Pinus* species (*Picea abies, Picea glauca, Picea sitchensis, Pinus bankdiana, Pinus contorta, Pinus pinaster, Pinus sylvestris* and *Pinus tadea*) were downloaded from the PlantGDB database (Duvick *et al.*, 2008; http://www.plant-gdb.org/). Transcriptomes of other Gymnosperm species (*Cycas rumphii, Ginkgo biloba, Podocarpus macrophyllus, Cryptomeria japonica, Sequoia sempervirens, Sciadopitys verticillata, Taxus baccata, Gnetum gnemo*n) and representatives of ferns (*Ceratopteris richardii*), lycophytes (*Selaginella moellendorffii*), mosses (*Physcomitrella patens*), liverworts (*Marchantia polymorpha*) and algae (*Chlamydomonas reinhardtii*) were downloaded from either the PlantGDB or Dendrome databases (http://dendrome.ucdavis.edu/) (Supporting Information Table S1). In addition, raw data from transcriptome/RNA sequencing using Roche 454 technology were downloaded from the Sequence Read Archive (SRA; http://www.ncbi.nlm.nih.gov/sra), when available. If possible, at least one million reads were retrieved for each species. The number of sequences and cumulative length of all databases used for homology search are listed in Table S1. Each database was

analyzed separately. First, scaffold/transcript with best BLAST hit was retrieved for each *A. thaliana* Lhcb protein using TBLASTN with default parameters, but e-value = 1e-10. Subsequently, a particular scaffold/transcript was compared with the full set of *A. thaliana* proteins (TAIR.10) using the BLASTX algorithm with default parameters, but e-value = 1e-10. Best hits for all Lhcb proteins in each database as well as best hits of particular scaffolds/transcripts in TAIR.10 are listed in Table S2. Scaffolds/transcripts matching reciprocally with a single *A. thaliana* Lhcb protein were considered as representatives of a particular gene in the analyzed species. The same strategy and dataset (transcriptomes and raw 454 data) were used to reveal the presence of transcripts for homologues of *A. thaliana* PGR5 (AT2G05620.1; retrieved from TAIR.10) and *C. reinhardtii* Lhcsr proteins (Lhcsr1, Cre08.g365900.t1.2; Lhcsr2, Cre08.g367500.t1.1; Lhcsr3, Cre08.g367400.t1.1; retrieved from PHYTOZOME v.11; Goodstein *et al.*, 2012; https://phytozome.jgi.doe.gov). In the case Lhcsr-like transcripts, a particular scaffold/transcript was compared with the complete *C. reinhardtii* proteome v.5.5 (Merchant *et al.*, 2007; downloaded from PHYTOZOME v.11) using the BLASTX algorithm with default parameters, but e-value = 1e-10.

Results and Discussion

Here we present for the first time the structure of the PSII supercomplex in a representative of gymnosperms, Norway spruce (*P. abies*). Mildly solubilized PSII-enriched thylakoid membranes were electrophoresed using CN-PAGE, which resulted in the separation of PSII supercomplexes into three bands (Fig. 1a). The largest PSII supercomplexes, present in the band with the shortest migration distance, were analyzed by single particle electron microscopy and image processing. Inspection of raw electron micrographs indicated the presence of several forms of the PSII supercomplex, which differed in the size of their antenna (Fig. 1b). Image analysis of *c.* 80 000 single particle projections revealed structures $C_2S_2M_2$, C_2S_2M and C_2S_2 (Fig. 1b–e). The largest, that is the most intact, supercomplex ($C_2S_2M_2$) was further analyzed in detail. The smaller supercomplexes represent degradation products of $C_2S_2M_2$ supercomplexes, which disintegrate during the preparation of the samples for electron microscopy analysis.
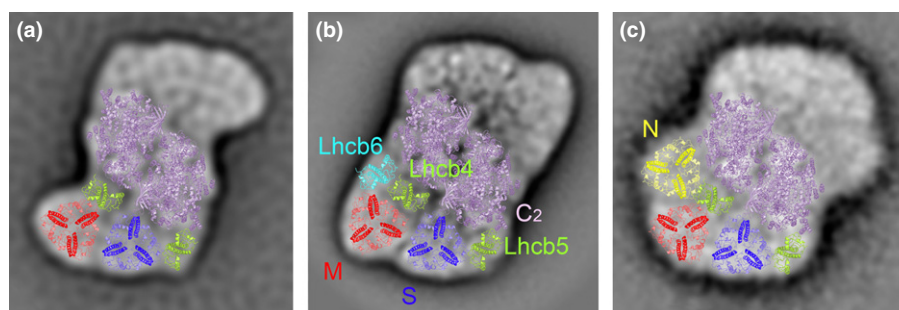
Fig. 2 Structural assignment of protein subunits of the photosystem II (PSII) supercomplex. (a) PSII supercomplexes from Norway spruce (*Picea abies*) and its counterparts from (b) *Arabidopsis thaliana* and (c) *Chlamydomonas reinhardtii*. Averaged projection maps are shown for the $C_2S_2M_2$ supercomplexes from Norway spruce and *A. thaliana*, and $C_2S_2M_2N_2$ from *C. reinhardtii* (adapted from Drop *et al.*, 2014). High-resolution structures were fitted to the projection maps; the PSII core complex (C_2, light violet) (Guskov *et al.*, 2009), trimeric (the S, M and N trimer in blue, red and yellow, respectively) and monomeric (Lhcb4 and Lhcb5 in green, Lhcb6 in cyan) Lhcb proteins (Liu *et al.*, 2004).

We constructed a pseudo-atomic model of the $C_2S_2M_2$ supercomplex from spruce by fitting the electron microscopy projection map with known PSII and Lhcb X-ray structures and compared it with the models of the $C_2S_2M_2$ supercomplex from *A. thaliana*, a representative of angiosperms, and with $C_2S_2M_2N_2$ from *C. reinhardtii* (Fig. 2). It is clear that the position occupied by the minor antenna protein Lhcb6 in *A. thaliana* remains unoccupied in the spruce PSII supercomplex. Due to the absence of Lhcb6, the M trimer associates to the PSII core complex in a different orientation, which has never been observed in land plants before. The rotation of the M trimer by *c.* 52° enables its tighter association with the S trimer, decreasing their mutual distance by *c.* 7 Å (for details see the Materials and Methods section). Interestingly, the same orientation of the M and S trimers was recently observed in an evolutionarily older organism, the green alga *C. reinhardtii*, which also lacks the Lhcb6 protein (Fig. 2c) (Tokutsu *et al.*, 2012; Drop *et al.*, 2014).

The reason for the observed absence of the Lhcb6 protein in separated PSII supercomplexes from spruce could either be the downregulation of its transcription or translation or the absence of the *lhcb6* gene. To distinguish between these possibilities, we have performed *in silico* analysis of the *P. abies* genome (Nystedt *et al.*, 2013) and transcriptome using the Lhcb6 protein sequence from *A. thaliana*. Basic local alignment search tool (BLAST) was used to retrieve best reciprocal BLAST hits for Lhcb1–6. The analysis clearly reveals the absence of a genomic sequence corresponding to *lhcb6* as well as of its transcript in *P. abies*. As in land plants the appearance of Lhcb6 coincides with Lhcb3 (see earlier), we performed the same analysis for *lhcb3* and obtained the same results. Moreover, we have also observed the loss of the *lhcb6* and *lhcb3* gene products in the transcriptomes of other *Picea* and *Pinus* species, which implies that this loss affects the whole pine family (Pinaceae) (Table 1). The absence of transcripts for Lhcb6 and Lhcb3 proteins was also observed in *G. gnemon* (Table 1), a representative of Gnetales (Fig. 3). Importantly, we have found the *lhcb6* and *lhcb3* transcripts in transcriptomes of representatives of all other groups of gymnosperms (cupressophytes, cycads, Ginkgoales) and of evolutionarily older land plant groups (mosses, liverworts, lycophytes, ferns) (Table 1; Fig. 3).

Although the absence of the Lhcb6 protein in the structure of PSII supercomplex from spruce is clearly visible, the absence of the Lhcb3 protein in the PSII structure is not so evident (Fig. 2). The Lhcb3 protein in the M trimer seems to be replaced by another Lhcb protein, as was observed in the PSII supercomplex isolated from *A. thaliana* mutant lacking Lhcb3 (Damkjær *et al.*, 2009). In spruce, however, the nature of the Lhcb3-replacing protein could be unique as it enables a stable binding of the M trimer to the PSII core complex at the absence of Lhcb6 protein (Fig. 2a) (see the

Table 1 The presence of homologs of *Arabidopsis thaliana* lhcb1–6 genes identified by the best reciprocal basic local alignment search tool (BLAST) hit in transcriptomes of selected organisms

Organism	lhcb1	lhcb2	lhcb3	lhcb4	lhcb5	lhcb6	Group
Chlamydomonas reinhardtii		(+)		+	+		Algae
Marchantia polymorpha		(+)	+	+	+	+	Liverworts
Physcomitrella patens		(+)	+	+	+	+	Mosses
Selaginella moellendorffii		(+)	+	+	+	+	Lycophytes
Ceratopteris richardii	+	+	+	+	+	+	Ferns
Cycas rumphii	+	+	+	+	+	+	Cycads
Ginkgo biloba	+	+	+	+	+	+	Gingkoales
Podocarpus macrophillus	+	+	+	+	+	+	Cupressophytes
Cryptomeria japonica	+	+	+	+	+	+	Cupressophytes
Sequoia sempervirens	+	+	+	+	+	+	Cupressophytes
Sciadopitys verticillata	+	+	+	+	+	+	Cupressophytes
Taxus baccata	+	+	+	+	+	+	Cupressophytes
Picea abies (genome)	+	+		+	+		Pinaceae
Picea abies (transcriptome)	+	+		+	+		Pinaceae
Picea glauca	+	+		+	+		Pinaceae
Picea sitchensis	+	+		+	+		Pinaceae
Pinus banksiana	+	+		+	+		Pinaceae
Pinus contorta	+	+		+	+		Pinaceae
Pinus pinaster	+	+		+	+		Pinaceae
Pinus sylvestris	+	+		+	+		Pinaceae
Pinus taeda	+	+		+	+		Pinaceae
Gnetum gnemon	+	+		+	+		Gnetales
Arabidopsis thaliana	+	+	+	+	+	+	Angiosperms

Note: In the case of *P. abies*, the analysis was also performed within its genome. Homologs of *lhcb6* and *lhcb3* are clearly missing in the genome of *P. abies* (see Supporting Information Table S1) and in the transcriptomes of *Picea*, *Pinus* and *Gnetum* species (see Table S2). Color coding corresponds to different plants groups: bryophyte (orange), lycophytes (light blue), ferns (violet), gymnosperms (light green), gymnosperms lacking the lhcb3 and lhcb6 genes (dark green), angiosperms (gray). Homologs of *A. thaliana* lhcb2 but not *lhcb1* were revealed for representatives of algae, liverworts, mosses and lycophytes by best reciprocal BLAST hit. However, in *C. reinhardtii* and *P. patens* LHCII trimeric proteins are encoded by *lhcbm* genes (*C. reinhardtii*), and *lhcbm* and *lhcb3* (*P. patens*) genes, respectively (Ballottari *et al.*, 2012). Generally, Lhcbm proteins could not be specifically associated with individual Lhcb proteins in *A. thaliana*. Thus, the identified *lhcb2* homologs (+) are most probably representatives of *lhcbm* genes.
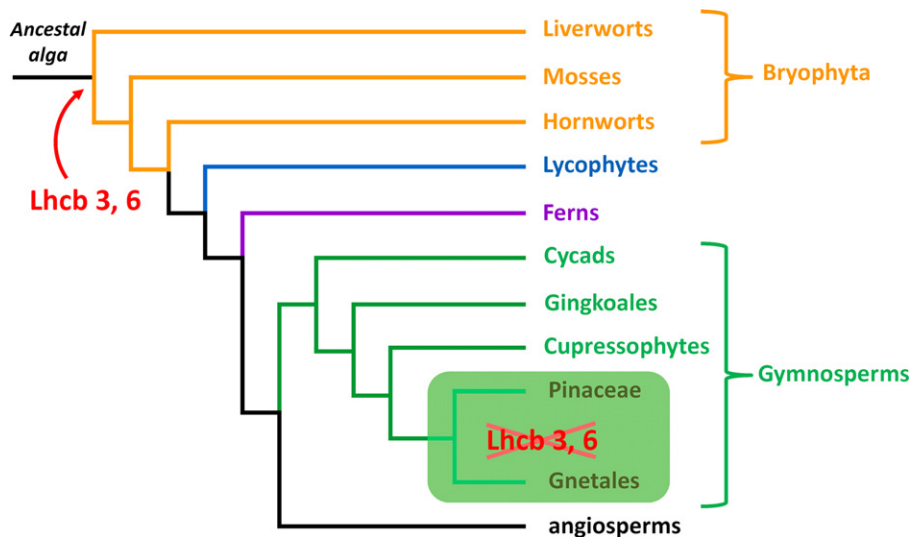
Fig. 3 Phylogenetic tree of land plant groups with indicated appearance and loss of Lhcb3 and Lhcb6 proteins. The tree was made according to Clarke *et al.* (2011).

Introduction section). The origin of the substitute of the Lhcb3 in spruce remains an intriguing question.

The sequence analysis, together with the structural changes in the PSII supercomplex in spruce, indicates that the evolution of Pinaceae and Gnetales is associated with significant modification of the light-harvesting antenna system of PSII. According to current phylogeny of plants, these groups are, despite their morphological differences, considered to be sister groups and represent a crown group of gymnosperms (Fig. 3) (see Bowe *et al.*, 2000; Chaw *et al.*, 2000; Clarke *et al.*, 2011; Wang & Ran, 2014, and references cited therein). In the light of this phylogenetic tree it is reasonable to assume that the loss of the genes for Lhcb6 and Lhcb3 proteins has occurred in a common ancestor of these groups, although individual losses of the genes in each group cannot be excluded.

During evolution, every important mutation/genetic change that is transferred to following generations offers some evolutionary advantage. The question arises what could be the cause(s) for the loss of Lhcb6 and Lhcb3 and what benefit would it provide? An important finding which offers the answer comes from the analysis of PSII supercomplex of angiosperms acclimated to high light conditions. Kouřil *et al.* (2013) have observed that long-term acclimation of *A. thaliana* to excess light leads to a selective downregulation of the Lhcb6 and Lhcb3 proteins, which further leads to a transition of the most abundant PSII supercomplex $C_2S_2M_2$ to C_2S_2. This indicates that long-term high light conditions in the past might be the environmental factor that affected the evolution of the common ancestor of Pinaceae and Gnetales. These gymnosperm families evolved most probably in the Triassic (Miller, 1999; Clarke *et al.*, 2011; He *et al.*, 2012), that is, after the greatest extinction event in Earth history (Great Dying). This catastrophe probably opened the canopy for a very long time period (until middle Triassic) (Retallack *et al.*, 1996; McElwain & Punyasena, 2007), exposing those surviving plants to high light.

It is also important to mention that in contrast to all other land plant groups, Pinaceae and Gnetales have also lost an entire set of plastid genes for NAD(P)H dehydrogenase (NDH) (Braukmann

et al., 2009). The NDH enzyme participates in one of two main pathways of cyclic electron flow (CEF) around PSI. On the contrary to the proton gradient regulation 5 protein (PGR5) dependent pathway (Munekage *et al.*, 2002), which was found to be essential for photosynthesis (Munekage *et al.*, 2004) and which seems to be operational in Pinaceae and Gnetales families (based on the presence of PGR5 in their transcriptomes, Table S2), the NDH-dependent electron pathway is not functional in these plant groups. The NDH pathway is used by photosynthetic machinery of stressed plants when the chloroplast stroma becomes over-reduced (for review see Shikanai, 2007). This pathway is very important for plants grown at low light, but for high light grown plants it does not have significant physiological function (Yamori *et al.*, 2015). This finding again supports our hypothesis that the common ancestor of Pinaceae and Gnetales evolved in high light conditions. It is also of note that extant species of Pinaceae and Gnetales are high-light tolerant, even though some of the evolutionarily more recent ones (e.g. *Gnetum* species, *Pinus krempfii*) prefer shade conditions (Brodribb & Feild, 2008; Feild & Balun, 2008).

The absence of the Lhcb6 protein in Pinaceae and Gnetales also evokes a question related to the nonphotochemical quenching (NPQ) of excess light energy, as Lhcb6 is known to play an important role in NPQ of land plants. Based on a dramatic decrease in NPQ observed in *A. thaliana* mutant lacking Lhcb6, it has been suggested that the Lhcb6, with associated M trimer, provides an interaction site for PsbS (Kovács *et al.*, 2006), a protein indispensable for fast and full activation of NPQ (Li *et al.*, 2000). Thus, it can be assumed that in Pinaceae and Gnetales, the mode of action of PsbS is different (due to the lack of Lhcb6) and/or that an additional protein is involved in the NPQ process. The structural similarities between the PSII supercomplexes from green alga *C. reinhardtii* and Norway spruce (Fig. 2) raise a question whether they also share similar NPQ features. In all photosynthetic organisms evolutionarily older than vascular plants (except of red algae), the NPQ depends on stress-related light harvesting complex (Lhcsr) (Koziol *et al.*, 2007; Peers *et al.*, 2009). Therefore, we performed additional

analysis of transcriptomes, which revealed *lhcsr*-like transcripts in some species of Pinaceae family (*P. glauca*, *P. sitchensis*, *P. abies* and *P. pinaster*) (Table S2). Thus, both the lack of the Lhcb6 protein and a possible presence of the Lhcsr protein indicate that Pinaceae can have a different mechanism of NPQ, which requires further in-depth investigation.

In conclusion, our results show that Pinaceae and Gnetales are exceptional land plant groups that deserve particular attention in plant physiology. The absence of Lhcb6 and Lhcb3 proteins revealed in this work changes the organization of antenna complexes in PSII supercomplex, which indicate that these plants use a different strategy to cope with changing light conditions.

Acknowledgements

Author contributions

R.K., L.N., J.B. and P.I. planned and designed the research. R.K., L.N., and E.J.B. performed experiments. R.K., L.N., J.B., E.J.B. and P.I. analyzed the data. R.K., L.N., J.B. and P.I. wrote the manuscript and all authors revised and approved it.

References

Alboresi A, Caffarri S, Nogue F, Bassi R, Morosinotto T. 2008. *In silico* and biochemical analysis of *Physcomitrella patens* photosynthetic antenna: identification of subunits which evolved upon land adaptation. *PLoS ONE* 3: e2033.

Ballottari M, Girardon J, Dall'osto L, Bassi R. 2012. Evolution and functional properties of photosystem II light harvesting complexes in eukaryotes. *Biochimica et Biophysica Acta – Bioenergetics* 1817: 143–157.

de Bianchi S, Dall'Osto L, Tognon G, Morosinotto T, Bassi R. 2008. Minor antenna proteins CP24 and CP26 affect the interactions between photosystem II subunits and the electron transport rate in grana membranes of Arabidopsis. *Plant Cell* 20: 1012–1028.

Bowe LM, Coat G, De Pamphilis CW. 2000. Phylogeny of seed plants based on all three genomic compartments: extant gymnosperms are monophyletic and Gnetales' closest relatives are conifers. *Proceedings of the National Academy of Sciences, USA* 97: 4092–4097.

Braukmann TWA, Kuzmina M, Stefanovic S. 2009. Loss of all plastid *ndh* genes in Gnetales and conifers: extent and evolutionary significance for the seed plant phylogeny. *Current Genetics* 55: 323–337.

Brodribb TJ, Feild TS. 2008. Evolutionary significance of a flat-leaved *Pinus* in Vietnamese rainforest. *New Phytologist* 178: 201–209.

Büchel C. 2015. Evolution and function of light harvesting proteins. *Journal of Plant Physiology* 172: 62–75.

Caffarri S, Kouřil R, Kereiche S, Boekema EJ, Croce R. 2009. Functional architecture of higher plant photosystem II supercomplexes. *EMBO Journal* 28: 3052–3063.

Chaw SM, Parkinson CL, Cheng Y, Vincent TM, Palmer JD. 2000. Seed plant phylogeny inferred from all three plant genomes: monophyly of extant gymnosperms and origin of Gnetales from conifers. *Proceedings of the National Academy of Sciences, USA* 97: 4086–4091.

Clarke JT, Warnock RCM, Donoghue PCJ. 2011. Establishing a time-scale for plant evolution. *New Phytologist* 192: 266–301.

Dainese P, Bassi R. 1991. Subunit stoichiometry of the chloroplast photosystem-II antenna system and aggregation state of the component chlorophyll-*a*/*b* binding proteins. *Journal of Biological Chemistry* 266: 8136–8142.

Damkjær JT, Kereiche S, Johnson MP, Kovacs L, Kiss AZ, Boekema EJ, Ruban AV, Horton P, Jansson S. 2009. The photosystem II light-harvesting protein Lhcb3 affects the macrostructure of photosystem II and the rate state transitions in *Arabidopsis*. *Plant Cell* 21: 3245–3256.

Drop B, Webber-Birungi M, Yadav SK, Filipowicz-Szymanska A, Fusetti F, Boekema EJ, Croce R. 2014. Light-harvesting complex II (LHCII) and its supramolecular organization in *Chlamydomonas reinhardtii*. *Biochimica et Biophysica Acta – Bioenergetics* 1837: 63–72.

Duvick J, Fu A, Muppirala U, Sabharwal M, Wilkerson MD, Lawrence CJ, Lushbough C, Brendel V. 2008. PlantGDB: a resource for comparative plant genomics. *Nucleic Acids Research* 36: 959–965.

Feild TS, Balun L. 2008. Xylem hydraulic and photosynthetic function of *Gnetum* (Gnetales) species from Papua New Guinea. *New Phytologist* 177: 665–675.

Goodstein DM, Shu S, Howson R, Neupane R, Hayes RD, Fazo J, Mitros T, Dirks W, Hellsten U, Putnam N et al. 2012. Phytozome: a comparative platform for green plant genomics. *Nucleic Acids Research* 40: 1178–1186.

Guskov A, Kern J, Gabdulkhakov A, Broser M, Zouni A, Saenger W. 2009. Cyanobacterial photosystem II at 2.9-Å resolution and the role of quinones, lipids, channels and chloride. *Nature Structural & Molecular Biology* 16: 334–342.

Harrer R. 2003. Association between light-harvesting complexes and photosystem II from *Marchantia polymorpha* L. determined by two- and three-dimensional electron microscopy. *Photosynthesis Research* 75: 249–258.

He T, Pausas JG, Belcher CM, Schwilk DW, Lamont BB. 2012. Fire-adapted traits of *Pinus* arose in the fiery Cretaceous. *New Phytologist* 194: 751–759.

Jansson S. 2006. A protein family saga: from photoprotection to light-harvesting (and back?). In: Demmig-Adams B, Adams WW III, Mattoo AK, eds. *Photoprotection, photoinhibition, gene regulation, and environment. Advances in photosynthesis and respiration.* Dordrecht, the Netherlands: Springer, 145–153.

Kouřil R, Dekker JP, Boekema EJ. 2012. Supramolecular organization of photosystem II in green plants. *Biochimica et Biophysica Acta – Bioenergetics* 1817: 2–12.

Kouřil R, Strouhal O, Nosek L, Lenobel R, Chamrád I, Boekema EJ, Šebela M, Ilík P. 2014. Structural characterization of a plant photosystem I and NAD(P)H dehydrogenase supercomplex. *Plant Journal* 77: 568–576.

Kouřil R, Wientjes E, Bultema JB, Croce R, Boekema EJ. 2013. High-light vs. low-light: effect of light acclimation on photosystem II composition and organization in *Arabidopsis thaliana*. *Biochimica et Biophysica Acta – Bioenergetics* 1827: 411–419.

Kovács L, Damkjær J, Kereïche S, Ilioaia C, Ruban AV, Boekema EJ, Jansson S, Horton P. 2006. Lack of the light-harvesting complex CP24 affects the structure and function of the grana membranes of higher plant chloroplasts. *Plant Cell* 18: 3106–3120.

Koziol AG, Borza T, Ishida K, Keeling P, Lee RW, Durnford DG. 2007. Tracing the evolution of the light-harvesting antennae in chlorophyll *a*/*b*-containing organisms. *Plant Physiology* 143: 1802–1816.

Lamesch P, Berardini TZ, Li D, Swarbreck D, Wilks C, Sasidharan R, Muller R, Dreher K, Alexander DL, Garcia-Hernandez G et al. 2012. The Arabidopsis information resource (TAIR): improved gene annotation and new tools. *Nucleic Acids Research* 40: 1202–1210.

Li XP, Björkman O, Shih C, Grossman AR, Rosenquist M, Jansson S, Niyogi KK. 2000. A pigment-binding protein essential for regulation of photosynthetic light harvesting. *Nature* 403: 391–395.

Lichtenthaler H, Buschmann C. 2001. Chlorophylls and carotenoids: measurement and characterization by UV-VIS spectroscopy. In: Wrolstad RE, Acree TE, An H, Decker EA, Penner MH, Reid DS, Schwartz SJ, Shoemaker CF, Sporns P, eds. *Current protocols in food analytical chemistry.* New York, NY, USA: John Wiley & Sons, F4.3.1–F4.3.8.

Liu Z, Yan H, Wang K, Kuang T, Zhang J, Gui L, An X, Chang W. 2004. Crystal structure of spinach major light-harvesting complex at 2.72 Å resolution. *Nature* **428**: 287–292.

McElwain JC, Punyasena SW. 2007. Mass extinction events and the plant fossil record. *Trends in Ecology & Evolution* **22**: 548–557.

Merchant SS, Prochnik SE, Vallon O, Harris EH, Karpowicz SJ, Witman GB, Terry A, Salamov A, Fritz-Laylin LK, Maréchal-Drouard L *et al.* 2007. The *Chlamydomonas* genome reveals the evolution of key animal and plant functions. *Science* **318**: 245–250.

Miller CN. 1999. Implications of fossil conifers for the phylogenetic relationships of living families. *Botanical Review* **65**: 239–277.

Munekage Y, Hashimoto M, Miyake C, Tomizawa KI, Endo T, Tasaka M, Shikanai T. 2004. Cyclic electron flow around photosystem I is essential for photosynthesis. *Nature* **429**: 579–582.

Munekage Y, Hojo M, Meurer J, Endo T, Tasaka M, Shikanai T. 2002. *PGR5* is involved in cyclic electron flow around photosystem I and is essential for photoprotection in Arabidopsis. *Cell* **110**: 361–371.

Nystedt B, Street NR, Wetterbom A, Zuccolo A, Lin YC, Scofield DG, Vezzi F, Delhomme N, Giacomello S, Alexeyenko A *et al.* 2013. The Norway spruce genome sequence and conifer genome evolution. *Nature* **497**: 579–584.

Oostergetel GT, Keegstra W, Brisson A. 1998. Automation of specimen selection and data acquisition for protein electron crystallography. *Ultramicroscopy* **74**: 47–59.

Peers G, Truong TB, Ostendorf E, Busch A, Elrad D, Grossman AR, Hippler M, Niyogi KK. 2009. An ancient light-harvesting protein is critical for the regulation of algal photosynthesis. *Nature* **462**: 518–521.

Retallack GJ, Veevers JJ, Morante R. 1996. Global coal gap between Permian–Triassic extinction and Middle Triassic recovery of peatforming plants. *Geological Society of America Bulletin* **108**: 195–207.

Shikanai T. 2007. Cyclic electron transport around photosystem I: genetic approaches. *Annual Review of Plant Biology* **58**: 199–217.

Tokutsu R, Kato N, Bui KH, Ishikawa T, Minagawa J. 2012. Revisiting the supramolecular organization of Photosystem II in *Chlamydomonas reinhardtii*. *Journal of Biological Chemistry* **287**: 31574–31581.

Vanheel M. 1987. Angular reconstitution – *a posteriori* assignment of projection directions for 3-D reconstruction. *Ultramicroscopy* **21**: 111–123.

Wang XQ, Ran JH. 2014. Evolution and biogeography of gymnosperms. *Molecular Phylogenetics and Evolution* **75**: 24–40.

Wittig I, Karas M, Schägger H. 2007. High resolution clear native electrophoresis for In-gel functional assays and fluorescence studies of membrane protein complexes. *Molecular & Cellular Proteomics* **6**: 1215–1225.

Yamori W, Shikanai T, Makino A. 2015. Photosystem I cyclic electron flow via chloroplast NADH dehydrogenase-like complex performs a physiological role for photosynthesis at low light. *Scientific Reports* **5**: 13908.

Supporting Information

Additional supporting information may be found in the online version of this article.

Table S1 Number of sequences, cumulative length and source of databases used for the identification of Lhcb transcripts in analyzed species using basic local alignment search tool (BLAST)

Table S2 Best hits for *Arabidopsis thaliana* Lhcb proteins and PGR5 and *Chlamydomonas reinhardtii* Lhcsr proteins in transcriptomes of selected species, particular scaffolds/transcripts in TAIR.10 or *C. reinhardtii* proteome and between scaffolds/transcript and proteins

Please note: Wiley Blackwell are not responsible for the content or functionality of any supporting information supplied by the authors. Any queries (other than missing material) should be directed to the *New Phytologist* Central Office.

About *New Phytologist*

- *New Phytologist* is an electronic (online-only) journal owned by the New Phytologist Trust, a **not-for-profit organization** dedicated to the promotion of plant science, facilitating projects from symposia to free access for our Tansley reviews.

- Regular papers, Letters, Research reviews, Rapid reports and both Modelling/Theory and Methods papers are encouraged. We are committed to rapid processing, from online submission through to publication 'as ready' via *Early View* – our average time to decision is <27 days. There are **no page or colour charges** and a PDF version will be provided for each article.

- The journal is available online at Wiley Online Library. Visit **www.newphytologist.com** to search the articles and register for table of contents email alerts.

- If you have any questions, do get in touch with Central Office (np-centraloffice@lancaster.ac.uk) or, if it is more convenient, our USA Office (np-usaoffice@lancaster.ac.uk)

- For submission instructions, subscription and all the latest information visit **www.newphytologist.com**

Publication 7

Structural variability of plant photosystem II megacomplexes in thylakoid membranes

Lukáš Nosek[1], Dmitry Semchonok[2], Egbert J. Boekema[2], Petr Ilík[1] and Roman Kouřil[1],*

[1]*Centre of the Region Haná for Biotechnological and Agricultural Research, Department of Biophysics, Faculty of Science, Palacký University, Šlechtitelů 27, 783 71 Olomouc, Czech Republic, and*
[2]*Electron Microscopy Group, Groningen Biomolecular Sciences and Biotechnology Institute, University of Groningen, Nijenborgh 7, 9747 AG Groningen, The Netherlands*

SUMMARY

Plant photosystem II (PSII) is organized into large supercomplexes with variable levels of membrane-bound light-harvesting proteins (LHCIIs). The largest stable form of the PSII supercomplex involves four LHCII trimers, which are specifically connected to the PSII core dimer via monomeric antenna proteins. The PSII supercomplexes can further interact in the thylakoid membrane, forming PSII megacomplexes. So far, only megacomplexes consisting of two PSII supercomplexes associated in parallel have been observed. Here we show that the forms of PSII megacomplexes can be much more variable. We performed single particle electron microscopy (EM) analysis of PSII megacomplexes isolated from *Arabidopsis thaliana* using clear-native polyacrylamide gel electrophoresis. Extensive image analysis of a large data set revealed that besides the known PSII megacomplexes, there are distinct groups of megacomplexes with non-parallel association of supercomplexes. In some of them, we have found additional LHCII trimers, which appear to stabilize the non-parallel assemblies. We also performed EM analysis of the PSII supercomplexes on the level of whole grana membranes and successfully identified several types of megacomplexes, including those with non-parallel supercomplexes, which strongly supports their natural origin. Our data demonstrate a remarkable ability of plant PSII to form various larger assemblies, which may control photochemical usage of absorbed light energy in plants in a changing environment.

Keywords: clear native polyacrylamide electrophoresis, *Arabidopsis thaliana*, photosystem II, megacomplex, single particle electron microscopy, grana membrane.

INTRODUCTION

Photosystem II (PSII) is one of the key protein complexes involved in light reactions of photosynthesis. It is embedded in thylakoid membranes of cyanobacteria, algae and higher plants, where it uses captured light energy for splitting water molecules. In cooperation with other protein complexes such as photosystem I (PSI) and cytochrome b_6f complex, it participates in the production of energetically rich molecules of ATP and NADPH, which drive reactions of CO_2 assimilation.

Plant PSII consists of a dimeric core complex (C_2) and a variable number of light-harvesting proteins (Lhcb1–Lhcb6), which form light-harvesting complex II (LHCII). The major part of the plant LHCII is represented by LHCII trimers, which consist of three Lhcb proteins (Lhcb1–Lhcb3), and which are associated with C_2 via monomeric antenna proteins Lhcb4 (also called CP29), Lhcb5 (CP26) and Lhcb6

(CP24). According to the strength of their binding to C_2, the LHCII trimers were designated as 'S' and 'M' (strongly and moderately bound LHCII, respectively; Dekker and Boekema, 2005; Kouřil *et al.*, 2012). Occasionally, C_2 can also associate with the 'L' (loosely bound) trimers (Boekema *et al.*, 1999a). Single-particle electron microscopy (EM) analysis of PSII in various land plant species indicates that the $C_2S_2M_2$ supercomplex is the largest stable form of the PSII supercomplex. In this supercomplex, C_2 associates with four LHCII trimers: two of them are strongly bound (S trimers) at the side of Lhcb5, and two of them are moderately bound (M trimers) via Lhcb4 and Lhcb6 (Boekema *et al.*, 1995; Caffarri *et al.*, 2009). A recent finding has revealed that the composition and architecture of the $C_2S_2M_2$ supercomplex is not conserved through all land plant species. Two land plant groups lack Lhcb3

(a constituent of the M trimer) and Lhcb6 proteins: the pine family (Pinaceae) and Gnetales. Apart from as yet unspecified physiological consequences, the absence of these proteins results in a structural modification of the $C_2S_2M_2$ supercomplex. This modified supercomplex is unique among land plants (Kouřil *et al.*, 2016) and resembles its counterpart in green alga *Chlamydomonas reinhardtii* (Tokutsu *et al.*, 2012; Drop *et al.*, 2014).

Despite progress in the specification of the positions of Lhcb proteins in PSII supercomplexes, there are still some Lhcb proteins with unclear localization. Biochemical analysis indicates that in the thylakoid membrane, up to eight LHCII trimers can be present per C_2 (Peter and Thornber, 1991; van Oort *et al.*, 2010; Kouřil *et al.*, 2013); however, the binding capacity of C_2 is limited to six LHCII trimers (including the L trimers). The remaining LHCIIs have so far been considered to be 'free' in the thylakoid membrane.

Besides a demand for the improvement of structural information about the PSII supercomplexes, the investigation of their organization in thylakoid membranes is also highly relevant. Considering that the excitation energy transfer between pigment-protein complexes strongly depends on their mutual distances, the interactions and connectivity between adjacent PSII complexes in the thylakoid membrane are very important for the regulation and optimization of their photochemical yield (e.g. van Oort *et al.*, 2010; Amarnath *et al.*, 2016). Most of the EM studies suggest that the organization of PSII supercomplexes in the thylakoid membrane is random (Dekker and Boekema, 2005; Kouřil *et al.*, 2012); however, in some cases a preference for a parallel association of PSII supercomplexes into megacomplexes was observed both on the level of isolated protein complexes (see Dekker and Boekema, 2005) and in isolated grana membranes (Kirchhoff *et al.*, 2008). The mutual interaction between two parallel PSII supercomplexes involves C_2, the M trimers, and the minor antenna proteins Lhcb5 and Lhcb6. S trimers and the Lhcb4 protein were also shown to be able to mediate the interaction between supercomplexes, but only in the case of the smaller C_2S_2 supercomplexes (Boekema *et al.*, 1999a,b; Yakushevska *et al.*, 2001a). The megacomplexes can further associate into various semi-crystalline arrays, which have been often observed in grana thylakoid membranes (Boekema *et al.*, 1999a,b, 2000; Yakushevska *et al.*, 2001a,b; Kirchhoff *et al.*, 2007; Daum *et al.*, 2010; Kouřil *et al.*, 2013). A mechanism controlling the formation of the megacomplexes and semi-crystalline arrays, as well as their functional relevance, is still not fully understood; however, there is increasing evidence that these structures, in analogy with respiratory megacomplexes in mitochondria (see e.g. Dudkina *et al.*, 2010 for review), are important for the regulation and optimization of photosynthetic processes and small protein traffic (for reviews, see e.g. Kouřil *et al.*,

2012; Kirchhoff, 2013; Tietz *et al.*, 2015), and may also contribute to grana formation (Daum *et al.*, 2010).

In this work, we have revealed a remarkable ability of PSII supercomplexes from *Arabidopsis thaliana* to form variable types of megacomplexes. Apart from the known parallel association of two PSII supercomplexes, we have also found variable associations between two non-parallel PSII supercomplexes. In some megacomplexes, novel binding positions for additional LHCII trimers (including the LHCII trimers so far considered to be 'free') were revealed at the sides of the S and M trimers. Importantly, we have also found some of these megacomplexes on the level of grana membranes, which evidences their natural origin. We propose that a dynamic formation of different types of PSII megacomplexes can optimize photochemical utilization of absorbed light energy under variable environmental conditions.

RESULTS

Separation of PSII megacomplexes using CN-PAGE

The PSII supercomplexes and megacomplexes can be separated from gently solubilized thylakoid membranes by ultracentrifugation using sucrose gradient (Caffarri *et al.*, 2009) or by clear/blue-native polyacrylamide gel electrophoresis (CN/BN-PAGE; e.g. Järvi *et al.*, 2011). The advantage of CN/BN-PAGE is that it provides well-focused protein zones. In order to preserve the integrity and to maximize the yield of PSII megacomplexes, a mild detergent such as *n*-dodecyl α-D-maltoside is often used. We solubilized thylakoid membranes from *A. thaliana* leaves using this detergent and modified the gradient of the resolving gel in order to achieve the optimal resolution of pigment-protein complexes of the highest molecular weight. Figure 1(a) shows that a combination of these approaches ensured a clear separation of PSII- and PSI-containing supercomplexes and PSII megacomplexes at the expense of the small protein complexes/proteins, such as trimeric or monomeric LHCII (see the band at the bottom part of the gel).

To clarify the band assignment, we measured chlorophyll fluorescence from the whole gel at room temperature (22 °C) using a gel imager (Figure 1a). As the quantum yield of PSII fluorescence at room temperature is much higher than the quantum yield of PSI fluorescence, this measurement enabled us to identify both types of photosystems. Using this approach, PSI supercomplexes (PSI core with LHCI) were identified in a relatively dense band with undetectable fluorescence (see Figure 1a). In native electrophoresis of pigment-protein complexes from thylakoid membranes (BN-PAGE and CN-PAGE), the PSII core dimer migrates close to the PSI supercomplex because it has similar molecular weight (e.g. Lípová *et al.*, 2010; Järvi *et al.*, 2011). In our gel, the PSII core dimer is represented
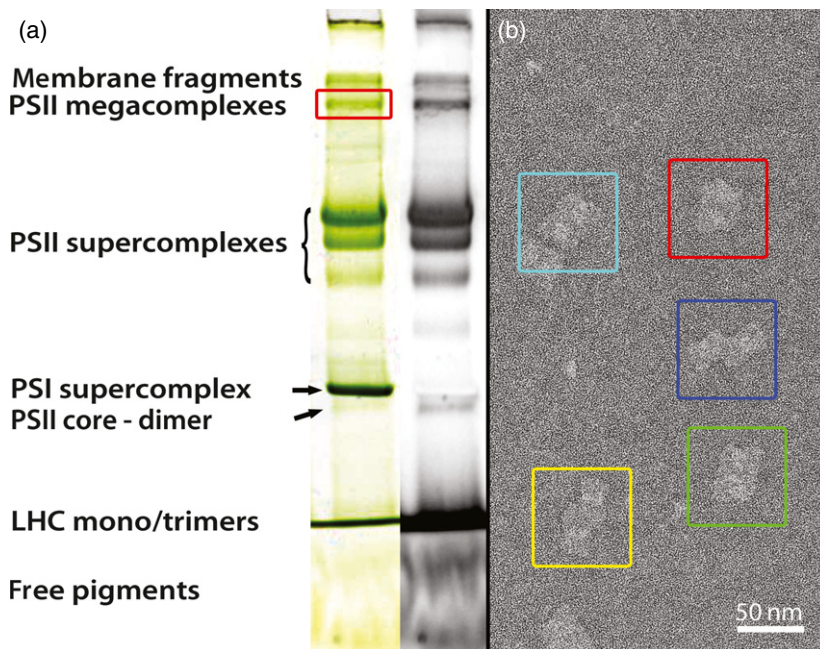
Figure 1. Separation and imaging of *Arabidopsis thaliana* pigment-protein complexes. (a) Clear-native polyacrylamide gel electrophoresis (CN-PAGE) separation of pigment-protein complexes from thylakoid membranes solubilized by *n*-dodecyl α-D-maltoside. The red frame indicates the band with megacomplexes subjected to elution and subsequent single-particle electron microscopy analysis. The black and white image represents the chlorophyll fluorescence emission detected from the same gel. The fluorescence signal was detected through a bandpass filter (690–720 nm); the excitation wavelength was 460 nm. (b) Part of the electron micrograph of a negatively stained specimen with photosystem II (PSII) megacomplexes. The colour frames highlight different forms of PSII megacomplexes.

by a very faint green band, which can be observed just below the PSI supercomplex band and which has high chlorophyll fluorescence yield. The fluorescence imaging of the gel further revealed that the green bands above the PSI supercomplex band are highly fluorescent, i.e. that they contain PSII. Based on the analogy with many papers dealing with native electrophoresis of chlorophyll-containing proteins from thylakoids (e.g. Järvi *et al.*, 2011; Albanese *et al.*, 2016), we designated the group of bands above the PSI supercomplex band as PSII supercomplexes and PSII megacomplexes.

It is clearly visible that the yield of isolated PSII megacomplexes is much smaller compared with the yield of supercomplexes. The lower yields of PSII megacomplexes can be caused either by lower stability during the isolation procedure (both solubilization and separation by CN-PAGE) or by a lower abundance in the thylakoid membrane. In order to characterize the structure and the composition of the separated megacomplexes, we excised the corresponding green band from the gel, extracted the pigment-protein megacomplexes by spontaneous elution and performed their detailed structural characterization by single-particle EM and image analysis.

PSII megacomplexes with specifically associated supercomplexes

Figure 1(b) shows an electron micrograph of a negatively stained specimen, where several PSII megacomplexes of different shape can be distinguished. Image processing of a large number of projections (about 50 000) selected from almost 12 000 micrographs revealed the presence of 13 different types of megacomplexes. Each megacomplex

consisted of two PSII supercomplexes. Based on the mutual position of individual PSII supercomplexes, the PSII megacomplexes could be divided into two groups. Whereas the first group represents the majority of megacomplexes (about 80% of the data set), with the PSII supercomplexes associated in parallel (Figure 2a–f), the second group (about 20% of the data set) represents PSII supercomplexes interacting in a non-parallel manner (Figure 2g–m). In order to reveal the architecture of individual megacomplexes in detail, the EM projection maps were fitted with the pseudo-atomic X-ray model of the PSII supercomplex (Caffarri *et al.*, 2009). It is obvious that most of the megacomplexes are formed by two copies of the complete $C_2S_2M_2$ supercomplex (Figure 3), with the exception of one megacomplex that lacks one M trimer (Figure 3l). Interestingly, the detailed image analysis revealed the presence of additional LHCII trimers in some of the megacomplexes (Figure 3e,f,g,k). These LHCII trimers are not regular constituents of PSII supercomplexes and so far have been assumed to be 'free' in the thylakoid membrane. Our results indicate that these trimers can interact with PSII supercomplexes at as yet uncharacterized binding sites.

Electron microscopy of grana membranes

In order to investigate the physiological relevance of the PSII megacomplexes separated using CN-PAGE, we also searched for megacomplexes on the level of isolated grana membranes. Figure 4(a) shows an example of an electron micrograph of the grana membrane with resolved densities of PSII complexes. Projections of individual PSII complexes were selected and processed by image analysis. If there are any specific interactions between some of these
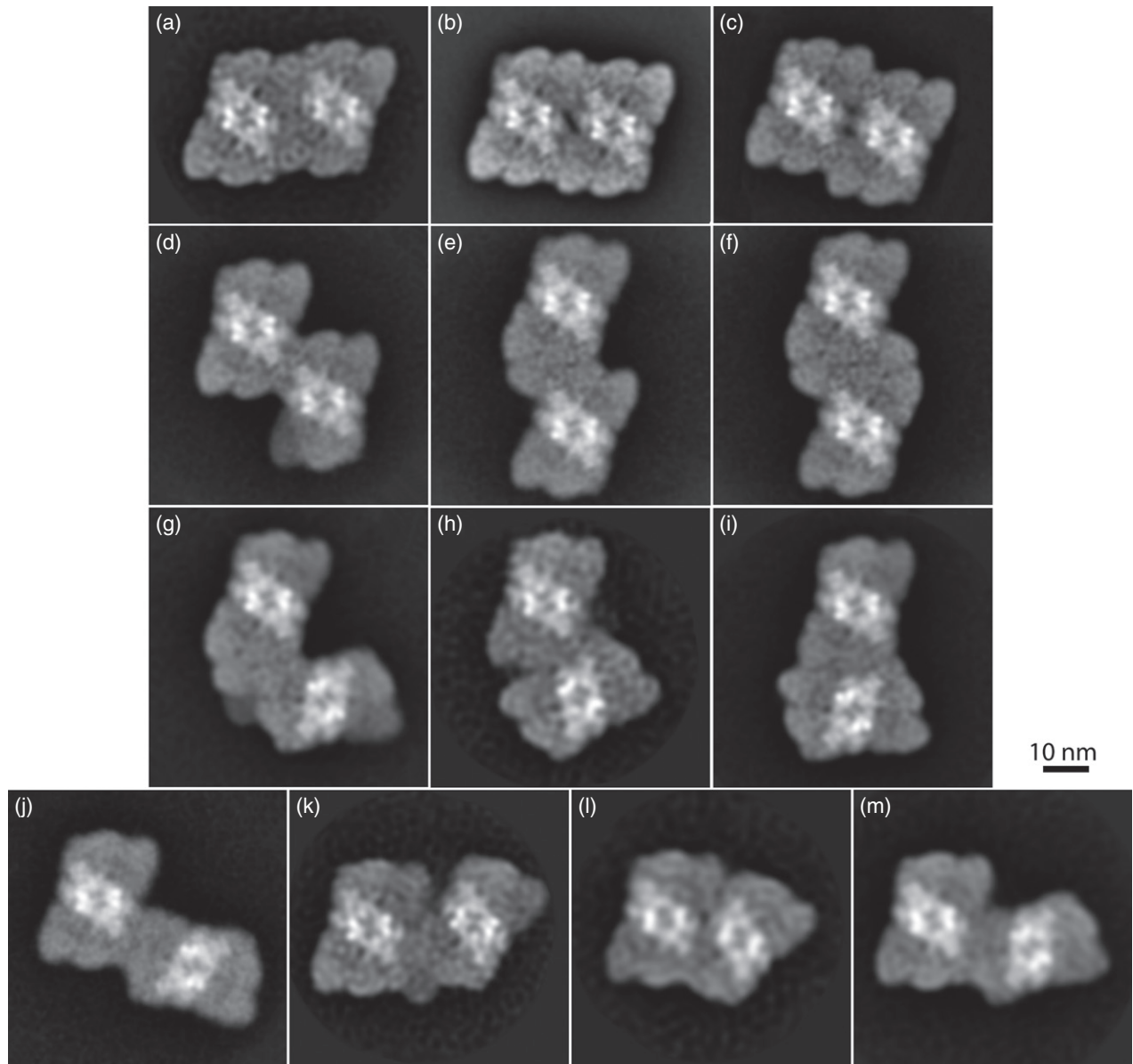
Figure 2. Structural characterization of photosystem II (PSII) megacomplexes: (a–f) represent the megacomplexes with parallel orientation of PSII supercomplexes, whereas (g–m) represent the megacomplexes formed by two supercomplexes associated in non-parallel manner. The total sums of particles contributing to the final images: (a) 1637, 4%; (b) 8411, 22%; (c) 16 928, 45%; (d) 2105, 6%; (e) 378, 1%; (f) 779, 2%; (g) 1640, 4%; (h) 418, 1%; (i) 2789, 7%; (j) 506, 1%; (k) 582, 2%; (l) 488, 1%; (m) 1082 (3%). The percentages indicate the relative abundance of the particular form of PSII megacomplex.

neighbouring PSII complexes in the grana membrane, they should be revealed as distinct classes after image processing. Indeed, image analysis revealed five specific classes with resolved densities of pairs of PSII core complexes (Figure 4b–f). Based on their mutual distance and orientation, we were able to link these pairs to the corresponding class averages of PSII megacomplexes separated using CN-PAGE (Figure 4g–k). Using this approach, the PSII megacomplexes with both parallel and non-parallel association of PSII supercomplexes were identified in the granal thylakoid membrane, with the parallel associations being about two times more abundant than the non-parallel associations. This result provides evidence that the PSII megacomplexes separated using CN-PAGE represent native PSII structures appearing in thylakoid membranes.

DISCUSSION

Structural studies of plant PSII revealed its remarkable ability to form variable types of PSII supercomplexes, consisting of PSII core and Lhcb proteins. Moreover, the proximity of PSII supercomplexes in the grana membrane enables the formation of larger assemblies, i.e. PSII
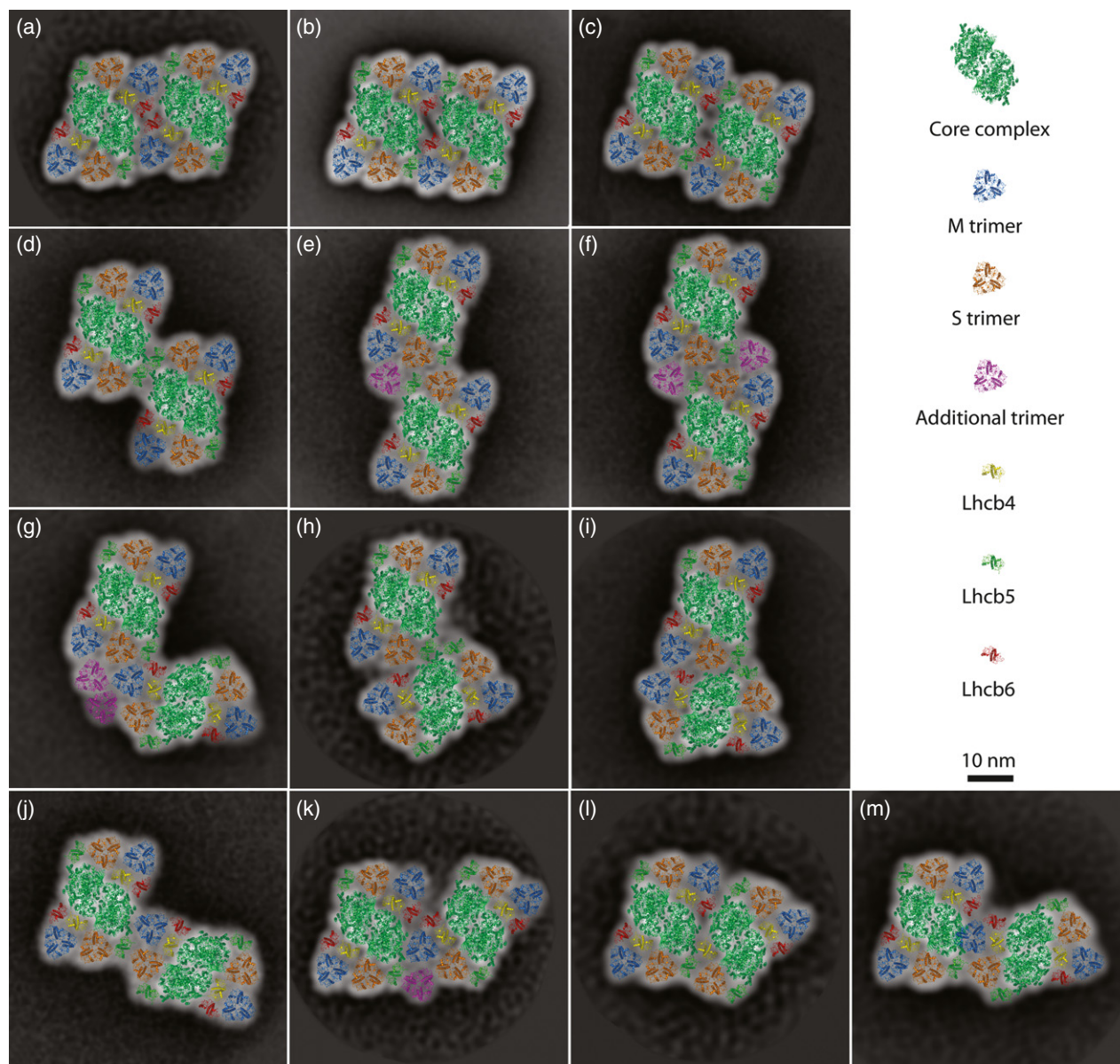
Figure 3. Structural models of the PSII megacomplexes shown in Figure 2. (a–m) Photosystem II (PSII) megacomplexes fitted with the proposed PSII crystalline structure, as published by Caffarri *et al.* (2009). Individual PSII subunits are color-coded in the following manner: pale green, core complex; blue, M trimer; orange, S trimer; magenta, additional LHCII trimers; yellow, Lhcb4; green, Lhcb5; red, Lhcb6.

megacomplexes or even structures of higher order (see Dekker and Boekema, 2005; Kouřil *et al.*, 2012 for reviews). Assembly/disassembly of PSII supercomplexes or megacomplexes modulates the antenna size of PSII, which was found to have an influence on the overall photochemical yield (e.g. Amarnath *et al.*, 2016). These changes of higher PSII organization can represent one of the responses of plants to dynamic changes of environmental conditions, such as light intensity (Ballottari *et al.*, 2007; Kouřil *et al.*, 2013). A recent theoretical study indicates that the excitation can move diffusively through the antenna proteins within a radius of about 50 nm until it reaches the reaction

center (Amarnath *et al.*, 2016). As the dimensions of the PSII supercomplex $C_2S_2M_2$ are 20 nm $\times$ 33 nm, the excitation can thus be shared within the whole megacomplex formed by two supercomplexes.

Our structural analysis of PSII megacomplexes separated using CN-PAGE revealed that a majority of them is formed by the parallel association of two PSII supercomplexes (Figures 2a–f and 3a–f). The reason for their abundance can be their higher structural stability when compared with the megacomplexes formed by the non-parallel association of PSII supercomplexes. Alternatively, it could reflect the fact that the megacomplexes with PSII

Figure 4. Photosystem II (PSII) megacomplexes found within an intact thylakoid membrane. (a) An example of an electron micrograph of negatively stained thylakoid membrane isolated from *Arabidopsis thaliana*, with densities corresponding to the PSII core complex indicated by white arrows. (b–f) PSII megacomplexes found within the thylakoid membrane (the number of summed projections was 1838, 2620, 940, 682 and 825, respectively). (g–k) PSII megacomplex analogs found in the sample separated by clear-native polyacrylamide gel electrophoresis (CN-PAGE). (g–k) Megacomplexes (a), (b), (h), (i) and (j), respectively, from Figure 2. The red frames surround core complexes of individual PSII supercomplexes and highlight that the megacomplexes found in the thylakoid membrane match with those obtained using CN-PAGE.
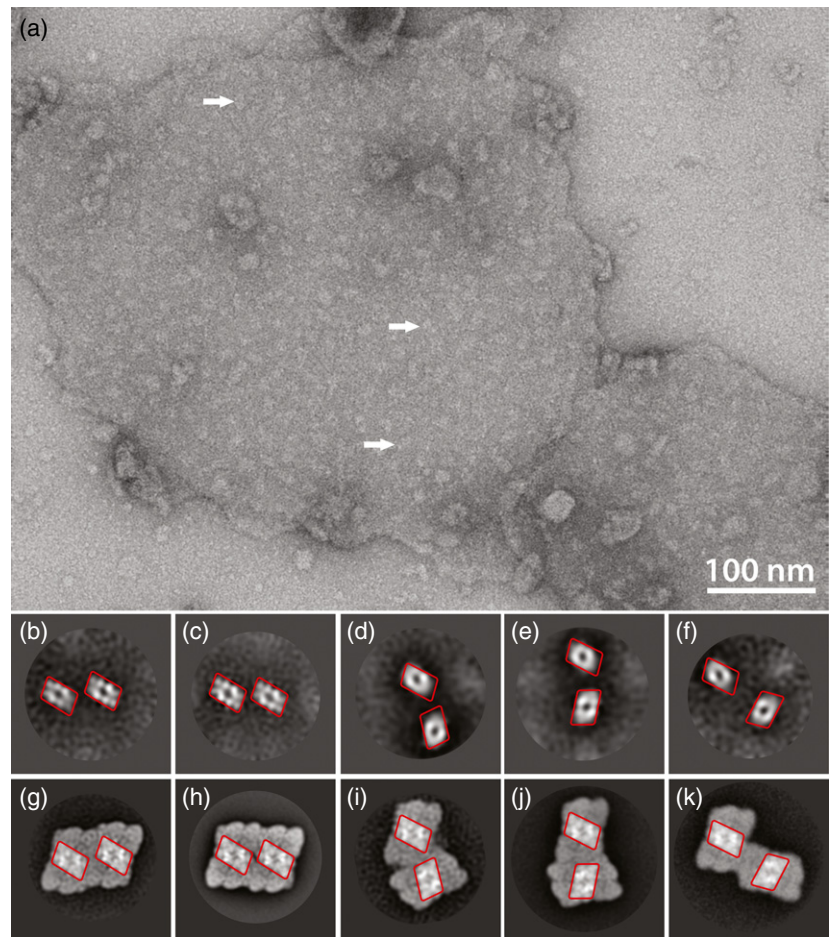
supercomplexes associated in parallel originate from solubilized semi-crystalline arrays, which appear occasionally in grana membranes (Boekema *et al.*, 1999a,b, 2000; Yakushevska *et al.*, 2001a,b; Kirchhoff *et al.*, 2007; Daum *et al.*, 2010; Kouřil *et al.*, 2013).

In the most abundant megacomplexes, PSII supercomplexes interact in parallel via core complexes, M trimers, and Lhcb5 and Lhcb6 proteins (Figure 3a–c). Obviously, the involvement of all these components in the interaction increases the overall stability of megacomplexes, resulting in their relatively high abundance; however, it seems that the interaction between Lhcb5 and the core complex alone is strong enough for the formation of the 'parallel' PSII megacomplex (Figure 3d). Moreover, novel types of PSII megacomplexes that consist of the parallel supercomplexes and additional LHCII trimers were revealed (Figure 3e,f). The additional LHCII trimers seem to be indispensable for the stability of these megacomplexes, as no analogous PSII megacomplexes lacking these additional trimers were detected.

In addition to the parallel association of the PSII supercomplexes into megacomplexes, the PSII megacomplexes with non-parallel orientation of supercomplexes were

detected for the first time (Figure 3g–m). As in the previous case, the supercomplex interactions within these megacomplexes are mediated by core complexes, S and M trimers, Lhcb5 and Lhcb6 proteins, and additional LHCII trimers, although not all components are always involved in the megacomplex formation. As a result of the asymmetric structure, these megacomplexes lack the possibility to form an arrangement similar to two-dimensional crystals.

Another interesting question that can be at least partially answered by our structural study is which subunits are, in general, essential for the formation of PSII megacomplexes. Their identification will help to understand a regulatory mechanism controlling the formation and dissociation of these megacomplexes. We propose that the contribution of Lhcb5 to PSII megacomplex formation is the most significant, as it participates to some extent in the formation of all types of PSII megacomplexes, even in those where Lhcb6 and the M trimer are not involved (Figure 3d–f).

In the grana membrane, most of the PSII supercomplexes seem to be randomly organized (Figure 4; see also Kouřil *et al.*, 2013); however, the observed variability in the architecture of the PSII megacomplexes separated using

CN-PAGE indicates that what originally looked like complete randomness can at least partially be explained by the abundance of specific megacomplex forms. Image analysis of PSII supercomplexes within the grana membrane revealed specific associations of PSII supercomplexes (both parallel and non-parallel interactions), which nicely corresponds with the structures of PSII megacomplexes isolated using CN-PAGE (Figure 4). In light of these results, we realize that the positions of interacting PSII supercomplexes that we observed previously in the cryo-tomogram of the grana membranes (Kouřil et al., 2011) do not have to be random, but can indeed be specific.

Taken together, the two sets of characterized PSII megacomplexes (with parallel and non-parallel arrangements of PSII supercomplexes) indicate that there are more LHCII trimers bound in specific positions to PSII than has been considered previously (Dekker and Boekema, 2005). This fact reduces the pool of 'free' LHCII trimers and supports the idea of a more defined packing of all PSII-related components in the grana membrane. The packing of PSII supercomplexes with 'free' LHCII trimers can be important for the regulation of effective PSII antenna size. The dynamic formation/disintegration of PSII megacomplexes can efficiently manage the utilization of absorbed light energy by PSII supercomplexes, as it enables the contact points between PSII reaction centers and adjacent antenna proteins to change. Nevertheless, the physiological significance and potential benefit of the formation of PSII megacomplexes under varying environmental conditions remains to be elucidated.

EXPERIMENTAL PROCEDURES

Plant material and sample preparation

Arabidopsis thaliana plants were grown in a growth chamber at 21°C, with an 8-h light/16-h dark photoperiod, at an irradiance of 100 μmol photons m^{-2} s^{-1} of photosynthetically active radiation (400–700 nm). Thylakoid membranes were isolated from 8-week-old plants using the protocol described by Dau et al. (1995). The chlorophyll content in the final thylakoid membrane suspension was determined by a pigment extraction into 80% acetone (Lichtenthaler, 1987). Thylakoid membranes with 10 μg of chlorophylls were solubilized with *n*-dodecyl α-D-maltoside using a detergent: chlorophyll mass ratio of 20, and supplemented with sample buffer (50 mM HEPES, pH 7.2, 400 mM sucrose, 5 mM MgCl$_2$, 15 mM NaCl, 10% glycerol) to a final volume of 30 μl. Non-solubilized membranes were removed by a short centrifugation (22 000 *g*, 4°C). After centrifugation, the supernatant was immediately loaded onto a polyacrylamide gel with 4–8% gradient resolving gel and 4% stacking gel (Wittig et al., 2007). The electrophoretic separation was conducted in a Bio-Rad Mini protean tetra cell system (Bio-Rad, http://www.bio-rad.com), starting with a constant current of 4 mA for 15 min and then continuing with a constant current of 7 mA until the front reached the bottom of the resolving gel. The CN-PAGE gel was analyzed using a gel scanner Amersham Imager 600RGB (GE HealthCare Life Sciences, http://www.gelifesciences.com). To visualize all the bands, the gel was scanned in transmission mode using white light illumination. The black and white image of the same gel was acquired in fluorescent mode to identify PSI- and PSII-containing bands. The excitation wavelength was 460 nm and the fluorescence signal was detected through a bandpass filter (690–720 nm). Subsequent elution of protein complexes from the gel and the preparation of the specimen for EM analysis was performed according to the procedure described by Kouřil et al. (2014).

Grana membranes were obtained by the solubilization of thylakoid membranes using digitonin (0.5 mg of chlorophylls per ml, 0.5% digitonin in buffer; 20 mM HEPES, pH 7.5, 5 mM MgCl$_2$). Incubation (20 min at 4°C while slowly stirred) was followed by centrifugation in an Eppendorf table centrifuge (5 min, 12 000 *g*, 4°C). The pellet with the non-solubilized grana thylakoid membranes was used for EM analysis.

Electron microscopy and image processing

Electron microscopy was performed on a Tecnai G2 20 Twin electron microscope (FEI, http://www.fei.com) equipped with a LaB$_6$ cathode, operated at 200 kV. Images were recorded with an UltraScan 4000 UHS CCD camera (Gatan, http://www.gatan.com), either at 130 000× magnification (in the case of isolated PSII megacomplexes) or at 80 000× magnification (in the case of grana membranes), with a pixel size of 0.224 and 0.375 nm, respectively, at the specimen level after binning the images to 2048 × 2048 pixels. GRACE (Oostergetel et al., 1998) was used for the semi-automated acquisition of about 12 000 images, from which a data set of about 50 000 single-particle projections of PSII megacomplexes separated by CN-PAGE was obtained. Single-particle image analysis (see e.g. Boekema et al., 2009) was performed using GRIP and RELION (Scheres, 2012). Image analysis revealed that about 75% of the projections from the data set could be assigned to one of the distinct classes. The remaining 25% of the data set represented projections of the PSI-NDH supercomplex (Kouřil et al., 2014), which co-migrated with the PSII megacomplexes during CN-PAGE separation, and projections of other unassigned particles. In the case of grana membranes, about 800 images were recorded and about 20 000 projections of PSII particles were manually selected. Image analysis using RELION revealed that about 35% of the projections from the data set could be resolved into five specific classes, for which we were able to reliably determine the mutual orientation of the PSII core complexes. The remaining 65% of the projections represented classes where the orientation could not be determined, either because of a low signal to noise ratio (i.e. a small number of particles) or because of non-specific interactions between the adjacent PSII complexes.

ACKNOWLEDGEMENTS

REFERENCES

Albanese, P., Manfredi, M., Meneghesso, A., Marengo, E., Saracco, G., Barber, J., Morosinotto, T. and Pagliano, C. (2016) Dynamic reorganization

of photosystem II supercomplexes in response to variations in light intensities. *Biochim. Biophys. Acta* **1857**, 1651–1660.

Amarnath, K., Bennet, D.I.G., Schneider, A.R. and Fleming, G.R. (2016) Multiscale model of light harvesting by photosystem II in plants. *Proc. Natl Acad. Sci. USA* **113**, 1156–1161.

Ballottari, M., Dall'Osto, L., Morosinotto, T. and Bassi, R. (2007) Contrasting behavior of higher plant photosystem I and II antenna systems during acclimation. *J. Biol. Chem.* **282**, 8947–8958.

Boekema, E.J., Hankamer, B., Bald, D., Kruip, J., Nield, J., Boonstra, A.F., Barber, J. and Rögner, M. (1995) Supramolecular structure of the photosystem II complex from green plants and cyanobacteria. *Proc. Natl Acad. Sci. USA* **92**, 175–179.

Boekema, E.J., van Roon, H., Calkoen, F., Bassi, R. and Dekker, J.P. (1999a) Multiple types of association of photosystem II and its light-harvesting antenna in partially solubilized photosystem II membranes. *Biochemistry*, **38**, 2233–2239.

Boekema, E.J., van Roon, H., van Breemen, J.F.L. and Dekker, J.P. (1999b) Supramolecular organization of photosystem II and its light-harvesting antenna in partially solubilized photosystem II membranes. *Eur. J. Biochem.* **266**, 444–452.

Boekema, E.J., van Breemen, J.F.L., van Roon, H. and Dekker, J.P. (2000) Arrangement of photosystem II supercomplexes in crystalline macrodomains within the thylakoid membrane of green plant chloroplasts. *J. Mol. Biol.* **301**, 1123–1133.

Boekema, E.J., Folea, M. and Kouřil, R. (2009) Single particle electron microscopy. *Photosynth. Res.* **102**, 189–196.

Caffarri, S., Kouril, R., Kereiche, S., Boekema, E.J. and Croce, R. (2009) Functional architecture of higher plant photosystem II supercomplexes. *EMBO J.* **28**, 3052–3063.

Dau, H., Andrews, J., Roelofs, T., Latimer, M., Liang, W., Yachandra, V., Sauer, K. and Klein, M. (1995) Structural consequences of ammonia binding to the manganese center of the photosynthetic oxygen-evolving complex: an X-ray absorption spectroscopy study of isotropic and oriented photosystem II particles. *Biochemistry*, **34**, 5274–5287.

Daum, B., Nicastro, D., Austin, J., McIntosh, J. and Kühlbrandt, W. (2010) Arrangement of photosystem II and ATP synthase in chloroplast membranes of spinach and pea. *Plant Cell*, **22**, 1299–1312.

Dekker, J.P. and Boekema, E.J. (2005) Supramolecular organization of thylakoid membrane proteins in green plants. *Biochim. Biophys. Acta* **1706**, 12–39.

Drop, B., Webber-Birungi, M., Yadav, S.K., Filipowicz-Szymanska, A., Fusetti, F., Boekema, E.J. and Croce, R. (2014) Light-harvesting complex II (LHCII) and its supramolecular organization in *Chlamydomonas reinhardtii*. *Biochim. Biophys. Acta* **1837**, 63–72.

Dudkina, N.V., Kouřil, R., Peters, K., Braun, H.P. and Boekema, E.J. (2010) Structure and function of mitochondrial supercomplexes. *Biochim. Biophys. Acta* **1797**, 664–670.

Järvi, S., Suorsa, M., Paakkarinen, V. and Aro, E.M. (2011) Optimized native gel systems for separation of thylakoid protein complexes: novel super- and mega-complexes. *Biochem. J.* **439**, 207–214.

Kirchhoff, H. (2013) Architectural switches in plant thylakoid membranes. *Photosynth. Res.* **116**, 481–487.

Kirchhoff, H., Haase, W., Wegner, S., Danielsson, R., Ackermann, R. and Albertsson, P.A. (2007) Low-light-induced formation of semicrystalline photosystem II arrays in higher plant chloroplast. *Biochemistry*, **46**, 11169–11176.

Kirchhoff, H., Lenhert, S., Büchel, C., Chi, L. and Nield, J. (2008) Probing the organization of photosystem II in photosynthetic membranes by atomic force microscopy. *Biochemistry*, **47**, 431–440.

Kouřil, R., Oostergetel, G.T. and Boekema, E.J. (2011) Fine structure of granal thylakoid membrane organization using cryo electron tomography. *Biochim. Biophys. Acta* **1807**, 368–374.

Kouřil, R., Dekker, J.P. and Boekema, E.J. (2012) Supramolecular organization of photosystem II in green plants. *Biochim. Biophys. Acta* **1817**, 2–12.

Kouřil, R., Wientjes, E., Bultema, J.B., Croce, R. and Boekema, E.J. (2013) High-light vs. low-light: effect of light acclimation on photosystem II composition and organization in *Arabidopsis thaliana*. *Biochim. Biophys. Acta* **1827**, 411–419.

Kouřil, R., Strouhal, O., Nosek, L., Lenobel, R., Chamrád, I., Boekema, E.J., Šebela, M. and Ilík, P. (2014) Structural characterization of a plant photosystem I and NAD(P)H dehydrogenase supercomplex. *Plant J.* **77**, 568–576.

Kouřil, R., Nosek, L., Bartoš, J., Boekema, E.J. and Ilík, P. (2016) Evolutionary loss of light-harvesting proteins Lhcb6 and Lhcb3 in major land plant groups - break-up of current dogma. *New Phytol.* **210**, 808–814.

Lichtenthaler, H.K. (1987) Chlorophylls and carotenoids. Pigments of photosynthetic biomembranes. In *Methods in Enzymology* (Colowick, S.P. and Kaplan, N.O., eds). San Diego/New York: Academic Press, pp. 350–382.

Lípová, L., Krchňák, P., Komenda, J. and Ilík, P. (2010) Heat-induced disassembly and degradation of chlorophyll-containing protein complexes *in vivo*. *Biochim. Biophys. Acta* **1797**, 63–70.

van Oort, B., Alberts, M., de Bianchi, S., Dall'Osto, L., Bassi, R., Trinkunas, G., Croce, R. and van Amerongen, H. (2010) Effect of antenna-depletion in photosystem II on excitation energy transfer in *Arabidopsis thaliana*. *Biophys. J*. **98**, 922–931.

Oostergetel, G.T., Keegstra, W. and Brisson, A. (1998) Automation of specimen selection and data acquisition for protein electron crystallography. *Ultramicroscopy*, **74**, 47–59.

Peter, G.F. and Thornber, J.P. (1991) Biochemical composition and organization of higher plant photosystem II light harvesting pigment-proteins. *J. Biol. Chem.* **266**, 16745–16754.

Scheres, S.H. (2012) RELION: implementation of a Bayesian approach to cryo-EM structure determination. *J. Struct. Biol.* **180**, 519–530.

Tietz, S., Puthiyaveetil, S., Enlow, H.M. *et al.* (2015) Functional implications of photosystem II crystal formation in photosynthetic membranes. *J. Biol. Chem.* **290**, 14091–14106.

Tokutsu, R., Kato, N., Bui, K.H., Ishikawa, T. and Minagawa, J. (2012) Revisiting the supramolecular organization of Photosystem II in *Chlamydomonas reinhardtii*. *J. Biol. Chem.* **287**, 31574–31581.

Wittig, I., Karas, M. and Schagger, H. (2007) High resolution clear native electrophoresis for in-gel functional assays and fluorescence studies of membrane protein complexes. *Mol. Cell Proteomics* **6**, 1215–1225.

Yakushevska, A.E., Jensen, P.E., Keegstra, W., van Roon, H., Scheller, H.S., Boekema, E.J. and Dekker, J.P. (2001a) Supermolecular organization of photosystem II and its associated light-harvesting antenna in *Arabidopsis thaliana*. *Eur. J. Biochem.* **268**, 6020–6028.

Yakushevska, A.E., Ruban, A.V., Jensen, P.E., van Roon, H., Niyogi, K.K., Horton, P., Dekker, J.P. and Boekema, E.J. (2001b) Supermolecular organization of photosystem II and its associated light-harvesting antenna in the wild- type and *npq4* mutant of *Arabidopsis thaliana*. In *Proceedings: 12th International Congress on Photosynthesis*. Melbourne, Australia: CSIRO Publishing, pp. S5-006.

Publication 8

Subunit and chlorophyll organization of the plant photosystem II supercomplex

Laura S. van Bezouwen[1][†], Stefano Caffarri[2], Ravindra S. Kale[3], Roman Kouřil[3], Andy-Mark W. H. Thunnissen[1], Gert T. Oostergetel[1] and Egbert J. Boekema[1]*

Photosystem II (PSII) is a light-driven protein, involved in the primary reactions of photosynthesis. In plant photosynthetic membranes PSII forms large multisubunit supercomplexes, containing a dimeric core and up to four light-harvesting complexes (LHCs), which act as antenna proteins. Here we solved a three-dimensional (3D) structure of the $C_2S_2M_2$ supercomplex from *Arabidopsis thaliana* using cryo-transmission electron microscopy (cryo-EM) and single-particle analysis at an overall resolution of 5.3 Å. Using a combination of homology modelling and restrained refinement against the cryo-EM map, it was possible to model atomic structures for all antenna complexes and almost all core subunits. We located all 35 chlorophylls of the core region based on the cyanobacterial PSII structure, whose positioning is highly conserved, as well as all the chlorophylls of the LHCII S and M trimers. A total of 13 and 9 chlorophylls were identified in CP26 and CP24, respectively. Energy flow from LHC complexes to the PSII reaction centre is proposed to follow preferential pathways: CP26 and CP29 directly transfer to the core using several routes for efficient transfer; the S trimer is directly connected to CP43 and the M trimer can efficiently transfer energy to the core through CP29 and the S trimer.

The photosynthetic reactions in plants, cyanobacteria and algae are catalysed by four major protein complexes, photosystem I (PSI), PSII, cytochrome $b_6 f$ and ATPase. These proteins are embedded in the thylakoid membranes, and in plants these membranes are located in a special organelle, the chloroplast. The primary photosynthetic reactions are light driven, and the harvested energy is used by PSI and PSII to transport electrons over the membranes and to establish a membrane proton gradient[1,2].

To understand the photosynthetic reactions, detailed knowledge about the structure of these protein complexes is necessary. For plant PSI high-resolution structures are known[3], but for plant PSII the structural information is limited. For cyanobacteria[4–6] and red algae[7] there is a high-resolution PSII structure based on X-ray crystallography, but no high-resolution structure for higher plants could be obtained by protein crystallography. Very recently this goal was achieved by single-particle cryo-EM and image processing[8].

PSII is a large multisubunit protein complex containing a dimeric core and a number of peripheral membrane-embedded antenna complexes. The core complex comprises between 20 and 23 protein subunits, depending on the organism. The catalytic heart of the core is the reaction centre, which is highly conserved between plants, algae and cyanobacteria. The reaction centre consists of four subunits, PsbA (D1), PsbB (CP47), PsbC (CP43) and PsbD (D2), which are also the largest membrane-intrinsic subunits. PsbA and PsbD form the photochemical reaction centre where the charge separation takes place as well as electron transfer over the membrane. Both subunits bind in total six chlorophylls (Chls), and PsbA has in addition two pheophytins. PsbB and PsbC are the internal antenna proteins, which bind several chlorophylls. These two subunits are involved in light harvesting and transporting excitation energy from peripheral antenna subunits towards the photochemical reaction centre[1]. In addition

to the reaction centre there are several other small intrinsic subunits, which are present in all organisms: PsbE, PsbF, PsbH, PsbI-M, PsbTc, PsbX, PsbY and PsbZ. These subunits are structurally and functionally conserved but less strongly related between organisms than those of the reaction centre. Plant PsbY has, for instance, an additional membrane spanning helix as compared to its bacterial counterpart. Plants lack the cyanobacterial subunit Ycf12 but have two additional subunits, PsbTn and PsbW. Their location could be established in the plant supercomplex structure[8].

PSII has a special set of three to four extrinsic subunits of the oxygen-evolving complex (OEC) which shields the water splitting machinery[9]. The 33 kDa subunit PsbO, which stabilizes the manganese complex, is present in all organisms. The set of smaller subunits is variable. Plants have PsbP, PsbQ and PsbR[10] of which PsbP and PsbQ subunits are involved in optimizing the oxygen evolution at physiological concentrations of calcium and chloride[9]. PsbR needs PsbJ for stabilization and seems important for the assembly of PsbP[9]. The location of the extrinsic subunits for plants is now largely established[8].

The dimeric plant core complex (C_2) can form supercomplexes with up to six LHCII trimers, which are the major components of the antenna system. LHCII consists of heterotrimers composed of different combinations of Lhcb1, Lhcb2 and Lhcb3[11]. These trimers are linked to the core complex by the minor monomeric antenna proteins Lhcb4 (CP29), Lhcb5 (CP26) and Lhcb6 (CP24)[12]. At present, the largest purifiable PSII supercomplex, the $C_2S_2M_2$ particle, binds four LHCII trimers, two strongly bound (S) and two moderately strongly bound (M) trimers. Two additional, loosely bound (L), trimers could be detected in spinach supercomplexes (indicated as $C_2S_2M_2L_2$) and *A. thaliana* supercomplexes and megacomplexes[13].

The light-harvesting proteins have been the subject of many studies. Over the years several crystal structures were solved for

[1]Electron microscopy and Protein crystallography group, Groningen Biomolecular Sciences and Biotechnology Institute, University of Groningen, 9747 AG Groningen, The Netherlands. [2]Aix Marseille Université, CEA, CNRS, BIAM, Laboratoire de Génétique et Biophysique des Plantes, 13009 Marseille, France. [3]Centre of the Region Haná for Biotechnological and Agricultural Research, Department of Biophysics, Faculty of Science, Palacký University, Šlechtitelů 27, 783 71 Olomouc, Czech Republic. [†]Present address: Cryo-Electron Microscopy, Bijvoet Centre for Biomolecular Research, Faculty of Science, Utrecht University, 3584 CH Utrecht, Netherlands (L.S.v.B.). *e-mail: e.j.boekema@rug.nl
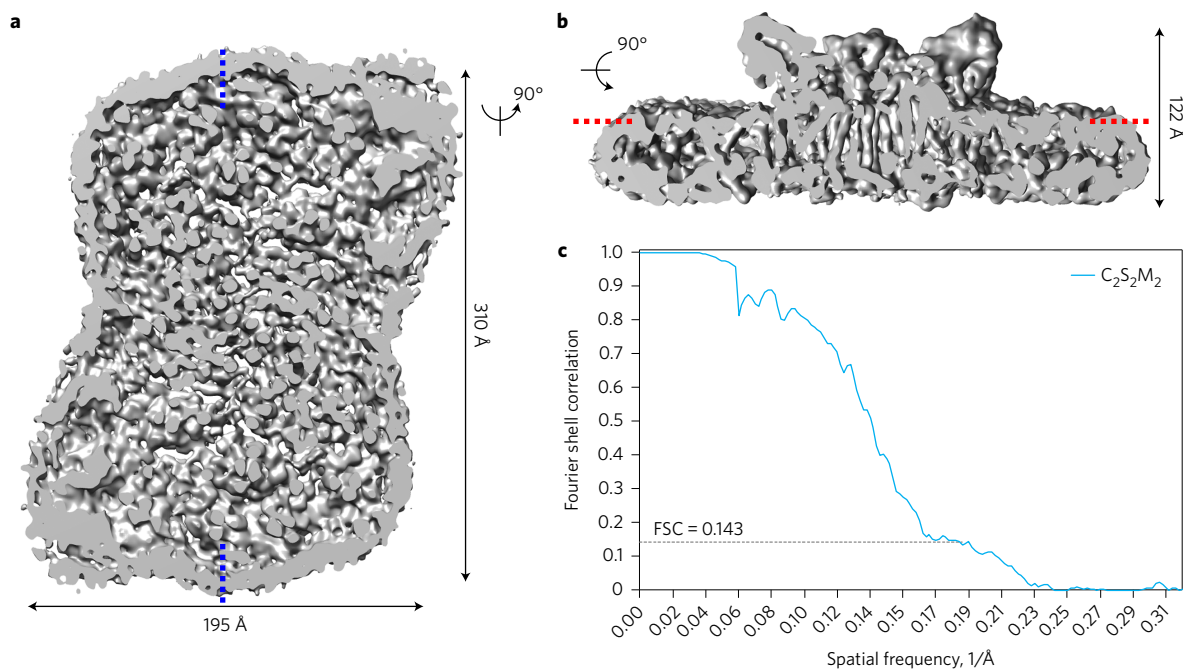
Figure 1 | Architecture of the $C_2S_2M_2$ particle at an average resolution of 5.3 Å. a, Cryo-EM density map of the final supercomplex. Blue lines indicate where the protein was sliced as shown in **b**. **b**, Density inside the complex shown vertical to the membrane plane. Red lines indicate where the protein was sliced as shown in **a**. **c**, FSC curve of two independently refined half datasets of the $C_2S_2M_2$ supercomplex (blue). The resolution based on the gold-standard criterion (0.143) is 5.3 Å.

both the LHCII trimers from spinach and pea[14,15] and for the monomeric CP29 from spinach[16]. The monomeric LHCII subunit and CP29 show significant homology in amino acid sequence and overall structure, but there are some relevant differences[17], in particular with respect to carotenoid and chlorophyll composition. The monomeric antenna CP29 binds three carotenoids (one lutein, one violaxanthin and one neoxanthin), and LHCII binds four carotenoids per monomer (two luteins and one neoxanthin as in CP29, plus one violaxanthin/lutein in an additional peripheral mixed site). Each LHCII monomer contains 14 chlorophylls, of which eight are Chl *a* and six are Chl *b*. On the other hand, CP29 has 13 chlorophylls, of which eight are Chl *a* and four are Chl *b* with a mixed Chl *a/b* site present at binding site 610. In addition to a variable number of chlorophylls there is a difference in their location within the antenna proteins. In comparison to a LHCII monomer, CP29 is lacking chlorophylls at binding sites 601 and 605. Conversely, in CP29 a chlorophyll is present at binding site 615, which is absent in the LHCII monomers[17]. Monomeric CP26 and CP24 are predicted to contain 13 and 10/11 chlorophylls, respectively, based on sequence homology and biochemical evidence[18]. In the absence of crystal structures of CP26 and CP24, it is unclear which chlorophylls are present, and what is their exact location and orientation in these antenna proteins.

To fully understand the flow of excitation energy within plant PSII, it is crucial to have a high-resolution 3D structure of a PSII supercomplex. Because of recent developments in electron detectors and in image processing[19], single-particle electron microscopy is nowadays able to solve structures at near-atomic resolution. The spinach C_2S_2 supercomplex, lacking a large part of the antenna system, was the first plant PSII supercomplex to be determined at high resolution[8]. The largest PSII supercomplex, the $C_2S_2M_2$, is more abundant in *Arabidopsis*, but only a negative stain projection map at a 12 Å resolution is available[20]. Based on the new electron microscopy developments we managed to obtain a 3D cryo-EM map of the $C_2S_2M_2$ supercomplex from *Arabidopsis* at an overall resolution of 5.3 Å, allowing reconstruction of its 3D structure.

The structure contains all the membrane-bound core subunits conserved in different PSII complexes, except PsbJ and PsbY, as well as the LHCII trimers and minor antenna complexes. The supramolecular organization of the subunits in the $C_2S_2M_2$ is described in particular with respect to the location and orientation of LHCII trimers and minor antenna complexes. We also discuss the location of all the chlorophylls in the subunits and their role in the energy flow from the peripheral antennae to the core.

Results

To gain an insight in the plant PSII function we determined the structure of a $C_2S_2M_2$ particle by single-particle cryo-EM. For this purpose, a large dataset with movie frames was collected (Supplementary Fig. 1) and processed (Supplementary Figs 2 and 3). We used particles purified from a *npq4* mutant, lacking PsbS which was found to be present in sub-stoichiometric amount in $C_2S_2M_2$ particles purified from wild-type membranes[20,21]. Though high purity is not a prerequisite, it is considered to be advantageous in 3D single-particle analysis. The final structure with a twofold symmetry imposed has an overall resolution of 5.3 Å (Fig. 1). At this resolution the transmembrane helices of the subunits are resolved and therefore the location of all the different subunits could be determined. The overall resolution is 5.3 Å, but there is a large variance within the map (Supplementary Fig. 4). The core region is well determined, with a local resolution between 4 Å and 5 Å, but the resolution in the periphery of the complex, where the antenna proteins are located, is not as high as in the centre.

To allow a reliable reconstruction of the 3D structure of the $C_2S_2M_2$ particle, the cryo-EM map was divided into different regions of more or less uniform resolution. Three regions were identified in the cryo-EM map, encompassing the core, the S trimers with subunits CP26 and CP29, and the M trimers with subunits CP24. First, a 3D structure of the core region was built and fitted into the cryo-EM map, using the 1.9 Å cyanobacterial PSII structure[4] as a starting model. The core of cyanobacterial PSII, without the extrinsic subunits PsbU and PsbV, was placed
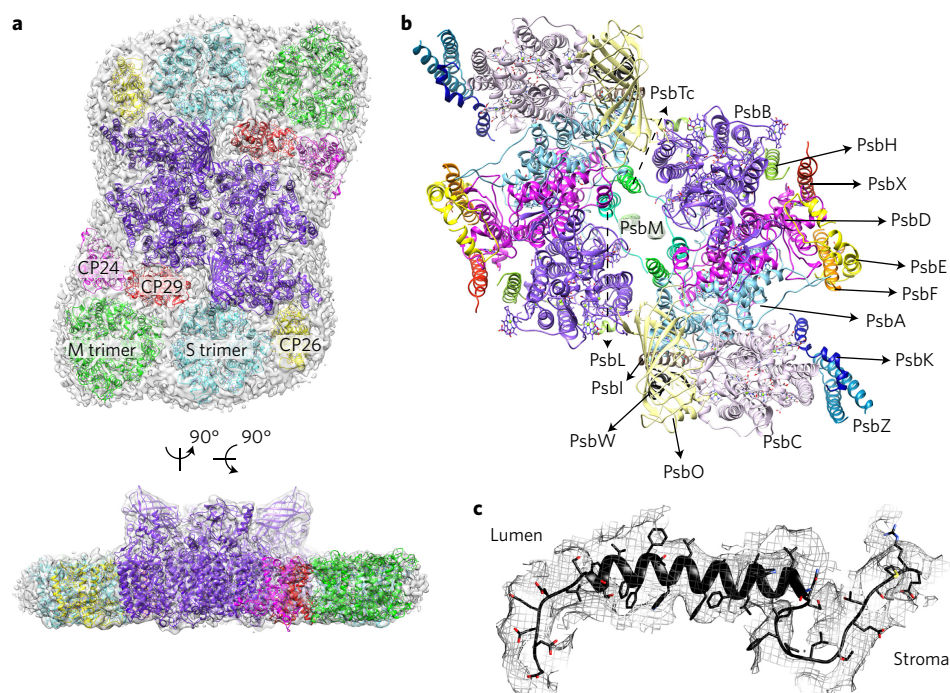
Figure 2 | Location of all the different subunits of the $C_2S_2M_2$ particle. a, Overviews with the location of the core region (purple), the S-LHCII trimer, the M-LHCII trimer, CP29, CP26 and CP24 indicated. The top view shows PSII from the lumenal side, normal to the membrane plane; the bottom view is along the membrane plane. **b**, Assigned subunits of the core, individually indicated in the figure. **c**, Close-up of the fit of PsbW in our structure. The lumen and stroma are indicated.

into the density map using a rigid body fit. Based on this initial fit, the homology models for the *Arabidopsis* subunits were then placed into the density map and refined as individual rigid bodies to adjust their relative positions and orientations. Each fit was examined individually, to determine whether the corresponding subunit was indeed present in the cryo-EM density map. The local fit and geometry of the core subunits were then optimized by model building and real space refinement at 4.5 Å resolution, using tight secondary structure restraints, side chain rotamer restraints and restraints to maintain a proper geometry and binding mode of the chlorophylls. Using a similar approach, separate 3D structures were obtained of the S trimers with subunits CP26 and CP29, and of the M trimers with subunits CP24, improving local fit and geometry by real space restrained refinement at 5.5 Å and 6.5 Å, respectively. The final PSII model was obtained by assembly of the separately built and refined regions (Fig. 2).

In the cryo-EM density map all the transmembrane helices of PsbA, PsbB, PsbC and PsbD are clearly visible and well defined. Whereas the helices are clearly visible, the termini are more difficult to assign. The region around these subunits is the best resolved part, and the porphyrin ring of the chlorophylls can be fitted accurately in the right plane.

The small intrinsic subunits were analysed one by one. In the centre of the core the helices are well defined and the subunits PsbL, PsbM and PsbTc were easy to place. Towards the outside of the core it was more difficult, but overall most subunits could be assigned. The location of PsbE and PsbF, which coordinate the cytochrome *b*-559, could be confirmed by the clear presence of a density for the haem. The subunits PsbH, PsbI, PsbK, PsbX and PsbZ are clearly present as well. For the extrinsic subunits the density for PsbO has been assigned. The β-barrel is well organized, but for the loops not all densities are resolved. In the density map at each location of PsbO a single copy is present (Fig. 2a,b), as in the recent model of the C_2S_2 particle from spinach[8].

The other three extrinsic subunits, PsbQ, PsbP and PsbR, are absent in our map. The location of PsbP and PsbQ has been recently proposed for the spinach PSII-C_2S_2 supercomplex[8], but the location of PsbR remains still unknown. One unassigned density, in between PsbA, PsbC and the S trimer, is likely to be the subunit PsbW (Fig. 2c)[8]. To further confirm this assignment, the known amino acid sequence has been fitted in by taking into account the expected structure[22]. The full transmembrane part and a large part of the amino (N) terminus is modelled, starting from amino acid 9. The model indicates that PsbW has interactions with PsbA, PsbC and PsbI, and via its N terminus with PsbO. Possibly there is an interaction with a cofactor of the S trimer, because an unassigned density is present between PsbW and the S trimer subunit, above Chl *a*612. At the current resolution it is not possible to identify this density. Based on the size of the extra density we do not expect a chlorophyll at that location.

Two small membrane subunits, PsbJ and PsbY, could not be detected in the 3D map. No unassigned density was present in the electron microscopy density map at the position where PsbJ was expected according to the cyanobacterial structure. It should be noted that in the recent spinach PSII structure[8], PsbJ has been assigned to a density between PsbK and PsbE. However this density is very weak, suggesting a sub-stoichiometric amount of PsbJ. To determine the location of PsbY, the cyanobacterial core structure[5] was used as a reference (pdb: 4UB6). At the putative location of PsbY (next to PsbK and PsbZ) a weak density is present. However, considering that the second transmembrane helix predicted in *Arabidopsis* (in cyanobacteria PsbY has only one helix) is not visible and that the resolution in the map at the possible location of PsbY is low, PsbY was not placed in the $C_2S_2M_2$ model.

The structure gives insight into the location of the many pigments and co-factors, in particular for the four large subunits of the reaction centre that contain all the chlorophylls of the core. All 35 chlorophylls, the two pheophytins and the haem, which are present in cyanobacteria, were identified in the plant PSII core (Fig. 3). The chlorin rings of both the chlorophylls and the
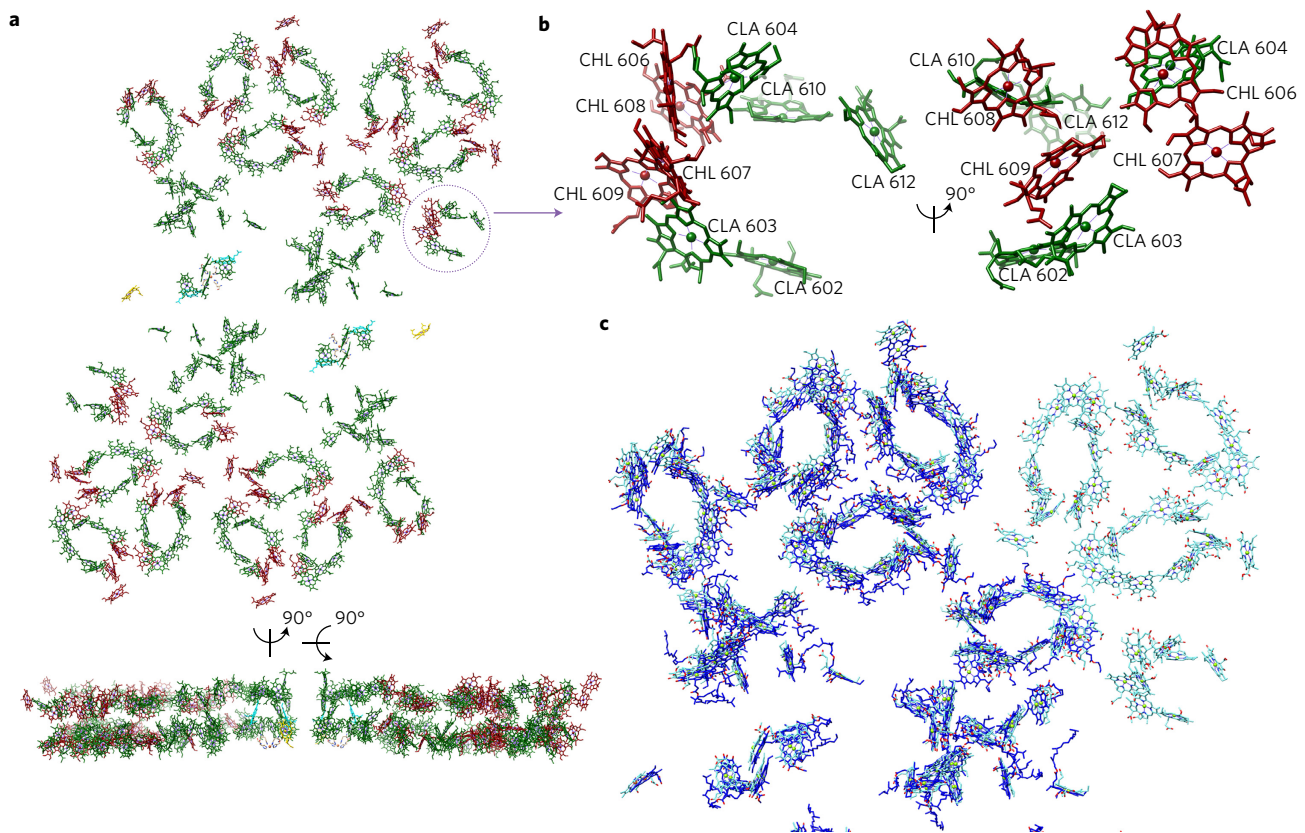
Figure 3 | Chlorophylls of the supercomplex. a, Overview of all chlorophylls in the supercomplex shown from the lumenal side and along the membrane plane. Chlorophyll *a* is depicted in green, chlorophyll *b* in dark red, pheophytins in cyan and haem in yellow. **b**, Close-up of CP24; a view from the lumen (left) and along the membrane plane (right). **c**, Overlay of the chlorophylls of the *Arabidopsis* $C_2S_2M_2$ particle (light blue) and the spinach C_2S_2 particle (dark blue)[8].

pheophytins are easy to locate, but for the phytol tails there is no clear density present and therefore they were removed from the model during the refinement. Owing to the missing phytol tails, it is not possible to determine the exact orientation of the chlorophylls, but there are no differences in distances between the chlorophylls in plants and cyanobacteria. This indicates that these chlorophylls are highly conserved between distant species.

All chlorophylls in the core could be localized, but other densities smaller than a chlorophyll remain unassigned. To have an idea where other pigments and lipids are located, pigments and lipids of cyanobacteria were overlaid on top of the unassigned densities. Based on this analysis, it is possible to locate eight β-carotenes. In the cyanobacterial structure there are more than 20 lipids present[4] and in spinach there are 16 lipids, 10 carotenoids and 1 plastoquinone[8]; in our map the partial density of 10 of them could be assigned (data not shown). None of these pigments or lipids was included in the refined 3D model of PSII, as only partial densities are present in the electron microscopy map and the resolution is a limiting factor as well (Supplementary Fig. 5). The presence of a number of pigments or lipids could be confirmed, but the presence of the manganese cluster could not (Supplementary Fig. 6). All the amino acids which coordinate manganese, calcium or oxygen atoms are conserved in *Arabidopsis*. But the carboxy (C) terminus of PsbA (amino acids 335–344), important for the binding of the manganese cluster, appears to be disordered, as there is no density present in that region.

In this structure of the $C_2S_2M_2$ particle the location and orientation of the antenna proteins could be unambiguously determined although the overall resolution of the antenna region is not as high as in the core and among the different antenna proteins the resolution is not consistent as well. The S trimer, CP26 and CP29 are the best-resolved components compared with the M trimer and CP24 (Supplementary Fig. 4). Therefore these regions were analysed separately. Chlorophylls could be detected in all these proteins, but no distinction could be made between Chl *a* and Chl *b*. The phytol tails of the chlorophylls were not used for the model as there is no density present. The carotenoids could not be detected at all. There are some unassigned densities in the S trimer, and it is possible that one pigment molecule is located there. But based on the current resolution it is impossible to determine if this is an extra pigment molecule or just a tail from one of the assigned chlorophylls.

Crystal structures of both the LHCII trimer and CP29 are available[15,16] and these were placed at the location of the S trimer and CP29. The trimer was analysed as a homotrimer with only Lhcb1 because of limited resolution of the S trimer, which does not allow a determination of the side chains of the amino acids. The individual amino acids that differ between pea and *Arabidopsis* were replaced; the same was done for the amino acids of CP29 that differ between spinach and *Arabidopsis*. Although the side chains of the amino acids are not resolved in the density, a rigid body fit followed by a real space refinement determined the precise orientation and location of both the S trimer and CP29. The root mean squared deviations (r.m.s.d.) between the backbone Cα atoms of PSII-CP29 and those of the 3PL9 (ref. 16) and 2BHW (ref. 15) structures are 1.1 Å and 1.5 Å, respectively. Based on the location of the helices the structures could be placed rather exactly (Supplementary Fig. 7). Once the helices were placed, the location of the chlorophylls could be determined. In both structures all the chlorophyll binding sites, based on the

Table 1 | Detected chlorophylls of CP26 and CP24 and the chlorophyll binding site.

CP26[*]	CP24[*]	Coordinating residues (CP26/C24)
b601[†]		–
a602	a602	GLU114/GLU102
a603	a603	HIS117/HIS105
a604	a604	–/–
b606	b606	GLU178/GLN149
b607	b607	–/–
b608	b608	–/–
a609	b609	GLU186/GLU157
a610	a610	GLU225/GLU228
a611		–/–
a612	a612	ASN228/HIS231
a613		GLN242/–
a614		HIS257/–

*Chlorophyll types are based on the chlorophylls of CP29 (ref. 16) and biochemical data[27]. †Chlorophyll type is based on the trimer structure[14].

backbone, are conserved. For the S trimer all 14 chlorophylls per monomer are present. For CP29, 13 chlorophylls were located, including Chl a601 and Chl a614, of which the last one is missing in the spinach CP29 cryo-EM map[8]. Chl a615 from the crystal structure[16] could not be located, as well as Chl a616 from spinach PSII[8]. The identity of chlorophyll 601 is based on the CP29 crystal structure and the identity of Chl 615, which is a Chl a assigned to a new site near to Chl 601 site in the N-terminal region. However, the N terminus in the CP29 crystal was severely affected during CP29 purification and crystallization, and Chl a615 was very likely to be a displaced Chl a601.

For CP26 a homology model was built, as there is no crystal structure available for this subunit. Once the exact location and orientation was determined, the chlorophylls could be located (Fig. 3). As the resolution does not allow differentiation between Chl a and Chl b, the same type of chlorophyll was assigned to every position as in CP29 or the LHCII trimer, although some adjustments were made based on biochemical data[18,23,24]. In this map 13 chlorophylls are detected. The chlorophyll binding sites are listed in Table 1. Based on the trimer structures, CP26 has a Chl b601. For all other locations the chlorophyll binding sites from the backbone are conserved. Just like CP29 there is no Chl 605 present. No other pigments could be detected in CP26.

The chlorophylls of the *Arabidopsis* and spinach structures were overlaid (Fig. 3c). When comparing these two plant structures there are hardly any differences. In both structures 35 chlorophylls in the core region are detected as well as all 14 chlorophylls of a single trimer subunit. Before these structures were solved it was assumed that there were 13 chlorophylls in CP29. The crystal structure contained a chlorophyll at location 615 which was unknown. In none of the plant structures a density was found for this chlorophyll but a density is present for a chlorophyll 601. The major difference between the two plant structures are the chlorophylls at location 614 and 616. In our structure we have found a chlorophyll at location 614 but none at location 616. Also there is no density that indicates that the presence of a chlorophyll at location 616. Conversely, in the spinach structure chlorophyll 614 is lost during purification but there is an extra chlorophyll present at location 616. This chlorophyll needs to be confirmed with biochemical data. For CP26 the same 13 chlorophylls have been found in both plant structures. This number of chlorophylls was expected based on the biochemical data[18].

The density at the region for both the M trimer and CP24 is less ordered than in the other map regions (Supplementary Fig. 4). The M trimer was analysed as a homotrimer with only Lhcb1. A rigid
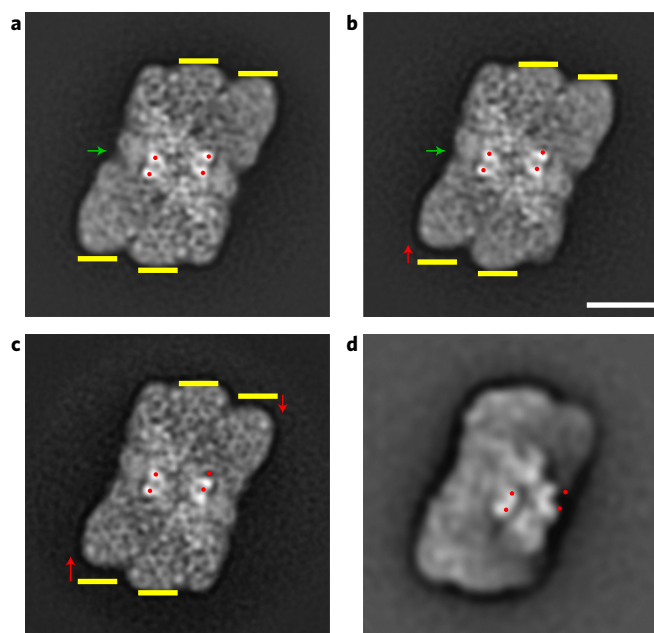
Figure 4 | Flexibilities in the C2S2M2 supercomplex from *Arabidopsis* investigated by negative stain single-particle electron microscopy. a, The sum of 28,048 particles of the standard C2S2M2 supercomplex. **b**, The sum of 22,626 particles of the supercomplex in which one M trimer is moved upward. Green arrows indicate a variable gap between CP24 and the core. **c**, The sum of 7,629 particles of the supercomplex in which both M trimers and the two halves of the core complex have been shifted, as can be seen from the positions of the central bright densities (red dots). **d**, The sum of 1,000 particles at a tilted view, in which the stain-excluding extrinsic subunits and the lumenal-protruding domains of CP47 and CP43 are apparent. Scale bar, 100 Å.

body fit could be applied for both CP24 and the M trimer. In the M trimer all the densities for the chlorophylls are present in all three individual monomers. For CP24 the individual chlorophylls had to be determined. The assignment of Chl a or Chl b was based on biochemical data[24] and the crystal structure of the homologue monomeric CP29 antenna[16]. For CP24, nine chlorophylls were detected (Table 1 and Fig. 3b). The chlorophyll binding sites of the backbone are conserved for the detected chlorophylls[24]. From biochemical data and sequence alignment, Chl 601, 613, 614 are likely absent in CP24[24], and indeed these chlorophylls were not found in our electron microscopy map. In contrast, Chl 611 should be present[24], but no density was detected for this pigment.

The flexibility within the peripheral antenna, apparently leading to a lower overall resolution in our map and in particular the flexibility of the M trimer/ CP24 region is an interesting topic on its own. In addition to the cryo-electron microscopy data, we have analysed a set of 400,000 negatively stained *Arabidopsis* supercomplex projections (Fig. 4). Flexibility leads to a number of different, but specific conformations. It is found that the M trimer can have two clearly different positions, in contrast to the S trimer. When one of the two M trimers is shifted, there is a displacement of CP24 (Fig. 4b), leading to a smaller gap with the core (green arrow). This could explain a lower resolution of CP24 and the M trimer, than the PSII core complex and the S trimer/ CP29 domain in the cryo-structure. In smaller numbers of particles, both M trimers are displaced (Fig. 4c). This leads to lateral movement of the two halves of the dimeric core complex, as indicated by the positions of red dots on the highest densities of the core part. These densities also change position on tilting (Fig. 4d), but not vertically as in Fig. 4b,c. The nature of the

5

M trimer flexibility is not understood since it is observed with a similar abundance in both dark-adapted plants and plants with light-induced non-photochemical quenching.

Discussion

Over the years protein crystallization attempts have been made to obtain a high-resolution 3D structure for plant PSII, but the high flexibility and heterogeneity of PSII supercomplexes has prevented success. Single-particle cryo-EM was applied on a homogeneous sample of $C_2S_2M_2$ particles from a *npq4* mutant, lacking PsbS. Use of the mutant is justified because previous electron microscopy analyses on PSII particles and membranes from wild-type and *npq4* plants did not reveal any structural difference in isolated PSII[20]. Moreover, it was shown that maximum quantum yield of PSII, quantum yield of oxygen evolution, maximal oxygen production rate and pigment content are identical in wild-type and *npq4* plants[21,25–27]. We managed to determine a 3D structure for the $C_2S_2M_2$ supercomplex to 5.3 Å resolution. Based on the structure we are able to describe the location of almost all expected intrinsic membrane embedded subunits of the core. In this electron microscopy map the location of the 35 chlorophylls of the core based on the cyanobacterial structure[4] were confirmed. This result matches the results of the spinach structure as well[8], indicating that these chlorophylls are highly conserved between different organisms. Of the extrinsic subunits only PsbO is present. PsbQ, PsbP and PsbR are absent in our map: the location of PsbP and PsbQ has been recently proposed[8], but the location of PsbR remains unknown. The absence of three of the extrinsic subunits and some other small intrinsic subunits, as discussed below, is a consequence of the way to keep the particles in a monodisperse state for cryo-EM. Hence the structure does not provide insight into the oxygen evolution, which has been described in detail for the system from cyanobacteria[4,5]. The location of the chlorophylls, however, provides insight into the antenna organization and the energy flow in the membrane compartment of PSII.

In addition, the position of all peripheral antenna proteins in the largest purifiable PSII supercomplex could be determined, including CP24 and CP26. Since no crystal structure is available for these two subunits, electron microscopy densities allowed significant information to be obtained about protein structure and pigment organization to build a 3D model of these proteins.

All densities could be assigned to the small subunits, but PsbJ and PsbY are missing from the map. It is unlikely that one of these subunits is present. PsbJ is a very hydrophobic chloroplast-encoded protein and operates in a gene cluster with *psbE*, *psbF* and *psbL*. In the structures of *Thermosynechococcus vulcanus* PsbJ is placed between PsbE/PsbF and PsbK[4,5] and, as PsbJ functions in cyanobacteria and higher plants in a similar way[28], there is no indication that it is relocated to a position elsewhere. PsbW was assigned next to PsbA, PsbC, PsbI and S-LHCII based on a good match with the expected structure (Fig. 2d). This location of PsbW, between the core and the antenna proteins, is in agreement with the map of spinach PSII[8] and previous results because in the absence of PsbW no supercomplexes are formed[29].

The aim of this study was to perform a reconstruction on a purified supercomplex particle with a complete set of subunits, including the four extrinsic subunits of the OEC (PsbO, PsbP, PsbQ and PsbR). The sucrose gradient centrifugation and concentration step were carried out at pH 7.5, to prevent aggregation. As indicated elsewhere, this relatively high pH value may destabilize the OEC[9], which appears to be the case for our digitonin preparation[30]. This could explain why both PsbP and PsbQ are missing from the structure. PsbR is absent as well, although it is more difficult to wash off this subunit[30]. PsbR needs PsbJ for its assembly into the PSII core[31], and the structure clearly shows the absence of PsbJ. Moreover, the absence of PsbR further affects its neighbours PsbP

and PsbQ[10]. The fact that most extrinsic subunits are missing from our structure could probably have destabilized the domain around the manganese cluster, explaining why the cluster is not visible in the 3D map.

It should be noted that biochemical characterization of digitonin-purified PSII particles from *Arabidopsis* suggests that PsbR (and possibly also PsbP and PsbQ) is present in substoichiometric amount[30], not only in the purified PSII supercomplex, but also in PSII in leaves[30]. PsbR is also lacking in the recent cryo-EM structure of the smaller C_2S_2 PSII complex of spinach[8], possibly for the same reason as for *Arabidopsis* particles (substoichiometric amount of PsbR). Thus, further investigation is needed to understand the stoichiometry, function and location of PsbR. Conversely, in the α-dodecyl maltoside-purified PSII particles of spinach, PsbP and PsbQ are visible[8]. However also in this case PsbP and PsbQ are present in substoichiometric amount. Indeed their visualization requires decreasing the level of electron microscopy density threshold to a very low value. This usually significantly increases the noise signal, but the fact that these peripheral subunits do not bind detergent allows their visualization with little noise compared with the rest of the PSII. It is also possible that PsbP and PsbQ are more strongly bound to the PSII core in spinach than in *Arabidopsis*.

The PsbS protein has the key function of activating the fast energy dissipation at the level of PSII in a still unknown way. Thus, localization of PsbS in the supercomplex is necessary to understand its mechanism of action. In our work, we cannot provide data about PsbS localization since, as discussed above, we chose to use PSII from *npq4* plants lacking PsbS. So far no data show a role of PsbS in electron transfer mechanisms or its inter-action with OEC subunits, but rather recent biochemical evidences support the fact that PsbS could interact with the external antennas[32,33], as proposed for some time. Moreover, previous work by us and other groups did not show any difference in functioning and structure between wild-type and *npq4* PSII, as long as plants are grown in non-stressed conditions. This means that PsbS does not have an evident structural role in PSII, at least under non stressing conditions. Intriguingly, the localization of PsbS remains elusive despite the fact that this is an objective of several groups for over 15 years. All assays to localize PsbS in the supercomplex by electron microscopy have not had success[13,34], indicating that PsbS is not or just very weakly bound to PSII. It should also be noted that in the recent spinach cryo-EM structure[8], PsbS was present in the fraction containing the C_2S_2 particles (although the stoichiometry was not calculated), but it was not found in the density map of the complex, further indicating that PsbS is not, or very weakly, bound to PSII. Another possibility might be that PsbS is bound at several different positions around PSII.

Not all protein subunits were identified, but all chlorophylls present in cyanobacteria are identified in the plant PSII map and all chlorophyll positions of cyanobacterial PSII are highly conserved in plants. These are the same chlorophylls as in the spinach structure, and all the chlorophylls have the same orientation in the two plant structures. In our density map there are unassigned densities in the core. According to their size it is likely to be that these unassigned densities are carotenoids and lipids, rather than chlorophylls although it has been suggested earlier that PSII core complexes in plants would have extra chlorophylls compared with cyanobacteria PSII[18].

Orientation and structure of antenna proteins

The location and orientation of the antenna complexes could be determined unambiguously from our map. The positions of most of the antenna complexes are similar to those proposed earlier in the 2D negative stain map[20], but the current data are much more accurate. Only a 3D map with a resolution sufficient to at least resolve individual α-helices allows modelling the correct location

and orientation of LHCII and the minor antenna subunits. Moreover, membrane proteins cannot be determined accurately from negative stain data because the stain does not penetrate the hydrophobic membrane. A comparison of the two models shows that the S- and M trimers are rotated by approximately 5° (Supplementary Fig. 8). The exact orientation of CP26 and CP29 is slightly different from the previous model, but the orientation of CP24 is significantly different. We can now also compare the positions of CP26 and CP29 with those of a high-resolution structure of the smaller C_2S_2 particle from spinach[8]. Although at low resolution the spinach C_2S_2 particle often looks closer to a rectangle than the *Arabidopsis* C_2S_2 particle[20], it now appears that in both supercomplexes the CP26 subunit and the S trimer are in a very similar position.

Compared to the S trimer, the M trimer is not well resolved, although all chlorophylls could be detected. There is good evidence from the negative stain maps (Fig. 4) that the position of the M trimer/CP24 is variable, leading to a lower local resolution. In a small number of supercomplexes there is also an additional shift of the two halves of the core. Therefore the exact orientation and location in the model for the supercomplex may change once this region of the map becomes resolved at a higher resolution. In the current map it is possibly a mixture of two or more conformations, but to separate them a larger dataset is necessary. LHCII-M specifically contains one Lhcb3 monomer, an LHCII isoform evolved in land plants in parallel with CP24 (ref. 35). In some plant clade, Lhcb3 recently disappeared together with CP24 (ref. 36), indicating a relationship between these two Lhcb complexes. The resolution of the M-LHCII is not good enough to distinguish the specific Lhcb3 features (like a shorter N terminus and the specific amino acid substitutions with respect to Lhcb1). However, the relative orientation of M-LHCII and CP24 obtained from the PSII model indicates that a contact of CP24 with M-LHCII involves the region between helix B and helix E of the LHCII monomer facing CP24. Interestingly, this is the most variable region between Lhcb1 and Lhcb3, suggesting that the monomer in contact with CP24 is indeed Lhcb3 and its specific residues are important for the interaction.

CP29 is slightly tilted relative to the plane of the membrane, which may have implications for the expected energy flow within PSII. 13 chlorophylls were detected for CP29 in our density map, and the same number was also present in the crystal structure. However, there are important differences. First, Chl 615 is missing in the electron microscopy structures of *Arabidopsis* and spinach PSII, and there is no unassigned density near the expected location of Chl 615 that could account for a chlorophyll molecule. Our results support the conclusion that the position of Chl 615 in the crystal structure is an artefact, because the N terminus of CP29 is not intact as it is in the cryo-EM structures. Second, at the position corresponding to Chl 601 in LHCII there is density for an extra chlorophyll. The resolution in the *Arabidopsis* and spinach maps is not high enough for identification of the Chl species. We assigned Chl 601 as Chl *a*, based on the identify of Chl 615 in the spinach CP29 crystal structure, since it is very likely to be that Chl 615 is Chl 601 displaced during CP29 purification and crystallization. This is the same assignment as in CP29 in the spinach PSII structure[8]. In LHCII this chlorophyll was however assigned as Chl *b*[14,15]. Higher resolution is necessary to solve this question.

There are two significant differences between CP29 in *Arabidopsis* and spinach PSII: Chl614 is present in CP29 of *Arabidopsis*, but absent in in the spinach CP29. For Chl 616, it is the opposite situation, because we have not found any extra density that could indicate the presence of Chl 616. Since the Chl614 presence is proven from biochemical experiments[37] and the crystal structure[14], it is likely to be that this chlorophyll is lost from spinach PSII during preparation.

In our map 13 chlorophylls are detected in CP26. The same number of chlorophylls was predicted earlier[18]. The known crystal structures of both CP29 and a single subunit of the LHCII trimer where overlaid on the location of CP26 to identify the chlorophylls. Based on these overlays we concluded that a chlorophyll is present at position 601. Similar to CP29, there is no chlorophyll present at position 605. All other chlorophyll binding sites are conserved. When comparing this structure with the one from spinach[8], there is no significant difference in chlorophyll location or orientation between the two structures.

The location and the most likely orientation of the CP24 protein were determined. Of the 10–11 predicted chlorophylls[18,24], 9 were detected at conserved binding sites. Surprisingly, Chl 611 was not detected. This chlorophyll, which is not coordinated by a protein residue, is predicted from biochemical data[24] and conserved in other Lhc complexes. Therefore, it is possible that a density was not found for the low resolution of this part of the complex and/or its loss during PSII purification. Chl 614 is absent, in accordance with the lack of the binding site due to a shorter C terminus. A residue for Chl 613 binding could be present in the protein sequence[24], but there is no density for this chlorophyll in the 3D map. This result supports biochemical results proposing its absence[24]. Concerning Chl 601, no biochemical or structural data allow concluding about its presence or not. The density of Chl *a*603 is weak, but based on its conserved binding site in all Lhcs, it was placed in the map. To identify possible missing chlorophylls in this minor antenna protein a better resolution is required.

Excitation energy transfer

Detailed investigation and simulation of energy transfer kinetics in large pigment systems as plant PSII, which contains >300 chlorophylls, are extremely complex and require precise orientations of the chlorophylls and approaches beyond the scope of this article. Recent examples focus on plant PSII kinetics using an advanced modelling approach[38,39] based on a previous pseudo-atomic model of PSII[20] and exciton systems of individual subunits. However, the improved PSII structural model here presented allows providing qualitative information and preferential pathways for energy transfer between Lhc antennas and from Lhc towards the core (Fig. 5 and Table 2) based on the Chl species and distances between the nearest chlorophylls in adjacent complexes. This is the same approach as used for pea PSI[40] and spinach PSII complexes[8]. The almost identical organization of the *Arabidopsis* and spinach PSII core complex, as well as the further similarity between plant and cyanobacterial PSII, make it very likely that energy transfer inside the core complexes is similar between plant and cyanobacteria PSII. This topic has been investigated previously[41] and therefore we limit our discussion to the Lhc antenna system.

Efficient connection and energy transfer between S- and M-LHCII trimers is more likely to be provided between three couples of Chl *a*: Chl $a611_{(S3)}$/Chl $a610_{(M2)}$, Chl $a612_{(S3)}$/Chl $a612_{(M2)}$ and Chl $a614_{(S3)}$/Chl $a604_{(M2)}$ (Fig. 5 and Table 2). It should be noted that Chls 611 and 612, located near the stromal side of LHCII, have the lowest energy states in all Lhcb complexes and are the most populated at equilibrium. From the S trimer, excitation energy can directly and efficiently flow to CP43 from Chl $a611$/$a612_{(S1)}$ to Chl $a506_{(CP43)}$, and from Chl $a614_{(S1)}$ to Chl $a501_{(CP43)}$. From M trimer to CP29, energy migration involves the lowest energy chlorophylls of this two complexes, in particular Chl $a611_{(M1)}$ and Chl $a611_{(CP29)}$. It should be noted that the shortest distance between chlorophylls of the M trimer and CP29 is between Chl $a614_{(M1)}$ and Chl $b614_{(CP29)}$ on the lumenal side of LHCII, but likely this pathway is less populated since it involves in CP29 a Chl *b*, which has a higher energy level than Chl *a*. However it should be noted that a recent hypothesis suggests that conformational changes in the helix 5/Chl 614 domain may form an energization quenching (qE) site in Lhc antennas[42].

Figure 5 | Energy flow within C$_2$S$_2$M$_2$ particles. Lhc antenna complexes are labelled in blue. The monomers of S- and M-LHCII trimers are named for clarity in the text and in Table 2. Core complex antennas (CP47 and CP43) and the reaction centre (RC) are labelled in red. Chlorophyll couples probably involved in energy transfer between adjacent complexes are indicated with blue and red lines. Red lines connect couples involving only Chl *a*. Blue lines are couples involving one or two Chl *b*, which have a higher energy level than Chl *a* and thus are less efficient in receiving energy.

Thus Chl614$_{(M1)}$ and Chl614$_{(CP29)}$ may have a significant role in excitation energy transfer and quenching. From the monomeric antenna CP29, energy can reach the core via at least three couples of Chl *a*: Chl *a*603$_{(CP29)}$ to Chl *a*610$_{(CP47)}$, Chl *a*609$_{(CP29)}$ to Chl *a*616$_{(CP47)}$ and Chl *a*613$_{(CP29)}$ to Chl *a*602$_{(CP47)}$. The presence of multiple pathways suggests that CP29 is energetically very well connected to the core. In contrast, energy connection between the S trimer and CP29 seems weak, since Chl *b* is involved (Fig. 5 and Table 2).

Similarly to CP29, also the monomeric antenna CP26 is well connected with the core (CP43) through Chl *a* couples at a short distance: Chl *a*611$_{(CP26)}$ to Chl *a*513/*a*512$_{(CP43)}$ and Chl *a*614$_{(CP26)}$ to Chl *a*503$_{(CP43)}$. The couple Chl *b*601$_{(CP26)}$/ Chl *a*513$_{(CP43)}$ could be also important, considering the very short distance between the two chlorophylls. Connection of S-LHCII with CP26, as in the case of CP29, is likely to be weaker and rather directional (LHCII to CP26), since it involves Chl *b*605 and Chl *b*608 of the S trimer at ~20 Å distance from Chl *a*604 and Chl *a*610/612 of CP26, respectively. The nearest Chl *a* couples, Chl *a*610$_{(S2)}$/Chl *a*610$_{(CP26)}$ and Chl *a*604$_{(S2)}$/Chl *a*604$_{(CP26)}$, are at ~25 Å away each other.

Finally, CP24, which is particularly enriched in Chl *b*, would transfer energy to CP29 from Chl *b*606$_{(CP24)}$ to Chl *b*614$_{(CP29)}$ and Chl *b*608/*b*609$_{(CP24)}$ to Chl *a*601$_{(CP29)}$. This transfer is rather directional, since involving Chl *b* in CP24 and Chl *a* in CP29. Energy transfer via Chl *a* is possible towards M-LHCII from Chl *a*610$_{(CP24)}$ to Chl *a*612$_{(M1)}$ and from Chl *a*604$_{(CP24)}$ to Chl *a*604$_{(M1)}$. From the Chl *b* domain of CP24, energy can be directionally transferred to M-LHCII from Chl *b*608$_{(CP24)}$ to Chl *a*612$_{(M1)}$.

It is interesting to observe that most of the Chl *a* of CP24 is located towards the exterior of PSII, and Chl *b* is facing CP29 and LHCII-M. Since Chl *b* has a higher energy level than Chl *a*, this could in principle cause a relatively slow energy transfer from Chl *a* of CP24 to the rest of PSII. However, based on recent results showing various types of PSII megacomplexes found *in vitro* and *in vivo* in *Arabidopsis*[13], in which CP24 occupies a position in between two PSII, we can speculate that that such a particular organization of the chlorophylls in CP24 can improve PSII connectivity by helping energy transfer between adjacent PSII.

In short, energy transfer between trimers should be fast, and from the S trimer energy would flow directly to the core via

Table 2 | Distance between the Mg–Mg of the chlorophylls involved in the energy transfer.

(A)				(B)			
Subunit and Chl	Subunit and Chl	Mg–Mg distance (Å)	Location	Subunit and Chl	Subunit and Chl	Mg–Mg distance (Å)	Location
M2-LHCII	S3-LHCII						
Chl a610	Chl a611	19.8	Stroma				
Chl a612	Chl a612	23.1	Stroma				
Chl a604	Chl a614	20.9	Lumen				
M1-LHCII	CP29			M1-LHCII	CP29		
Chl a611	Chl a611	17.1	Stroma	Chl a614	Chl b614	13.8	Lumen
CP29	CP47						
Chl a603	Chl a610	18.2	Stroma				
Chl a609	Chl a616	19.8	Stroma				
Chl a613	Chl a602	20.5	Lumen				
S1-LHCII	CP43			S1-LHCII	CP29		
Chl a611	Chl a506	17.2	Stroma	Chl b605	Chl b606	19.1	Lumen
Chl a612	Chl a506	20.2	Stroma	Chl b605	Chl a604	17.3	Lumen
Chl a614	Chl a501	24.5	Lumen				
S2-LHCII	CP26			S2-LHCII	CP26		
Chl a604	Chl a604	24.4	Lumen	Chl b605	Chl a604	19.5	Lumen
Chl a610	Chl a610	25.0	Stroma	Chl b608	Chl a610	20.5	Stroma
				Chl b608	Chl a612	20.7	Stroma
CP26	CP43			CP26	CP43		
Chl a611	Chl a513	15.0	Stroma	Chl b601	Chl a513	11.1	Stroma
Chl a611	Chl a512	18.2	Stroma				
Chl a614	Chl a503	15.9	Lumen				
CP24	M1-LHCII			CP24	M1-LHCII		
Chl a610	Chl a612	24.2	Stroma	Chl b608	Chl a612	20.8	Stroma
Chl a604	Chl a604	25.9	Lumen				
				CP24	CP29		
				Chl b606	Chl b614	19.0	Lumen
				Chl b608	Chl a601	18.2	Stroma
				Chl b609	Chl a601	20.1	Stroma

(A) Energy transfer pathways involving couples of Chl a. (B) Energy transfer pathways involving one or two Chl b. In each case, the nearest chlorophyll of two adjacent subunits is indicated together with the Mg–Mg distance and the lumenal or stromal location. The names of the single LHCII monomers are given as indicated in Fig. 5.

CP43, while from the M trimer it needs to pass through CP29 to reach the core on CP47 or through S-LHCII to reach CP43. Despite the fact that PSII is considered rather isoenergetic and thus energy can move randomly between subunits, the fact that monomeric CP26 and CP29 seem well connected with the core and less well connected with S trimer could provide some directionality of the energy migration towards the core and limit the equilibration on the antenna system.

Lastly, it is worth noting that the distances between chlorophylls in PSII antennas are larger than in PSI[3,40], which indeed, despite the presence of low energy chlorophylls (red forms) in the antenna system, has a very fast energy transfer from LHCI to the core, faster than the one proposed between Lhcb antennas and the PSII core[43]. It is also worth noting that most of the energy connections are on the stromal side of the Lhc complexes. This could facilitate *in vivo* energy exchange between PSII located in opposite highly stacked grana membranes, further increasing the connectivity of PSII.

Methods

Protein purification. PSII-enriched membranes (BBY)[44] were prepared from *A. thaliana npq4* plants, following the same protocol[20]. PSII-C$_2$S$_2$M$_2$ particles were prepared as by Crepin and coworkers[30], where further biochemical characterization is provided. In short, aliquots of 200 μg (in chlorophylls) of BBY membranes were washed with 10 mM Hepes KOH pH 7.5, resuspended at a concentration of 1 mg ml^{-1} in 10 mM Hepes KOH pH 7.5 and solubilized by adding an equal volume of 1% digitonin and 0.4% α-dodecylmaltoside to a final clorophyll concentration of 0.5 mg ml^{-1} and a final detergent concentration of 0.5% digitonin and 0.2% α-dodecylmaltoside. The samples were incubated on ice in the dark for 30 min and then centrifuged at 12,000g for 10 min to eliminate unsolubilized material. PSII supercomplexes were purified by sucrose gradient centrifugation with a sucrose gradient containing 0.65 M sucrose, 10 mM Hepes KOH pH 7.5 and 0.01% digitonin. Gradients were formed by freezing and thawing. Ultracentrifugation was performed in a Beckmann SW41 rotor, at 41,000 r.p.m. for 17 h.

PSII supercomplexes for electron microscopy of negatively stained specimens were isolated using clear-native polyacrylamide gel electrophoresis[45] with the following modifications. Thylakoid membranes with 10 μg of chlorophylls were solubilized with α-dodecylmaltoside using a detergent/chlorophyll mass ratio of 40 and supplemented with sample buffer (50 mM HEPES pH 7.2, 400 mM sucrose, 5 mM MgCl$_2$, 15 mM NaCl, 10% glycerol) to the final volume of 30 μl.

Sample preparation and electron microscopy. A volume of 6 ml of sucrose PSII solution at a concentration of 0.033 μg ml^{-1} chlorophyll was concentrated about 100× to a final concentration of 3.5 mg ml^{-1} chlorophyll. The sample was placed on a Millipore Amicon filter (10 kDa cut-off) and centrifuged at 3,500g for 20 min per round. After every washing round the sample was diluted with 2 ml of buffer (10 mM Hepes, 0.01% digitonin). This was repeated six times, a final seventh run was used to concentrate the sample to a final volume of 60 μl. Aliquots of 3 μl of the concentrated PSII sample were applied onto glow-discharged holey carbon grids (Quantifoil R1.2/1.3). Grids were blotted for 8 s at 100% humidity, before being plunge-frozen in a FEI Vitrobot using liquid ethane. Grids were transferred to a G2-Polara (FEI), operating at 300 kV, equipped with a Gatan energy filter and a Gatan 4000 SP 2 K CCD camera. Micrographs were recorded with a pixel size of 2.63 Å at the specimen level, with a defocus of 3 μm and with a dose of 25 e$^-$ Å^{-2} (electrons per square Ångström) and 25,996 particles were manually selected with Xmipp 3.0[46] or RELION-1.3[47].

For high-resolution electron microscopy, grids were transferred to a FEI Titan Krios (NeCEN, Leiden), operating at 300 kV, equipped with a Falcon 2 direct electron detector. Micrographs were collected at a pixel size of 1.105 Å at the specimen level and an exposure time of 1 s, corresponding with an electron dose of 28, 38 or 49 e$^-$ Å^{-2} for the integrated image. The frames had a dose of 3, 4.2 and 5.4 e$^-$ Å^{-2}, respectively. A total of 5,198 images, with a defocus range of 1.2–3.0 μm, were collected with EPU software (FEI) and 104,025 particles selected.

Single-particle electron microscopy of negatively stained specimens was performed on a Tecnai G2 20 Twin transmission electron microscope (FEI, Eindhoven, the Netherlands), operated at 200 kV. Images were recorded with an UltraScan 4000UHS CCD camera (Gatan, Pleasanton, CA, USA) with a pixel size of 2.24 Å at the specimen level after binning the images to 2048 × 2048 pixels.

Data processing. From the G2-Polara dataset the best 13,570 particles were used for an initial 3D model, made with Ransac[48], using C2 symmetry. During every 3D

classification and 3D refinement C2 symmetry was applied. This initial 3D model was further refined and used as a reference for the dataset of the Titan Krios. The contrast transfer function parameters of the G2-Polara micrographs were determined with CTFFIND3[49]. CTFFIND4[50] was used on the summed images of the frames aligned by MOTIONCORR[51], to correct for beam induced motion and drift. The dataset was processed with RELION-1.3, two initial 3D classifications were used to clean the datasets based on a three times binned pixel (3.32 Å), to select the best 23,434 particles combined for a 3D refinement. Many of the rejected particles lacked a LHCII trimer. As a reference a 40 Å low-pass filtered initial model was used. The 3D classification parameters were used for a 3D refinement at twice-binned pixel (2.21 Å) and on the original pixel (1.105 Å). With a twice-binned pixel size the resolution after 3D refinement was 7.0 Å. For the original pixel after particle polishing and refinement[52] the best particles gave a resolution of 5.3 Å. At the original pixel size a map with a resolution of 7.0 Å was low-pass filtered to 40 Å and used as a reference. All density maps were corrected with the modulation transfer function of the detector and sharpened by applying a negative B-factor (−60)[53]. All resolutions are based on the gold-standard Fourier shell correlation (FSC) = 0.143 criterion[54]. Local resolutions of the density maps were calculated in ResMap[55]. From the Tecnai G2 data set almost 400,000 particles were analysed using Xmipp[56] and Relion software[47].

Modelling and bioinformatics tools. Initial fitting of the subunits in the cryo-EM map was performed by rigid body real space refinement in Chimera[57], using as templates the high-resolution crystal structures of *Thermosynechococcus vulcanus* PSII (PDB code 3WU2)[4], pea LHC-II (PDB code 2BHW[15]) for the S- and M trimers and spinach CP29 (PDB code 3PL9[16]) for CP29, CP26 and CP24. Local fitting and adjustment of the subunits in the cryo-EM maps was performed using the programs Coot[58] and phenix.real_space_refine[59,60], starting from homology models constructed using the Phyre2 server[61]. Model refinement was carried out using symmetry and geometry restraints, including secondary structure, rotamer and Ramachandran plot restraints. Secondary structure assignments were based on analysis of the structures with DSSP[62]. Geometries of the chlorophylls and haems were strictly restrained towards those found in the high-resolution crystal structures, including correct coordination geometry of the metals with protein residues. A model of PsbW was obtained by fitting a polyalanine α-helix into the empty density for a transmembrane helix. After one round of model building and refinement, side chains were replaced to match the actual amino acid sequence of PsbW. Owing to large differences in local resolution of the cryo-EM map, refinement of the PSII core, the S trimer with CP26/CP29 and the M trimer with CP24 was performed separately in excised parts of the cryo-EM map. Refinement of the PSII core was carried out at 4.5 Å resolution; the S trimer with CP26/CP29 and the M trimer with CP24 were refined at 5.5 Å and 6.5 Å resolution, respectively. The final model was created by reassembling the independently refined structural regions without further refinement of the complete structure. The overall clashscore of the complete PSII structure is 8, with 0.0% Ramachadran outliers and 0.1% side chain rotamer outliers, as calculated by Molprobity[63], indicated that the geometry of the structure is acceptable. High-resolution images for publication were prepared with Chimera[57] and PyMOL (Molecular Graphics System, version 1.8 Schrödinger, LLC).

Data availability. The data that support the findings of this study are available from the corresponding author upon request. The Cryo-EM map and refined 3D structure of PSII were deposited at the Electron Microscopy Data Bank (EMDB) and Protein Data Bank (PDB) with accession codes EMD-3491 and 5MDX, respectively.

References

1. Dekker, J. P. & Van Grondelle, R. Primary charge separation in photosystem II. *Photosynth. Res.* **63,** 195–208 (2000).
2. Nelson, N. & Yocum, C. F. Structure and function of photosystems I and II. *Ann. Rev. Plant Biol.* **57,** 521–565 (2006).
3. Mazor, Y., Borovikova, A. & Nelson, N. The structure of plant photosystem I super-complex at 2.8 Å resolution. *eLife* **4,** 213 (2015).
4. Ferreira, K. N., Iverson, T. M., Maghlaoui, K., Barber, J. & Iwata, S. Architecture of the photosynthetic oxygen-evolving center. *Science* **303,** 1831–1838 (2004).
5. Umena, Y., Kawakami, K., Shen, J. & Kamiya, N. Crystal structure of oxygen-evolving photosystem II at a resolution of 1.9 Å. *Nature* **473,** 55–60 (2011).
6. Suga, M. *et al.* Native structure of photosystem II at 1.95 Å resolution viewed by femtosecond X-ray pulses. *Nature* **517,** 99–103 (2014).
7. Ago, H. *et al.* Novel features of eukaryotic photosystem II revealed by its crystal structure analysis from a red alga. *J. Biol. Chem.* **291,** 5676–5687 (2016).
8. Wei, X. *et al.* Structure of spinach photosystem II–LHCII supercomplex at 3.2 Å resolution. *Nature* **534,** 69–74 (2016).
9. Bricker, T. M., Roose, J. L., Fagerlund, R. D., Frankel, L. K. & Eaton-Rye, J. J. The extrinsic proteins of photosystem II. *Biochim. Biophys. Acta* **1817,** 121–142 (2012).
10. Ifuku, K. Localization and functional characterization of the extrinsic subunits of photosystem II: an update. *Biosc. Biotechnol. Biochem.* **79,** 1223–1231 (2015).
11. Caffarri, S., Croce, R., Cattivelli, L. & Bassi, R. A look within LHCII: differential analysis of the Lhcb1−3 complexes building the major trimeric antenna complex of higher-plant photosynthesis†. *Biochemistry* **43,** 9467–9476 (2004).
12. Kouřil, R., Dekker, J. P. & Boekema, E. J. Supramolecular organization of photosystem II in green plants. *Biochim. Biophys. Acta* **1817,** 2–12 (2012).
13. Nosek, L., Semchonok, D., Boekema, E. J., Ilik, P. & Kouril, R. Structural variability of plant photosystem II megacomplexes in thylakoid membranes. *Plant J.* **89,** 104–111 (2017).
14. Liu, Z. F. *et al.* Crystal structure of spinach major light-harvesting complex at 2.72 Å resolution. *Nature* **428,** 287–292 (2004).
15. Standfuss, J., Terwissscha van Scheltinga, A. C., Lamborghini, M. & Kühlbrandt, W. Mechanisms of photoprotection and nonphotochemical quenching in pea light-harvesting complex at 2.5 Å resolution. *EMBO J.* **24,** 919–928 (2005).
16. Pan, X. *et al.* Structural insights into energy regulation of light-harvesting complex CP29 from spinach. *Nat. Struct. Mol. Biol.* **18,** 309–315 (2011).
17. Pan, X., Liu, Z., Li, M. & Chang, W. Architecture and function of plant light-harvesting complexes II. *Curr. Opin. Struct. Biol.* **23,** 515–525 (2013).
18. Caffarri, S., Tibiletti, T., Jennings, R. C. & Santabarbara, S. A. Comparison between plant photosystem I and photosystem II architecture and functioning. *Curr. Protein Pept. Sci.* **15,** 296–331 (2014).
19. Nogales, E. & Scheres, S. H. W. Cryo-EM: a unique tool for the visualization of macromolecular complexity. *Mol. Cell* **58,** 677–689 (2015).
20. Caffarri, S., Kouřil, R., Kereiche, S., Boekema, E. J. & Croce, R. Functional architecture of higher plant photosystem II supercomplexes. *EMBO J.* **28,** 3052–3063 (2009).
21. Li, X. P., Muller-Moule, P., Gilmore, A. M. & Niyogi, K. K. PsbS-dependent enhancement of feedback de-excitation protects photosystem II from photoinhibition. *Proc. Natl Acad. Sci. USA* **99,** 15222–15227 (2002).
22. Shi, L. X., Lorkovic, Z. J., Oelmüller, R. & Schröder, W. P. The low molecular mass PsbW protein is involved in the stabilization of the dimeric photosystem II complex in *Arabidopsis thaliana*. *J. Biol. Chem.* **275,** 37945–37950 (2000).
23. Caffarri, S., Passarini, F., Bassi, R. & Croce, R. A specific binding site for neoxanthin in the monomeric antenna proteins CP26 and CP29 of photosystem II. *FEBS Lett.* **581,** 4704–4710 (2007).
24. Passarini, F., Wientjes, E., Hienerwadel, R. & Croce, R. Molecular basis of light harvesting and photoprotection in CP24: unique features of the most recent antenna complex. *J. Biol. Chem.* **284,** 29536–29546 (2009).
25. Golan, T., Muller-Moule, P. & Niyogi, K. K. Photoprotection mutants of *Arabidopsis thaliana* acclimate to high light by increasing photosynthesis and specific antioxidants. *Plant Cell Environ.* **29,** 879–887 (2006).
26. Li, X. P. *et al.* A pigment-binding protein essential for regulation of photosynthetic light harvesting. *Nature* **403,** 391–395 (2000).
27. Roach, T. & Krieger-Liszkay, A. The role of the PsbS protein in the protection of photosystems I and II against high light in *Arabidopsis thaliana*. *Biochim. Biophys. Acta* **1817,** 2158–2165 (2012).
28. Shi, L., Hall, M., Funk, C. & Schröder, W. P. Photosystem II, a growing complex: updates on newly discovered components and low molecular mass proteins. *Biochim. Biophys. Acta* **1817,** 13–25 (2012).
29. Garcia-Cerdan, J. G. *et al.* The PsbW protein stabilizes the supramolecular organization of photosystem II in higher plants. *Plant J.* **65,** 368–381 (2011).
30. Crepin, A., Santabarbara, S. & Caffarri, S. Biochemical and spectroscopic characterization of highly stable photosystem II supercomplexes from *Arabidopsis*. *J. Biol. Chem.* **291,** 19157–19171 (2014).
31. Suorsa, M. *et al.* Psbr, a missing link in the assembly of the oxygen-evolving complex of plant photosystem II. *J. Biol. Chem.* **281,** 145–150 (2006).
32. Gerotto, C., Franchin, C., Arrigoni, G. & Morosinotto, T. *In vivo* identification of photosystem II light harvesting complexes interacting with Photosystem subunit S. *Plant Physiol* **168,** 1747–1761 (2015).
33. Correa-Galvis, V., Poschmann, G., Melzer, M., Stuehler, K. & Jahns, P. Psbs interactions involved in the activation of energy dissipation in *Arabidopsis*. *Nat. Plants* **2,** 15225 (2016).
34. Pagliano, C. *et al.* Proteomic characterization and three-dimensional electron microscopy study of PSII-LHCII supercomplexes from higher plants. *Biochim. Biophys. Acta* **1837,** 1454–1462 (2014).
35. Alboresi, A. *et al. In silico* and biochemical analysis of *Physcomitrella patens* photosynthetic antenna: identification of subunits which evolved upon land adaptation. *PloS ONE* **3,** e2033 (2008).
36. Kouřil, R., Nosek, L., Bartos, J., Boekema, E. J. & Ilík, P. Evolutionary loss of light-harvesting proteins Lhcb6 and Lhcb3 in major land plant groups—break-up of current dogma. *New Phytol.* **210,** 808–814 (2016).
37. Bassi, R., Croce, R., Cugini, D. & Sandona, D. Mutational analysis of a higher plant antenna protein provides identification of chromophores bound into multiple sites. *Proc. Natl Acad. Sci. USA* **96,** 10056–10061 (1999).
38. Kreisbeck, C. & Aspuru-Guzik, A. Efficiency of energy funneling in the photosystem II supercomplex of higher plants. *Chemical Sci.* **7,** 4174–4183 (2016).
39. Bennet, D. I. G., Amarnath, K. & Fleming, G. R. A structure-based model of energy transfer reveals the principles of light harvesting in photosystem II supercomplexes. *J. Am. Chem. Soc.* **135,** 9164–9173 (2013).

40. Qin, X., Suga, M., Kuang, T. & Shen, J. R. Structural basis for energy transfer pathways in the plant PSI–LHCI supercomplex. *Science* **348,** 989–995 (2015).
41. Raszewski, G. & Renger, S. Light harvesting in photosystem II core complexes is limited by the transfer to the trap: can the core complex turn into a photoprotective mode? *J. Am. Chem. Soc.* **130,** 4431–4446 (2008).
42. Ioannidis, N. E. & Kotzabasis, K. Could structural similarity of specific domains between animal globins and plant antenna proteins provide hints important for the photoprotection mechanism? *J. Theor. Biol.* **364,** 71–79 (2015).
43. van Amerongen, H. & Croce, R. Light harvesting in photosystem II. *Photosynth. Res.* **116,** 251–263 (2013).
44. Berthold, D. A., Babcock, G. T. & Yocum, C. F. A highly resolved, oxygen-evolving photosystem II preparation from spinach thylakoid membranes. *FEBS Lett.* **134,** 231–234 (1981).
45. Kouřil, R. *et al.* Structural characterization of a plant photosystem I and NAD(P)H dehydrogenase supercomplex. *Plant J.* **77,** 568–576 (2014).
46. Sorzano, C. O. S., de la Rosa-Trevin, J. M., Tama, F. & Jonic, S. Hybrid electron microscopy normal mode analysis graphical interface and protocol. *J. Struct. Biol.* **188,** 134–141 (2014).
47. Scheres, S. H. W. RELION: implementation of a Bayesian approach to cryo-EM structure determination. *J. Struct. Biol.* **180,** 519–530 (2012).
48. Vargas, J., Álvarez-Cabrera, A.-L., Marabini, R., Carazo, J. M. & Sorzano, C. O. S. Efficient initial volume determination from electron microscopy images of single particles. *Bioinformatics* **30,** 2891–2898 (2014).
49. Mindell, J. A. & Grigorieff, N. Accurate determination of local defocus and specimen tilt in electron microscopy. *J. Struct. Biol.* **142,** 334–347 (2003).
50. Rohou, A. & Grigorieff, N. CTFFIND4: fast and accurate defocus estimation from electron micrographs. *J. Struct. Biol.* **192,** 216–221 (2015).
51. Li, X. *et al.* Electron counting and beam-induced motion correction enable near-atomic-resolution single-particle cryo-EM. *Nat. Methods* **10,** 584–590 (2013).
52. Scheres, S. H.W. Beam-induced motion correction for sub-megadalton cryo-EM particles. *eLife* **3,** e03665 (2014).
53. Rosenthal, P. B. & Henderson, R. Optimal determination of particle orientation, absolute hand, and contrast loss in single-particle electron cryomicroscopy. *J. Mol. Biol.* **333,** 721–745 (2003).
54. Scheres, S. H. W. & Chen, S. Prevention of overfitting in cryo-EM structure determination. *Nat. Methods* **9,** 853–854 (2012).
55. Kucukelbir, A., Sigworth, F. J. & Tagare, H. D. Quantifying the local resolution of cryo-EM density maps. *Nat. Methods* **11,** 63–65 (2013).
56. de la Rosa-Trevin, J. M. *et al.* Xmipp 3.0: an improved software suite for image processing in electron microscopy. *J. Struct. Biol.* **184,** 321–328 (2013).
57. Pettersen, E. F. *et al.* UCSF chimera? A visualization system for exploratory research and analysis. *J. Comput. Chem.* **25,** 1605–1612 (2004).
58. Emsley, P., Lohkamp, B., Scott, W. G. & Cowtan, K. Features and development of coot. *Acta Crystallogr. D* **66,** 486–501 (2010).
59. Adams, P. D. *et al.* PHENIX: building new software for automated crystallographic structure determination. *Acta Crystallogr. D* **58,** 1948–1954 (2002).
60. Afonine, P. V. *et al.* Towards automated crystallographic structure refinement with phenix.refine. *Acta Crystallogr. D* **68,** 352–367 (2012).
61. Kelley, L. A., Mezulis, S., Yates, C. M., Wass, M. N. & Sternberg, M. J. E. The Phyre2 web portal for protein modeling, prediction and analysis. *Nat. Protoc.* **10,** 845–858 (2015).
62. Touw, W. G. *et al.* A series of PDB-related databanks for everyday needs. *Nucleic Acids Res.* **43,** D364–D368 (2015).
63. Chen, V. B. *et al.* Molprobity: all-atom structure validation for macromolecular crystallography. *Acta Crystallogr. D* **66,** 12–21 (2010).

Acknowledgements

Author contributions

L.S.v.B., G.T.O. and E.J.B. designed the research. S.C. isolated the supercomplex, L.S.v.B. and G.T.O. collected the data. L.S.v.B. performed the single-particle analysis. L.S.v.B., S.C., G.T.O. and A.-M.W.H.T. analysed the data. R.S.K and R.K. analysed the negative stain supercomplex data. L.S.v.B., S.C., G.T.O., A.-M.W.H.T. and E.J.B. wrote the article.

Additional information

Supplementary information is available for this paper.

Reprints and permissions information is available at www.nature.com/reprints.

Correspondence and requests for materials should be addressed to E.J.B.

How to cite this article: van Bezouwen, L. S. *et al.* Subunit and chlorophyll organization of the plant photosystem II supercomplex. *Nat. Plants* **3,** 17080 (2017).

Publisher's note: Springer Nature remains neutral with regard to jurisdictional claims in published maps and institutional affiliations.

Competing interests

The authors declare no competing financial interests.

Publication 9

Chapter 9
Organization of Plant Photosystem II and Photosystem I Supercomplexes

Roman Kouřil, Lukáš Nosek, Dmitry Semchonok, Egbert J. Boekema, and Petr Ilík

Abstract In nature, plants are continuously exposed to varying environmental conditions. They have developed a wide range of adaptive mechanisms, which ensure their survival and maintenance of stable photosynthetic performance. Photosynthesis is delicately regulated at the level of the thylakoid membrane of chloroplasts and the regulatory mechanisms include a reversible formation of a large variety of specific protein-protein complexes, supercomplexes or even larger assemblies known as megacomplexes. Revealing their structures is crucial for better understanding of their function and relevance in photosynthesis. Here we focus our attention on the isolation and a structural characterization of various large protein supercomplexes and megacomplexes, which involve Photosystem II and Photosystem I, the key constituents of photosynthetic apparatus. The photosystems are often attached to other protein complexes in thylakoid membranes such as light harvesting complexes, cytochrome b_6f complex, and NAD(P)H dehydrogenase. Structural models of individual supercomplexes and megacomplexes provide essential details of their architecture, which allow us to discuss their function as well as physiological significance.

R. Kouřil (✉) · L. Nosek · P. Ilík
Department of Biophysics, Faculty of Science, Centre of the Region Haná for Biotechnological and Agricultural Research, Palacký University, Olomouc, Czech Republic
e-mail: roman.kouril@upol.cz; lukas.nosek@upol.cz; petr.ilik@upol.cz

D. Semchonok · E. J. Boekema
Electron Microscopy Group, Groningen Biomolecular Sciences and Biotechnology Institute, University of Groningen, Groningen, The Netherlands
e-mail: d.o.semchonok@rug.nl; e.j.boekema@rug.nl

9.1 Introduction to Molecular Organization of Photosynthetic Apparatus

The apparatus responsible for primary photosynthetic reactions is embedded in the thylakoid membrane (Fig. 9.1). The membrane forms a flexible, three-dimensional network, in which regular stacks of thylakoids (grana) are interconnected by unstacked (stroma) thylakoids. Thylakoids enclose a single aqueous space – the thylakoid lumen, whereas the chloroplast space outside the thylakoids is called the stroma. Major components of the photosynthetic apparatus in thylakoids are integral membrane protein complexes Photosystem II (PSII) and Photosystem I (PSI), which form, together with other protein complexes, the core of the photosynthetic apparatus. PSI and PSII together with the light harvesting complex (LHC) and cytochrome b_6/f (Cytb_6f) complex mediate linear electron transport across the thylakoid membrane leading to the reduction of NADP$^+$ to NADPH. Except of these four major complexes, there are also other protein components in the thylakoid membrane, such as the PROTON GRADIENT REGULATION 5 (PGR5) complex, PGR5-LIKE1 (PGRL1) complex and NAD(P)H dehydrogenase (NDH) complex, which mediate cyclic electron transport (Kramer et al. 2004; Munekage et al. 2004; Shikanai 2016). Both linear and cyclic electron transport pathway are coupled to the translocation of protons across the thylakoid membrane, which leads to the generation of a transmembrane ΔpH gradient utilized by ATP synthase to produce ATP (Albertsson 2001; Nelson and Yocum 2006).

In thylakoid membranes of plants, PSII and PSI are spatially separated. PSII complexes are preferentially embedded in the grana regions, although a minor fraction of the PSII complexes is present also in the stroma membranes in the form of monomers, where they participate in the PSII repair cycle (see e.g. Baena-Gonzalez and Aro 2002; Järvi et al. 2015). On the other hand, PSI complexes are confined exclusively to the stroma thylakoids and grana margins. The presence of PSI
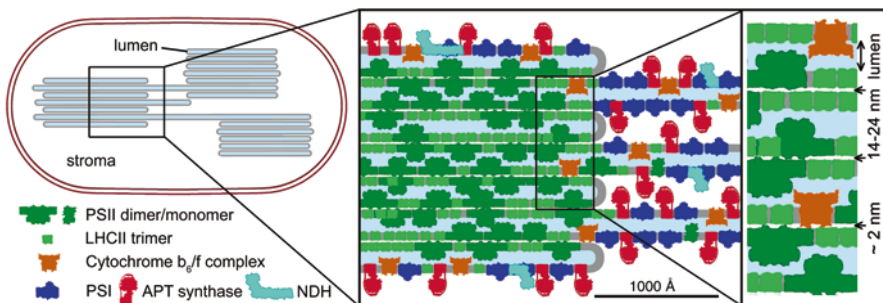
Fig. 9.1 Model of the thylakoid membrane organization within the chloroplast. The model shows a chloroplast with three stacks of grana membranes, connected by stroma membranes. A cross-section of the granum shows a specific distribution of major components of photosynthetic apparatus such as Photosystem II, Photosystem I, cytochrome b_6f complex, NDH dehydrogenase and ATP-synthase (Modified from Dekker and Boekema 2005)

extrinsic subunits, which face the stroma, precludes the entry of the PSI complexes into the grana stacks and similar limitation applies also to ATP synthase and NDH dehydrogenase. In the case of the Cytb_6f complex there is no such structural limitation and this complex is considered to be evenly distributed in the thylakoid membrane (Fig. 9.1) (Albertsson 2001; Dekker and Boekema 2005).

Organization of both PSII and PSI complexes shares a common motif, as both these complexes consist of two functional moieties – a core complex and a peripheral antenna system. The core complex contains the reaction center with all the cofactors necessary for photochemical reactions, whereas the peripheral antenna system optimizes and regulates the light harvesting capacity of the photosystems. The core complexes are highly conserved among prokaryotic and eukaryotic photosynthetic organisms, but the organization and composition of the light harvesting antenna system (LHCs) show a great variability.

The core complex of PSII is present as a homodimer. In land plants, this dimer is specifically associated with a variable number of monomeric and trimeric Lhcb antenna proteins (LHCII), forming together various types of large PSII-LHCII supercomplexes. The ability of PSII to control and regulate the antenna size and thus also the amount of absorbed light energy is extremely important for plants experiencing varying natural light conditions. The PSI core complex is present in the form of a monomer in the thylakoid membrane (Boekema et al. 2001; Kouřil et al. 2005a). However, isolated plant PSI complexes have been also found in larger oligomeric forms such as dimers, trimers and tetramers, which resemble trimeric and tetrameric forms of cyanobacterial PSI (Boekema et al. 1987; Semchonok et al. 2016). The native origin of plant PSI oligomers has not been clearly confirmed yet, therefore they are still considered to be artificial (Boekema et al. 2001, Kouřil et al. 2005a). The light harvesting capacity of the plant PSI core complex is increased by four attached Lhca proteins (LHCI), which form a crescent-shaped belt associated with the core complex (Boekema et al. 2001). In contrast to PSII complexes, where the LHCII antenna size is very variable, the LHCI antenna size and the stoichiometry of Lhca proteins of the plant PSI-LHCI supercomplex remains very stable even under different light conditions (Ballottari et al. 2007) (*see* the Sects. 9.3 and 9.4 below for details about structural organization of PSII and PSI).

In the last few decades, extensive biochemical evidence has been provided of the ability of photosynthetic proteins to form different supercomplexes, in analogy with respiratory proteins in mitochondria (*see* Dudkina et al. 2010a, b). For example, the PSI-LHCI supercomplex is known to form larger assemblies with other protein complexes, such as LHCII trimers, the Cytb_6f complex and NDH dehydrogenase. On the other hand, PSII-LHCII supercomplexes are known to form larger megacomplexes only via association with each other. A direct proof of the existence of the PSI-containing supercomplexes and the PSII megacomplexes can be obtained by clarification of their structures. However, structural characterization of large protein assemblies is often a very challenging task, because they are formed only transiently in the membrane and they are very fragile, which makes their purification in native form difficult. Here we describe our current experimental approach for the isolation and structural characterization of large photosynthetic supercomplexes or

even megacomplexes. We use optimized clear native polyacrylamide gel electrophoresis (CN-PAGE) for their separation and single particle electron microscopy for their structural characterization. The current knowledge about their structure, function and physiological significance is summarized in the following text.

9.2 Separation of Native Photosynthetic Supercomplexes for Their Structural Analysis

The first step to structural analysis of photosynthetic supercomplexes using electron microscopy (EM) is their isolation in sufficient quantity and homogeneity by a procedure that preserves their native form. Nowadays, two separation techniques are used most frequently – sucrose gradient ultracentrifugation and native polyacrylamide gel electrophoresis. Ultracentrifugation on a sucrose gradient allows an efficient separation of different types of photosynthetic protein complexes, as has been shown in several structural studies (e.g. Caffarri et al. 2009; Albanese et al. 2016; Wei et al. 2016). However, this technique is very time-consuming, as a single run may take about 10–20 h, and requires expensive equipment. In addition, prior to the preparation of the specimen for electron microscopy, a dialysis step is often indispensable to lower the sucrose concentration, which can severely reduce contrast of individual particles in electron micrographs. The main advantage of this method is the possibility to separate a large amount of sample in one separation run. Native electrophoresis also allows very efficient separation of native photosynthetic supercomplexes and megacomplexes of high molecular weight. Recent studies clearly show that separated protein complexes can be easily extracted from a gel and analyzed by EM (e.g. Knispel et al. 2012; Kouřil et al. 2014, 2016; Nosek et al. 2017). Although the electrophoretic technique enables separation of rather small sample volumes compared to the ultracentrifugation, the yield of isolated protein complexes is still sufficient for the EM technique. Moreover, a short separation time (about 2–3 h) and inexpensive equipment make the technique very attractive.

Undoubtedly, the above-mentioned techniques are gradually replacing other separation techniques such as gel filtration or affinity chromatography (e.g. van Roon et al. 2000; Drop et al. 2011). While the gel filtration suffers from a lower resolution and undesirable dilution of separated protein complexes, the affinity chromatography requires construction of a tag (e.g. the His6-tag) with no adverse effect on functional and structural properties of the tagged protein. Nevertheless, there is a continuous effort to search for mild separation techniques, which would further shorten the separation time and would allow the separation of fragile protein assemblies. Recently, free-flow electrophoresis was shown to be a promising technique (Yadav et al. 2017).

9.2.1 Native Polyacrylamide Gel Electrophoresis

Considering both scientific and practical aspects of the purification of photosynthetic supercomplexes, including time necessary for one separation and equipment expenses, native electrophoresis appears to be the best compromise. There are two variants of native electrophoresis, known as blue native electrophoresis (BN-PAGE) and clear native electrophoresis (CN-PAGE). Both native electrophoretic techniques differ in the agent used to provide the solubilized complexes the negative charge necessary for their movement in the electric field. While BN-PAGE uses an anionic dye Coomassie Brilliant blue (CBB), CN-PAGE applies a mild anionic detergent sodium deoxycholate.

The separation of protein complexes using BN-PAGE provides very good resolution, as the negatively charged CBB dye is directly adsorbed on the protein complexes. However, there are some indications that CBB disturbs the weakest protein-protein interactions. Moreover, the estimation of enzymatic activity of separated protein complexes and detection of fluorescently labeled proteins can be also hampered due to the presence of CBB (Wittig and Schägger 2005). To avoid this undesirable effect, a high-resolution CN-PAGE has been developed (Wittig et al. 2007), where CBB was replaced by the mild anionic detergent sodium deoxycholate, which is able to provide the negative charge without the disturbance of weak protein-protein interactions.

9.2.2 Solubilization of Photosynthetic Supercomplexes

Prior to the electrophoretic separation, the protein complexes have to be efficiently extracted from the lipid biological membranes. For this purpose, it is necessary to use mild detergents that are able to disrupt lipid-lipid and lipid-protein interactions on one hand and preserve protein-protein interactions on the other hand. Nowadays, a broad spectrum of different detergents can be used for this purpose (*see* Crepin et al. 2016), however, a screening of their solubilization properties indicates that non-ionic surfactants, like the dodecyl-maltosides (DDM) (the α- and β- anomers) and digitonin, are the most suitable for the solubilization of protein complexes from the thylakoid membranes. While there is a negligible difference in the α-DDM and β-DDM chemical structure, there is a considerable difference in their physical properties, which is evidenced by the stronger solubilizing power of β-DDM compared to α-DDM (see e.g. Pagliano et al. 2012; Barera et al. 2012).

It is important to keep in mind that both the lipid composition and lipid/protein ratio in the thylakoid membrane are species dependent and can also strongly vary under different environmental conditions. The same holds for the stability and abundance of a given type of photosynthetic protein complex. Therefore, to achieve an optimal solubilization of thylakoid membranes in each particular case, not only the type of the detergent has to be selected, but also its concentration has to be carefully

determined. The response of a sample to a detergent can be screened using so-called detergent concentration line, when a defined amount of sample is treated with a gradually increasing amount of the selected detergent. Using this approach it is possible to find the optimal solubilization conditions, which provide a maximal yield of a desired protein complex.

An example of this optimization procedure is shown for a solubilization of thylakoid membranes from *Arabidopsis thaliana* with a focus on large PSI-containing supercomplexes. In our optimization approach, we have decided to test both α- and β-DDM as solubilization agents (Figs. 9.2 and 9.3, respectively). Figure 9.2a shows that in the molecular weight range above 1 MDa (approx. The upper half of the gel), a milder solubilization using α-DDM was efficient for the isolation of larger forms of PSII supercomplexes or even PSII megacomplexes, which was further confirmed by the measurement of PSII fluorescence at room temperature (Fig. 9.2b). Fluorescence measurement enables unambiguous distinction between PSII and PSI containing complexes, as the fluorescence quantum yield of PSI is very low at room temperature, whereas the yield of PSII is high. Although the amount of separated PSII supercomplexes and megacomplexes significantly increased with increasing concentration of the detergent, the amount of PSI-containing high molecular weight bands (PSI hmw) increased only negligibly. A less mild solubilization of the thylakoid membrane using β-DDM led to a complete disappearance of the PSII megacomplex band and a substantial disruption of the largest PSII supercomplex into smaller forms. The yield of PSI-containing supercomplexes was still rather low (Fig. 9.3).
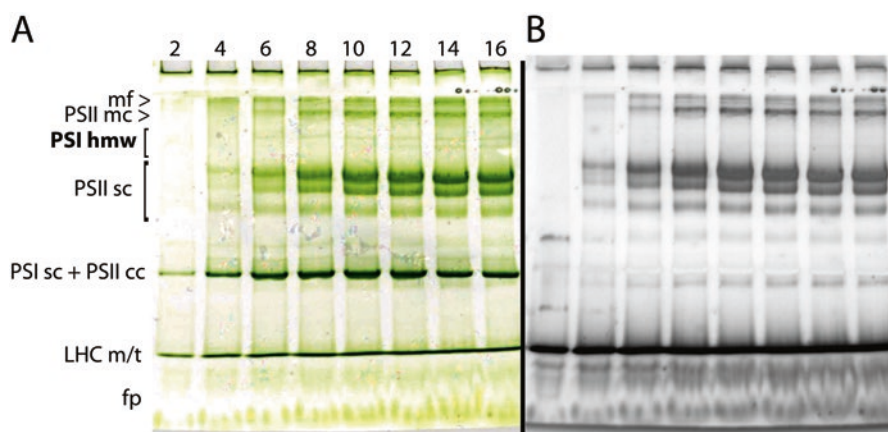
Fig. 9.2 Electrophoretic separation of *Arabidopsis thaliana* thylakoid membranes solubilized by increasing amount of α-DDM. (**a**) colour image of the gel, (**b**) room temperature fluorescence of supercomplexes from the same gel. 2–16: DDM/chl ratio, *mf* membrane fragments, *PSII mc* megacomplexes of PSII, *PSI hmw* high molecular weight PSI-containing bands, *PSII sc* supercomplexes of PSII, *PSI sc* supercomplex of PSI, *PSII cc* core complex of PSII, *LHCm/t* LHC monomers and trimers, *fp* free pigments. For a better resolution of hmw protein complexes, a polyacrylamide gel with 4–8% gradient was used
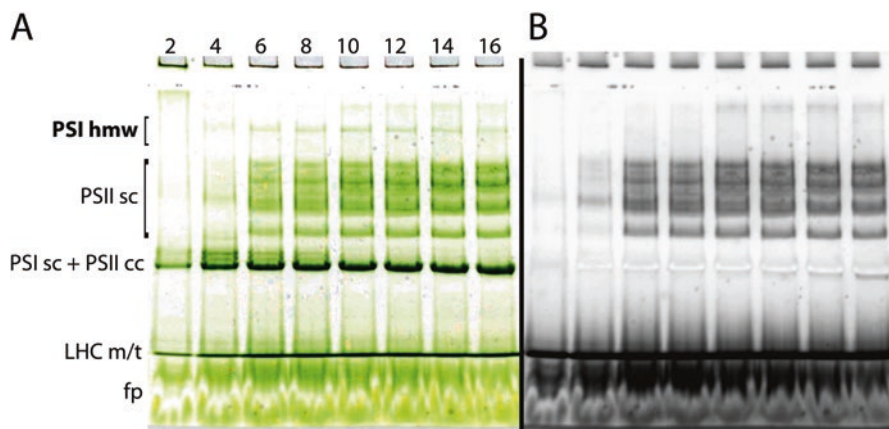
Fig. 9.3 Electrophoretic separation of *Arabidopsis thaliana* thylakoid membranes solubilized by increasing amount of β-DDM. (**a**) colour image of the gel, (**b**) room temperature fluorescence of supercomplexes from the same gel. 2–16: DDM/chl ratio, *PSI hmw* high molecular weight PSI-containing bands, *PSII sc* supercomplexes of PSII, *PSI sc* supercomplex of PSI, *PSII cc* core complex of PSII, *LHCm/t* LHC monomers and trimers, *fp* free pigments. For a better resolution of hmw protein complexes, a polyacrylamide gel with 4–8% gradient was used

As the yield of high molecular weight (hmw) PSI-containing complexes from *Arabidopsis thaliana* was very small, we decided to test another plant species. Figures 9.4 and 9.5 show repeated electrophoretic separations of photosynthetic complexes from thylakoid membranes isolated from barley leaves (*Hordeum vulgare*) after solubilization with α- and β-DDM. Inspection of obtained results indicates that in the barley sample solubilized with β-DDM, two dense PSI hmw bands were detected. After evaluating the effect of detergent concentration on the band densities (Fig. 9.5, values 2–16), the DDM/chl ratio 8 was selected as optimal. At this ratio, we obtained the highest densities of both the PSI hmw bands. After a brief screening of the two bands by electron microscopy, we found the PSI-NDH supercomplex in the lower one. The upper band was found to contain oligomers of PSI complexes. In conclusion, despite the fact that the PSI-NDH supercomplex was initially discovered in *Arabidopsis thaliana* (Peng et al. 2008), we found that barley was a more suitable plant material for the isolation and structural characterization of this supercomplex (Kouřil et al. 2014). This demonstrates the importance of optimization of isolation and separation conditions preceding the structural analysis.
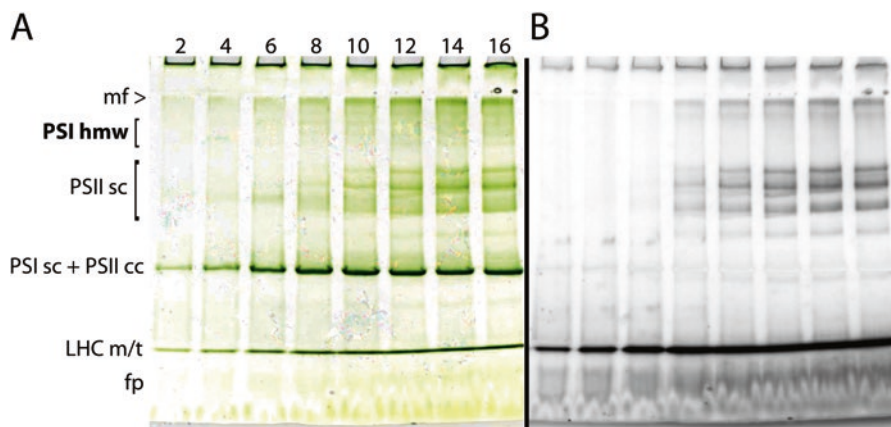
Fig. 9.4 Electrophoretic separation of barley (*Hordeum vulgare*) thylakoid membranes solubilized by increasing amount of α-DDM. (**a**) colour image of the gel, (**b**) room temperature fluorescence of supercomplexes from the same gel. 2–16: DDM/chl ratio, mf: membrane fragments, *PSI hmw* high molecular weight PSI-containing bands, *PSII sc* supercomplexes of PSII, *PSI sc* supercomplex of PSI, *PSII cc* core complex of PSII, *LHCm/t* LHC monomers and trimers, *fp* free pigments. For a better resolution of hmw protein complexes, a polyacrylamide gel with 4–8% gradient was used
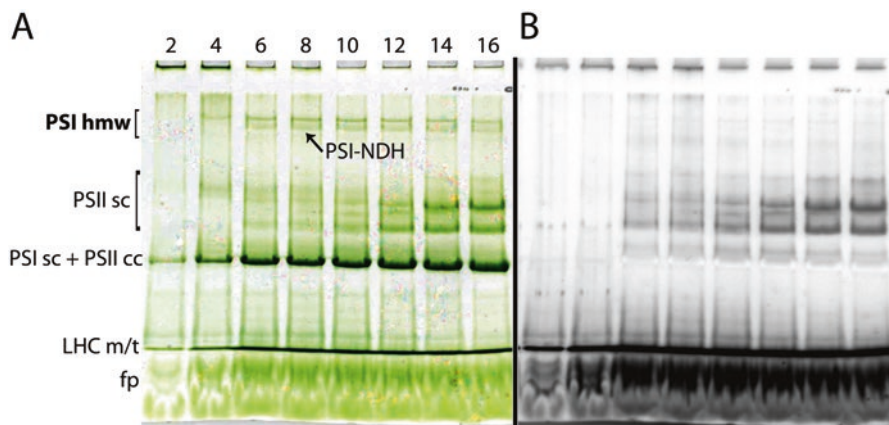
Fig. 9.5 Electrophoretic separation of barley (*Hordeum vulgare*) thylakoid membranes solubilized by increasing amount of β-DDM. (**a**) colour image of the gel, (**b**) room temperature fluorescence of supercomplexes from the same gel. 2–16: DDM/chl ratio, *PSI hmw* high molecular weight PSI-containing bands, *PSI-NDH* PSI-NDH supercomplex, *PSII sc* supercomplexes of PSII, *PSI sc* supercomplex of PSI, *PSII cc* core complex of PSII, *LHCm/t* LHC monomers and trimers, *fp* free pigments. For a better resolution of hmw protein complexes, a polyacrylamide gel with 4–8% gradient was used

9.2.3 Preparation of Specimens for Structural Analysis

Once the separation of desired protein complexes using CN-PAGE is optimized, the proteins have to be extracted from the gel prior to specimen preparation for single particle electron microscopy (Boekema et al. 2009). There are several methods available.

A procedure allowing a direct transfer of separated complexes from a native gel to the carbon coated grid was developed by Knispel and colleagues (2012). They placed the grid directly on the gel band with proteins of interest and relied on a spontaneous adsorption of protein complexes on the grid surface. This method is indeed very simple, however, its efficiency can be hampered by physical properties of separated complexes (i.e. size and shape), as we observed e.g. for large PSII supercomplexes.

Another option is the extraction of protein complexes into a buffer solution prior to specimen preparation. Generally, there are two methods: electro elution and spontaneous elution. Using the electro elution, the complexes are electrically forced from the gel and retained on a hydrophobic membrane, where they get concentrated. This method is fast, effective and quantitative, but requires specific and costly equipment. In addition, for our purpose it appears unsuitable, because the predominantly hydrophobic photosynthetic complexes can irreversibly aggregate on the hydrophobic membrane, which is highly undesirable for structural studies. On the other hand, spontaneous elution represents a convenient method with no special demands. It is based on simple free elution of complexes from the excised gel band into an elution buffer during a couple of hours. When spontaneous elution is performed, the excised gel band with complexes of interest is cut into small pieces and fully immersed into a small amount of elution buffer. We found this method to be very effective, as evidenced by several structural studies (i.e. Nosek et al. 2017; Kouřil et al. 2014, 2016). Once the complexes are extracted from the gel into solution, the electron microscopy specimen is prepared by a pipetting of the eluate on the glow-discharged carbon coated grid.

9.3 Structural Characterization of Plant Photosystem II Supercomplexes

The plant PSII is a large and highly variable multi-subunit protein supercomplex. The variability originates in the capability of the PSII core dimer to associate with a variable amount of LHCII proteins. This, together with a low stability of isolated PSII-LHCII supercomplexes, makes the structural analysis of this supercomplex via X-ray crystallography very difficult, because this technique requires a highly purified and concentrated sample. So far, X-ray crystallography was employed to obtain high resolution structures of some PSII components, including two extrinsic subunits of the plant PSII core complex, PsbP (Ifuku et al. 2004) and PsbQ (Calderone

et al. 2003; Balsera et al. 2005), and two types of antenna proteins, LHCII trimer (Liu et al. 2004; Standfuss et al. 2005) and Lhcb4 (Pan et al. 2011). On the other hand, single particle electron microscopy, which is less demanding with respect to sample homogeneity and quantity, turned out to be an indispensable technique in the structural research of the plant PSII-LHCII supercomplexes (*see* Kouřil et al. 2012; Pagliano et al. 2013; Caffarri et al. 2014 for recent reviews).

9.3.1   Composition and Organization of Photosystem II Supercomplex in Land Plants

PSII core complex functions as a homo-dimer (C_2) (Hankamer et al. 1997). Each monomer contains a reaction center (RC), which is formed by two large intrinsic subunits PsbA and PsbD (also called D1 and D2 protein, respectively), PsbE and PsbF subunits (the cytochrome b559 complex), and PsbI. These subunits bind most of the redox cofactors and pigments that are necessary for the photochemical reactions and initiation of the electron transport across the thylakoid membrane. The absorption cross-section of the RC is further increased by its association with inner antenna proteins PsbB and PsbC (also called CP47 and CP43, respectively). RC is also associated with about a dozen low-molecular weight pigment-free subunits, which are important for the stabilization of the entire C_2 and for its association with additional peripheral light harvesting proteins. Finally, there are three extrinsic subunits, PsbO, PsbP and PsbQ, which associate to the PSII core complex from the lumenal site and constitute the oxygen evolving complex with the Mn_4CaO_5 cluster that is responsible for water oxidation (*see* e.g. Pagliano et al. 2013; Caffarri et al. 2014 for more details).

The light harvesting capacity of the C_2 is significantly enhanced by the peripheral LHCII complex, which is composed of six pigment-binding proteins, Lhcb1-6. In addition to supplying the RC with excitation energy, these proteins also play an important structural role in the photo-protection of PSII against photo-oxidative damage by excessive light. Lhcb1-3 proteins are the most abundant and they form several types of trimers. As the ratio between Lhcb1, Lhcb2, and Lhcb3 proteins is about 8:3:1 (Jansson 1994), this implies that they can form either homotrimers (composed of either Lhcb1 or Lhcb2) or heterotrimers (composed of Lhcb1, Lhcb2 and Lhcb3). Lhcb4-6 proteins (also called CP29, CP26, and CP24, respectively) represent a minor fraction of LHCII. They are present as monomers and mediate the specific association of LHCII trimers to the PSII core complex and thus are important for the formation of the PSII-LHCII supercomplex. According to the character of the binding to C_2, the LHCII trimers were designated as "S" and "M" (Strongly and Moderately bound LHCII trimers, respectively) (Dekker and Boekema 2005; Kouřil et al. 2012), occasionally C_2 can associate also with "L" trimers (Loosely bound) (Boekema et al. 1999a, b). However, biochemical data indicate that in the thylakoid membrane, up to eight LHCII trimers can be present per C_2 (Peter and Thornber 1991; Broess et al. 2008; van Oort et al. 2010), which implies that there is probably a pool of "extra" LHCII, which has unknown location with respect to the C_2.

Our knowledge of the architecture of the PSII-LHCII supercomplexes has been significantly improved over the last 20 years (*see* Dekker and Boekema 2005; Kouřil et al. 2012; Pagliano et al. 2013). Single particle EM revealed 2D projection maps of different types of PSII-LHCII supercomplexes (Boekema et al. 1995, 1998, 1999a, b) and a gradual improvement of their resolution allowed a precise localization of individual subunits (Yakushevska et al. 2003; Caffarri et al. 2009). Figure 9.6 shows three forms of the PSII-LHCII supercomplex, which can be separated by CN-PAGE after a mild solubilization of thylakoid membranes using α-DDM (Fig. 9.2). The largest and the most abundant form of the supercomplex consists of PSII core complex with two copies of the S trimers and two copies of the M trimers, the so-called $C_2S_2M_2$ supercomplex (Fig. 9.2, the top PSII sc band). The binding of the S trimer is mediated by Lhcb5 and Lhcb4, while the M trimer binds with the help of the Lhcb6 protein (Fig. 9.6c, f). The smaller forms of the PSII-LHCII supercomplex, which are less abundant (*see* Fig. 9.2), lack either one or both M trimers (Fig. 9.6a, b, d, e). Experiments with barley *viridis zb63* mutant, which is character-
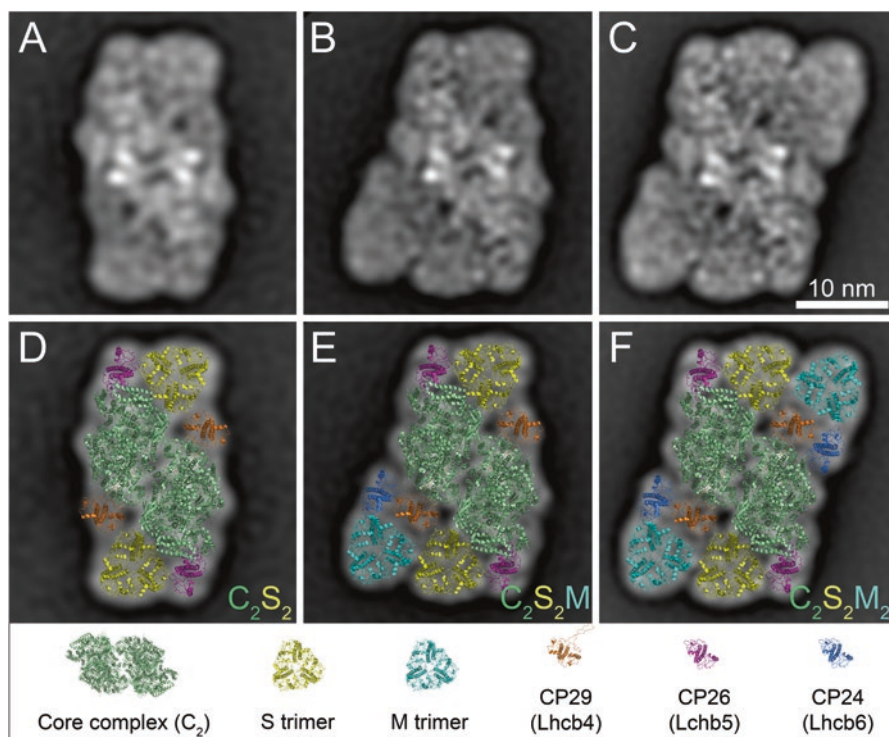
Fig. 9.6 Projection maps of different forms of PSII supercomplexes from *Arabidopsis thaliana* revealed by single particle electron microscopy and image analysis. (**a**) Projection map of PSII C_2S_2 supercomplex, (**b**) C_2S_2M supercomplex and (**c**) $C_2S_2M_2$ supercomplex. (**d–f**) Structural models of the PSII supercomplexes obtained by fitting the high resolution structures of the plant PSII supercomplex (Caffarri et al. 2009; Wei et al. 2016)

ized by a reduced LHCII to a minimal size due to the lack of PSI, indicate that the C_2S_2 supercomplex (Fig. 9.6a, d) represents the smallest physiologically relevant form of the supercomplex (Morosinotto et al. 2006).

Interestingly, the peripheral PSII antenna system can not only vary in its size, but it exhibits also small structural flexibility (Fig. 9.7). The flexibility within the peripheral antenna and, in particular, the flexibility of the M-trimer, Lhcb4, and Lhcb6 proteins, leads to several distinct conformations of the PSII supercomplex. Image analysis of a large data set (about 400,000 particles) shows that in the most abundant form of PSII supercomplex (approx. 60%), there is a gap between the Lhcb4, the S trimer and the core complex (Fig. 9.7a, d). A shift of the M trimer together with the Lhcb4/Lhcb6 region induces a small displacement of the S trimer and Lhcb5 (Fig. 9.7b, e), which leads to a tighter packing of the antenna in about 25% of analyzed projections. In the remaining 15% of analyzed data, the rotational shift of both the M trimers with the Lhcb4/Lhcb6 proteins induces additional lateral movement of the two halves of the dimeric core complex (Fig. 9.7c, f). The origin of the antenna flexibility still remains unknown. Single particle EM analysis of samples from dark-adapted plants and plants with light-induced NPQ excluded a
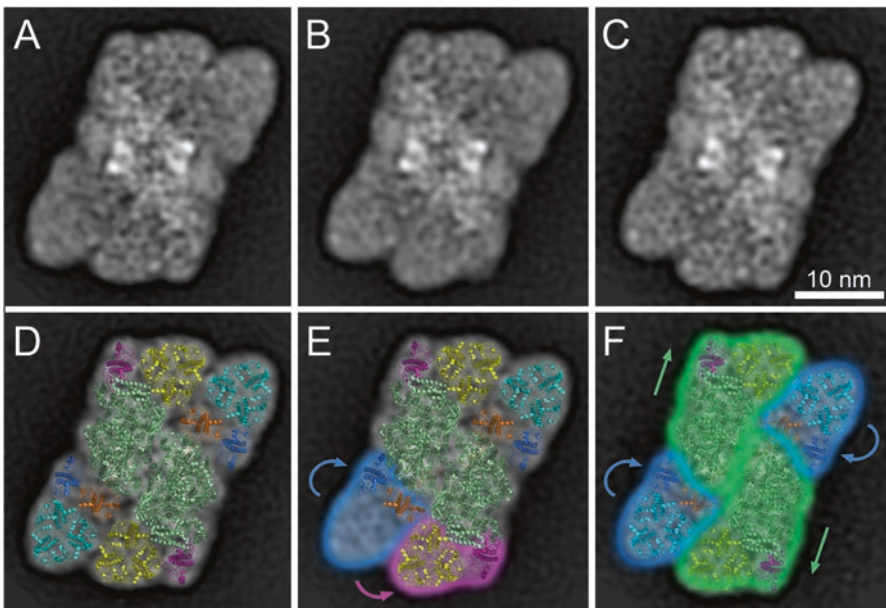
Fig. 9.7 Structural flexibility of the PSII $C_2S_2M_2$ supercomplexes from *Arabidopsis thaliana* revealed by single particle electron microscopy and image analysis. Projection maps of a standard PSII $C_2S_2M_2$ supercomplex (**a**) and the $C_2S_2M_2$ supercomplexes with slightly different organization of LHCII antenna proteins and PSII core complex (**b, c**). (**d–f**) Structural models of the PSII super-complexes obtained by fitting the high resolution structures of the plant PSII supercomplex (Caffarri et al. 2009, Wei et al. 2016). (**e, f**) The flexible parts of the PSII supercomplex and their movements with respect to the standard $C_2S_2M_2$ supercomplex are highlighted (See Fig. 9.6 for color coding)

direct relation between the particular antenna conformation and a light treatment (data not shown). Similarly, no direct connection with the presence of PsbS or zeaxanthin was observed (data not shown).

Recently, a breakthrough in the structural characterization of the PSII supercomplex was achieved, when the 3D structure of the C_2S_2 supercomplex was obtained using cryo electron microscopy at 3.2 Å resolution (Wei et al. 2016). This study significantly improved the resolution of the previous 3D structures (Nield et al. 2000; Nield and Barber 2006) and improved our knowledge about the organization of the whole supercomplex. A precise localization of individual Lhcb proteins shed more light on a possible energy transfer pathways between antenna and core complex. Nevertheless, solving the 3D structure of the complete $C_2S_2M_2$ supercomplex remains a challenging task for future research, especially due to the fragility of the supercomplex and the antenna flexibility.

9.3.2   Organization of Photosystem II Supercomplex in Pinaceae

The $C_2S_2M_2$ supercomplex was first found in representatives of flowering plants (angiosperms), the phylogenetically youngest land plants (e.g. spinach, pea, *Arabidopsis*) (Boekema et al. 1999a; Caffarri et al. 2009; Pagliano et al. 2014). Until recently, it had been assumed that the overall architecture of the $C_2S_2M_2$ supercomplex is conserved throughout the evolution of land plants, as the structure of this supercomplex in liverworts (Harrer 2003), the evolutionary oldest land plants, is similar to $C_2S_2M_2$ in angiosperms. Surprisingly, our recent study on PSII-LHCII supercomplexes in Norway spruce (*Picea abies*) revealed that the architecture and the subunit composition of PSII-LHCII supercomplex are not uniform in all land plants (Kouřil et al. 2016). Genome and transcriptome analysis of Norway spruce showed a lack of functional *Lhcb6* and *Lhcb3* genes, which notably changes the structural organization of the $C_2S_2M_2$ supercomplex (Fig. 9.8) (Kouřil et al. 2016). Due to the absence of Lhcb3 (a constituent of the M trimer, Dainese and Bassi 1991) and Lhcb6, the M trimer associates to the PSII complex in a different manner, which has never been observed in land plants before. Interestingly, the same orientation of the M and S trimers has been recently described in an evolutionarily older organism, the green alga *Chlamydomonas reinhardtii*, which also lacks the Lhcb6 protein (Fig. 9.8c, f) (Tokutsu et al. 2012; Drop et al. 2014).

The Lhcb6 and Lhcb3 proteins are known to be crucial for the management of absorbed light in land plants. The interaction between these proteins is important for the stable attachment of the M trimers to PSII complex (Kovacs et al. 2006; Caffarri et al. 2009; Kouřil et al. 2013). Therefore, these proteins can control the PSII antenna size during both plant adaptation and acclimation to different light conditions (Bailey et al. 2001; Ballottari et al. 2007; Betterle et al. 2009; Kouřil et al. 2013), optimize macro-organization of PSII supercomplexes and control connectiv-
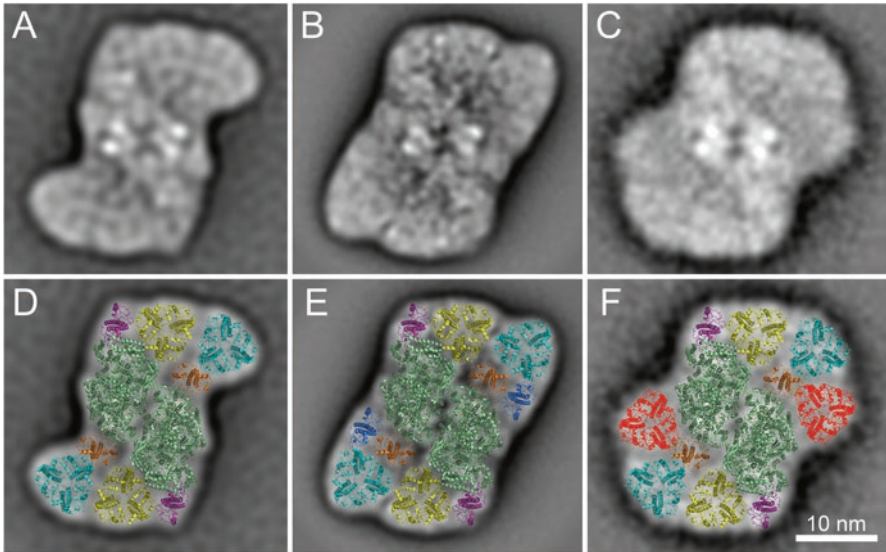
Fig. 9.8 Projection maps of PSII supercomplexes from different plant species revealed by single particle electron microscopy and image analysis. Projection maps of (**a**) PSII supercomplex ($C_2S_2M_2$) from Norway spruce (*Picea abies*), (**b**) PSII supercomplex ($C_2S_2M_2$) from *Arabidopsis thaliana*, (**c**) PSII supercomplex ($C_2S_2M_2N_2$) from green alga *Chlamydomonas reinhardtii* (Adapted from Drop et al. 2014). (**d**–**f**) Structural models of different forms of the PSII supercomplexes obtained by fitting the high resolution structures of the plant PSII supercomplex (Caffarri et al. 2009; Wei et al. 2016) (See Fig. 9.6 for color coding)

ity between PSII cores (Kovacs et al. 2006; Caffarri et al. 2009). These factors are crucial to accomplish a maximum efficiency of PSII photochemistry and play a key role in effective photo-protective dissipation of absorbed light energy (so-called non-photochemical quenching, NPQ) (Kovacs et al. 2006). Namely Lhcb6 is known to play an important role in NPQ of land plants, as it provides an interaction site for PsbS (Kovacs et al. 2006), a protein that is essential for the induction of NPQ (Li et al. 2000). The current model of NPQ suggests that upon exposure to excessive light, a part of the PSII-LHCII supercomplex containing Lhcb6, Lhcb4 and the M trimer dissociates, which leads to the PsbS-dependent NPQ (Betterle et al. 2009; Johnson et al. 2011).

A thorough genome and transcriptome analysis revealed that the absence of the Lhcb3 and Lhcb6 proteins is not limited to *Picea abies*. We have shown that these proteins are also absent in the gymnosperm genera *Picea* and *Pinus* (family Pinaceae) and *Gnetum* (Gnetales) (Kouřil et al. 2016). This is quite surprising, as the appearance of both Lhcb3 and Lhcb6 had been assumed to be crucial for the transition of photosynthetic organisms from aquatic habitat to land (Koziol et al. 2007; Alboresi et al. 2008; de Bianchi et al. 2008; Büchel 2015). A possible physiological benefit of the loss of these proteins in Pinaceae and Gnetales families remains to be clarified.

9.3.3 Association of Photosystem II Supercomplexes into Megacomplexes

The ability of the plant PSII-LHCII supercomplexes to associate with other proteins of the photosynthetic apparatus and to form even larger assemblies is rather limited. To our knowledge, there is only indirect biochemical evidence of the interactions of PSII-LHCII supercomplexes with PsbS protein (Gerotto et al. 2015; Correa-Galvis et al. 2016) or PSI complex (Yokono et al. 2015; Chen et al. 2016), which is still awaits a structural elucidation.

However, there is structural evidence of specific associations between two copies of PSII-LHCII supercomplexes into PSII megacomplexes (Boekema et al. 1999a, b; Yakushevska et al. 2001b; Caffarri et al. 2009; Jarvi et al. 2011; Albanese et al. 2016; Nosek et al. 2017). The PSII-LHCII supercomplexes associated in parallel can further associate into larger semi-crystalline arrays, which can be occasionally observed in grana membranes and which are believed to be important for the optimization and regulation of photosynthetic processes (Boekema et al. 1999a, b, 2000; Yakushevska et al. 2001a, b; Kirchhoff et al. 2007; Daum et al. 2010; Kouřil et al. 2012, 2013; Kirchhoff 2013; Tietz et al. 2015).

Recently, optimization of isolation of PSII megacomplexes using CN-PAGE (Fig. 9.2) allowed us to perform their thorough analysis. Single particle EM revealed a large variability in their formation (Nosek et al. 2017). A majority of analyzed PSII megacomplexes (about 80%) were formed by various parallel associations of two PSII-LHCII supercomplexes (Fig. 9.9a–e), which has been observed in previous studies. Structural models of their interactions indicate that the megacomplexes are formed by interactions between core complexes, M trimers and monomeric antenna proteins Lhcb5 and Lhcb6. Interestingly, the interaction between the core complex and Lhcb6 protein is already strong enough to form a stable megacomplex (Fig. 9.9d). Moreover, the involvement of additional LHCII trimers in the binding interactions gave rise to a unique type of the parallel PSII megacomplex (Fig. 9.9e). The additional LHCII trimers seem to be crucial for the formation of this type of the megacomplex (Fig. 9.9e), as no analogous PSII megacomplexes without these trimers were observed. Furthermore, single particle image analysis revealed novel variable associations between two non-parallel PSII-LHCII supercomplexes (Fig. 9.9f–l). Their structural models indicate that core complexes, S and M trimers, monomeric antenna proteins Lhcb5 and Lhcb6, and additional LHCII trimers are involved, to a different extent, in the mutual interactions between the two supercomplexes.

As the PSII megacomplexes were observed in several plant species (Boekema et al. 1999a, b; Yakushevska et al. 2001b; Caffarri et al. 2009; Jarvi et al. 2011; Nosek et al. 2017), their formation can be considered as a general property of the plant PSII-LHCII supercomplex. A successful identification of PSII megacomplexes in isolated grana membranes (Kirchhoff et al. 2008; Kouřil et al. 2011; Nosek et al. 2017) strongly supports their natural origin and physiological significance. A reversible formation of PSII megacomplexes can effectively modulate and control
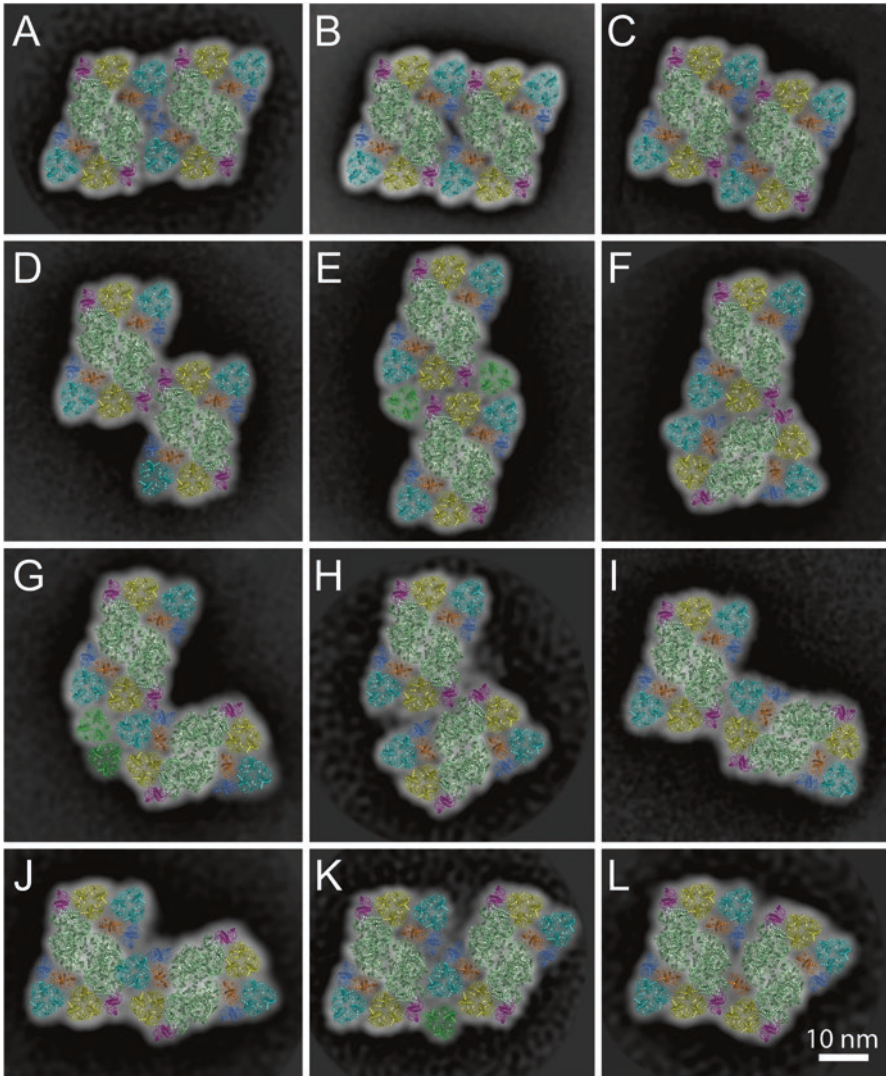
Fig. 9.9 Projection maps of *Arabidopsis thaliana* PSII megacomplexes revealed by single particle electron microscopy and image analysis. (**a–l**) Structural models of different forms of the PSII megacomplexes obtained by fitting the high resolution structures of the plant PSII supercomplex (Caffarri et al. 2009, Wei et al. 2016) (See Fig. 9.6 for color coding. The additional LHCII trimers are depicted in green)

the overall antenna size and effectively regulate a photochemical usage of absorbed light energy by plants in a changing environment (Ballottari et al. 2007; Kouřil et al. 2013; Albanese et al. 2016).

9.4 Structural Characterization of Plant Photosystem I Supercomplexes

PSI is a pigment-binding supercomplex, which works as a light-driven plastocyanin:ferredoxin oxidoreductase. The PSI core complex coordinates the components responsible for a light-driven electron transfer and specifically associates with a membrane-embedded light harvesting complex, LHCI, which extends its light-harvesting capacity. Initial structural research of a plant PSI-LHCI supercomplex largely profited from a high structural homology of the plant core complex with the cyanobacterial counterpart, as the latter was successfully studied using X-ray crystallography at atomic resolution (Krauss et al. 1996; Schubert et al. 1997; Jordan et al. 2001). The first structural details of the organization of the entire plant PSI-LHCI supercomplex were provided by single particle EM, which revealed an asymmetric binding of the LHCI proteins to one side of the core complex (Boekema et al. 2001). Due to an extensive effort of the research group of Nathan Nelson, the first high-resolution structure of the PSI-LHCI supercomplex was solved by X-ray crystallography at 4.4 Å (Ben-Shem et al. 2003) and a gradually improved up to 2.8 Å (Amunts et al. 2007, 2010; Mazor et al. 2015; Qin et al. 2015). As we show below, a combination of X-ray data and single particle EM maps is very advantageous for solving the structures of even larger assemblies between the PSI-LHCI supercomplex and additional proteins of the plant photosynthetic apparatus like the NDH complex, LHCII or Cytb_6f complex.

9.4.1 Composition and Organization of Photosystem I Supercomplex in Land Plants

X-ray structures of the plant PSI-LHCI supercomplex show that a stable form of the PSI core complex consists of 12 subunits PsaA – PsaL (Ben-Shem et al. 2003; Amunts et al. 2007, 2010; Mazor et al. 2015; Qin et al. 2015). There are only a few core subunits (PsaG, H, N-P, R), which are specific to green plants. Both PsaG and PsaH are stably bound to the core and were found to play important roles in the stabilization of the core complex (Varotto et al. 2002; Jensen et al. 2002), and in the docking of phosphorylated LHCII during state transitions, respectively (Lunde et al. 2000, Kouřil et al. 2005b, see also Sect. 9.4.3). PsaN-PsaP and PsaR subunits were found to occasionally associate with the PSI core complex. As both PsaN and PsaR subunits were identified in the crystal structure of the core complex only under specific crystallization conditions, they are not considered as its stable parts and their exact functions remain unclear (Amunts et al. 2010). PsaO and PsaP are subunits which have not been identified in any crystal structure of plant PSI-LHCI supercomplex yet (see also Nelson and Yocum 2006, Busch and Hippler 2011 for reviews).

The light harvesting complex of PSI consists of four peripheral light harvesting proteins Lhca1-4. They are evenly expressed and form two heterodimers, which create together a crescent-shaped belt at the PsaF/J site of the core complex (Boekema et al. 2001; Ben-Shem et al. 2003). One dimer is composed of Lhca1 and Lhca4 proteins and interacts with PSI core complex via PsaG and PsaB subunits (Lhca1) and via the PsaF subunit (Lhca4). The other dimer is formed by Lhca2 and Lhca3 proteins. Lhca2 associates with PSI core complex via PsaA and PsaJ and Lhca3 interacts via PsaA and PsaK (Jansson et al. 1996; Ben-Shem et al. 2003). The individual Lhca proteins in the PSI-LHCI supercomplex are not mutually interchangeable, which was demonstrated on mutants lacking individual Lhca subunits (Wientjes et al. 2009). In addition, there are two light harvesting proteins, Lhca5 and Lhca6, which are expressed at a very low level and bind, in contrast to other Lhca1-4 proteins, to PSI in a sub-stoichiometric amount (Klimmek et al. 2006). The exact role of Lhca5 and Lhca6 was unclear, until the mutants lacking these subunits were constructed. Analysis of these mutants indicated direct involvement of Lhca5 and Lhca6 in the formation and stabilization of the PSI-NDH supercomplex (Peng et al. 2008, 2009; Kouřil et al. 2014) (see the Sect. 9.4.2).

9.4.2   *Structure of Photosystem I and NAD(P)H Dehydrogenase Supercomplex*

The chloroplast NDH complex, which is similar to bacterial respiratory complex I, mediates one type of cyclic electron transport around PSI (Burrows et al. 1998; Kofer et al. 1998; Shikanai et al. 1998). This pathway is highly important for plants especially under stress conditions, as it helps to protect the photosynthetic apparatus against oxidative stress by preventing over-reduction of the chloroplast stroma (see Yamori and Shikanai 2016 for recent review). Biochemical analysis of the NDH complex revealed its association with PSI in the thylakoid membrane (Aro et al. 2005; Peng et al. 2008), and one NDH complex was proposed to associate with up to two copies of PSI (Peng and Shikanai 2011). The formation of the PSI-NDH supercomplex was found to be a prerequisite for the efficient operation of the NDH cyclic electron pathway (Peng et al. 2009). Surprisingly, two minor light harvesting proteins, Lhca5 and Lhca6, whose roles in relation to PSI had been enigmatic, were found to be directly involved in the formation of the PSI-NDH supercomplex (Peng et al. 2009). Thus, revealing the structure of the giant PSI-NDH supercomplex was keenly awaited.

Single particle EM analysis provided the first structural evidence of the presence of the PSI$_2$-NDH supercomplex in barley plants and its role in electron transport was proposed (Kouřil et al. 2014). In agreement with the former biochemical data, the supercomplex was formed by two copies of PSI, which were attached to one NDH complex. In addition, a smaller sub-complex, formed by one PSI associated to one NDH, was also found (Kouřil et al. 2014). A pseudo-atomic model of the

PSI$_2$-NDH supercomplex, constructed by a fitting the EM projection map with the X-ray structures of PSI and the bacterial respiratory complex (Amunts et al. 2010; Baradaran et al. 2013), indicates that the PSI complexes interact with the NDH complex through sites on LHCI (Fig. 9.10h). Our recent structural analysis revealed the same two types of the PSI-NDH supercomplexes in *Arabidopsis thaliana* (Fig. 9.10a, b). In addition, in Arabidopsis we have found even larger assemblies of the PSI-NDH supercomplex, where up to four PSI were associated to one copy of the NDH complex (Fig. 9.10c–f). However, due to a lower resolution, we were not able to unambiguously determine how the extra PSI complexes associate to the PSI$_2$-NDH supercomplex. Interestingly, we observed a unique association of two PSI to two NDH complexes (Fig. 9.10g), which indicate that these complexes might be able to form large PSI-NDH clusters in the thylakoid membrane.

9.4.3 Structure of Photosystem I and Light Harvesting Complex II Supercomplex

Optimal photosynthetic performance is achieved when the light absorption by both PSII and PSI is balanced. As the absorption properties of the two photosystems are different and the spectral composition and intensity of the sunlight can considerably vary during the day, plants have developed a mechanism of a rapid adjustment of the relative absorption cross-sections of both photosystems called state transitions (Bonaventura and Myers 1969; Bennett 1977). The adjustment involves a reversible migration of phosphorylated LHCII between PSII and PSI, which compensates for the absorption imbalance (Allen 1992; Wollman 2001; Minagawa 2011). Under a
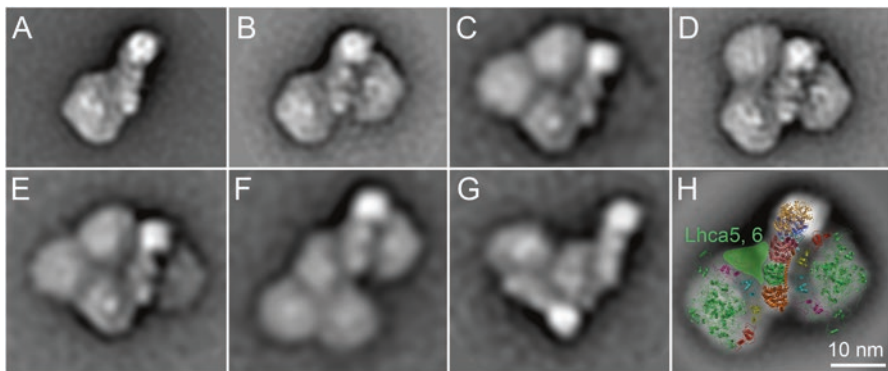
Fig. 9.10 Projection maps of different *Arabidopsis thaliana* PSI-NDH supercomplexes revealed by single particle electron microscopy and image analysis. (**a**) Projection map of the PSI$_1$-NDH supercomplex, (**b**) projection map of the PSI$_2$-NDH supercomplex, (**c**, **d**) projection maps of two different PSI$_3$-NDH supercomplexes, (**e**, **f**) projection maps of two different PSI$_4$-NDH supercomplexes, (**g**) projection map of dimeric PSI$_1$-NDH supercomplexes, (**h**) structural model of the PSI$_2$-NDH supercomplexes according to Kouřil et al. (2014)

preferential excitation of PSII, the activated Stn7 kinase (Bellafiore et al. 2005) phosphorylates LHCII, which subsequently moves from PSII and associates with PSI (state 2). Conversely, under a preferential excitation of PSI, the Stn7 kinase is inactivated and the LHCII phosphatase (Pribil et al. 2010; Shapiguzov et al. 2010) dephosphorylates LHCII, inducing its return back to PSII (state 1).

Although there is ample functional evidence for the occurrence of state transitions, the structure of the PSI-LHCII supercomplex remained uncharacterized for a long time, especially due to difficult purification of the supercomplex with yield too low for structural analysis. The first structural details about the architecture of the PSI-LHCII supercomplex were revealed by single particle EM of a crude, non-purified protein extract, obtained via mild solubilization of Arabidopsis thylakoid membranes using digitonin (Kouřil et al. 2005b). We have found that the PSI-LHCII supercomplex forms a pear-shaped particle, where the LHCII associates with PSI at the PsaA site between the PsaK and PsaH subunits (Fig. 9.11a, e). Recent structural analysis of free-flow electrophoretic fractions revealed even larger forms of the PSI-LHCII supercomplexes (Yadav et al. 2017). The largest assembly represented a dimer of the PSI-LHCII particles (Fig. 9.11b). A pseudo-atomic model indicates that the two PSI-LHCI complexes interact with each other from the PsaH side and the LHCII trimers also considerably contribute to the dimer formation (Fig. 9.11f). In addition, PSI-LHCII supercomplexes containing two LHCII trimers were also identified (Fig. 9.11c, d). The second LHCII binds at the peripheral antenna LHCI
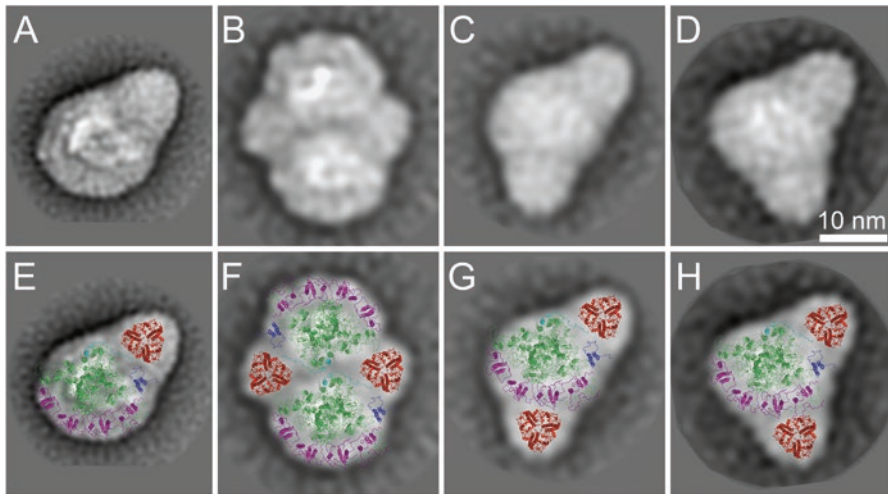
Fig. 9.11 Projection maps of different *Arabidopsis thaliana* PSI-LHCII supercomplexes revealed by single particle electron microscopy and image analysis. (**a**) PSI-LHCII supercomplex, (**b**) dimer of the PSI-LHCII supercomplex, (**c, d**) PSI-LHCII supercomplexes with additional LHCII trimer attached. (E-H) Structural models of the PSI-LHCII supercomplexes obtained by fitting the high resolution structures of the plant PSI complex (Mazor et al. 2015) (PSI core complex in green, PsaH in cyan, PsaK in blue, LHCI in magenta) and LHCII trimer (red) (Standfuss et al. 2005). LHCII trimer binds to the PSI core complex at the PsaH/PsaK side (**e, f**), additional LHCII trimer associates with the PSI complex at the LHCI site (**g, h**) (Adapted from Yadav et al. 2017)

of PSI (Fig. 9.11g, h). Our structural data clearly show that different types of the PSI-LHCII supercomplexes can be formed during state transitions and more than one LHCII trimer can associate with PSI. The novel associations indicate that our current view of the state transitions is rather limited and deserves further attention.

One of the still unanswered questions related to state transitions is where do the migrating LHCII trimers come from? Do the phosphorylated LHCII trimers represent the M trimers from $C_2S_2M_2$ supercomplexes or rather trimers from the free pool of LHCII? Based on a higher ratio of the $C_2S_2M/C_2S_2M_2$ particles in state 2 it has been proposed that the M trimer is involved in the association with PSI (Kouřil et al. 2005b; Dietzel et al. 2011). However, further experiments questioned the proposed scenario, as a lower amount of the $C_2S_2M_2$ supercomplexes in state 2 could be explained just by a higher sensitivity of the supercomplexes to a detergent treatment upon phosphorylation and the L trimers or LHCII from the free pool were proposed to play a key role in state transitions (Galka et al. 2012; Wientjes et al. 2013).

9.4.4 Structure of Photosystem I and Cytochrome b_6f Supercomplex

PSI has the ability to form supercomplexes with Cytb_6f complex. Several years ago, a supercomplex composed of PSI and Cytb_6f complex was biochemically described in the green alga *Chlamydomonas reinhardtii* (Iwai et al. 2010). This PSI-Cytb_6f supercomplex was proposed to contain three additional minor components – LHCII, FNR and PGRL1 – and was considered to play a role in cyclic electron flow. The first structural evidence of this supercomplex was obtained from a study of *Arabidopsis thaliana* membrane protein complexes, quickly purified with free-flow electrophoresis (Yadav et al. 2017). Electron microscopy analysis indicated that the Cytb_6f complex binds to PSI either as a monomer or as a dimer. The interaction between PSI and Cytb_6f is very loose and can be easily disrupted by detergents during purification, which could probably be explained by the fact that the rectangular-shaped Cytb_6f dimer binds to PSI at its short side (Fig. 9.12a).

A low-resolution 3D model was calculated from filtered projection maps, obtained by single particle EM (Fig. 9.12d). The high-resolution structures of PSI (Mazor et al. 2015) and the Cytb_6f complex (Stroebel et al. 2003; Kurisu et al. 2003) have been characterized before and could be modeled into the electron microscopy density map (Yadav et al. 2017). The shape of the Cytb_6f complex is highly asymmetrical with respect to the membrane (Stroebel et al. 2003, Kurisu et al. 2003), because unlike PSI, it protrudes strongly on the lumenal side of the membrane. This was very helpful to establish the binding position of Cytb_6f complex (Fig. 9.12d). Modelling shows that the Cytb_6f complex binds on the side of the PsaB subunit, next to the PsaG subunit of PSI core and the Lhca1 subunit of the peripheral antenna (Fig. 9.12e). The small protein plastocyanin functions as an electron transporter between the cytochrome f subunit of Cytb_6f complex and PSI. Minimizing this distance (black circles, Fig. 9.12e) could be the reason why the Cytb_6f complex binds to PSI with its short side rather than with its long side.
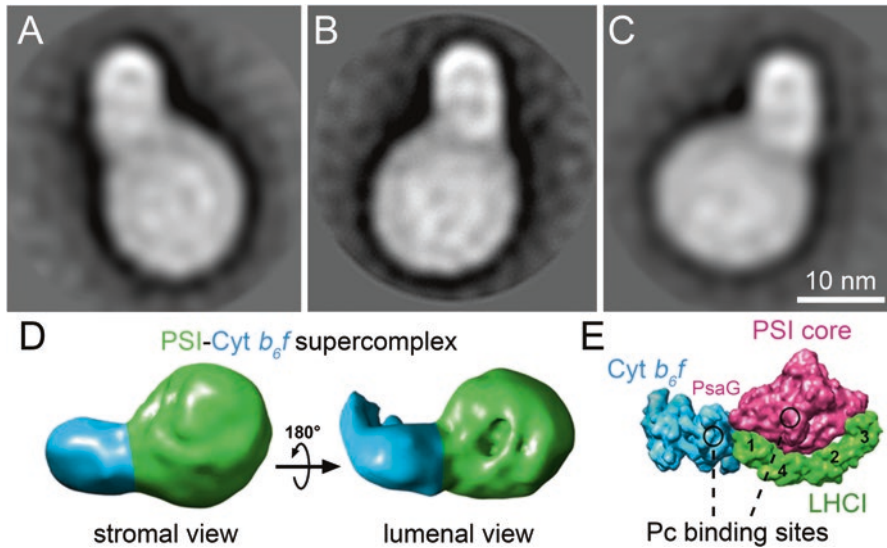
Fig. 9.12 Projection maps of *Arabidopsis thaliana* PSI-Cyt*b₆f* supercomplexes revealed by single particle electron microscopy and image analysis. (**a–c**) Different views of the supercomplexes consisting of PSI complex and a dimer of the Cyt*b₆f* complex. (**d**) Reconstructed 3D model of the PSI-Cyt*b₆f* supercomplex visualized from the stromal and lumenal sides, PSI complex in green, Cyt*b₆f* complex in light blue. (**e**) Model of the PSI-Cyt*b₆f* supercomplex with the PSI core (purple), LHCI (green, positions of the Lhca1-4 proteins is indicated by numbers), and Cyt*b₆f* complex (light blue) (Adapted from Yadav et al. 2017)

Over the last years it became obvious that PSI is undoubtedly a key protein in the regulation of electron flow. As PSI is involved in linear electron flow and two types of cyclic electron flow, it is important for modulation of the ATP:NADPH production and for the prevention of photo-oxidative damage under stress conditions (Burrows et al. 1998; Shikanai et al. 1998; Munekage et al. 2004). PSI uses light energy to mediate electron transfer from plastocyanin to ferredoxin, which then transports electrons from PSI to FNR in linear electron flow or to either Cyt*b₆f* complex or NDH in cyclic electron flow. This electron transport via plastocyanin and ferredoxin is diffusion-limited. Therefore, the regulation of the distances between electron carriers via the formation of supercomplexes of PSI with NDH or Cyt*b₆f* complex can control kinetics of the cyclic electron flows. We hypothesize that fine tuning of distances between PSI, NDH and Cyt*b₆f* complex in supercomplexes and/ or small membrane domains can control activity of the two types of cyclic electron flow. However, how this works in detail is not clear yet. So far, the analysis of the structures of the supercomplexes has not revealed the localization of small but essential components of the two types of cyclic electron flow, such as PGRL1, PGRL5 and FNR. Also LHCII was not found to be a component of the plant PSI-Cyt*b₆f* supercomplex, although PSI-LHCII supercomplexes are present in fair amounts in plant thylakoid membranes.

9.5 Future Perspectives

Currently, we have a very good knowledge of the architecture of all main components of the photosynthetic apparatus in thylakoid membranes at near atomic resolution. Single particle EM revealed the ability of the components to associate into large assemblies, which were shown to have physiological relevance. In our opinion, future structural studies on photosynthetic complexes should be more focused on the organization of photosynthetic complexes in the thylakoid membrane. Recent cryo electron tomography studies indicate that it is possible to resolve PSII core complexes directly in the membrane (Daum et al. 2010; Kouřil et al. 2011). This is largely due to a presence of extrinsic subunits of oxygen evolving complex, which enhance the contrast of the PSII particles with respect to the surrounding membrane. Recent instrumentation development in the field of cryo EM, leading to a significant improvement of a contrast in electron micrographs (see e.g. Fernandez-Leiro and Scheres 2016 for a recent review), is promising with respect to the possibility to visualize also other photosynthetic complexes with large hydrophilic domains (e.g. Cytb_6f complex and NDH complex). A visual monitoring of photosynthetic complexes and their distribution in the thylakoid membrane under different environmental conditions would open up a whole new chapter in photosynthesis research.

References

Albanese P, Nield J, Alejandro J et al (2016) Isolation of novel PSII-LHCII megacomplexes from pea plants characterized by a combination of proteomics and electron microscopy. Photosynth Res 130(1–3):19–31

Albertsson PÅ (2001) A quantitative model of the domain structure of the photosynthetic membrane. Trends Plant Sci 6(8):349–354

Alboresi A, Caffarri S, Nogue F et al (2008) In silico and biochemical analysis of *Physcomitrella patens* photosynthetic antenna: identification of subunits which evolved upon land adaptation. PLoS One 3:e2033

Allen JF (1992) Protein phosphorylation in regulation of photosynthesis. Biochim Biophys Acta 1098:275–335

Amunts A, Drory O, Nelson N (2007) The structure of a plant photosystem I supercomplex at 3.4 Å resolution. Nature 447:58–63

Amunts A, Toporik H, Borovikova A et al (2010) Structure determination and improved model of plant photosystem I. J Biol Chem 285:3478–3486

Aro EM, Suorsa M, Rokka A et al (2005) Dynamics of photosystem II: a proteomic approach to thylakoid protein complexes. J Exp Bot 56:347–356

Baena-Gonzalez E, Aro EM (2002) Biogenesis, assembly and turnover of photosystem II units. Phil Trans R Soc Lond B 357:1451–1460

Bailey S, Walters RG, Jansson S et al (2001) Acclimation of Arabidopsis thaliana to the light environment: the existence of separate low light and high light responses. Planta 213:794–801

Ballottari M, Dall'Osto L, Morosinotto T et al (2007) Contrasting behavior of higher plant photosystem I and II antenna systems during acclimation. J Biol Chem 282:8947–8958

Balsera M, Arellano JB, Revuelta JL et al (2005) The 1.49 Å resolution crystal structure of PsbQ from photosystem II of *Spinacia oleracea* reveals a PPII structure in the N-terminal region. J Mol Biol 350:1051–1060

Baradaran R, Berrisford JM, Minhas GS et al (2013) Crystal structure of the entire respiratory complex I. Nature 494:443–448

Barera S, Pagliano C, Pape T et al (2012) Characterization of PSII-LHCII supercomplexes isolated from pea thylakoid membrane by one-step treatment with alpha- and beta-dodecyl-D-maltoside. Philos Trans R Soc Lond Ser B Biol Sci 367(1608):3389–3399

Bellafiore S, Barneche F, Peltier G et al (2005) State transitions and light adaptation require chloroplast thylakoid protein kinase STN7. Nature 433:892–895

Bennett J (1977) Phosphorylation of chloroplast membrane polypeptides. Nature 269:344–346

Ben-Shem A, Frolow F, Nelson N (2003) Crystal structure of plant photosystem I. Nature 426:630–635

Betterle N, Ballottari M, Zorzan S et al (2009) Light-induced dissociation of an antenna hetero-oligomer is needed for non-photochemical quenching induction. J Biol Chem 284(22):15255–15266

Boekema EJ, Dekker JP, van Heel MG et al (1987) Evidence for a trimeric organization of the photosystem I complex from the thermophililc cyanobacterium *Synechococcus* sp. FEBS Lett 217(2):283–286

Boekema EJ, Hankamer B, Bald D et al (1995) Supramolecular structure of the photosystem-II complex from green plants and cyanobacteria. Proc Natl Acad Sci U S A 92(1):175–179

Boekema EJ, van Roon H, Dekker JP (1998) Specific association of photosystem II and light-harvesting complex II in partially solubilized photosystem II membranes. FEBS Lett 424:95–99

Boekema EJ, van Roon H, Calkoen F et al (1999a) Multiple types of association of photosystem II and its light-harvesting antenna in partially solubilized photosystem II membranes. Biochemistry 38:2233–2239

Boekema EJ, van Roon H, van Breemen JFL et al (1999b) Supramolecular organization of photosystem II and its light-harvesting antenna in partially solubilized photosystem II membranes. Eur J Biochem 266:444–452

Boekema EJ, van Breemen JFL, van Roon H et al (2000) Arrangement of photosystem II supercomplexes in crystalline macrodomains within the thylakoid membrane of green plant chloroplasts. J Mol Biol 301:1123–1133

Boekema EJ, Jensen PE, Schlodder E et al (2001) Green plant photosystem I binds light-harvesting complex I on one side of the complex. Biochemistry 40:1029–1036

Boekema EJ, Folea M, Kouřil R (2009) Single particle electron microscopy. Photosynth Res 102:189–196

Bonaventura C, Myers J (1969) Fluorescence and oxygen evolution from *Chlorella pyrenoidosa*. Biochim Biophys Acta 189:366–383

Broess K, Trinkunas G, van Hoek A et al (2008) Determination of the excitation migration time in photosystem II – consequences for the membrane organization and charge separation parameters. Biochim Biophys Acta 1777:404–409

Büchel C (2015) Evolution and function of light harvesting proteins. J Plant Physiol 172:62–75

Burrows PA, Sazanov LA, Svab Z et al (1998) Identification of a functional respiratory complex in chloroplasts through analysis of tobacco mutants containing disrupted plastid ndh genes. EMBO J 17:868–876

Busch A, Hippler M (2011) The structure and function of eukaryotic photosystem I. Biochim Biophys Acta 1807:864–877

Caffarri S, Kouřil R, Kereïche S et al (2009) Functional architecture of higher plant photosystem II supercomplexes. EMBO J 28:3052–3063

Caffarri S, Tibiletti T, Jennings RC (2014) A comparison between plant photosystem I and photosystem II architecture and functioning. Curr Protein Pept Sci 15(4):296–331

Calderone V, Trabucco M, Vujicić A et al (2003) Crystal structure of the PsbQ protein of photosystem II from higher plants. EMBO Rep 4(9):900–905

Chen F, Dong G, Wu L et al (2016) A nucleus-encoded chloroplast protein YL1 is involved in chloroplast development and efficient biogenesis of chloroplast ATP synthase in rice. Sci Rep 6:32295

Correa-Galvis V, Poschmann G, Melzer M et al (2016) PsbS interactions involved in the activation of energy dissipation in *Arabidopsis*. Nat Plants 2:15225

Crepin A, Santabarbara S, Caffarri S (2016) Biochemical and spectroscopic characterization of highly stable photosystem II supercomplexes from Arabidopsis. J Biol Chem 291(36):19157–19171

Dainese P, Bassi R (1991) Subunit stoichiometry of the chloroplast photosystem-II antenna system and aggregation state of the component chlorophyll-a/b binding-proteins. J Biol Chem 266:8136–8142

Daum B, Nicastro D, Austin J et al (2010) Arrangement of photosystem II and ATP synthase in chloroplast membranes of spinach and pea. Plant Cell 22:1299–1312

de Bianchi S, Dall'Osto L, Tognon G et al (2008) Minor antenna proteins CP24 and CP26 affect the interactions between photosystem II subunits and the electron transport rate in grana membranes of Arabidopsis. Plant Cell 20:1012–1028

Dekker JP, Boekema EJ (2005) Supermolecular organization of the thylakoid membrane proteins in green plants. Biochim Biophys Acta 1706:12–39

Dietzel L, Bräutigam K, Steiner S et al (2011) Photosystem II supercomplex remodeling serves as an entry mechanism for state transitions in *Arabidopsis*. Plant Cell 23(8):2964–2977

Drop B, Webber-Birungi M, Fusetti F et al (2011) Photosystem I of Chlamydomonas reinhardtii contains nine light-harvesting complexes (Lhca) located on one side of the core. J Biol Chem 286(52):44878–44887

Drop B, Webber-Birungi M, Yadav SKN et al (2014) Light-harvesting complex II (LHCII) and its supramolecular organization in *Chlamydomonas reinhardtii*. Biochim Biophys Acta 1837:63–72

Dudkina NV, Oostergetel GT, Braun HP et al (2010a) Row-like organization of ATP synthase in intact mitochondria determined by cryo-electron tomography. Biochim Biophys Acta 1797:272–277

Dudkina NV, Kouřil R, Bultema JB et al (2010b) Imaging of organelles by electron microscopy reveals protein-protein interactions in mitochondria and chloroplasts. FEBS Lett 584:2510–2515

Fernandez-Leiro R, Scheres SH (2016) Unravelling biological macromolecules with cryo-electron microscopy. Nature 537:339–346

Galka P, Santabarbara S, Thi THK et al (2012) Functional analyses of the plant photosystem I-light-harvesting complex II supercomplex reveal that light-harvesting complex II loosely bound to photosystem II is a very efficient antenna for photosystem I in state II. Plant Cell 24:2963–2978

Gerotto C, Franchin C, Arrigoni G et al (2015) In vivo identification of photosystem II light harvesting complexes interacting with photosystem II subunit S. Plant Physiol 168:1747–1761

Hankamer B, Barber J, Boekema EJ (1997) Structure and membrane organization of photosystem II in green plants. Annu Rev Plant Physiol Plant Mol Biol 48:641–671

Harrer R (2003) Associations between light-harvesting complexes and photosystem II from *Marchantia polymorpha* L. determined by two- and three-dimensional electron microscopy. Photosynth Res 75:249–258

Ifuku K, Nakatsu T, Kato H et al (2004) Crystal structure of the PsbP protein of photosystem II from *Nicotiana tabacum*. EMBO Rep 5(4):362–367

Iwai M, Takizawa K, Tokutsu R et al (2010) Isolation of the elusive supercomplex that drives cyclic electron flow in photosynthesis. Nature 464(7292):1210–1203

Jansson S (1994) The light–harvesting chlorophyll a/b binding-proteins. Biochim Biophys Acta 1184:1–19

Jansson S, Andersen B, Scheller HV (1996) Nearest-neighbor analysis of higher-plant photosystem I holocomplex. Plant Physiol 112:409–420

Jarvi S, Suorsa M, Paakkarinen V et al (2011) Optimized native gel systems for separation of thylakoid protein complexes: novel super- and mega-complexes. Biochem J 439:207–214

Järvi S, Suorse M, Aro EM (2015) Photosystem II repair in plant chloroplasts – regulation, assisting proteins and shared components with photosystem II biogenesis. Biochim Biophys Acta 1847:900–909

Jensen PE, Rosgaard L, Knoetzel J et al (2002) Photosystem I activity is increased in the absence of the PSI-G subunit. J Biol Chem 277(4):2798–2803

Johnson MP, Goral TK, Duffy CD et al (2011) Photoprotective energy dissipation involves the reorganization of photosystem II light-harvesting complexes in the grana membranes of spinach chloroplasts. Plant Cell 23(4):1468–1479

Jordan P, Fromme P, Witt HT et al (2001) Three-dimensional structure of photosystem I at 2.5 Å resolution. Nature 411:909–917

Kirchhoff H (2013) Architectural switches in plant thylakoid membranes. Photosynth Res 116:481–487

Kirchhoff H, Haase W, Wegner S et al (2007) Low-light-induced formation of semicrystalline photosystem II arrays in higher plant chloroplasts. Biochemistry 46:11169–11176

Kirchhoff H, Lenhert S, Büchel C et al (2008) Probing the organization of photosystem II in photosynthetic membranes by atomic force microscopy. Biochemistry 47:431–440

Klimmek F, Sjodin A, Noutsos C et al (2006) Abundantly and rarely expressed Lhc protein genes exhibit distinct regulation patterns in plants. Plant Physiol 140:793–804

Knispel RW, Kofler C, Boicu M et al (2012) Blotting protein complexes from native gels to electron microscopy grids. Nat Methods 9:182–184

Kofer W, Koop HU, Wanne G et al (1998) Mutagenesis of the genes encoding subunits A, C, H, I, J and K of the plastid NAD(P)H-plastoquinone-oxidoreductase in tobacco by polyethylene glycol-mediated plastome transformation. Mol Gen Genet 258:166–173

Kouřil R, van Oosterwijk N, Yakushevska AE et al (2005a) Photosystem I: a search for green plant trimers. Photochem Photobiol Sci 4:1091–1094

Kouřil R, Zygadlo A, Arteni AA et al (2005b) Structural characterization of a complex of photosystem I and light-harvesting complex II of *Arabidopsis thaliana*. Biochemistry 44:10935–10940

Kouřil R, Oostergetel GT, Boekema EJ (2011) Fine structure of granal thylakoid membrane organization using cryo electron tomography. Biochim Biophys Acta 1807:368–374

Kouřil R, Dekker JP, Boekema EJ (2012) Supramolecular organization of photosystem II in green plants. Biochim Biophys Acta 1817:2–12

Kouřil R, Wientjes E, Bultema JB et al (2013) High-light vs. low-light: effect of light acclimation on photosystem II composition and organization in *Arabidopsis thaliana*. Biochim Biophys Acta 1827:411–419

Kouřil R, Strouhal O, Nosek L et al (2014) Structural characterization of a plant photosystem I and NAD(P)H dehydrogenase supercomplex. Plant J 77:568–576

Kouřil R, Nosek L, Bartoš J et al (2016) Evolutionary loss of light-harvesting proteins Lhcb6 and Lhcb3 in major land plant groups – break-up of current dogma. New Phytol 210:808–814

Kovacs L, Damkjær J, Kereïche S (2006) Lack of the light-harvesting complex CP24 affects the structure and function of the grana membranes of higher plant chloroplasts. Plant Cell 18:3106–3120

Koziol AG, Borza T, Ishida KI et al (2007) Tracing the evolution of the light-harvesting antennae in chlorophyll a/b-containing organisms. Plant Physiol 143:1802–1816

Kramer DM, Avenson TJ, Edwards GE (2004) Dynamics flexibility in the light reactions of photosynthesis governed by both electron and proton transfer reactions. Trends Plant Sci 9:349–357

Krauss N, Schubert WD, Klukas O et al (1996) Photosystem I at 4 Å resolution represents the first structural model of a joint photosynthetic reaction centre and core antenna system. Nat Struct Biol 3(11):965–973

Kurisu G, Zhang H, Smith JL et al (2003) Structure of the cytochrome b6f complex of oxygenic photosynthesis: tuning the cavity. Science 302:1009–1014

Li XP, BjörkmanO Shich C et al (2000) A pigment-binding protein essential for regulation of photosynthetic light harvesting. Nature 403:391–395

Liu Z, Yan H, Wang K et al (2004) Crystal structure of spinach light-harvesting complex at 2.72 Å resolution. Nature 428:287–292

Lunde C, Jensen PE, Haldrup A et al (2000) The PSI-H subunit of photosystem I is essential for state transitions in plant photosynthesis. Nature 408:613–615

Mazor Y, Borovikova A, Nelson N (2015) The structure of plant photosystem I super-complex at 2.8 Å resolution. Elife 4:e07433

Minagawa J (2011) State transitions – the molecular remodeling of photosynthetic supercomplexes that controls energy flow in the chloroplast. Biochim Biophys Acta 1807:897–905

Morosinotto T, Bassi R, Frigerio S et al (2006) Biochemical and structural analyses of a higher plant photosystem II supercomplex of a photosystem I-less mutant of barely. Consequences of a chronic over-reduction of the plastoquinone pool. FEBS J 273:4616–4630

Munekage Y, Hashimoto M, Miyake C et al (2004) Cyclic electron flow around photosystem I is essential for photosynthesis. Nature 429:579–582

Nelson N, Yocum CF (2006) Structure and function of photosystems I and II. Ann Rev Plant Biol 57:521–565

Nield J, Barber J (2006) Refinement of the structural model for the photosystem II supercomplex of higher plants. Biochim Biophys Acta 1757:353–361

Nield J, Orlova EV, Morris EP et al (2000) 3D map of the plant photosystem II supercomplex obtained by cryoelectron microscopy and single particle analysis. Nat Struct Biol 7(1):44–47

Nosek L, Semchonok D, Boekema EJ et al (2017) Structural variability of plant photosystem II megacomplexes in thylakoid membranes. Plant J 89:104–111

Pagliano C, Barera S, Chimirri F et al (2012) Comparison of the alpha and beta isomeric forms of the detergent n-dodecyl-D-maltoside for solubilizing photosynthetic complexes from pea thylakoid membranes. Biochim Biophys Acta 1817:1506–1515

Pagliano C, Saracco G, Barber J (2013) Structural, functional and auxiliary proteins of photosystem II. Photosynth Res 116:167–188

Pagliano C, Nield J, Marsano F et al (2014) Proteomic characterization and three-dimensional electron microscopy study of PSII-LHCII supercomplexes from higher plants. Biochim Biophys Acta 1837:1454–1462

Pan X, Li M, Wan T et al (2011) Structural insights into energy regulation of light-harvesting complex CP29 from spinach. Nat Struct Mol Biol 18:309–315

Peng LW, Shikanai T (2011) Supercomplex formation with photosystem I is required for the stabilization of the chloroplast NADH dehydrogenase-like complex in Arabidopsis. Plant Physiol 155:1629–1639

Peng LW, Shimizu H, Shikanai T (2008) The chloroplast NAD(P)H dehydrogenase complex interacts with photosystem I in Arabidopsis. J Biol Chem 283:34873–34879

Peng LW, Fukao Y, Fujiwara M et al (2009) Efficient operation of NAD(P)H dehydrogenase requires supercomplex formation with photosystem I via minor LHCI in Arabidopsis. Plant Cell 21:3623–3640

Peter GF, Thornber JP (1991) Biochemical-composition and organization of higher-plant photosystem-II light-harvesting pigment-proteins. J Biol Chem 266:16745–16754

Pribil M, Pesaresi P, Hertle A et al (2010) Role of plastid protein phosphatase TAP38 in LHCII dephosphorylation and thylakoid electron flow. PLoS Biol 8:e1000288

Qin X, Suga M, Kuang T et al (2015) Structural basis for energy transfer pathways in the plant PSI-LHCI supercomplex. Science 348(6238):989–995

Schubert WD, Klukas O, Krauss N et al (1997) Photosystem I of *Synechococcus elongatus* at 4 Å resolution: comprehensive structure analysis. J Mol Biol 272(5):741–769

Semchonok DA, Li M, Bruce BD et al (2016) Cyro-EM structure of a tetrameric cyanobacterial photosystem I complex reveals novel subunit interactions. Biochim Biophys Acta 1857:1619–1626

Shapiguzov A, Ingelsson B, Samol I et al (2010) The PPH1 phosphatase is specifically involved in LHCII dephosphorylation and state transitions in Arabidopsis. Proc Natl Acad Sci U S A 107:4782–4787

Shikanai T (2016) Chloroplast NDH: a different enzyme with a structure similar to that of respiratory NADH dehydrogenase. Biochim Biophys Acta 1857:1015–1022

Shikanai T, Endo T, Hashimoto T et al (1998) Directed disruption of the tobacco ndhB gene impairs cyclic electron flow around photosystem I. Proc Natl Acad Sci U S A 95:9705–9709

Standfuss R, van Scheltinga ACT, Lamborghini M et al (2005) Mechanisms of photoprotection and nonphotochemical quenching in pea light harvesting complex at 2.5 Å resolution. EMBO J 24:919–928

Stroebel D, Choquet Y, Popot JL et al (2003) An atypical haem in the cytochrome b_6f complex. Nature 426:413–418

Tietz S, Puthiyaveetil S, Enlow HM et al (2015) Functional implications of photosystem II crystal formation in photosynthetic membranes. J Biol Chem 290:14091–14106

Tokutsu R, Kato N, Bui KH et al (2012) Revisiting the supramolecular organization of photosystem II in *Chlamydomonas reinhardtii*. J Biol Chem 287:31574–31581

van Oort B, Alberts M, de Bianchi S et al (2010) Effect of antenna-depletion in photosystem II on excitation energy transfer in *Arabidopsis thaliana*. Biophys J 98:922–931

van Roon H, van Breemen JFL, de Werd FL et al (2000) Solubilization of green plant thylakoid membranes with *n*-dodecyl-α,D-maltoside. Implications for the structural organization of the photosystem II, photosystem I, ATP synthase and cytochrome b_6f complexes. Photosynth Res 64:155–166

Varotto C, Pesaresi P, Jahns P et al (2002) Single and double knockouts of the genes for photosystem I subunits G, K, and H of Arabidopsis. Effects on photosystem I composition, photosynthetic electron flow, and state transitions. Plant Physiol 129:616–624

Wei X, Su X, Cao P et al (2016) Structure of spinach photosystem II-LHCII supercomplex at 3.2 Å resolution. Nature 534(7605):69–74

Wientjes E, Oostergetel GT, Jansson S et al (2009) The role of Lhca complexes in the supramolecular organization of higher plant photosystem I. J Biol Chem 284:7803–7810

Wientjes E, Drop B, Kouřil R et al (2013) During state 1 to state 2 transition in *Arabidopsis thaliana*, the photosystem II supercomplex gets phosphorylated but does not disassemble. J Biol Chem 288:32821–32826

Wittig I, Schägger H (2005) Advantages and limitations of clear-native PAGE. Proteomics 5:4338–4346

Wittig I, Karas M, Schägger H (2007) High resolution clear native electrophoresis for in-gel functional assays and fluorescence studies of membrane protein complexes. Mol Cell Proteomics 6:1215–1225

Wollman FA (2001) State transitions reveal the dynamics and flexibility of the photosynthetic apparatus. EMBO J 20:3623–3630

Yadav KNS, Semchonok DA, Nosek L et al (2017) Supercomplexes of plant photosystem I with cytochrome b6f, light-harvesting complex II and NDH. Biochim Biophys Acta 1858:12–20

Yakushevska AE, Jensen PE, Keegstra W et al (2001a) Supermolecular organization of photosystem II and its associated light-harvesting antenna in *Arabidopsis thaliana*. Eur J Biochem 268:6020–6021

Yakushevska AE, Ruban AV, Jensen PE et al (2001b) Supermolecular organization of photosystem II and its associated light-harvesting antenna in the wild- type and npq4 mutant of *Arabidopsis thaliana*. In: PS2001 proceedings: 12th international congress on photosynthesis. CSIRO Publishing, Melbourne, p S5

Yakushevska AE, Keegstra W, Boekema EJ et al (2003) The structure of photosystem II in Arabidopsis: localization of the CP26 and CP29 antenna complexes. Biochemistry 42:806–813

Yamori W, Shikanai T (2016) Physiological functions of cyclic electron transport around photosystem I in sustaining photosynthesis and plant growth. Annu Rev Plant Biol 67:81–106

Yokono M, Takabayashi A, Akimoto S et al (2015) A megacomplex composed of both photosystem reaction centres in higher plants. Nat Commun 6:6675

Publication 10

Unique organization of photosystem II supercomplexes and megacomplexes in Norway spruce

Roman Kouřil[1],* iD, Lukáš Nosek[1] iD, Monika Opatíková[1] iD, Rameez Arshad[1,2] iD, Dmitry A. Semchonok[2], Ivo Chamrád[3], René Lenobel[3], Egbert J. Boekema[2] and Petr Ilík[1] iD

[1]Department of Biophysics, Centre of the Region Haná for Biotechnological and Agricultural Research, Faculty of Science, Palacký University, Šlechtitelů 27, Olomouc 783 71, Czech Republic,

[2]Electron Microscopy Group, Groningen Biomolecular Sciences and Biotechnology Institute, University of Groningen, Nijenborgh 7, Groningen 9747 AG, The Netherlands, and

[3]Department of Protein Biochemistry and Proteomics, Centre of the Region Haná for Biotechnological and Agricultural Research, Faculty of Science, Palacký University, Šlechtitelů 27, Olomouc 783 71, Czech Republic

SUMMARY

Photosystem II (PSII) complexes are organized into large supercomplexes with variable amounts of light-harvesting proteins (Lhcb). A typical PSII supercomplex in plants is formed by four trimers of Lhcb proteins (LHCII trimers), which are bound to the PSII core dimer via monomeric antenna proteins. However, the architecture of PSII supercomplexes in Norway spruce[*Picea abies* (L.) Karst.] is different, most likely due to a lack of two Lhcb proteins, Lhcb6 and Lhcb3. Interestingly, the spruce PSII supercomplex shares similar structural features with its counterpart in the green alga *Chlamydomonas reinhardtii* [Kouřil *et al*. (2016) *New Phytol*. 210, 808–814]. Here we present a single-particle electron microscopy study of isolated PSII supercomplexes from Norway spruce that revealed binding of a variable amount of LHCII trimers to the PSII core dimer at positions that have never been observed in any other plant species so far. The largest spruce PSII supercomplex, which was found to bind eight LHCII trimers, is even larger than the current largest known PSII supercomplex from *C. reinhardtii*. We have also shown that the spruce PSII supercomplexes can form various types of PSII megacomplexes, which were also identified in intact grana membranes. Some of these large PSII supercomplexes and megacomplexes were identified also in *Pinus sylvestris*, another representative of the Pinaceae family. The structural variability and complexity of LHCII organization in Pinaceae seems to be related to the absence of Lhcb6 and Lhcb3 in this family, and may be beneficial for the optimization of light-harvesting under varying environmental conditions.

Keywords: clear native polyacrylamide electrophoresis, *Picea abies*, *Pinus sylvestris*, photosystem II, megacomplex, supercomplex, single-particle electron microscopy, grana membrane.

INTRODUCTION

Photosystem II (PSII) is a large multi-subunit pigment−protein complex embedded in the thylakoid membrane of cyanobacteria, algae and plants. It is a key player in light reactions of photosynthesis due to its ability to split water into oxygen, protons and electrons, which are further utilized in photosynthetic reactions (Barber, 2003).

A core complex of PSII forms a dimer (C_2), which contains pigments and redox cofactors necessary for the photochemical reactions. In land plants, C_2 associates with light-harvesting complex II (LHCII), consisting of a variable number of membrane-embedded light-harvesting proteins (Lhcb1−6). The variability of LHCII composition and size is important for the optimization of the absorption cross-section of the PSII core complex under different light conditions (Bailey *et al*., 2001; Ballottari *et al*., 2007; Kouřil *et al*., 2013; Albanese *et al*., 2016). Lhcb1−3 proteins are present only in the trimeric form (Jansson, 1994). Lhcb1 and Lhcb2 can form homotrimers, but they are also able to form heterotrimers with each other or with Lhcb3. These trimers specifically bind to C_2 core with the help of monomeric proteins Lhcb4−6 (also called CP29, CP26 and CP24, respectively).

Depending on the strength of the association of the trimers to C_2, we distinguish between strongly (S), moderately (M) and loosely (L) bound LHCII trimers (Dekker and

Boekema, 2005; Kouřil *et al.*, 2012, 2018; see also Figure 5). The S trimer consists of Lhcb1 and Lhcb2 proteins at different ratios and is attached to C_2 via Lhcb5 and Lhcb4 proteins. The M trimer is formed by one copy of Lhcb3 and two Lhcb1/2 proteins (Caffarri *et al.*, 2004, 2009; Su *et al.*, 2017; Crepin and Caffarri, 2018). Lhcb3 is a structurally important component of the M trimer (Caffarri *et al.*, 2009; Su *et al.*, 2017), as it can interact with Lhcb6, one of the minor antenna proteins. Lhcb6, together with Lhcb4, plays a crucial role in the binding of M trimer to C_2 (Kovács *et al.*, 2006; de Bianchi *et al.*, 2008, 2011).

In plants grown under optimal light conditions, the most abundant form of PSII is the $C_2S_2M_2$ supercomplex, containing two strongly and two moderately bound trimers (Kouřil *et al.*, 2013). Namely in plants grown under high light conditions, the size of the supercomplex can be reduced to C_2S_2, the smallest physiologically relevant form of PSII that binds just two S trimers (Morosinotto *et al.*, 2006; Ballottari *et al.*, 2007; Kouřil *et al.*, 2013; Albanese *et al.*, 2016). On the other hand, the $C_2S_2M_2$ supercomplex can be occasionally further extended by the presence of an L trimer; however, the $C_2S_2M_2L_{1-2}$ supercomplexes are very rare. Up to today, they have been found only in spinach and only as a very minor fraction of all supercomplexes (Boekema *et al.*, 1999a,b). Recently, an additional LHCII trimer was found to be associated with $C_2S_2M_2$ in Arabidopsis as well, but in a different position than in spinach and only as a part of PSII megacomplexes (Nosek *et al.*, 2017).

Our understanding of the assembly and structure of plant PSII supercomplexes has significantly increased during the last 10 years. High-resolution structures uncovered details of subunit positions and arrangement of pigment molecules, which are crucial for the identification of possible energy transfer pathways within the PSII supercomplex (Caffarri *et al.*, 2009; Wei *et al.*, 2016; van Bezouwen *et al.*, 2017; Su *et al.*, 2017). At the same time, the generally accepted hypothesis that the architecture of the PSII supercomplex is uniform in land plants has been recently disproved by our work showing the surprising absence of Lhcb3 and Lhcb6 proteins in some gymnosperm genera (Kouřil *et al.*, 2016). The lack of these proteins, which had been considered as essential components of LHCII in all land plants, has apparent consequences for the structure of PSII supercomplex in these species, including Norway spruce (*Picea abies*; Kouřil *et al.*, 2016).

Structural analysis of PSII supercomplex from spruce provided direct evidence that the M trimer (or rather the pseudo-M trimer without Lhcb3) can bind to C_2 even in the absence of Lhcb6 (Kouřil *et al.*, 2016). However, the absence of Lhcb3 and Lhcb6 changes the orientation of the M trimer with respect to the C_2 core, and this unique position of the M trimer has never been observed in any other land plant species. Interestingly, the orientation of the M trimer in spruce is similar to the position of the M trimer

in the PSII supercomplex from the green alga *Chlamydomonas reinhardtii* (Kouřil *et al.*, 2016). Compared with spruce, however, the PSII supercomplexes from *C. reinhardtii* are larger, because they contain two additional LHCII trimers and form $C_2S_2M_2N_2$ supercomplexes (Tokutsu *et al.*, 2012; Drop *et al.*, 2014; Shen *et al.*, 2019; Sheng *et al.*, 2019). The two additional trimers attached to the $C_2S_2M_2$ in the alga were designated as N (naked) trimers, because – unlike S and M trimers – they bind directly to C_2 core without the involvement of any monomeric antenna (Drop *et al.*, 2014). Actually, the N trimers bind to C_2 at the position that is in land plants occupied by Lhcb6 (CP24; Drop *et al.*, 2014). Therefore, as the absence of Lhcb6 seems to be a prerequisite of the binding of this additional trimer, it is reasonable to ask whether the N trimer can be found in the spruce PSII supercomplex as well.

Plant PSII supercomplexes exhibit variability not only in their composition and structure, but they can also form variable higher order structures in the thylakoid membrane. Neighboring individual supercomplexes can interact with each other, forming so-called PSII megacomplexes, which can be isolated from thylakoid membranes using mild solubilization conditions. Different types of interactions then result in different long-distance arrangement of supercomplexes within the thylakoids (Kirchhoff *et al.*, 2004, 2008; Nosek *et al.*, 2017). Random PSII organization, as well as highly ordered (crystalline) arrays of PSII, have been observed, each characterized by different interactions between the supercomplexes (for reviews, see Kouřil *et al.*, 2012; Kirchhoff, 2013). Structural analysis revealed that pairs of neighboring PSII supercomplexes can interact in two ways. The first one involves interaction between stromal sides of PSII supercomplexes located in two adjacent grana membranes (Daum *et al.*, 2010; Albanese *et al.*, 2016, 2017; Su *et al.*, 2017), the second one takes place in the membrane plane and is mediated by the interaction between LHCII and C_2 (Nosek *et al.*, 2017). The physiological relevance of the formation of PSII megacomplexes *in vivo* was supported by their identification on the level of the thylakoid membrane (Daum *et al.*, 2010; Nosek *et al.*, 2017).

In the present work, we study the consequences of the loss of Lhcb3 and Lhcb6 proteins for the organization of PSII supercomplexes and megacomplexes in Norway spruce. As the spruce $C_2S_2M_2$ supercomplex shares some structural features with the PSII supercomplex from *C. reinhardtii*, we focused on the question whether the additional N trimers typical for this alga could attach also to spruce PSII supercomplex. As we have shown, the absence of the Lhcb6 and Lhcb3 proteins also results in a loss of a rectangular shape of the $C_2S_2M_2$ supercomplex, which is typical for other land plants (Kouřil *et al.*, 2016). We were thus interested in how the modified shape of spruce

supercomplexes affects their ability to form megacomplexes and higher order assemblies in thylakoid membranes.

RESULTS

Separation of large spruce PSII assemblies

A necessary prerequisite of our search for larger assemblies of PSII complexes in Norway spruce was the optimization of the solubilization and separation protocols. The solubilization was achieved using detergent α-DDM, which is milder than β-DDM used in our previous study (Kouřil *et al.*, 2016). The concentration of α-DDM was optimized to maximize the yield of high-molecular-mass bands (PSII megacomplexes and larger PSII supercomplexes) in clear native−polyacrylamide gel electrophoresis (CN−PAGE). Interestingly, the optimal detergent: chlorophyll ratio (w/w) for spruce appeared to be 50, whereas similar optimization performed for separation of larger PSII assemblies from *Arabidopsis thaliana* led to a ratio of 20 (Nosek *et al.*, 2017). Therefore, the solubilization protocol is not universal and should be optimized for each plant species separately.

Figure 1 shows a typical separation profile of mildly solubilized thylakoid membranes from Norway spruce using CN−PAGE. Most PSII supercomplexes were separated into three dense bands in the central part of the gel. They differed in their antenna size and were assigned as the $C_2S_2M_2$, C_2S_2M and C_2S_2 supercomplexes, in analogy with our previous paper (Kouřil *et al.*, 2016). The use of mild detergent α-DDM and optimized solubilization conditions allowed us to observe two additional high-molecular-weight bands in the upper part of the gel (the bands I and II; Figure 1). These bands contain larger PSII supercomplexes and megacomplexes, as mass spectrometry (MS) analysis revealed a high abundance of the proteins related

to PSII and LHCII in these bands (Table S1). Both bands were excised from the gel, protein content was extracted by spontaneous elution and the obtained protein solution was subjected to structural analysis by single-particle electron microscopy.

Structural characterization of PSII supercomplexes

Image analysis of particle projections selected from electron micrographs revealed that PSII supercomplexes are present in both high-molecular-weight CN−PAGE bands (the bands I and II; Figure 1). Although various forms of large supercomplexes were found predominantly in band I, the largest PSII supercomplexes were so big that they co-migrated with PSII megacomplexes in band II.

Single-particle analysis of the samples prepared from band I resulted in the selection of 163 447 particle projections that were subsequently classified into 80 classes (Figure S1). In addition to the standard spruce $C_2S_2M_2$ supercomplex, where the core complex C_2 binds four LHCII trimers (Figure 2a), we observed novel types of PSII supercomplexes with up to six LHCII trimers (Figure 2b,c,g,h). The identified forms of PSII supercomplexes (Figure S1) differ significantly in their size, although they were obtained from the same highly focused band after CN−PAGE. Thus, it is probable that the smaller supercomplexes in Figure S1 (e.g. C_2S_2) are degradation products of the larger supercomplexes, which disintegrated during the elution of supercomplexes from the gel and/or during the preparation of samples for electron microscopy.

The samples obtained from band II (Figure 1) contained mainly PSII megacomplexes (Figure S2, detailed analysis follows), but a substantial part of the dataset contained various types of PSII supercomplexes. Except for several smaller PSII supercomplexes (C_2S_2, C_2S_2M and $C_2S_2M_2$), which probably originate from the break-up of less stable megacomplexes during the elution step and/or the specimen preparation, we observed very unique very large PSII supercomplexes that contain up to seven−eight LHCII trimers (Figure 2d–f), and have not been observed in any other plant species yet.

To examine the architecture of the large PSII supercomplexes and especially to analyze novel binding positions of LHCII trimers in detail, we fitted the electron microscopy projection maps with a recent molecular model of the PSII supercomplex (van Bezouwen *et al.*, 2017). Structural models show the organization of LHCII trimers within the supercomplexes (Figure 2i–p). In addition to the standard S and M trimers (Figure 2i), in some supercomplexes we were able to identify the N trimers, typical for supercomplexes from *C. reinhardtii* (Figure 2j,l–p). The orientation of the N trimer with respect to C_2 core was determined in the best-resolved projection map of the $C_2S_2M_2N$ supercomplex (Figure 2b,j), and this orientation seems to be the same in all other supercomplexes but one (Figure 2l–o).

Figure 1. Separation of photosystem II (PSII) supercomplexes and megacomplexes from Norway spruce using clear native−polyacrylamide gel electrophoresis (CN−PAGE).

Isolated thylakoid membranes were mildly solubilized by *n*-dodecyl α-D-maltoside. The red and blue asterisks (the bands I and II) indicate the high-molecular-weight bands containing large PSII supercomplexes and megacomplexes, which were subjected to structural analysis by single-particle electron microscopy. The bands of lower molecular weight represent different forms of PSII supercomplexes, PSI complex and PSII core complex, and LHCII proteins, respectively.

Figure 2. The large photosystem II (PSII) supercomplexes from Norway spruce.

The supercomplexes were eluted from the band I (a–c, g, h) and the band II (d–f) in Figure 1. Projection maps of individual types of the PSII supercomplexes represent the best class averages of: (a) 12 015; (b) 9847; (c) 6356; (d) 622; (e) 1298; (f) 1018; (g) 1554; (h) 1219 particles.

(i–p) Structural models of PSII supercomplexes were obtained by a fit of the high-resolution structure (van Bezouwen *et al.*, 2017). Individual PSII subunits are color-coded: dark green – core complex; yellow – S trimer; cyan – M trimer; red – N trimer; green – L trimer; magenta – Lhcb5; orange – Lhcb4.

The exception is the C_2S_2MN supercomplex (Figure 2p), where the orientation of the N trimer is different, probably due to the absence of the M trimer in the vicinity of the N trimer. Our analysis also revealed the presence of the L trimer in some of the supercomplexes (Figure 2m,o), and we were even able to see supercomplexes where there was a row of four LHCII trimers (S, M, N and L) around one side of the PSII core complex (Figure 2m,o). Moreover, our data show that the spruce PSII supercomplex has a unique ability to extend the antenna size even more by binding additional LHCII trimers. These trimers, which we term as the L_a trimers (additional loosely bound trimers), bind to the supercomplexes at different positions via the S, M, N and L trimers, and form the second row of LHCII trimers around the PSII core complex (Figure 2k–n).

To investigate whether the presence of larger PSII supercomplexes is a unique feature of Norway spruce or whether these structures can be found also in other members of the Pinaceae family (lacking the Lhcb3 and Lhcb6 proteins), we performed an analogical structural analysis of PSII supercomplexes isolated from Scots pine (*Pinus sylvestris*; Figure S3). Single-particle image analysis revealed several larger forms of pine PSII supercomplexes (Figure S4a–f), which were identical to their counterparts

in spruce (Figure 2a–d,h). This finding indicates that the unique ability to form larger antenna around the PSII core complex is likely a general property of the species from the Pinaceae family.

Structural characterization of PSII megacomplexes

The inspection of electron micrographs of the sample prepared from the high-molecular-weight band depicted as band II (Figure 1) resulted in the selection of 66 650 particle projections, which were subjected to image analysis and classification into 64 classes (Figure S2). Visual analysis of the classification file (Figure S2) allowed us to estimate that the PSII megacomplexes account for about 30% of the whole dataset. Approximately half of the dataset contained various types of PSII supercomplexes (see above). The rest of the structures (about 20%) in Figure S2 contained other types of unspecific protein complexes (e.g. dimers/monomers of ATP synthase), which co-migrated with the PSII megacomplexes in the gel.

Figure 3 shows the best-resolved classes of PSII megacomplexes. Each megacomplex consists of two copies of PSII supercomplexes, which associate with each other through their antenna complexes. Based on the orientation of PSII cores, the associations of the pairs of PSII

Figure 3. Various photosystem II (PSII) megacomplexes from Norway spruce.

The megacomplexes were eluted from the band II (Figure 1). Projection maps of individual types of the PSII megacomplexes represent the best class averages of: (a) 1549; (b) 3118; (c) 1095; (d) 724; (e) 1178; (f) 915; (g) 1103 particles.

(h–n) Structural models of the PSII megacomplexes obtained by a fit of the high-resolution structure of PSII (van Bezouwen *et al.*, 2017). Individual PSII subunits are color-coded: dark green – core complex; yellow – S trimer; cyan – M trimer; green – L trimer; magenta – Lhcb5; orange – Lhcb4.
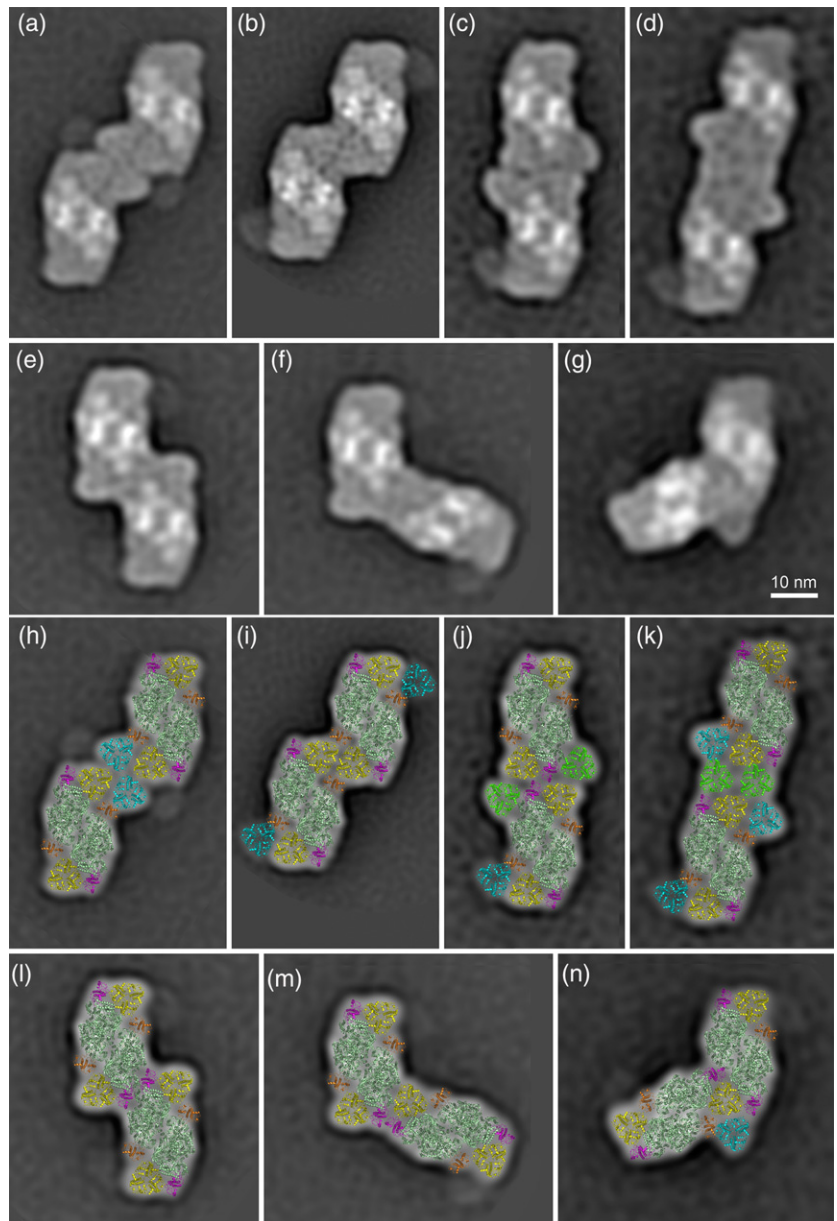
supercomplexes were either parallel (Figure 3a–e) or non-parallel (Figure 3f,g). The parallel associations were more abundant (70%) than the non-parallel ones (30%).

Structural models of the projection maps of the PSII megacomplexes show that the megacomplexes are formed by variable interactions between $C_2S_2M_2$ (Figure 3k), C_2S_2M (Figure 3h–k) and C_2S_2 (Figure 3j,l,m) supercomplexes. In some cases, PSII megacomplexes are formed with the help of the additional L trimers (Figure 3j,k). A closer view at the models of the identified megacomplexes (Figure 3) shows that the S trimer is most frequently involved in the megacomplex formation. Thus, the S trimer mediates probably the strongest binding between PSII supercomplexes within the PSII megacomplexes. However,

also other subunits were found to participate in the association of supercomplexes into megacomplexes – Lhcb5 (CP26), Lhcb4 (CP29), C_2, L and M trimers (in order of decreasing importance). Similar forms of PSII megacomplexes were also observed in Scots pine (Figure S4g–i).

Interaction between PSII complexes in grana membranes

Isolated grana membranes were analyzed using electron microscopy in order to characterize the organization and interaction between the neighboring PSII supercomplexes in the membrane. Visual screening of the electron micrographs revealed a random distribution of PSII complexes in the grana membranes (Figure 4a). The organization of PSII complexes into 2D crystalline arrays was not observed

in analyzed micrographs, which is somewhat surprising as the array formation is quite common in other plant species (Kouřil *et al.*, 2012). In order to confirm the physiological relevance of the PSII megacomplexes, which were observed after CN−PAGE separation, we investigated specific interactions between individual PSII complexes in the grana membranes. Indeed, image analysis of the PSII projections revealed several conserved mutual positions of PSII core complexes (Figure 4b). These pairs can be considered as PSII megacomplexes as the projection maps can be fitted with the model of the $C_2S_2M_2$ supercomplex with tight interactions between the LHCII trimers or PSII core complexes (Figure 4c).

DISCUSSION

Structural characterization of large spruce PSII supercomplexes

Our previous study showed that the absence of Lhcb6 and Lhcb3 in the PSII complex of spruce results in a specific assembly of $C_2S_2M_2$, which has never been found in land plants before (Kouřil *et al.*, 2016). Here we show that the unique organization of the $C_2S_2M_2$ supercomplex seems to be characteristic for the Pinaceae family, as we have found the identical architecture of this supercomplex also in Scots pine (Figure S4a). This unique organization of the PSII supercomplex brought several questions about the possible consequences for the attachment of additional LHCII trimers and the formation of larger super- and megacomplexes.

As the spruce PSII supercomplex shares some features with PSII supercomplex in *C. reinhardtii* (Kouřil *et al.*, 2016), the first hypothesis we wanted to verify was whether the spruce $C_2S_2M_2$ supercomplex is able to bind additional LHCII trimer (N trimer) in the same way as *C. reinhardtii* (Tokutsu *et al.*, 2012; Drop *et al.*, 2014; Shen *et al.*, 2019; Sheng *et al.*, 2019). The outcome of single-particle analysis unequivocally confirmed that the $C_2S_2M_2$ supercomplex is indeed able to bind the N trimer; however, its precise orientation depends on the presence of the M trimer. In supercomplexes where both the N and M trimers are present (Figure 2j,l–o), the N trimer is rotated clockwise by 63° compared with *C. reinhardtii*. This rotation could be most probably explained by the differences in the structure of the M and N trimers themselves. While the LHCII trimers in Norway spruce are formed by Lhcb1 and Lhcb2 proteins (Kouřil *et al.*, 2016) with possible involvement of Lhcb5 (Grebe *et al.*, 2019), the LHCII trimers in *C. reinhardtii* are formed by Lhcbm1/2/3/6/7 proteins (Drop *et al.*, 2014; Shen *et al.*, 2019). In Scots pine, the orientation of the N trimer in PSII supercomplexes is the same as in spruce (Figure S4b,e). Interestingly, in both spruce and pine, we have also found supercomplex where the N trimer is bound to the PSII core without the presence

of the M trimer (Figures 2p and S4f, respectively). In this case, the N trimer binds to the PSII core complex in the same orientation as in *C. reinhardtii* (Figure 5). This finding indicates that the mutual interaction between the M and N trimer determines the orientation of the N trimer in PSII supercomplexes in Pinaceae. However, due to the lack of high-resolution structural details of the spruce and pine PSII supercomplexes, we cannot exclude the possibility that some PSII core subunits are involved in the binding of the N trimer – namely PsbH and PsbX, which are involved in the binding of the N trimer in *C. reinhardtii* (Shen *et al.*, 2019; Sheng *et al.*, 2019). A high-resolution cryo-electron microscopy structure of spruce/pine supercomplex will be necessary to unequivocally resolve this question.

The optimization of the separation procedure allowed us not only to find supercomplexes with attached N trimer, but also PSII supercomplexes that are even larger than the $C_2S_2M_2N$. In some of these supercomplexes from Norway spruce, another LHCII trimer binds in the vicinity of the N trimer (Figure 2m,o). As the position of this trimer is similar to the position of the L trimer observed in the very small fraction of isolated PSII supercomplexes from spinach (Boekema *et al.*, 1999a,b; see also Figure 5), we tentatively named it as the L trimer. Such a large PSII supercomplex with four LHCII trimers (S, M, N, L) bound around the PSII core has never been found in any plant species so far. There are some indications that this structure might exist in *C. reinhardtii*, as Kawakami *et al.* (2019) recently found that there are four types of LHCII trimers in *C. reinhardtii*. Nevertheless, their work was based on biochemical methods, and the attachment of the L trimer to the $C_2S_2M_2N_{1-2}$ supercomplex in *C. reinhardtii* is yet to be confirmed experimentally. It is possible that the difference in the orientation of the N trimer in spruce and in *C. reinhardtii* affects the strength of the binding of the L trimer, making it more labile and thus more prone to dissociation in the latter.

Surprisingly, we have found out that even the large PSII supercomplex with attached S, M, N and L trimers is not the largest one that could be found in spruce. Our structural analysis revealed for the first time that the PSII supercomplex is able to bind LHCII trimers in two rows. The LHCII trimers of the second (outer) row, which we named L_a (additional L) trimers, can bind to PSII at five specific positions along the inner row of the S, M, N and L trimers. The largest spruce PSII supercomplex identified in our study binds seven or eight LHCII trimers (Figure 2l–n), which exceeds the antenna size of $C_2S_2M_2N_2$ supercomplex in *C. reinhardtii*, currently considered to be the largest known PSII supercomplex. Considering the twofold symmetry of the PSII supercomplex, we can hypothesize that the most complete spruce PSII supercomplex would have the ability to bind up to 18 LHCII trimers (Figure 5). The hypothetical model can be applied also for Scots pine,

Figure 4. Distribution of photosystem II (PSII) complexes and their association into megacomplexes in isolated grana membranes.

(a) An example of the electron micrograph of negatively stained grana membranes isolated from Norway spruce showing a density and distribution of PSII complexes. White arrow indicates a typical density of the PSII core complex.

(b) Most abundant associations of PSII complexes into different types of megacomplexes found within the grana membranes after image analysis.

(c) Structural models of the PSII megacomplexes obtained by a fit of the high-resolution structure (van Bezouwen *et al.*, 2017). Individual PSII subunits are color-coded: dark green – core complex; yellow – S trimer; cyan – M trimer; magenta – Lhcb5; orange – Lhcb4.
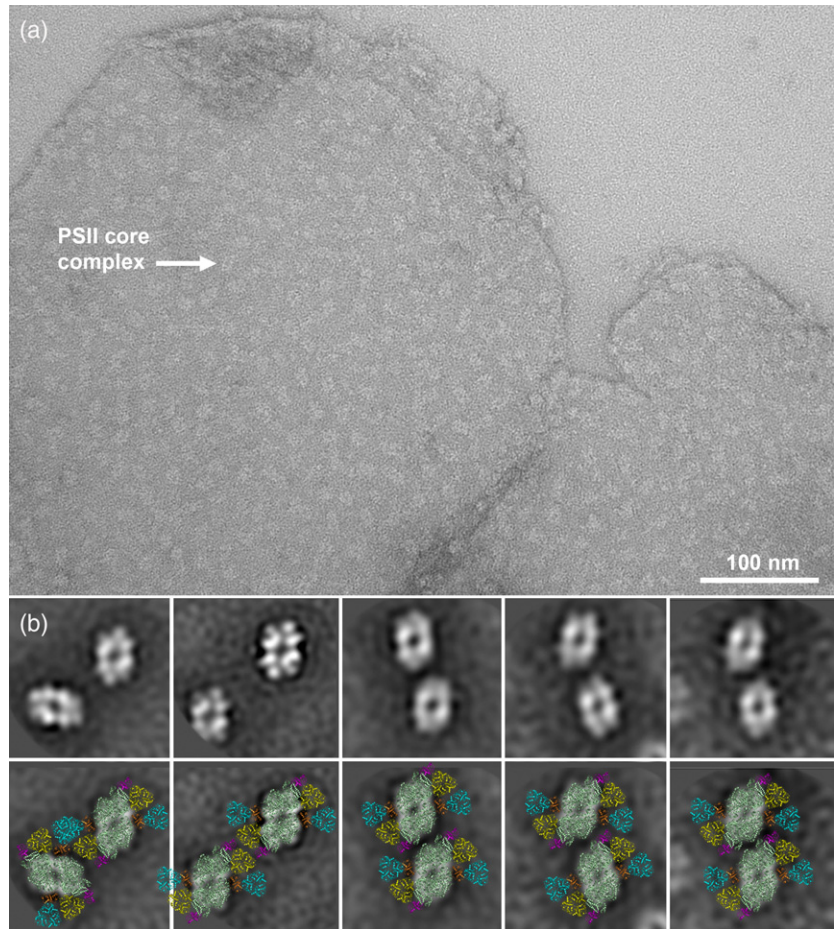
where the largest identified form of the PSII supercomplex binds seven LHCII trimers (Figure S4e). Interestingly, the antenna organization in this large PSII supercomplex would still keep free the path for plastoquinone to the acceptor sites in the PSII core complex (van Eerden *et al.*, 2017), which gives the hypothetical model a physiological relevance.

Structural characterization of spruce PSII megacomplexes

It is well known that plant PSII supercomplexes can further associate into larger assemblies, forming PSII megacomplexes. Our work shows that the species from Pinaceae family are no exception. Single-particle electron microscopy analysis revealed several distinct types of spruce and pine PSII megacomplexes, which were formed either by parallel or non-parallel associations between two PSII supercomplexes (Figures 3 and S4g–i). The main distinctive feature of the spruce and pine PSII megacomplexes, when compared with those from Arabidopsis (Nosek *et al.*, 2017), is their lower structural variability. While we found only seven types of megacomplexes in spruce and three in pine, their number in Arabidopsis was significantly higher (13; Nosek *et al.*, 2017). This finding can be simply

explained by the lower stability of PSII megacomplexes in Pinaceae. This explanation is supported, for example, by our finding that during the image analysis of the sample from the high-molecular-weight band II (Figure 1), we have observed classes of the C_2S_2, C_2S_2M and $C_2S_2M_2$ PSII supercomplexes, which are the building blocks of the megacomplexes (Figure S2). As these supercomplexes cannot co-migrate in the gel with megacomplexes, which have roughly twice the size and weight, the only feasible explanation of the presence of these supercomplexes in this sample is that they originate from the break-up of megacomplexes during the elution step and specimen preparation for electron microscopy.

In our previous study with Arabidopsis, we have successfully identified some forms of megacomplexes also on the level of the thylakoid membrane (Nosek *et al.*, 2017), and therefore we have employed this approach also for spruce. Image analysis of the PSII distribution in thylakoid membranes from spruce revealed five well-resolved specific associations between the adjacent PSII supercomplexes (Figure 4b,c), which strongly indicates that PSII megacomplexes in spruce exist *in vivo*. The proposed structural models of these megacomplexes show that they can be
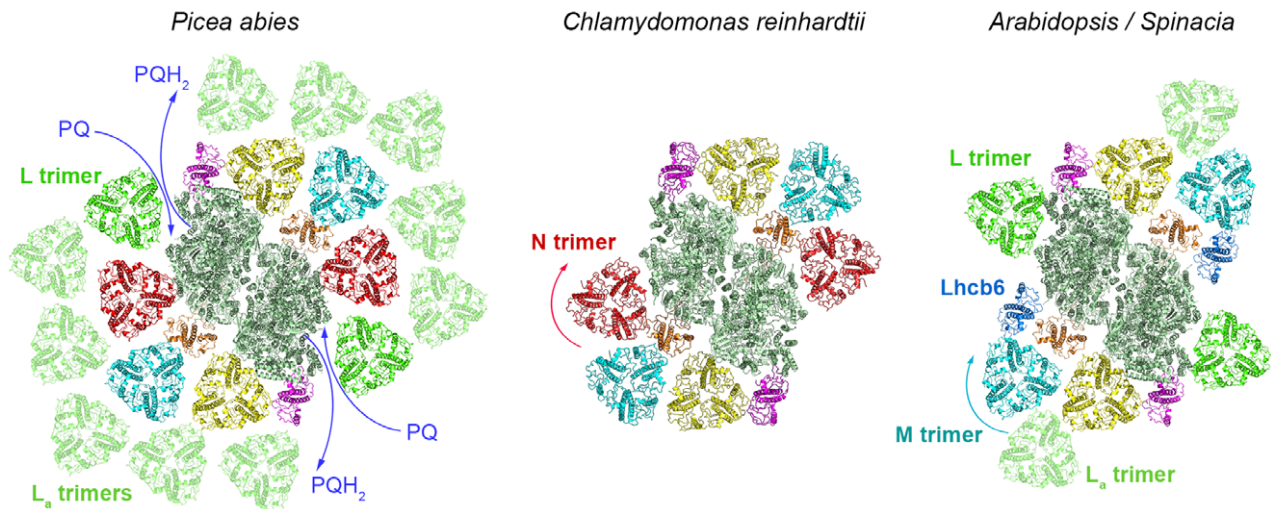
Figure 5. A hypothetical model of photosystem II (PSII) supercomplex from Norway spruce (*Picea abies*) and its comparison with evolutionary different organisms.

The model of the complete PSII supercomplex in Norway spruce is based on the structures of different forms of PSII supercomplexes revealed by single-particle electron microscopy. The specific orientation of the N trimer in Norway spruce probably enables a stable binding of the L trimer and formation of the second row of additional L$_a$ trimers along the PSII core complex, but still keeps the path for plastoquinone molecules free. Different orientation of the N trimer in *Chlamydomonas reinhardtii* (Shen *et al.*, 2019) likely does not support the binding of the L trimer. In the majority of land plants, the binding site for the N trimer is occupied by the Lhcb6 protein, which probably modifies the binding of the M trimer. The L trimer can very occasionally bind to the PSII core complex (e.g. in spinach; Boekema *et al.*, 1999a,b) or additional L$_a$ trimers can associate with PSII at the site of the S/M trimers (e.g. Arabidopsis; Nosek *et al.*, 2017). Individual PSII subunits are color-coded: dark green – core complex; yellow – S trimer; cyan – M trimer; red – N trimer; green – L trimer; light green – L$_a$ trimers; magenta – Lhcb5; orange – Lhcb4.

formed, for example, by $C_2S_2M_2$ supercomplexes (Figure 4c), but we cannot exclude the involvement of even larger forms of the PSII supercomplexes. Three types of the megacomplexes represent an almost parallel association of the PSII supercomplexes along the core complex, which is similar to the megacomplex formations observed in Arabidopsis (Nosek *et al.*, 2017).

It is, however, important to note that - unlike in Arabidopsis (Nosek *et al.*, 2017) – in spruce the PSII associations observed in thylakoid membranes do not correspond to any spruce PSII megacomplexes that we were able to isolate and separate. The interactions between the neighboring PSII supercomplexes in the membrane seem to be too weak to keep the megacomplexes intact during the separation procedure and/or specimen preparation for electron microscopy analysis. Thus, it is likely that the separated PSII megacomplexes (Figure 3) represent the most stable megacomplex forms, but they do not represent the most frequent type of megacomplexes found in the thylakoid membrane.

We assume that the lower stability of the bigger PSII megacomplexes could be closely related to the overall architecture of individual PSII supercomplexes. While a majority of the isolated spruce and pine megacomplexes are formed by pairs of smaller forms of PSII supercomplexes (C_2S_2 or C_2S_2M; Figures 3 and S4g–i), in Arabidopsis the megacomplexes are formed by the larger, $C_2S_2M_2$, supercomplexes. Considering a different shape of the

$C_2S_2M_2$ supercomplexes in spruce and Arabidopsis (Figure 5), it becomes obvious that the rectangular shape of the $C_2S_2M_2$ in Arabidopsis can provide more stable interaction between adjacent supercomplexes. Indeed, a majority of the Arabidopsis megacomplexes were formed by parallel associations of two PSII supercomplexes along their longer sides, which probably represents a relatively stable configuration. The shape of the $C_2S_2M_2$ supercomplex in Pinaceae, modified by the absence of Lhcb3 and Lhcb6 proteins (Kouřil *et al.*, 2016), cannot provide the same interaction interface, which could potentially explain the lower stability of the PSII megacomplexes.

In summary, the structural analysis of PSII from two species from the Pinaceae family, Norway spruce and Scots pine, further extended our knowledge about the architecture of PSII supercomplexes. Our results clearly show that there are more binding sites for LHCII trimers than it was originally thought. We suggest that the evolutionary loss of Lhcb6 in Pinaceae resulted in the ability of PSII core to bind the N trimer as in the case of green alga *C. reinhardtii* (Figure 5). A unique orientation of the N trimer in Pinaceae probably supports the binding of the L trimer and additional L$_a$ trimers, thus leading to the formation of larger PSII supercomplexes. A different orientation of the N trimer in *C. reinhardtii* or the absence of the N trimer in other land plant species (e.g. Arabidopsis, spinach) likely results in a loose binding of the L trimer to the PSII core (Figure 5).

The interesting question to answer is what environmental conditions would lead to a formation of such giant PSII supercomplexes, hypothetically up to the $C_2S_2M_2N_2L_2L_{a10}$ supercomplex. Formation of these giant supercomplexes would require LHCII trimers to be in great excess of PSII core complexes. Acclimation of land plants to low light intensity is well known to induce a higher LHCII/PSII core ratio (Bailey *et al.*, 2001; Ballottari *et al.*, 2007; Kouřil *et al.*, 2013); however, for example Norway spruce does not follow this strategy, as the antenna size remains almost unchanged during acclimation (Kurasová *et al.*, 2003; Štroch *et al.*, 2008). Nevertheless, there are indications that the acclimation of conifers to winter conditions can lead to the enhanced LHCII/PSII core ratio (Verhoeven, 2014), which may create favorable conditions for the formation of large PSII supercomplexes.

EXPERIMENTAL PROCEDURES

Plant material and isolation of PSII megacomplexes and supercomplexes

Norway spruce [*Picea abies* (L.) Karst.] and Scots pine [*Pinus sylvestris* (L.); Semenoles, Liptovský Hrádok, Slovakia] seedlings were grown in a growth chamber with 16 h: 8 h, light: dark photoperiod at 21°C for 4 weeks. Plants were illuminated with white light at 100 µmol photons m^{-2} sec^{-1} (400–700 nm). Isolation of thylakoid membranes and electrophoretic separation of solubilized membranes using CN−PAGE were performed according to a protocol described by Nosek *et al.* (2017) with one modification in the solubilization condition, that is spruce and pine thylakoid membranes with 10 µg of chlorophylls were solubilized with *n*-dodecyl α-D-maltoside (α-DDM) using a detergent: chlorophyll mass ratio of 50.

Spruce PSII membranes were isolated using mild solubilization of thylakoid membranes with digitonin (0.5 mg of chlorophylls per ml and 0.5% digitonin) in a buffer containing 20 mM HEPES, pH 7.5, 5 mM $MgCl_2$ and 15 mM NaCl. Solubilization was performed for 20 min at 4°C with slow stirring, and was followed by centrifugation (5 min, 12 000 *g*, 4°C). The pellet with the non-solubilized PSII grana membranes was washed twice with the buffer mentioned above, spun down again for 5 min (12 000 *g*, 4°C) and then used for electron microscopy analysis.

Single-particle electron microscopy and image analysis

The PSII megacomplexes and supercomplexes were eluted from excised CN−PAGE gel bands according to Kouřil *et al.* (2014). Obtained protein solutions were directly used for electron microscopy specimen preparations by negative staining with 2% uranyl acetate on glow-discharged carbon-coated copper grids. Electron microscopy of spruce PSII supercomplexes and megacomplexes was performed on a Tecnai G2 F20 microscope (FEI) equipped with a LaB$_6$ cathode, operated at 200 kV. Images were recorded with an UltraScan 4000 UHS CCD camera (Gatan, Pleasanton, CA, USA) at 130 000 × magnification with a pixel size of 0.224 nm at the specimen level after binning the images to 2048 × 2048 pixels. GRACE software (Oostergetel *et al.*, 1998) was used for semi-automated acquisition of 14 000 and 11 000 images of PSII complexes eluted from the bands I and II, respectively, and two datasets of approx. 163 447 (band I) and 66 650 (band II) single-particle

projections were selected and subjected to several rounds of single-particle image analysis and classification (Boekema *et al.*, 2009) using RELION software (Scheres, 2012) and reference-free 2D classification using SCIPION image processing framework (De La Rosa-Trevín *et al.*, 2016). Pseudo-atomic models of obtained PSII projection maps were created using PYMOL (DeLano, 2002).

Electron microscopy of isolated grana membranes from Norway spruce and eluted PSII megacomplexes and supercomplexes from Scots pine was performed on a Tecnai G2 F20 microscope (FEI) equipped with a field emission gun operated at 200 kV. Images were recorded with an Eagle 4K CCD camera (FEI) at 83 000 × magnification with a pixel size of 0.36 nm (spruce grana membrane), and at 130 000 × magnification with a pixel size of 0.226 nm (pine PSII super-/megacomplexes) at the specimen level after binning the images to 2048 × 2048 pixels. In total, 150 micrographs were recorded and about 13 000 manually selected projections of PSII particles were analyzed using RELION software (Scheres, 2012) to reveal the specific formation of PSII megacomplexes in the spruce grana membrane. Two datasets of approx. 73 000 and 310 000 single-particle projections were selected from 8000 and 7000 electron micrographs of pine PSII megacomplexes and PSII supercomplexes, respectively, and analyzed using reference-free 2D classification using SCIPION image processing framework (de la Rosa-Trevín *et al.*, 2016).

Proteomic characterization of spruce PSII supercomplexes and megacomplexes

The electroeluted PSII super- and megacomplexes were first concentrated and transferred to a denaturing buffer using a centrifugal filter unit with 3K cut-off. Next, in-solution protein digestion was performed with commercially available trypsin, as described previously (León *et al.*, 2013). The tryptic peptides were desalted and fractionated with the use of a custom reversed-phase (C18) microcolumn (Franc *et al.*, 2012) and subsequently analyzed by LC-MS (Simerský *et al.*, 2017). The acquired MS data were searched against *P. abies*-specific protein database (Grebe *et al.*, 2019) employing MaxQuant software v.1.6.10.43 (Beck *et al.*, 2015; Tyanova *et al.*, 2016) with Andromeda search engine (Cox *et al.*, 2011). To evaluate the abundances of the identified proteins, the well-established iBAQ method (Schwanhäusser *et al.*, 2011) was applied. Missing protein annotations were assigned by pBLAST homology searches. Details for all described methods can be found in the Supporting Information (Methods S1).

AUTHOR CONTRIBUTIONS

RK, LN, PI planned and designed the research. RK, LN, MO, RA, DS, IC, RL performed experiments. RK, LN, MO, RA, DS, IC, R.L., EJB and PI analyzed the data. RK and PI wrote the manuscript, and all authors revised and approved it.

CONFLICT OF INTEREST

The authors have no conflict of interest to declare.

DATA AVAILABILITY STATEMENT

All relevant data can be found within the manuscript and its supporting materials. The mass spectrometry proteomics data have been deposited to the ProteomeXchange Consortium via the PRIDE (Perez-Riverol *et al.*, 2019) partner repository with the dataset identifier PXD020138.

SUPPORTING INFORMATION

Additional Supporting Information may be found in the online version of this article.

Figure S1. Single-particle image analysis and classification of PSII supercomplexes from Norway spruce extracted from CN−PAGE band I.

Figure S2. Single-particle image analysis and classification of PSII supercomplexes and megacomplexes from Norway spruce extracted from CN−PAGE band II.

Figure S3. Separation of pigment−protein complexes from Scots pine using CN−PAGE.

Figure S4. Structural characterization of PSII supercomplexes and megacomplexes from Scots pine.

Data S1. Complete protein identification data and other files containing information related to protein identification as exported from MaxQuant software v. 1.6.10.43.

Table S1. An overview of protein composition of the PSII supercomplex and megacomplex bands (CN−PAGE bands I and II).

Table S2. A list of all identified proteins from CN−PAGE bands I and II with corresponding characteristics and annotations.

Methods S1. Proteomic characterization of Norway spruce PSII supercomplexes and megacomplexes.

REFERENCES

Albanese, P., Nield, J., Tabares, J.A.M., Chiodoni, A., Manfredi, M., Gosetti, F., Marengo, E., Saracco, G., Barber, J. and Pagliano, C. (2016) Isolation of novel PSII-LHCII megacomplexes from pea plants characterized by a combination of proteomics and electron microscopy. *Photosynth. Res.* **130**, 19–31.

Albanese, P., Melero, R., Engel, B.D. *et al*. (2017) Pea PSII-LHCII supercomplexes form pairs by making connections across the stromal gap. *Sci. Rep.* **7**, 10067.

Ballottari, M., Dall'Osto, L., Morosinotto, T. and Bassi, R. (2007) Contrasting behavior of higher plant photosystem I and II antenna systems during acclimation. *J. Biol. Chem.* **282**, 8947–8958.

Barber, J. (2003) Photosystem II: the engine of life. *Q. Rev. Biophys.* **36**, 71–89.

Bailey, S., Walters, R.G., Jansson, S. and Horton, P. (2001) Acclimation of *Arabidopsis thaliana* to the light environment: the existence of separate low light and high light responses. *Planta*, **213**, 794–801.

Beck, S., Michalski, A., Raether, O. *et al*. (2015) The impact II, a very high-resolution Quadrupole Time-of-Flight Instrument (QTOF) for deep shotgun proteomics. *Mol. Cell. Proteomics*, **14**, 2014–2029.

Boekema, E.J., van Roon, H., Calkoen, F., Bassi, R. and Dekker, J.P. (1999a) Multiple types of association of photosystem II and its light-harvesting antenna in partially solubilized photosystem II membranes. *Biochemistry*, **38**, 2233–2239.

Boekema, E.J., van Roon, H., van Breemen, J.F.L. and Dekker, J.P. (1999b) Supramolecular organization of photosystem II and its light-harvesting antenna in partially solubilized photosystem II membranes. *Eur. J. Biochem.* **266**, 444–452.

Boekema, E.J., Folea, M. and Kouřil, R. (2009) Single particle electron microscopy. *Photosynth. Res.* **102**, 189–196.

Caffarri, S., Kouřil, R., Kereiche, S., Boekema, E.J. and Croce, R. (2009) Functional architecture of higher plant photosystem II supercomplexes. *EMBO J.* **28**, 3052–3063.

Caffarri, S., Croce, R., Cattivelli, L. and Bassi, R. (2004) A look within LHCII: Differential analysis of the Lhcbl-3 complexes building the major trimeric antenna complex of higher-plant photosynthesis. *Biochemistry*, **43**, 9467–9476.

Cox, J., Neuhauser, N., Michalski, A., Scheltema, R.A., Olsen, J.V. and Mann, M. (2011) Andromeda: a peptide search engine integrated into the MaxQuant environment. *J. Proteome Res.* **10**, 1794–1805.

Crepin, A. and Caffarri, S. (2018) Functions and evolution of Lhcb isoforms composing LHCII, the major light harvesting complex of photosystem II of green eukaryotic organisms. *Curr. Protein Pept. Sci.* **19**, 699–713.

Daum, B., Nicastro, D., Austin, J., McIntosh, J. and Kühlbrandt, W. (2010) Arrangement of photosystem II and ATP synthase in chloroplast membranes of spinach and pea. *Plant Cell*, **22**, 1299–1312.

de Bianchi, S., Dall'Osto, L., Tognon, G., Morosinotto, T. and Bassi, R. (2008) Minor antenna proteins CP24 and CP26 affect the interactions between photosystem II subunits and the electron transport rate in grana membranes of Arabidopsis. *Plant Cell*, **20**, 1012–1028.

DeLano, W.L. (2002) *The PyMOL Molecular Graphics System*. San Carlos, CA: DeLano Scientific.

de Bianchi, S., Betterle, N., Kouřil, R., Cazzaniga, S., Boekema, E., Bassi, R. and Dall'Osto, L. (2011) Arabidopsis mutants deleted in the light-harvesting protein Lhcb4 have a disrupted photosystem II macrostructure and are defective in photoprotection. *Plant Cell*, **23**, 2659–2679.

de la Rosa-Trevín, J.M., Quintana, A., Del Cano, L. *et al*. (2016) Scipion: a software framework toward integration, reproducibility and validation in 3D electron microscopy. *J. Struct. Biol.* **195**, 93–99.

Dekker, J.P. and Boekema, E.J. (2005) Supramolecular organization of thylakoid membrane proteins in green plants. *Biochim. Biophys. Acta*, **1706**, 12–39.

Drop, B., Webber-Birungi, M., Yadav, S.K., Filipowicz-Szymanska, A., Fusetti, F., Boekema, E.J. and Croce, R. (2014) Light-harvesting complex II (LHCII) and its supramolecular organization in *Chlamydomonas reinhardtii*. *Biochim. Biophys. Acta-Bioenergetics*, **1837**, 63–72.

Franc, V., Šebela, M., Řehulka, P., Končitíková, R., Lenobel, R., Madzak, C. and Kopečný, D. (2012) Analysis of N-glycosylation in maize cytokinin oxidase/dehydrogenase 1 using a manual microgradient chromatographic separation coupled offline to MALDI-TOF/TOF mass spectrometry. *J. Proteomics*, **75**, 4027–4037.

Grebe, S., Trotta, A., Bajwa, A.A., Suorsa, M., Gollan, P.J., Jansson, S., Tikkanen, M. and Aro, E.M. (2019) The unique photosynthetic apparatus of Pinaceae: analysis of photosynthetic complexes in *Picea abies*. *J. Exp. Bot.* **70**, 3211–3225.

Jansson, S. (1994) The light−harvesting chlorophyll a/b binding-proteins. *Biochim. Biophys. Acta*, **1184**, 1–19.

Kawakami, K., Tokutsu, R., Kim, E. and Minagawa, J. (2019) Four distinct trimeric forms of light-harvesting complex II isolated from the green alga *Chlamydomonas reinhardtii*. *Photosynth. Res.* **142**, 195–201.

Kirchhoff, H. (2013) Architectural switches in plant thylakoid membranes. *Photosynth. Res.* **116**, 481–487.

Kirchhoff, H., Tremmel, I., Haase, W. and Kubitscheck, U. (2004) Supramolecular photosystem II organization in grana thylakoid membranes: evidence for a structured arrangement. *Biochemistry*, **43**, 9204–9213.

Kirchhoff, H., Lenhert, S., Büchel, C., Chi, L. and Nield, J. (2008) Probing the organization of photosystem II in photosynthetic membranes by atomic force microscopy. *Biochemistry*, **47**, 431–440.

Kouřil, R., Dekker, J.P. and Boekema, E.J. (2012) Supramolecular organization of photosystem II in green plants. *Biochim. Biophys. Acta-Bioenergetics*, **1817**, 2–12.

Kouřil, R., Wientjes, E., Bultema, J.B., Croce, R. and Boekema, E.J. (2013) High-light vs. low-light: effect of light acclimation on photosystem II composition and organization in *Arabidopsis thaliana*. *Biochim. Biophys. Acta-Bioenergetics*, **1827**, 411–419.

Kouřil, R., Strouhal, O., Nosek, L., Lenobel, R., Chamrád, I., Boekema, E.J., Šebela, M. and Ilík, P. (2014) Structural characterization of a plant photosystem I and NAD(P)H dehydrogenase supercomplex. *Plant J.* **77**, 568–576.

Kouřil, R., Nosek, L., Bartoš, J., Boekema, E.J. and Ilík, P. (2016) Evolutionary loss of light-harvesting proteins Lhcb6 and Lhcb3 in major land plant groups - break-up of current dogma. *New Phytol.* **210**, 808–814.

Kouřil, R., Nosek, L., Semchonok, D., Boekema, E.J. and Ilík, P. (2018) Organization of plant photosystem II and photosystem I supercomplexes. *Subcell. Biochem.* **87**, 259–286.

Kovács, L., Damkjær, J., Kereïche, S., Ilioaia, C., Ruban, A.V., Boekema, E.J., Jansson, S. and Horton, P. (2006) Lack of the light-harvesting complex CP24 affects the structure and function of the grana membranes of higher plant chloroplasts. *Plant Cell*, **18**, 3106–3120.

Kurasová, I., Kalina, J., Urban, O., Štroch, M. and Špunda, V. (2003) Acclimation of two distinct plant species, spring barley and Norway spruce, to combined effect of various irradiance and CO_2 concentration during cultivation in controlled environment. *Photosynthetica*, **41**, 513–523.

León, I.R., Schwämmle, V., Jensen, O.N. and Sprenger, R.R. (2013) Quantitative assessment of in-solution digestion efficiency identifies optimal protocols for unbiased protein analysis. *Mol. Cell. Proteomics*, **12**, 2992–3005.

Morosinotto, T., Bassi, R., Frigerio, S., Finazzi, G., Morris, E. and Barber, J. (2006) Biochemical and structural analyses of a higher plant photosystem II supercomplex of a photosystem I-less mutant of barely. Consequences of a chronic over-reduction of the plastoquinone pool. *FEBS J.* **273**, 4616–4630.

Nosek, L., Semchonok, D., Boekema, E.J., Ilík, P. and Kouřil, R. (2017) Structural variability of plant photosystem II megacomplexes in thylakoid membranes. *Plant J.* **89**, 104–111.

Oostergetel, G.T., Keegstra, W. and Brisson, A. (1998) Automation of specimen selection and data acquisition for protein electron crystallography. *Ultramicroscopy*, **74**, 47–59.

Perez-Riverol, Y., Csordas, A., Bai, J. *et al*. (2019) The PRIDE database and related tools and resources in 2019: improving support for quantification data. *Nucleic Acids Res.* **47**, D442–D450.

Scheres, S.H. (2012) RELION: implementation of a Bayesian approach to cryo-EM structure determination. *J. Struct. Biol.* **180**, 519–530.

Schwanhäusser, B., Busse, D., Li, N., Dittmar, G., Schuchhardt, J., Wolf, J., Chen, W. and Selbach, M. (2011) Global quantification of mammalian gene expression control. *Nature*, **473**, 337–342.

Shen, L., Huang, Z., Chang, S., Wang, W., Wang, J., Kuang, T., Han, G., Shen, J.R. and Zhang, X. (2019) Structure of a $C_2S_2M_2N_2$-type PSII–LHCII supercomplex from the green alga *Chlamydomonas reinhardtii. Proc. Natl. Acad. Sci. USA*, **116**, 21246–21255.

Sheng, X., Watanabe, A., Li, A., Kim, E., Song, C., Murata, K., Song, D., Minagawa, J. and Liu, Z. (2019) Structural insight into light harvesting for photosystem II in green algae. *Nat. Plants*, **5**, 1320–1330.

Simerský, R., Chamrád, I., Kania, J., Strnad, M., Šebela, M. and Lenobel, R. (2017) Chemical proteomic analysis of 6-benzylaminopurine molecular partners in wheat grains. *Plant Cell Rep.* **36**, 1561–1570.

Štroch, M., Kuldová, K., Kalina, J. and Špunda, V. (2008) Dynamics of the xanthophyll cycle and non-radiative dissipation of absorbed light energy during exposure of Norway spruce to high irradiance. *J. Plant Physiol.* **165**, 612–622.

Su, X., Ma, J., Wei, X., Cao, P., Zhu, D., Chang, W., Liu, Z., Zhang, X. and Li, M. (2017) Structure and assembly mechanism of plant $C_2S_2M_2$-type PSII-LHCII supercomplex. *Science*, **357**, 815–820.

Tokutsu, R., Kato, N., Bui, K.H., Ishikawa, T. and Minagawa, J. (2012) Revisiting the supramolecular organization of photosystem II in *Chlamydomonas reinhardtii. J. Biol. Chem.* **287**, 31574–31581.

Tyanova, S., Temu, T. and Cox, J. (2016) The MaxQuant computational platform for mass spectrometry-based shotgun proteomics. *Nat. Protoc.* **11**, 2301–2319.

van Bezouwen, L.S., Caffarri, S., Kale, R.S., Kouřil, R., Thunnissen, A.M.W.H., Oostergetel, G.T. and Boekema, E.J. (2017) Subunit and chlorophyll organization of the plant photosystem II supercomplex. *Nat. Plants*, **3**, 17080.

van Eerden, F.J., Melo, M.N., Frederix, P.W.J.M., Periole, X. and Marrink, S.J. (2017) Exchange pathways of plastoquinone and plastoquinol in the photosystem II complex. *Nat. Commun.* **8**, 15214.

Verhoeven, A. (2014) Sustained energy dissipation in winter evergreens. *New Phytol.* **201**, 57–65.

Wei, X., Su, X., Cao, P., Liu, X., Chang, W., Li, M., Zhang, X. and Liu, Z. (2016) Structure of spinach photosystem II-LHCII supercomplex at 3.2Å resolution. *Nature*, **534**, 69–74.

Publication 11

Plant Physiology®

Research Article

Towards spruce-type photosystem II: consequences of the loss of light-harvesting proteins LHCB3 and LHCB6 in Arabidopsis

Iva Ilíková [ID],[1] Petr Ilík [ID],[2] Monika Opatíková [ID],[2] Rameez Arshad [ID],[2,3] Lukáš Nosek [ID],[2] Václav Karlický [ID],[4,5] Zuzana Kučerová [ID],[2] Pavel Roudnický [ID],[6] Pavel Pospíšil [ID],[2] Dušan Lazár [ID],[2] Jan Bartoš [ID][1] and Roman Kouřil [ID][2,†,*]

1 Institute of Experimental Botany of the Czech Academy of Sciences, Centre of the Region Haná for Biotechnological and Agricultural Research, 783 71 Olomouc, Czech Republic

2 Department of Biophysics, Centre of the Region Haná for Biotechnological and Agricultural Research, Palacký University, 783 71 Olomouc, Czech Republic

3 Electron Microscopy Group, Groningen Biomolecular Sciences and Biotechnology Institute, University of Groningen, Nijenborgh 7, 9747 AG Groningen, The Netherlands

4 Department of Physics, Faculty of Science, University of Ostrava, 710 00 Ostrava, Czech Republic

5 Global Change Research Institute of the Czech Academy of Sciences, 603 00 Brno, Czech Republic

6 Central European Institute of Technology, Masaryk University, 625 00 Brno, Czech Republic

*Author for communication: roman.kouril@upol.cz

†Senior author.

R.K., I.I., and P.I. planned and designed the research. All authors performed experiments and analyzed the data. I.I., R.K., and P.I. wrote the manuscript with input from all authors, and all authors revised and approved it.

The author responsible for distribution of materials integral to the findings presented in this article in accordance with the policy described in the Instructions for Authors (https://academic.oup.com/plphys/pages/General-Instructions) is: Iva Ilíková (ilikova@ueb.cas.cz).

Abstract

The largest stable photosystem II (PSII) supercomplex in land plants ($C_2S_2M_2$) consists of a core complex dimer (C_2), two strongly (S_2) and two moderately (M_2) bound light-harvesting protein (LHCB) trimers attached to C_2 via monomeric antenna proteins LHCB4–6. Recently, we have shown that LHCB3 and LHCB6, presumably essential for land plants, are missing in Norway spruce (*Picea abies*), which results in a unique structure of its $C_2S_2M_2$ supercomplex. Here, we performed structure–function characterization of PSII supercomplexes in Arabidopsis (*Arabidopsis thaliana*) mutants *lhcb3*, *lhcb6*, and *lhcb3 lhcb6* to examine the possibility of the formation of the "spruce-type" PSII supercomplex in angiosperms. Unlike in spruce, in Arabidopsis both LHCB3 and LHCB6 are necessary for stable binding of the M trimer to PSII core. The "spruce-type" PSII supercomplex was observed with low abundance only in the *lhcb3* plants and its formation did not require the presence of LHCB4.3, the only LHCB4-type protein in spruce. Electron microscopy analysis of grana membranes revealed that the majority of PSII in *lhcb6* and namely in *lhcb3 lhcb6* mutants were arranged into C_2S_2 semi-crystalline arrays, some of which appeared to structurally restrict plastoquinone diffusion. Mutants without LHCB6 were characterized by fast induction of non-photochemical quenching and, on the contrary to the previous *lhcb6* study, by only transient slowdown of electron transport between PSII and PSI. We hypothesize that these functional changes, associated with the arrangement of PSII into C_2S_2 arrays in thylakoids, may be important for the photoprotection of both PSI and PSII upon abrupt high-light exposure.

Open Access

Introduction

Photosynthesis is a very complex process that relies on a synergistic function of large multi-subunit pigment–protein complexes of photosystem II (PSII) and photosystem I (PSI), which are embedded in specific regions of the thylakoid membrane called grana and stroma lamellae, respectively. Photosystems mediate a light-driven electron transport from water molecules across the thylakoid membrane, leading to the reduction of $NADP^+$ to NADPH and generation of a proton gradient across the membrane, subsequently utilized by ATP-synthase in the production of ATP. The basic concepts of photosynthesis are shared by the majority of photosynthesizing organisms and the individual photosynthetic proteins and their organization into higher complexes are usually highly conserved.

In land plants, PSII is present in the form of supercomplexes, consisting of a dimeric core complex (C_2) and light-harvesting antenna (LHC) II. The light-harvesting system is formed by a variable amount of antenna proteins organized into LHCII trimers (LHCB1–3), which are functionally attached to the core via minor antennae (LHCB4–6). The most abundant light-harvesting protein in land plants is LHCB1, its content being about two-fold and eight-fold higher compared with the other two trimer-forming proteins, LHCB2 and LHCB3 (Peter and Thornber, 1991). LHCB1 and LHCB2 can form both homo- and heterotrimers, while LHCB3 is present only in heterotrimers together with two copies of LHCB1/LHCB2 (Caffarri et al., 2004; Standfuss and Kühlbrandt, 2004). The monomeric LHCB4–6 proteins, which represent a minor fraction of LHCII, mediate a specific association of LHCII trimers to the PSII core complex and are crucial for the formation of the PSII supercomplex. The LHCII trimers are designated as "S" and "M" based on the strength of their binding to the core dimer (strongly and moderately bound, Dekker and Boekema, 2005; Kouřil et al., 2018). The S trimers bind to the core complex with the help of LHCB5 and LHCB4, whereas the binding of the M trimers is mediated by LHCB4 and LHCB6. Apart from the different binding sites, the trimers also differ in their protein composition, as the M trimer specifically contains one copy of LHCB3 monomer (Caffarri et al., 2009; Su et al., 2017; van Bezouwen et al., 2017). The largest stable form of PSII in land plants is the $C_2S_2M_2$ supercomplex, where C_2 binds two copies of both the S and M trimers (Dekker and Boekema, 2005; Kouřil et al., 2018). Occasionally, the binding of the "L" (loosely bound) and "N" (naked) trimers can further extend the size of the light-harvesting antenna (Boekema et al., 1999; Kouřil et al., 2020). Our knowledge about the composition and architecture of the $C_2S_2M_2$ supercomplex has gradually improved and we have gained substantial information about the structural details of interactions between individual subunits and pigment arrangements within the supercomplex monomer (Caffarri et al., 2009; Su et al., 2017; van Bezouwen et al., 2017).

A generally accepted dogma that the composition and structure of PSII supercomplexes is uniform and strongly conserved in all land plants was refuted by our finding that LHCB3 and LHCB6 proteins, which had been considered as essential components of LHCII in land plants, are missing in gymnosperm families Pinaceae and Gnetales (Kouřil et al., 2016). In these plants, in the absence of LHCB3 and LHCB6, the M trimer binds to the C_2 in a different orientation, which results in a specific form of PSII supercomplex that is unique among land plants (henceforth, termed "spruce-type" in this work; Kouřil et al., 2016). It is currently difficult to speculate what was the evolutionary factor that led to the loss of LHCB3 and LHCB6 in these plant families, as we do not have enough information about the physiological consequences of the absence of these two important proteins. Norway spruce (*Picea abies*) and other representatives of Pinaceae and Gnetales are not very convenient model plants and therefore their photosynthetic performance and characteristics have not been extensively analyzed yet. At the same time, even if such study had been performed, it would be extremely difficult to decipher which features of the photosynthetic response of these plants are linked to the loss of LHCB3 and LHCB6 (i.e. linked to the unique structure of their PSII supercomplex) and which are related to other specific properties of these plant groups, including the loss of LHCB4.1/4.2 (Grebe et al., 2019), the loss of the NDH complex (Nystedt et al., 2013), and the presence of flavodiiron protein (Allahverdiyeva et al., 2015; Ilík et al., 2017). To investigate the putative physiological benefits and drawbacks of the unique composition of the light-harvesting system in Norway spruce, we have attempted to create a first approximation of the "spruce-type" PSII supercomplex in Arabidopsis (*Arabidopsis thaliana*) by preparing a double mutant *lhcb3 lhcb6* line.

Arabidopsis single mutant lines lacking either LHCB6 or LHCB3 have already been characterized and the studies have revealed some interesting properties of these mutants. Analysis of the Arabidopsis *lhcb3* mutant has shown that the absence of LHCB3 is compensated by LHCB1 and/or LHCB2 proteins and that the $C_2S_2M_2$ supercomplexes can be formed in this mutant, as electron microscopy (EM) of *lhcb3* grana membrane fragments revealed semi-crystalline arrays of $C_2S_2M_2$ supercomplexes (Damkjær et al., 2009). Even though the resolution of the PSII supercomplex structure in this study was very low, the analysis of these arrays suggested that the position of the M trimer in $C_2S_2M_2$ is modified, but that its binding to C_2 is probably still mediated by LHCB6 (Damkjær et al., 2009).

The loss of LHCB6 appears to have a much stronger detrimental effect on the photosynthetic performance of Arabidopsis plants than the loss of LHCB3, as strong reduction of plant growth, permanent limitation of electron transport, and impairment of non-photochemical quenching (NPQ) has been reported in *lhcb6* (Kovács et al., 2006; de Bianchi et al., 2008). The analysis of the *lhcb6* mutant revealed
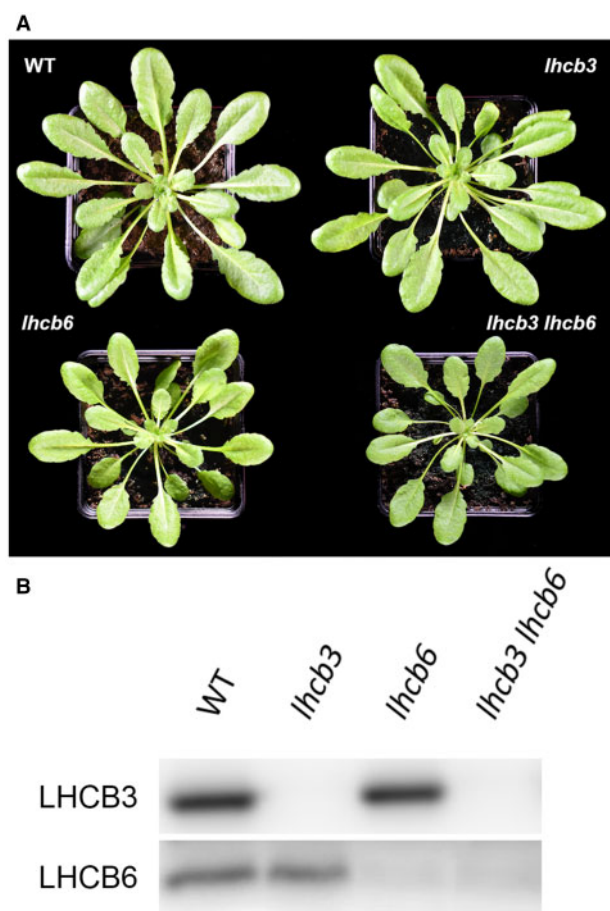
Figure 1 Phenotype and immunoblot analysis. A, Phenotype of *A. thaliana* WT and mutant plants (*lhcb3*, *lhcb6*, *lhcb3 lhcb6*) grown in control conditions for 6 weeks (120 μmol photons m^{-2} s^{-1}, 22 °C, 8/16 h day/night, and 60% humidity). B, Immunoblot analysis of thylakoid membranes of WT and mutant plants (*lhcb3*, *lhcb6*, *lhcb3 lhcb6*) with antibodies directed against minor light-harvesting proteins LHCB3 and LHCB6.

that in Arabidopsis, LHCB6 might be important for the binding of the M trimer to C_2, as no $C_2S_2M_2$ supercomplexes were observed in the *lhcb6* mutant (Kovács et al., 2006; Caffarri et al., 2009).

It has been suggested that the strong impairment of photosynthesis in *lhcb6* is not primarily caused by the loss of LHCB6 per se, but that it results from the relatively high proportion of PSII arranged into so-called PSII semi-crystalline arrays, which in turn may result in severe and permanent limitation of plastoquinone (PQ) diffusion between PSII and PSI (de Bianchi et al., 2008). The ability of PSII complexes to form semi-crystalline arrays has been known for a long time, the early evidence coming from freeze-fracture experiments. In one of the first studies, Park and Biggins (1964) have reported that the "quantasomes" (i.e. PSII supercomplexes) could exist in thylakoids in a variety of arrangements, from random through linear arrays to crystalline arrays, although the crystals were reported to be rather rare. Despite the lack of any structural details and limited knowledge on the structure and composition of PSII

particles at that time, there have already been data suggesting that there are various types of semi-crystals (Miller et al., 1976; Simpson, 1979; Tsvetkova et al., 1995; Semenova, 1995). Currently, we know that all types of PSII supercomplexes observed in land plants ($C_2S_2M_2$, C_2S_2M, and C_2S_2) are able to form semi-crystalline arrays (Boekema et al., 2000; Yakushevska et al., 2001), but the mechanism and regulation of their formation, as well as their physiological function, importance, and putative benefits, are still very poorly understood.

In our study, we have prepared Arabidopsis double mutant line lacking LHCB3 and LHCB6 in an attempt to reproduce the unique "spruce-type" PSII supercomplex in Arabidopsis, which would help us to obtain valuable information about the possible physiological benefits of this type of supercomplex. From the published studies, we already know that in the absence of LHCB6, the "regular" M trimer containing LHCB3 is not able to bind to the supercomplex. Our primary question thus was whether the additional loss of LHCB3 in *lhcb6* mutant line can facilitate the binding of the M trimer to C_2S_2 and if not, what could be the possible factors preventing its appearance in Arabidopsis. It appears that indeed, in Arabidopsis the loss of both LHCB3 and LHCB6 is not sufficient for the stable formation of "spruce-type" supercomplex. At the same time, we have found that in the Arabidopsis double mutant *lhcb3 lhcb6*, the majority of PSII are arranged into C_2S_2 semi-crystalline arrays. Therefore, we have used this mutant for an extensive analysis of its primary photosynthetic reactions in order to shed some light on the possible physiological/regulatory role of PSII ordering into C_2S_2 semi-crystalline arrays.

Results

The additional loss of LHCB3 does not change the phenotype of Arabidopsis *lhcb6* mutant

Arabidopsis *lhcb3 lhcb6* double mutant was prepared via the crossing of two SALK T-DNA insertion lines, SALK_020314c (*lhcb3*) and SALK_077953 (*lhcb6*), which were already used in several previous studies. Western blot analysis confirmed a complete absence of LHCB3 in both *lhcb3* and *lhcb3 lhcb6* mutants (Figure 1, B), which agrees with the findings of other authors and confirms that the SALK_020314c is indeed a knockout line (Damkjær et al., 2009; Adamiec et al., 2015). However, in the case of LHCB6, we were able to observe a weak antibody signal in the Western blots, suggesting either cross-reactivity of the used antibody or the presence of some residual amount of LHCB6 in both *lhcb6* and *lhcb3 lhcb6* mutants (Figure 1, B). Closer examination of the T-DNA insertion site in the SALK_077953 line reveals that the T-DNA insertion is localized in the 5′-UTR region of the lhcb6 gene (AT1G15820), which frequently leads to knockdowns rather than knockouts (Wang, 2008). Other authors who have previously used this insertion line and performed Western blots either failed to detect this residual amount of LHCB6 (de Bianchi et al., 2008; Chen et al., 2018), or observed it but disregarded it as
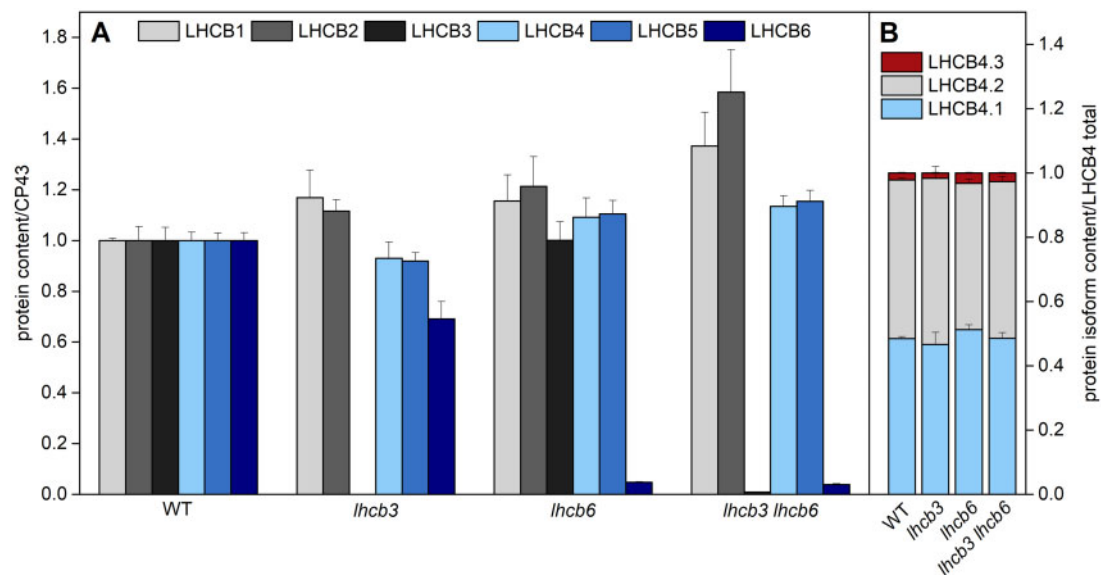
Figure 2 Relative content of light-harvesting proteins in thylakoid membranes of WT and mutant plants (*lhcb3*, *lhcb6*, *lhcb3 lhcb6*). A, The content of individual light-harvesting proteins LHCB1-6 evaluated relatively to the content of chlorophyll protein 43 (CP43, the inner antenna of PSII), and subsequently normalized to WT. B, The content of individual LHCB4 isoforms (LHCB4.1, LHCB4.2, LHCB4.3) related to the sum of all LHCB4 isoforms. The protein content was determined in isolated thylakoid membranes by LC–MS/MS. The presented values are means ± SD from four replicates.

Table 1 Growth parameter and pigment content

	Fresh weight (g)	Chl $a + b$	Chl a/b	Car	Vio	Ant	Zea
WT	1.4 ± 0.2	960 ± 190	2.79 ± 0.09	169 ± 26	15 ± 4	2.0 ± 0.5	ND
lhcb3	1.4 ± 0.3	910 ± 73	2.84 ± 0.04	165 ± 8	18 ± 2	2.4 ± 0.4	ND
lhcb6	0.6 ± 0.2	820 ± 85	2.94 ± 0.07	149 ± 14	18 ± 2	3.1 ± 0.2	ND
lhcb3 lhcb6	0.7 ± 0.2	800 ± 68	2.96 ± 0.05	148 ± 12	17 ± 2	3.1 ± 2.1	ND

Notes: Presented values are means ± SD. Fresh weight of individual rosettes was measured (n = 13–15). Pigment content is expressed in µg g^{-1} fresh weight (n = 4). Chl, chlorophyll; Car, carotenoids; Vio, violaxanthin; Ant, antheraxanthin; Zea, zeaxanthin; and ND, not detectable.

non-detectable (3% ± 1% of wild-type (WT) level, Kovács et al., 2006), and therefore the insertion line has been widely used as a knockout mutant for LHCB6. Nevertheless, we have confirmed the presence of the residual amount of LHCB6 in the presumed knockout line also by the mass spectrometry analysis, which revealed a low, but unequivocally detectable amount of LHCB6 in both *lhcb6* and *lhcb3 lhcb6* (4%–5% of WT level, Figure 2, A). Thus, unlike *lhcb3* (SALK_020314c), *lhcb6* (SALK_077953) is a strong knockdown line rather than a complete knockout.

In agreement with a previous study (Damkjær et al., 2009), a phenotypic characterization of mutant plants lacking LHCB3 did not show any distinct changes compared with WT, either in growth rate or pigment composition (Figure 1, A and Table 1). Plants of *lhcb6* line were visibly smaller (Figure 1, A), but their chlorophyll and carotenoid content did not significantly differ from WT and *lhcb3* (Table 1). The double mutant *lhcb3 lhcb6* plants grown under controlled conditions in the phytotron were indistinguishable from the *lhcb6* plants (Figure 1, A), indicating that the additional loss of LHCB3 did not have a substantial effect on the plant visual phenotype.

The changes in LHCB protein levels in individual mutant lines were assessed using mass spectrometry and expressed relative to protein levels in WT. The loss of LHCB3 in *lhcb3* led to a slight increase in the amount of LHCB1 and LHCB2 proteins (Figure 2, A), which probably replace LHCB3 in the M trimer. At the same time, the amount of LHCB6 decreased to approximately 70% of WT level (Figure 2, A), which has not been observed on Western blots from *lhcb3* plants in previous studies (Damkjær et al., 2009; Adamiec et al., 2015). In *lhcb6* mutant plants, we have found again a slight increase in the amount of LHCB1 and LHCB2 (Figure 2, A), which is in agreement with previously observed trends (Kovács et al., 2006; de Bianchi et al., 2008). The level of LHCB3 did not change (Figure 2, A), although literature suggests a decrease to 70% (Kovács et al., 2006; Chen et al., 2018) or even 25% (de Bianchi et al., 2008) of the WT level. LHCB4 and LHCB5 did not show any distinct change in abundance (Figure 2, A). Mass spectrometry analysis confirmed the presence of a residual amount of LHCB6 protein in the *lhcb6* line (less than 5% of the WT level, Figure 2, A), which was already observed in immunoblots (Figure 1, B). The protein composition of the
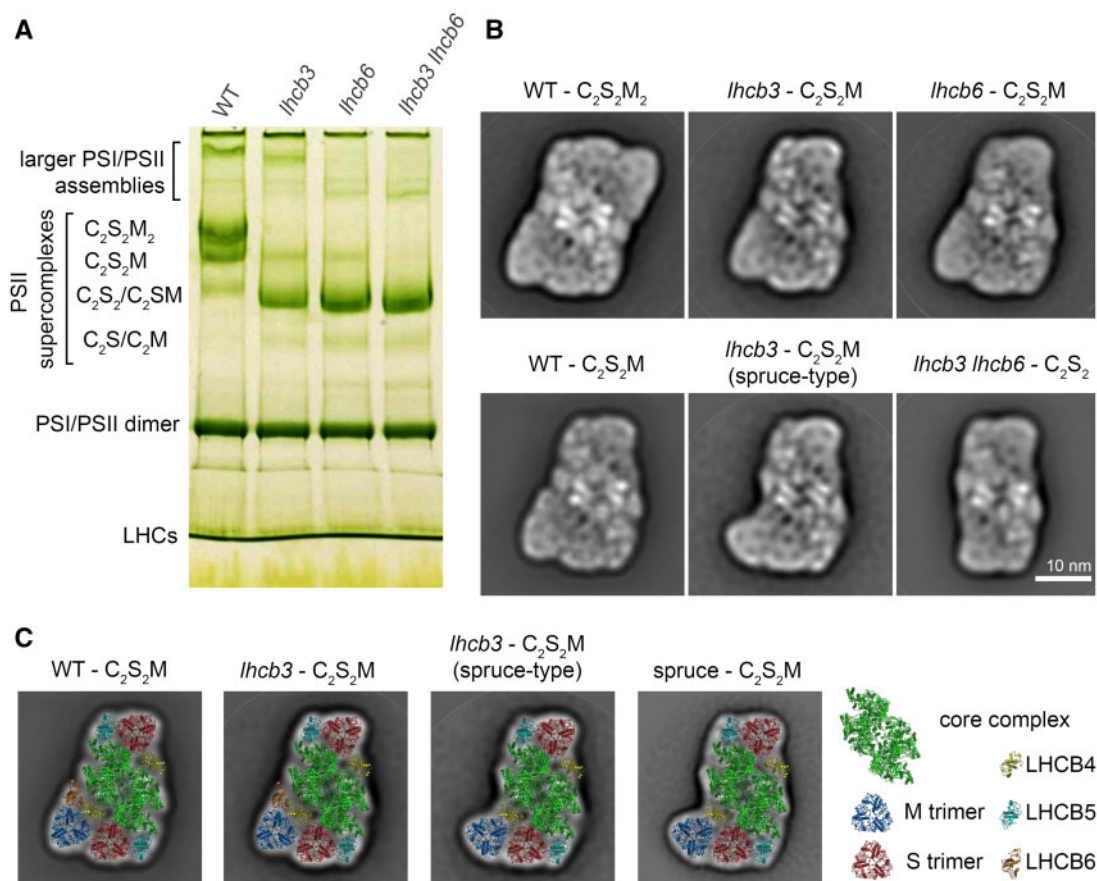
Figure 3 Separation and structural characterization of PSII (PSII) supercomplexes from WT and mutant plants (*lhcb3*, *lhcb6*, *lhcb3 lhcb6*). A, CN polyacrylamide gel electrophoresis separation of pigment–protein complexes from thylakoid membranes from *A. thaliana* WT, *lhcb3*, *lhcb6*, and *lhcb3 lhcb6* mutants solubilized by *n*-dodecyl α-D-maltoside. Different forms of separated PSII supercomplexes consist of PSII core dimer (C_2) and one and/or two copies of strongly (S) and moderately (M) bound light-harvesting trimers. B, Structural characterization of the largest forms of PSII supercomplexes revealed in WT and *lhcb3*, *lhcb6*, and *lhcb3 lhcb6* mutants. In WT, the gel bands designated as $C_2S_2M_2$ and C_2S_2M were analyzed. In *lhcb3* and *lhcb6*, the C_2S_2M gel bands, and the C_2S_2 gel band in *lhcb3 lhcb6* were analyzed. C, Structural models of C_2S_2M PSII supercomplexes from WT and *lhcb3* mutant shown in (B) supplemented with the model of C_2S_2M separated from thylakoid membranes of spruce (Kouřil et al. 2016). The models were obtained by a fit of the high-resolution structure from van Bezouwen et al. (2017). Individual PSII subunits are color-coded.

double mutant plants *lhcb3 lhcb6* was similar to *lhcb6* plants, except for the absence of LHCB3 and a slightly more pronounced increase in LHCB1 and LHCB2 abundance (Figure 2, A).

Out of all assessed LHCB proteins, LHCB4 and LHCB5 were affected the least. It is of note that these two proteins can be considered as a part of the "functional core" of the PSII antenna system in all organisms from the green lineage (Alboresi et al., 2008), and unlike the rest of the LHCB proteins, their content is not readily affected by environmental conditions (Ballottari et al., 2007). As LHCB4 is known to be present in Arabidopsis in three isoforms (LHCB4.1, LHCB4.2, and LHCB4.3), we used mass spectrometry to analyze the relative contribution of individual isoforms to the total amount of LHCB4. In WT, LHCB4.1 and LHCB4.2 isoforms were present in approximately equimolar amounts, which agrees with the recently published data (McKenzie et al.,

2020), and the loss of LHCB3 and/or LHCB6 did not significantly change this ratio (Figure 2, B). The relative contribution of the third isoform, LHCB4.3, was very low in all analyzed plants (Figure 2, B).

C_2S_2 is the main stable form of PSII supercomplex in Arabidopsis *lhcb3 lhcb6* mutant

To analyze the impact of the loss of LHCB3 and/or LHCB6 proteins on the formation and structure of PSII supercomplexes in Arabidopsis, we have used clear-native PAGE (CN-PAGE), which enabled us to separate individual photosynthetic protein complexes from thylakoid membranes mildly solubilized with *n*-dodecyl α-D-maltoside (α-DDM). The separation profile of PSII supercomplexes from WT (Figure 3, A) agrees with our previously published data (Nosek et al., 2017) and confirms that $C_2S_2M_2$ is the most abundant form of PSII supercomplex present

in Arabidopsis plants grown under normal light conditions (Kouřil et al., 2013). Other forms (C_2S_2M and namely C_2S_2/C_2SM) are not so frequent and may also originate from the disassembly of the $C_2S_2M_2$ complex during sample preparation.

In plants lacking LHCB3, we did not observe any distinct band that would correspond to $C_2S_2M_2$, instead, the dominant form appeared to be the small C_2S_2 supercomplex (Figure 3, A). However, the presence of a faint, but clearly visible band at the position corresponding to C_2S_2M supercomplexes suggests that even in the absence of LHCB3, the M trimer is able to bind to C_2S_2. The data obtained by Damkjær et al. (2009) on fragments of granal membranes with crystalline arrays indicate that the $C_2S_2M_2$ supercomplex is indeed present in lhcb3 in vivo. It seems that in the absence of LHCB3, the binding of the M trimer to C_2S_2 is very weak and the fragile $C_2S_2M_2$ supercomplexes are easily disrupted to smaller supercomplexes during the solubilization. In the previous report, where sucrose gradient fractionation was used instead of CN-PAGE to analyze lhcb3 PSII supercomplexes, even the C_2S_2M supercomplexes were not detectable and C_2S_2/C_2SM was the only detected form of PSII supercomplex (Caffarri et al., 2009).

The separation profile of PSII supercomplexes isolated from lhcb6 is very similar to lhcb3 (Figure 3, A). In agreement with a previous study (Caffarri et al., 2009), we have found out that the band corresponding to $C_2S_2M_2$ is absent and that the major form of PSII supercomplex in this mutant is C_2S_2. However, in addition to this, we were able to observe also a faint band at the position of C_2S_2M supercomplexes. This again suggests the superiority of our CN-PAGE purification approach, as this form of PSII supercomplexes was not detectable in lhcb6 via sucrose gradient fractionation (Caffarri et al., 2009). We have assumed that the formation of a small amount of C_2S_2M was enabled by the presence of the residual amount of LHCB6 (Figures 1, B, 2, A) in the lhcb6 mutant. This hypothesis has been indeed confirmed by mass spectrometry analysis of this band, as it contained LHCB6 and had the same protein composition as C_2S_2M from WT plants (Supplemental Figure S1). In contrast to lhcb3, in lhcb6, the $C_2S_2M_2$ supercomplexes are probably not present even in the membrane, as the previous EM analysis of PSII supercomplexes in lhcb6 thylakoids revealed more than 95% of C_2S_2 (Kovács et al., 2006). Thus, in the absence of LHCB6, the only stable form of PSII supercomplex appears to be C_2S_2 (Figure 3, A).

CN-PAGE analysis of PSII supercomplexes from the double mutant lhcb3 lhcb6 revealed only one strong PSII band, corresponding to C_2S_2 (Figure 3, A). This is interesting in the light of the data obtained from Norway spruce. This representative of Pinaceae lacks both LHCB3 and LHCB6 (Kouřil et al., 2016), but at the same time, the CN-PAGE separation of its thylakoid membranes provides clear evidence of the presence of large forms of PSII supercomplexes (Kouřil et al.,

2016, 2020). However, based solely on electrophoretic analysis, it was not possible to decide whether the larger forms of PSII supercomplexes are absent in lhcb3 lhcb6 mutant or whether they are just too unstable to be isolated via CN-PAGE as in the case of lhcb3.

The appearance of "spruce-type" PSII supercomplex in Arabidopsis lhcb3 mutant

The largest forms of PSII supercomplexes separated by CN-PAGE from thylakoid membranes of individual lines were analyzed using single-particle EM. The analysis of the supercomplexes from $C_2S_2M_2$ and C_2S_2M WT bands showed the presence of typical forms of supercomplexes (Figure 3, B; Caffarri et al., 2009), which was also confirmed by the fitting of our projection maps with a structural model of PSII supercomplex from Arabidopsis (van Bezouwen et al., 2017) and by detailed protein analysis of individual supercomplexes (Supplemental Figure S1).

The analysis of a faint CN-PAGE band from lhcb3 that is present at the tentative position of C_2S_2M confirmed that it indeed contained C_2S_2M supercomplexes. The proteomic data suggest that the absence of LHCB3, normally present in the LHCII trimer at M position, is in lhcb3 compensated by increased amounts of LHCB1/LHCB2 (Figure 2, A). Detailed single particle EM image analysis revealed the presence of two different forms of the C_2S_2M supercomplex in lhcb3. About 90% of the particles were represented by a C_2S_2M supercomplex where the M trimer binds to the PSII core complex with the help of both LHCB4 and LHCB6 subunits (Figure 3, B and C). This type of supercomplex is similar to the C_2S_2M present in WT, the only difference being a slight change in the position of the M trimer with respect to the S trimer (rotation by ca 10°, Figure 3, B and C). This result is in agreement with the previous report, where the change in the orientation of the M trimer was suggested from the analysis of semi-crystalline arrays of $C_2S_2M_2$ supercomplexes in lhcb3 granal membranes (Damkjær et al., 2009). In the second type of C_2S_2M present in lhcb3, however, the M trimer is attached to the core complex only via LHCB4, without the participation of LHCB6. Single particle analysis revealed that in this type of supercomplex, the position normally occupied by LHCB6 is empty (Figure 3, B and C). In this case, the structure closely resembles the C_2S_2M supercomplex observed previously in Norway spruce (Kouřil et al., 2016); therefore, we term it "spruce-type." Although this "spruce-type" supercomplex represents only about 10% of all the analyzed supercomplexes from the lhcb3 C_2S_2M band, it is not possible to draw any reliable conclusions about its natural abundance in lhcb3 thylakoids. PSII supercomplexes appear to be very fragile in the absence of LHCB3, as evidenced by the disruption of $C_2S_2M_2$ supercomplexes from lhcb3 by even very mild solubilization (Figure 3, A). Therefore, any differences in the stability of the two forms of C_2S_2M during the preparation of the sample for

CN-PAGE and EM can easily distort the estimation of their relative abundance in intact thylakoids. However, irrespective of its relative occurrence in vivo, our finding demonstrates that even in Arabidopsis, the absence of LHCB3 and LHCB6 can lead to the formation of the "spruce-type" C_2S_2M supercomplexes. The presence of this LHCB6-less "spruce-type" C_2S_2M supercomplex could contribute to the observed decrease in the relative amount of LHCB6 in *lhcb3* thylakoids (Figure 2, A).

Single particle analysis of the C_2S_2M band from *lhcb6* revealed a typical form of the C_2S_2M supercomplex observed in WT, without any structural modification (Figure 3, B). The projection map shows a density at the position of LHCB6, which could in theory indicate that there is a replacement of LHCB6 by some other LHC protein. However, the mass spectrometry analysis of supercomplexes eluted from this *lhcb6* CN-PAGE band unequivocally confirmed that these C_2S_2M supercomplexes indeed contain LHCB6 (Supplemental Figure S1) and that the appearance of the faint C_2S_2M band is a direct consequence of the presence of the residual amount of LHCB6. This band would probably be absent in a complete LHCB6 knockout and the only stable form of PSII supercomplex would be C_2S_2.

The analysis of the C_2S_2 band from *lhcb3 lhcb6* revealed a typical form of C_2S_2 (Figure 3, B). Although we have confirmed the ability of Arabidopsis to form "spruce-type" C_2S_2M (see above, Figure 3, B and C), these larger forms of PSII supercomplexes were completely absent in the CN-PAGE of the thylakoids from the double mutant. We have concluded that either $C_2S_2M_{(2)}$ supercomplexes are not formed in this mutant at all, or are present in thylakoid membranes, but are too fragile to be isolated by CN-PAGE. To resolve this issue, it was necessary to perform EM analysis of granal thylakoid membranes.

The majority of PSII supercomplexes in Arabidopsis *lhcb3 lhcb6* mutant are organized into C_2S_2 semi-crystalline arrays

EM analysis of isolated grana membranes of individual Arabidopsis mutant lines can bring additional information about the arrangement of PSII supercomplexes in vivo. In WT plants, the arrangement of PSII supercomplexes in thylakoid membranes is mostly random (Supplemental Figure S2, A), but supercomplexes can also specifically interact to form various megacomplexes (e.g. Nosek et al., 2017). Some of these megacomplexes could originate from the disassembly of semi-crystalline arrays of $C_2S_2M_2$, which are occasionally present in WT thylakoids (Supplemental Figure S2, A; e.g. Kouřil et al., 2013). The arrangement of PSII supercomplexes into semi-crystalline arrays was observed also in grana membranes isolated from *lhcb3* (Supplemental Figure S2, B). Previously, it has been shown that these arrays have slightly higher abundance in *lhcb3* and that they also consist of $C_2S_2M_2$ (Damkjær et al., 2009).

In *lhcb6*, the PSII arrays are formed by C_2S_2 rather than $C_2S_2M_2$ supercomplexes (Kovács et al., 2006; de Bianchi et
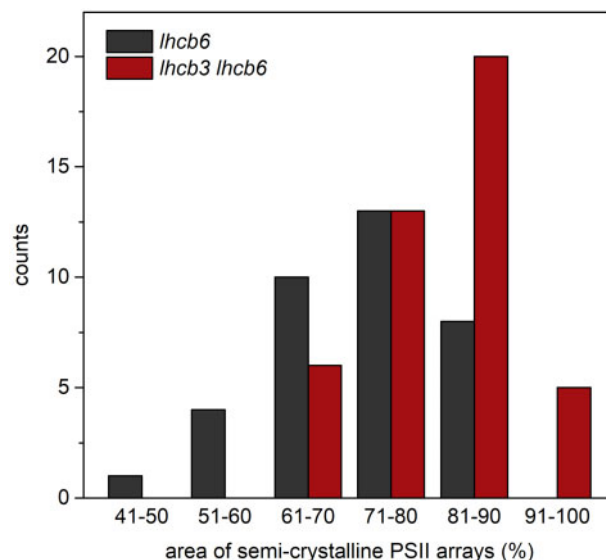
Figure 4 Histogram of a relative representation of two-dimensional semi-crystalline arrays of PSII in the grana membranes from *lhcb6* and *lhcb3 lhcb6* mutants. Area of semi-crystalline arrays of PSII per a total area of the grana membranes was determined in 30 electron micrographs of grana membranes from each type of mutants.

al., 2008) and their abundance is relatively high (Supplemental Figure S2, C). Based on the analysis of freeze–fracture electron micrographs of *lhcb6* thylakoids, the fraction of PSII present in arrays has been previously estimated to be 25% (Goral et al., 2012). Our EM data, however, suggest that the arrays are much more frequent. In the majority of electron micrographs randomly selected for analysis, semi-crystalline arrays were present in 60%–90% of the area of granal thylakoid membranes of *lhcb6* (Figure 4). The remaining membrane areas without arrays were usually represented by low PSII density regions, where randomly oriented PSII complexes were surrounded by seemingly free space (low PSII density areas, Supplemental Figure S2, C). These parts of the granal membrane most likely contained free LHCII trimers, which could not be directly resolved in the membrane by EM due to their low contrast.

In the grana membranes isolated from the double mutant *lhcb3 lhcb6*, the degree of the arrangement of PSII supercomplexes into arrays was very high, with only a minor representation of LHCII-rich regions (Supplemental Figure S3). In most of the analyzed granal membranes, 80%–100% of the area was occupied by semi-crystalline arrays and we did not observe any membrane where the relative contribution of the arrays was lower than 60% (Figure 4). The average parameters of the lattice unit cell of these arrays, calculated from the analyzed crystals, were (243 ± 4) $\times$ (165 ± 3) Å with lattice angles $82°$ or $98° \pm 2°$. Very similar lattice parameters were reported for C_2S_2 arrays in PSI-less *viridis zb63* barley (*Hordeum vulgare*) mutant (250×165 Å, angles $80°$ and $100°$; Morosinotto et al., 2006), and also the C_2S_2 arrays observed in *lhcb6* appear to be of the same type (de Bianchi et al., 2008). Indeed, fitting of the arrays in *lhcb3*
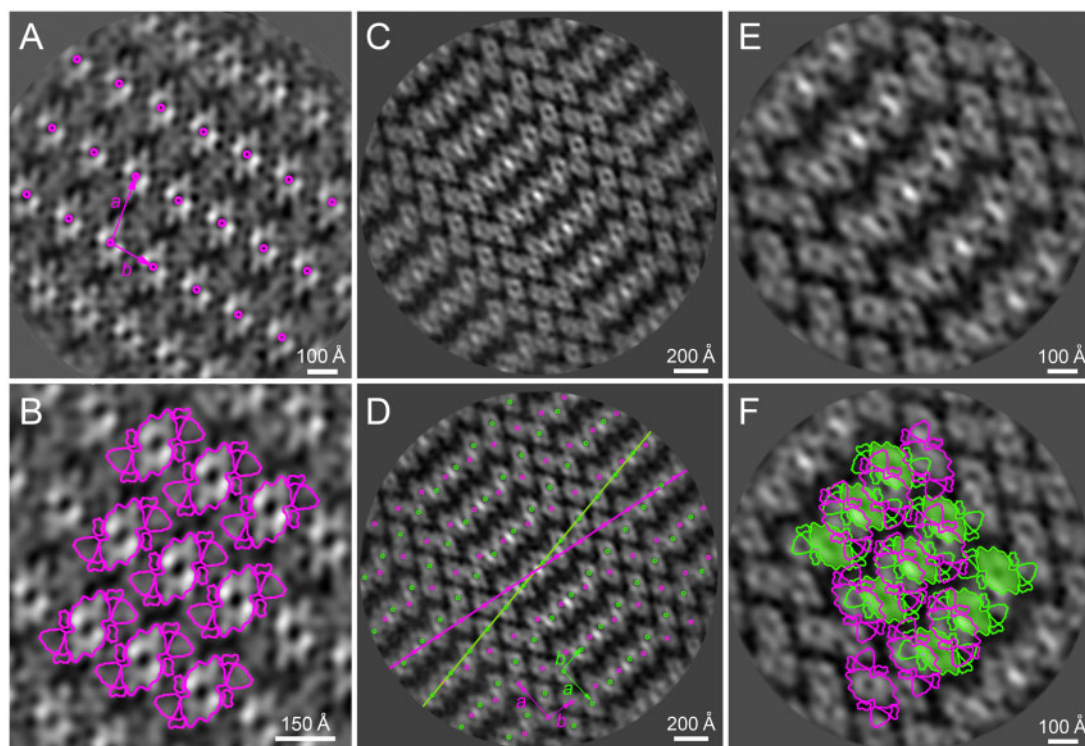
Figure 5 Different types of the two-dimensional semi-crystalline arrays of PSII in the grana membranes from *lhcb3 lhcb6* mutant. A, Image analysis of grana membrane sub-areas (1,320 × 1,320 Å) with semi-crystalline array of PSII complexes revealed a projection map of one layer of PSII complexes ordered into the regular array viewed from the lumen side. The centers of the PSII core complexes represent the lattice points of the PSII arrays (magenta). The unit cell is defined by the *a* and *b* parameters. B, Enlarged central parts of the PSII arrays shown in A. The cartoon model shows that the semi-crystalline array is formed by PSII C_2S_2 supercomplexes viewed from the lumen side. C, Image analysis of larger sub-areas (2,160 × 2,160 Å) of another type of semi-crystalline array, a carpet-like motive, of PSII complexes revealed a projection map of two translationally and rotationally shifted layers of ordered PSII complexes. D, The lattice points of the PSII arrays viewed from the lumen and stroma sides are indicated by magenta and green points, respectively. A mutual rotation of the two layers is indicated by the two magenta and green lines and it is about 17°. The unit cells are defined by the *a* and *b* parameters. E, Image analysis focused on smaller sub-areas (1,230 × 1,230 Å) of the semi-crystalline array presented in (C) revealed interactions between the two PSII layers in more details. F, A cartoon model shows variable interactions between PSII C_2S_2 supercomplexes from the two adjacent layers viewed from the lumen and stroma sides (in magenta and green, respectively).

lhcb6 (Figure 5) by a cartoon model of PSII supercomplex (Figure 6) confirms that they consist of C_2S_2. Based on this observation, we can conclude that the absence of the $C_2S_2M_2$ band in CN-PAGE of *lhcb3 lhcb6* (Figure 3, A) cannot be ascribed to the disintegration of the large supercomplexes during sample preparation and that, on the contrary to *lhcb3*, the $C_2S_2M_{(2)}$ supercomplexes are not present even in the granal membranes of *lhcb3 lhcb6*.

Previously, it has been shown that in barley *viridis zb63* mutant, PSII can be arranged in several crystal forms (Stoylova et al., 2000), and therefore we have performed a detailed analysis of crystalline arrays in order to find out whether such variability exists also in *lhcb3 lhcb6* mutant. Indeed, we have identified at least three types of C_2S_2 arrays, which differ in the dimensions and angle of the lattice unit cell, whereas the tilting of the C_2S_2 with respect to the vector of the lattice cell was similar in all three types (Figure 6 and Table 2). The models of individual crystal forms clearly show that although all of them consist of C_2S_2, the different tightness of supercomplex packing is likely to have different consequences for the diffusion rate of PQ molecules. Therefore, different types

of C_2S_2 crystal arrangement can have different effects on PSII photochemical activity.

The analysis of EM micrographs of granal thylakoid membranes from *lhcb3 lhcb6* (Supplemental Figures S3–S5) also revealed the presence of membrane stacks consisting of pairs of membrane layers interacting through their stromal sides. The layers are attached to each other via two types of interactions between PSII supercomplexes—regular and variable. Regular interactions between PSII supercomplexes in adjacent layers lead to a regular pattern in EM micrographs (Figure 5, A and B and Supplemental Figure S4), which closely resembles the pattern already observed in *viridis zb63* barley mutant (Morosinotto et al., 2006). It remains an open question which component mediates the interaction of PSII supercomplexes over the stromal gap. Unfortunately, in the regular arrays, the mutual orientation of PSII supercomplexes in the interacting layers is difficult to analyze because the interacting supercomplexes vertically overlap each other. It has been suggested that the stacking might be mediated by interactions between adjacent PSII core complexes (PSII sandwiches, Albanese et al., 2016b, 2017) or between
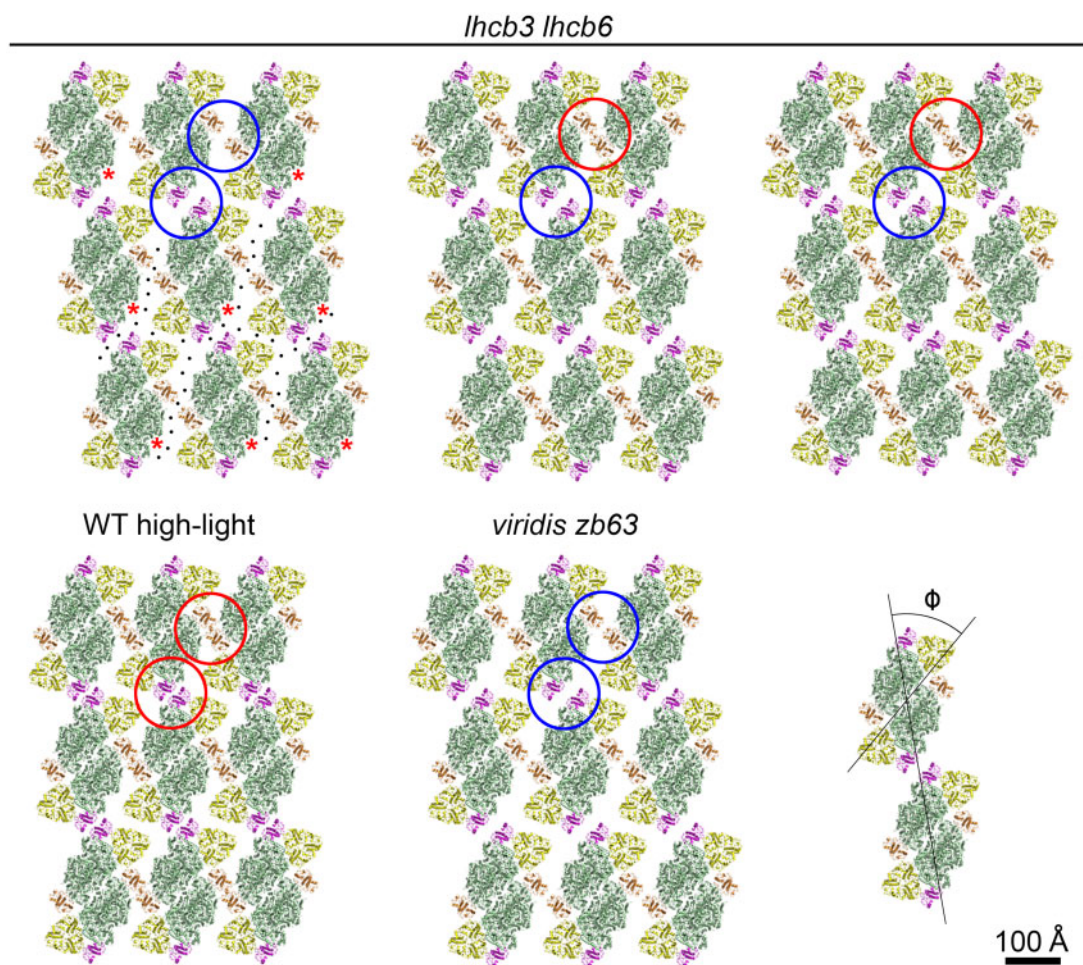
Figure 6 Structural models of different types of packing of PSII C_2S_2 complexes into two-dimensional semi-crystalline arrays. A–C, Structural models of C_2S_2 arrays in grana membranes of Arabidopsis *lhcb3 lhcb6* mutant with different lattice unit cell parameters (Table 2). The model (A) represents an open conformation with a larger distance between LHCB4 and LHCB5 proteins of neighboring C_2S_2 supercomplexes (see blue circles), which is favorable for free diffusion of PQ molecules (black on-scale dots) to/from the Q_B binding pockets (indicated by red asterisks). On the contrary, the models (B) and (C) show a closer contact between the neighboring C_2S_2 supercomplexes, especially between LHCB4 proteins (see red circles), which can hamper a free diffusion of PQ molecules. D, Structural model of C_2S_2 arrays in Arabidopsis WT acclimated to high-light intensity indicates even closer contact between neighboring C_2S_2 supercomplexes (adopted from Kouřil et al., 2013). E, Structural model of C_2S_2 arrays in barley mutant, *viridis zb63*, grown under optimal light conditions shows an open conformation similar to the open conformation (A) in Arabidopsis *lhcb3 lhcb6*. F, Determination of the ϕ angle, which is defined as the angle between the vector *a* of the lattice unit cell and the diagonal of the C_2S_2 supercomplex. Lattice unit cell parameters of all presented models are shown in Table 2. Structural model of the C_2S_2 supercomplex was obtained from Wei et al. (2016). Individual PSII subunits are color-coded: dark green, core complex; yellow, S trimer; magenta, LHCB5; and orange, LHCB4.

overlapping S trimers (Grinzato et al., 2020). Except for the regular arrays, where all PSII supercomplexes in one layer appear to interact in a periodically repeating manner with their counterparts in the second layer, we have also observed "variable" arrays. In these arrays, the interactions between PSII supercomplexes in the adjacent membrane layers are less specific, as the vertically overlapping (i.e. potentially interacting) proteins are variable. These arrays originate via interaction of two translationally and rotationally (about 17°) shifted layers of PSII complexes and are recognizable through the appearance of a "carpet-like" motive in electron micrographs (Figure 5, B–E and Supplemental Figure S5).

C_2S_2 arrays are present in vivo in Arabidopsis *lhcb6* and *lhcb3 lhcb6* mutants

Higher organization of photosynthetic complexes can be sometimes affected by isolation procedures, which are necessary for the preparation of samples for EM. Therefore, we have complemented our study by circular dichroism (CD) spectroscopy, a method that can be used to assess the macro-organization of pigment–protein complexes in thylakoid membrane in vivo (Garab and van Amerongen, 2009). Complex systems such as granal thylakoid membranes provide a complex CD spectrum, consisting of a superposition of signals induced by the intrinsic asymmetry of molecules, excitonic short-range interactions, and so-called psi-type

Table 2 Lattice unit cell parameters of C_2S_2 arrays in Arabidopsis *lhcb3 lhcb6*, Arabidopsis WT acclimated to high light and barley *vir-zb63* mutant

Plant	a (Å)	b (Å)	α (°)	ϕ (°)[a]	Type of C_2S_2 double layer	Source
Arabidopsis *lhcb3 lhcb6*	244	170	80	50	Carpet	This study, Figure 6, A
	233	162	84	51	Regular	This study, Figure 6, B
	245	155	83	50	Regular	This study, Figure 6, C
Arabidopsis WT (high light)	234 ± 5[b]	154 ± 1[b]	86 ± 1[b]	48	–	This study, Figure 6, D (data from Kouřil et al. 2013)
Barley *vir-zb63*	250	165	80	–	–	Morosinotto et al. (2006)
	244 ± 3[b]	170 ± 3[b]	82 ± 0[b]	51	–	This study, Figure 6, E
Barley *vir-zb63* (far-red light)	234 ± 0.3[b]	162 ± 0.2[b]	81.2 ± 1.9[b]	–	–	Stoylova et al. (2000)
	243 ± 0.4[b]	162 ± 0.2[b]	81.1 ± 1.9[b]	–	–	Stoylova et al. (2000)
	235 ± 0.4[b]	158 ± 0.3[b]	80.5 ± 2.0[b]	–	–	Stoylova et al. (2000)
	215 ± 0.7[b]	175 ± 0.5[b]	87.1 ± 1.7[b]	–	–	Stoylova et al. (2000)

Notes: The a and b are lengths of vectors of lattice unit cells, α is the angle between these vectors, and ϕ is the angle between the a vector and the diagonal of C_2S_2 supercomplex (see Figure 6, F). Data for the evaluation of the lattice unit cell parameters for Arabidopsis acclimated to high light (800 μmol photons m^{-2} s^{-1}) was taken from Kouřil et al. (2013). For other details, see the legend to Figure 6 and Materials and Methods.
[a]Evaluated from the models presented in Figure 6.
[b]Values $\pm$ SD.

signals (polymer and salt-induced; Garab and van Amerongen, 2009). We are mostly interested in the psi-type signals, as they originate from three-dimensional aggregates, which contain a high number of interacting chromophores and whose dimensions are comparable to the wavelength of measuring light.

The main spectral features of the CD spectra of WT leaves (Figure 7) are three bands at wavelengths around (+)685, (–)673, and (+)505 nm, which are of psi-type origin and thus reflecting the supramolecular organization of pigment–protein complexes (Barzda et al., 1994; Dobrikova et al., 2003). It is well established that the (+)685 and (–)673 nm psi-type CD bands are associated with chlorophyll molecules while the (+)505 psi-type CD band mainly originates from a β-carotene bound to PSII core complexes (Kovács et al., 2006; Tóth et al., 2016). The psi-type CD (–)673 nm band is mostly associated with grana stacking (Garab et al., 1991), whereas the (+)505 and (+)685 nm bands are not linked directly to the granal stacking, but rather to the lateral supramolecular organization of PSII–LHCII supercomplexes (Kovács et al., 2006; Tóth et al., 2016).

In agreement with EM microscopy analysis, the absence of LHCB3 did not lead to a substantial change in long-range macroorganization of the thylakoid membranes compared with WT, which is evidenced by a very similar psi-type signal (Figure 7). On the other hand, the depletion of LHCB6 (in both *lhcb6* and *lhcb3 lhcb6*) led to an almost complete loss of the main positive psi-type band at 685 nm, whereas the 505-nm band was unaffected (Figure 7). This change, which agrees with previously published data obtained on *lhcb6* (Kovács et al., 2006; Tóth et al., 2016), was even more pronounced in leaves of *lhcb3 lhcb6* (Figure 7). The ratio CD_{685}/CD_{505}, suggested to be proportional to PSII nearest neighbor distance (Tóth et al., 2016), is also lower in the double mutant compared with *lhcb6* (Figure 7). CD data thus support our finding from EM analysis that the *lhcb3 lhcb6* mutants have an exceptionally high abundance of C_2S_2 semi-crystalline arrays in their granal thylakoid membranes.

C_2S_2 arrays transiently slow down the electron flow from PSII to PSI

To examine the functional state of the donor and acceptor sides of the PSII complex in the LHCB mutants, the kinetics of the Q_A^- reoxidation after a single-turnover saturating flash was measured on intact leaves (Supplemental Figure S6). For WT and mutant leaves, we have observed very similar multiphasic fluorescence decay kinetics of variable fluorescence, which could be deconvoluted into three different exponential decays (Supplemental Table S1). The fast decay component (time constant ~460–490 μs, relative amplitude ~ 62%–65%), which arises from Q_A^- to Q_B/Q_B^- electron transfer (Vass et al., 1999), was similar in all plants, which indicates that the redox gap between the two quinone acceptors is largely unaffected in the studied LHCB mutants. The middle decay phase (~70–80 ms, 14%–16%), reflecting the Q_A^- reoxidation in the PSII centers with an empty Q_B pocket (Deák et al., 2014), was also unchanged, suggesting a very similar redox state of PQ in the dark in WT and the mutants. Only very minor differences were observed in the slow phase of the decay (~3.6–4 s, 20%–23%), arising from $S_2(Q_AQ_B)^-$ charge recombination, indicating that also the donor side of PSII in the mutants is not substantially different from WT. Thus, we can conclude that no substantial changes in the properties of both the acceptor and donor side of PSII were observed.

Although the function of PSII per se was not affected by the loss of LHCB3 and/or LHCB6 or by the arrangement of PSII into C_2S_2 arrays, the mesoscopic arrangement of PSII has important consequences for the functionality of the electron transport chain. To analyze the electron transport balance between PSII and PSI, we have simultaneously measured chlorophyll fluorescence and P700 oxidation, reflecting the photochemical activity of PSII and PSI (Figure 8). Upon switching on the actinic light, P700 is gradually oxidized due to PSI photochemistry and subsequent outflow of electrons from the acceptor side of PSI, but at the same time, it is reduced by electrons from PSII or cyclic electron flow around PSI. The balance between these processes shapes the final P700 signal.
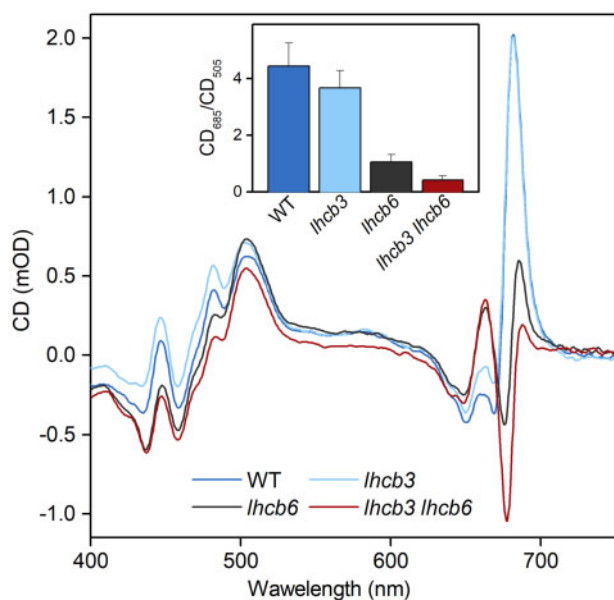
Figure 7 CD Spectra of intact leaves of WT and mutant plants (*lhcb3*, *lhcb6*, *lhcb3 lhcb6*). Averaged spectra from four leaves of each genotype (WT, *lhcb3*, *lhcb6*, *lhcb3 lhcb6*) are shown, for each leaf three scans were collected and averaged. CD spectra were normalized to the Chl Q_y absorption band. The inset presents the ratio of amplitudes of positive psi-type CD bands (CD_{685}/CD_{505}), mean $\pm$ SD is shown ($n = 4$).

In WT leaves, the full stable oxidation of P700 is reached after ca 60 s of light exposure (Figure 8, A). Within this period, the limitation of electron flow at the acceptor side of PSI is replaced by the limitation of electron flow at the donor side of PSI (Figure 9, D and E). This response probably reflects the induction of so-called photosynthetic control, that is the slowing of electron flow on the level of the cytochrome $b_6 f$ complex due to lumen acidification induced by cyclic electron flow around PSI (Yamamoto and Shikanai, 2019). The P700 kinetics is the same in the leaves of *lhcb3* mutants (Figure 8, B), indicating that the electron transport is similar to WT plants. In *lhcb6* and *lhcb3 lhcb6* mutants, however, the light-induced oxidation of P700 is much faster, as P700 is fully oxidized already within the first ca 15 s of illumination (Figure 8, C and D). Although in principle this type of response can result from faster activation of electron outflow from the acceptor side of PSI, the most likely explanation of this phenomenon is the limited supply of electrons to PSI. A very similar acceleration of P700 oxidation upon transition to high light was observed also in *pgr1* Arabidopsis mutant (Yamamoto and Shikanai, 2019), in which the sensitivity of the activation of photosynthetic control to lumen acidification is enhanced due to a mutation of the Rieske protein in the cytochrome $b_6 f$ complex (Munekage et al., 2001).

The fast activation of photosynthetic control in mutants without LHCB6 is supported by the highly retarded electron transport rate through PSI (ETR-I, Figure 9, C), accompanied by a strong limitation of electron transport on the donor side of PSI (Y(ND), Figure 9, D). Chlorophyll fluorescence

data used for the monitoring of the PSII functioning show that in the first minutes of light exposure, the electron transport rate of PSII is reduced (ETR-II, Figure 9, B). Taking into account that the PSII function per se is not affected by the mutations (see above), these lower values of ETR-II indicate a higher reduction of the PQ pool. In principle, the lower ETR-II could also reflect a lower supply of excitations to PSII due to the smaller light-harvesting capacity of the mutants, but this was not confirmed (see below). The higher values of the parameter $1-qP$ (reflecting higher reduction of PQ pool) in the first minutes of light exposure in *lhcb6* and *lhcb3 lhcb6* (Figure 10) further support the view that in this time range, the PQ pool in thylakoid membranes of *lhcb6* and *lhcb3 lhcb6* is more reduced than in WT and *lhcb3*. The discrepancy between the transient higher reduction of PQ pool and the pronounced limitation of PSI electron transport due to a shortage of electrons on the donor side of PSI in *lhcb6* and *lhcb3 lhcb6* could be a result of the organization of PSII into $C_2 S_2$ arrays in these mutants. However, it is important to stress that this restriction is only transient, as the PSII and PSI electron transport rates reach the WT values after several minutes of light exposure (Figure 9, B and C). This result agrees with the results by Chen et al. (2018), who observed WT level of ETR-II at steady-state conditions in *lhcb6* mutant, but disagrees with the results by de Bianchi et al. (2008), who observed in *lhcb6* mutant a permanent restriction of electron transport.

The induction of NPQ of excitations in *lhcb6* and *lhcb3 lhcb6* mutants was different from the WT and *lhcb3*. The absence of LHCB6 resulted in fast induction of NPQ in the first 30 s of light exposure, even faster than in WT and *lhcb3*, followed by a slow rise in NPQ till the end of light exposure (Figure 9, A), at which point its value reached 80%–85% of the WT and *lhcb3* value. Again, these findings correspond with the results by Chen et al. (2018), who observed similar level of the steady-state NPQ in *lhcb6* and WT, but disagrees with the results obtained by de Bianchi et al. (2008), who have reported much lower NPQ values. de Bianchi et al. (2008) explained their NPQ data by permanent restriction in electron transport leading to lower lumen acidification. However, our NPQ data indicate that there is only transient limitation in electron transport rates upon the dark-to-light transition described above.

The effective antenna size of PSII is not reduced in the mutants

The data from CN-PAGE and EM show that PSII supercomplexes in *lhcb6* and *lhcb3 lhcb6* lack the M trimer, that is the supercomplexes have smaller apparent antenna compared with WT. However, at the same time, our mass spectrometry data clearly indicate that in all mutants, the relative amount of light-harvesting proteins per RC PSII is very similar to WT (Figure 2, A). We can thus ask where these unbound LHCII trimers are located and whether they are functionally connected to PSII. As they cannot be present within the $C_2 S_2$ arrays in *lhcb6* and *lhcb3 lhcb6*, they

Table 3 Chlorophyll fluorescence induction parameters

	F_V/F_M	F_O (r.u.)	F_M (r.u.)	ACS PSII (r.u.)	TR_0/RC (r.u.)
WT	0.836 ± 0.003	1.00 ± 0.03	1.00 ± 0.03	1.00 ± 0.03	1.00 ± 0.06
lhcb3	0.819 ± 0.011	1.07 ± 0.01	0.97 ± 0.05	0.97 ± 0.06	1.04 ± 0.05
lhcb6	0.749 ± 0.014	1.33 ± 0.04	0.87 ± 0.06	1.00 ± 0.07	1.06 ± 0.09
lhcb3 lhcb6	0.731 ± 0.011	1.41 ± 0.01	0.86 ± 0.05	1.15 ± 0.11	1.19 ± 0.05

Notes: Absorption cross-section of PSII was estimated using the area above the chlorophyll fluorescence induction curve in DCMU-treated leaves (ACS PSII) and the initial slope of the O–J rise in the chlorophyll fluorescence induction normalized to the fluorescence intensity at the J step (TR_0/RC). The parameters, except for the F_V/F_M, are normalized to the values of WT. Presented values are means $\pm$ SD ($n = 5$–8).

are most probably concentrated in areas with low PSII density sometimes observed at the edge of the arrays (low PSII density area, see Supplemental Figures S2, C, S3). The question is whether they are functionally attached to PSII in crystalline arrays.

To resolve this issue, we have decided to estimate the effective antenna size of PSII via the measurement of chlorophyll fluorescence induction curves. The maximal quantum yield of PSII photochemistry for dark-adapted samples, expressed as the F_V/F_M ratio (Kitajima and Butler, 1975; Lazár, 1999), is ≈0.83, which is a typical value for healthy leaves (Björkman and Demmig, 1987; Lazár and Nauš, 1998). The mutants without LHCB6 have lower values of the quantum yield, which is caused by a simultaneous increase in minimal chlorophyll fluorescence (F_O) and a decrease in maximal fluorescence (F_M) (Table 3). The effective antenna size, estimated from the O–J phase of the O–J–I–P chlorophyll fluorescence induction curves (TR_0/RC parameter), was unexpectedly slightly higher in the mutants, and the increase was the highest for the lhcb3 lhcb6 mutant (119% of WT, Table 3). Similar results have been obtained using estimation of PSII absorption cross-section based on chlorophyll fluorescence induction measured with electron-blocking agent DCMU (ACS PSII). Also, this method indicates that the absorption cross-section of the lhcb3 lhcb6 mutant is slightly higher than in WT (115% of WT, Table 3).

Based on our data we can conclude that the domains of unbound LHCII, which we assume to be present at grana margins in lhcb3 lhcb6, are most likely responsible for the mild increase in the minimal fluorescence F_O. However, considering the supposed large number of unbound LHCII, they are either very effectively quenched, or are functionally connected to PSII arrays. The estimation of absorption cross-section indicates that the latter possibility is more likely. If only S trimers were involved in light-harvesting, the absorption cross-section should be considerably smaller than in WT, where the predominant form of PSII is $C_2S_2M_2$. The fact that the absorption cross-section in the mutants without LHCB6 did not decrease compared with WT is a clear indication that the pool of unbound LHCII can supply excitations to PSII in the arrays. The existence of a large fraction of LHCII weakly connected to PSII in thylakoid membranes of the lhcb6 mutant is also supported by fluorescence lifetime measurements at different excitation wavelengths performed earlier for lhcb6 mutant by van Oort et al. (2010).

These weakly bound LHCIIs characterized by high fluorescence lifetime are probably the reason for the observed higher F_O values in lhcb6 and lhcb3 lhcb6 mutants, which can lower the F_V/F_M ratio and thus underestimate the real maximum yield of PSII photochemistry.

As the effective antenna of PSII, as well as the functionality of RC PSII, are very similar in WT and all mutants, the transient retardation of the electron transport observed in lhcb6 and lhcb3 lhcb6 is most likely a result of limited mobility of electron carriers involved in the transfer of electrons to PSI. In our case, cytochrome b_6f complex is most likely localized at grana margins (it is probably not a part of arrays) and thus it seems unlikely that the transfer from cytochrome b_6f complex to PSI via plastocyanin would be largely affected. The most probable electron carrier that would be affected by the arrangement of PSII into semi-crystalline arrays is PQ (Morosinotto et al., 2006; de Bianchi et al., 2008).

Lateral separation of LHCII results in faster state transitions

It can be expected that the lateral separation of PSII supercomplexes from a substantial part of LHCII trimers would have functional consequences, namely on processes that largely involve LHCII. Assuming that free LHCII trimers are preferentially localized at the periphery of the PSII arrays, likely at grana margins, this localization should affect the process of state transitions. To verify this assumption, we have measured both the extent and rate of state transitions in WT as well as in all the mutants. State transitions were successfully induced in all plants (Supplemental Figure S7) and the changes of absorption cross-sections of PSII upon State I to State II transition were similar in all genotypes (Table 4).

However, the rate of state transitions (characterized by $t_{1/2}$ of the fluorescence decay upon switching off far-red light) was significantly different in individual mutants. In lhcb3, the rate was almost two times faster compared with WT (Table 4). This is in agreement with the previous study, where higher phosphorylation of LHCII (due to the replacement of LHCB3 by LHCB1/2) was identified as a possible cause of faster state transitions (Damkjær et al., 2009). In the lhcb6 and lhcb3 lhcb6 mutants, we have found that the rates were about four times faster compared with WT (Table 4), which agrees with faster state transitions in lhcb6 reported by de Bianchi et al. (2008).
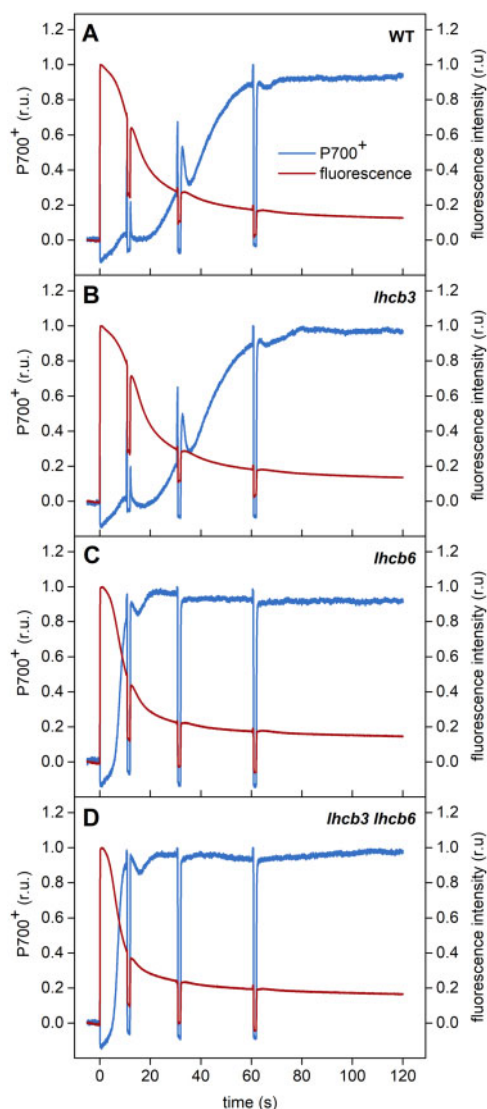
Figure 8 Representative P700 oxidation and chlorophyll fluorescence induction curves of WT and mutant plants (*lhcb3*, *lhcb6*, *lhcb3 lhcb6*). The induction curves were recorded in leaves dark-adapted for 30 min and then exposed to actinic light (800 μmol photons m^{-2} s^{-1}). The induction curves were interrupted by saturating red light pulses (300 ms, 10,000 μmol photons m^{-2} s^{-1}) followed by switching off the actinic light for 1 s, which were necessary for the calculation of PSII and PSI activity parameters presented in Figure 9. Representative curves are shown.

As similarly fast state transitions were observed in *lhcb6* and *lhcb3 lhcb6*, it is not likely that the effect is related to the replacement of LHCB3. The reason for such substantially faster state transition in *lhcb6* and *lhcb3 lhcb6* might be the involvement of free LHCII trimers localized at the periphery of the PSII arrays. Due to their peripheral location, they would have a substantially shorter migration distance to PSI than free trimers in WT, where they are probably dispersed in the whole area of the granum. At the same time, the free LHCIIs are most likely co-localized with the cytochrome $b_6 f$ complex, which is required for

the activation of the kinase responsible for state transitions. Therefore, once activated, it can directly phosphorylate LHCII located conveniently at its vicinity and the phosphorylated LHCII then can quickly attach to PSI which is located nearby.

Discussion

"Spruce-type" C_2S_2M supercomplex appears in Arabidopsis lacking LHCB3

Since the emergence of LHCB3 and LHCB6 proteins at the dawn of plant land colonization, the structure of the $C_2S_2M_2$ supercomplex had been thought to be highly conserved. However, recently we have broken this dogma and have shown that LHCB3 and LHCB6 proteins, whose presence had been considered as a fingerprint of all land plants, are absent in several gymnosperm families. The loss of these two light-harvesting proteins is reflected in a unique structure of PSII supercomplex in these plant species ("spruce-type" $C_2S_2M_2$ supercomplex). In this supercomplex, the position usually occupied by LHCB6 is empty and the binding of the M trimer to the PSII core complex is modified, resulting in its tighter association with the S trimer (Kouřil et al., 2016).

It is not clear why such specific photosynthetic adaptation has developed in this group of plants. As LHCB3 and LHCB6 proteins are known to be downregulated during high light stress (Kouřil et al., 2013), it is possible that this adaptation could be connected with environmental conditions in which the ancestors of these plant groups have evolved. This would also partially explain the unusual responses of spruce photosynthetic apparatus to changes in light intensity, some of them being typical for high-light adapted plants (Kurasova et al., 2003).

To shed some light on the evolutionary and physiological implications of the "spruce-type" form of PSII supercomplex, we have prepared a double mutant of *A. thaliana* lacking LHCB3 and LHCB6 proteins. It has been shown that in the absence of LHCB3, the M trimer can bind to C_2S_2, but in a slightly different rotational position than in WT (Damkjær et al., 2009). Nevertheless, this change does not correspond with the binding mode of the M trimer within the "spruce-type" $C_2S_2M_2$ (Kouřil et al., 2016). At the same time, in Arabidopsis, the $C_2S_2M_2$ supercomplex with LHCB3-less M trimer is very fragile, a feature not observed in the "spruce-type" supercomplex. The loss of LHCB6 is known to induce much more serious disturbance of photosynthetic apparatus of Arabidopsis than the loss of LHCB3 (Kovács et al., 2006; de Bianchi et al., 2008). It has been shown that the absence of LHCB6 leads to the dissociation of the M trimer, leaving C_2S_2 as the main form of supercomplex in the *lhcb6* mutant (Kovács et al., 2006). By creating a double *lhcb3 lhcb6* mutant, we wanted to find out whether the modified LHCII trimer without LHCB3 is able to bind to C_2S_2 in the absence of LHCB6 and whether the resulting supercomplex will mimic the structure of the "spruce-type" $C_2S_2M_2$.
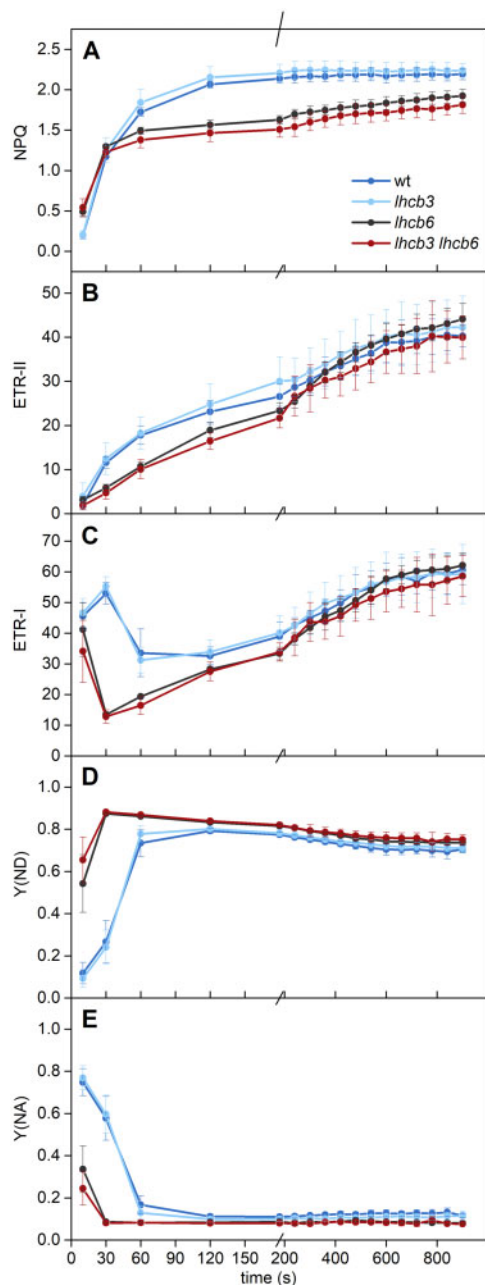
Figure 9 Photosynthetic control parameters in WT and mutant plants (*lhcb3*, *lhcb6*, *lhcb3 lhcb6*) during light exposure. The parameters of (A) NPQ in PSII, electron transport rates through (B) PSII and (C) PSI (ETR-II and ETR-I), and quantum yields of non-photochemical energy dissipation in PSI due to (D) donor and (E) acceptor side limitation (Y(ND) and Y(NA)) were recorded in leaves dark-adapted for 30 min and then exposed to actinic light (800 μmol photons m^{-2} s^{-1}). The parameters were calculated using saturating red light pulses (300 ms, 10,000 μmol photons m^{-2} s^{-1}) applied during 16-min actinic light exposure. The presented values are means ± SD from four plants.

Our results revealed that the "spruce-type" supercomplex without LHCB3 and LHCB6 can be formed even in in Arabidopsis (Figure 3, B), but at the same time, it appears that there are other important factors that are playing role in its formation and stability. Nevertheless, we were able to

observe and identify the "spruce-type" supercomplex in an angiosperm plant, in particular in the *lhcb3* mutant. It is obvious that this type of supercomplex can be formed only when LHCB6 is absent along with LHCB3 (Figure 3, B), whereas in the presence of LHCB6, the LHCB3-less supercomplex closely resembles the supercomplex from WT. It is difficult to make any estimation of the abundance of "spruce-type" supercomplex in *lhcb3* in vivo, as the results of CN-PAGE and single particle analysis can be distorted by different stabilities of individual types of supercomplexes. However, the mass spectrometry data show that thylakoid membranes from *lhcb3* have a lower relative amount of LHCB6 (70% of WT, Figure 2, A), so it is tempting to hypothesize that in vivo, the fraction of supercomplexes that lack LHCB6 might correspond to the fraction of "spruce-type" supercomplexes.

We have confirmed that in Arabidopsis, "spruce-type" supercomplexes without LHCB3 and LHCB6 can be formed, but why these supercomplexes are not found in the double mutant *lhcb3 lhcb6*? As has been mentioned, it appears that without LHCB3, the attachment of the M trimer to C_2S_2 is much weaker than in WT—in the CN-PAGE of mildly solubilized *lhcb3* thylakoids we did not see any $C_2S_2M_2$ band (Figure 3, A), although we know that this type of supercomplex is present in vivo in this mutant (Damkjær et al., 2009). No such disassembly was observed for WT $C_2S_2M_2$ (Figure 3, A). The combined absence of LHCB3 and LHCB6 may lead to so strong destabilization of the M trimer, that the resulting structure is not advantageous. It might be possible that the binding of the M trimer to C_2S_2 is so weak that it cannot ensure efficient energy transfer and in such situation, the formation of C_2S_2 arrays functionally connected to a large pool of unbound LHCII trimers might represent a preferable, more efficient arrangement.

There is, however, an inevitable question—what is the factor that makes this particular form of supercomplex stable in spruce? It is possible that the key to its different stability in Arabidopsis and spruce is the type of minor antenna protein LHCB4. Due to its prominent position in the PSII supercomplex, LHCB4 is responsible for proper binding of the S and M trimers to the PSII core dimer (de Bianchi et al., 2011; van Bezouwen et al., 2017; Su et al., 2017) and plays a key role in both the energy transfer and PSII photoprotection (de Bianchi et al., 2011). Recently, it has been found that the Pinaceae and Gnetales families lack not only LHCB3 and LHCB6, but also the LHCB4.1/4.2 proteins, which have so far been thought to be the dominant isoforms of LHCB4 in land plants (Grebe et al., 2019). It appears that in spruce, only the gene for the isoform LHCB4.3 (later renamed LHCB8) is present, which has for a long time been considered as a peculiar, rarely expressed gene restricted only to angiosperm clade Eurosids (Klimmek et al., 2006). In spruce PSII, LHCB8 replaces LHCB4.1/4.2 at its binding site in the $C_2S_2M_2$, which could contribute to the stability of the "spruce-type" supercomplex.

In Arabidopsis, LHCB4 is present in three isoforms coded by three separate genes—LHCB4.1 (AT5G01530), LHCB4.2
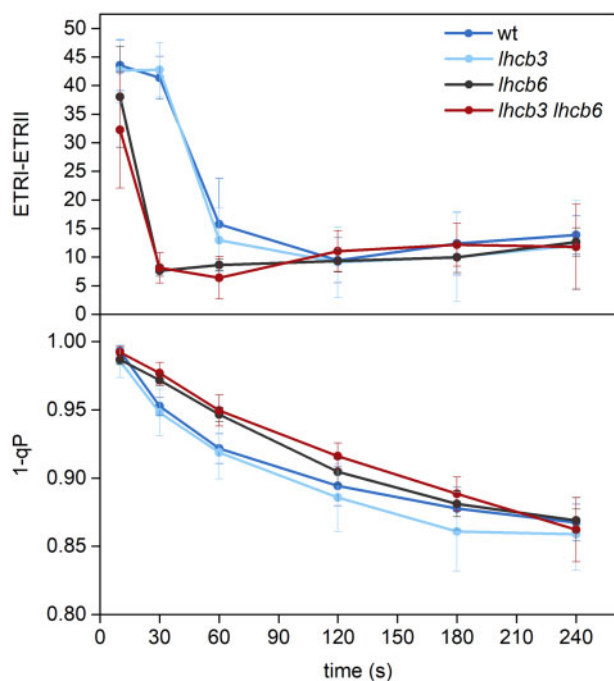
Figure 10 Cyclic electron flow around PSI and redox state of the PQ pool in WT and mutant plants (*lhcb3*, *lhcb6*, *lhcb3 lhcb6*). The extent of cyclic electron flow around PSI was estimated as a difference between ETR-I and ETR-II shown in Figure 9. The fraction of reduced PQ pool in thylakoid membranes was evaluated as 1–qP, where qP is the photochemical quenching coefficient calculated as $(F_M'-F)/(F_M'-F_O')$. The intensity of actinic light was 800 μmol photons m^{-2} s^{-1}. The presented values are means ± SD from four plants.

(AT3G08940), and LHCB4.3 (AT2G40100). All LHCB4.1/4.2 proteins from various plants have a strictly conserved 15-amino-acid motif at their C-terminus (WxTHLxDPLHTTIxD; Grebe et al., 2019). This motif has been proposed as the site of the interaction of LHCB4.1/4.2 with LHCB6 and LHCB3 (i.e. the M trimer; Su et al., 2017). This C-terminal motif is completely absent in LHCB4.3, which could explain why the evolution pressure in plant species without LHCB3 and LHCB6 led to the loss of LHCB4.1/4.2, whereas LHCB4.3 has been retained. The proteins LHCB4.1 and LHCB4.2 have high sequence homology (89% identity) and similar structure, function, and regulation (Jansson, 1999; de Bianchi et al., 2011), whereas there are strong indications that LHCB4.3 is functionally different from LHCB4.1/4.2, at least in angiosperms (Klimmek et al., 2006).

To explore possible changes in the relative amount of individual LHCB4 isoforms in the mutants, we have performed a detailed analysis of the mass spectrometry data. The amount LHCB4.3 was not increased in any of the mutants compared with WT, which indicates that in Arabidopsis, the loss of LHCB3 and/or LHCB6 does not stimulate the synthesis of LHCB4.3 (Figure 2, B). Even in a very detailed proteomic analysis of the supercomplexes eluted from the *lhcb3* $C_2S_2M_2$ band, which contains a fraction of "spruce-type" C_2S_2M, we did not see any change in the relative LHCB4.3 content (Figure 11). It seems that in Arabidopsis, the

regulation of gene expression of *LHCB4.3* is completely different from spruce. The main role of LHCB4.3 in Eurosids is probably related to photoprotection, as there is an up-regulation of the LHCB4.3 gene expression under high-light conditions (Klimmek et al., 2006; Albanese et al., 2016a, 2018, 2019).

We can thus hypothesize that the reason why we were not able to observe "spruce-type" PSII supercomplexes in Arabidopsis *lhcb3 lhcb6* double mutant is the presence of LHCB4.1/4.2 proteins, which are replaced by LHCB4.3 (LHCB8) in spruce. Analysis of the double mutant grown under specific conditions leading to the accumulation of LHCB4.3 might clarify whether LHCB4.3 is indeed the key to the stability of "spruce-type" PSII supercomplex or whether some other factors stabilize this unusual PSII supercomplex structure in spruce (e.g. differences in amino-acid composition of PSII proteins in spruce and Arabidopsis, different phosphorylation pattern, etc.). Physiological characterization of Arabidopsis plants with high abundance of "spruce-type" PSII would be important for our understanding of the specifics of photosynthesis in spruce and could provide valuable clues about the possible evolutionary advantage of the loss of LHCB3 and LHCB6 in some gymnosperm groups.

Semi-crystalline arrays of PSII supercomplexes

Today we have a lot of information about photosynthetic complexes at the level of individual proteins or protein complexes (high-resolution crystal structures). However, their organization into higher order assemblies and their cooperation within them is still poorly understood, although it is clear that these processes play a key role in the highly organized and strongly regulated process of photosynthesis.

It has been known for a very long time that PSII supercomplexes in granal membranes are able to spontaneously order into semi-crystalline arrays. However, only after solving the PSII supercomplex crystal structure, it was possible to identify particular types of supercomplexes that are involved in array formation. In an extensive study, Boekema et al. (2000) were able to unequivocally distinguish two types of crystals in spinach thylakoids. The more abundant crystals with wider spacing (27.3 × 18.3 nm, 74.5°, unit area 481 nm^2) were shown to consist of the array of C_2S_2M, whereas the rare (1% abundance), more tightly packed crystals (23 × 16.9 nm, unit area of 389 nm^2) were formed by C_2S_2. On the contrary to spinach, the analysis of thylakoid membranes in Arabidopsis revealed only one type of semi-crystalline arrays, which have a bigger unit cell (25.6 × 21.4 nm, 77°, 534 nm^2) that has been identified as $C_2S_2M_2$ (Yakushevska et al., 2001). These data indicate that all forms of PSII supercomplexes (i.e. C_2S_2, C_2S_2M, and $C_2S_2M_2$) are capable of forming semi-crystalline arrays, although different types of arrays may have different properties and function. Since then, a number of studies have described the presence of the arrays in several plant species grown under various conditions (Kirchhoff et al., 2007; Daum et al., 2010; Sznee et al., 2011; Kouřil et al., 2013; Wientjes et al., 2013; Charuvi et al., 2015) or in various mutants (Ruban et al., 2003; Yakushevska et al., 2003;

Table 4 State transition parameters

	$t_{1/2}$ (s)	qT (%)
WT	124 ± 14	11.7 ± 0.4
lhcb3	75 ± 12	12.9 ± 0.4
lhcb6	26 ± 1	8.7 ± 1.3
lhcb3 lhcb6	28 ± 1	9.2 ± 1

Notes: The rate of state transition from State I to State II was characterized as the half-time ($t_{1/2}$) of a gradual fluorescence decay upon switching off far-red light according to Damkjær et al. (2009). Parameter qT, which reflects the decrease in the LHCII antenna size, was calculated as $(F_M' - F_M'')/F_M'$. Presented values are means ± SD ($n = 5$).

Morosinotto et al., 2006; Kovács et al., 2006; de Bianchi et al., 2008; Damkjær et al., 2009; Kereïche et al., 2010; Goral et al., 2012; Onoa et al., 2014; Tietz et al., 2015). Thus, it appears that the formation of PSII arrays is a relatively widespread phenomenon.

The heterogeneity in PSII packing, that is the simultaneous existence of "random" and "arrayed" PSII in thylakoid membranes, makes it difficult to analyze the specific properties of PSII in the arrays. The proportion of PSII present in the crystal phase is usually relatively low (around or below 10%), although there are some mutants where the fraction of arrays is reported to be higher (Morosinotto et al., 2006; Goral et al., 2012; Tietz et al., 2015). The double mutant lhcb3 lhcb6 prepared in this study is unique as it has the majority of PSII supercomplexes packed into C_2S_2 semi-crystalline arrays (Figure 4), that is it represents a very good model for the investigation of formation, regulation, and properties of C_2S_2 PSII arrays.

It has been suggested that one of the functions of C_2S_2 arrays might be related to more efficient energy transfer among different supercomplexes (Morosinotto et al., 2006). As high protein density is a prerequisite for efficient energy transfer (Haferkamp et al., 2010), it can be speculated that the tight packing of C_2S_2 supercomplexes improves energy equilibration within interconnected antenna and makes the distribution of excitations to PSII more efficient. As the relative amount of LHCII per reaction center in both lhcb6 and lhcb3 lhcb6 is approximately the same as in WT (Figure 2 and Table 1), the LHCII trimers, which in WT are bound within $C_2S_2M_2$, have to contribute to the pool of "free" LHCII in the mutants. As the free trimers are not part of the arrays, they most likely create LHCII-only areas outside the arrays at the grana margins. The presence of these unattached LHCII is probably responsible for slightly higher minimal fluorescence F_O observed in the mutants (Table 3). However, it appears that this pool of LHCII has to be functionally connected with PSII in the arrays, as the effective absorption cross-section of PSII in lhcb6 and lhcb3 lhcb6 is comparable, or even slightly higher than in WT (Table 3). We can hypothesize that the packing of C_2S_2 supercomplexes into arrays and their functional attachment to the pool of free LHCII might represent a compensatory mechanism, which can substitute the binding of M trimers to individual PSII in the form of $C_2S_2M_2$.

The "separation" of the pool of free LHCII at the grana margins can also explain faster kinetics of state transitions. Due to space restrictions, it is obvious that the cytochrome b_6f complex is not a part of the arrays and thus it is probably located close to the LHCII pool at grana margins. It has been suggested that the kinase involved in state transitions cannot enter the closely stacked areas in the grana and that it is able to phosphorylate only LHCII in stroma or on the interface between grana and stroma (Dekker and Boekema, 2005). The activation of the kinase thus probably takes place in the same area (or very close) to the pool of free LHCII and, once phosphorylated, LHCII will have a short diffusion distance from the grana margins to stromal thylakoids. As a result, we can expect significantly faster state transition kinetics, which is indeed a phenomenon we have observed in both mutants without LHCB6 (Table 4).

Another of the frequently discussed issues related to PSII arrays is their large effect on the mobility of PQ and thus on the overall electron transport rate. There is an emerging evidence that different types of PSII arrays ($C_2S_2M_2$ and C_2S_2) may actually have the opposite effect on the effectivity of PQ diffusion. It is well known that the granal membrane is highly crowded by proteins (70%–80% of the membrane area, Kirchhoff, 2008) and that the protein concentration is very close to a critical threshold above which the long-range diffusion coefficient drops to zero (Tremmel et al., 2003). It has been proposed that the arrangement of $C_2S_2M_2$ PSII supercomplexes into crystalline arrays can lead to the formation of a kind of lipidic channel, which might be viewed as a diffusion highway facilitating fast diffusion of PQ molecules to the cytochrome b_6f complex localized outside the arrays (Tietz et al., 2015). However, on the other hand, it has been argued that in C_2S_2 arrays the packing is so tight that there is very limited space for PQ diffusion. Indeed, plants with extensive C_2S_2 arrays (Arabidopsis lhcb6, barley viridis zb63) have been previously reported to suffer from retarded linear electron transport, lower PSII yield, and impaired NPQ (Kovács et al., 2006; Morosinotto et al., 2006; de Bianchi et al., 2008).

However, the situation appears to be much more complex, as a detailed analysis of multiple crystalline arrays in the lhcb3 lhcb6 mutant revealed that there is a substantial degree of variability in the types of C_2S_2 arrays (Table 2). It appears that while some of the C_2S_2 arrays are indeed very tightly packed, leaving very small space for the diffusion of PQ, there are also other types of arrays where the diffusion restriction is not so severe. As in all types of the observed crystals the Q_B pocket (red asterisk, Figure 6) is freely accessible to PQ (black dots, Figure 6), the main factor affecting the PQ diffusion appears to be the spatial "bottleneck" between LHCB4 and LHCB5 in the neighboring supercomplexes (red and blue circles, Figure 6). Figure 6, A shows a type of crystal where the packing of C_2S_2 supercomplexes is relatively loose, with enough space left between individual protein complexes to enable diffusion of PQ in all directions. A similar type of crystal was observed in barley mutant without PSI (viridis zb63) (Figure 6, E). However, in lhcb3
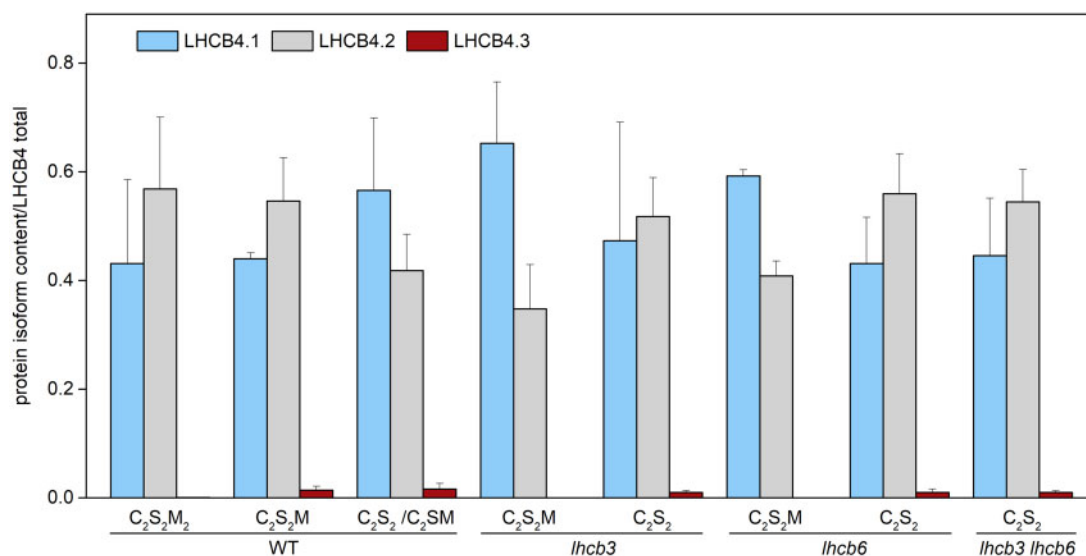
Figure 11 Content of individual LHCB4 isoforms in PSII supercomplexes isolated from *A. thaliana* WT and mutant plants (*lhcb3*, *lhcb6*, *lhcb3 lhcb6*). The relative content of individual LHCB4 isoforms was determined by LC–MS/MS in samples prepared from gel bands excised from CN-PAGE (see Figure 3, A). The contribution of LHCB4.1, 4.2 and 4.3 isoforms, evaluated from normalized PG intensities, is shown relatively to the overall content of LHCB4. The presented values are means ± SD from four replicates. Different forms of separated PSII supercomplexes consist of PSII core dimer (C_2) and one and/or two copies of strongly (S) and moderately (M) bound light-harvesting trimers.

lhcb6, we have also found crystals with smaller lattice units (Table 2), where the PQ diffusion pathway was partially closed due to the very close contact between LHCB4 subunits of neighboring C_2S_2 supercomplexes (red circle, Figure 6, B and C). As a result, the PQ diffusion is more restricted in these types of crystals as PQ can move only in one direction (horizontally, considering the crystal orientation shown in Figure 6, B and C). An example of an extremely tightly packed C_2S_2 crystal is shown in Figure 6, D. In this PSII arrangement, previously sporadically observed in high-light acclimated WT Arabidopsis (Kouřil et al., 2013), the diffusion of PQ is completely restricted, as the possible pathways are closed in both directions by a tight contact between LHCB4 and LHCB5 antennae (red circles, Figure 6, D). It can be assumed that the PSII supercomplexes arranged into this type of crystal do not contribute to linear electron transport and could represent an operative storage structure of PSII with their own quenching mechanism.

Our data indicate that there is a variety of C_2S_2 crystal types, which largely vary with respect to the degree of the restriction of PQ diffusion. It appears that a very small rearrangement of the PSII crystalline arrays can have a large effect on their photochemical activity, as it can lead to the opening or closing of two apparent "bottlenecks" for PQ diffusion, localized between LHCB4 and LHCB5 subunits of the neighboring supercomplexes. It is possible that such crystal rearrangement can be a part of the fine-tuning mechanism by which plants regulate and optimize electron transport under various conditions.

Formation of C_2S_2 arrays—a strategy for the protection of both PSI and PSII upon abrupt high light exposure?

Analysis of the photosynthetic response of *lhcb6* and *lhcb3 lhcb6* mutants revealed significant retardation of the electron transport rate in the first minutes of light exposure. Interestingly, after this transient slow-down, the electron transport parameters in both mutants reached the values of WT and *lhcb3* (Figure 9). This finding contradicts the result obtained by de Bianchi et al. (2008), who have reported that considerable suppression of the PSII electron transport rate of *lhcb6* persists even at steady-state conditions. The reason for the discrepancy is not clear, but it could be associated with different growth conditions leading to substantially higher overall fitness of our *lhcb6* (and *lhcb3 lhcb6*) mutants, which is evidenced by, for example better growth (Figure 1, A), higher F_V/F_M ratio (Table 3) or NPQ values (Figure 9, A). Obviously, in our case, the transient retardation of electron flow between PSII and PSI in mutants without LHCB6 cannot be attributed to any permanent damage of the electron transport pathway, but seems to be rather a result of altered dynamics of regulatory processes. One of the feasible hypotheses that could possibly explain the dynamic changes in electron transport restriction is the light-induced rearrangement/disordering of the C_2S_2 arrays.

It has been shown that immediately after the exposure of dark-adapted plants to light, when the outflow of electrons from the acceptor side of PSI is restricted, the cyclic electron transport (CET) around PSI is highly stimulated (Joliot and Joliot, 2002). As a result, P700 becomes gradually fully oxidized (Figure 8), which is crucial for the protection of PSI against photoinhibition (for a recent review, see Miyake, 2020). The lumen acidification induced by CET then leads to the suppression of electron transport from PSII to PSI on the level of the cytochrome b_6f complex (photosynthetic control, see Yamamoto and Shikanai, 2019), which, together with the gradual activation of electron outflow at the acceptor side of PSI, leads to the suppression of CET. The activity

of CET can be estimated from the difference between electron transport rates ETR I and ETR II and the evaluation of this parameter revealed that the activation and dynamics of CET are the same in WT and *lhcb3* mutant (Figure 10). However, in *lhcb6* and *lhcb3 lhcb6* mutants, the suppression of CET was much faster, within the first 30 s of illumination (Figure 10). The reason for this result is not clear, but could be somehow associated with the transient limitation of PQ diffusion due to the arrangement of PSII into C_2S_2 arrays. As the over-reduction of the PQ pool is thought to suppress CET (Allen, 2003; Miyake, 2010), the higher reduction of the PQ pool observed in the first minutes of illumination in *lhcb6* and *lhcb3 lhcb6* (Figure 10) can be connected with the faster inactivation of CET in these mutants. However, it is important to stress that even when CET is activated for a substantially shorter time in *lhcb6* and *lhcb3 lhcb6* mutants, P700 is oxidized in these plants much faster than in WT (Figure 8). It is tentative to speculate that the transient restriction of PQ diffusion, likely resulting from the packing of PSII into C_2S_2 arrays, can substitute CET in the photoprotection of PSI.

Another interesting phenomenon that might be connected with the arrangement of PSII in C_2S_2 arrays is related to the dynamics of the induction of NPQ. In both *lhcb6* and *lhcb3 lhcb6*, the induction of NPQ in the first seconds of light exposure was faster compared with WT and *lhcb3* (Figure 9, A). The light-induced induction of energy-dependent NPQ (qE) in plants is a strictly regulated and complex process triggered by lumen acidification. Lowering lumen pH leads to several processes, including the dissociation of LHCIIs from PSII supercomplexes, activation of xanthophyll cycle (deepoxidation of violaxanthin (Vio) to zeaxanthin (Zea) by violaxanthin deepoxidase (VDE)), and formation of quenching centers in the aggregated LHCIIs (for a recent review, see Ruban and Wilson, 2020). It has been proposed that the light-induced dissociation of LHCIIs from PSII supercomplexes is represented by a detachment of the M trimer and LHCB6 from the $C_2S_2M_2$ supercomplex and that this process is induced by protonated PsbS (Betterle et al., 2009; Dall'Osto et al., 2017). As the pK$_a$ of PsbS protonation is relatively low (about 5.2, Li et al., 2002), considerably pronounced lumen acidification is necessary for the light-induced disassembly of $C_2S_2M_2$, that is for the induction of NPQ in plants where $C_2S_2M_2$ is the major form of PSII supercomplex. As the dissociation of LHCIIs from PSII supercomplexes is necessary to make Vio in LHCIIs available for the conversion to Zea by activated VDE (for a review, see Morosinotto et al., 2003), pronounced lumen acidification (inducing LHCII dissociation) is also required for the effective function of the xanthophyll cycle, although VDE itself is activated already at higher luminal pH (pKa about 6, Günther et al., 1994; Bratt et al., 1995). Therefore, the dynamics of LHCII detachment appears to be the main factor determining the dynamics/kinetics of NPQ.

Recent findings evidenced that only separated LHCIIs and light-induced lumen acidification are the crucial factors that are necessary for qE (Johnson, 2020; Saccon et al., 2020). Therefore, it is natural to expect that in plants exposed to stress factors that lead to the detachment of LHCII from PSII supercomplexes, the dynamics of qE will be affected. Indeed, faster induction of qE has been observed for example in plants preheated in the dark (Ilík et al., 2010), where the disassembly of PSII supercomplexes is well known (e.g. Lípová et al., 2010). This scenario matches also the results obtained in this work for the *lhcb6* and *lhcb3 lhcb6* Arabidopsis mutants. As the $C_2S_2M_2$ supercomplexes are replaced by C_2S_2 and a large pool of separated LHCII trimers, the dissociation is already achieved and therefore we can observe very fast qE induction in the first seconds of illumination, even though the overall rate of electron transport is retarded. These results are supported by a paper by Townsend et al. (2018), who have observed pronounced initial phase of qE induction in Arabidopsis mutants NoM that lack minor PSII antenna complexes and have a large pool of free LHCIIs. Taking into account the facts above, it appears that PSII arranged into C_2S_2 arrays with a pool of detached LHCII trimers at the array margins represents the arrangement that is "pre-prepared" for the formation of quenching centers and thus is beneficial for very fast induction of NPQ.

Conclusions

Our experiments have shown that the loss of LHCB3 has surprisingly strong destabilizing effect on $C_2S_2M_2$ supercomplexes, as the binding of the LHCB3-less M trimer to C_2S_2 is very weak. A very small part of the PSII supercomplexes in Arabidopsis *lhcb3* mutant appeared to adopt unique structure previously observed only in Norway spruce ("spruce-type" supercomplex), where LHCB6 is missing but the LHCB3-less M trimer is still attached to the PSII core. The absence of the "spruce-type" PSII supercomplexes in the *lhcb6* and *lhcb3 lhcb6* mutants indicates that on the contrary to spruce, in Arabidopsis both LHCB3 and LHCB6 proteins are needed for stable binding of the M trimer to PSII core. As the minor antenna LHCB4 is in direct contact with both the M trimer and LHCB6, we can speculate that the clue to the different stability of the "spruce-type" PSII supercomplex in Arabidopsis and spruce could be different isoform of this protein. The only isoform of LHCB4 in spruce is of LHCB4.3 type (renamed LHCB8), which is characteristic by the loss of a highly conserved motif at its C-terminus. On the other hand, in WT Arabidopsis as well as in all the analyzed mutants, the most populated isoforms were LHCB4.1 and LHCB4.2, with only negligible contribution of LHCB4.3. Further studies are needed to identify factors that are crucial for the formation and stabilization of PSII supercomplex with "spruce-like" structure in Arabidopsis. We are just beginning to understand the unique physiological benefits of the "spruce-like" PSII structure and more effort will be necessary to fully fathom the reasons that led a group of plants to "abandon" the widely conserved and evolutionary optimized PSII structure adopted by all other land plants.

PSII supercomplexes in Arabidopsis *lhcb6* and *lhcb3 lhcb6* mutants were present almost exclusively in the C_2S_2 form, which in WT plants appears primarily at high light conditions when LHCB3 and LHCB6 are downregulated. The C_2S_2 supercomplexes were arranged into very large semi-crystalline arrays, which can be connected with some interesting physiological features we have observed in *lhcb6* and *lhcb3 lhcb6* plants. These mutants showed fast activation of photosynthetic control of electron transport in thylakoid membranes, which can protect PSI against photoinhibition upon a sudden rise in light intensity, and even faster induction of NPQ, protecting PSII against overexcitation. Both these responses, which would be especially helpful in fluctuating light conditions, are probably associated with the restriction of electron transport between PSII and PSI resulting from the semi-crystalline arrangement of C_2S_2. However, on the contrary to the previous study on the *lhcb6* mutant (de Bianchi et al., 2008), we show that this restriction is only transient, as both PSI and PSII electron transport rates in *lhcb6* and *lhcb3 lhcb6* reach WT values after approximately 4 min of continuous illumination. It is tempting to hypothesize that this transient slowdown in electron transport between PSII and PSI could be controlled by light-dependent rearrangement of C_2S_2 semi-crystalline arrays, which would also explain the considerable variability in the types of C_2S_2 arrays we have observed in grana membranes of *lhcb3 lhcb6* mutants. Detailed structural analysis of the dynamics of C_2S_2 arrays in response to light could further contribute to the uncovering of the still enigmatic function of PSII crystalline arrangement in plants.

Material and methods

Plant material and growth conditions

Arabidopsis (*A. thaliana*) WT (accession Columbia) and T-DNA insertion lines *lhcb3* (SALK_020314c), *lhcb6* (SALK_077953) were obtained from Arabidopsis Biological Resource Center collection. Plants carrying double mutation (*lhcb3 lhcb6*) were prepared by crossing homozygous *lhcb3* and *lhcb6* plants. Plants from the F_1 generation were self-fertilized and double homozygous plants were selected from the F_2 generation via PCR genotyping (Thermo Scientific Phire Plant Direct PCR Kit) using the combination of gene-specific primers and universal T-DNA primer LBb1. Primer sequences were as follows: lhcb3_FP: AGAATTCCCTGGCGATTATGG; lhcb3_RP: ATAAAGGTCGTCACCGGAAATG; lhcb6_FP: GGTGAGGAACGAAGAACCAA; lhcb6_RP: CCAAACTCCCGACTTTACCA; and LBb1: GCGTGGACCGCTTGCTGCAACT. Arabidopsis plants were grown in a walk-in phytoscope (Photon Systems Instruments, Drásov, Czech Republic) at 22 °C, with an 8-h light/16-h dark cycle (light intensity 120 μmol photons m^{-2} s^{-1}), and 60% humidity. All experiments were performed with 6–7-week-old plants. Barley (*H. vulgare*) mutant *viridis zb63* was grown hydroponically (Knop solution) in a growth chamber (PGC-40L2, Percival Scientific, USA) at 21 °C, with a 16-h light/8-h dark cycle (light intensity 100 μmol photons m^{-2} s^{-1}) and 50% humidity for 2 weeks.

Fresh weight determination and isolation of thylakoid membranes

Prior to isolation, plants were dark-adapted for 30 min. Arabidopsis rosettes or primary leaves of barley were cut and used for the determination of fresh weight. Subsequently, thylakoid membranes were isolated using the protocol described by Dau et al. (1995). All procedures were performed under green light on ice or at 4 °C. The chlorophyll content in the final thylakoid membrane suspension was determined spectrophotometrically by a pigment extraction in 80% acetone (Lichtenthaler, 1987).

Pigment analysis

Leaves were collected from dark-adapted plants (30 min), weighed, and frozen in liquid nitrogen. After homogenization in 80% acetone with a small amount of $MgCO_3$ and centrifugation (3,600 g, 5 min, 4°C), the obtained supernatant was used for spectrophotometric (Unicam UV 500, Thermo Spectronics, UK) determination of chlorophyll and carotenoid content (Lichtenthaler, 1987). Quantification of xanthophyll content (violaxanthin, antheraxanthin, zeaxanthin) was performed by a reversed-phase high-performance liquid chromatography (HPLC) using Alliance e 2695 HPLC System (Waters, Milford, MA, USA) equipped with 2,998 Photodiode Array detectors. The separation was carried out using a gradient system (1.5 mL min^{-1} at 25 °C) on a LiChrospher 100 RP-18 (5 μm) LiChroCART 250-4 (Merck, Darmstadt, Germany) with acetonitrile:methanol:water (87:10:3; v/v) and methanol:*n*-hexane (80:20; v/v) as solvent systems. Quantification of the xanthophylls was based on the comparison of their absorbance (441 nm violaxanthin, 446 nm antheraxanthin, and 454 nm zeaxanthin) with corresponding standards purchased from DHI Lab Products (Hørsholm, Denmark).

Western blot analysis

Thylakoid membranes (100 μg of chlorophyll) were mixed with 1 mL of extraction buffer (14 mM DL-dithiothreitol, 28 mM Na_2CO_3, 175 mM sucrose, 5% (w/v) SDS, and 10 mM EDTA-Na_2), incubated at 70 °C for 30 min, and centrifuged for 10 min at 19,200 g. The supernatant containing isolated proteins was used for blotting. Isolated proteins (corresponding to 1 μg of chlorophyll) were supplemented with sample buffer (Tricine Sample Buffer, BioRad; 3× diluted) and dH$_2$O to a total volume of 20 μL. After 10 min incubation at 70 °C, samples were loaded onto 10% gel (Mini-PROTEAN TGX Precast Protein Gel, Bio Rad, Hercules, USA). Electrophoretic buffers were prepared according to Schägger (2006). Electrophoresis was performed at RT with a constant voltage of 100 V for 45 min.

The separated proteins were transferred to a polyvinylidene fluoride membrane using Trans-Blot Turbo RTA Mini 0.2 μm PVDF Transfer Kit (Bio Rad) and detected using specific antibodies. All antibodies used in the

present study were purchased from Agrisera (Vännäs, Sweden). The presence of primary antibodies Anti-LHCB3 (AS01 002) and Anti-LHCB6 (AS01 010) was detected with a secondary antibody with conjugated HRP enzyme and a chemiluminescent signal was recorded after developing with Immobilon Western Chemiluminescent HRP Substrate (Merck, Darmstadt, Germany) and visualized using gel scanner Amersham Imager 600RGB (GE HealthCare Life Sciences, Tokyo, Japan).

CN-PAGE

CN-PAGE (CN-page) was performed according to Nosek et al. (2017) with minor modifications. Thylakoid membranes (10 µg of chlorophyll) were solubilized with *n*-dodecyl α-D-maltoside using a detergent:chlorophyll mass ratio of 15, and supplemented with sample buffer (50 mM HEPES/NaOH, pH 7.2, 0.4 M sucrose, 5 mM MgCl$_2$, 15 mM NaCl, 10% glycerol) to a final volume of 30 µL. After short gentle mixing (approximately for 2 s), samples were immediately centrifuged at 20,000 g/4 °C for 10 min to remove non-solubilized membranes. The supernatant was loaded onto a polyacrylamide gel with 4%–8% gradient (Wittig et al., 2007), stacking gel was not used. The electrophoretic separation was conducted in a Bio-Rad Mini protean tetra cell system (Bio Rad), starting with a constant current of 3.5 mA for 15 min and then continuing with a constant current of 7 mA until the front reached the bottom of the gel. The CN-PAGE gel was analyzed using a gel scanner Amersham Imager 600RGB (GE HealthCare Life Sciences, Tokyo, Japan). Transmission mode using white light illumination was used for the visualization of all bands.

Mass spectrometry analysis

Isolated thylakoid membranes were subjected to filter-aided sample preparation as described elsewhere (Wiśniewski et al., 2009). The resulting peptides were analyzed by liquid chromatography–tandem mass spectrometry (LC–MS/MS) performed using UltiMate 3000 RSLCnano system (Thermo Fisher Scientific, Waltham, USA) on-line coupled with Orbitrap Elite hybrid spectrometer (Thermo Fisher Scientific).

Bands with desired PSII supercomplexes separated by CN-PAGE were excised and after washing procedures, each gel band was incubated with trypsin. LC–MS/MS analysis was performed using UltiMate 3000 RSLCnano system (Thermo Fisher Scientific) on-line coupled with Orbitrap Q Exactive HF-X spectrometer (Thermo Fisher Scientific). See the section Supplemental Methods S1 for full details regarding the analyses and data evaluation.

EM and single particle analysis

Elution of isolated PSII supercomplexes from the gel and preparation of specimens for single particle EM was performed according to a procedure described by Kouřil et al. (2014). Electron micrographs were collected using a Tecnai G2 F20 microscope (FEI Technologies, Hillsboro, USA) with an Eagle 4K CCD camera (FEI Technologies) at 133,000× magnification. The pixel size at the specimen level after

binning the images to 2,048 × 2,048 pixels was 0.218 nm. Approximately 92.000, 293.000, 42.000, 33.000, and 61.000 PSII projections were picked in semi-automated mode from 2,128, 7,642, 4,447, 2,311, and 1,925 micrographs of specimens prepared from the gel bands assigned as WT $C_2S_2M_2$, WT C_2S_2M, *lhcb3* $C_2S_2M_2$, *lhcb6* $C_2S_2M_2$, and *lhcb3 lhcb6* C_2S_2, respectively. Individual datasets were subjected to reference-free two-dimensional classification using SCIPION image processing framework (de la Rosa-Trevín et al., 2016). The structure of the $C_2S_2M_2$ supercomplex (van Bezouwen et al., 2017) was used to fit the projection maps of analyzed PSII supercomplexes.

EM of isolated grana membranes from *A. thaliana* WT, *lhcb3*, *lhcb6*, and *lhcb3 lhcb6* mutants, isolated according to Kouřil et al. (2013), was performed on a Jeol JEM2010 (Jeol, Tokyo, Japan) with a Quemesa CCD camera (EMSIS, Muenster, Germany) and a Jeol 2100 (Jeol, Japan) with a Tengra CCD camera (EMSIS, Muenster, Germany). Sub-areas (1,320 × 1,320 Å, 2,160 × 2,160 Å) of two-dimensional crystalline arrays of PSII C_2S_2 supercomplexes from *lhcb3 lhcb6* were analyzed using a single particle approach using RELION software (Scheres, 2012). The structure of the C_2S_2 supercomplex (Wei et al., 2016) was used to fit the two-dimensional arrays. Lattice parameters of the crystalline arrays and a ratio of the area of semi-crystalline PSII arrays per total area of the grana membranes were analyzed using ImageJ software (Schneider et al., 2012).

Chlorophyll fluorescence and P700 measurements

Minimal chlorophyll fluorescence F_O, maximal chlorophyll fluorescence F_M, and maximum quantum yield of PSII photochemistry F_V/F_M (where $F_V = F_M - F_O$) for the dark-adapted state were evaluated from a fast chlorophyll fluorescence induction transients measured for 5 s on pre-darkened (30 min) Arabidopsis leaves using a Plant Efficiency Analyzer—PEA (Hansatech, King's Lynn, Norfolk, UK). The parameters were calculated using Biolyzer software (R.M. Rodriguez, University of Geneva, Switzerland). Chlorophyll fluorescence was excited using red light adjusted to the relative intensity of 45%.

PSII and PSI functions were simultaneously recorded on whole leaves (pre-darkened for 30 min) using a Dual-PAM100 measuring system (Heinz Walz, Effeltrich, Germany) during light exposure by red actinic light (800 µmol photons m^{-2} s^{-1}) for 16 min and using 300 ms saturating red light pulses (10,000 µmol photons m^{-2} s^{-1}). PSII function and induction of NPQ in PSII were detected and calculated as the effective yield of PSII photochemistry for light-adapted state Y(II) = $(F_M' - F)/F_M'$ (F_M' is the maximum chlorophyll fluorescence intensity at a light-adapted state and F is related chlorophyll fluorescence level at the state induced by the actinic light) and NPQ = $(F_M - F_M')/F_M'$ (F_M is the maximum chlorophyll fluorescence intensity at dark-adapted state; Genty et al., 1989; Bilger and Björkman, 1990). Parameters related to PSI function, Y(I), Y(ND), and Y(NA), that is the effective quantum yield of PSI photochemistry, and the quantum yields of non-

photochemical energy dissipation due to donor and acceptor side limitation, respectively, were calculated using the Dual-PAM100 software according to Klughammer and Schreiber (2008). The electron transport rate through PSII and PSI (ETR-II and ETR-I) are directly related to Y(II) a Y(I), respectively (= PAR × Y(II) or Y(I) × 0.84 × 0.5, where PAR is the irradiation level at 400–700 nm and the constants represent the assumed average leaf absorptance of PAR and the fraction of the light absorbed by given photosystem). The fraction of reduced PQ pool in thylakoid membranes was estimated as 1−qP, where qP is the photochemical quenching coefficient calculated as $(F_M'−F)/(F_M'−F_O')$. F_O' represents related minimal chlorophyll fluorescence level during the light exposure and was calculated according to Oxborough and Baker (1997).

Estimation of effective antenna size of PSII

Chlorophyll fluorescence induction was measured with a Dual-PAM100 system (Heinz Walz) on leaves that were excised from dark-adapted (30 min) Arabidopsis plants and subsequently infiltrated with 50 µM 3-(3,4-dichlorophenyl)-1,1-dimethylurea (DCMU) using five low-pressure shockwaves. This treatment was sufficient to block the PSII electron transport from Q_A to Q_B. The fluorescence induction was excited by red light (12 µmol photons $m^{−2}s^{−1}$) according to Belgio et al. (2014). Evaluation of effective absorption cross-section (σ, denoted as ACS PSII in Table 3) of PS II in the samples was estimated from fluorescence induction curves measured for 450 ms and double-normalized to obtain relative variable Chl fluorescence $V(t)$ as

$$V(t) = (F(t)−F_0)/(F_M−F_0),$$

where F_0 and F_M are minimal and maximal Chl fluorescence, respectively, and $F(t)$ is Chl fluorescence at time t.

According to the theory of Malkin et al. (1981), the complementary area (CA, area between the $V(t)$ measured with DCMU-treated samples and the horizontal line at the F_M level) of dark-adapted sample is related to σ as follows:

$$CA = 1/\sigma I,$$

where I is the incident light intensity. Since I was the same for all measured samples, we get

$$\sigma \approx 1/CA.$$

The CA has been calculated using Microsoft Excel.

Another estimation of effective antenna size of PSII of the samples was performed from the measurement of chlorophyll fluorescence curves of dark-adapted (30 min) leaves (without DCMU) measured using a PEA (Hansatech) under high intensity of incident light (adjusted to 45%). Under these conditions, a typical O–J–I–P Chl fluorescence induction curve is measured (Strasser and Srivastava, 1995; Lazár, 2006). According to the theory of energy fluxes and the JIP test (Strasser et al., 2004; Stirbet et al., 2018), maximal trapping flux at time zero TR_0/RC (corresponding to the rate by

which an incident light is trapped by the reaction centers of PSII resulting in the reduction of Q_A) can be expressed as $TR_0/RC = M_0/V_J$, where M_0 and V_J are defined as follows:

$$M_0 = 4(F_{300µs}−F_{50µs})/(F_M−F_0)$$

$$V_J = (F_J−F_0)/(F_M−F_0),$$

where $F_{50µs}$, $F_{300µs}$, and F_J are values of Chl fluorescence signal at 50 and 300 µs and at the position of the J step (at 2 ms), respectively, of the O–J–I–P curve. Since the initial rate of Q_A reduction reflects the effective antenna size of PSII of the sample (Lazár et al., 2001), TR_0/RC was used as another way to estimate the effective antenna size of PSII. The TR_0/RC was calculated using Biolyzer software (R.M. Rodriguez, University of Geneva, Switzerland).

Measurement of state transitions

State transitions were induced and monitored via the measurement of chlorophyll fluorescence using a Dual-PAM100 (Heinz Walz) according to de Bianchi et al. (2008) with modifications. A measurement protocol started with a preferential excitation of PSII by illumination with red light (13 µmol photons $m^{−2}$ $s^{−1}$) for 15 min. Then PSI was excited by far-red light for 15 min simultaneously with the red light, which was followed by 800 ms saturating red light pulse (10,000 µmol photons $m^{−2}$ $s^{−1}$) to determine the F_M' level in State I. A transition from State I to State II was achieved by red light illumination for 15 min, followed by a saturating light pulse to determine the F_M'' level in State II. The half-time of state transition from State I to State II was evaluated as the half-time of a gradual fluorescence decay upon switching off far-red light according to Damkjær et al. (2009). Parameter qT, which reflects the decrease in the LHCII antenna size, was calculated as $(F_M'−F_M'')/F_M'$ according to Ruban and Johnson (2009).

CD spectroscopy

Room temperature CD spectra of intact leaves were recorded in the range of 400–750 nm with a J-815 spectropolarimeter (Jasco, Tokyo, Japan). Intact leaves were supported by a flat cell and CD spectra were measured perpendicularly to the optical path. Measurements were carried out at room temperature with 0.5 nm step, 1 s integration time, 3 nm band-pass, and scanning speed 100 nm $min^{−1}$. To improve the signal-to-noise ratio, leaves were infiltrated with distilled water prior to the measurements using a 2-min interval at low pressure, and three scans were collected and averaged. CD spectra were normalized to the Chl Q_y absorption band. In order to minimize the influences of the overlapping excitonic CD bands, the amplitudes of the (+)685 nm and (+)505 nm psi-type CD bands were calculated as the difference between the CD signal at 685 and 750 nm and between 505 and 620 nm, respectively.

Chlorophyll fluorescence decay after a single-turnover saturating flash

The kinetics of the Chl fluorescence decay after a single-turnover saturating flash was monitored using Joliot-type kinetic spectrometer JTS-100 (Biologic, Seyssinet-Pariset, France). Arabidopsis plants were dark-adapted for 30 min, individual leaves were detached and immediately used for the measurement. Single turnover saturating (0.5 J) actinic flashes of 2 μs duration at half-peak intensity were provided by a xenon lamp (Hamamatsu LF1 L-11730-04-01-1, Shimokanzo, Japan) with Schott BG39 filter (Schott, Mainz, Germany), whereas the instruments LED system with a narrow bandpass filter centered at 650 nm (XHQA650; FWHM of 12 nm) provided measuring flashes. Fluorescence decay was recorded in the time range 15 μs to 50 s. Multicomponent deconvolution of the obtained fluorescence decay curves was achieved by fitting the experimental data with two exponential components (fast and middle phase) and one hyperbolic component (slow phase) as described earlier (Vass et al., 1999):

$$F_V = A_0 + A_1 \cdot e^{\frac{-t}{T_1}} + A_2 \cdot e^{\frac{-t}{T_2}} + \frac{A_3}{1 + \frac{t}{T_3}}$$

where $F_V = F(t) - F_0$, $F(t)$ is the fluorescence yield at time t, F_0 is the basic fluorescence level before the flash, A_1–A_3 are the amplitudes, T_1–T_3 are the time constants and A_0 describe non-decaying fluorescence component in the time span of the measurement.

Accession numbers

The accession numbers are as follows: LHCB3 (AT5G54270), LHCB6 (AT1G15820), LHCB4.1 (AT5G01530), LHCB4.2 (AT3G08940), and LHCB4.3 (AT2G40100). The mass spectrometry proteomic data have been deposited to the ProteomeXchange Consortium via the PRIDE partner repository with the identifiers: PXD023071 (thylakoid membranes) and PXD026019 (PSII supercomplexes).

Supplemental data

Supplemental Figure S1. Relative content of light-harvesting proteins in PSII supercomplexes separated by CN-PAGE.

Supplemental Figure S2. Gallery of electron micrographs of grana membranes isolated from Arabidopsis WT, *lhcb3* and *lhcb6* mutants.

Supplemental Figure S3. Electron micrograph of grana membranes isolated from Arabidopsis *lhcb3 lhcb6* mutant.

Supplemental Figure S4. Electron micrograph of grana membranes isolated from Arabidopsis *lhcb3 lhcb6* mutant—regular arrays.

Supplemental Figure S5. Electron micrograph of grana membranes isolated from Arabidopsis *lhcb3 lhcb6* mutant—carpet-like motive.

Supplemental Figure S6. Kinetics of Q_A^- reoxidation following a single turnover saturating flash.

Supplemental Figure S7. Measurements of state transitions in WT and mutant plants (*lhcb3*, *lhcb6*, *lhcb3 lhcb6*).

Supplemental Table S1. Decay kinetics of flash-induced variable fluorescence in Arabidopsis leaves.

Supplemental Methods S1. Mass spectrometry analysis of isolated thylakoid membranes and PSII supercomplexes.

References

Adamiec M, Gibasiewicz K, Luciński R, Giera W, Chełminiak P, Szewczyk S, Sipińska W, van Grondelle R, Jackowski G (2015) Excitation energy transfer and charge separation are affected in *Arabidopsis thaliana* mutants lacking light-harvesting chlorophyll a/b binding protein Lhcb3. J Photochem Photobiol B **153:** 423–428

Albanese P, Manfredi M, Meneghesso A, Marengo E, Saracco G, Barber J, Morosinotto T, Pagliano C (2016a) Dynamic reorganization of photosystem II supercomplexes in response to variations in light intensities. Biochim Biophys Acta **1857:** 1651–1660

Albanese P, Nield J, Tabares JAM, Chiodoni A, Manfredi M, Gosetti F, Marengo E, Saracco G, Barber J, Pagliano C (2016b) Isolation of novel PSII-LHCII megacomplexes from pea plants characterized by a combination of proteomics and electron microscopy. Photosynth Res **130:** 19–31.

Albanese PMelero REngel BDGrinzato ABerto PManfredi MChiodoni AVargas JSorzano CÓSMarengo E, et al. (2017) Pea PSII–LHCII supercomplexes form pairs by making connections across the stromal gap. Sci Rep. **7:** 10067.

Albanese P, Manfredi M, Re A, Marengo E, Saracco G, Pagliano C (2018) Thylakoid proteome modulation in pea plants grown at different irradiances: quantitative proteomic profiling in a non-model organism aided by transcriptomic data integration. Plant J **96:** 786–800

Albanese P, Manfredi M, Marengo E, Saracco G, Pagliano C (2019) Structural and functional differentiation of the light-harvesting protein Lhcb4 during land plant diversification. Physiol Plant **166:** 336–350

Alboresi A, Caffarri S, Nogue F, Bassi R, Morosinotto T (2008) In silico and biochemical analysis of *Physcomitrella patens* photosynthetic antenna: Identification of subunits which evolved upon land adaptation. PLoS ONE **3:** e2033

Allahverdiyeva Y, Isojärvi J, Zhang P, Aro E-M (2015) Cyanobacterial oxygenic photosynthesis is protected by flavodiiron proteins. Life Basel Switz 5: 716–743

Allen JF (2003) Cyclic, pseudocyclic and noncyclic photophosphorylation: New links in the chain. Trends Plant Sci 8: 15–19

Ballottari M, Dall'Osto L, Morosinotto T, Bassi R (2007) Contrasting behavior of higher plant photosystem I and II antenna systems during acclimation. J Biol Chem 282: 8947–8958

Barzda V, Mustárdy L, Garab G (1994) Size dependency of circular dichroism in macroaggregates of photosynthetic pigment–protein complexes. Biochemistry 33: 10837–10841

Belgio E, Kapitonova E, Chmeliov J, Duffy CDP, Ungerer P, Valkunas L, Ruban AV (2014) Economic photoprotection in photosystem II that retains a complete light-harvesting system with slow energy traps. Nat Commun 5: 4433.

Betterle N, Ballottari M, Zorzan S, de Bianchi S, Cazzaniga S, Dall'Osto L, Morosinotto T, Bassi R (2009) Light-induced dissociation of an antenna hetero-oligomer is needed for non-photochemical quenching induction. J Biol Chem 284: 15255–15266

van Bezouwen LS, Caffarri S, Kale RS, Kouřil R, Thunnissen A-MWH, Oostergetel GT, Boekema EJ (2017) Subunit and chlorophyll organization of the plant photosystem II supercomplex. Nat. Plants 3: 17080

de Bianchi S, Betterle N, Kouril R, Cazzaniga S, Boekema E, Bassi R, Dall'Osto L (2011) Arabidopsis mutants deleted in the light-harvesting protein Lhcb4 have a disrupted photosystem II macrostructure and are defective in photoprotection. Plant Cell 23: 2659–2679

de Bianchi S, Dall'Osto L, Tognon G, Morosinotto T, Bassi R (2008) Minor antenna proteins CP24 and CP26 affect the interactions between photosystem II subunits and the electron transport rate in grana membranes of Arabidopsis. Plant Cell 20: 1012–1028

Bilger W, Björkman O (1990) Role of the xanthophyll cycle in photoprotection elucidated by measurements of light-induced absorbance changes, fluorescence and photosynthesis in leaves of Hedera canariensis. Photosynth Res 25: 173–185

Björkman O, Demmig B (1987) Photon yield of O_2 evolution and chlorophyll fluorescence characteristics at 77 K among vascular plants of diverse origins. Planta 170: 489–504

Boekema EJ, van Roon H, Calkoen F, Bassi R, Dekker JP (1999) Multiple types of association of photosystem II and its light-harvesting antenna in partially solubilized photosystem II membranes. Biochemistry 38: 2233–2239

Boekema EJ, van Breemen JFL, van Roon H, Dekker JP (2000) Arrangement of photosystem II supercomplexes in crystalline macrodomains within the thylakoid membrane of green plant chloroplasts. J Mol Biol 301: 1123–1133

Bratt CE, Arvidsson PO, Carlsson M, Akerlund HE (1995) Regulation of violaxanthin de-epoxidase activity by pH and ascorbate concentration. Photosynth Res 45: 169–175

Caffarri S, Croce R, Cattivelli L, Bassi R (2004) A look within LHCII: Differential analysis of the Lhcb1–3 complexes building the major trimeric antenna complex of higher-plant photosynthesis. Biochemistry 43: 9467–9476

Caffarri S, Kouřil R, Kereïche S, Boekema EJ, Croce R (2009) Functional architecture of higher plant photosystem II supercomplexes. EMBO J 28: 3052–3063

Charuvi D, Nevo R, Shimoni E, Naveh L, Zia A, Adam Z, Farrant JM, Kirchhoff H, Reich Z (2015) Photoprotection conferred by changes in photosynthetic protein levels and organization during dehydration of a homoiochlorophyllous resurrection plant. Plant Physiol 167: 1554–1565

Chen Y-E, Ma J, Wu N, Su Y-Q, Zhang Z-W, Yuan M, Zhang H-Y, Zeng X-Y, Yuan S (2018) The roles of Arabidopsis proteins of Lhcb4, Lhcb5 and Lhcb6 in oxidative stress under natural light conditions. Plant Physiol Biochem 130: 267–276

Dall'Osto L, Cazzaniga S, Bressan M, Paleček D, Židek K, Niyogi KK, Fleming GR, Zigmantas D, Bassi R (2017) Two mechanisms for dissipation of excess light in monomeric and trimeric light-harvesting complexes. Nat Plants 3: 17033.

Damkjær JT, Kereiche S, Johnson MP, Kovács L, Kiss AZ, Boekema EJ, Ruban AV, Horton P, Jansson S (2009) The photosystem II light-harvesting protein Lhcb3 affects the macrostructure of photosystem II and the rate of state transitions in Arabidopsis. Plant Cell 21: 3245–3256

Dau H, Andrews JC, Roelofs TA, Latimer MJ, Liang W, Yachandra VK, Sauer K, Klein MP (1995) Structural consequences of ammonia binding to the manganese center of the photosynthetic oxygen-evolving complex: An X-ray absorption spectroscopy study of isotropic and oriented photosystem II particles. Biochemistry 34: 5274–5287

Daum B, Nicastro D, Austin J, McIntosh JR, Kühlbrandt W (2010) Arrangement of photosystem II and ATP synthase in chloroplast membranes of spinach and pea. Plant Cell 22: 1299–1312

Deák Z, Sass L, Kiss É, Vass I (2014) Characterization of wave phenomena in the relaxation of flash-induced chlorophyll fluorescence yield in cyanobacteria. Biochim Biophys Acta 1837: 1522–1532

Dekker JP, Boekema EJ (2005) Supramolecular organization of thylakoid membrane proteins in green plants. Biochim Biophys Acta 1706: 12–39

Dobrikova AG, Várkonyi Z, Krumova SB, Kovács L, Kostov GK, Todinova SJ, Busheva MC, Taneva SG, Garab G (2003) Structural rearrangements in chloroplast thylakoid membranes revealed by differential scanning calorimetry and circular dichroism spectroscopy. Thermo-optic effect. Biochemistry 42: 11272–11280

Garab G, Kieleczawa J, Sutherland JC, Bustamante C, Hind G (1991) Organization of pigment–protein complexes into macrodomains in the thylakoid membranes of wild-type and chlorophyll-b less mutant of barley as revealed by circular dichroism. Photochem Photobiol 54: 273–281

Garab G, van Amerongen H (2009) Linear dichroism and circular dichroism in photosynthesis research. Photosynth Res 101: 135–146

Genty B, Briantais J-M, Baker NR (1989) The relationship between the quantum yield of photosynthetic electron transport and quenching of chlorophyll fluorescence. Biochim Biophys Acta 990: 87–92

Goral TK, Johnson MP, Duffy CDP, Brain APR, Ruban AV, Mullineaux CW (2012) Light-harvesting antenna composition controls the macrostructure and dynamics of thylakoid membranes in Arabidopsis. Plant J 69: 289–301

Grebe S, Trotta A, Bajwa AA, Suorsa M, Gollan PJ, Jansson S, Tikkanen M, Aro E-M (2019) The unique photosynthetic apparatus of Pinaceae: Analysis of photosynthetic complexes in Picea abies. J Exp Bot 10: 3211–3225

Grinzato A, Albanese P, Marotta R, Swuec P, Saracco G, Bolognesi M, Zanotti G, Pagliano C (2020) High-light versus low-light: Effects on paired photosystem II supercomplex structural rearrangement in pea plants. Int J Mol Sci 21: 8643

Günther G, Thiele A, Laasch H (1994) A new method for the determination of the transthylakoid pH gradient in isolated chloroplasts: The pH-dependent activity of violaxanthin de-epoxidase. Plant Sci 102: 19–30

Haferkamp S, Haase W, Pascal AA, van Amerongen H, Kirchhoff H (2010) Efficient light harvesting by photosystem II requires an optimized protein packing density in grana thylakoids. J Biol Chem 285: 17020–17028

Ilík P, Kotabová E, Spundová M, Novák O, Kana R, Strzałka K (2010) Low-light-induced violaxanthin de-epoxidation in shortly preheated leaves: uncoupling from Delta pH-dependent nonphotochemical quenching. Photochem Photobiol 86: 722–726

Ilík P, Pavlovič A, Kouřil R, Alboresi A, Morosinotto T, Allahverdiyeva Y, Aro E-M, Yamamoto H, Shikanai T (2017) Alternative electron transport mediated by flavodiiron proteins is operational in organisms from cyanobacteria up to gymnosperms. New Phytol 214: 967–972

Jansson S (1999) A guide to the Lhc genes and their relatives in Arabidopsis. Trends Plant Sci 4: 236–240

Johnson MP (2020) Just the essentials: Photoprotective energy dissipation pared-down. J Exp Bot 71: 3380–3382

Joliot P, Joliot A (2002) Cyclic electron transfer in plant leaf. Proc Natl Acad Sci USA 99: 10209–10214

Kereïche S, Kiss AZ, Kouřil R, Boekema EJ, Horton P (2010) The PSBS protein controls the macro-organisation of photosystem II complexes in the grana membranes of higher plant chloroplasts. FEBS Lett 584: 759–764

Kirchhoff H (2008) Significance of protein crowding, order and mobility for photosynthetic membrane functions. Biochem Soc Trans 36: 967–970

Kirchhoff H, Haase W, Wegner S, Danielsson R, Ackermann R, Albertsson P-A (2007) Low-light-induced formation of semicrystalline photosystem II arrays in higher plant chloroplasts. Biochemistry 46: 11169–11176

Kitajima M, Butler WL (1975) Quenching of chlorophyll fluorescence and primary photochemistry in chloroplasts by dibromothymoquinone. Biochim Biophys Acta 376: 105–115

Klimmek F, Sjödin A, Noutsos C, Leister D, Jansson S (2006) Abundantly and rarely expressed LHC protein genes exhibit distinct regulation patterns in plants. Plant Physiol 140: 793–804

Klughammer C, Schreiber U (2008) Saturation pulse method for assessment of energy conversion in PS I. PAM Appl Notes 1: 11–14.

Kouřil R, Wientjes E, Bultema JB, Croce R, Boekema EJ (2013) High-light vs. low-light: Effect of light acclimation on photosystem II composition and organization in Arabidopsis thaliana. Biochim Biophys Acta 1827: 411–419

Kouřil R, Strouhal O, Nosek L, Lenobel R, Chamrád I, Boekema EJ, Šebela M, Ilík P (2014) Structural characterization of a plant photosystem I and NAD(P)H dehydrogenase supercomplex. Plant J 77: 568–576

Kouřil R, Nosek L, Bartoš J, Boekema EJ, Ilík P (2016) Evolutionary loss of light-harvesting proteins Lhcb6 and Lhcb3 in major land plant groups—break-up of current dogma. New Phytol 210: 808–814

Kouřil R, Nosek L, Semchonok D, Boekema EJ, Ilík P (2018) Organization of plant photosystem II and photosystem I supercomplexes. In JR Harris, EJ Boekema, eds, Membrane Protein Complexes: Structure and Function, Vol. Subcellular Biochemistry. Springer, Singapore, pp 259–286

Kouřil R, Nosek L, Opatíková M, Arshad R, Semchonok DA, Chamrád I, Lenobel R, Boekema EJ, Ilík P (2020) Unique organization of photosystem II supercomplexes and megacomplexes in Norway spruce. Plant J 104: 215–225

Kovács L, Damkjær J, Kereiche S, Ilioaia C, Ruban AV, Boekema EJ, Jansson S, Horton P (2006) Lack of the light-harvesting complex CP24 affects the structure and function of the grana membranes of higher plant chloroplasts. Plant Cell 18: 3106–3120

Kurasova I, Kalina J, Urban O, Stroch M, Spunda V (2003) Acclimation of two distinct plant species, Spring Barley and Norway Spruce, to combined effect of various irradiance and CO_2 concentration during cultivation in controlled environment. Photosynthetica 41: 513–523

Lazár D (1999) Chlorophyll a fluorescence induction 1. Biochim Biophys Acta 1412: 1–28

Lazár D (2006) The polyphasic chlorophyll a fluorescence rise measured under high intensity of exciting light. Funct Plant Biol 33: 9–30.

Lazár D, Nauš J (1998) Statistical properties of chlorophyll fluorescence induction parameters. Photosynthetica 35: 121–127

Lazár D, Tomek P, Ilík P, Nauš J (2001) Determination of the antenna heterogeneity of photosystem II by direct simultaneous fitting of several fluorescence rise curves measured with DCMU at different light intensities. Photosynth Res 68: 247–257

Li X-P, Gilmore AM, Niyogi KK (2002) Molecular and global time-resolved analysis of a psbS gene dosage effect on pH- and xanthophyll cycle-dependent nonphotochemical quenching in photosystem II. J Biol Chem 277: 33590–33597

Lichtenthaler HK (1987) Chlorophylls and carotenoids: Pigments of photosynthetic biomembranes. In: R Douce and L Packer, eds, Methods in Enzymology, Academic Press Inc., New York, pp 350–382

Lípová L, Krchnák P, Komenda J, Ilík P (2010) Heat-induced disassembly and degradation of chlorophyll-containing protein complexes in vivo. Biochim Biophys Acta 1797: 63–70

Malkin S, Armond PA, Mooney HA, Fork DC (1981) Photosystem II photosynthetic unit sizes from fluorescence induction in leaves: Correlation to photosynthetic capacity. Plant Physiol 67: 570–579

McKenzie SD, Ibrahim IM, Aryal UK, Puthiyaveetil S (2020) Stoichiometry of protein complexes in plant photosynthetic membranes. Biochim Biophys Acta 1861: 148141

Miller KR, Miller GJ, McIntyre KR (1976) The light-harvesting chlorophyll–protein complex of photosystem II. Its location in the photosynthetic membrane. J Cell Biol 71: 624–638

Miyake C (2010) Alternative electron flows (water–water cycle and cyclic electron flow around PSI) in photosynthesis: Molecular mechanisms and physiological functions. Plant Cell Physiol 51: 1951–1963

Miyake C (2020) Molecular mechanism of oxidation of P700 and suppression of ROS production in photosystem I in response to electron–sink limitations in C3 plants. Antioxidants 9: 230

Morosinotto T, Caffarri S, Dall'Osto L, Bassi R (2003) Mechanistic aspects of the xanthophyll dynamics in higher plant thylakoids. Physiol Plant 119: 347–354

Morosinotto T, Bassi R, Frigerio S, Finazzi G, Morris E, Barber J (2006) Biochemical and structural analyses of a higher plant photosystem II supercomplex of a photosystem I-less mutant of barley. FEBS J 273: 4616–4630

Munekage Y, Takeda S, Endo T, Jahns P, Hashimoto T, Shikanai T (2001) Cytochrome b(6)f mutation specifically affects thermal dissipation of absorbed light energy in Arabidopsis. Plant J 28: 351–359

Nosek L, Semchonok D, Boekema EJ, Ilík P, Kouřil R (2017) Structural variability of plant photosystem II megacomplexes in thylakoid membranes. Plant J 89: 104–111

Nystedt BStreet NRWetterbom AZuccolo ALin Y-CScofield DGVezzi FDelhomme NGiacomello SAlexeyenko A, et al. (2013) The Norway spruce genome sequence and conifer genome evolution. Nature 497: 579–584

Onoa B, Schneider AR, Brooks MD, Grob P, Nogales E, Geissler PL, Niyogi KK, Bustamante C (2014) Atomic force microscopy of photosystem II and its unit cell clustering quantitatively delineate the mesoscale variability in Arabidopsis thylakoids. PLoS ONE 9: e101470

van Oort B, Alberts M, de Bianchi S, Dall'Osto L, Bassi R, Trinkunas G, Croce R, van Amerongen H (2010) Effect of antenna-depletion in photosystem II on excitation energy transfer in Arabidopsis thaliana. Biophys J 98: 922–931

Oxborough K, Baker NR (1997) Resolving chlorophyll a fluorescence images of photosynthetic efficiency into photochemical and non-photochemical components—calculation of qP and F_v'/F_m'; without measuring F_o'. Photosynth Res 54: 135–142

Park RB, Biggins J (1964) Quantasome: size and composition. Science 144: 1009–1011

Peter GF, Thornber JP (1991) Biochemical composition and organization of higher plant photosystem II light-harvesting pigment–proteins. J Biol Chem 266: 16745–16754

de la Rosa-Trevín JMQuintana ADel Cano LZaldívar AFoche IGutiérrez JGómez-Blanco JBurguet-Castell JCuenca-Alba JAbrishami V, et al. (2016) Scipion: A software framework toward integration, reproducibility and validation in 3D electron microscopy. J Struct Biol 195: 93–99

Ruban AV, Johnson MP (2009) Dynamics of higher plant photosystem cross-section associated with state transitions. Photosynth Res 99: 173–183

Ruban AV, Wentworth M, Yakushevska AE, Andersson J, Lee PJ, Keegstra W, Dekker JP, Boekema EJ, Jansson S, Horton P (2003)

Plants lacking the main light-harvesting complex retain photosystem II macro-organization. Nature **421**: 648–652

Ruban AV, Wilson S (2020). The mechanism of non-photochemical quenching in plants: Localisation and driving forces. Plant Cell Physiol (doi: 10.1093/pcp/pcaa155)

Saccon F, Giovagnetti V, Shukla MK, Ruban AV (2020) Rapid regulation of photosynthetic light harvesting in the absence of minor antenna and reaction centre complexes. J Exp Bot **71**: 3626–3637

Schägger H (2006) Tricine-SDS-PAGE. Nat Protoc **1**: 16–22.

Scheres SHW (2012) RELION: Implementation of a Bayesian approach to cryo-EM structure determination. J Struct Biol **180**: 519–530

Schneider CA, Rasband WS, Eliceiri KW (2012) NIH Image to ImageJ: 25 years of image analysis. Nat Methods **9**: 671–675

Semenova GA (1995) Particle regularity on thylakoid fracture faces is influenced by storage conditions. Can J Bot **73**: 1676–1682

Simpson DJ (1979) Freeze–fracture studies on barley plastid membranes. III. Location of the light-harvesting chlorophyll-protein. Carlsberg Res Commun **44**: 305–336

Standfuss J, Kühlbrandt W, (2004) The three isoforms of the light-harvesting complex II: Spectroscopic features, trimer formation, and functional roles. J Biol Chem **279**: 36884–36891

Stirbet A, Lazár D, Kromdijk J, Govindjee (2018) Chlorophyll a fluorescence induction: Can just a one-second measurement be used to quantify abiotic stress responses? Photosynthetica **56**: 86–104.

Stoylova S, Flint TD, Ford RC, Holzenburg A (2000) Structural analysis of photosystem II in far-red-light-adapted thylakoid membranes: New crystal forms provide evidence for a dynamic reorganization of light-harvesting antennae subunits. Eur J Biochem **267**: 207–215

Strasser RJ, Srivastava A (1995) Polyphasic chlorophyll a fluorescence transient in plants and cyanobacteria. Photochem Photobiol **61**: 32–42

Strasser RJ, Tsimilli-Michael M, Srivastava A (2004) Analysis of the chlorophyll a fluorescence transient. *In* GC Papageorgiou and Govindjee, eds, Chlorophyll a Fluorescence: A Signature of Photosynthesis. Advances in Photosynthesis and Respiration. Springer, Dordrecht, Netherlands, pp 321–362

Su X, Ma J, Wei X, Cao P, Zhu D, Chang W, Liu Z, Zhang X, Li M (2017) Structure and assembly mechanism of plant $C_2S_2M_2$-type PSII–LHCII supercomplex. Science **357**: 815–820

Sznee K, Dekker JP, Dame RT, van Roon H, Wuite GJL, Frese RN (2011) Jumping mode atomic force microscopy on grana membranes from Spinach. J Biol Chem **286**: 39164–39171

Tietz S., Puthiyaveetil SEnlow HMYarbrough RWood MSemchonok DALowry TLi ZJahns PBoekema EJ, et al. (2015) Functional implications of photosystem II crystal formation in photosynthetic membranes. J Biol Chem **290**: 14091–14106

Tóth TN, Rai N, Solymosi K, Zsiros O, Schröder WP, Garab G, van Amerongen H, Horton P, Kovács L (2016) Fingerprinting the macro-organisation of pigment–protein complexes in plant thylakoid membranes in vivo by circular-dichroism spectroscopy. Biochim Biophys Acta **1857**: 1479–1489

Townsend AJ, Saccon F, Giovagnetti V, Wilson S, Ungerer P, Ruban AV (2018) The causes of altered chlorophyll fluorescence quenching induction in the Arabidopsis mutant lacking all minor antenna complexes. Biochim Biophys Acta **1859**: 666–675

Tremmel IG, Kirchhoff H, Weis E, Farquhar GD (2003) Dependence of plastoquinol diffusion on the shape, size, and density of integral thylakoid proteins. Biochim Biophys Acta **1607**: 97–109

Tsvetkova NM, Apostolova EL, Brain APR, Patrick Williams W, Quinn PJ (1995) Factors influencing PS II particle array formation in *Arabidopsis thaliana* chloroplasts and the relationship of such arrays to the thermostability of PS II. Biochim Biophys Acta **1228**: 201–210.

Vass I, Kirilovsky D, Etienne AL (1999) UV-B radiation-induced donor- and acceptor-side modifications of photosystem II in the cyanobacterium *Synechocystis* sp. PCC 6803. Biochemistry **38**: 12786–12794

Wang YH (2008) How effective is T-DNA insertional mutagenesis in Arabidopsis? J Biochem Technol **1**: 11–20.

Wei X, Su X, Cao P, Liu X, Chang W, Li M, Zhang X, Liu Z (2016) Structure of spinach photosystem II—LHCII supercomplex at 3.2 Å resolution. Nature **534**: 69–74

Wientjes E, Drop B, Kouřil R, Boekema EJ, Croce R (2013) During state 1 to state 2 transition in *Arabidopsis thaliana*, the photosystem II supercomplex gets phosphorylated but does not disassemble. J Biol Chem **288**: 32821–32826

Wiśniewski JR, Zougman A, Nagaraj N, Mann M (2009) Universal sample preparation method for proteome analysis. Nat Methods **6**: 359–362

Wittig I, Karas M, Schägger H (2007) High resolution clear native electrophoresis for in-gel functional assays and fluorescence studies of membrane protein complexes. Mol Cell Proteomics **6**: 1215–1225

Yakushevska AE, Jensen PE, Keegstra W, van Roon H, Scheller HV, Boekema EJ, Dekker JP (2001) Supermolecular organization of photosystem II and its associated light-harvesting antenna in *Arabidopsis thaliana*: Supermolecular organization of photosystem II. Eur J Biochem **268**: 6020–6028.

Yakushevska AE, Keegstra W, Boekema EJ, Dekker JP, Andersson J, Jansson S, Ruban AV, Horton P (2003) The structure of photosystem II in *Arabidopsis*: localization of the CP26 and CP29 antenna complexes. Biochemistry **42**: 608–613

Yamamoto H, Shikanai T (2019) PGR5-dependent cyclic electron flow protects photosystem I under fluctuating light at donor and acceptor sides. Plant Physiol **179**: 588–600

Publication 12

Cryo-EM structure of a plant photosystem II supercomplex with light-harvesting protein Lhcb8 and α-tocopherol

Check for updates

Monika Opatíková [1,10], Dmitry A. Semchonok[2,10], David Kopečný [3], Petr Ilík [1], Pavel Pospíšil [1], Iva Ilíková [4], Pavel Roudnický [5], Sanja Ćavar Zeljković[6,7], Petr Tarkowski [6,7], Fotis L. Kyrilis [2], Farzad Hamdi [2], Panagiotis L. Kastritis [2,8,9] & Roman Kouřil [1] ✉

The heart of oxygenic photosynthesis is the water-splitting photosystem II (PSII), which forms supercomplexes with a variable amount of peripheral trimeric light-harvesting complexes (LHCII). Our knowledge of the structure of green plant PSII supercomplex is based on findings obtained from several representatives of green algae and flowering plants; however, data from a non-flowering plant are currently missing. Here we report a cryo-electron microscopy structure of PSII supercomplex from spruce, a representative of non-flowering land plants, at 2.8 Å resolution. Compared with flowering plants, PSII supercomplex in spruce contains an additional Ycf12 subunit, Lhcb4 protein is replaced by Lhcb8, and trimeric LHCII is present as a homotrimer of Lhcb1. Unexpectedly, we have found α-tocopherol (α-Toc)/α-tocopherolquinone (α-TQ) at the boundary between the LHCII trimer and the inner antenna CP43. The molecule of α-Toc/α-TQ is located close to chlorophyll a614 of one of the Lhcb1 proteins and its chromanol/quinone head is exposed to the thylakoid lumen. The position of α-Toc in PSII supercomplex makes it an ideal candidate for the sensor of excessive light, as α-Toc can be oxidized to α-TQ by high-light-induced singlet oxygen at low lumenal pH. The molecule of α-TQ appears to shift slightly into the PSII supercomplex, which could trigger important structure–functional modifications in PSII supercomplex. Inspection of the previously reported cryo-electron microscopy maps of PSII supercomplexes indicates that α-Toc/α-TQ can be present at the same site also in PSII supercomplexes from flowering plants, but its identification in the previous studies has been hindered by insufficient resolution.

Photosynthesis is essential for the majority of organisms living on Earth. This process, employed by (cyano-)bacteria, algae and land plants, is crucial for the conversion of water and carbon dioxide molecules into oxygen and organic substances and is enabled by the cooperative function of two pigment–protein complexes—photosystem (PS) II and I.

PSII is a supramolecular pigment–protein complex embedded in the thylakoid membrane. Upon absorption of light, it splits water

molecules into oxygen, electrons and protons, and creates the proton gradient across the thylakoid membrane, which is the driving power for ATP synthase. Over the past few years, an extensive effort of several research groups in the field of cryo-electron microscopy (cryo-EM) has led to the description of the structure of eukaryotic PSII supercomplexes at near-atomic resolution in representatives of green algae (*Chlamydomonas reinhardtii* (*Cr*))[1,2] and flowering plants (angiosperms)[3–5]. All the PSII structures so far confirm the dimeric nature of the PSII core (C₂). The structure of C_2 is highly conserved across photosynthetic species and its pigment–protein composition arrangement is strikingly similar to its evolutionarily older counterpart in thermophilic cyanobacteria[6–8]. Unlike C_2, the light-harvesting complexes (LHCII) that bind to C_2 in the form of LHCII trimers and monomers are the source of variability of PSII structure in different organisms. For instance, in *Cr* the LHCII trimers consist of a combination of LhcbM1–9 proteins[9], while in land plants they are formed by a variable combination of only three proteins Lhcb1–3 (ref. 10).

Differences in the type and number of LHCII trimers attached to C_2 result in different forms of PSII supercomplexes. Three types of LHCII trimer are recognized, based on the strength of their attachment to C_2—strongly (S), moderately (M) and loosely (L) bound trimers. The most abundant form of PSII supercomplex in land plants is the $C_2S_2M_2$ supercomplex, where two copies of each S and M trimers are bound to C_2 via monomeric antenna proteins Lhcb4, Lhcb5 and Lhcb6 (see below for exceptions). In *Cr*, however, the Lhcb6 protein is missing, which results in a slightly altered binding position of LHCII trimers in the PSII supercomplex[11,12]. This modification may also be the reason why large $C_2S_2M_2L_2$ supercomplexes are common in *Cr*, whereas in land plants they are usually very rare. Different organization of PSII supercomplexes in *Cr* and land plants has a direct impact on the major excitation energy transfer (EET) pathways between chlorophyll (Chl) molecules from LHCII to the reaction centre of C_2 (ref. 13), which can have important consequences for the adjustment of the absorption cross-section of PSII in the dynamic light environment.

Recently, we have found that the composition and arrangement of PSII supercomplexes in land plant species are not as conserved and uniform as initially hypothesized. The gymnosperm genera *Picea* and *Pinus* (family Pinaceae) and *Gnetum* (clade Gnetales) have lost light-harvesting proteins Lhcb3 and Lhcb6 during evolution. As a consequence, the organization of their PSII supercomplexes is different from other land plants and shares some common features with the supercomplex from the green alga *Cr*[14,15]. In addition, these genera have retained only one isoform of the Lhcb4 protein, namely Lhcb4.3, also referred to as Lhcb8 (ref. 16). Lhcb8 is a specific isoform of Lhcb4 that has been observed so far only in a subgroup of dicotyledonous plants and only under high-light conditions[17], suggesting its important role in plants coping with excess light[18]. However, even the exposure of plants to high light intensity does not lead to a complete replacement of Lhcb4 by Lhcb8 in the PSII supercomplex, and their simultaneous presence does not allow a structural study focused purely on the structure and role of Lhcb8 in the organization of the PSII supercomplex[19].

In this Article, we present a cryo-EM density map and structural model of the PSII C_2S_2 supercomplex from Norway spruce (*Picea abies*, hereinafter referred to as spruce) at 2.8 Å resolution. The obtained model with near-atomic resolution provides structural insight into subunit composition and pigment arrangements, enabling analysis of EET pathways within the supercomplex. The PSII structure from a gymnosperm representative partially fills the gap between the known PSII structures from green algae and angiosperm species and enables their detailed structural and functional comparison. Analysis of cryo-EM density map of the PSII supercomplex revealed a specific density at the boundary between the LHCII trimer and the inner antenna CP43, which was assigned to α-tocopherol (α-Toc)/α-tocopherolquinone (α-TQ). The possible role of α-Toc in the protection of PSII against photo-oxidative damage is discussed.

Results and discussion
Overall structure

The structure of the PSII supercomplex from Norway spruce, a model organism of gymnosperms, was studied using single-particle cryo-EM. PSII supercomplexes were purified from solubilized thylakoid membranes by sucrose gradient ultracentrifugation. A gradient fraction of PSII supercomplexes was collected (Fig. 1a), concentrated, and used for cryo specimen preparation and data acquisition (Fig. 1b). A visual analysis of 2D classes of aligned particle projections showed that the best-resolved densities were obtained for the C_2S_2 form of the PSII supercomplex (Supplementary Fig. 1). The larger forms of PSII supercomplexes (that is, $C_2S_2M_2$ and C_2S_2M) were underrepresented in the obtained dataset, leading to the absence of their homogeneous classes with well-resolved projections. This is in agreement with our previous report indicating a higher abundance of smaller forms of PSII supercomplexes (C_2S_2) in spruce[14] compared with other plant species, for example, *Arabidopsis thaliana* (*At*). The best-resolved 2D classes of C_2S_2 supercomplexes were used for the 3D reconstruction, which generated a final map of the PSII C_2S_2 supercomplex at 2.8 Å resolution (equal to Fourier shell correlation at 0.143; Fig. 1c,d, Supplementary Fig. 2 and Supplementary Table 1).

Spruce PSII C_2S_2 supercomplex consists of the dimeric core complex, which binds two S-LHCII trimers and two of each minor antenna proteins Lhcb5 and Lhcb8 (Fig. 1c,d). It binds 204 chlorophylls, 4 pheophytins, 56 carotenoids and a number of lipids and co-factor molecules (Supplementary Table 2). The calculated root-mean-square deviation values between the spruce PSII C_2S_2 supercomplex and supercomplexes from other plant species[1–5,19] ranged from 1.4 Å to 2.4 Å, indicating similar structural features between spruce PSII and PSII from other organisms (Supplementary Table 3). The structural similarities are also apparent from the superposition of the structural model of the spruce PSII C_2S_2 supercomplex with those from other photosynthetic organisms, including *Cr*, *At*, spinach, and pea (Supplementary Fig. 3).

Structure of the core complex of PSII

As in other plant species, the core complex of spruce forms a homodimer with characteristic two-fold symmetry (Fig. 2). Each monomer is composed of four major intrinsic subunits PsbA (D1), PsbB (CP47), PsbC (CP43) and PsbD (D2). The rest of the core complex is formed by smaller low-molecular-weight subunits, namely PsbE, PsbF (cytochrome b_{559} alpha and beta subunit, respectively), PsbH, PsbI, PsbK-M, PsbO, PsbT$_c$, PsbT$_n$, Ycf12, PsbW, PsbX and PsbZ (Fig. 2c). A comparison of the subunit composition of the core complex from spruce and its counterparts from angiosperm species (*Arabidopsis*, pea and spinach) revealed the presence of one subunit specific for the spruce core complex, Ycf12. This protein has so far been found only in the PSII structure from green alga *Cr*[1,2], as the corresponding gene is missing in angiosperms[20]. The position of Ycf12 in spruce closely corresponds with its position in *Cr*. It strongly interacts with PsbK and PsbZ with an interface area of 446 Å² and 347 Å², respectively. On the stromal side, the C-terminal tail of Ycf12 interacts with the N-terminus of PsbC. In *Cr*, Ycf12 is also in contact with PsbJ[1,2], which is, however, missing in our structure, together with PsbP and PsbQ subunits. PsbJ is a low-molecular-mass subunit represented by a single transmembrane α-helix localized at the periphery of the core complex close to the cyt b_{559}. PsbP and PsbQ are extrinsic subunits of the oxygen-evolving complex. As the mass spectrometry analysis has confirmed the presence of these three protein subunits in the fraction of purified spruce PSII supercomplexes (Supplementary Table 4), their absence in the obtained PSII supercomplex structure is most likely caused by their loose binding to the core complex. The absence of these labile subunits has also been observed to some extent in other PSII structures from *At*, pea and *Cr* (Protein Data Bank (PDB) ID 5mdx, 6yp7 and 6kad,
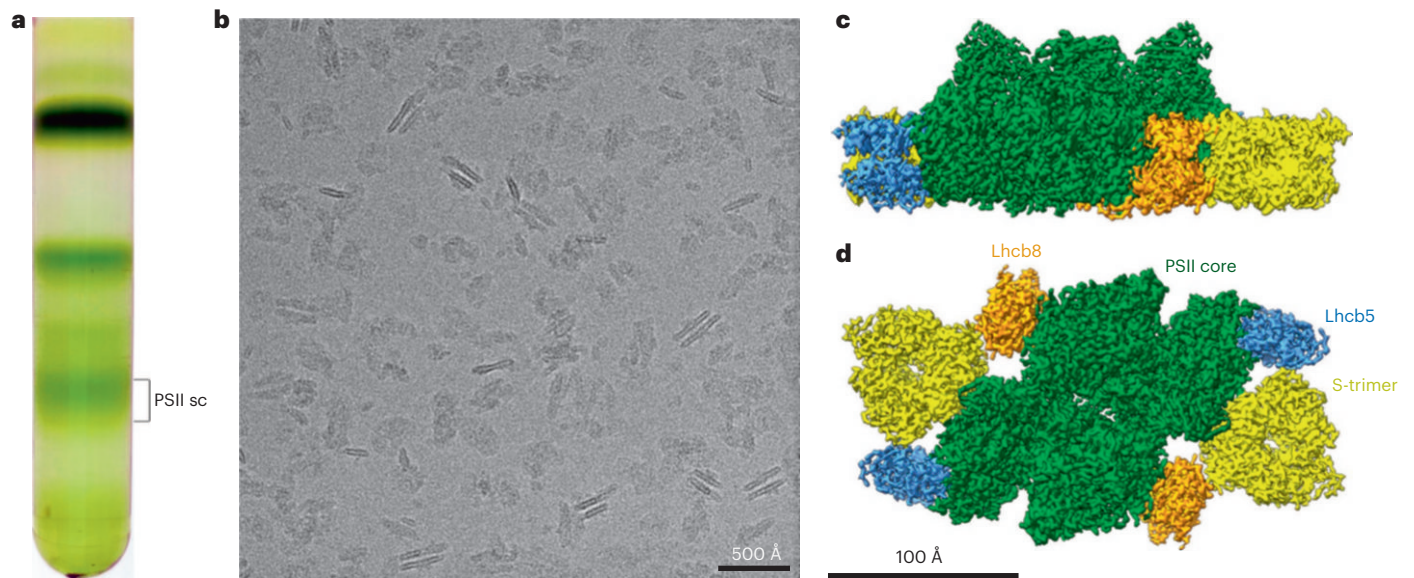
Fig. 1 | Separation and single-particle cryo-EM analysis of spruce PSII C$_2$S$_2$ supercomplex. a, Separation of the PSII supercomplexes using sucrose gradient ultracentrifugation of solubilized thylakoid membranes from spruce. The fraction marked 'PSII sc' was used for the cryo specimen preparation. The experiment was repeated nine times independently with similar results. **b**, Representative electron micrograph of a cryo-EM specimen of the spruce PSII supercomplexes. In total, 2,392 electron micrographs were recorded. **c**,**d**, 3D cryo-EM density map of the spruce C$_2$S$_2$ supercomplex side view (along the membrane plane) (**c**) and top view (lumenal side) (**d**). The PSII dimeric core complex C$_2$ is shown in green, Lhcb5 in light blue, Lhcb8 in orange and the S-LHCII trimer in yellow.
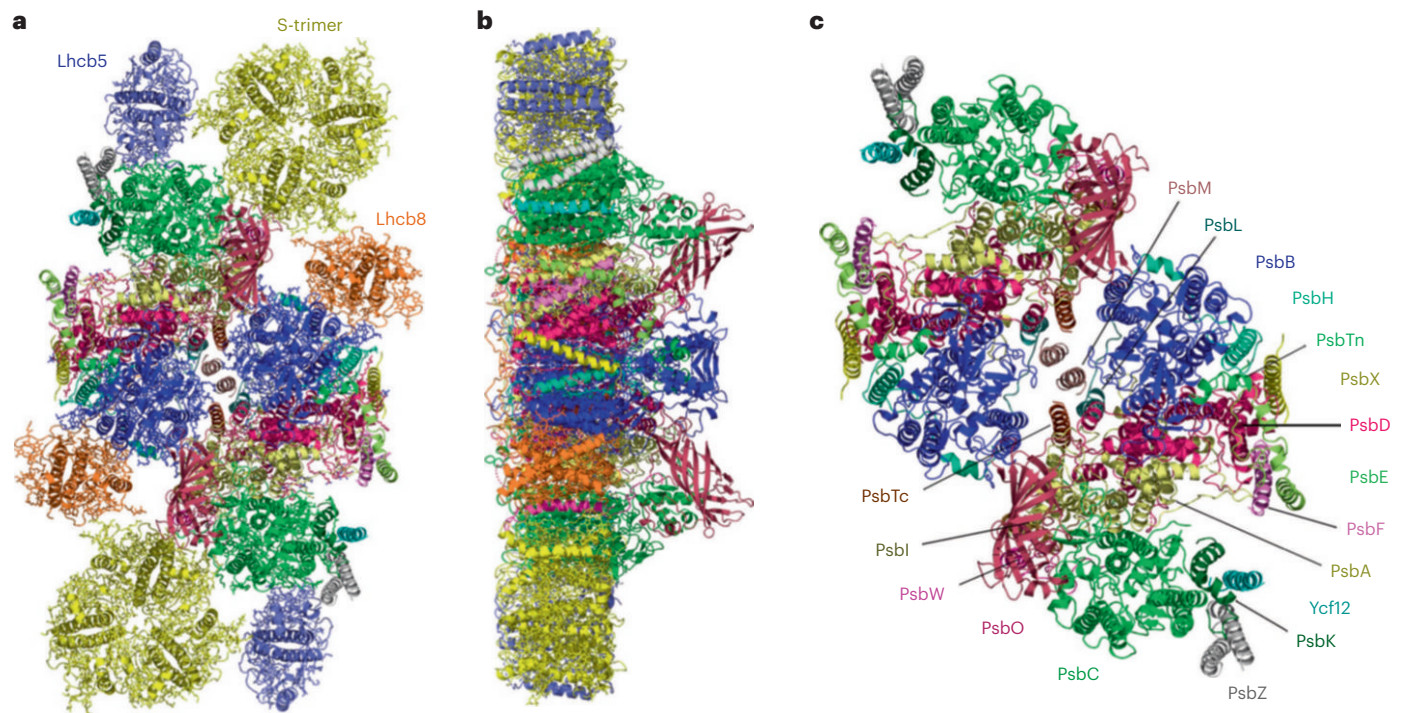
Fig. 2 | Overall architecture of the spruce PSII C$_2$S$_2$ supercomplex. a, The view of the C$_2$S$_2$ supercomplex from the lumenal side with indicated subunits of light-harvesting antenna, Lhcb5, Lhcb8 and the S-LHCII trimer, bound to the dimeric core complex. **b**, The side view of the C$_2$S$_2$ supercomplex along the membrane plane. **c**, Assigned subunits of the core complex.

respectively). These subunits thus either dissociate from the supercomplexes during sample handling before/during cryo-EM specimen preparation or are bound to the supercomplex sub-stoichiometrically, and thus their presence in the density map is suppressed during image analysis.

Structure of the PSII peripheral antenna

Light-harvesting antenna of the spruce PSII C$_2$S$_2$ supercomplex consists of two S-LHCII trimers bound to the PSII core complex via two monomeric antennae, Lhcb5 and Lhcb8 (Fig. 2). The spruce S-LHCII trimer shows similar structural features as LHCII trimers from other
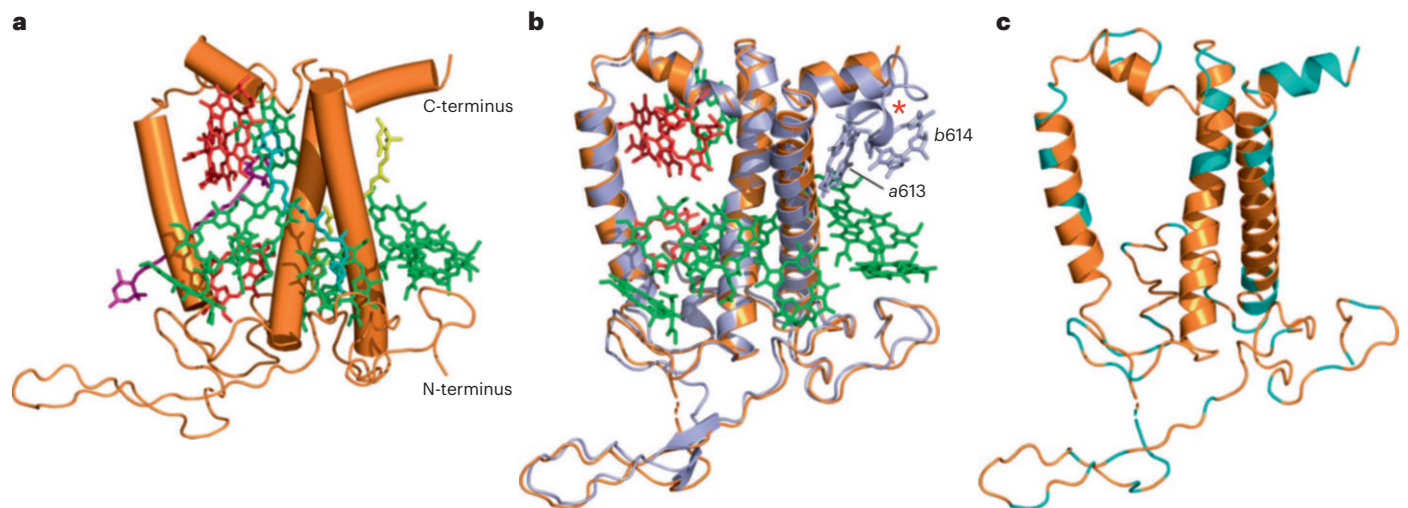
Fig. 3 | Structure of the Lhcb8 subunit. a, A cartoon representation of spruce Lhcb8 with bound pigments (Chl *a*, green; Chl *b*, red; lutein, yellow; violaxanthin, cyan; neoxanthin, magenta). **b**, A structural comparison of spruce Lhcb8 (orange) and Lhcb4 (light blue) from pea (PDB code: 5xnl). Chlorophylls of spruce Lhcb8 are shown in green (Chl *a*) and red (Chl *b*). The red asterisk indicates a longer C-terminus of pea Lhcb4, which supports the binding of two additional chlorophylls, Chl *a* (*a*613) and Chl *b* (*b*614) (in light blue). **c**, Spruce Lhcb8 with highlighted regions of amino acid sequence (cyan) that differ from pea Lhcb4 (PDB code: 5xnl).

representatives of land plants or green algae. It has identical pigment composition, and the localization of the pigment molecules is also very similar to other species (Supplementary Fig. 4). In each monomer, we have identified 14 Chl binding sites (8 Chl *a*, 6 Chl *b*) and 4 carotenoid binding sites (two luteins, one violaxanthin and one neoxanthin) (Supplementary Table 2).

In land plants, the S-LHCII trimer is formed by various combinations of Lhcb1 and Lhcb2 proteins, forming either homotrimers or heterotrimers[10]. Moreover, both Lhcb1 and Lhcb2 are usually present in several isoforms[21] with very high homology, and the separation of PSII supercomplexes with S-LHCII with different isoform composition is virtually impossible. Therefore, the samples for cryo-EM analysis always contain the sum of PSII complexes with various types of the S-LHCII trimers, that is, the structure of the S-LHCII trimer in the resulting cryo-EM density maps represents a superposition of all present Lhcb1 and Lhcb2 isoforms. This in turn lowers the resolution at the isoform-specific amino acid positions, and thus the distinction of present isoforms is impossible. This effect, however, was not observed in the case of spruce S-LHCII trimer. Its cryo-EM density map has unusually high resolution, which indicates that its isoform composition is rather uniform.

On the basis of the detailed comparison of the cryo-EM structure with the amino acid composition of the trimer-forming proteins Lhcb1 and Lhcb2, we were able to identify the spruce S-LHCII trimer as a homotrimer, composed solely of Lhcb1. In spruce, Lhcb1 protein can be present in five isoforms (Lhcb1-A1, -A2 and -A3; Lhcb1-B1 and -B2) and Lhcb2 in three isoforms (Lhcb2-A1, -A2 and -A3) (ref. 16). By tracing the amino acid densities of individual monomers in the S-LHCII trimer, we were able to exclude the presence of all isoforms of Lhcb2 (Supplementary Fig. 5). Namely, Glu64 and Leu171 of Lhcb2 do not fit the corresponding densities in any of the three proteins/monomers forming the S-LHCII trimer (chain G/g, N/n and Y/y in the structure file, respectively) (for sequence comparison, see Supplementary Fig. 6). Instead, these densities in all three monomers were reliably fitted by amino acids from the sequence of Lhcb1 (Gly73 and Ala180) (Supplementary Fig. 5a,b). Using this approach, we were able to narrow the number of possible isoforms even further. The presence of both Lhcb1-B1 and Lhcb1-B2 isoforms in the S-LHCII trimer was excluded as Leu174 (present in Lhcb1-B1 and Lhcb1-B2) does not fit the corresponding density in the

map, whereas Trp171 (present in Lhcb1-A1, -A2 and -A3) matches it perfectly. The presence of isoform Lhcb1-A3 is also unlikely, at least in chain G, as there is no corresponding density for Tyr253, whereas Ala253 fits nicely. Nevertheless, as the same confirmation cannot be achieved for the chains N and Y, the presence of this isoform in the S-LHCII trimer cannot be excluded. According to the systematic annotation by model refinement, the EM map was best matched by the Lhcb1-A1/A2 isoforms, and the Lhcb1-A1 isoform was used in the structural model. Thus, to our knowledge, this is the first specific identification of a LHCII homotrimer as a component of PSII supercomplex in any photosynthetic organism studied so far. As the mass spectrometry analysis of the fraction of PSII supercomplexes also revealed the presence of Lhcb2 protein (Supplementary Table 4), it can be deduced that Lhcb2 is a building component of the M-LHCII trimer, because the PSII supercomplexes with M-LHCII trimers were also partially present in the isolated PSII fraction (Supplementary Fig. 1). However, the question of whether the spruce M-LHCII trimer is a homotrimer of Lhcb2 or a heterotrimer composed of Lhcb1/Lhcb2 can be answered only by detailed structural analysis of spruce $C_2S_2M_2$ supercomplex.

Spruce Lhcb5 antenna protein exhibits typical structural features of Lhcb5 in other land plants and has identical pigment composition. It binds nine Chl *a*, four Chl *b* and three carotenoids (Supplementary Table 2). The comparison of Lhcb5 from spruce and *Cr* shows that the algal Lhcb5 protein has longer loops between the helixes C and A and the helixes E and C, allowing it to bind one extra Chl *a* (Supplementary Fig. 7).

The structure of the monomeric antenna protein found at the binding position between the S-LHCII trimer and CP47 in spruce is different from other land plants. While this position in the C_2S_2 supercomplex from spinach and pea is occupied by the Lhcb4 (refs. 3,5), in spruce Lhcb4 is replaced by Lhcb8 (formerly known as Lhcb4.3 isoform), the only Lhcb4-type protein present in spruce (Fig. 3a). Lhcb8 has a slightly different amino acid sequence from Lhcb4, but its most distinctive feature is its shorter C-terminus (Fig. 3b,c). Lhcb8 binds nine Chl *a*, three Chl *b* and three carotenoids (Supplementary Table 2), and the binding positions and orientations of these pigment molecules are very similar to land plant Lhcb4 protein. However, due to its shorter C-terminus, Lhcb8 has lost two Chl molecules that are present in land plant Lhcb4 (Supplementary Fig. 8), namely Chl*a*613 and Chl*b*614
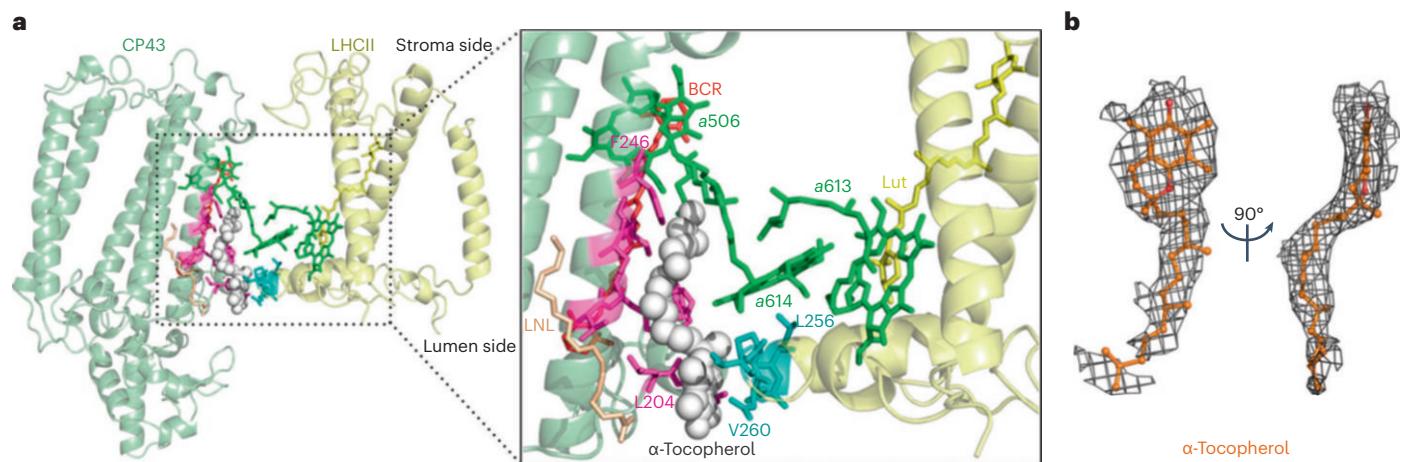
Fig. 4 | Localization of α-Toc in spruce PSII C₂S₂ supercomplex. a, α-Toc is localized between the S-LHCII trimer and CP43, the inner antenna of the core complex, close to the lumenal side of the thylakoid membrane. α-Toc interacts with CP43 via several specific amino acids in the region between Leu204 to Phe246 (magenta), Chl*a*506 and LNL, and with one monomer of the S-LHCII trimer through the amino acid region from Leu256 to Val260 (cyan) and Chl*a*614. Lutein (Lut) is shown in yellow, and β-carotene (BCR) in red. **b**, The density identified in the cryo-EM density map of the spruce PSII supercomplex fitted by α-Toc (orange).

(Fig. 3b). It is interesting to note that Lhcb4 from green alga *Cr*[1,2] also has a shorter C-terminus (Supplementary Fig. 8d,e), but its C-terminal α-helix is rotated slightly clockwise compared with spruce, which probably allows the binding of one extra Chl *a* molecule compared with Lhcb8. The exclusive presence of Lhcb8 is probably connected with the evolutionary loss of Lhcb3 and Lhcb6 proteins in spruce and other representatives of the Pinaceae and Gnetales families[14], as in other land plants, the longer C-terminus of Lhcb4 is involved in the direct interaction with Lhcb3 and Lhcb6 (ref. 22).

Antenna–core interactions

The binding of light-harvesting proteins in the spruce PSII C₂S₂ supercomplex is similar to other known PSII structures from land plant species and a green alga. The binding of Lhcb5 to the PSII core is supported mainly by PsbZ subunit with an interface area of 295 Å². The association is supported by a salt bridge between Asp100 (Lhcb5) and Lys37 (PsbZ) on the stromal side and a hydrogen bond between Leu290 (Lhcb5) and Ser59 (PsbZ) on the lumenal side. The interface area of Lhcb5 with CP43 is 189 Å². Interestingly, the interaction of Lhcb5 with the S-LHCII trimer is apparently weaker compared with other plant species, as the interface area is only about 100 Å², that is, approximately 1/3 of the interface area observed in other plant PSII structures. The binding of Lhcb8 to the PSII core is similar to that of Lhcb4 in plant and algal PSII C₂S₂ supercomplex. It involves interactions with PsbB, PsbH, PsbA and PsbL subunits via several specific hydrogen bonds and a salt bridge (Supplementary Table 5). The attachment of the S-LHCII trimer to the core complex is controlled mainly by the PsbW subunit and CP43 with interaction areas of 116 Å² and 41 Å², respectively. The precise position of the S-LHCII is also supported by Lhcb8 with an interface area of 86 Å².

Analysis of the density map between CP43 and S-LHCII (Y/y chain) revealed a specific density not described in any previous cryo-EM structures of PSII. The first possible candidate for this density could be the detergent molecule *n*-dodecyl α-D-maltoside (α-DDM), which has already been detected in several cryo-EM structures, including PSII C₂S₂ supercomplex from *Cr*[2]. However, when α-DDM is refined to the corresponding density, it is clear that the hydroxyl groups and carbon atoms of the pyranose ring of the second glucose of the maltoside protrude from the density map (Supplementary Fig. 9). Since we are not aware of any lipid molecules that could match the density map, we fitted the density map with the molecule of α-Toc (Fig. 4) and refined. Its presence in the fraction containing PSII C₂S₂ supercomplexes was confirmed by liquid chromatography–tandem mass spectrometry (LC–MS/MS) analysis (Supplementary Fig. 10). The molecule of α-Toc is fully embedded in the thylakoid membrane with its chromanol ring facing the lumenal side. It interacts with CP43 (Leu204–Pro206, Phe210, Val238, Trp239, Ser242, Ile243 and Phe246), Lhcb1 of the S-LHCII (Leu256–Val260) and linolenic acid (LNL526_CP43), and is close to two chlorophylls *a*506_CP43 and *a*614_S-LHCII (Fig. 4a).

To support the attribution of the electron density to α-Toc, we calculated the interaction energies $\Delta^i G$ for the most relevant interaction interface (based on the interface area) of both α-Toc and α-DDM with adjacent surroundings in the PSII supercomplex. The calculations resulted in the interaction with CP43 for both molecules. However, whereas the major surface area buried by α-Toc was predicted to be favourable ($\Delta^i G = -2.0$ kcal mol⁻¹), the opposite was true for both possible conformations of α-DDM ($\Delta^i G = 1.7$ kcal mol⁻¹ and $\Delta^i G = 2.3$ kcal mol⁻¹).

Except of α-Toc, the LC–MS/MS analysis of the fraction of spruce PSII C₂S₂ supercomplexes also revealed the presence of a substantial amount of α-TQ (Supplementary Fig. 10). α-TQ is the oxidation product of α-Toc, which has been previously identified in chloroplasts and thylakoid membrane[23,24]. The relative amount of α-TQ was slightly lower compared with α-Toc (45% and 55%, respectively). The quantification analysis of the PSII fraction also shows that the ratio of the sum of α-Toc and α-TQ per C₂S₂ supercomplex is approximately 0.9. Although this quantitative estimation indicates that in our sample, α-Toc with α-TQ were present at a sub-stoichiometric amount with respect to C₂S₂ supercomplex, the occupancy of the binding site by these molecules was still high enough to enable the detection of this specific density in the PSII structure. The shape and the fitting of the density map suggest that the α-Toc is more abundant in our sample, but α-TQ can be fitted as well (Supplementary Fig. 11b).

The inspection of the cryo-EM density 3D maps of PSII supercomplexes from other organisms revealed that α-Toc at this position might not be unique to spruce, as we have observed a trace of similar density in the pea PSII supercomplex[5] (EMD-6741) as well. A striking similarity between the shapes of these spruce and pea density maps could indicate their common origin in α-Toc/α-TQ molecules (Supplementary Fig. 11). The resolution of the cryo-EM density 3D maps from *At* (EMD-3491) and spinach (EMD-6617) was insufficient for the
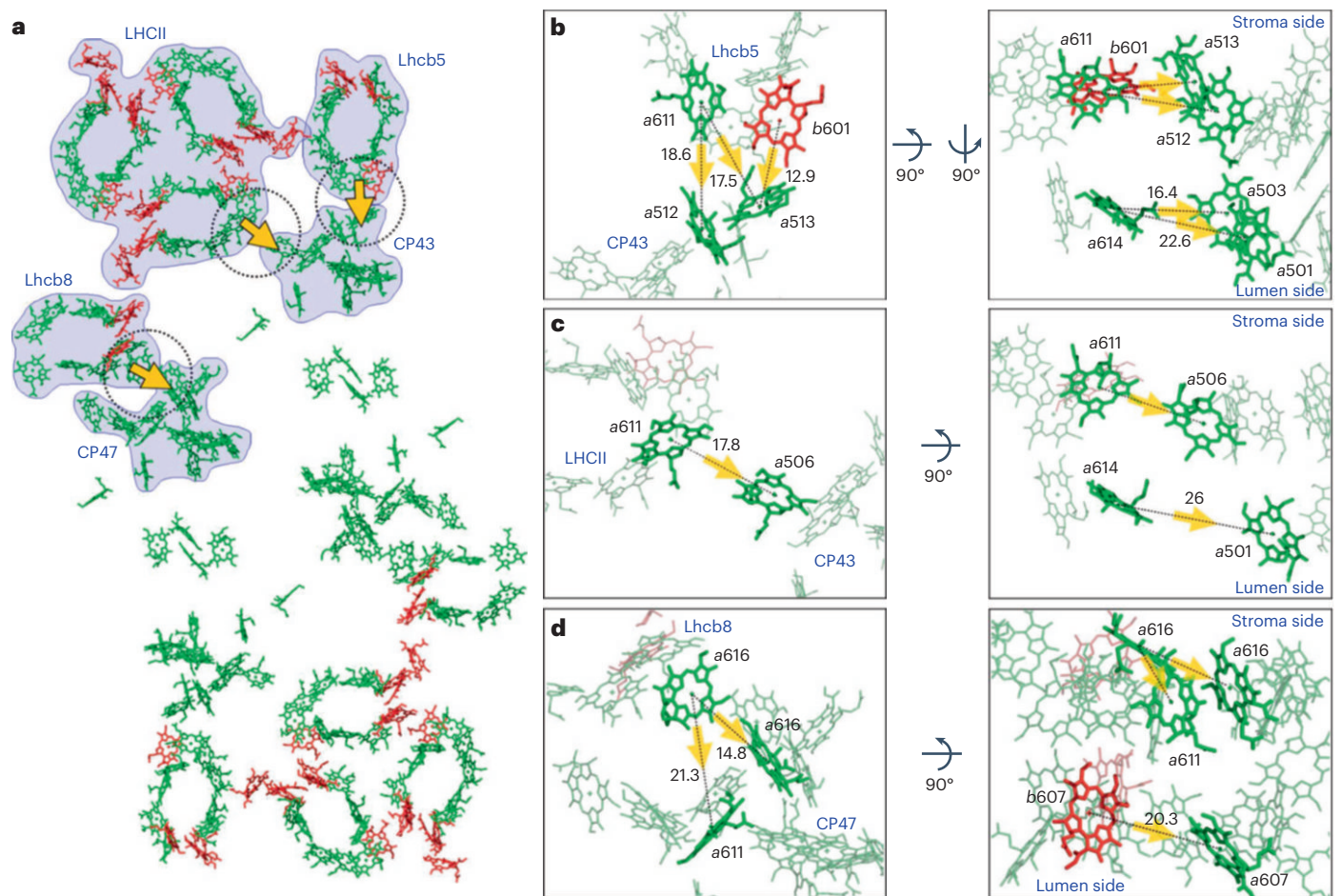
Fig. 5 | Major energy transfer pathways within the spruce PSII C$_2$S$_2$ supercomplex. a, Overview of all chlorophylls in the spruce C$_2$S$_2$ supercomplex shown from the stromal side, Chl *a* in green and Chl *b* in red. Major energy transfer pathways between the highlighted LHCII subunits (Lhcb5, Lhcb8 and S-LHCII trimer) and the core complex (CP43 and CP47) are indicated by yellow arrows. **b–d**, Chlorophylls involved in the energy transfer from Lhcb5 to CP43 (**b**), S-LHCII trimer to CP43 (**c**) and Lhcb8 to CP47 (**d**). Chlorophylls, which are the most prominent in the EET, are highlighted. The numbers at the dotted lines indicate the Mg-to-Mg distances in Å between two adjacent chlorophylls. The left figures in **b–d** show the view from the stromal side.

analysis of the same area with a representable outcome. On the other hand, the inspection of PSII supercomplexes from *Cr* (EMD-9955, EMD-9956 and EMD-9957) revealed the unequivocal absence of this density, which results in a closer contact between the S-LHCII trimer with the CP43 subunit. Nevertheless, it is impossible to draw any firm conclusion about the absence of α-Toc/α-TQ in *Cr*. Both molecules could have been lost during the isolation procedure, which probably happened in a recent structural study of the PSII supercomplex from *At*[25]. The analysis of amino acid sequence, however, suggests that the regions of CP43 and S-LHCII (Lhcb1 or LhcbM1) that are involved in the interaction with α-Toc are relatively conserved in spinach, pea and *At*, whereas in *Cr* there are more substantial changes (Supplementary Figs. 12 and 13). These findings could indicate that the presence of α-Toc/α-TQ at the interface between S-LHCII and CP43 might be specific to land plants.

EET pathways

Localization and assignments of chlorophyll molecules in the spruce PSII allow a calculation of the EET pathways in the C$_2$S$_2$ supercomplex. We have used a recently proposed approach[13], based on the calculation of EET between the entire individual light-harvesting proteins (Lhcb5, Lhcb8 and S-LHCII trimer) and the inner antenna of the PSII core complex (CP43 and CP47). When calculating the main pathway for EET, this approach considers the contribution of all chlorophylls of given light-harvesting proteins, but at the same time, it allows the identification of key pairs of chlorophylls that mediate EET between the subunits.

As expected, the calculated Förster resonance energy transfer (FRET) rates show that EET from monomeric antennae Lhcb5 and Lhcb8 to S-LHCII trimer is highly improbable (Supplementary Table 6). The main EET pathways from these minor antenna proteins are directed to inner antenna complexes CP43 and CP47, respectively (Fig. 5). The energy absorbed by S-LHCII trimer is directed mainly to inner antenna CP43 (Fig. 5), and EET to Lhcb5 and Lhcb8 is negligible (Supplementary Table 6). Similar pathways of the main EET have been described in PSII supercomplexes of other land plants and green algae, but our data indicate that the majority of FRET rates of spruce EET pathways are slightly slower (Supplementary Table 6). This is most likely due to the subtle changes in the positions of participating chlorophylls, as the FRET rate is inversely proportional to the sixth power of the distance between them.

A detailed inspection of the chlorophylls that mediate EET from the peripheral antenna proteins (Lhcb5, Lhcb8 and trimer S-LHCII) to the internal antenna complexes (CP43 and CP47) shows that, as in other plants, EET is mediated primarily through chlorophylls localized on the stromal side of the thylakoid membrane. This is due to their closer contact compared with chlorophylls localized on the lumenal side. Detailed information about chlorophylls involved in the main EET pathways, their localization, orientation and mutual distances can be found in Fig. 5b–d.
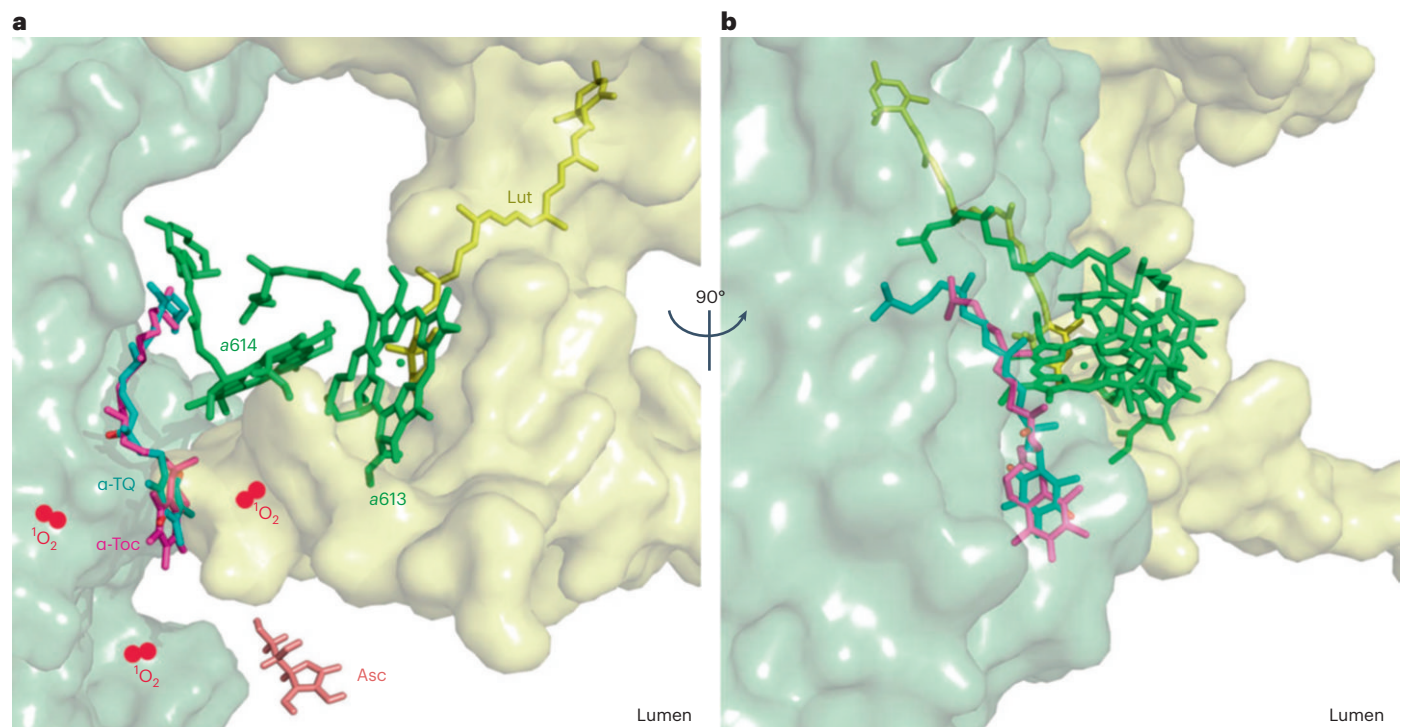
Fig. 6 | Position of α-Toc/α-TQ in the structure of spruce PSII supercomplex. a,b, A detail of membrane side view (**a**) and the same detail rotated by 90° (**b**) with embedded α-Toc/α-TQ in PSII supercomplex. A cluster of chlorophylls a614, a613 and lutein (Lut) in the Lhcb1 protein of trimeric LHCII is close to the α-Toc/α-TQ. Ascorbate (Asc) molecule in the thylakoid lumen can reach and reduce the chromanol head of the α-Toc oxidized by singlet oxygen ($^1O_2$) (for details, see the text).

What is the role of α-tocopherol(quinone) in PSII?

It is well known that $^1O_2$ formed in photosynthetic organisms exposed to excessive light is most effectively eliminated by carotenoids[26]. However, they are not the only $^1O_2$-detoxifying compounds in plants. The second line of defence against $^1O_2$ is represented by tocopherols, namely α-Toc, which can react with $^1O_2$ forming hydroperoxide (α-Toc-OOH). This compound can be either regenerated back to α-Toc by reducing agents (for example, ascorbate), or irreversibly converted to α-TQ. This conversion is known to be promoted under acidic conditions, that is, conditions typically present in the lumen of light-exposed thylakoids[27].

In light of these facts, it is very interesting to note that the chromanol head of the α-Toc molecule newly identified in the PSII supercomplex of spruce is exposed to the lumen. This position indicates that whenever this α-Toc is oxidized by $^1O_2$ produced by PSII (in excessive light), it can be readily regenerated by ascorbate present in the lumen. At the same time, when the lumenal pH becomes acidic, this regeneration pathway could be surpassed by the irreversible conversion of the hydroperoxide α-Toc-OOH to α-TQ. It appears that a minor shift occurs between the two-ring chromanol head and quinone head when refined as α-TQ or α-Toc, respectively, in the PSII supercomplex (Fig. 6). We hypothesize that the conversion of α-Toc to α-TQ can lead to conformational changes in PSII supercomplex with possible functional consequences. The conversion of α-Toc to α-TQ could be, for example, sensed by the neighbouring PSII subunit PsbW, which is known to be crucial for the proper assembly of proteins into PSII supercomplexes[28,29], and could therefore act as a molecular switch triggering the high-light adjustment of PSII.

The molecule of α-TQ itself is an effective quencher of chlorophyll fluorescence from PSII (ref. [30]), and therefore it can contribute to the quenching of excessive excitations in the PSII supercomplex. However, the involvement of α-Toc/α-TQ in the frequently discussed quenching of excitations in PSII supercomplex[31] can also be indirect. The molecule is localized in the proximity of the Chl$a$614–Chl$a$613 cluster in the Lhcb1 antenna of the S-trimer of LHCII (Fig. 6). In the context of LHCII, the chlorophylls in this cluster are of middle energy[32] and therefore this cluster is not likely to act as a quenching centre, although it is well coupled with the carotenoid lutein. However, it is tempting to suggest that the oxidation of α-Toc to α-TQ induced by lumen acidification under excessive light can lead to a conformation change of the supercomplex, which could lower the energy levels of the Chl$a$614–Chl$a$613 cluster and turn the cluster into an effective quenching site in PSII supercomplex. Indeed, recent in silico predictions suggest that the Chl$a$614–Chl$a$613 cluster might serve as a quenching centre upon protonation of the D-helix in the Lhcb1 antenna[33].

Our hypothesis that α-Toc/α-TQ has not only structural, but also functional role in PSII supercomplex is supported by the analysis of *Arabidopsis vte1* mutant, defective in the synthesis of α-Toc. It has been reported that this mutant has probably impaired turnover of D1 protein both at high[34] and low[35] irradiation, which supports that the α-Toc/α-TQ localized within the supercomplex could be important for the proper function of PSII.

Methods

Plant material and isolation of thylakoid membranes

Seedlings of Norway spruce (*Picea abies* L. Karst.) were grown in a growth chamber for 3 weeks at 120 µmol photons $m^{-2}s^{-1}$, 22 °C, with a 16 h light/8 h dark cycle. Before the isolation procedure, spruce seedlings were dark-adapted for 30 min. Subsequently, seedlings were cut approximately 2 cm above the soil, and thylakoid membranes were isolated according to the protocol described by Dau et al.[36] with one modification. All buffers used for the isolation were complemented with phosphatase inhibitor sodium fluoride (NaF) at a final concentration of 10 mM. The isolation was performed under

green light and samples were kept on ice during the whole procedure. The chlorophyll content in the final thylakoid membrane suspension was determined spectrophotometrically by a pigment extraction in 80% acetone[37].

Ultracentrifugation and sample preparation for cryo-EM

Ultracentrifugation was performed according to Caffarri et al.[38] with minor modifications. For the preparation of the PSII supercomplexes fraction, thylakoid membranes (corresponding to 200 µg of chlorophyll $a + b$) were centrifuged at 4,600g (4 °C, 4 min). The resulting pellet was resuspended in 10 mM HEPES (pH 7.5) to a chlorophyll concentration of 2 mg ml^{-1} and solubilized by adding α-DDM in 10 mM HEPES (pH 7.5) to the final detergent concentration of 1% and final chlorophyll concentration of 0.5 mg ml^{-1} (final detergent/chlorophyll mass ratio of 20) and vortexed gently for a few seconds. The solubilized thylakoid membranes were immediately centrifuged at 18,000g (4 °C, 10 min) to remove insolubilized membranes and then fractionated by ultracentrifugation on a sucrose gradient at 284,000g (4 °C, 18 h). The sucrose gradients were prepared in tubes containing 0.65 M sucrose solution in 10 mM HEPES (pH 7.5) with critical micelle concentration of α-DDM (0.008%). Tubes were frozen (−80 °C) and subsequently thawed at 4 °C. A total volume of 5.4 ml of the sucrose fraction with PSII supercomplexes was collected from nine tubes (0.6 ml from each tube) and concentrated using a 50 kDa cut-off Millipore Amicon filter at 14,000g (4 °C, 5 min) and washed twice in 400 µl of 10 mM HEPES (pH 7.5) buffer with a critical micelle concentration concentration of α-DDM to remove sucrose. The obtained fraction with a chlorophyll concentration of 3 mg ml^{-1} was directly used for cryo specimen preparation.

Sample preparation for electron microscopy

Aliquots (3.5 µl) containing PSII supercomplexes were applied to the glow-discharged (PELCO easiGlow, 15 mA, 25 s) Quantifoil holey carbon-supported copper grids (R 2/1, 200 mesh). The sample excess was blotted away (TFS 595 type Φ55/20 filter paper, blot force 2, blotting time of 6 s) and plunge-frozen in liquid ethane using a TFS Vitrobot Mark IV at 4 °C and 95% humidity.

Electron microscopy data acquisition

Image acquisition was performed on the Thermo Fisher Scientific Glacios cryogenic electron microscope equipped with a field emission gun (ThermoFisher X-FEG) and operated at 200 kV in bright field imaging mode. In total, 2,392 movies were recorded using a Thermo Scientific Falcon 3EC Direct electron Detector in linear mode at a nominal magnification of 150,000× and a true magnification of 145,641× at the camera level, corresponding to a pixel size of 0.96127 Å per pixel with 120 frames at a dose of 0.9215 e$^-$ Å^{-2} per frame and an exposure time of 108 s per movie. The acquisition was performed using TFS EPU2 (Supplementary Table 1).

Image processing

The raw movies were imported into SCIPION 3.0 (ref. [39]). The motion correction for drift correction and dose weighting was performed with MotionCor2-plugin[40] and GCTF-plugin[41] for contrast transfer function estimation. During the previous step, the 2,100 micrographs with well-estimated parameters were further subjected to the manual/auto Xmipp particle picking[42]. Extracted 202,251 particles were 2D classified using cryoSPARC-plugin[43], and the best classes were selected for ab initio map generation with cryoSPARC-plugin. Then 118,509 particles from the best 2D class averages were taken for 3D classification using Relion 3.1-plugin[44] with two classes. The best resulting 3D class containing C_2S_2 supercomplexes was further taken to 3D non-uniformed refinement in cryoSPARC-plugin, resulting in a 3D map of 3.32 Å resolution. The subsequent particles have undergone Bayesian polishing using Relion 3.1-plugin[44] and further 3D non-uniformed refinement

with cryoSPARC-plugin[43] resulting in a 2.785 Å resolution 3D map (Supplementary Fig. 2 and Supplementary Table 1).

Modelling, structure and FRET analysis

Initial fitting of the subunits in the cryo-EM map was performed by rigid body real-space refinement in Chimera[45], using the high-resolution crystal structure of PSII from *Spinacia oleracea* (PDB code 3JCU). Several linear-shaped electron densities were fitted with linolenic acid (LNL) in line with its high abundance among fatty acid esters identified in the PSII supercomplex fraction (Supplementary Fig. 14). Fatty acids in the final model are assumed to belong to membrane lipids, which were not possible to model fully due to a poor density. Local fitting of the subunits in the cryo-EM map was performed using the program Coot. Refinement was performed at 2.8 Å resolution (Fourier shell correlation at 0.143) in Phenix using the real-space refinement module and applying geometry, secondary structure, rotamer and Ramachandran plot restraints. A model of chain V was obtained by fitting a polyalanine α-helix into the empty density for a transmembrane helix and side chains were subsequently updated to the protein sequence (UniProt accession R4ZGY5_PICAB). The validation statistics calculated by MolProbity provided the final score value of 1.6, the overall clash score of 8, Ramachandran outliers of 0.06% and the CC (mask) value of 0.85 (Supplementary Table 1). Images were prepared with PyMOL[46].

To evaluate the structural similarity between spruce and other plant PSII supercomplexes, the average deviation between the corresponding atoms of two superimposed proteins/supercomplexes (root-mean-square deviation values) was calculated from structural files[47,48] using CCP4 software. The interface area between specific protein subunits and between co-factors and $Δ^iG$ (the solvation free energy gain upon interface formation) was calculated from structural files using the Pisa software[49]. FRET analysis was performed according to Sheng et al.[2] and Croce and Amerongen[13]. Multiple sequence alignments were performed with BioEdit software using ClustalW algorithm.

Analysis of separated PSII supercomplexes from spruce by MS

Isolated PSII supercomplexes from spruce (*P. abies*) seedlings were subjected to filter-aided sample preparation based on Wisniewski et al.[50]. The resulting peptides were analysed by LC–MS/MS performed using UltiMate 3000 RSLCnano system (Thermo Fisher Scientific) on-line coupled with Orbitrap Exploris 480 spectrometer (Thermo Fisher Scientific) using Thermo Scientific Xcalibur software. The sample was processed and measured in technical triplicates. For complete details regarding the analyses and data evaluation, see Supplementary Information.

Detection of α-Toc and α-TQ by LC–MS/MS

n-Hexane (200 µl) was added into a fraction of isolated PSII supercomplexes (10 µl, chlorophyll concentration of 3.075 mg ml^{-1}), sonicated for 3 min at 25 °C, and the upper layer was transferred into a new vial. Extraction was repeated three times, and collected n-hexane extracts were evaporated to dryness under a vacuum at 40 °C and redissolved in 40 µl of acetonitrile. For the quantification, ultra-high-performance liquid chromatography–MS/MS analysis was performed using Nexera X2 UHPLC (Shimadzu Handels), coupled with MS-8050 (Shimadzu Handels GmbH). Chromatographic separation was performed on an Acquity UPLC BEH C18 (50 × 2.1 mm; 1.7 µm particle size; Waters) with the corresponding pre-column. Target compounds were separated using a binary gradient consisting of 15 mM formic acid, pH 3 (adjusted with NH$_4$OH) (component A), and 0.1% formic acid in acetonitrile (component B) at a flow rate of 0.4 ml min^{-1}. The column temperature was maintained at 40 °C. The linear gradient consisted of 75% B for 2 min, 75–100% B for 9 min, isocratic for 0.3 min, back to 75% B within 0.2 min, and equilibration for 2 min. Injected volume was 5 µl. The effluent was introduced into an electrospray source (interface temperature of 300 °C, heat block temperature of 400 °C and interface

capillary voltage of 5.0 kV). Argon was used as the collision gas, and nitrogen was used as the nebulizing gas. To achieve high specificity in addition to the high sensitivity, the analysis was performed in the multiple reaction monitoring mode alternating the following transitions 431.30 > 165.10, 431.30 > 134.05 and 431.30 > 68.95 for α-Toc, and 429.00 > 164.95, 429.00 > 163.20 and 429.00 > 191.20 for α-TQ. The calculated amount of α-Toc and α-TQ in the analysed PSII fraction was 100 pmol and 81 pmol, respectively, indicating that the chls/(α-Toc + α-TQ) ratio in the fraction is 188/1. Both data collection and data analysis were performed via Lab Solutions software (Shimadzu Corporation 2008–2019).

Fatty acid composition

Extraction solvent [CHCl₃:MeOH (2:1, v-v)] was added into membrane extract and sonicated for 10 min at room temperature. The extract was centrifuged for 5 min at 14,500g and the supernatant was evaporated at 40 °C under a vacuum. Methylation of fatty acids was performed with 1 M NaOMe/MeOH for 5 min at room temperature. After the addition of 200 µl of saturated NaCl, fatty acid methyl esters (FAME) were extracted with 2 × 500 µl of n-hexane. The solvent was evaporated under a vacuum, and the residuum was dissolved into 20 µl of n-hexane. The resulting FAMEs were analysed via gas-chromatography–mass spectrometry using the Agilent system (GC 7890A; MSD 5975 C series II) on a fused silica HP-5MS UI column (30 m × 0.25 mm × 0.25 mm) and carrier gas He (1.1 ml min⁻¹). The temperature was programmed at 120 °C for 3 min, 5 °C min⁻¹ to 180 °C, then held for 10 min, 10 °C min⁻¹ to 220 °C, and finally 2 °C min⁻¹ to 250 °C and held for 5 min. The temperature of the injection port and detector was 230 °C. Ionization was performed in the electron impact mode (70 eV). Injection (1 µl) was done in splitless mode. Identification was performed by comparing retention times, indices and mass spectra with the mixture of authentic standards (Supelco 37 Component FAME Mix, Merck). Pinolenic acid (Cayman) was also derivatized using the above protocol. All compounds' linear retention indices were determined via the Kovats method by injecting homologous series of C8–C40 n-alkanes (Merck) in n-hexane solution. Other compounds detected in the sample were identified by comparison of their mass spectra with those found in the database (NIST/EPA/NIH Mass Spectral Library v.2.0). Results are presented as percentage content calculated according to the area of the chromatographic peaks. Both data collection and data analysis were performed via MSD ChemStation software (Agilent Technologies, 1989–2011).

Reporting summary

Further information on research design is available in the Nature Portfolio Reporting Summary linked to this article.

Data availability

The mass spectrometry proteomic data have been deposited to the ProteomeXchange Consortium via the PRIDE partner repository with the identifier PXD035272. The cryo-EM map of the spruce PSII supercomplex has been deposited in the Electron Microscopy Data Bank with accession code EMD-16389. The corresponding structure model has been deposited in the PDB under PDB code 8C29.

References

1. Shen, L. et al. Structure of a C₂S₂M₂N₂-type PSII–LHCII supercomplex from the green alga *Chlamydomonas reinhardtii*. *Proc. Natl Acad. Sci. USA* **116**, 21246–21255 (2019).
2. Sheng, X. et al. Structural insight into light harvesting for photosystem II in green algae. *Nat. Plants* **5**, 1320–1330 (2019).
3. Wei, X. et al. Structure of spinach photosystem II–LHCII supercomplex at 3.2 Å resolution. *Nature* **534**, 69–74 (2016).
4. van Bezouwen, L. S. et al. Subunit and chlorophyll organization of the plant photosystem II supercomplex. *Nat. Plants* **3**, 17080 (2017).
5. Su, X. et al. Structure and assembly mechanism of plant C2S2M2-type PSII–LHCII supercomplex. *Science* **357**, 815–820 (2017).
6. Kamiya, N. & Shen, J.-R. Crystal structure of oxygen-evolving photosystem II from *Thermosynechococcus vulcanus* at 3.7-Å resolution. *Proc. Natl Acad. Sci. USA* **100**, 98–103 (2003).
7. Ferreira, K. N., Iverson, T. M., Maghlaoui, K., Barber, J. & Iwata, S. Architecture of the photosynthetic oxygen-evolving center. *Science* **303**, 1831–1838 (2004).
8. Loll, B., Kern, J., Saenger, W., Zouni, A. & Biesiadka, J. Towards complete cofactor arrangement in the 3.0 Å resolution structure of photosystem II. *Nature* **438**, 1040–1044 (2005).
9. Minagawa, J. & Takahashi, Y. Structure, function and assembly of photosystem II and its light-harvesting proteins. *Photosynth. Res.* **82**, 241–263 (2004).
10. Jansson, S. The light-harvesting chlorophyll *a/b*-binding proteins. *Biochim. Biophys. Acta* **1184**, 1–19 (1994).
11. Kouřil, R., Nosek, L., Semchonok, D., Boekema, E. J. & Ilík, P. Organization of plant photosystem II and photosystem I supercomplexes. *Subcell. Biochem.* **87**, 259–286 (2018).
12. Cao, P., Pan, X., Su, X., Liu, Z. & Li, M. Assembly of eukaryotic photosystem II with diverse light-harvesting antennas. *Curr. Opin. Struct. Biol.* **63**, 49–57 (2020).
13. Croce, R. & van Amerongen, H. Light harvesting in oxygenic photosynthesis: structural biology meets spectroscopy. *Science* **369**, eaay2058 (2020).
14. Kouřil, R., Nosek, L., Bartoš, J., Boekema, E. J. & Ilík, P. Evolutionary loss of light-harvesting proteins Lhcb6 and Lhcb3 in major land plant groups—break-up of current dogma. *N. Phytol.* **210**, 808–814 (2016).
15. Kouřil, R. et al. Unique organization of photosystem II supercomplexes and megacomplexes in Norway spruce. *Plant J.* **104**, 215–225 (2020).
16. Grebe, S. et al. The unique photosynthetic apparatus of Pinaceae: analysis of photosynthetic complexes in *Picea abies*. *J. Exp. Bot.* **70**, 3211–3225 (2019).
17. Klimmek, F., Sjödin, A., Noutsos, C., Leister, D. & Jansson, S. Abundantly and rarely expressed Lhc protein genes exhibit distinct regulation patterns in plants. *Plant Physiol.* **140**, 793–804 (2006).
18. Albanese, P. et al. Dynamic reorganization of photosystem II supercomplexes in response to variations in light intensities. *Biochim. Biophys. Acta Bioenerg.* **1857**, 1651–1660 (2016).
19. Grinzato, A. et al. High-light versus low-light: effects on paired photosystem II supercomplex structural rearrangement in pea plants. *Int. J. Mol. Sci.* **21**, 8643 (2020).
20. Kashino, Y. et al. Ycf12 is a core subunit in the photosystem II complex. *Biochim. Biophys. Acta* **1767**, 1269–1275 (2007).
21. Crepin, A. & Caffarri, S. Functions and evolution of Lhcb isoforms composing LHCII, the major light harvesting complex of photosystem II of green eukaryotic organisms. *Curr. Protein Pept. Sci.* **19**, 699–713 (2018).
22. Guardini, Z., Gomez, R. L., Caferri, R., Dall'Osto, L. & Bassi, R. Loss of a single chlorophyll in CP29 triggers re-organization of the photosystem II supramolecular assembly. *Biochim. Biophys. Acta Bioenerg.* **1863**, 148555 (2022).
23. Kruk, J. & Srzałka, K. Occurrence and function of alpha-tocopherol quinone in plants. *J. Plant Physiol.* **145**, 405–409 (1995).
24. Kumar, A., Prasad, A. & Pospíšil, P. Formation of α-tocopherol hydroperoxide and α-tocopheroxyl radical: relevance for photooxidative stress in Arabidopsis. *Sci. Rep.* **10**, 19646 (2020).
25. Graça, A. T., Hall, M., Persson, K. & Schröder, W. P. High-resolution model of *Arabidopsis* photosystem II reveals the structural consequences of digitonin-extraction. *Sci. Rep.* **11**, 15534 (2021).

26. Triantaphylides, C. & Havaux, M. Singlet oxygen in plants: production, detoxification and signaling. *Trends Plant Sci.* **14**, 219–228 (2009).

27. Krieger-Liszkay, A. & Trebst, A. Tocopherol is the scavenger of singlet oxygen produced by the triplet states of chlorophyll in the PSII reaction centre. *J. Exp. Bot.* **57**, 1677–1684 (2006).

28. Shi, L. X., Lorkovic, Z. J., Oelmuller, R. & Schroder, W. P. The low molecular mass PsbW protein is involved in the stabilization of the dimeric photosystem II complex in *Arabidopsis thaliana*. *J. Biol. Chem.* **275**, 37945–37950 (2000).

29. Granvogl, B., Zoryan, M., Plöscher, M. & Eichacker, L. A. Localization of 13 one-helix integral membrane proteins in photosystem II subcomplexes. *Anal. Biochem.* **383**, 279–288 (2008).

30. Kruk, J., Schmid, G. H. & Strzałka, K. Interaction of α-tocopherol quinone, α-tocopherol and other prenyllipids with photosystem II. *Plant Physiol. Biochem.* **38**, 271–277 (2000).

31. Bielczynski, L. W., Xu, P. & Croce, R. PSII supercomplex disassembly is not needed for the induction of energy quenching (qE). *Photosynth. Res.* **152**, 275–281 (2022).

32. Novoderezhkin, V., Marin, A. & van Grondelle, R. Intra- and inter-monomeric transfers in the light harvesting LHCII complex: the Redfield–Förster picture. *Phys. Chem. Chem. Phys.* **13**, 17093–17103 (2011).

33. Papadatos, S., Charalambous, A. C. & Daskalakis, V. A pathway for protective quenching in antenna proteins of photosystem II. *Sci. Rep.* **7**, 2523 (2017).

34. Hakala-Yatkin, M. et al. Magnetic field protects plants against high light by slowing down production of singlet oxygen. *Physiol. Plant.* **42**, 26–34 (2011).

35. Niewiadomska, E. et al. Lack of tocopherols influences the PSII antenna and the functioning of photosystems under low light. *J. Plant Physiol.* **223**, 57–64 (2018).

36. Dau, H. et al. Structural consequences of ammonia binding to the manganese center of the photosynthetic oxygen-evolving complex: an X-ray absorption spectroscopy study of isotropic and oriented photosystem II particles. *Biochemistry* **34**, 5274–5287 (1995).

37. Lichtenthaler, H. K. Chlorophylls and carotenoids: pigments of photosynthetic biomembranes. *Methods Enzymol.* **148**, 350–382 (1987).

38. Caffari, S., Kouril, R., Kereiche, S., Boekema, E. J. & Croce, R. Functional architecture of higher plant photosystem II supercomplexes. *EMBO J.* **28**, 3052–3063 (2009).

39. Sorzano, C. O. S. et al. A new algorithm for high-resolution reconstruction of single particles by electron microscopy. *J. Struct. Biol.* **204**, 329–337 (2018).

40. Zheng, A. Q. et al. MotionCor2: anisotropic correction of beam-induced motion for improved cryo-electron microscopy. *Nat. Methods* **4**, 331–332 (2017).

41. Zhang, K. Gctf: real-time CTF determination and correction. *J. Struct. Biol.* **193**, 1–12 (2016).

42. de la Rosa Tevín, J. M. et al. Xmipp 3.0: an improved software suite for image processing in electron microscopy. *J. Struct. Biol.* **184**, 321–328 (2013).

43. Punjani, A., Rubinstein, J. L., Fleet, D. J. & Brubaker, M. A. cryoSPARC: algorithms for rapid unsupervised cryo-EM structure determination. *Nat. Methods* **14**, 290–296 (2017).

44. Scheres, S. H. RELION: implementation of a Bayesian approach to cryo-EM structure determination. *J. Struct. Biol.* **180**, 519–530 (2012).

45. Pettersen, E. F. et al. UCSF Chimera—a visualization system for exploratory research and analysis. *J. Comput. Chem.* **25**, 1605–1612 (2004).

46. DeLano, W. L. The PyMOL Molecular Graphics System (DeLano Scientific, 2002).

47. Winn, M. D. et al. Overview of the CCP4 suite and current developments. *Acta Crystallogr. D* **67**, 235–242 (2011).

48. Krissinel, E. & Henrick, K. Secondary-structure matching (SSM), a new tool for fast protein structure alignment in three dimensions. *Acta Crystallogr. D* **60**, 2256–2268 (2004).

49. Krissinel, E. & Henrick, K. Inference of macromolecular assemblies from crystalline state. *J. Mol. Biol.* **372**, 774–797 (2007).

50. Wiśniewski, J. R., Zougman, A., Nagaraj, N. & Mann, M. Universal sample preparation method for proteome analysis. *Nat. Methods* **6**, 359–362 (2009).

Acknowledgements

Author contributions

M.O., D.K., P.I., P.P, P.L.K. and R.K., study design. M.O., D.A.S., F.L.K. and F.H., sample preparation for cryo-EM. D.A.S., image analysis of cryo-EM data. D.K. and R.K., model building. M.O. and I.I., amino acid sequence analysis. P.R., mass spectrometry analysis. P.T. and S.Ć.Z., fatty acid composition. P.T. and S.Ć.Z., α-tocopherol(quinone) analysis. M.O., D.K., P.I., P.P. I.I. and R.K., data interpretation. M.O., D.A.S., P.I., I.I. and R.K. wrote the main body of the paper, and all authors revised and approved it.

Competing interests

The authors declare no competing interests.

Additional information

Supplementary information The online version contains supplementary material available at https://doi.org/10.1038/s41477-023-01483-0.

Correspondence and requests for materials should be addressed to Roman Kouřil.

[1]Department of Biophysics, Faculty of Science, Palacký University, Olomouc, Czech Republic. [2]Interdisciplinary Research Center HALOmem, Charles Tanford Protein Center, Martin Luther University Halle-Wittenberg, Halle/Saale, Germany. [3]Department of Experimental Biology, Faculty of Science, Palacký University, Olomouc, Czech Republic. [4]Institute of Experimental Botany of the Czech Academy of Sciences, Centre of Plant Structural and Functional Genomics, Olomouc, Czech Republic. [5]Central European Institute of Technology, Masaryk University, Brno, Czech Republic. [6]Czech Advanced Technology and Research Institute, Palacký University, Olomouc, Czech Republic. [7]Centre of the Region Haná for Biotechnological and Agricultural Research, Department of Genetic Resources for Vegetables, Medicinal and Special Plants, Crop Research Institute, Olomouc, Czech Republic. [8]Institute of Biochemistry and Biotechnology, Martin Luther University Halle-Wittenberg, Halle/Saale, Germany. [9]Institute of Chemical Biology, National Hallenic Research Foundation, Athens, Greece. [10]These authors contributed equally: Monika Opatíková, Dmitry A. Semchonok. ✉e-mail: roman.kouril@upol.cz